Sound propagation in woodland

Thesis

Sound Propagation in Woodland

Thesis Submitted By
Margaret Anne (Williams) Price BSc(Hons).
for the degree of
Doctor of Philosophy
June 1986

Department of Engineering Mechanics
Faculty of Technology
Open University
Milton Keynes
England.

Abstract

A review of past research into sound propagation in woodland is presented. The attenuation of sound in woodland is small between about 800 and 2000Hz and greater at low and high frequencies.

Attenuation measurements made in three contrasting woodlands are presented and compared with theoretical models. Propagation models using simple one- and two-parameter impedance models are used to calculate appropriate ground parameters for the prediction of impedance of the woodland soils. The ground parameters varied on different days in a single stand due to differences in moisture content and compaction. The overall differences between the stands are not significant. The woodland soil has a considerably lower impedance than other outdoor ground surfaces such as grassland or sand.

A theoretical model for the attenuation of sound by thermoviscous absorption and scattering within an array of cylinders is assessed by means of a model experiment with wooden rods in an anechoic chamber. An input density 60% lower than the actual density gives a good agreement with measured attenuation. This modified model also predicts the attenuation by the cylinders in the presence of a ground surface.

The scattering model is compared with the high frequency attenuation measured in the woodland, using sampled trunk densities and radius, this underpredicts the observed attenuation, particularly in the stands with a dense branch and foliage structure. Addition of a second, dense, array of non rigid scatterers gives a good agreement with the measured data, thus modelling the scattering and absorbing effects of trunks, branches and leaves, in the high frequencies.

Finally, a combined model is presented in which the attenuation caused by ground interference effects, at low frequencies, is added to a prediction of attenuation by the scattering model, across the whole frequency range. This model reproduces the frequency dependence of the attenuation of sound in woodland.

Acknowledgements

The author is indebted to her supervisors, Dr Keith Attenborough and Dr Nick Heap for their guidance and support throughout the course of this research and records her sincere gratitude, to them and to Ms Heather Hess, Ms Jeanette Vaughan and Mr Brendan Aengenheister for their assistance in the woods and Mr Philip Payne and the Technical Staff of the Technology Faculty for their help in making up experimental equipment.

This research was supported by studentship grants from the Science and Engineering Research Council, the Forestry Commission and the Open University.

Table of Contents.

Figure Captions For Chapter 2

Figure Captions For Chapter 3

Figure Captions For Chapter 4

100 Figure 4.23: Attenuation function, using homogeneous approximation. σ_e = 100,000 mks rayls σ_e = 200,000 mks rayls σ_e =1,000,000 mks rayls Reference microphone:- hs=1.3m, hr=1.3m, r=2m. Test microphone:- hs=1.3m, hr=1.2m, r=96m.

100 Figure 4.24: Attenuation function, using rigid-backed layer approximation. σ_e = 100,000 mks rayls (homogeneous) σ_e = 100,000 mks rayls de = 0.01 σ_e = 100,000 mks rayls de = 0.1 σ_e = 100,000 mks rayls de = 0.02 Experimental geometry as in figure 4.23.

101 Figure 4.25: Attenuation function, using variable porosity approximation. σ_e = 100,000 mks rayls α_e = 0 (homogeneous) σ_e = 100,000 mks rayls α_e = 100 σ_e = 100,000 mks rayls α_e = 200 Experimental geometry as in figure 4.23.

101 Figure 4.26: Attenuation function, using Delany and Bazley model. σ_e = 100,000 mks rayls σ_e = 200,000 mks rayls σ_e =1,000,000 mks rayls Experimental geometry as in figure 4.23.

Figure Captions For Chapter 5

Figure Captions For Chapter 6.

185 Figure 6.4.15: 2/7/85 mean of 4 attenuation measurements, microphone at F26, source at FS and source at FS microphone at d (16.8m).

Figure Captions For Chapter 7.

Figure Captions For Chapter 8

Page

259 Figure 8.22: Range of attenuation (dB per 24m) for all Wetleys Wood measurements. With 'trunk scattering' predictions.

radius=0.059, density=0.303 (measured).

radius=0.059, density=0.1212 (-60%).

259 Figure 8.23: Range of attenuation (dB per 24m) for all Bucknell Wood measurements. With 'trunk scattering' predictions.

radius=0.066, density=0.181 (measured).

radius=0.066, density=0.0724 (-60%).

260 Figure 8.24: Predicted attenuation over 24m using sum of 2 arrays and 'mean array'.

261 Figure 8.25: Mean measured attenuation (dB per 24m) for Hazelborough Wood. summer measurements.

is sum of predictions for 2 arrays. Mean difference=0.62dB. a) radius=0.045, density=0.1068 rigid cylinders and b) radius=0.0131, density=1.5, rigid cylinders.

261 Figure 8.25a: Prediction for 2 arrays

radius=0.045, density=.1068 rigid cylinders and radius=0.0131, density=1.5, rigid cylinders.

262 Figure 8.26: Mean measured attenuation (dB per 24m) for Hazelborough Wood. winter measurements.

is prediction for sum of 2 arrays, mean difference=0.89. 2 arrays a) radius=0.045, density=0.1068 rigid cylinders and

b) radius=0.001, density=2, rigid cylinders.

262 Figure 8.26a: Prediction for 2 arrays

radius=0.045, density=0.1068 rigid cylinders and radius=0.001, density=2, rigid cylinders

263 Figure 8.27: Mean measured attenuation (dB per 24m) for Wetleys Wood.

is sum of predictions for 2 arrays. Mean difference=0.80dB. a) radius=0.059, density=0.1212 rigid cylinders and b) radius=0.0019, density=80, rigid cylinders

263 Figure 8.27a: Prediction for 2 arrays

radius=0.059, density=0.1212, rigid cylinders and radius=0.0019, density=80, rigid cylinders.

264 Figure 8.28: Mean measured attenuation (dB per 24m) for Bucknell Wood.

is sum of predictions for 2 arrays. Mean difference=6.04dB. a) radius=0.066, density=0.0724 rigid cylinders and b) radius=0.0021, density=340, rigid cylinders

272 Figure 8.34: Measured attenuation from Hazelborough Wood 9/8/84; Separation distance 48m, H track, 1.2m microphone height, Prediction using homogeneous approximation σ_e = 40,000; to 2kHz. + scattering radius= 0.045, density = 0.1068, rigid cylinders

+ radius= 0.001, density = 70 , σ_e = 1,900,000

273 Figure 8.35: Range of values for Bucknell Wood 12m separation. Prediction using homogeneous approximation σ_e = 68,000; to 2kHz. + scattering radius= 0.066, density = 0.0724, rigid cylinders

+ radius= 0.001, density = 100 , σ_e = 860,000

273 Figure 8.36: Range of values for Bucknell Wood 24m separation. Prediction using homogeneous approximation σ_e = 68,000; to 2kHz. + scattering radius= 0.066, density = 0.0724, rigid cylinders

+ radius= 0.001, density = 100 , σ_e = 860,000

274 Figure 8.37: Range of values for Bucknell Wood 40m separation. Prediction using homogeneous approximation σ_e = 68,000; to 2kHz. + scattering radius= 0.066, density = 0.0724, rigid cylinders

+ radius= 0.001, density = 100 , σ_e = 860,000

274 Figure 8.38: Range of values for Wetleys Wood 12m separation. Prediction using homogeneous approximation σ_e = 68,000; to 2kHz. + scattering radius= 0.059, density = 0.1212, rigid cylinders

+ radius= 0.001, density = 100 , σ_e = 10,000,000

275 Figure 8.39: Range of values for Wetleys Wood 24m separation. Prediction using homogeneous approximation σ_e = 68,000; to 2kHz. + scattering radius= 0.059, density = 0.1212, rigid cylinders

+ radius= 0.001, density = 100 , σ_e = 10,000,000

275 Figure 8.40: Range of values for Wetleys Wood 48m separation. Prediction using homogeneous approximation σ_e = 68,000; to 2kHz. + scattering radius= 0.059, density = 0.1212, rigid cylinders

+ radius= 0.001, density = 100 , σ_e = 10,000,000

276 Figure 8.41: Range of values for Wetleys Wood 96m separation. Prediction using homogeneous approximation σ_e = 68,000; to 2kHz. + scattering radius= 0.059, density = 0.1212, rigid cylinders

+ radius= 0.001, density = 100 , σ_e = 10,000,000

283 Figure 8.51: Excess attenuation at 50m, as in figure 8.49. With predictions from Kragh et al (1982) and ISO (1986).

283 Figure 8.52: Excess attenuation at 100m, as in figure 8.50. With predictions from Kragh et al (1982) and ISO (1986).

Chapter 1: Introduction.

The increasing problem of noise as an environmental pollutant, has lead to the development of standards of acceptable noise levels and legislation concerning noise control. In order to assess the possible impact of new developments such as motorways on the acoustic environment of an area, prediction schemes have been developed to determine the sound pressure levels which would be expected at a given location, calculated from the noise source and the terrain over which the sound travels. Most such prediction schemes disregard the presence of woodland since there is relatively little detailed knowledge about the precise effects of woodland on the propagation of sound, and the evidence obtained by different studies often gives rise to different conclusions. The use of a belt of woodland as a barrier to screen a problematic noise source is an attractive proposition from an aesthetic and ecological point of view, but again there is some debate about the effectiveness of such a screen due to the high porosity of a belt of trees compared to conventional noise control screens.

Measurements of sound propagation are generally quoted as 'attenuation' ie the amount by which sound is reduced when passing through a woodland, this is because the main applications are concerned with noise control. Many studies of sound propagation in woodland have described the pattern of the attenuation spectrum as having greater attenuation in the high and low frequencies with little or no attenuation in the mid-frequencies, in fact, an increase in sound pressure over the free field level has been reported by some authors. The prediction of propagation over a flat, acoustically rather soft, ground surface, has been suggested as the main mechanism operating at low frequencies. Various theoretical models have been suggested to account for the observed high frequency attenuation, generally in terms of scattering and absorption by the trunks, branches, and leaves of the trees.

The purpose of this thesis is to assess the various theoretical models presented in the literature, and their applicability to the description, and prediction, of sound propagation within and through wooded areas, in an attempt to elucidate the physical mechanisms acting on a sound wave as it passes through a woodland. An attempt is made at combining the high and low frequency effects into a model which could be used to predict the sound

pressure level at a known distance, in particular to reproduce the typical frequency dependence of the attenuation spectra measured in woodland.

Layout of the Thesis.

The background to this study is described in chapter 2, in the form of a general review of published literature relating to the propagation of sound in woodland. This review assesses the various approaches which have been adopted by research workers. Several studies carried out to assess the use of trees in noise control have used broad band sources, such as traffic noise and measured the overall attenuation, others have investigated the frequency dependence of the attenuation of sound by the woodland, which is applicable to a wider range of uses. Knowledge of the frequency dependence of the sound propagation in woodland has enabled theoretical studies to be carried out into the possible mechanisms of sound attenuation acting in woodland, some of which are also reviewed in chapter 2. The theoretical studies assessed include the effect of the ground, related to the type of ground surface, which is evidently different in woodland to farmland, grassland, pavement, etc. and has different acoustic properties. Other mechanisms which have been suggested as explanations for the attenuation of sound in woodland include scattering and absorption by tree trunks, branches and leaves. Existing methods used to take account of the attenuation of sound by tree belts and woodland are also described in chapter 2.

The equipment and methods used in experiments carried out in woodland is described in chapter 3 along with a descripion of the software developed to analyse the data obtained.

In chapter 4 the theoretical models used to predict the propagation of sound over a ground surface are described in detail. The theoretical models are used to calculate an attenuation function which is directly comparable to the measurements carried out in woodland. The dependence of the attenuation function on the experimental geometry and the ground surface is illustrated.

The theoretical model for the second main mechanism of sound attenuation in woodland investigated in detail, ie. scattering of sound, is described in chapter 5, along with the software developed to calculate a prediction of attenuation from the model.

The results of attenuation measurements made in the woodland sites are described in chapter 6. Three contrasting sites were used, all are Forestry Commission plantations, on flat land near Silverstone in Northamptonshire. Each stand is treated individually in chapter 6, presenting the characteristics of the stand, description of the main measurements made and results for each measurement day. The results for the stand on different days are compared.

In order to investigate the applicability of the theoretical model of the attenuation of sound by scattering by an array of cylinders, both with, and without, a ground surface, a model experiment was carried out which is described in chapter 7. The attenuation caused by an array of cylindrical wooden rods was measured, both with the rods inserted into a tray of sand to simulate a ground surface and without the sand, so the rods were assumed to approximate to infinitely long rods. Theoretical model predictions were compared with the results.

In chapter 8 the two theoretical models are used to compare the attenuation effects of the different stands. A combined model of attenuation including the effects of both ground and scattering effects in presented and its applicability to the measured results assessed. The practical applications of the results of this study are presented and suggestions made for future work which would advance the understanding of sound propagation in woodland.

Chapter 2 : Background.

Various approaches have been used in studies of sound propagation within and through woodland, depending largely on the main application for which a study was conducted. Many have concentrated on the attenuation by a narrow belt of trees as this has obvious applications in outdoor noise control and planning. More extensive woodland has also been evaluated for planning purposes such as the prediction of noise contours from proposed motorway developments close to existing woodland. Studies for planning purposes tend to produce little or no information on the frequency dependence of the results beyond using an appropriate source eg. road traffic noise, or A-weighting the results. Studies which analyse the results in terms of frequency tend to have a wider application as the results can be extrapolated for different source spectra. Other reasons for carrying out research in this area have included the description of the acoustic environment relating to animal vocalisation and military applications. Theoretical studies investigating the physical properties of outdoor sound propagation in terms of ground reflection, scattering and absorption by vegetation and meteorological effects, are also relevant to sound propagation in woodland. Many studies have, of course, combined empirical measurements with theoretical predictions.

In this chapter, after defining some of the more important terms used in describing experimental results, I will summarise the findings of various empirical studies and then assess predictive models that have been applied to describe the ground effect and other attenuation mechanisms.

2.1 Definition of Terms.

The propagation of sound over a ground surface is most often quoted as the 'excess attenuation'. This is defined as the difference between the sound level (in decibels: dB), measured (or predicted) at a certain location above a surface, minus that which would be expected at that location in the absence of any ground surface (known as the 'free field' case). The free field case is calculated from the source level, and the reduction in sound level due to spherical spreading, and atmospheric absorption. The free field source level and spectrum have to be determined experimentally eg by measuring the source level in an anechoic chamber or with the source and receivers far from any reflecting surfaces. Some sources eg. traffic noise may be deduced from measurements made over a rigid surface, and corrected using certain assumptions about sound propagation over an acoustically hard surface to give a free field spectrum. Atmospheric absorption can be calculated from formulae such as those described by Bazley (1976) (see chapter 3).

Another way in which the attenuation due to woodland is often quoted is as an 'insertion loss'. The insertion loss is the level measured at a given separation distance and source and receiver height resulting from a source over 'open ground' minus the level measured using the same source and experimental geometry with the sound propagating through a belt, or stand, of trees. Another way of putting this is: the (excess) attenuation through woodland minus that across the open ground. The reference 'open ground' used evidently has a considerable effect on the insertion loss. Grassland is often used as the reference ground since it would be the most likely ground covering if the woodland or belt were not there. The reference ground is generally chosen to have a similar gradient for direct comparison between the two cases without consideration of the ground configuration. The measurements of attenuation over the reference ground and through the woodland are often made on the same day in order to minimise the effects which could be caused by different meteorological conditions, however, the vegetation itself affects the meteorological conditions so this assumption may not be valid. Other possible errors encountered in making insertion loss measurements include the differences between the properties of different reference grounds and the forest floor. The effect of different ground surfaces will be discussed later in this chapter.

2.2 Empirical Measurements of Sound Propagation Through Tree Belts and Woodlands.

Table 1 Summary of some results using broad-band source and analysis.

Author	Vegetation	Insertion Loss	Excess Attenuation	Sound Source
Kragh (1979)	Dense mixed belt 15 years old.	8 9dBA '50m		Railway
Kragh (1979)	Dense mixed belt 10 20 years.	6-7dBA '50m		Railway
Kragh (1981)	Deciduous trees and bushes 5-10 years.	0dB LAeq		Roads
Kragh (1981)	Very Dense white spruce belt 3m wide 40 years old.	3-5dB LAeq		Roads
Hess and Kursteiner (1961)	High mixed stand 200-250m belt.		35dB	Car engine
Hess and Kursteiner (1961)	Dense Oak thicket 200-250m belt.		45dB	Car engine
Whitcombe and Stowers (1973)	Illicum anisatum hedge	6 7dBA		Lawnmower
Whitcombe and Stowers (1973)	Illicum anisatum hedge.	10dBA		car at 60mph
Ozimek and Kobek (1970)	Dense Scots Pine stand.	15dB '25m		White Noise
Ozimek and Kobek (1970)	Birchwood with under-storey 12 years old.	15dB '14m		White Noise
Ozimek and Kobek (1970)	Scots pine with herbaceous ground vegetation 6 years old.	15dB '15m		White Noise
Visnapuu and Margus (1977)	7m belt of unbrashed spruce 2.5m high.	3-8dB		Traffic
Schiller, Schaudinschky and Keller (1981)	Conifer stands eg. Pinus spp. Callitris verrucosa, Thuya orientalis.	$\leqslant$0.1dBA/m		white noise
Schiller, Schaudinschky and Keller (1981)	Broadleaved stands eg Ficus retusa or Acacia saligna.	$\leqslant$0.2dBA/m		white noise

Table 1 summarises some reported results. This serves to illustrate the kind of measurements which have been made and the wide differences between methods and presentation of results. Interpretation of and comparison between such results is difficult due to differences in technique, and uncertainty about the actual techniques used, including such factors as the source spectrum, weighting used on the results, reference ground used for

insertion loss measurements etc. Differing results within the same study do, however,indicate that the attenuation does depend on the source spectrum (eg. Whitcombe and Stowers, Kragh) and the vegetation type (eg. Hess and Kursteiner, Ozimek and Kobek).

Cook and van Haverbeke (1971, 1974, 1976, 1977) carried out extensive measurements of attenuation through belts of trees in both rural and urban situations. They compared measurements of the drop in sound level with distance through tree belts with those over open ground and produced empirical equations to predict sound levels behind belts. They also produced recommendations for the planting of trees for traffic noise control. The empirical equations are limited to tree belts similar to the shelter-belts in agricultural land in Nebraska from which the equations were deduced. Different equations were constructed for each of three belt types (coniferous, mixed and deciduous) and three sound sources (truck noise, cars at 40 mph and the noise at a bus stop). These authors did observe that the attenuation was also dependent on belt density but were unable to find a satisfactory method of numerically evaluating belt density.

The following recommendations were made using the results from the initial study:-

Where possible taller varieties of trees which have dense foliage with a relatively uniform vertical foliage distribution (or a combination of trees and shrubs to give this effect) should be used.

Close planting is required to give a continuous, dense barrier, and evergreens or deciduous varieties which retain their leaves are recommended.

A tree belt should be approximately twice as long as the distance from the noise source to the receiver, and, when used as a screen parallel to a road, should extend equal distances along the road on both sides of the protected area.

The construction of a fence, wall or earth bank can be used to give immediate protection from noise and can later be supplemented as plantings of trees and shrubs grow to give a dense belt. This combination is recommended for urban sites with severe problems from a large road. A large landform of sufficient height to screen the traffic from view is recommended to reduce noise from high-speed car and truck traffic. with several rows of trees and shrubs planted on and adjacent to it.

In general the severity of the noise problem and land available will normally dictate the actual noise control barriers used, especially in urban areas. The visual screening of the sound is, however thought to be essential.

The conclusions and recommendations reached by Cook and van Haverbeke are based largely on their experimental results but also appear to draw heavily on 'common sense' conclusions since the experimental results have to be extrapolated from measurements made through very dense and wide rural belts and some dense urban belts. The use of a specific broad band source and analysis in terms of A-weighted decibels limits the extrapolation possible to account for sources with very different spectra.

Assessment of Stand Density

As mentioned above, Cook and van Haverbeke had some difficulty in relating vegetation density to attenuation. These authors, and others, have studied various ways in which tree belts, and more extensive stands could be characterised in terms of their density for comparison with acoustical measurements.

Drawing from work carried out in other fields, Cook and van Haverbeke investigated the use of radioactive methods which give an estimate of the amount of matter between two points, this is generally only useful at short distances therefore not applicable in a woodland situation. Windbreak specialists use a measurement of the reduction of wind by a tree belt as an assessment of density, Cook and van Haverbeke did not find this to be a useful

technique in their studies, this may be due to the fact that their belts were probably wider than a typical windbreak.

Eyring (1946), one of the earliest authors investigating sound propagation in woodlands, used a measure of visual penetrability to assess density (figure 2.1) with an increase in visibility relating to an increase in attenuation. These experiments were carried out in tropical jungles consisting of large-leaved plants and in most of the results the visibility is mainly restricted by the leaves suggesting that they are also responsible for the attenuation, except in zone 5 of figure 2.1 in which the visibility is greater than in zones 3 and 4 but the attenuation is greater, apparently due to the large size of the tree trunks.

Most noise propagation prediction schemes such as that of Kragh et al (1982a) state that to be at all effective in reducing noise a tree belt should prevent the sound source being seen from the receiver. This is related not only to the observed fact that a denser stand provides more attenuation but also the secondary, psychological effect, that is, a noise source is perceived to be less intrusive if it is screened from view. A popularly held belief that vegetation is an effective controller of noise also contributes to this 'psychological attenuation' effect (eg. Lim 1981).

Embleton (1963) found no correlation between visibility and attenuation in measurements of attenuation in homogeneous deciduous and evergreen woods, and Leonard and Herrington (1971) found no significant difference between a 'good' and 'poor' pine stand.

Cook and van Haverbeke stated that they had not found an estimate of ground cover significantly correlated with attenuation. The experiments of Kellomaki et al (1976), however, did correlate various numerical descriptors of ground cover and vertical structure of the stand with the measured attenuations. These measurements were made in stands of three different species (pine, spruce and mixed birch/conifer) and at different stages of growth. The sound source was white noise (20Hz to 100kHz) played through an amplifier and loudspeaker to produce a signal at 100 dBA 1m from the speaker. The resulting level was measured at distances of 12 to 96m from the source, by a sound level meter reading in

dBA. The densities were investigated in terms of total stem number per hectare, basal are of the stand (m^2 /ha) and volume (m^3 /ha). Contrary to the results of Cook and van Haverbeke, two of these were found to be significantly correlated with attenuation. A positive correlation of logarithmic form was found between the total stem number (trees over 2m high) and attenuation and there was also a positive correlation between the basal area of the stand and attenuation.

The vertical structure was investigated in terms of a lower tree storey (% of trees of height h, 2m $<$ h $<$ ¾ height of dominating trees), the percentage of self-pruned stems and the density of the bush storey (number of stems per ha). The regressions for the first two were found to be significant but the bush storey density did not appear to be significant. As the other two parameters showed that the presence of branches at lower levels increases attenuation, it is thought that the nature of the bush storey or experimental technique used account for the lack of a significant effect of the bush storey. There is no reason to suppose that stands with several storeys would not be more efficient in attenuation than a single storey.

The relationship between the height of the stands and attenuation is approximately parabolic, the attenuation increasing with height up to about 12m and decreasing as the stand gets higher. This is related to the growth stages of the trees which also reflect the vertical structure. The shorter trees are in the seedling and middle aged stage with branches down to ground level, whereas in mature stands the percentage of bare stem area is high. The correlations obtained from these results were used to construct equations from which the sound pressure can be predicted. Measured and predicted values were very highly correlated (correlation coefficient = 0.984).

The conclusions of Kellomaki et al are broadly in agreement with Cook and van Haverbeke and also of Beck (1968) that a large amount of foliage at low levels of the stand is important in stands planted for noise attenuation purposes. The differences in the detailed conclusions can be traced to the differences in the sources and stands used, and illustrate the limitations of such studies which do not investigate the frequency dependence of attenuation.

The fact that Kellomaki et al used white noise and Cook and van Haverbeke used traffic noise or a lawnmower account. in part. for the differences in the conclusions drawn about the correlation between density and attenuation. The attenuation caused by the scattering and absorption of sound by tree trunks. leaves and branches is largely a high frequency phenomenon. therefore the white noise source would have been affected more than the sources with little energy in the high frequencies. the use of A-weighting will only partially account for this difference. This clearly illustrates the need for more information about frequency dependence to be gathered in experiments. The predictions of Cook and van Haverbeke are evidently more applicable to noise control since they did use a common noise source. traffic noise. in some of their experiments. The use of three different traffic noise spectra in the construction of the prediction equations recognises that attenuation is dependent on frequency; but only partially accounts for factors affecting the frequency spectra of traffic noise. Measurements of sound propagation vs frequency such as those made through roadside tree belts in Denmark by Kragh (1982) are more applicable to a generalised noise prediction scheme.

A further reason for the differences between the conclusions of different studies is the vast diversity in what is termed a 'woodland' or 'forest' and the further complication introduced when the inhomogeneous structure of a tree belt is used. The tall, well-established shelterbelts used by Cook and van Haverbeke gave an increased attenuation with height because the dense shrub and understorey layers at the edge of the belt could continue to grow and develop as the trees in the centre grew to give attenuation to a greater height; whereas as the stands of Kellomaki et al grew taller, the lower layers became progressively more shaded and their growth was therefore inhibited giving rise to the parabolic relationship of attenuation vs height observed in this study.

The lack of undergrowth and living branches in mature forestry stands affects many studies of sound propagation in woodland since such stands are generally the most readily available. Deciduous plantations are more likely to have an understorey since more light is able to reach the ground levels particularly in spring, but they are still less dense than the woodland edges where the lower levels can develop under good light conditions. A belt of trees can be considered as two woodland edges which may have a 'hollow' area similar to a

forest stand in between.

Physical density, ie. the ratio of solid matter and air, is used in the characterisation of materials such as fibreglass for comparison with acoustic properties. The problems of obtaining such a value for woodland are evidently quite considerable. Martens (1980) has however described measurements of this kind on a smaller scale in a paper reporting on the attenuation of 'model forests' ie. small trees in pots in an anechoic chamber. It was concluded that there is a positive correlation between the total biomass of the leaves and attenuation, and also between the maximum size of the leaves and the frequency at which high frequency filtering of the sound starts. The results are illustrated in figure 2.2 it is evident from this figure that different species have a different effect on attenuation. Aylor (1972a) gives a similar relationship for very different vegetation type, ie maize and phragmites beds, this is reproduced as figure 2.3, these two species give a similar relationship with attenuation and frequency. Aylor and Martens used different parameters to describe the 'amount' of material present, ie the leaf area density and the total biomass, respectively. Martens states that the relationship obtained in the model forests is rather different to that obtained by Aylor, but Aylor (1981) later points out that if the values of F from figure 2.3 are converted to total biomass, the two papers are in closer agreement. The conclusions reached by these authors are that foliage is an effective filter of sound, absorbing the high frequencies and that, given knowledge of the total biomass (or leaf area density) and the dimensions of the leaves, the attenuation can be predicted. Martens further concludes that the physical differences between the leaves of different species also affects attenuation.

Kellomaki et al (1976) described differences between different species with their mixed and spruce woodlands giving more attenuation than pine. Mitscherlich and Scholzke (1977) also found spruce forests to be more effective in attenuating sound than either broadleaved trees or Scots pine; oak was found to be more effective than beech, and Scots pine the worst of the stands studied. It is not clear, however, whether these specific differences are due to actual differences between foliage types or simply an increase in biomass in the propagation path due to the different growth habits.

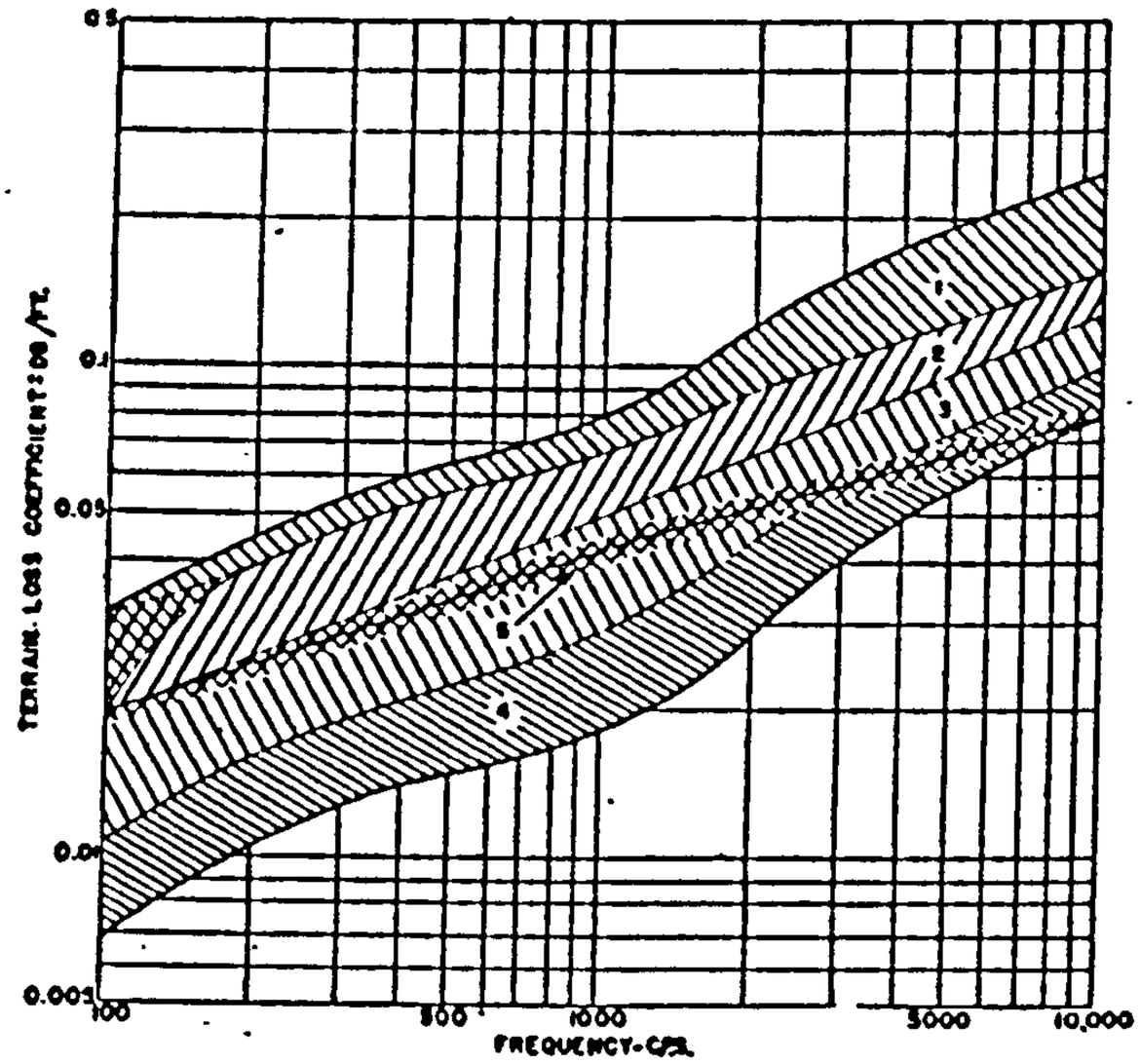

FIG. 10. A chart from which to estimate terrain loss coefficients for tropical jungles. Zone 1, very leafy, one sees a distance of approximately 20 ft., penetration by cutting; zone 2, very leafy, one sees approximately 50 ft., penetrated with difficulty but without cutting; zone 3, leafy, one sees a distance of approximately 100 ft., free walking if care is taken; zone 4, leafy, one sees a distance of approximately 200 ft., penetration is rather easy; zone 5, little leafy undergrowth, large bracketed trunks, one sees a distance of approximately 300 ft., penetration is easy.

Figure 2.1
Relationship between terrain loss and visibility, from Eyring(1946).

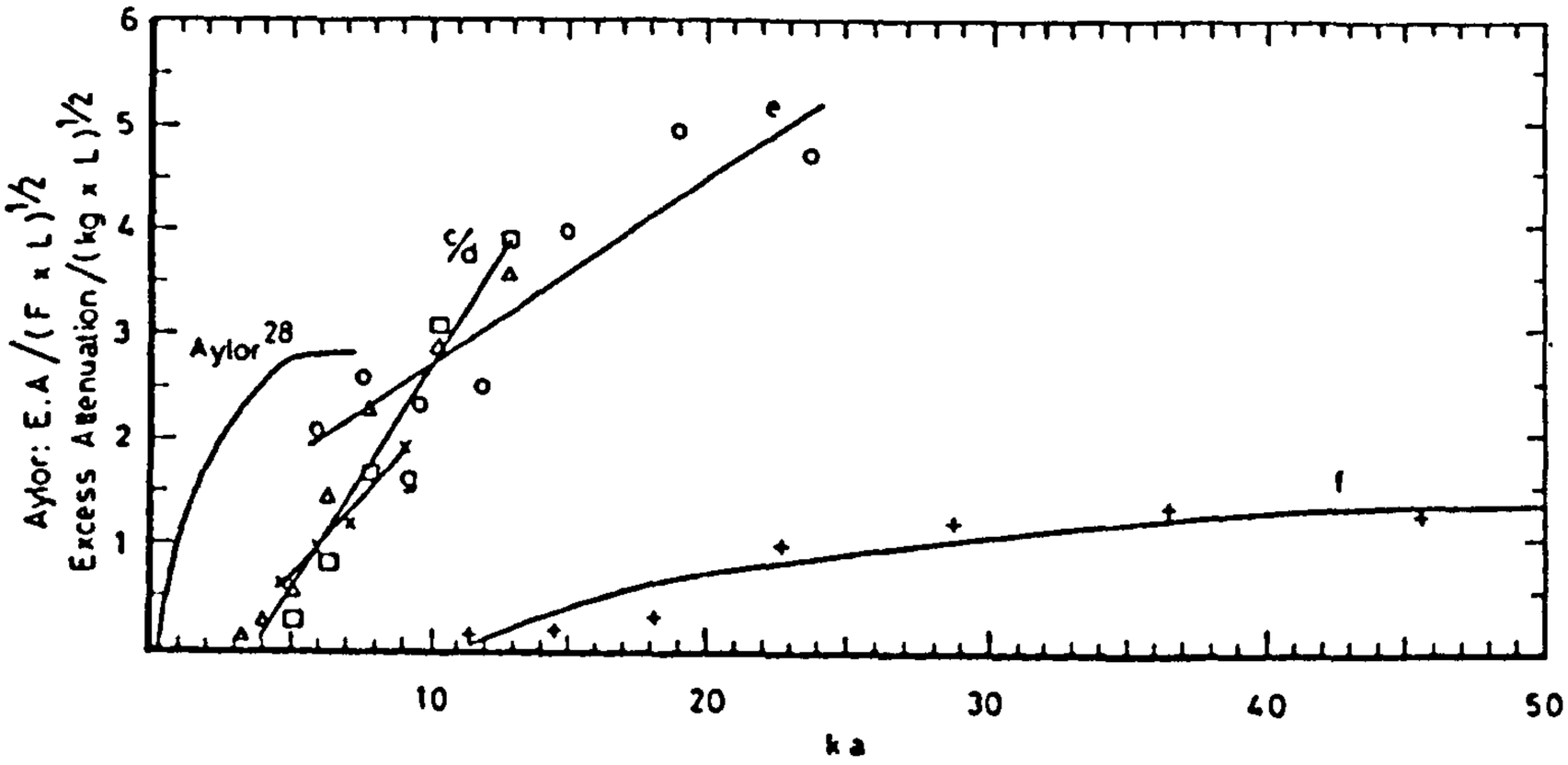

FIG. 4. Relation between excess attenuation, biomass of the plants in kg, length of model forest (L = 4.5 m), maximum dimension of leaves in cm, a, and wave-number (k = 2π divided by the wavelength). Curve c/d for the birch trees, e for the hazeltrees, f for the tropical plants, and g for the privets. For comparison Aylor's curve [28] is given; note that Aylor used the leaf area density (F), instead of the plant biomass.

Figure 2.2
Relationship between excess attenuation and plant physical parameters, from Martens(1980).

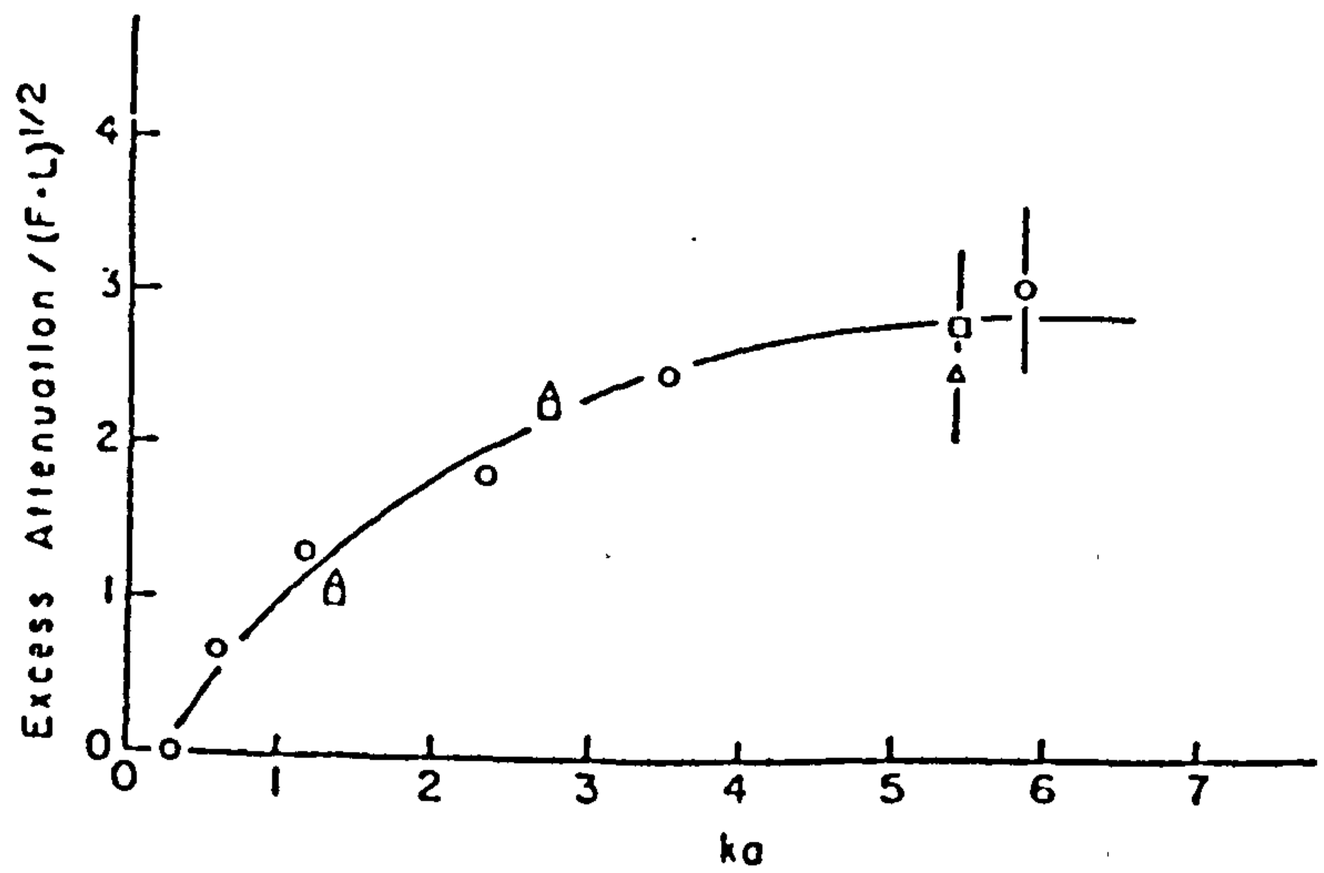

FIG. 3. Excess attenuation divided by $(F \cdot L)^{\frac{1}{2}}$ vs ka for *Phragmites* with an $F = 3\ m^{-1}$ (○), corn with an $F = 6.3\ m^{-1}$ (□), and corn with an $F = 3\ m^{-1}$ (△).

Figure 2.3
Relationship between excess attenuation and plant physical parameters, from Aylor(1972a).

2.3 Frequency Dependence of Sound Propagation in Woodland.

The results reported by Eyring (1946) of sound propagation in tropical forests are quoted as a Terrain Loss Coefficient in dB/ft as illustrated in figure 2.1. The terrain loss is approximately the same as excess attenuation since attenuation due to spherical spreading was accounted for. Later studies have shown that the attenuation in woodland is not a linear relationship with distance because of the effects of interferences between the waves travelling in a direct sound path and those reflected from the ground, as well as the differences between woodland edges and more extensive woodlands described above. The reason that Eyring's results could effectively be constrained to a linear relationship with distance is probably due to the nature of the forests studies ie. dense, uniform tropical forest with large leaves. The source and receivers may also have been sufficiently high above the ground to reduce the ground effect to a relatively small effect. The height of the transmission path above the ground is not quoted in this paper since, presumably, the significance of the ground effect and therefore the exact experimental geometry were not appreciated at the time.

Many later studies have shown the characteristic pattern of attenuation in woodland which does not follow the increase of attenuation with frequency shown in Eyring's results probably for the same reasons as the linear relationship with distance discussed above. The results such as those of Aylor (1972), Linskens et al (1976), Martens (1981), Lanphear (1971) and others show a marked peak in attenuation at low frequencies (200 to 500 Hz) with a dip in the mid-frequencies and a further increase in the higher frequencies. Figures 2.4 to 2.6, show some of these results. Marten et al (1977 and 1977a) do not observe the low frequency peak, this is probably because the peak for the ground surfaces used occured below the lowest frequency measured ie. 350Hz.

The results of the measurements carried out using traffic noise as a source by Kragh (1982) show that a similar pattern of attenuation can be detected in tree belts (see figures 2.7 and 2.8). The expected attenuation from grassland is compared with that measured through dense roadside belts. These results elucidate the reasons for the discrepancies between the results from different studies using belts of trees and calculating insertion loss.

The insertion loss would, in fact, be negative in the frequency range 500Hz to 1250Hz of figure 2.7 using the grassland attenuation as the reference, therefore sounds with much energy in this frequency range could be attenuated less by the tree belt than by the grassland. Other belts investigated in this study did show a greater, or very similar attenuation through the belt than across grassland at all frequencies (eg. figure 2.8).

Much effort has been spent, by many authors, on explaining the mid-frequency dip but the low frequency peak and mid-frequency dip are now known to be a result of the ground interference effects. The high frequency attenuation has been shown in many studies to be well above that explained by ground effects or that measured over open grassland, and is therefore thought to be more directly attributable to the presence of the trees.

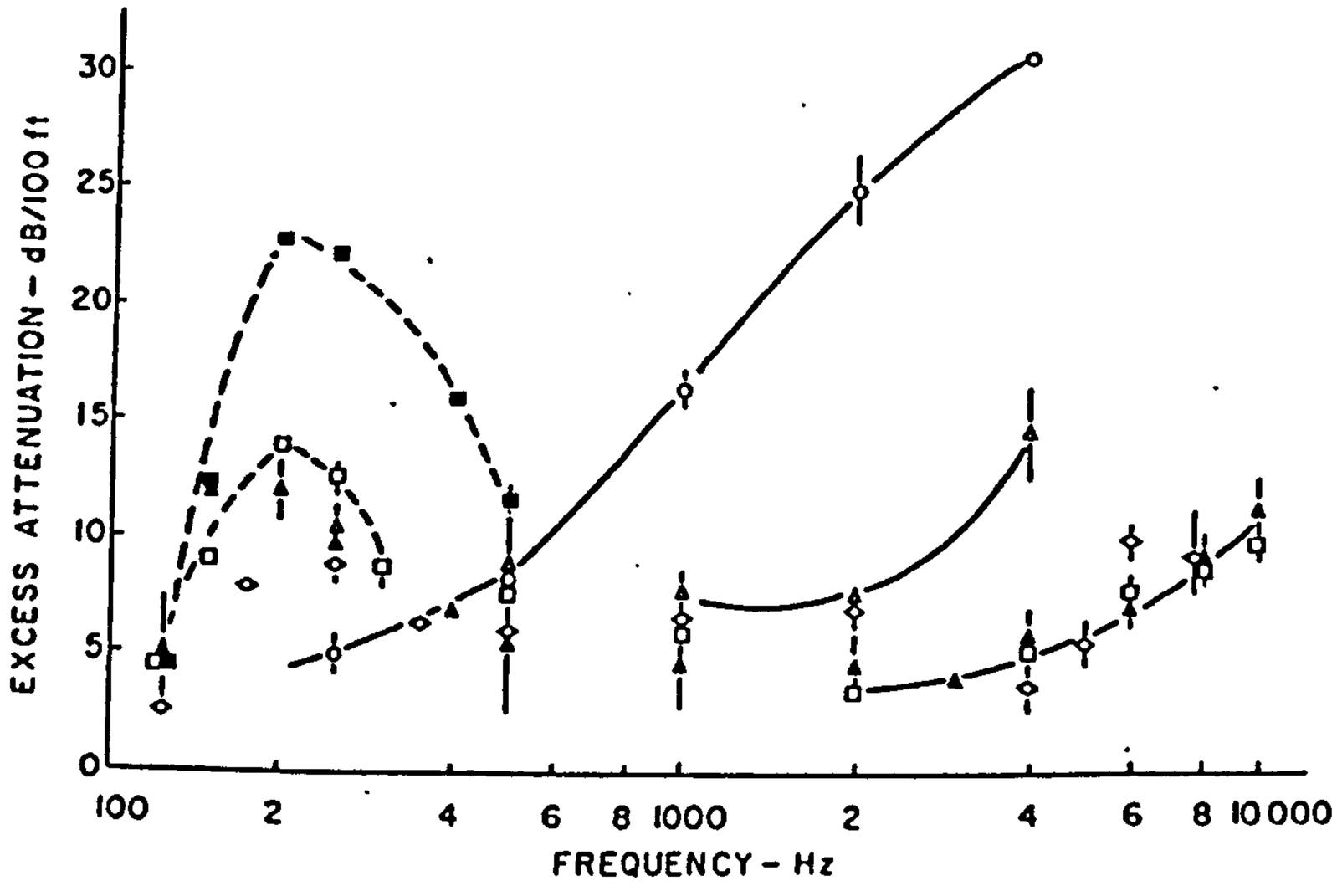

FIG. 1. Excess attenuation in decibels/100 ft for corn (○), hemlock (◇), pine measured at 200 ft (□), pine measured at 100 ft (■), brush in summer (△), and brush in autumn (▲) at frequencies of 100 to 10 000 Hz. The source height was 1 m for the corn and 1.5 m for the hemlock, pine, and brush.

Figure 2.4
Excess attenuation through vegetation. from Aylor(1972).

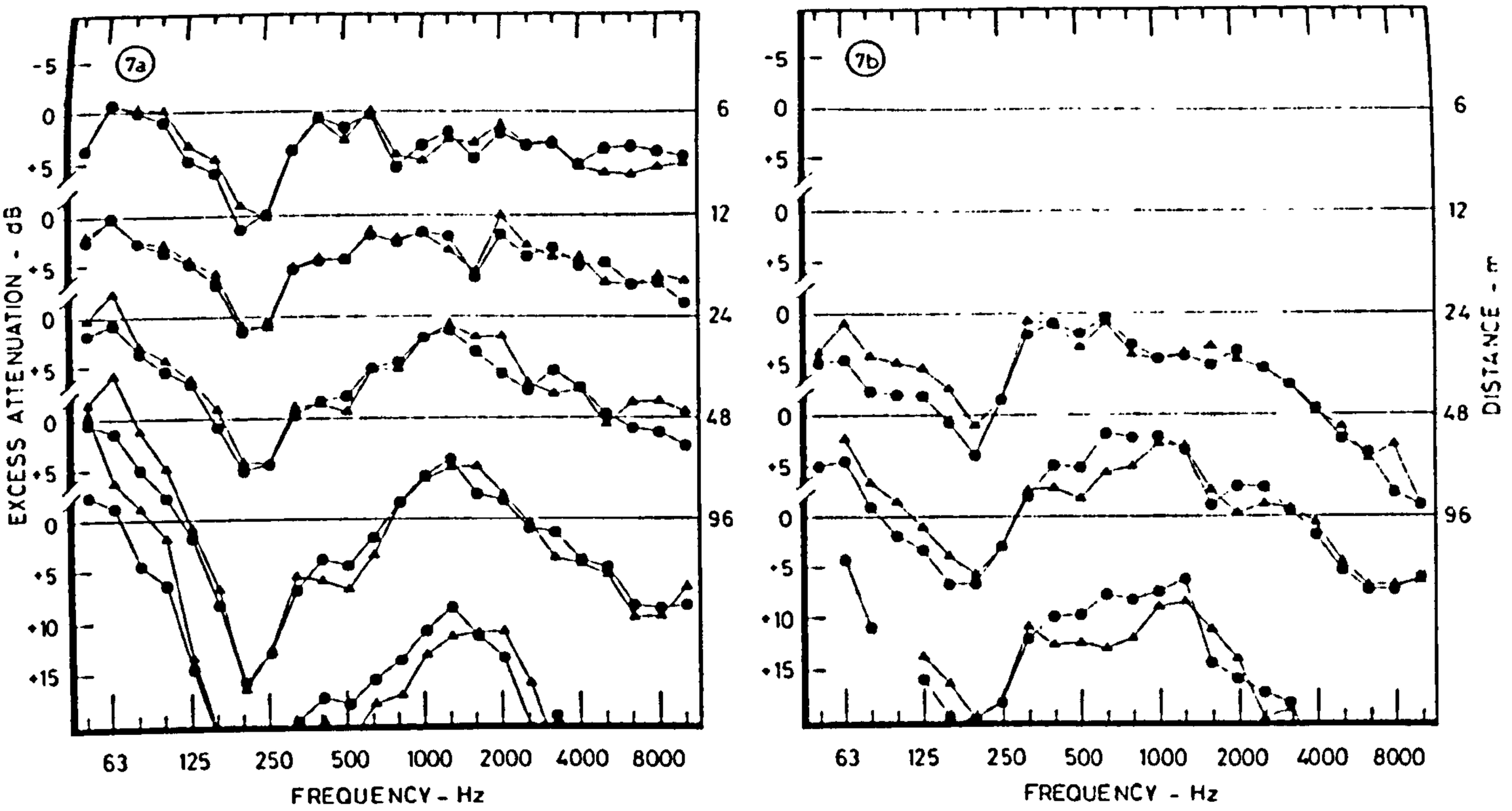

Fig. 7. Spruce fir forest. —●— 5 September 1978, —▲— 20 September 1978.

Figure 2.5
Excess attenuation in a spruce forest, from Martens(1981).

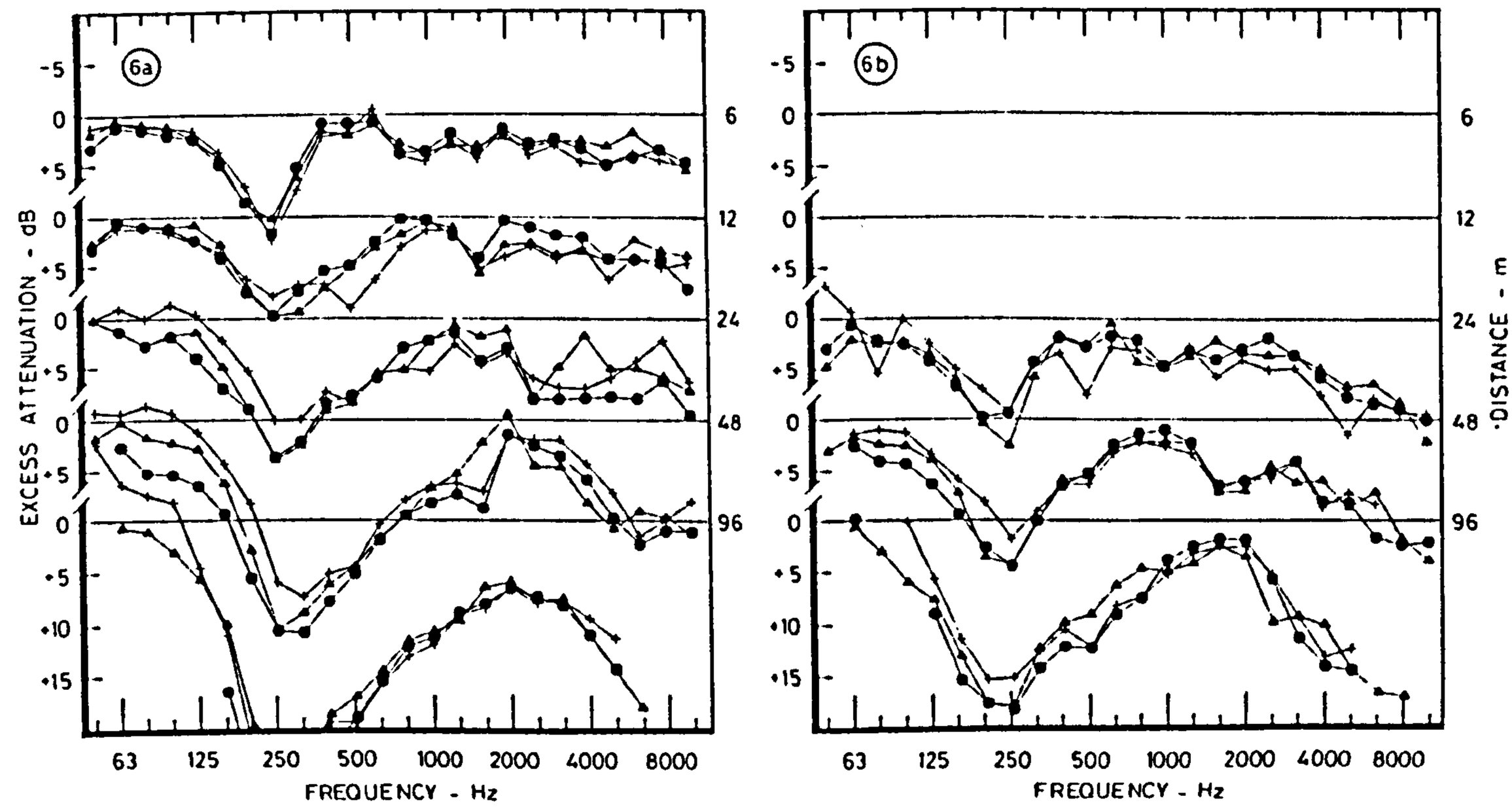

Fig. 6. Mixed poplar forest. ● 23 August 1978, - ▲ - - 7 September 1978, + 4 October 1978.

Figure 2.6
Excess attenuation in a mixed poplar forest, from Martens(1981)

16-22 years old, 23 m wide belt of 2-10 m high trees (oaks, spruces, larches, hornbeams, and alders) with edges of 1-5 m high bushes (roses, elders, and Amelanciers). This belt had a particularly dense overall structure.

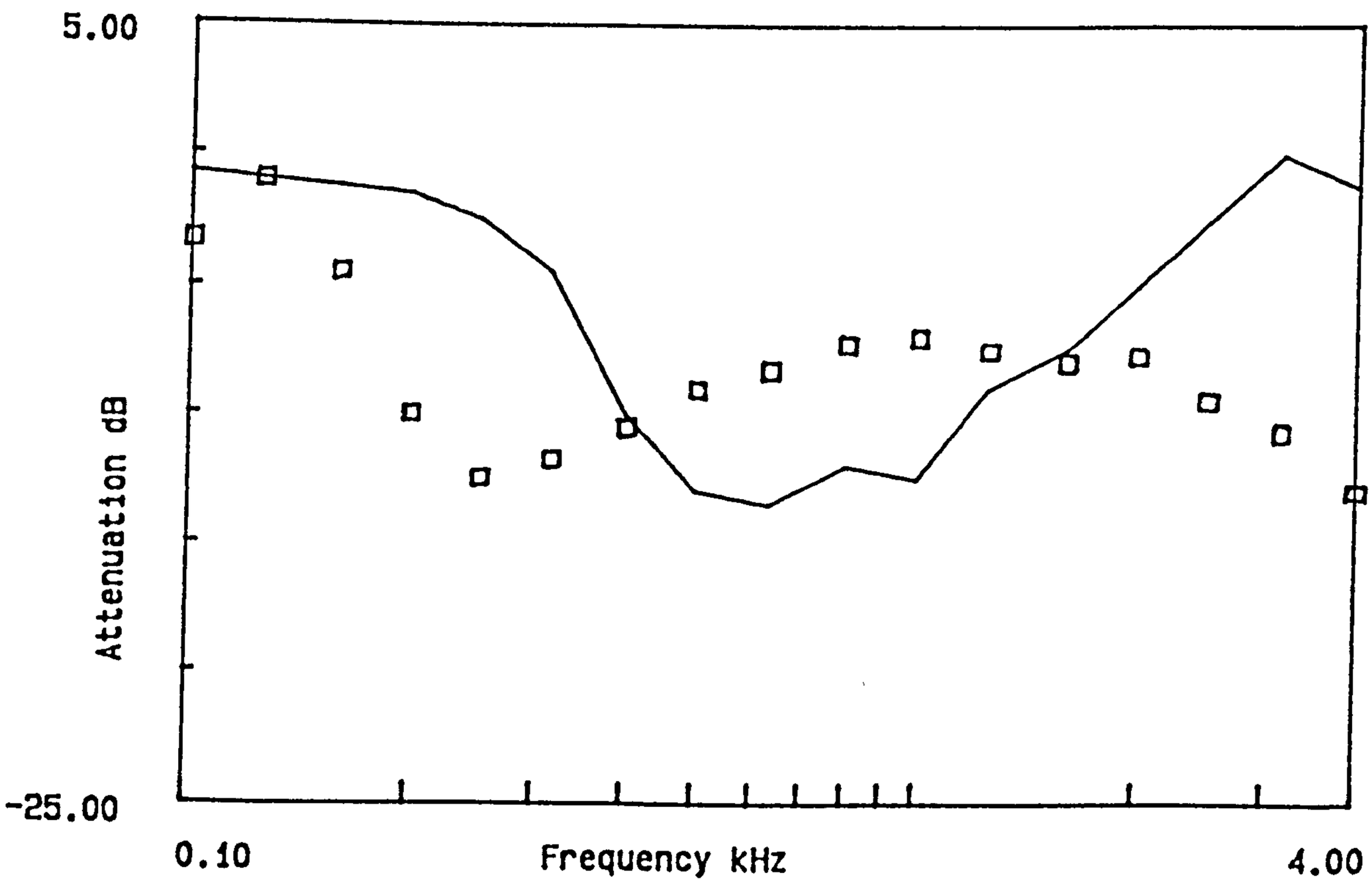

Figure 2.7
Attenuation by a roadside tree belt, from Kragh (1982).

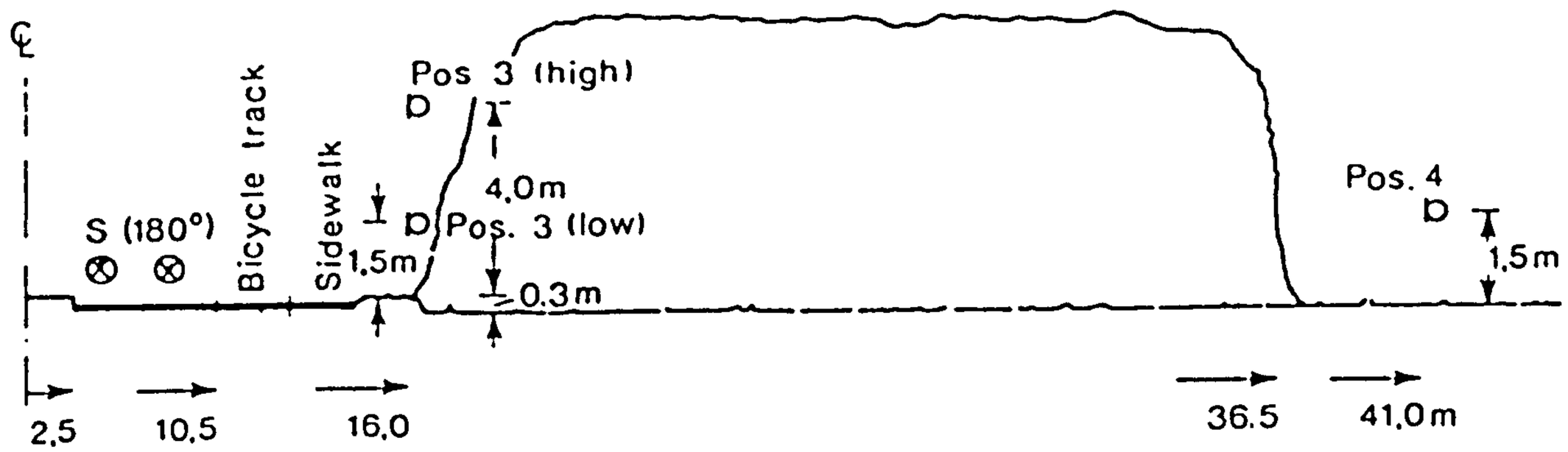

16 years old, 20 m wide belt of 7 m high common oaks, with 2 m high, extremely dense barberry bushes in front and in between. The rear edge consists of wild groups of sweetbriar.

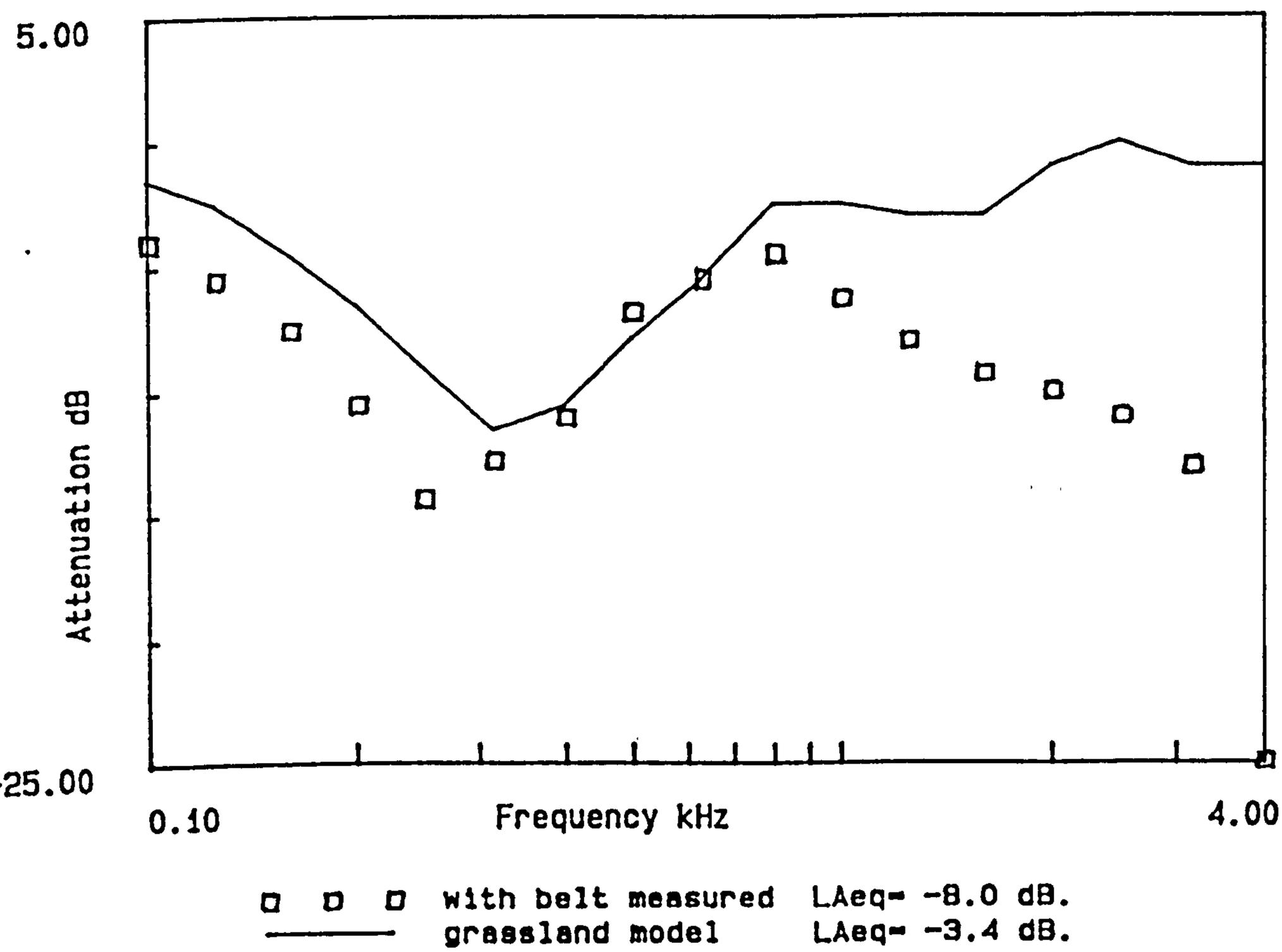

Figure 2.8
Attenuation by a roadside tree belt. from Kragh (1982).

2.4 Sound Reduction Due to the Forest Floor.

Knowledge of the effect of the ground is important in the interpretation of all outdoor sound propagation studies where the propagation path is close to the ground. It is evident that the ground surface in a woodland is markedly different in character to a grassland or other outdoor surfaces. This fact is important in the interpretation of insertion loss measurements and, indeed, all propagation results.

As mentioned above the low frequency peak in attenuation in woodland is now generally attributed to, so called, ground interference effects. Figure 2.9 shows a basic model of sound propagation over ground, the sound field at the receiver is a result of sound travelling both in a direct and a reflected path. The sound wave incident on a non-rigid ground is partially absorbed and changed in phase on reflection. The low frequency peak in attenuation can be explained by interference between the two waves reaching the receiver. At the frequency at which the two waves have a phase difference of 180 ° (π radians), destructive interference occurs and the sound waves cancel out causing a peak in excess attenuation. At frequencies either side of this peak the waves partially interfere with each other. The phase difference depends on the pathlength difference between the two wave paths, and the phase shift on reflection. The magnitude of the ground interference peak depends on the amount of energy absorbed at the surface.

Embleton (1963) presented measurements of excess attenuation in woodland with the source outside the wood. The results from the first 50 ft of vegetation gave a typical S-shaped pattern of excess attenuation. Embleton attempted to account for this in terms of mechanisms such as resonances by the branches. In the light of current knowledge these results can be shown to be simply the result of ground attenuation, and the reason the S-shaped pattern was only observed in the edge measurements, an artefact of the way in which the measurements were carried out and results presented. The peak in excess attenuation probably occurred in all the measurements but subtracting the excess attenuation spectra from two successive distances caused cancelling of the peak. This can be fairly accurately predicted using the prediction model described in chapter 4, as can be seen in figures

2.10 and 2.11 (calculated using the Delany and Bazley model with σ = 30,000 mks rayls). The high frequency part of figure 2.10 evidently diverges from the ground prediction and is therefore attributable to other attenuation effects. The measurements and ground prediction diverge less in the data of figure 2.11, this suggests a greater high frequency attenuation caused by a layer of dense edge vegetation.

The propagation model used in this study is presented in detail in chapter 4. The equations described originate from the Weyl-van der Pol formulations for a spherical wave incident on a hard boundary from electromagnetic wave theory (Weyl (1919) and van der Pol (1935)). They were first applied to sound wave theory by Rudnick (1947), and much has been written about the application of the theories in outdoor sound propagation and calculation of the various components of the equations; eg. by Ingard (1951), Attenborough and Heap (1975), Attenborough (1978 and 1982), Embleton et al (1976). The surface acoustic impedance is a complex value which is used in the propagation models as the main parameter characterising the ground surface, it describes the absorptive and phase-shifting properties of the ground surface, and is dependent on the physical properties of the ground.

Direct measurements of ground impedance have been described by various authors using techniques to detect the absorption and phase change caused by a surface. One technique which has been used to measure the impedance of woodland soils (eg by Talaske (1980) and Carlson et al (1976)) is an adaptation of a standard laboratory impedance tube. This device consists of a loudspeaker mounted at the end of a long tube, the other end of the tube is driven a few centimeters into the ground and pure tone sound waves projected down the tube so they reflect from the ground and cause a standing wave pattern which is detected by a probe microphone within the tube. The impedance can be deduced from a knowledge of the standing wave pattern. In an alternative impedance tube set-up, measurements are obtained from the transfer function between two small microphones mounted in the side of the tube, close to the ground, in this case white noise is used, not a pure tone (Chung and Blaser 1979). Studies carried out at Pennsylvania State University showed that differences in impedance measured using the two different types of impedance tube are negligible.

A technique which measures the impedance at oblique angles of incidence is described by Embleton et al (1976) and van der Hiejden (1984). In this technique an array of microphone positions is used to measure the changes in the interference pattern, of pure tones, along a straight inclined path ie the same acoustic 'ray' (as in figure 2.9) is followed by a moving microphone or array of microphones. The real and imaginary components of the normal surface impedance can be calculated from precise measurements of this interference pattern. Embleton et al (1976), and others, have shown that for outdoor ground surfaces, normal incidence techniques such as the impedance tube, and oblique incidence techniques such as the inclined track method give similar results. This shows that the ground can generally be assumed to be 'locally reacting'. The local reaction assumption is that the sound travelling inside the air spaces of a porous medium, travels into the ground normal to the surface whatever the angle of incidence of that sound wave is onto the ground. The alternative to the local reaction is the extended reaction in which the sound travels at an angle to the surface, that angle depending on the refractive index of the porous medium. The local and extended reaction assumptions are portrayed graphically in figure 2.12.

Some Measured Impedances

Research workers at Pennsylvania State University (eg. Talaske(1980), Carlson, McDaniel and Reethof (1976)) have described the forest floor as a two- layered medium with a top layer of a known depth and a semi-infinite lower layer. This model calculates the surface impedance from a knowledge of the characteristic impedance of the two layers. Talaske (1980) carried out impedance tube measurements of the surface impedance of forest floors and showed that the model is valid for a three-layered forest floor at two contrasting sites, the forest floors studied consisted of a litter layer and a humus layer of decaying litter over-lying the mineral soil. The characteristic impedance of the underlying mineral soil was measured by removing the litter and humus layers and using the impedance tube in-situ. The characteristic impedance of the top layers was measured using a thick sample of the litter and humus material, or comparing the surface impedance of one and two layers of the material with a rigid backing in a method described by Pyett(1953). The results of the measurements are illustrated in figure 2.13 along with some predictions from the two-

layered model. In a mature red pine stand the litter layer of fallen needles was shown to be virtually transparent, having a very low impedance, the top layer for the two-layered model was therefore assumed to be just the humus layer which did have a significant impedance value. The other site investigated was a mixed hardwood and white pine plantation. In this site the litter layer was found to have a significant acoustic impedance, which was similar in value to the impedance of the humus layer, therefore the top layer was assumed to consist of the litter and humus layers together. Figure 2.13 shows that the values predicted from the impedances of the two layers are generally within the scatter of the measured data points, except for the low frequency values of reactance in the pine plantation.

Figure 2.14 shows some impedance results reported by Martens, van der Heijden et al (1985) measured using the inclined track technique. The result from the pine wood with and without the litter layer only shows a slight influence of the litter layer on the acoustic impedance of the soil, and the result of removing first the litter then the humus layers of mixed wood indicate that the organic layers have little effect on the overall acoustic impedance, the stripped soil still having a low value of impedance. These authors state that their measurements do not reveal the reason for the acoustically soft nature of woodland soils. A real part of impedance which is relatively independent of frequency has been shown (eg. by Attenborough (1985)) to be characteristic of the impedance of a layered medium. The fact that the woodland soil impedance of these studies exhibits this kind of frequency dependence suggests that the soil is acting, acoustically, as a layered medium even with the organic layers removed, it is possible that this is due to the presence of a relatively porous 'A' layer or some other influence of the vegetation on the soil.

Measurements of ground impedance have been suggested eg by Attenborough and Hess (1985) as a means of deducing physical soil parameters such as the porosity, since the acoustic impedance is related to the volume, and configuration, of pores in a porous medium. Delany and Bazley (1970) described a method of relating acoustic impedance to the air flow resistance of fibreglass absorbents. The impedances of samples of fibreglass were measured using an impedance tube, the flow resistivity measured, and the two parameters compared by regression analysis. Approximately 200 data points were used to determine the following

power law relations for normalised resistance (R) and reactance (X) (impedance = R + iX).

$$R = 1+9.08\left[\frac{f}{\sigma}\right]^{-0.75} \quad \text{and} \quad X = -11.9\left[\frac{f}{\sigma}\right]^{-0.73} \tag{2.1}$$

f = frequency, σ = flow resistivity in cgs rayls. (The form of this equation given in chapter 4 is in mks units and a different convention for impedance used ie. a positive real part).

Chessel (1977) suggested the use of these equations in the prediction of impedance of outdoor ground surfaces for predictions of propagation. Piercy and Embleton (1979) presented the results of fitting predictions of sound propagation to their own, and other authors' propagation measurements using these formulae to calculate impedance and thereby deducing the most appropriate value of flow resistivity for that ground surface. Their results are presented in table 2.2

Table 2.2 Best Fit Effective Flow Resistivities of various ground Surface as Reported by Piercy and Embleton (1979).

Description of Surface	flow resistivity in mks rayls.
4 inches new fallen snow	10,000 to 30,000
Sugar snow	25,000 to 30,000
Forest floor, pine or hemlock	20,000 to 80,000
Grassland of various types	150,000 to 300,000
Roadside dirt,ill-defined, small rocks up to 4 inches.	300,000 to 800,000
Sandy silt, hard packed by vehicles	800,000 to 2,500,000
Earth, exposed and rain-packed	4,000,000 to 8,000,000
Asphalt, sealed by dust and use	>20,000,000

Experiments have shown that measured flow resistivities of soils are often around half of that predicted by propagation measurements, (results of flow resistivity measurements on soils are, however, very variable). The difference in porosity between the materials used by

Delany and Bazley (porosity $\Omega \simeq 1$) and soil ($\Omega \simeq 0.5$) accounts for this apparent discrepancy. Thus if the parameter $\frac{f}{\sigma}$ is replaced by $\frac{f}{\sigma\Omega}$ for the glass fibre materials this becomes $\frac{f}{\sigma}$ and for soil approximately $\frac{2f}{\sigma}$. Thus σ in equation 2.1 should be thought of as an 'acoustical' or 'effective' flow resistivity.

Considerably more complicated models relating the physical parameters of soils to the acoustic properties have recently been proposed, for example Attenborough (1985) describes a model which uses four physical characteristics, the flow resistivity, the porosity, the tortuosity (or 'twistiness') of the pores and a factor accounting for the shape of the pores. This four-parameter model could be extended to give a nine-parameter description of a two layered medium of the type described by Talaske each layer having four parameters. It is evident that this introduces an unwarranted level of complexity into the description of the ground for outdoor sound propagation prediction, since the results of Piercy and Embleton (1979) show fairly good agreement between measurement and prediction. One or two parameter approximations to the four-or-more parameter models are also presented by Attenborough (1985), these have the advantage of being theoretically derived rather than empirical (as the Delany and Bazley equations), and take account of different ground configurations. Equations are presented to calculate impedance for layered ground and ground which has an increasing porosity with depth as well as for a homogeneous ground. The different ground types give a different characteristic frequency dependence of impedance and therefore of excess attenuation. The equations of these one and two parameter models are given in chapter 4.

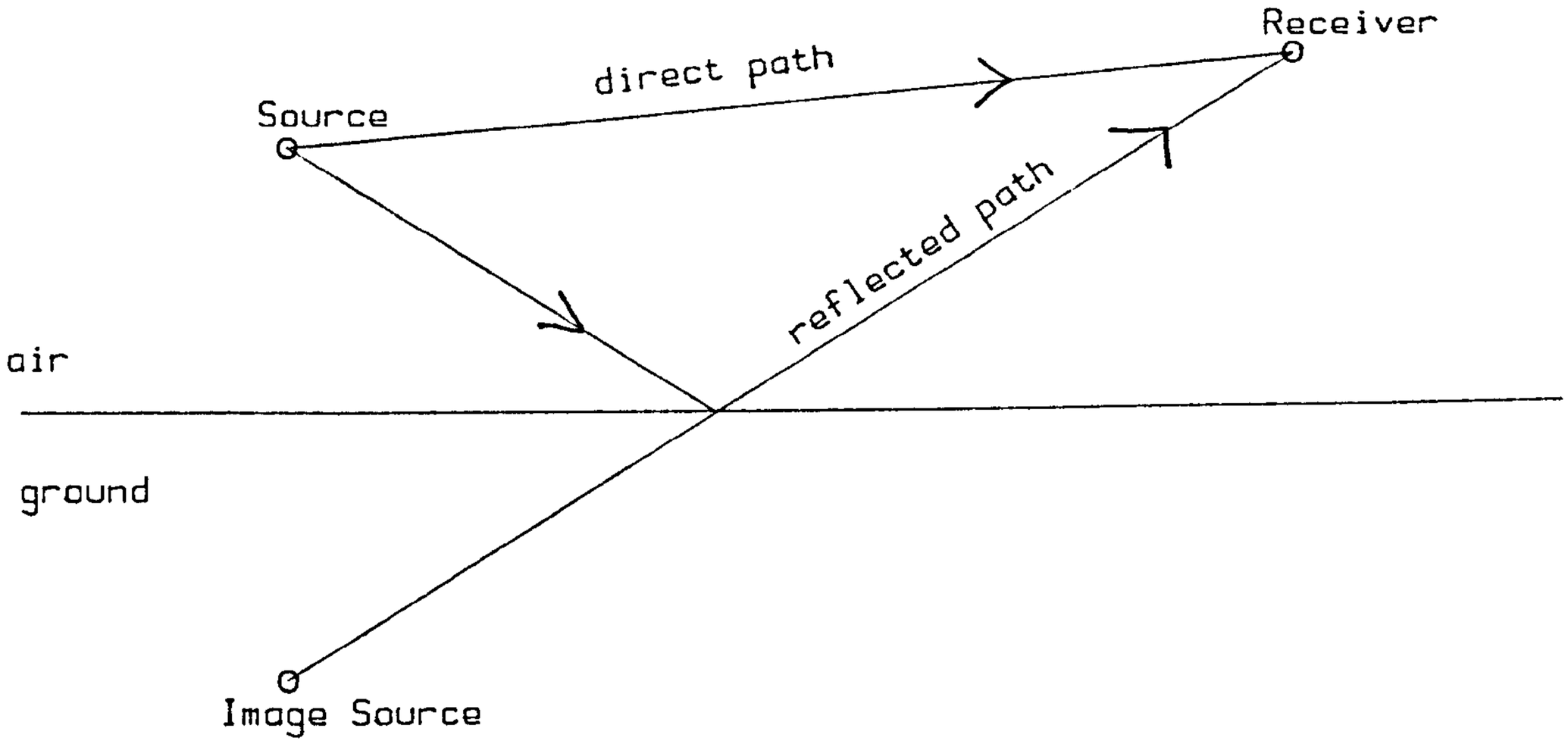

Figure 2.9
Diagrammatic representation of the propagation of sound above a ground surface.

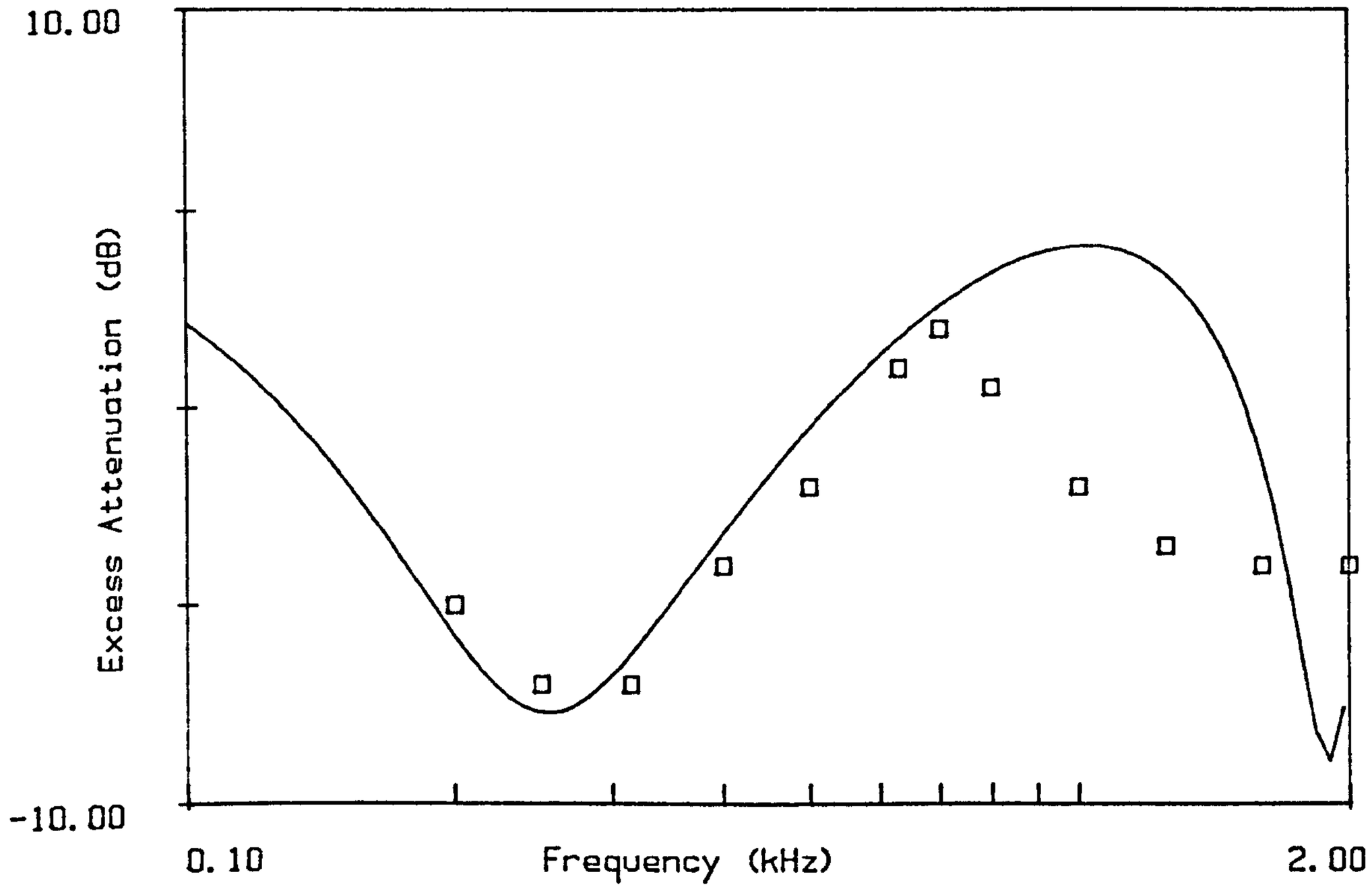

Figure 2.10
Predicted attenuation for 15.38m (50ft) of ground.
Points are mean measurements from Embleton (1963) for first 50ft of woodland corrected to dB/measurement distance.

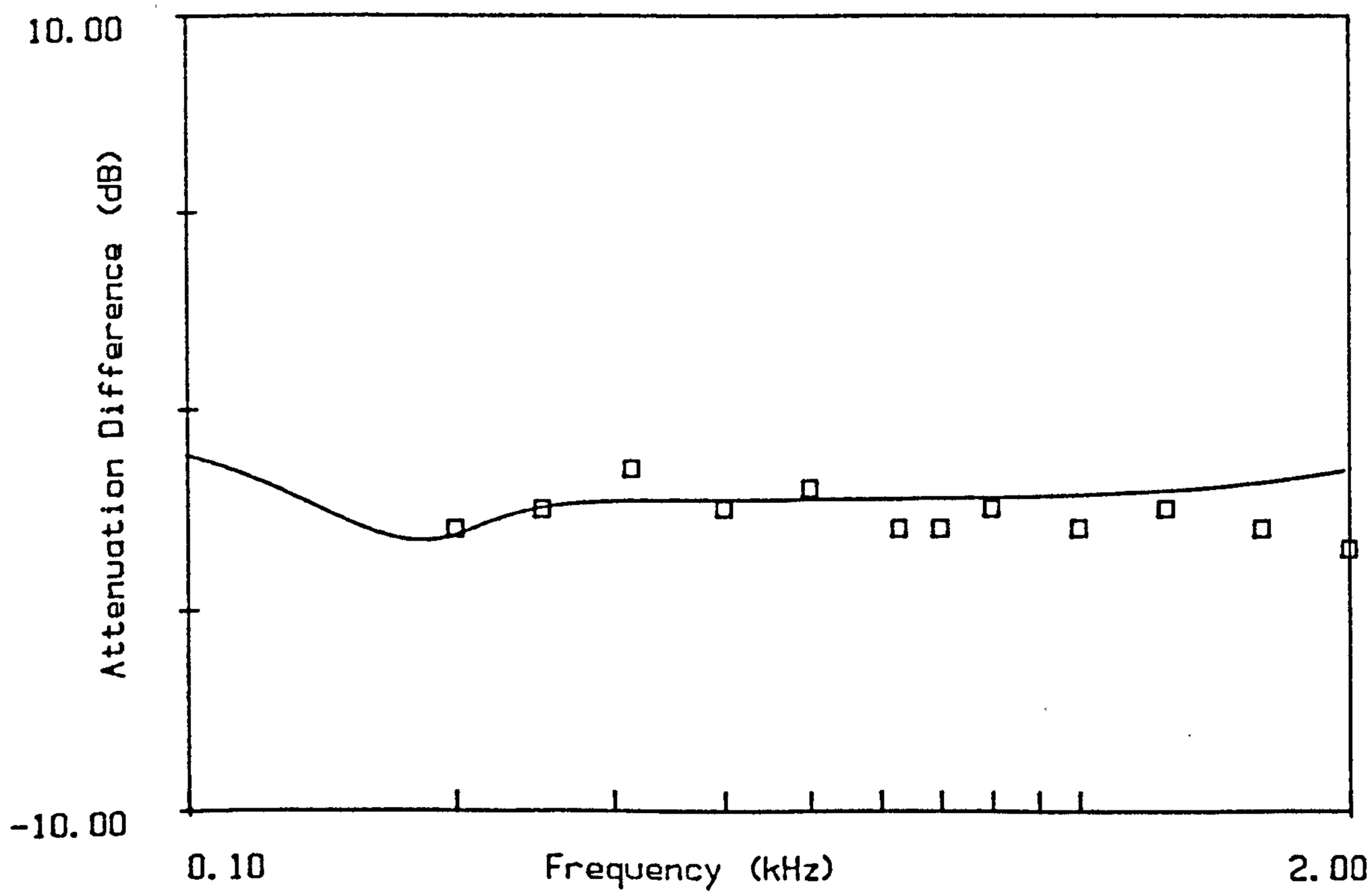

Figure 2.11
Predicted difference between excess attenuation at 150ft and 200ft.
Points are mean measurements from Embleton (1963) for corresponding 50ft of woodland corrected to dB/measurement distance (50ft).

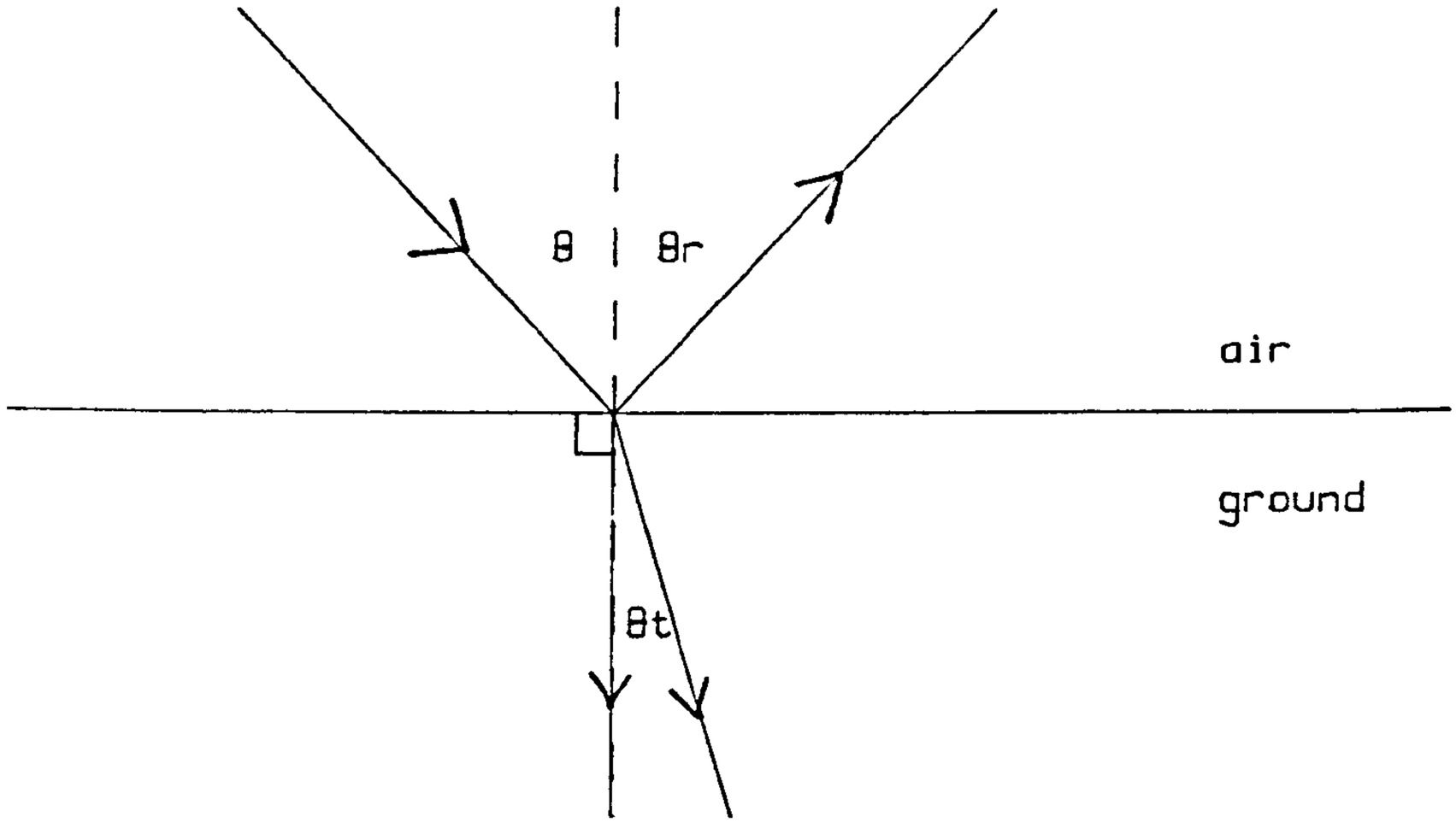

Figure 2.12 Diagrammatic representation of sound transmission into the ground.
Local reaction when $\theta t = 0$.
Extended reaction when $\theta t \neq 0$.

Figure 2.13
Real and imaginary parts of acoustic surface impedance of forest floors.
Impedance tube measurements compared with prediction from two-layered ground impedance model. from Talaske(1980).

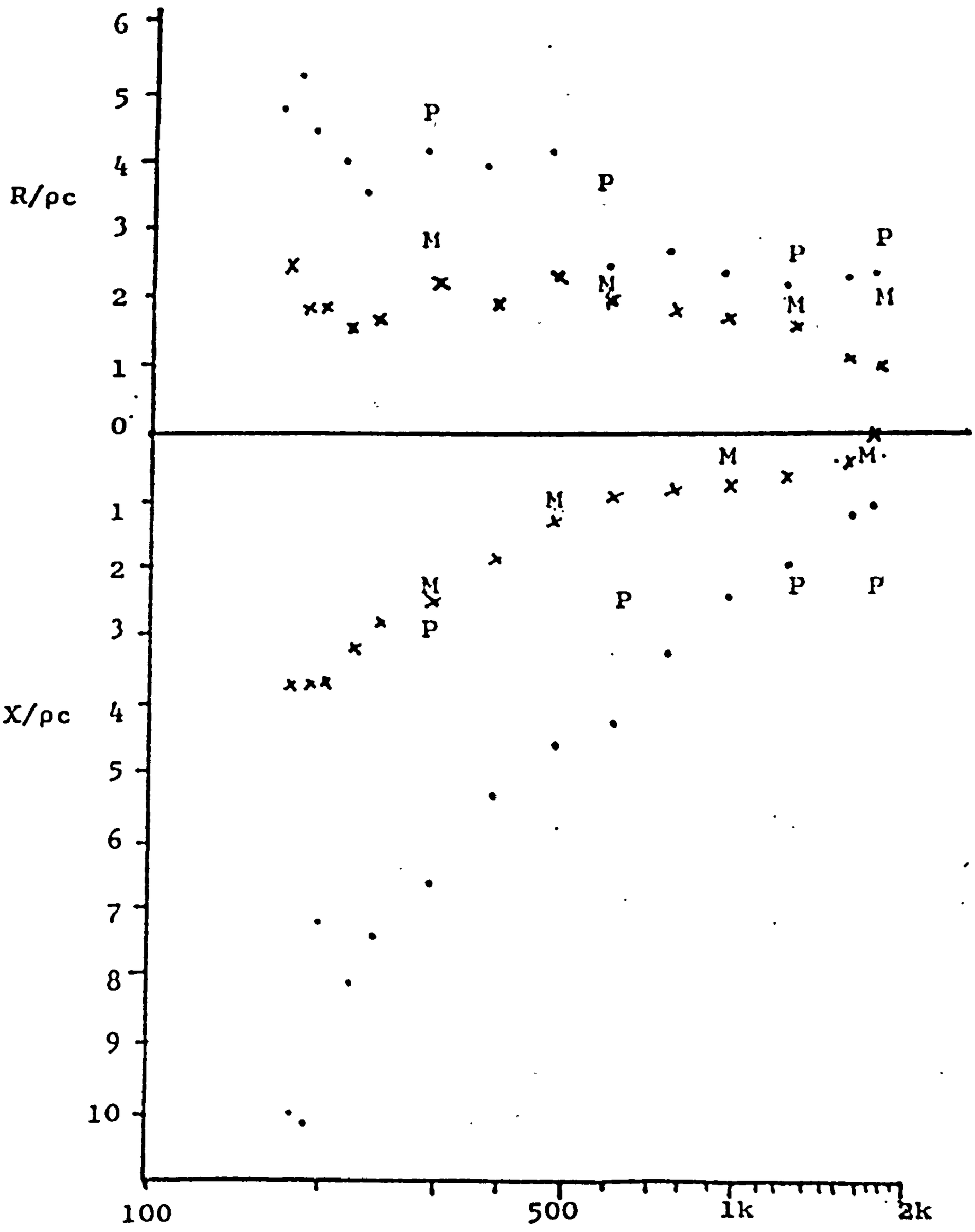

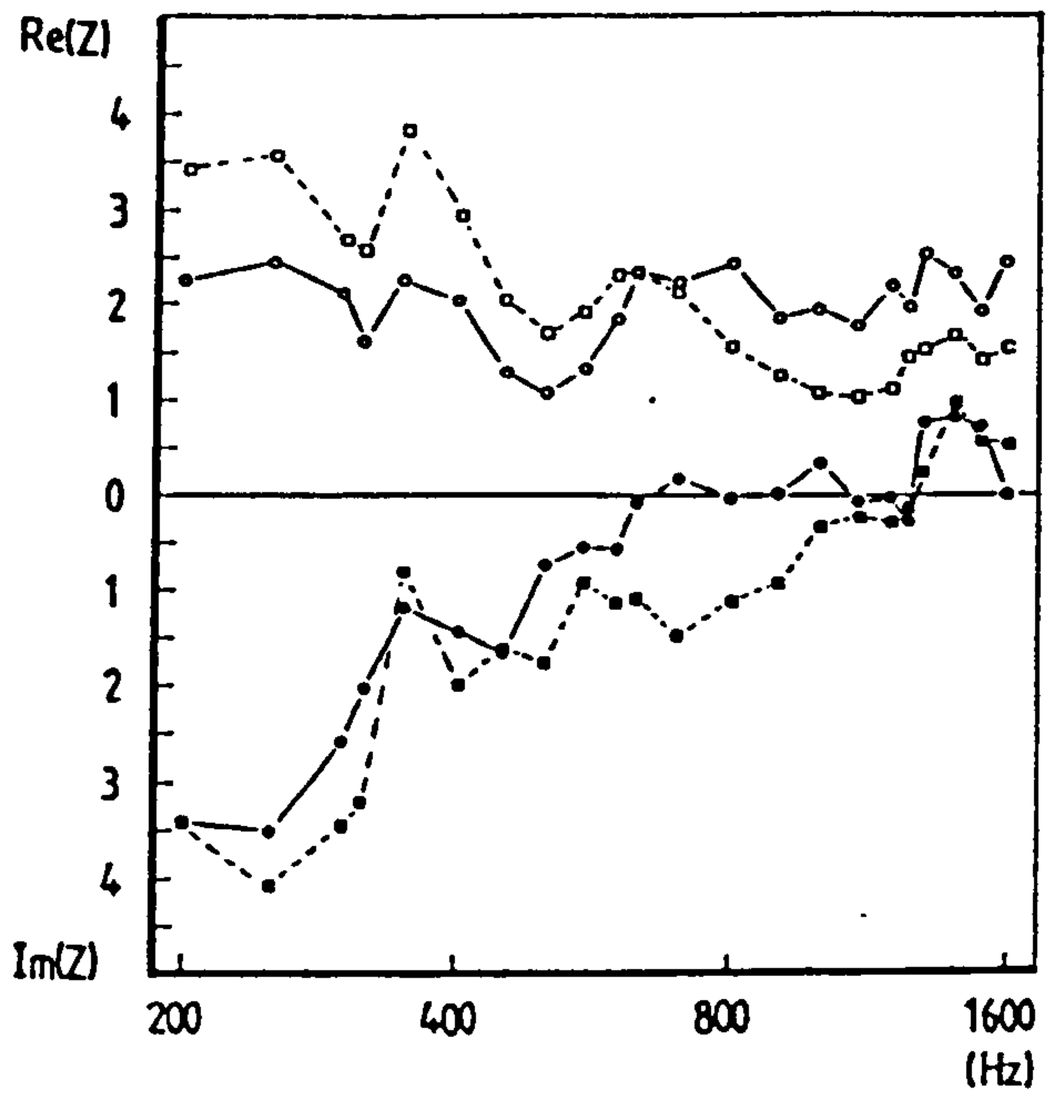

FIG. 4. Real and imaginary parts of the acoustic impedance versus frequency. Measurement 4a, pine forest, intact soil (circles). Measurement 4b, pine forest, without L layer (squares).

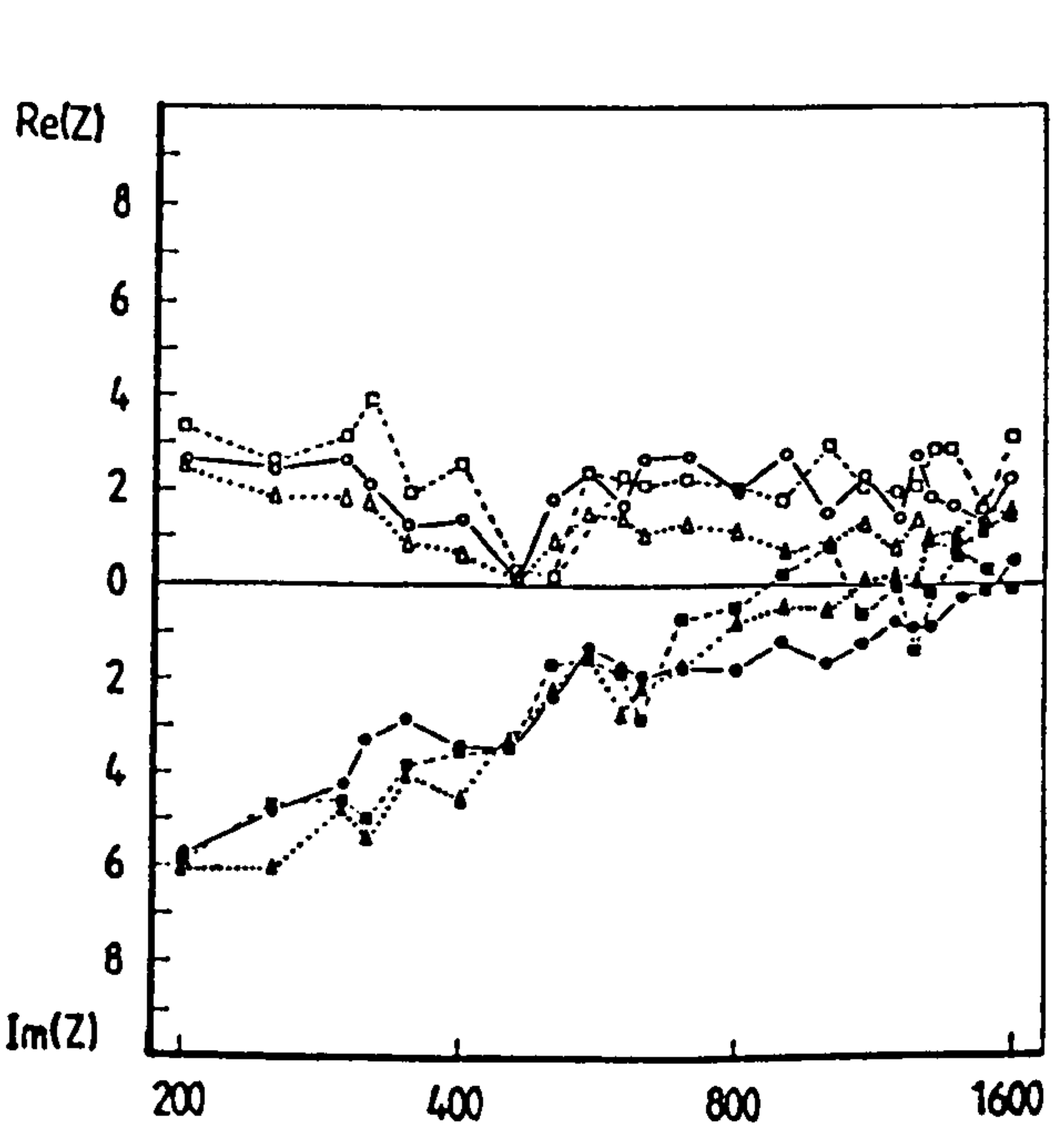

FIG. 11. Real and imaginary parts of the acoustic impedance versus frequency. Measurement 19a, mixed forest, intact floor (circles). $R_w = 53.8 \times 10^3$ Pa s m^{-2}, sum of squares = 1425. Measurement 19b, mixed forest, without L layer (squares). $R_w = 60.2 \times 10^3$ Pa s m^{-2}, sum of squares = 3234. Measurement 19c, mixed forest, without L and H layer. $R_w = 52.8 \times 10^3$ Pa s m^{-2}, sum of squares = 3527 (triangles).

Figure 2.14
Measured impedance of forest floors, from Martens et al (1985).

2.5 Other Mechanisms of Sound Attenuation by Trees and Shrubs

The attenuation of high frequency sound in woodland is variously attributed to absorption or scattering effects of the trunks, branches and foliage. The main possible absorbing elements of a wood are the surface of the trunks and the leaves, as well as the ground. Scattering effects are also thought to have a significant attenuating effect. Scattering occurs when a sound wave encounters a part of a tree (leaf, limb or trunk) which is of a comparable, or larger, size than the wavelength. Scattered sound waves have a greater likelihood of hitting the ground or other absorptive surfaces.

Lyon, Blair and de Jong (1977) have reported results of both field and scale model studies which demonstrate a greater high frequency attenuation in trees without leaves. It is suggested that the attenuation is due to back- scattering of sound from branches, leaves are thought to reduce this effect by deflecting sound towards the receiver. This result is evidently contrary to the results of most other studies. The model experiments also indicated that the planting of trees on or around a noise barrier reduces the effectiveness of the barrier, contrary to the results of Cook and van Haverbeke. Aylor (1972) found that foliage did cause significant high frequency attenuation, since the attenuation through a stand of deciduous brush was higher in summer than in winter (see figure 2.4)

Aylor (1972) and Yamada et al (1977) both propose what is effectively the same theoretical model for the absorption of sound energy by foliage. An equation is given for the energy dissipated due to viscosity by a single leaf, representing the leaf as a rectangular flat plate oscillating in a stationary fluid according to existing theory for fluid mechanics.

The single leaf case is quoted by Yamada et al as

$$E_1 = \frac{A}{2} V^2 S \left[\frac{\nu \rho \omega}{2} \right]^{1/2} \qquad (2.2)$$

Where E_1 = Energy loss per unit time

A = a constant describing the dimensions and shape of the leaf

V = particle velocity

S = surface area of the leaf (one side)

ρ = air density

ν = viscosity of air

ω = angular frequency = $2\pi f$

f = frequency (Hz)

and the random incident energy per unit time on the area S as

$$E_i = \frac{\rho c V^2 S}{\delta} \tag{2.3}$$

So an absorption coefficient for the leaf is

$$\alpha = \frac{E_1}{E_i} = 4A\left[\frac{\pi\nu f}{\rho c^2}\right]^{1/2} \tag{2.4}$$

The individual leaf case is extended to calculate the energy loss due to vegetation by integrating the single leaf case over the average leaf area density (F) to give absorption of energy by foliage per unit time as:

$$dI = \frac{A}{2}V^2\left[\frac{\nu\rho\omega}{2}\right]^{1/2}\cos^2(kx)F\,dx \tag{2.5}$$

Assuming plane waves are transmitted into the vegetation, attenuation over distance L can be shown to be:

$$A_e = 2.16A\left[\frac{\pi\nu f}{\rho c^2}\right]^{1/2}FL = 0.54FL\,\alpha \tag{2.6}$$

The parameter A does not appear in Aylor's model but a value of A = 2.2 gives a model identical to that described above.

Both authors point out that the attenuation accounted for by viscous and thermal dissipation, in this model, is considerably less than their own measured attenuation data and

also that of Embleton (1963) and Eyring (1946). It is evident that, according to this model, the absorption coefficient of foliage is proportional to the square root of the frequency. Yamada's data, obtained from four different species tested for absorption in a reverberant room indicated that the absorption coefficients are similar for the four species and that these are approximately proportional to the square root of frequency. Aylor, however, states that measured attenuation increases by about 6dB per doubling of frequency ie. A_e is proportional to $20\log_{10}f$ and suggests a formula of loss through a thin solid wall as a better model. In this model the canopy is represented by a single thin wall of unknown surface area density to sound transmission and

$$A_e = 20 \log_{10}\left(\frac{\pi S f}{41.5}\right) \tag{2.7}$$

for air at 20 ° C where S is the area density or the density times the thickness of the wall. This model appears to describe the qualitative aspects of the attenuation. Quantitatively an effective wall thickness needs to be about three leaf thicknesses to give the observed reduction at 1000Hz, this is thought to be a reasonable value.

Reethof, Frank and McDaniel (1976) present results of impedance tube measurements of the absorption coefficient of samples of the bark of six species of trees. The absorption was very low for most of the samples so the authors conclude that absorption at the surface of trees has little attenuating effect, although it is pointed out that the cumulative effect of many trees in a wood could be significant.

Embleton (1966) proposed a model to account for absorption and scattering by an array of cylinders which could have some application in describing scattering by tree trunks. The model is defined in terms of the surface impedance, and radius of the cylinders, in an array, of known density, of infinitely long, uniform sized cylinders with locally reacting surfaces. The model is based on the theoretical work of Twersky (1953) who considered the multiple scattering of plane waves by such an array. Twersky's expressions were simplified by assuming incident waves of unity amplitude propagated perpendicularly to the plane of the array. The expressions presented by Embleton are described in detail in chapter 5, together with another model proposed by Aylor(1972) to account for scattering by tree

trunks, and model studies carried out to assess their application are described in chapter 7.

Burns (1979) carried out some experiments to investigate thermoviscous absorption in the boundary layer around the branches and resonant effects of pine branches. Absorption was measured using a small reverberant chamber, the measured energy decay rate giving information on the absorbing capacity of the branches. Burns concludes that thermoviscous absorption in the boundary layer about idealised, smooth, rigid needles, and other surfaces of infinite heat capacity accounts, within experimental error for the magnitude of absorption observed within the reverberant box. The theoretical model of Attenborough and Walker (1972) was successfully used to predict the magnitude of absorption by the branches measured within the reverberant box. Burns also investigates the so called anomalous gain from Embleton's (1963) experiments but is unable to propose a mechanism for this due to resonances or scattering, (this gain has been explained above). Further investigation of the theoretical model within this study has shown that, when using the theoretical expressions of Attenborough and Walker, the input parameters proposed by Burns appear to produce some mathematical instability presumably because these parameters do not meet the inherent assumptions of the theoretical model. It is also unclear from Burns' paper how the information about thermoviscous absorption could be used to predict attenuation by a pine stand.

Bullen and Fricke (1982) proposed a model to combine the effects of scattering and absorption, in which they considered trees to act as cylindrical scatterers with a measurable 'scattering cross section' (σ_S) and 'absorption cross section' (σ_A). The scattering and absorption cross sections were calculated for a model of paper cylinders and various trees and it was suggested that the values of σ_S and σ_A could be used to predict sound propagation within woodland. In outline, the theory proposed is of a sound field within an infinitely wide belt of vegetation consisting of a number of sound particles or phonons. The scattering model is of a 2-dimensional situation and the phonon concept disregards the frequency and phase related effects. Both vertical scattering and frequency are, however, taken into account as they modify the values of σ_S and σ_A. It is also shown that this theory can be used to predict the attenuation for various configurations of scattering arrays such as tree belts. One conclusion reached from the study is that a greater attenuation can be expected

from a belt which is about as wide as it is deep than from an infinitely long belt of the same depth; the extra sound energy being scattered to the sides of the belt.

Values of σ_S and σ_A were determined experimentally for small trees of various species. The frequency at which the absorption cross section (measured in a reverberant room) was found to be greatest was 2kHz, dropping rapidly below this frequency. By stripping maple trees of their of their leaves it was shown that there is no measurable absorption by the trunk and branches. It is assumed that the absorption cross section can be directly scaled up for larger trees. The scattering cross section was measured for three kinds of trees, palm trees with and without foliage on the trunk and a fig tree with large branches. The resulting values of σ_S indicate that the foliage on the palm trunk had little effect on scattering and that the branches as well as the trunk of the fig tree contributed to the scattering.

In a later paper Fricke (1984) concludes that scattering rather than absorption is the more important attenuating phenomenon in the mid-frequencies while absorption becomes more dominant in the high frequencies, this agrees with the conclusion that the value of σ_A is greater in the higher frequencies. This conclusion is reached from measurements, made in pine plantations, of the rate of decay of sound within the forest compared with the attenuation with distance. An increase in time decay rate with increasing attenuation with distance is shown to occur at the high frequencies and demonstrate that the dominant mechanism is absorption. In the low and mid frequencies, however, the decay with time becomes less as the attenuation with distance increases, this is thought to be due to back-scattering of energy, this scattering is thought to be from both the ground and the vegetation.

Fricke (1984) also presents results of attenuation measurements made in three contrasting pine stands. The stand which had the greatest attenuation depended on frequency, again demonstrating that different mechanisms are important at different frequency ranges. The stands all had significantly different attenuation rates at the low frequencies demonstrating that the vegetation had a significant effect on the properties of the ground which contribute to attenuation. The differences in the high frequency attenuation could be explained by scattering and absorption effects. A third way in which Fricke (1984)

demonstrates the different mechanisms occurring at different frequencies is by looking at the ways in which attenuation data has been presented by different authors. The two main ways of expressing attenuation rates are as dB per doubling of distance (dB/dd) and dB per unit distance (dB/m). Using a least squares regression analysis it was shown that at low frequencies the use of dB/dd is more appropriate while at high frequencies dB/m gives a better fit and the mid-frequencies were no better correlated by using dB/dd or dB/m. This concurs with the supposition that low frequency attenuation is due to the interference between direct and ground-reflected sound and that high frequency attenuation is related to the quantity of biomass present to scatter and absorb the sound.

In addition to the thermal and viscous absorption effects discussed above. the absorption of sound due to friction within a leaf occurring when the leaf is caused to vibrate by a sound wave. has been suggested as a mechanism of absorption. Martens et al (1981 and 1986) have carried out experiments to detect the vibrational modes of leaves using laser-Doppler-vibrometer system. Sound is broadcast onto a leaf sample and the resulting vibrations detected by the vibrometer. Leaves were shown to act as linear mechanical systems ie no transformation of frequency was detected. The vibration measurements showed that the leaves behave conceptually as membranes or between membranes and plates. Using existing theory of dissipation of energy by vibrating membranes or plates. the absorption of energy by such vibrations is shown to be very small for a single leaf. Martens and Michelsen (1981) conclude, however, that the enormous number of leaves in a woodland could cause a significant cumulative effect by this mechanism. A further effect of leaves investigated by Martens et al (1985a) is the reflection of sound. Laboratory experiments showed that the reflection increases as a function of the square of the radius and that the mass of the leaf is also important. The authors suggest that in belts of trees used for screening. species with a larger diameter and a greater mass would be more effective. It seems, however, that, due to the random orientation of leaves on a tree the reflection of leaves could have other effects such as reflecting sound towards a receiver as is suggested by the paper of Lyon et al (1977) mentioned above. Any attenuation effects caused by leaf reflections are likely to be due to sound being reflected onto more absorptive surfaces such as the ground.

2.6 Existing Prediction Schemes

Confusion about the reliability of results of attenuation in woodland have led to their effect being generally neglected in practical prediction schemes. The Department of Transport, for example, do not consider the planting of trees to be an effective means of noise control, nor do they consider existing woodland in noise prognosis and planning matters. The results of experiments such as those described in sections 2.2 and 2.3 have, however, been suggested as a basis for practical prediction schemes.

In the T.S.C. report (Wesler (1972) described by Borthwick et al. (1978) the following values of attenuation are used:

$$A_c = 0.01(f)^{1/3}\frac{r}{3.28} \text{ dB/ foot for tree belts.} \qquad (2.8)$$

$$A_c = (0.18log(f)-0.31)\frac{r}{3.28} \text{ dB/ foot for shrubbery.} \qquad (2.9)$$

$$r = \frac{\pi WL}{2(L+W)}$$

Where a tree belt of width W is considered to be made up of sections of length L and f is the frequency. The attenuation of a number of sections can be calculated individually to convert the predicted attenuation of a point source into a result for a line source such as a road, without the use of integration. The maximum attenuation allowed by this scheme is 20 dB.

The same paper describes the NCHRP report (Kugler and Piersol (1973)) prediction scheme for traffic noise attenuation. This simply states that for a belt of trees at least 15ft tall with sufficient density to obscure the road from view, an attenuation of 5dB/100ft of

trees to a maximum of 10dB can be assumed.

Kragh et al (1982a) published a prediction scheme, mainly for industrial noise, which takes into account the attenuation caused by a belt of trees as long as the height is at least one metre above a curved transmission path and there is no visual path through it. The correction made for sound attenuation with the presence of a tree belt ΔL_r is

$$\Delta L_r = -n_r \alpha_r$$

Where n_r is the number of 'groups' of vegetation, if $n_r > 4$ then it is set to 4.

A dense forest is considered as a number of groups each of 50m. Thus if the transmission path through the forest is d_r metres $n_r = d_r / 50$. α_r is the attenuation coefficient per group from table 2.3.

Table 2.3: Attenuation Coefficients For Vegetation from Kragh et al (1982a).

Octave band (Hz)	63	125	250	500	1000	2000	4000	8000
α_r dB/group	0	0	1	1	1	1	2	3

The different characteristics of an extensive dense woodland and a tree belt is taken into account in this scheme, as a belt less than 50m wide is assumed to cause the same attenuation as 50m of dense woodland as long as the above conditions are fulfilled. The low frequency attenuation is not included here as there is a separate ground attenuation factor which accounts for this effect.

References Chapter 2.

[1] Attenborough, K. and Walker, L.A. 1972. Sound Dissipation by a Small Cylindrical Obstacle. J. ACOUST. SOC. AM. 51. 192-196

[2] Attenborough, K. and Heap, N. 1975. Sound Attenuation Over Ground Cover. SHOCK AND VIBRATION DIGEST 7(10) 73 - 83.

[3] Attenborough, K. 1978. Sound Attenuation Over Ground Cover. SHOCK AND VIBRATION DIGEST 10(7) 3 - 13.

[4] Attenborough, K. 1982. Predicted Ground Effect for Highway Noise. J. SOUND AND VIBRATION 81 (3) 413 - 424

[5] Attenborough, K. and Hess, H. 1985. Acoustical Surveying of Porous Soils. in ACOUSTICAL IMAGING; PROCEEDINGS OF THE FOURTEENTH INTERNATIONAL SYMPOSIUM. 111 - 122.

[6] Attenborough, K. 1985. Acoustical Impedance Models for Outdoor Ground Surfaces. J. SOUND AND VIBRATION 99(4) 521-544.

[7] Aylor, D.E. 1972 Noise reduction by vegetation and ground. J ACOUST SOC AM 51(1) 197 - 205

[8] Aylor, D.E. 1972a Sound transmission through vegetation in relation to leaf area density, leaf width, and breadth of canopy. J ACOUST SOC AM 51(1) 411 - 414

[9] Aylor, D.E. 1981 Comments on "Foliage as a low pass filter: experiments in an anechoic chamber". Letter to the editor. J ACOUST SOC AM 70(3) 891.

[10] Bazley, E.N. 1976 Sound absorption in air at frequencies up to 100kHz. NPL. ACOUSTICS REPORT. Ac 74.

[11] Beck, G. 1968 Plants as aids in noise abatement. PATZER-VERLAG HANOVER English summary in Forestry Abstracts.

[12] Borthwick, J., Halverson, H., Heisler, G.M., McDaniel, O.H., and Reethof G. 1978. Attenuation of Highway Noise by Narrow Forest Belts. FINAL REPORT ON FHWA CONTRACT. Report no FHWA-RD-77-140

[13] Bullen, R. and Fricke, F. 1982. Sound Propagation Through Vegetation. J. SOUND AND VIBRATION 80(1) 11-23

[14] Burns, S.H. 1979. The Absorption of Sound by Pine Trees. J. ACOUST. SOC AM 65(3) 658 - 661.

[15] Carlson, D.E. McDaniel, O.H. and Reethof, G. 1976. Theoretical and Experimental Research on the Acoustic Characteristics of Forests. USDA FOREST SERVICE REPORT.

[16] Chessel, C.I. 1977. Propagation of Noise Along a Finite Impedance Boundary. J. ACOUST. SOC. AM 62. 825 - 834.

[17] Chung, J.Y. and Blaser, D.A. 1979. Transfer Function Method of Measuring In-duct Acoustic Properties. J. ACOUST. SOC. AM. 68(3) 907 - 921.

[18] Cook, D.I. and van Haverbeke, D.F. 1971 Trees and shrubs for noise abatement. USDA. FOREST SERVICE AND UNIVERSITY OF NEBRASKA RESEARCH BULLETIN no 246.

[19] Cook, D.I. and van Haverbeke, D.F. 1974 Tree covered landforms for noise control. USDA FOREST SERVICE RESEARCH BULLETIN no 263.

[20] Cook, D.I. and van Haverbeke, D.F. 1976. Residential traffic noise control using tree-shrub-barrier combinations. In: Shelterbelts on the Great Plains. Proc. Symp. Great Plains Agric. Counc. 112-116

[21] Cook, D.I. and van Haverbeke, D.F. 1977. Suburban noise control with plantings and solid barrier combinations. UNIVERSITY OF NEBRASKA RESEARCH BULLETIN EM100.

[22] Delany, M.E. and Bazley, E.N. 1970. Acoustical Properties of Fibrous Absorbent Materials. APPLIED ACOUSTICS 3 309 - 322.

[23] Embleton, T.F.W. 1963 Sound Propagation in Homogeneous Deciduous and Evergreen Woods. J. ACOUST. SOC. AM. 35 1119 - 1125.

[24] Embleton, T.F.W. 1966 Scattering by an Array of Cylinders as a Function of Surface Impedance J. ACOUST. SOC. AM 40 667-670

[25] Embleton, T.F.W. Piercy, J. and Olson, N. 1976. Outdoor Sound Propagation Over Ground of Finite Impedance. J. ACOUST. SOC. AM. 59(2) 267 - 277.

[26] Eyring 1946. Jungle Acoustics. J ACOUST SOC AM 18(2) 257 - 270

[27] Fricke, F. 1984. Sound Attenuation in Forests. J. SOUND AND VIBRATION. 92(1) 149-158

[28] Hess and Kursteiner 1961. Traffic noise abatement by means of plantations. SCHWEIZ. Z. FORST. W. 112 English summary in Forestry Abstracts 23 No. 4560

[29] Ingard, U. 1951. On the Reflection of a Spherical Sound Wave From an Infinite Plane. J. ACOUST. SOC. AM. 23 329 - 335.

[30] Kellomaki, S. Haapenen, A. Salonen, H. 1976. Tree stands in urban noise abatement. SILVA FENNICA 10 (3) 237 - 256

[31] Kragh J. 1979. Pilot Studies on Railway Noise Attenuation by Belts of Trees. J. OF SOUND AND VIBRATION 66(3) 407 - 415.

[32] Kragh J. 1981. Road Traffic Noise Attenuation by Belts of Trees. J. OF SOUND AND VIBRATION 74(2) 235 - 241

[33] Kragh, J. 1982. Road Traffic Noise Attenuation by Belts of Trees and Bushes. DANISH ACOUSTICAL LABORATORY REPORT No. 31.

[34] Kragh, J. Andersen, and Jakobsen 1982a. Environmental Noise From Industrial Plants - General Prediction Method. DANISH ACOUSTICAL LABORATORY REPORT No. 32.

[35] Kugler, B.A. and Piersol, A.G. 1973. Highway Noise: A Field Evaluation of Traffic Noise Reduction Measures. NATIONAL COOPERATIVE HIGHWAY RESEARCH PROGRAM REPORT 144.

[36] Lanphear, F.O. 1971 Urban Vegetation: Values and Stresses HORT SCIENCE 6(4) 332 - 334.

[37] Leonard, R.E. and Herrington, L.P 1971. Noise Abatement in a Pine Plantation. USDA FOREST SERVICE RESEARCH NOTE NE - 140

[38] Lim, C.H. 1981. Some Aspects of Acoustical Privacy in Dwellings. PhD DISSERTATION, UNIVERSITY OF SYDNEY.

[39] Linskens, H.F. Martens, M.J.M. Hendriksen, H. Roestenberg-Sinnige,A. Brouwers, W. van der Staak, A. and Strik-Jansen, A. 1976. The Acoustic Climate of Plant Communities. OECOLOGIA 23 165 - 177

[40] Lyon, R., Blair, C. and de Jong, R. 1977. Evaluating Effects of Vegetation on the Acoustical Environment by Physical Scale Modelling. In USDA GENERAL TECHNICAL REPORT NE25.

[41] Marten, K. and Marler, P. 1977. Sound Transmission and its Significance for Animal Vocalization. 1 Temperate Habitats. BEHAV. ECOL. SOCIOBIOL. 2 271 - 290

[42] Marten, K. Quine, D. and Marler, P. 1977a. Sound Transmission and its Significance for Animal Vocalization. 2 Tropical Forest Habitats. BEHAV. ECOL. SOCIOBIOL 2 291 - 302

[43] Martens M.J.M. 1980. Foliage as a low pass filter: experiments with model forests in an anechoic chamber. J ACOUST SOC AM 67(1) 66 - 72

[44] Martens M.J.M 1981. Noise Abatement in Plant Monocultures and Plant Communities. APPLIED ACOUSTICS 14 167 - 189

[45] Martens, M.J.M. and Michelsen, A. (1981) Absorption of Acoustic Energy by Plant Leaves. J. ACOUST. SOC. AM. 69(1) 303-306

[46] Martens, M.J.M. van der Heijden, L.A.M. Walthus, H.H.J. and van Rens W.J.J.M. 1985. Classification of Soils Based on Acoustic Impedance, Air Flow Resistivity, and Other Physical Soil Parameters. J. ACOUST. SOC. AM. 78(3) 970 - 980.

[47] Martens, M., Severens, P., van Wissen, H., and van der Heijden, L., 1985a. Acoustic Reflection Characteristics of Deciduous Plant Leaves. ENVIRONMENTAL AND EXPERIMENTAL BOTANY 25(3). 285-292.

[48] Martens, M.J.M., Roebroek, J.G.H. and Geveling, S.M. 1986. Sound Induced Vibrations in Plant Leaves. PREPRINT PROC. 12TH INTERNATIONAL CONGRESS ON ACOUSTICS, TORONTO, CANADA, JULY 1986.

[49] Mitscherlich, G. and Scholzke, B. 1977. Noise Abatement by Forests. ALLG. FORST. U. J.ZTG 148(7) 125 - 143 (English Summary).

[50] Ozimek, E. and Kobek, W. 1970. Noise Reduction in Selected Types of Planted Areas. SYLWAN 114 49 - 63 (English Summary).

[51] Piercy, J.E. and Embleton, T.F.W. 1979. Excess Attenuation or Impedance of Common Ground Surfaces Characterised By Flow Resistance J. ACOUST. SOC. AM. 65(S1) S63.

[52] Pyett, J.S. 1953. The Acoustic Impedance of a Porous Layer at Oblique Incidence. ACUSTICA 3 375.

[53] Reethof, G., Frank, L. and McDaniel O.H. 1976. Absorption of sound by tree bark. USDA FOREST RESEARCH PAPER NE-341.

[54] Rudnick, I. 1947. The Propagation of an Acoustic Wave Along A Boundary. J. ACOUST. SOC. AM. 19 348 - 356.

[55] Schiller, G. Schaudinschky, L. and Keller, Y. 1981. The Acoustic Properties of Forest and Ornamental Trees. Hanot Directorate of Agricultural Research Part 5 No. 2162. Translated from Hebrew by Forestry Commission, Alice Holt, Surrey.

[56] Talaske, R. 1980. The Acoustic Impedance Of a Layered Forest Floor. USDA FOREST SERVICE AGREEMENT REPORT. Pennsylvania State University.

[57] Twersky,V. 1953. Multiple Scattering of Waves by a Volume Distribution of Parallel Cylinders. N.Y. RES. REPT. NO. EM-59 also J. MATH. PHYS. 3 700-715 (1962) and J. ACOUST. SOC. AM. 36 1314-1329 (1964).

[58] Van der Heijen, L.A.M. 1984. The Influence of Vegetation on Acoustic Properties of Soils. PhD THESIS; UNIVERSITY OF NIJMEGEN, NETHERLANDS.

[59] Van der Pol, B. 1935. Theory of the Reflection of the Light From a Point Source by a Finitely Conducting Flat Mirror With an Application to Radiotelegraphy. PHYSICA 2 843 - 853.

[60] Visnapuu, M. and Margus, M. 1977. Noise Abatement by Trees. METSANDUSLIKUD UURIMUSED 13 312 - 337 English Summary in Forestry Abstracts.

[61] Wesler, J.E. 1972. Manual For Highway Noise Prediction. US DEPARTMENT OF TRANSPORTATION, TRANSPORT SYSTEMS CENTRE, REPORT DOT-TSC-FHWA-72-1.

[62] Weyl, H. 1919. Ausbreitung Electromagnetischer Wellen Uber Einem Ebenen Leiter. ANN. Phys. 60 481 - 500.

[63] Whitcombe, C.E. and Stowers, J.F 1973. Sound Abatement With Hedges. HORT SCIENCE 8(2) 128 - 129

[64] Yamada, S. Watanabe, T. Nakamara, S. Yokoyama, H. and Takeoka, S. 1977. Noise Reduction by Vegetation. PROCEEDINGS OF INTERNOISE 1977.

Chapter 3 : Outdoor Measurement Technique

The Attenuation measurements form the most important part of this study as they are a measurement of the actual propagation of sound through a wooded area. These measurements were made with a 'reference microphone' close to the source and a 'test microphone' at a known distance, up to 96m, away from it. The source and receivers were usually both set up within the wood. The attenuation calculated was the measured level difference between the reference and test microphone corrected for the attenuation due to spherical spreading and atmospheric absorption.

Much of the published data quotes the results of outdoor sound propagation as the excess attenuation ie the total field at a receiver minus the free field level expected at that point. Such calculations assume a constant source strength and spectrum. Obtaining such a constant source poses many problems, so the attenuation measurements used in this study were based on a measurement of the difference between the field at two microphones recording the same source, simultaneously, thus eliminating any errors caused by an inconsistent source. This technique has also been used by other authors, most notably by Parkin and Scholes (1964). The attenuation measurements made have certain similarities with equivalent excess attenuation measurements since they were corrected for free field attenuation, and the reference microphone was close to the source, with a much larger distance between the two microphones than between the source and reference. They should not, however, be regarded as true excess attenuation measurements since two distinct receiver locations with attendant ground reflections are involved.

3.1 Equipment

Sound Generating System.

A random, approximately white, noise signal was produced electronically by a system made up by the Open University electronics department. This consisted of a noisy diode, and amplifier which combined to give an output signal of white noise, with an amplitude of between -1V and +1V. An amplifier (IIH S150 slave amplifier), powered by an inverter, amplified this signal to give a sound pressure level of about 112dB at 2m from the speaker unit.

The speaker unit was an Electrovoice S12-2 two-way speaker system. This has two speaker drivers, a 12 inch bass unit and a tweeter unit which produces the high frequencies. The crossover network of the speaker system has a nominal cutoff frequency of 3kHz. The centre of the high frequency speaker is 20cm above the centre of the bass unit. Pilot experiments showed that the centres of the speakers can safely be used as the effective source height ie the effective source height for the high frequencies is 20cm above that for the low frequencies, and that each acts as a separate point source. The frequency ranges at which the two speakers operate do overlap to some extent so the frequencies around 3kHz are produced by both speakers.

Test Microphone System.

A Nagra IV-SJ two-channel tape recorder was used in the experiments to record the 'test' signals ie those made at various distances from the speaker. The Nagra tape recorder has four inputs, 2 are line inputs which accept an a.c. signal from the two wires of a coaxial cable ie one live and one ground. The other two inputs are microphone inputs containing microphone power supplies which can be used to power a variety of microphones using special input adaptors. Each channel has stepped attenuators which can be adjusted in steps of 1 dB to adjust the recording level, indicated on a meter located on the front of the tape

recorder.

Two Bruel and Kjaer half-inch condenser microphones type 4165 with Bruel and Kjaer microphone preamplifiers type 2619 were used in most of the measurements, located at different heights during the measurements. The microphones were connected to the microphone input sockets of the tape recorder with adaptors type QSJP-BK. Ten metre extension cables were inserted between the preamplifier leads and the input adaptors where required. The microphones were protected with foam windshields. In some of the earlier measurements a sound level meter (Bruel and Kjaer type 2203 or 2218) was used, with a half inch microphone capsule (Bruel and Kjaer type 4165) connected via an extension cable. The a.c. output from the sound level meter was connected to the line input of the tape recorder to record the signal. The Nagra tape recorder also has a cue microphone to record a commentary on a third track of the tape, this was used to make a note of the attenuator settings, experimental geometry, weather conditions etc. in addition to written notes.

Reference Microphone System.

The system used to record the reference level 2m from the microphone consisted of a Bruel and Kjaer half-inch microphone capsule type 4165, or one-inch capsule type 4145, connected to the sound level meter type 2203 by the meter's adaptor and extension cable. The microphone was held on a tripod stand and was covered with a foam windshield. The attenuator control on the sound level meter was set at an appropriate level for the signal being recorded i.e. so the needle on the meter read between 0 and 10. The a.c. output socket was used to feed the output signal into a tape recorder. The signal was recorded on one channel of a Uher 4400 report stereo tape recorder. This tape recorder has a recording level attenuator which was used to ensure that the recordings were made when the meter was indicating an acceptable recording level. The attenuator control is continuous and not stepped so signal levels can only be directly compared if care is taken not to move this attenuator control between recordings as there is no means of recording the magnitude of the attenuation of the input signal.

3.2 Method.

The measurements of long range propagation in woodland were all carried out on days with little or no measurable wind. The wind was measured using a Vector Instruments D600 series wind measuring apparatus which comprises a 'Porton' anemometer with a self-referencing wind vane. The windspeed and direction are recorded on a paper chart recorder. The anemometer was normally set up in a slight clearing within the wood. The temperature and relative humidity were also measured during the experimental period in order to obtain input values for the calculation of atmospheric absorption. The relative humidity was measured with a whirling hygrometer. The temperature was measured using a mercury in glass thermometer. The temperature was usually measured at two or more heights and a mean value used.

Site Preparation

Experimental sites were chosen within an area of Forestry Commission land which was largely flat and planted with various types of trees. Detailed descriptions of the sites are included in chapter 6. At each of the compartments used a 'measuring track' was laid out. Positions within the stands were marked with short wooden posts, so that measurements could be repeated on different days, using exactly the same source and receiver positions. A source position was chosen well away from the edge of the stand, and a straight path measured with a 30m tape measure, keeping the whole measuring track within the stand. Microphone positions were marked at known distances with wooden posts. The measuring tracks are arranged so that the sound would propagate at an angle to the rows of trees rather than parallel to them ie the sound propagating through the most dense part of the stand. In most situations access to the source and receiver positions was fairly easily gained between the rows of trees.

Experimental Set-up

Figure 3.1 illustrates the configuration of the equipment used in the experiments.The source system was set up at an appropriate position marked by a wooden post. The speaker was put onto a tripod speaker stand with the amplifier and white noise source on the ground behind it. The reference recording system was set up with the microphone at two metres from the speaker and at the same height as the centre of the low frequency speaker cone.

The test signal recording system was set up at a wooden marker post at a known distance, with the two microphones attached to an adjustable microphone stand at 1.2m and 2.5m above the ground. The source height, to the centre of the low frequency speaker (hs - see figure 3.1), the reference microphone height (hrr), reference separation distance (rr), the test microphone height (hrt), and the test separation distance (rt), were written on the experimental data sheet and recorded on the cue track.

Calibration

Both the reference and test systems were calibrated using a pistonphone (B & K type 4220) which produces a sine wave at 250Hz with a level of 124dB, at the diaphragm of a microphone when the pistonphone is coupled to the microphone. The resulting signal was recorded onto the tape. In the reference system the sound level meter attenuator was set to 120dB and the recording level control on the Uher tape recorder adjusted so that the indicator needle was near the middle of its range, after the system had been calibrated care was taken not to alter this control. Calibration tones were recorded on this system frequently to check that the recording level control had not been moved, and also to separate the signals since there was no cue track on this system.

The test system was also calibrated using the pistonphone with the input attenuator on the Nagra tape recorder set to a level giving a reading in the middle of the range on the tape recorder meter. The Nagra has stepped attenuators so the recording level could be adjusted

to an appropriate reading for each recording without the need for recalibration. The resulting signal was again recorded.

Measurement

The background noise was recorded on the Nagra with appropriate attenuator settings. Two or three background noise recordings were made during a set of measurements to gain a representative sample.

The sound generating system was switched on and experimental results recorded. At each microphone location a total of six (in some cases four) measurements were made. At least one reference recording was made at the same time as the experimental recordings. Initially a reference recording was made simultaneously with all the experimental recordings, but the reference levels seemed to be fairly constant over a short time period, therefore the number of reference recordings made was reduced to one for each set of three test measurements. At one site it was not possible to locate the reference microphone directly in front of the speaker so the speaker had to be turned through 90 degrees to face the reference microphone: therefore reference recordings were made directly before or after experimental recordings at each location (details in Chapter 6.4). A calibration tone was recorded on the reference microphone system after each recording. The test microphone system was recalibrated at intervals during a set of measurements. Each of the recorded signals was approximately two minutes long, and the sound system was switched off between each one.

The sequence of test measurements made was:

i) 2 microphones set up at 1.2m and 2.5m above the white marker post.

ii) repeat with microphones displaced 0.5m to 1m to one side.

iii) repeat with microphones displaced 0.5m to 1m to the other side of the marker post.

iv) Move to another test microphone position and repeat the measurements.

Interpretation of Tape Recordings

Figure 3.2 is a block diagram illustrating the equipment used to analyse the calibrated tape recordings. In this set-up a program runs on the NOVA 4 minicomputer which remotely controls the Nicolet FFT analyser and reads the resulting data from it. The Nicolet FFT analyser calculates averaged rms spectra of the voltage of the signals as a function of frequency, from the signals played back from the tape recorder into each of the two input channels.

For these experiments the FFT analyser was set up to analyse frequencies up to 10kHz, the frequency range being covered by 400 points ie points at 25Hz spacing. The rms spectra were read by the NOVA 4 minicomputer, from the internal storage buffers of the Nicolet FFT analyser, and stored on floppy discs; together with information about the set-up of the FFT analyser and the Nagra tape recorder attenuator settings which were required in later analysis. The data was then transferred to a mainframe computer (VAX 11/780) where all further calculations were carried out. As the recording was played back the voltage output for the calibration tone (250Hz) was also noted so that the rms spectra could be converted to sound pressure levels, using the software described below.

Analysis of Data

The main parameter calculated is the attenuation which is, as described above, the difference between the sound pressure levels at two microphones corrected for the expected attenuation due to spherical spreading and atmospheric absorption. 'Raw data' files from the Nicolet are used in the FORTRAN program DIF2MK (source code listing in appendix A) to obtain the sound pressure level at each of the two microphones and the attenuation. A description of the program DIF2MK follows.

The raw data file names are first read into the program along with data about the instrumentation used in the data collection and analysis. Subroutine SLMSET calculates the

scaling parameters which are required to calculate the sound pressure levels from the voltage data obtained from the Nicolet. In order to calculate the sound pressure level for the measured spectra the voltage output by the tape recorder from the calibration tone (V_t) is used to calculate a reference voltage (V_{ref}).

The basic formula used is:

$$\text{Sound Pressure Level} = 120 + 20 \log_{10}\left(\frac{V_i}{V_{ref}}\right) \tag{3.1}$$

For the Nagra tape recorder the voltage into the tape recorder (V_i) is used to account for the fact that different attenuator settings are used for the calibration tone and the measurement. V_i is calculated from the tape recorder output voltage (V_o) using the formula

$$V_i = 10^{-A_t/20} V_o \tag{3.2}$$

Where A_t represents the Nagra tape recorder attenuator settings.

The recordings on the Uher are taken at the same recording level as the calibration tone, therefore the output voltages of the calibration tone and recorded signals are used directly, so $V_i = V_o$.

At the calibration level of 124dB equation 3.1 gives

$$V_{ref} = \frac{V_i}{10^{0.2}} \tag{3.3}$$

This value of V_{ref} is characteristic of the measuring system and is therefore used, in the main program, to calculate the sound pressure levels from the voltage data.

Subroutine SLMSET also sets the parameters used in the main program to account for the attenuator settings of the sound level meters. For the sound level meter type 2203 (used in the reference microphone system) the following formula is used, in place of equation 3.1 to calculate the dB level

$$\text{Sound Pressure Level} = \text{Attenuator setting} + 20 \log_{10}\left(\frac{V_i}{V_{ref}}\right) \qquad (3.4)$$

therefore the attenuator setting is used directly in the calculations to correct for differences between the setting for the calibration (120) and that for the measurement.

The sound level meter type 2218 has only three attenuator settings marked as dB ranges. The different settings effectively alter the value of V_{ref} by a factor of 10 or 100 compared with the highest setting used for the calibration tone; the modified value of V_{ref} and an 'attenuator setting' of 120 are used in the above equation. Where no sound level meter is used no further correction for V_{ref} is required and a notional 'attenuator setting' of 120 is returned to the main program to be used in equation 3.4 in further calculations, which is then evidently equal to equation 3.1.

The data from each file is then read into the program. The header block written onto the top of the data file by the NOVA routine is read first and the tape recorder attenuator settings read from it. The data is in the form of four columns the first two being the rms voltage spectra of the two channels. Only one column of the Nicolet data is required i.e. the rms. spectrum of either channel A or B therefore this is put into a new array with the appropriate frequency values for each point. The first four points corresponding to the dc. 25Hz. 50Hz and 75Hz measurement points are discarded. every point up to and including the 41st point are included in the array with every alternate point up to the 400th point. Thus an array with 2 columns and 216 rows is formed, the first column is the frequencies which range from 100Hz to 1kHz with 25Hz spacings and from 1050Hz to 10khz with 50 Hz spacings, and the second column is the voltage corresponding to that frequency.

This array provides the raw data used to calculate the sound pressure level at the microphones. The effect of the Nagra tape recorder is calculated by putting the tape attenuator setting (A_t), passed over from the Nova in the header block of the raw data file, into equation 3.2. The data is converted from volts to dB at the microphone using equation 3.4, the attenuator setting being the value returned from SLMSET. The level at each microphone is written to a data file. The difference between the two levels is calculated and corrected for the free field attenuation as described below, and the resulting attenuation value written to a data file.

The attenuation in the 'free field' case is well known as the attenuation due to spherical spreading and atmospheric absorption. The free field attenuation is calculated in subroutine CORFFAA. The reduction in sound pressure level due to the spreading of the wave front in a sphere from a point source is calculated as:

$$20 \log_{10}(rt / rr) \qquad (3.5)$$

where rr and rt are the source - receiver distance for the reference and test microphones, respectively.

Atmospheric absorption is calculated using the equations described by Bazley (1976) for absorption of pure tones. The total absorption is the sum of 'classical absorption' ie. losses due to viscous and thermal effects of sound travelling through a gaseous medium (M_{cl}): and the molecular absorption of the nitrogen and oxygen molecules (M_N and M_O respectively). The total absorption coefficient is the sum of the three components:

$$M = M_{cl} + M_N + M_O \ nepers / m \qquad (3.6)$$

or

$$M = 4.343(M_{cl} + M_N + M_O) \ dB / cm$$

where

$$M_{cl} = 3.6\times10^{-11}\frac{(1+0.001t)f^2}{P}$$

$$M_N = \frac{1.7\times10^{-8}}{(1+0.00366t)^{0.5}} \times \frac{hPf^2}{2.77\times10^{-5}f^2+h^2p^2}$$

$$h = \frac{RH}{P}T^{-4.922}\,10^{(20.5318-2939/T)}$$

$$M_O = \frac{2f}{(f/F)+(F/f)} \times 4.2425\times10^{-6} + 8.8168\times10^{-8}t + 5.4834\times10^{-10}t^2$$

$$F = 30560\times p\times h^{1.3}$$

f = frequency

t = temperature ° C

T = temperature ° K

RH = relative humidity

Since measurements of air pressure are not made during experiments the air pressure is assumed to be 1.

An example of a measured attenuation spectrum is illustrated in figure 3.3 it is evident that even with only half the original data points included at the higher frequencies the trends of the data are rather difficult to see due to the scatter of the data points. This is largely due to the fact that the FFT analyser calculates equally spaced frequencies on a linear scale, whereas this graph, following normal convention is plotted on a logarithmic

scale, giving a concentration of data points in the high frequency part of the graph. This is particularly troublesome when two or more spectra are to be plotted on the same graph; therefore a routine is used to 'smooth' the data. A simple wild point editing algorithm is used which smooths the graph of figure 3.3 to give figure 3.4. It is evident that little information is lost in this procedure and the resulting spectrum is considerably clearer. All the other measured data presented in this thesis has been smoothed in this way.

The measured attenuation can be used to compare different measuring situations and also to compare measurements with predictions from the ground and scattering models presented in Chapters 4 and 5, respectively.

References, Chapter 3.

[1] Bazley. E.N. 1976 Sound absorption in air at frequencies up to 100kHz. NPL ACOUSTICS REPORT. Ac 74.

[2] Parkin. P.H. and Scholes. W.E 1964. The Horizontal Propagation of Sound from a Jet Engine Close to the Ground at Radlett. J. SOUND. VIB 1 1-13.

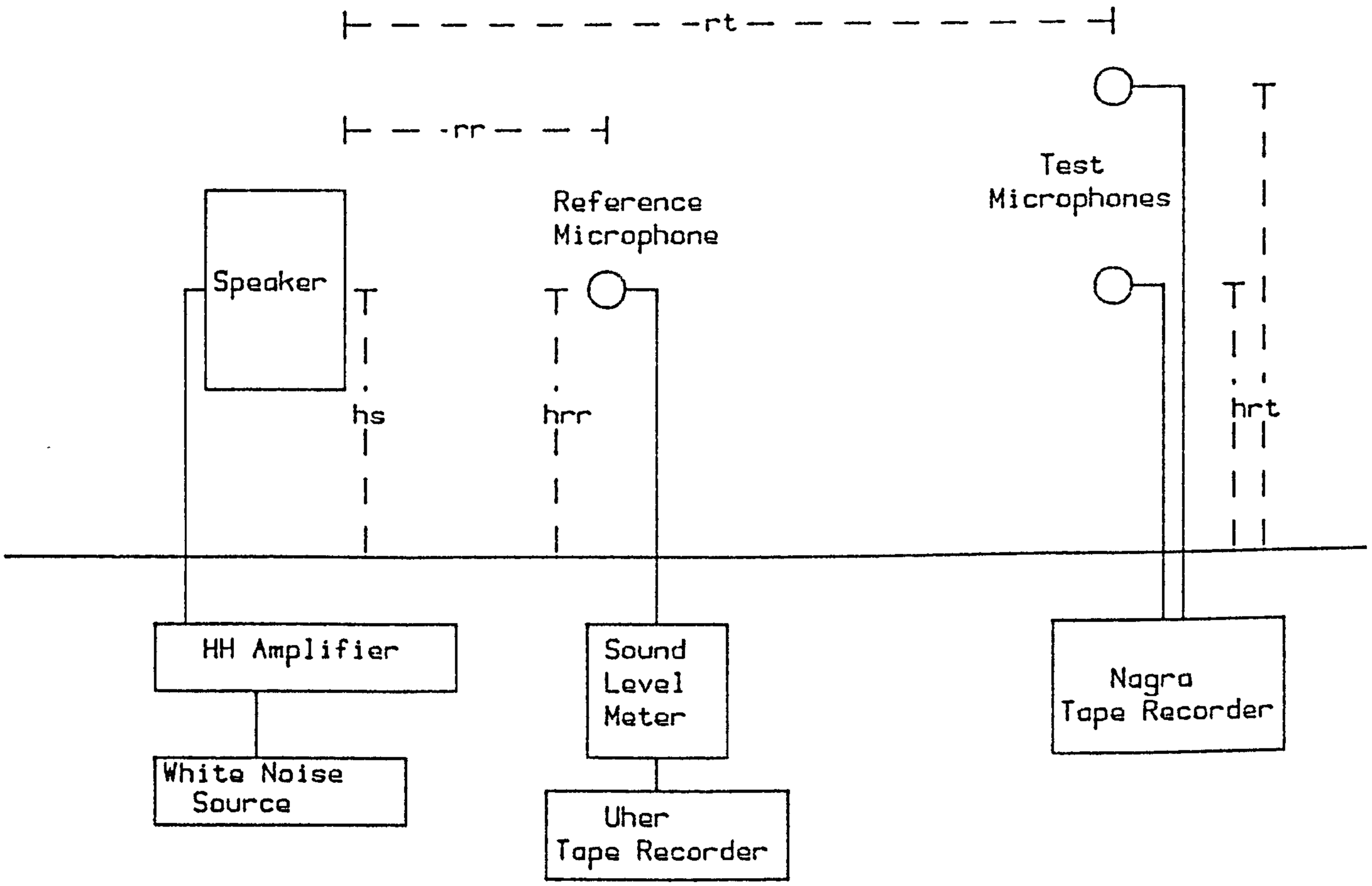

Figure 3.1 Apparatus used in outdoor experiments.

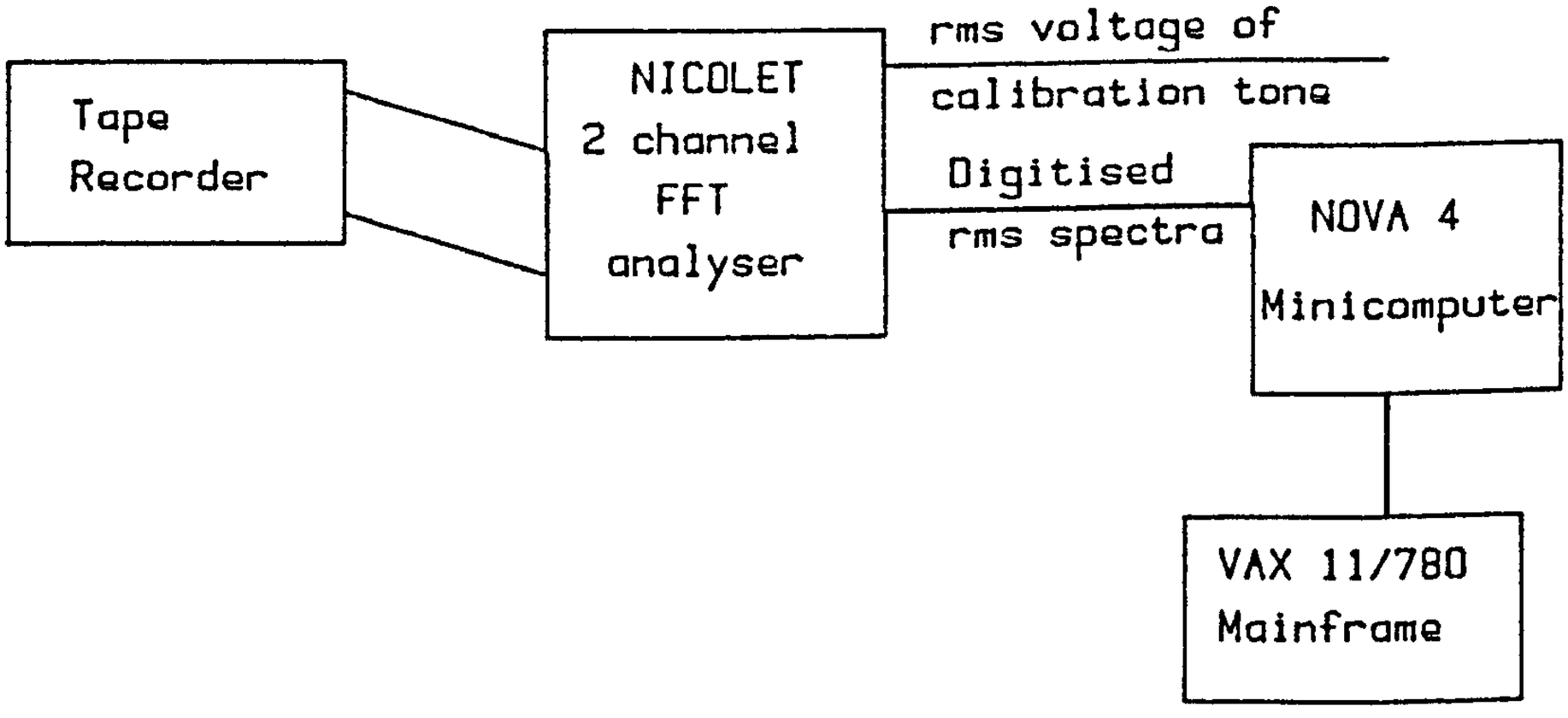

Figure 3.2 Apparatus for the analysis of tape recordings.

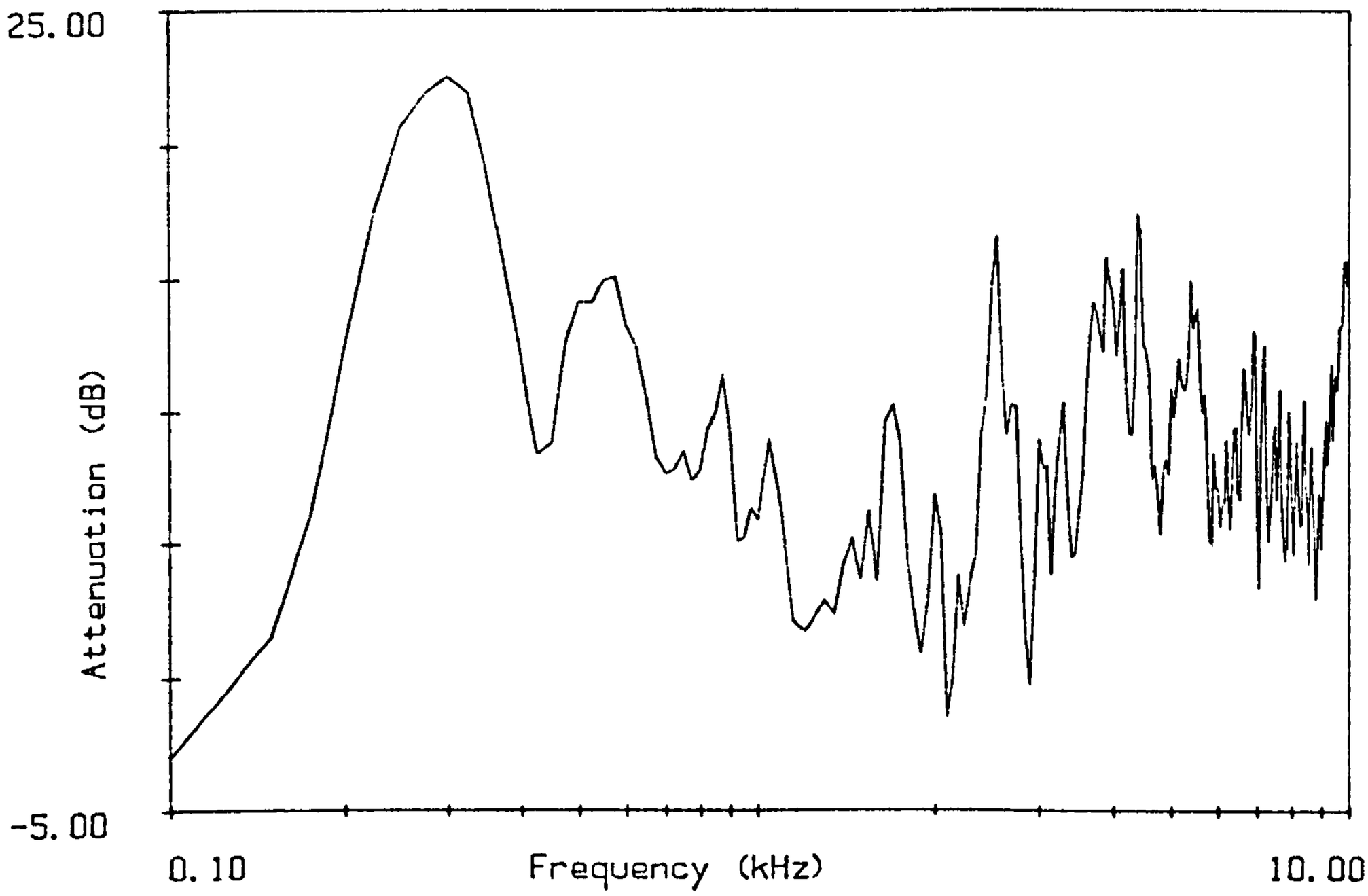

Figure 3.3
Example of attenuation measurement with 216 points.

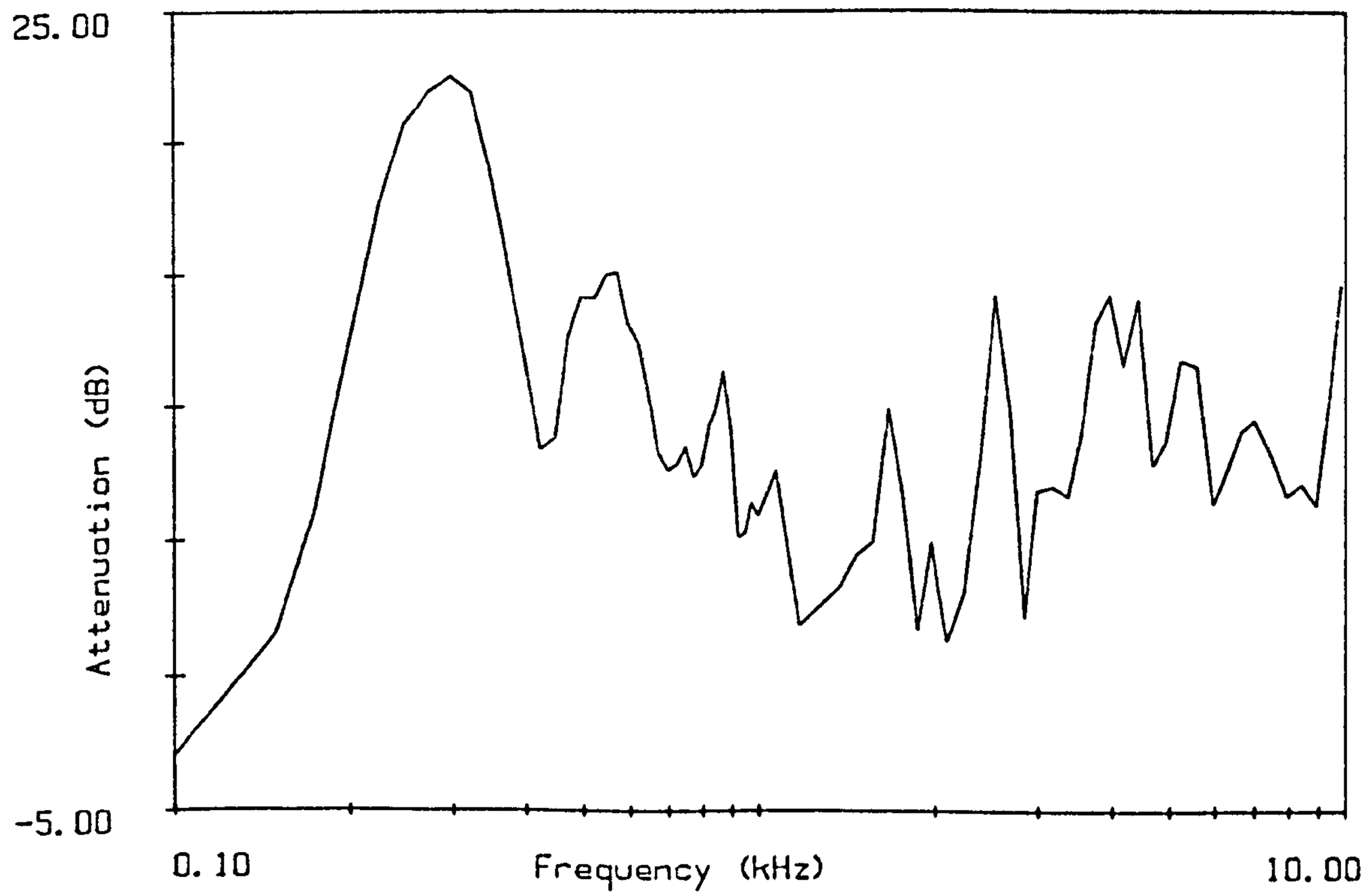

Figure 3.4
Attenuation measurement of figure 3.3 smoothed to 75 points.

Chapter 4 : Prediction of Sound Propagation Over Ground.

4.1 Propagation Prediction Model

The simplest model for a prediction of outdoor sound propagation is that of plane waves travelling over a flat, homogeneous ground surface, with the air assumed to be stationary and homogeneous. In this case the sound pressure at a receiver is the result of sound travelling as illustrated in the ray diagram in figure 4.1. The two paths by which the sound reaches the receiver are the direct path in a straight line between source and receiver, (distance r_1) and the reflected path (distance r_2), which can also be described as originating from an 'image source' from within the ground as illustrated in figure 4.1.

The result of an addition of the direct and reflected rays depends on the relative phase and magnitude of the two rays. If the phase of the two rays is the same the sound from the two ray paths will add coherently, giving an increase in the sound pressure which is twice that of a simple addition of the sound pressures, if they are 180 degrees out of phase the rays will cancel out, processes termed 'constructive and destructive interference' respectively. Where the phase difference is between 0 and 180 degrees the interference effects will be intermediate between the two. These interferences, and therefore the sound pressure levels are highly dependent on frequency.

Figure 4.2 shows the possible paths of a sound wave incident on the surface of a fluid; a porous medium such as a ground surface can be considered as a modified fluid since the penetration of sound into the medium is primarily through the air-filled pores, so this diagram is relevant for a porous ground surface. For a locally reacting surface $\theta_t = 0$. A non-zero value of θ_t is referred to as extended reaction. Extended reaction can be described in terms of the refractive index n.

$$n = \frac{k_1}{k_a} = \frac{\sin\theta}{\sin\theta_t} \tag{4.1}$$

k_0 and k_1 are the propagation constants of air and ground respectively (k_1 is complex). A high value of n indicates local reaction.

The total pressure at a receiver, of sound propagating from a point source over a flat surface is expressed as

$$P_t = \frac{P_i e^{ik w' 1}}{r_1} + Q\frac{P_i e^{ik w' 2}}{r_2} \qquad (4.2)$$

where P_i is source pressure, and Q is a correction for the change of phase and magnitude at the ground surface known as the reflection coefficient.

The reflection coefficient Q depends on whether local or extended reaction is assumed and whether the wave front is plane or spherical. The plane wave reflection coefficient (R_p) has been suggested as a useful approximation of Q, (eg by Delany and Bazley 1970a). The use of the plane wave reflection coefficient does not describe the propagation of plane waves, since equation 4.2 accounts for spherical spreading, but has been shown to adequately model the propagation of spherical waves in some situations (notably where θ is small). The extended reaction plane wave reflection coefficient is

$$R_p = \frac{Z\cos\theta - \left(1 - \sin^2\theta / n^2\right)^{0.5}}{Z\cos\theta + \left(1 - \sin^2\theta / n^2\right)^{0.5}} \qquad (4.3)$$

where

Z = the normalised surface impedance $\rho_1 c_1 / \rho_0 c_0$

ρ_0 and ρ_1 = density of air and ground.

c_0 and c_1 = sound velocity in air and ground.

It is evident that if θ_i is 0 ie. the local reaction case $\sin^2\theta / n^2=0$ so the plane wave reflection coefficient for a locally reacting surface is

$$R_p = \frac{Z\cos\theta - 1}{Z\cos\theta + 1} \tag{4.4}$$

Local reaction is usually assumed for outdoor sound propagation calculations because the ground surfaces generally have a much greater propagation constant than that of air, giving a large value of n in equation (4.1) and indicating local reaction. Impedance measurements made at oblique incidence have been shown (eg. Embleton et al 1976) to give similar results to those made using wave propagation normal to the surface in an impedance tube as described in chapter 2; this also indicates a locally reacting surface. Measurements made by Cramond and Don (1984) also indicate that the local reaction assumption holds for outdoor ground surfaces. Further reference to the plane wave reflection coefficient R_p can therefore be assumed to refer to the local reaction case.

The more complete representation of spherical wave propagation uses the above reflection coefficients incorporated into more complicated spherical wave reflection coefficient equations as described by Rudnick (1947), based on the Weyl-van der Pol formulation calculated for electromagnetic wave theory of the reflection of spherical waves incident on a hard boundary. A term often described as the ground wave term is added to the plane wave reflection coefficient to give the following expression for Q (local reaction case).

$$Q = R_p + (1-R_p)F(w) \tag{4.5}$$

$F(w)$ the boundary loss factor is defined as

$$F(w) = 1+2i\sqrt{w}e^{-w}\int_{-i\sqrt{w}}^{\infty} e^{-t^2}dt \tag{4.6}$$

which can also be expressed as

$$F(w) = 1+i\sqrt{\pi w}\ e^{-w}\ erfc(-i\sqrt{w}) \qquad (4.7)$$

where w, the numerical distance is approximated by Rudnick as

$$w = \frac{i\,2k_0 r_1}{\left(1-R_p\right)^2}\left(\frac{1}{Z}\right)^2\left(1-\left(\frac{k_0}{k_1}\right)^2\sin^2\theta\right) \qquad (4.8)$$

For local reaction case the final term can be neglected so w for the locally reacting ground surface can be expressed as

$$w = \frac{ik_0 r_1(\cos\theta+\beta)^2}{2} \qquad (4.9)$$

where β, the complex normalised admittance is 1/Z. The calculation of

$$e^{-w}erfc(-i\sqrt{w})$$

used in the analysis follows the method of Chien and Soroka (1975), modified in Chien and Soroka (1980).

The use of the calculation using the plane wave reflection coefficient with the local reaction assumption has been shown to agree well with measured data in many outdoor propagation situations. It is evident from equations (4.2) and (4.4) that this will predict complete cancellation of the sound at or near grazing incidence at all frequencies, since grazing incidence assumes a value of θ of 90 degrees giving a value of R_p of -1, and equal values of r_1 and r_2 causing a value of P_t of 0 in equation (4.2).

The spherical wave equations account for wave paths other than those illustrated in figure 4.1, ie the so called ground wave and surface wave. Figures 4.3 and 4.4 illustrate the range of validity of the plane wave assumption by plotting the difference, in decibels between the total pressure calculated using the plane wave and spherical wave reflection coefficients ie

$$20\log_{10}\left|\frac{\dfrac{e^{ikw1}}{r_1}+\dfrac{R_p e^{ikw2}}{r_2}}{\dfrac{e^{ikw1}}{r_1}+\left[R_p+\left(1-R_p\right)F(w)\right]\dfrac{e^{ikw2}}{r_2}}\right| \tag{4.10}$$

It is evident that at high frequencies and short separation distances the spherical wave and plane wave assumptions will give the same result. As the separation distance increases, ie the propagation path is closer to grazing incidence the difference between the calculations increases in both graphs. It should be noted that the source and receiver height are also important, the difference Δr between the distance r_1 and r_2 being the main geometrical parameter influencing sound propagation. Since the source and receiver heights are virtually constant for these graphs an increase in separation distance represents a decrease in Δr. The fact that the graphs show a zero difference at some frequencies, suggests that none of the experimental geometries illustrated are sufficiently close to grazing incidence to totally invalidate the plane wave assumption, on grounds of the cancellation effect. The two calculations do however give a significantly different result at the lower frequencies for the longer distances. The impedance of the ground also affects the range of frequencies over which the plane wave assumption holds. The ground parameters used in figure 4.4 represent a harder ground surface than that of figure 4.3 and the difference between the two assumptions although somewhat smaller, extends to a higher frequency.

The calculations used to predict sound propagation over ground, in this work, always use the spherical wave assumption since, where it is not required, the final term simply reduces to 0. The increased speed of computing which could be attained by using a plane wave assumption is not required as computing time is not critical.

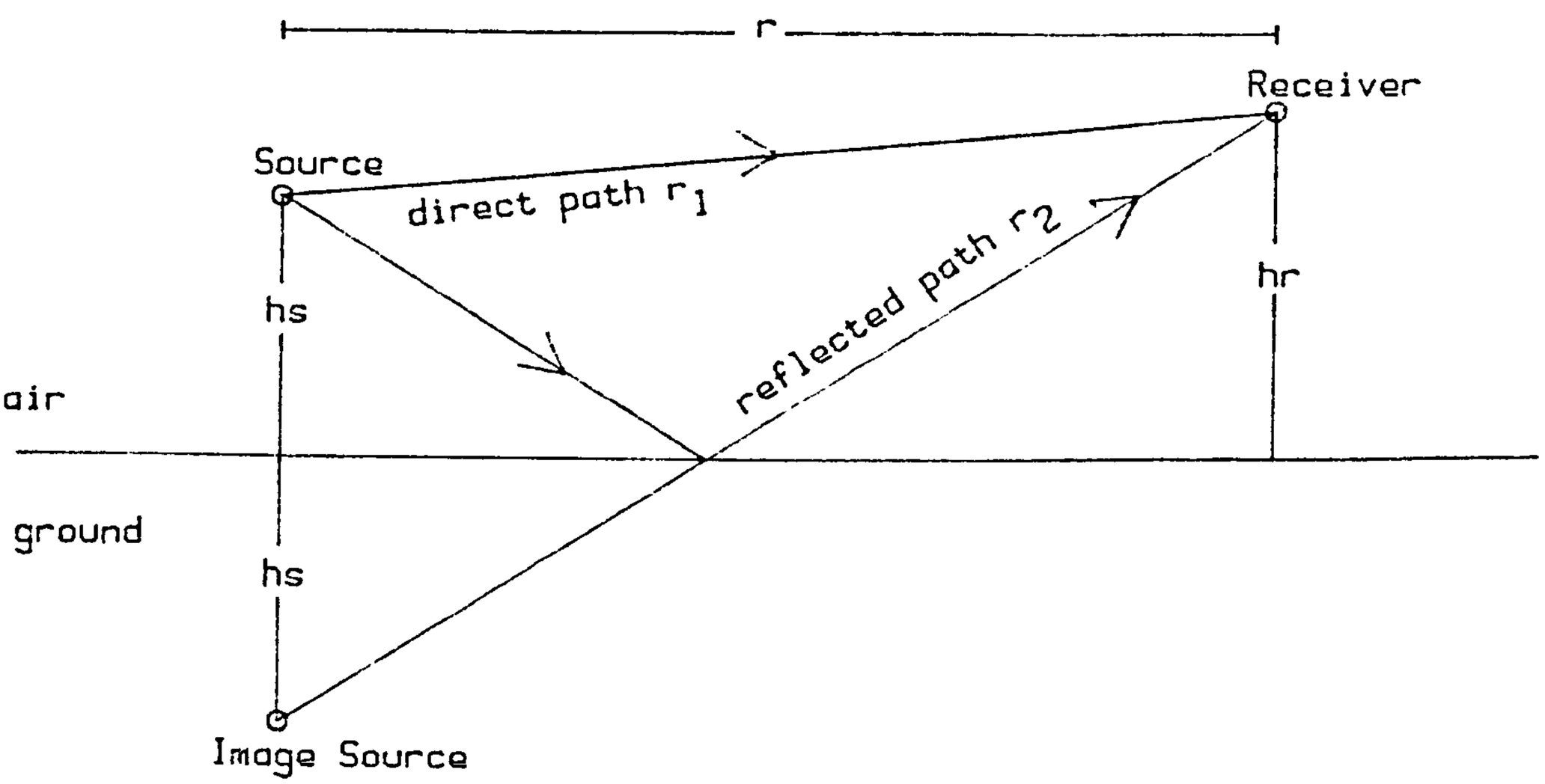

Figure 4.1. Diagrammatic representation of the propagation of sound above a ground surface.

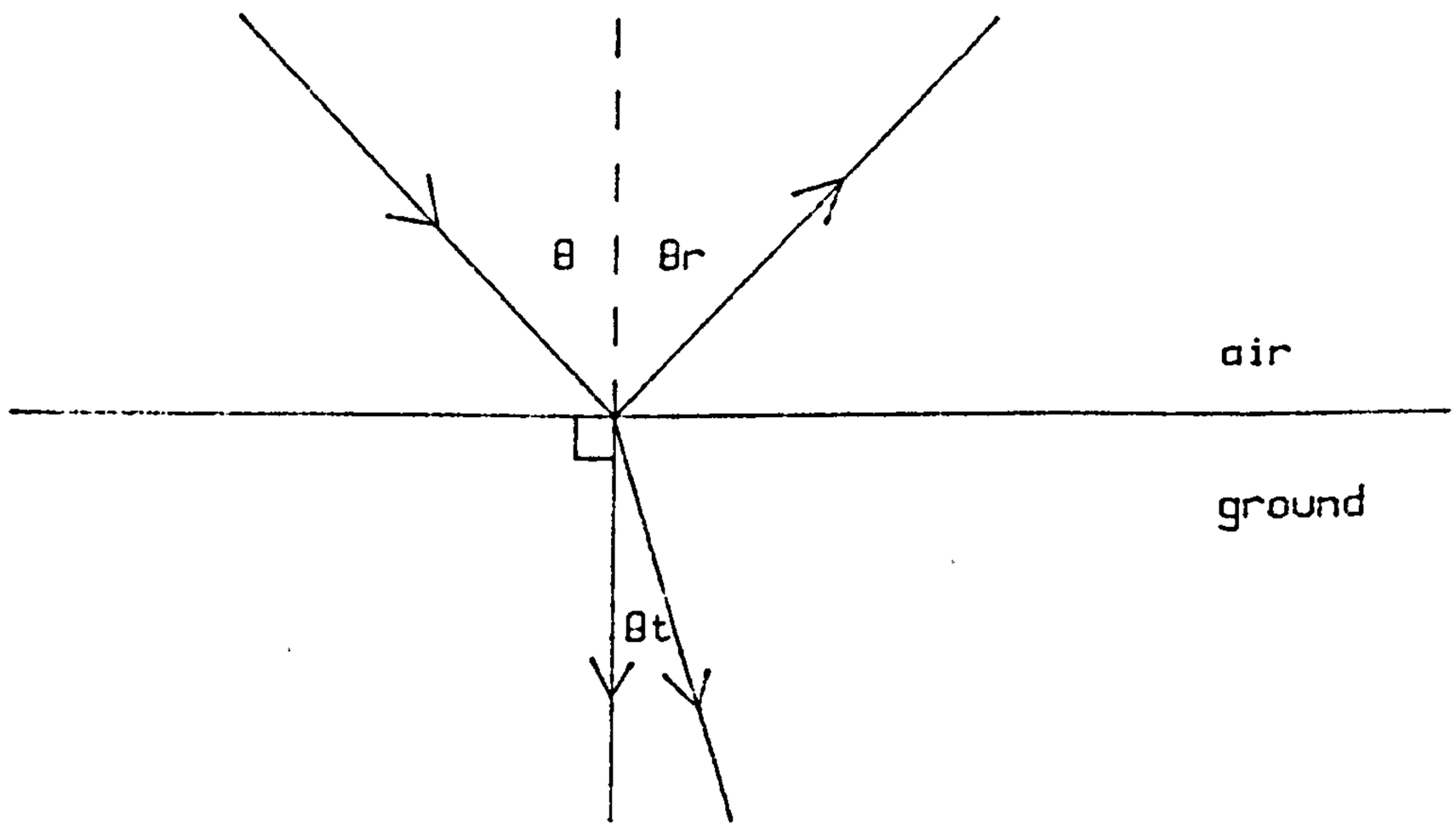

Figure 4.2 Diagrammatic representation of sound transmission into the ground.
Local reaction when $\theta t = 0$.
Extended reaction when $\theta t \neq 0$.

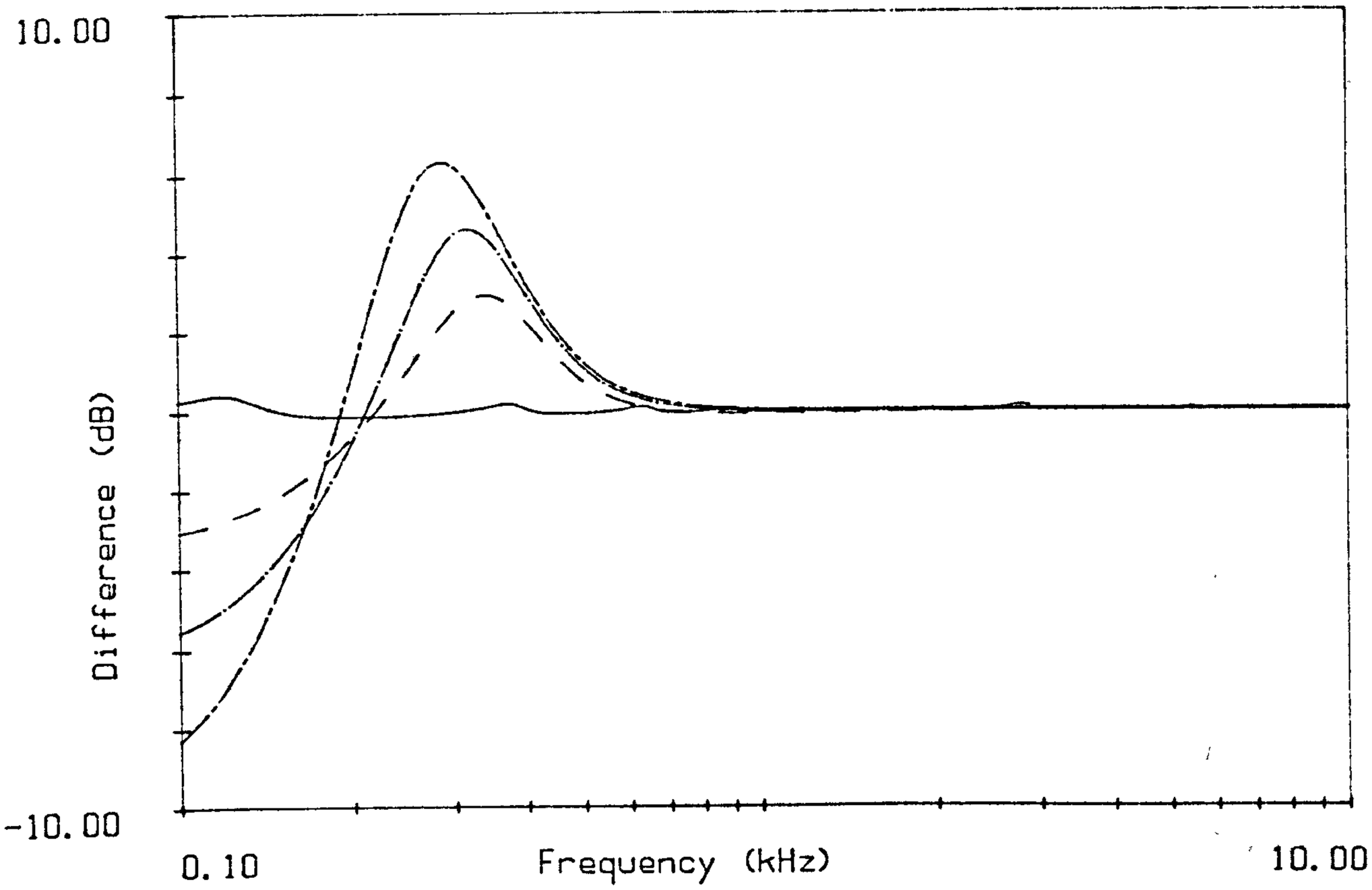

Figure 4.3 Difference between predictions using the plane wave and spherical wave reflection coefficients. Impedance predicted using equation 4.15, σe = 100,000.

——————— hs=1.3m, hr=1.3m, r=2m.
— — — — — hs=1.3m, hr=1.2m, r=24m.
———·———·——— hs=1.3m, hr=1.2m, r=48m.
——·——·——·—— hs=1.3m, hr=1.2m, r=96m.

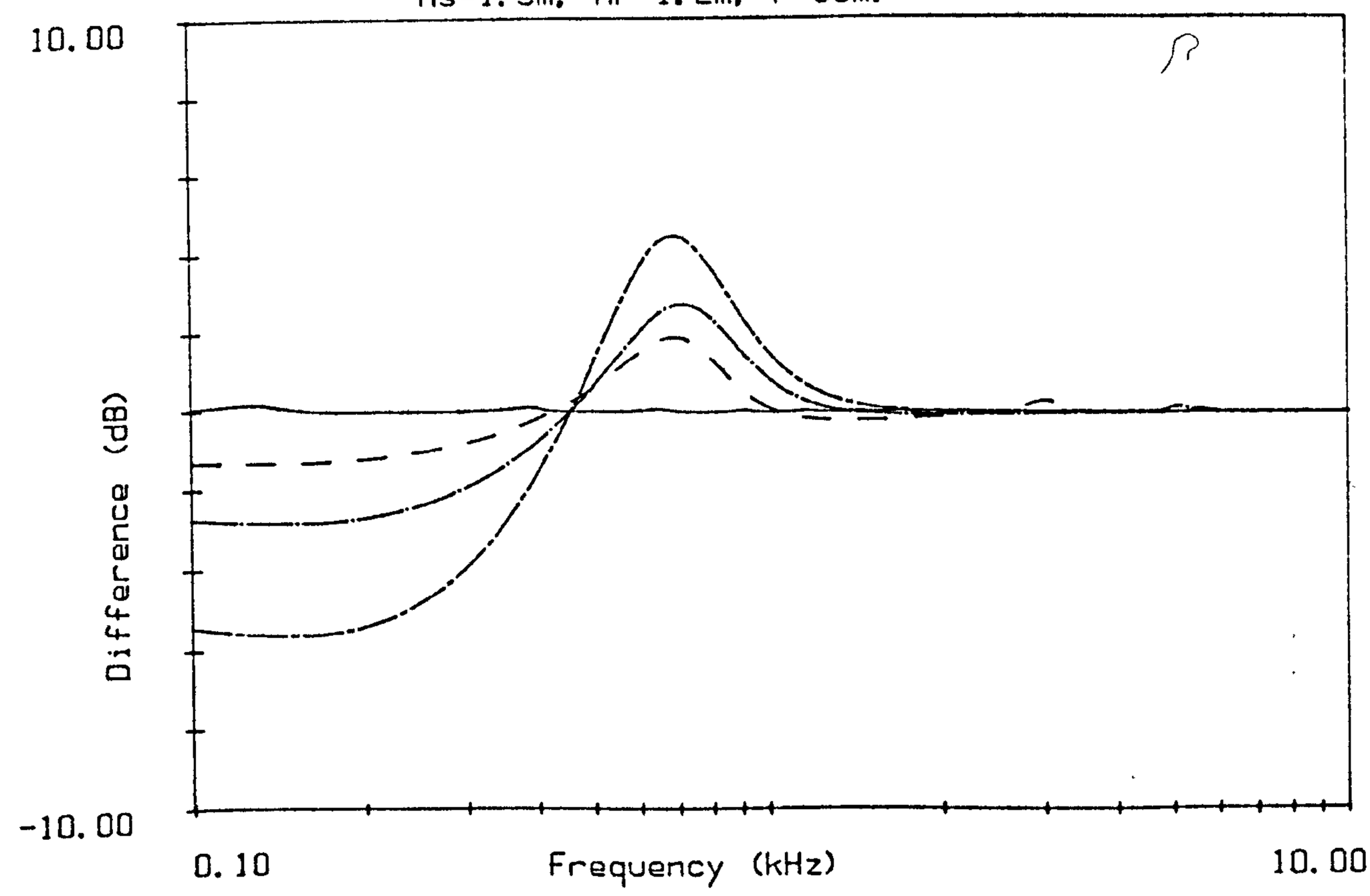

Figure 4.4 Difference between predictions using the plane wave and spherical wave reflection coefficients. Impedance predicted using equation 4.15, σe = 1,000,000. Geometry as in figure 4.3

4.2 Impedance predictions.

Impedance is a complex value which describes the acoustic properties of a material. The real part of impedance is termed the resistance and the imaginary part the reactance. In predictions of sound propagation above a ground surface, as described in section 4.1, a value of the normalised surface normal impedance (Z) is required. The normalised impedance is the specific acoustic impedance divided by the product of the density of, and sound velocity in, air. Various models are available which predict the surface impedance of ground surfaces, some of these are presented in this section.

4.2.1 Delany and Bazley Semi-empirical Model

Delany and Bazley (1970) carried out a series of impedance tube measurements of the surface impedance of porous fibrous materials and compared the results with measurements of the flow resistivity of the materials. They obtained the following relationships between flow resistivity and normalised surface impedance.

$$Z = 1+0.0571\left(\frac{\sigma}{f\rho}\right)^{0.754}+i\,0.087\left(\frac{\sigma}{f\rho}\right)^{0.732} \qquad (4.11)$$

where σ is the flow resistivity in mks rayls, f is the frequency and ρ is the density of air, normally taken as 1.21.

The bulk propagation constant k_b of the materials was also measured and used to calculate the following relationships between the flow resistivity and the normalised bulk propagation constant k_b thus:

$$k_b = 1+0.978\left(\frac{\sigma}{f\rho}\right)^{0.7}+i\,0.189\left(\frac{\sigma}{f\rho}\right)^{0.595} \qquad (4.12)$$

Experiments have shown that flow resistivity values deduced from this model are frequently around twice the value of measured flow resistivities for outdoor ground surfaces (flow resistivity measurements for soil are rather difficult to obtain and results tend to be very variable). This suggests that the value of σ in equations (4.11) and (4.12) should be regarded as an 'effective' flow resistivity. This effective flow resistivity is in fact closer to the product of the flow resistivity and the porosity, since the porosity of the materials used by Delany and Bazley was about 1 and that of soils is normally about 0.5.

4.2.2 Attenborough Four Parameter Model.

Attenborough (1983) has developed a model based on detailed theoretical analysis of the acoustical behaviour of rigid air- filled homogeneous granular materials. This uses four physical parameters of the granular material to predict the characteristic impedance. The four physical parameters used are: the flow resistivity (σ) the porosity (Ω), a pore shape factor (S_f), and a grain shape factor (n'). The characteristic impedance is defined as:

$$Z_c = \frac{\omega q^2}{k_b c\,\Omega\left[1-\frac{2}{Y}T'(Y)\right]} \tag{4.13}$$

$$Y = \left[\frac{8\rho q^2 \omega}{\Omega \sigma S_f^2}\right]^{0.5} \sqrt{i}$$

The normalised bulk propagation constant is expressed as:

$$k_b^2 = q^2 \frac{\left[1+2\left[\frac{\gamma-1}{Y\sqrt{N_{pr}}}\right]T'(Y\sqrt{N_{pr}})\right]}{1-\frac{2}{Y}T'(Y)}$$

$$T(x) = \frac{J_1(x)}{J_0(x)}$$

f = frequency

c = speed of sound in air

N_{pr} = Prandtl number in air

ρ = density of air

γ = ratio of specific heats of air

q^2 = tortuosity = $\Omega^{-n'}$

$J_1(x)$, $J_0(x)$ = First and zeroth order Bessel functions.

4.2.3 Rigid-Backed Layer Models.

The Delany and Bazley impedance model predicts the surface impedance since it is a result of empirical measurements of surface impedance, whereas the theoretical model calculates the characteristic impedance. The characteristic impedance is, however,equal to the surface impedance for a homogeneous layer of material sufficiently thick to be assumed infinite. Either model can also be extended to give the surface impedance of a thin layer of the material overlying a rigid backing, thus:

$$Z = Z_c \coth(-ik_1 d) \qquad (4.14)$$

where

$$k_1 = k_b \frac{\omega}{c}$$

and

d = layer depth.

The layer depth at which this equation becomes the homogeneous case ($Z = Z_c$) evidently depends on the flow resistivity as well as the layer depth. This agrees with the

physical reality, that sound is more likely to be reflected back to the surface from the rigid backing, in a medium with high porosity and flow resistivity ie one that is more 'transparent' to sound. For example, the results of Van der Heijden (1984) suggest that only the top 10cm affects the surface impedance, of sandy soils.

4.2.4 Approximations to the Four Parameter Theoretical Solutions

Attenborough (1985) has calculated approximations of the four parameter model for high flow resistivities and low frequencies. These result in calculations of surface impedance using only one or two parameters. The approximate models are:

Homogeneous Ground Approximation.

The characteristic and therefore surface impedance of a homogeneous or semi-infinite layer of ground is approximated as :

$$Z \approx 0.218 \left| \frac{\sigma_e}{f} \right|^{0.5} (1+i) \qquad (4.15)$$

effective flow resistivity $\sigma_e = \frac{S_f^2 \sigma}{\Omega}$

Thus the resistance and reactance are equal.

Variable Porosity Approximation.

Published data has shown that the porosity of natural and cultivated soils often decreases with increasing depth. The porosity is assumed to decrease exponentially with depth. A parameter α is used to describe this increase in porosity such that the porosity at a depth x is:

$$\Omega(x) = \Omega(0)\exp(-\alpha x) \tag{4.16}$$

The surface impedance for this approximation is defined as:

$$Z \approx 0.218\left[\frac{\sigma_e}{f}\right]^{0.5} + i\left[0.218\left[\frac{\sigma_e}{f}\right]^{0.5} + 9.74\left[\frac{\alpha_e}{f}\right]\right] \tag{4.17}$$

where σ_e is the value at the surface

and

$$\alpha_e = \frac{n'\alpha}{\Omega(0)}\, m^{-1}$$

It is evident that when α is 0 this is the same as the homogeneous approximation, as would be expected.

Rigid Backed Layer Approximations.

Attenborough (1985) uses an approximation for the surface impedance of a rigid-backed layer which has the form:

$$Z \approx 0.00082\sigma_e d_e + i\left|\frac{38.99}{f d_e}\right| \qquad (4.18)$$

effective depth $d_e = \Omega d$ metres

This is based on the first term of the series expansion for the hyperbolic cotangent (coth) used in equation (4.14). The resistance is independent of frequency. It is evident that increasing the layer depth to approximate to an infinite layer does not produce a result that is equal to the homogeneous approximation as the homogeneous model does not have a 'flat' resistance and frequency dependent reactance. Therefore this approximation is only valid for a thin layer, where $|k_1 d| \ll 1$.

An extension of this model can be made which equals equation (4.18) for a thin layer and low flow resistivity and equation (4.15) (homogeneous approximation) for a thicker layer and higher flow resistivity. This uses a direct calculation of the coth term of equation (4.14), which is easily achieved using the complex mathematics capability of FORTRAN. The surface impedance of a rigid backed layer can be expressed as:

$$Z \approx 0.218\left|\frac{\sigma_e}{f}\right|^{0.5}(1+i) \times \coth\left|-i\,5.59\times10^{-5}(1+i)(\sigma_e f)^{0.5} d_e\right| \qquad (4.19)$$

The layer depth corresponding to the value of d_e is dependent on the porosity, thus a 5cm layer of porosity 0.5 will have the same effect as a 6cm layer of porosity 0.42; except of course that the flow resistivity is likely to be different. In order to determine whether a particular value of d_e is likely to correspond physically to the homogeneous case, some knowledge of the likely porosity is required eg. a value of d_e of 0.08 will correspond to a layer depth of more than 10cm in a soil of porosity 0.5, and is therefore likely to approximate to the homogeneous case. Figure 4.6 shows a comparison between the approximations of equations (4.18) and (4.19). The two are similar at low frequencies, ie a smaller value of k_1 and diverge at high frequencies. It is evident from equation (4.19) that the 'coth term' is

dependent on frequency, flow resistivity, porosity and depth, an increase in any of these increasing the argument of coth, so that the coth term tends to 1 for high frequencies and large values of flow resistivity, porosity or depth. Thus this model encompasses both equations (4.18) and (4.15) for appropriate ranges of the various parameters.

4.2.5 Fitting Impedance vs Frequency Data

Several people have used the Delany and Bazley model to predict the surface impedance from propagation measurements over outdoor ground surfaces by deducing a flow resistivity value (eg Embleton et al. 1976). There have however been other results which cannot be adequately explained by this model. It is evident from equation (4.11) that at high frequencies the value of Z predicted by the Delany and Bazley model tends to $1 + i0$ the frequency response of the impedance predicted by this model can be seen in figure 4.5. Some measured impedance data has been shown to have the frequency dependence of this type of prediction, other measurements however do not follow this pattern.

The data of impedance of a forest floor from Van der Heijden(1984) shown in figure 4.6 can be more closely predicted by the rigid-backed layer approximations, in which the resistance is largely independent of frequency, and the reactance varies with the inverse of frequency. The data shown in figure 4.8 can be approximated by the homogeneous model in which the resistance and reactance are equal and vary with the inverse square root of frequency. The data and prediction of figure 4.7 show the frequency dependence of the variable porosity approximation. Figures 4.6 to 4.8 are taken from the paper by Attenborough (1985) in which the parameters used to calculate the predicted impedance are deduced from one particular point from the data, as indicated. The prediction in figure 4.6 which is calculated using equation (4.18) is the one corresponding to the prediction in Attenborough (1985) from which the input parameters are calculated.

The models described above all imply certain assumptions about the ground surface ie. whether it is homogeneous, layered or has a decreasing porosity with depth. The ground beneath trees can be seen to consist of a porous layer of fallen leaves and humus overlying a

layer of mineral soil.

The woodland floor data of figure 4.6 can be described acoustically as a thin layer with a rigid backing. The more detailed model described by Talaske(1980) for a thin layer overlying a semi-infinite porous layer, which is demonstrated as fitting impedance measurements of a forest floor, could be useful in deducing the characteristics of a forest floor given detailed impedance measurements. However it was not used in this study since the one and two parameter models described above are thought to be adequate for the deduction of impedance from propagation measurements, and models requiring more than two input parameters would present considerable difficulties in fitting predictions to measured data. The variable porosity approximation may, however, model a multi-layered situation in which deeper layers have successively higher porosities (and therefore higher flow resistivities). The use of the models presented in this section, in predicting sound propagation is described in section 4.3.

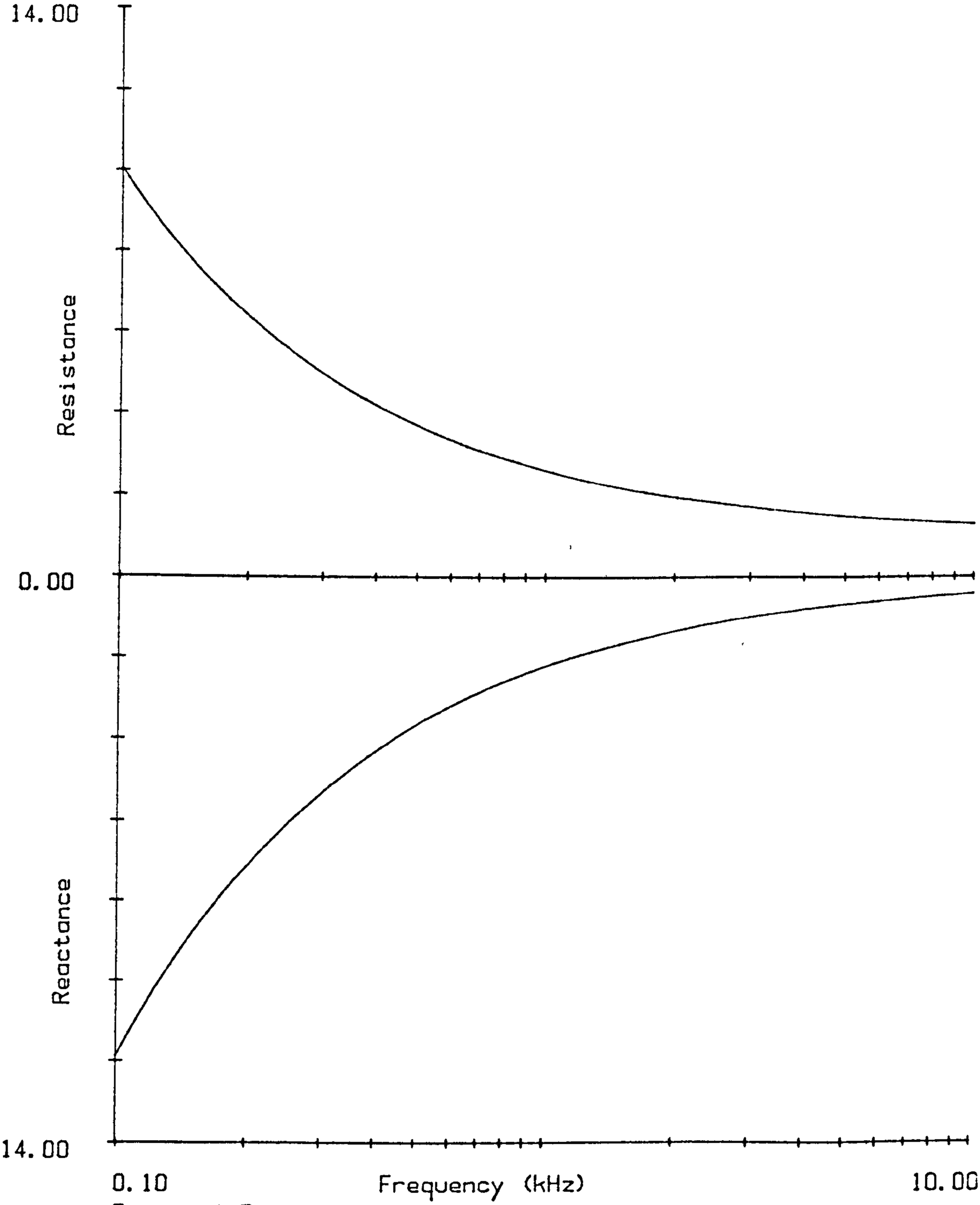

Figure 4.5.
Impedance predicted using the Delany and Bazley impedance model (equation 4.11) σ = 100,000 mks rayls.

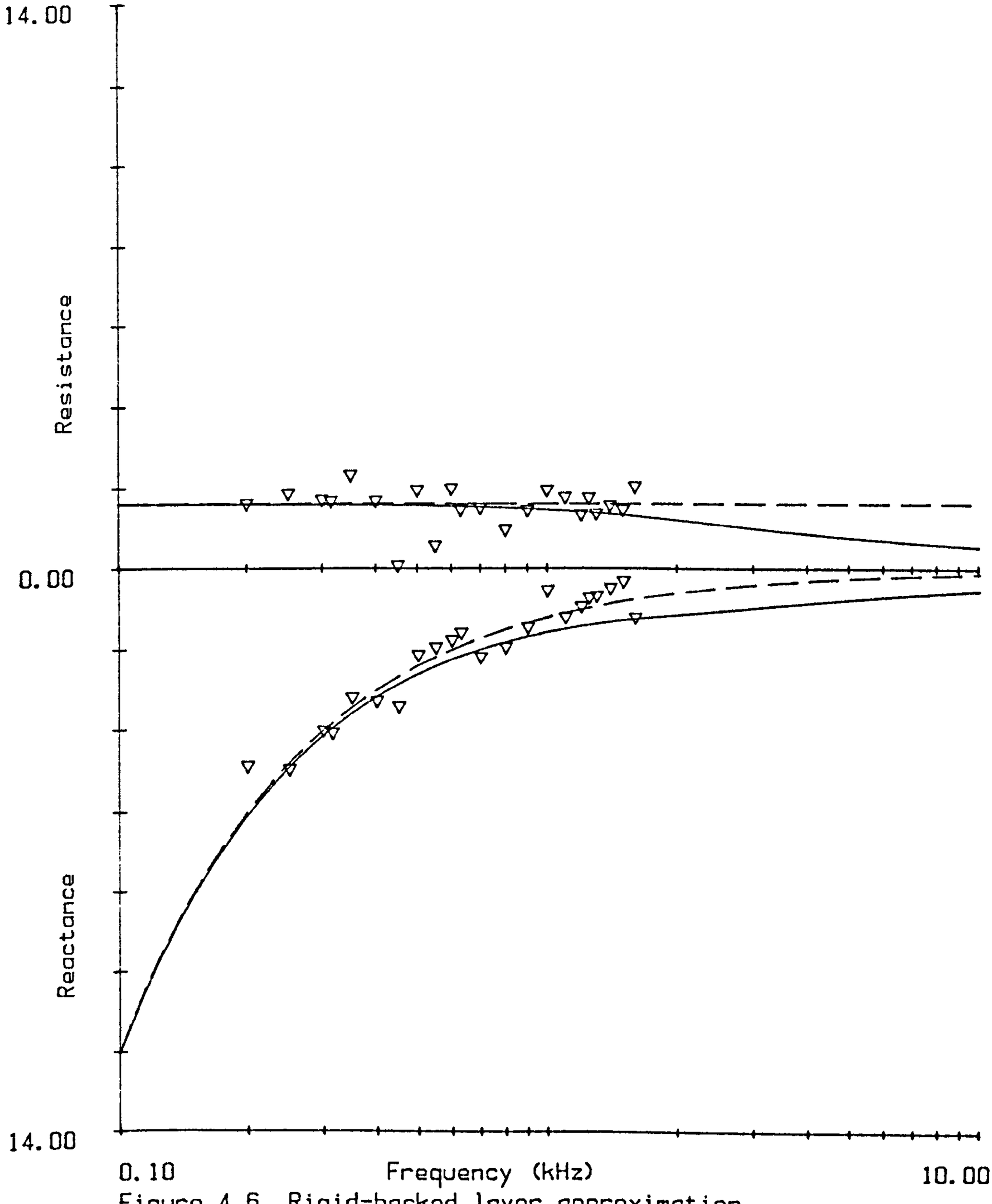

Figure 4.6. Rigid-backed layer approximation.
Measured impedance of forest floor from Van der Haijden (1984)
Predictions :
———— Equation 4.19 or e = 60.053 mks rayls, and de = 0.0325m.
— — — - Equation 4.18 using the same parameters.
Parameters calculated from equation 4.18 : z at 300Hz = (1.6+4i)

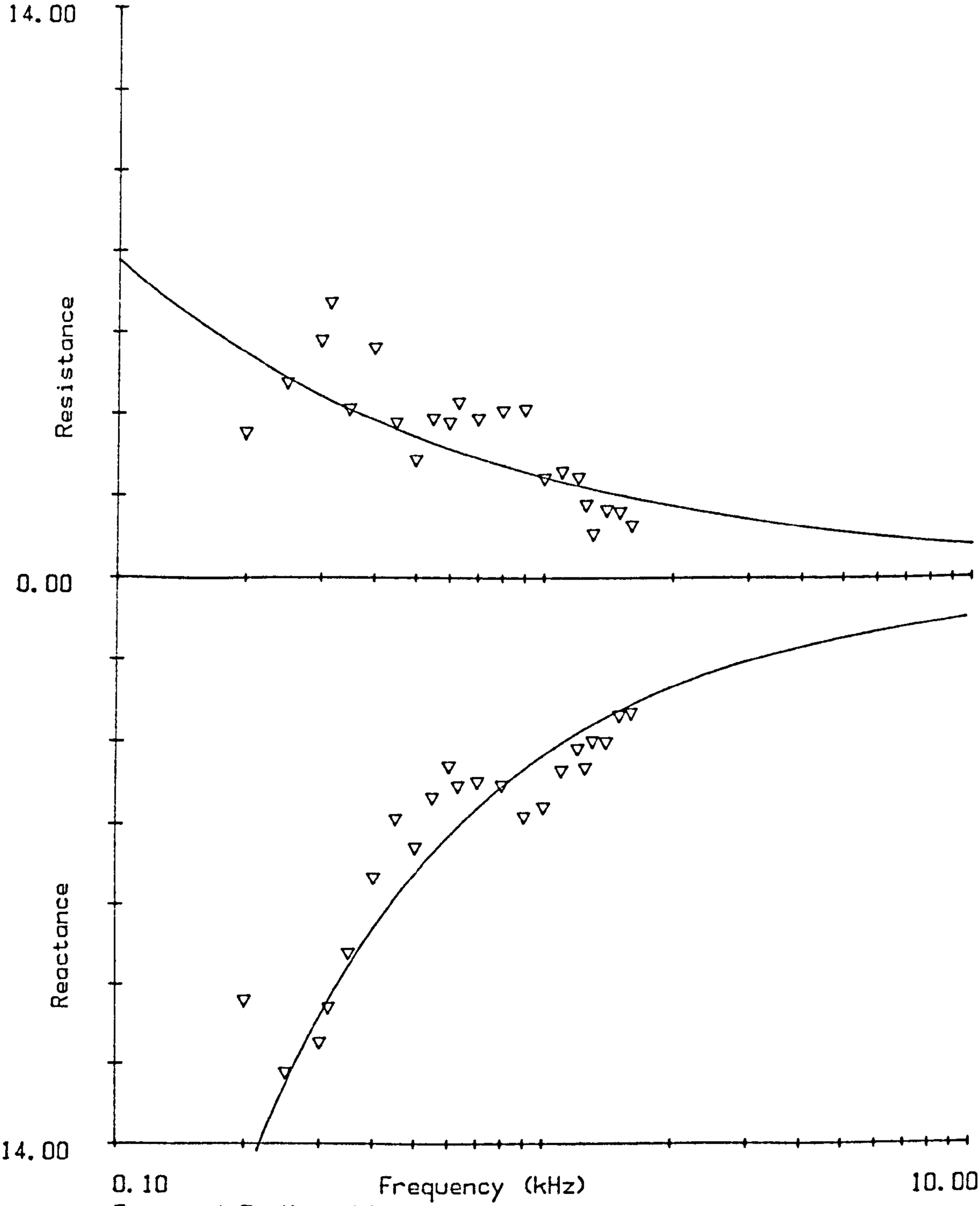

Figure 4.7. Variable porosity approximation.
Measured impedance of meadow from Van der Heijden (1984)
Prediction uses equation 4.17 σe = 126.824 mks rayls.
and αe = 195/m
Parameters calculated from : z at 250Hz = (4.9 + 12.2i)

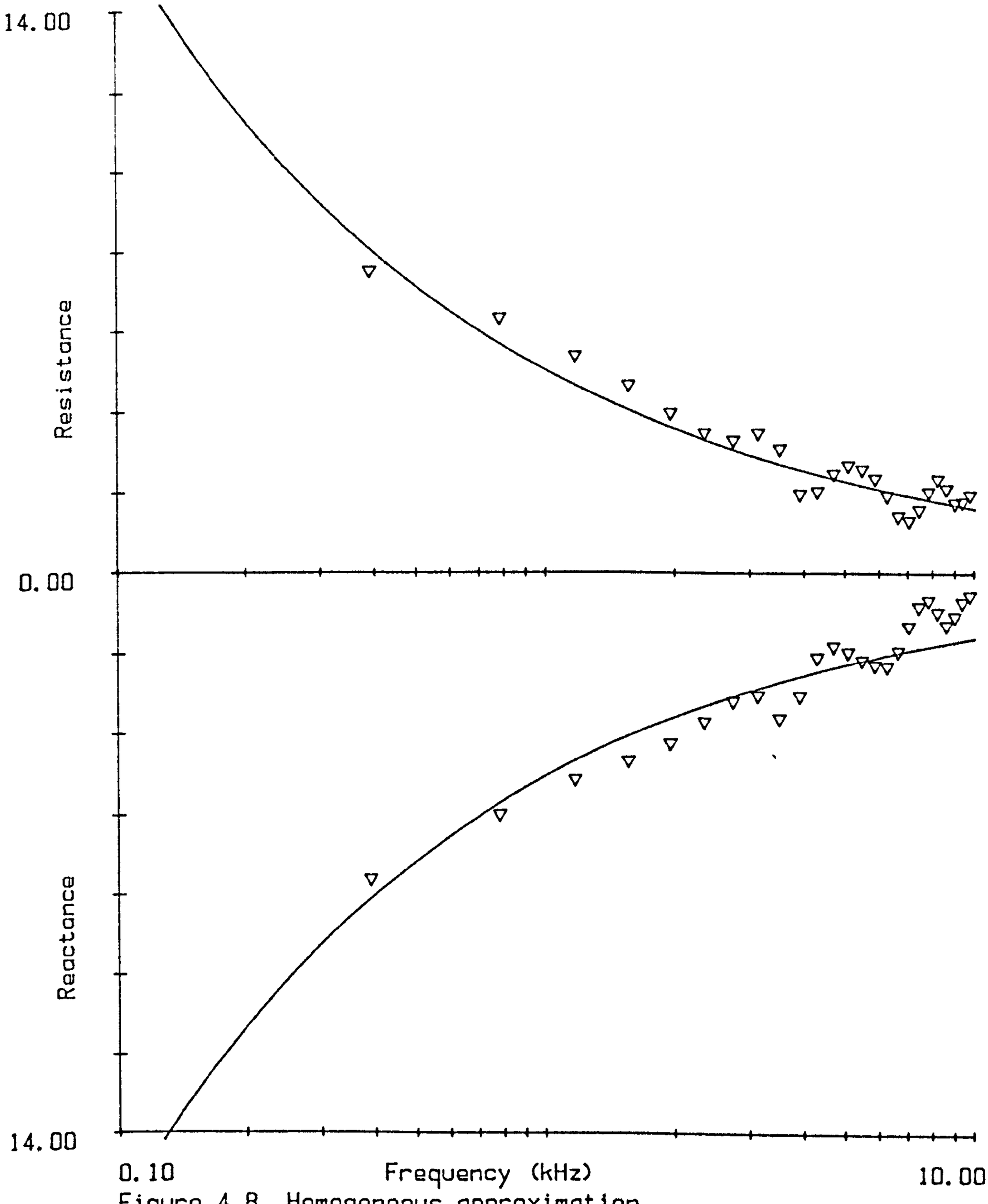

Figure 4.8. Homogeneous approximation.
Measured impedance of compacted earth from Don and Cramond
Prediction uses equation 4.15 σ e = 538.676 mks rayls.
Parameter calculated from : z at 400Hz = 8(1 + i)

4.3 Description of Attenuation Function

Equation (4.2) gives the total sound field at a receiver for a point source and a known source pressure level. To express the interference effects of a ground surface independently of source strength or spectrum, a ratio between two cases with the same source is used. The commonest ratio used is the excess attenuation ie. the total sound pressure minus the free field pressure.

$$Excess\ Attenuation\ A_e\ (dB) = 20 \log_{10} \left| \frac{\frac{e^{ik_0 r_1}}{r_1} + \frac{Q e^{ik_0 r_2}}{r_2}}{\frac{e^{ik_0 r_1}}{r_1}} \right| \qquad (4.20)$$

or

$$A_e = 20 \log_{10} \left| 1 + \frac{r_1}{r_2} Q e^{ik_0(r_2 - r_1)} \right| \qquad (4.21)$$

The attenuation function calculated from the measurements, as described in chapter 3 is the difference between the level at the reference microphone and that at the test microphone, minus the attenuation due to spherical spreading and atmospheric absorption. In order to predict this attenuation function the difference between the excess attenuations for the two microphones is calculated thus:

$$Attenuation\ (dB) = 20 \log_{10} \left| \left(\frac{\frac{e^{ik_0 r_1}}{r_1} + \frac{Q_r e^{ik_0 r_2}}{r_2}}{\frac{e^{ik_0 r_1}}{r_1}} \right) \left(\frac{\frac{e^{ik_0 t_1}}{t_1}}{\frac{e^{ik_0 t_1}}{t_1} + \frac{Q_t e^{ik_0 t_2}}{t_2}} \right) \right| \qquad (4.22)$$

where r_1 , r_2 and Q_r refer to the test microphone and r'_1 , r'_2 and Q_r refer to the reference microphone. The reflection coefficients Q_r and Q_r can be calculated using the same ground parameters or different ones depending on the situation. By definition

$$\left| e^{ik\,w'_1} \right| = 1 \text{ since } k_0 r'_1 \text{ is real}$$

and

$$\left| e^{ik\,w'_1} \right| = 1 \text{ since } k_0 r'_1 \text{ is real}$$

therefore the actual function calculated is:

$$Attenuation = 20 \log_{10} \left| \left(\frac{\dfrac{e^{ik\,w'_1}}{r_1} + \dfrac{Q_r\, e^{ik\,w'_2}}{r_2}}{\dfrac{e^{ik\,w'_1}}{t_1} + \dfrac{Q_r\, e^{ik\,w'_2}}{t_2}} \right) \left(\frac{t_1}{r_1} \right) \right| \qquad (4.23)$$

The attenuation due to spherical spreading of the direct path is accounted for in equation (4.23), in the term $\frac{t_1}{r_1}$. The resulting attenuation value calculated is therefore the difference in sound pressure level which could be measured between two microphones located above a flat surface of known surface impedance, assuming no atmospheric absorption: this is directly comparable to the measurements described in chapter 3. The microphone closest to the source is normally referred to as the reference microphone and the one further from the source as the test microphone, but the equations above are equally valid for any two receivers with the same source.

The prediction of attenuation is calculated using the FORTRAN program PREDDIFF (see Appendix A). PREDDIFF is designed to calculate attenuation in order to make

comparisons with the measured data. Since all the measurements are made using the Electrovoice S12-2 speaker, a correction is made for the fact that the unit consists of two speaker cones, one producing the high frequencies and the other the low frequencies. The nominal cutoff frequency for the crossover network is 3000Hz; ie the frequencies up to 3000Hz are mainly produced by the low frequency cone and those above 3000Hz by the high frequency cone. A correction is made for the fact that the two speaker cones are at different heights, by adding 0.2m to the source height when the frequency is above 3000Hz. The source height input to the program is the distance from the ground to the centre of the low frequency speaker. It should be noted that this correction does not mimic the action of the speaker exactly, since at the frequencies around 3000Hz sound is produced by both speaker cones.

Dependence of Attenuation Function on Geometry.

Figure 4.9 is an example of the predicted attenuation calculated using equation (4.23), the input source and receiver locations ('experimental geometry') used are commonly used in the experiments. The impedance is calculated using equation (4.15) with an effective flow resistivity of 100,000 mks rayls. The frequency dependence of the attenuation function is typical of those calculated for all the experimental geometries; it consists of an 'interference pattern ' of a number of large scale peaks which are made up of several small scale peaks and dips. The main low frequency peak is broader than those at the higher frequencies when plotted on the normal logarithmic frequency scale. To make further descriptions of the attenuation function clearer, the smaller scale peaks and dips which make up the large low frequency peak will be referred to as the 'lobes' of that peak. The narrow, high frequency peaks are often not observed in outdoor sound propagation measurements, due to large and small scale turbulent effects and scattering by vegetation, which disrupt the phase of the waves making destructive interference less likely.

Figures 4.10 to 4.14 show the dependence of the attenuation on the geometry of the system. Each of these figures has the attenuation function of figure 4.9 plotted as a solid line and two other attenuation graphs. The source and receiver locations used in the two

different graphs are a result of increasing only one of the dimensions by 10 and 50 per cent. a different dimension is varied in each figure.

Figure 4.10 shows the change in attenuation caused by increasing the test microphone height. the effect is to shift the high frequency peaks to a lower frequency. The low frequency peak and smaller peaks are not, however, shifted in frequency but the magnitude is slightly reduced by increasing the test microphone height.

Figure 4.11 shows the change in attenuation caused by increasing the test separation distance. the effect is to shift the high frequency peaks to a higher frequency. The low frequency peak and smaller peaks are again not shifted in frequency but the magnitude is increased by increasing the test separation distance.

Figure 4.12 shows the change in attenuation caused by increasing the reference microphone height. the effect is to shift the low frequency peaks and smaller peaks to a lower frequency and change their magnitudes. The high frequency peaks are only slightly altered in magnitude and the frequency at which they occur is unchanged.

Figure 4.13 shows the change in attenuation caused by increasing the reference microphone separation distance the effect is to shift the low frequency peaks and smaller peaks to a higher frequency and change their magnitudes. The high frequency peaks are again relatively unchanged.

Figure 4.14 shows the change in attenuation caused by increasing the source height. All the peaks are shifted to a lower frequency and altered in magnitude.

The shape of the attenuation spectra are evidently dependent on the locations of both the reference and test microphones. The shape and magnitude of the high frequency part is largely determined by the location of the test microphone whereas the low frequency part is more sensitive to changes in the location of the reference microphone. Altering the source height, of course, affects the geometry of both the test and the reference microphone system.

The shape of the attenuation function and its dependence on different dimensions of the system can be more clearly explained by examining the two excess attenuation spectra which make up the attenuation function.

Figures 4.15 and 4.16 illustrate the calculated excess attenuation function of the test and reference microphone positions respectively of figure 4.9. The correction for the change in source height at 3000Hz has been made in these calculations. The peaks and dips are caused by interference between the direct and reflected rays. It is evident from these figures that the large scale peaks of the attenuation function originate from the test microphone excess attenuation and the small scale ones from the reference microphone. Due to the subtraction of the test microphone signal from the reference microphone signal a dip in the test microphone excess attenuation gives rise to a peak in the attenuation function. The size and number of peaks and dips in the calculation of excess attenuation is highly dependent on the geometry of the system, in particular the difference in distance between the direct and reflected path (Δr). In general, increasing the value of Δr effectively shifts the peaks to a lower frequency and fewer peaks will occur in a given frequency range. It seems that the smaller the separation distance (or larger Δr) of a system the lower the frequency range in which the geometry has a significant effect on the excess attenuation and therefore the attenuation function. All the figures described in this section are calculated using the same assumed pattern of ground impedance, as will be seen in the next section the impedance model used, and parameters input to the impedance model, also affect the attenuation function; particularly the low frequency part.

Dependence of Attenuation Function on Impedance

Figure 4.17 shows the attenuation function of figure 4.9, compared with attenuation calculated using the homogeneous approximation with different values of effective flow resistivity. It is evident that the part of the attenuation function which is most affected by the change is the low frequency peak. The frequency at which the high frequency peaks occur is virtually unchanged, although the magnitude is somewhat altered.

A greater input flow resistivity ie harder ground surface, effectively shifts the low frequency peak to a higher frequency. The frequency at which each 'lobe' of the peak occurs is unchanged, but their magnitudes change so that, in this example, the first lobe is the highest for σ_e = 100,000, the second is the highest for σ_e = 200,000; giving a second lobe higher than the second lobe of the first graph, but lower than its first, highest lobe. In the third graph ie σ_e = 1,000,000 the third peak is the highest. Again it is higher than the corresponding lobe of the other two graphs, but lower in magnitude than the maxima for the two softer surfaces. The excess attenuation spectra from which figure 4.17 is calculated are plotted in figures 4.18 and 4.19. The excess attenuation graphs show that the shift in frequency and magnitude of the low frequency peak is due to a corresponding difference in the low frequency dip of the excess attenuation for the test microphone. The effect of the change in flow resistivity on the reference microphone follows a similar pattern but the magnitude of the change is very small. Thus the shape and location of the first peak in attenuation of a measurement gives information about the ground surface, particularly the ground between the reference and test microphones; when compared with, and fitted to, such model predictions (see section 4.4).

Figure 4.20 again shows the attenuation function of figure 4.9, this time compared with attenuation calculated using the rigid backed layer approximation (equation 4.19) with different values of effective flow resistivity and effective depth. The use of a thin layer (d_e = 0.01) has a similar effect to a high flow resistivity as seen in figure 4.17 ie the highest lobe of the attenuation is one at a higher frequency, and the highest value of attenuation is less. The frequency at which each of the lobes peak is slightly higher when the rigid-backed layer model is used. The spectrum of attenuation for d_e=0.1 is the same as the homogeneous approximation. This is as would be expected as a value of d_e of 0.1m corresponds to a layer depth of 0.2m assuming a porosity of 0.5; a layer this deep would be expected to approximate to an infinite medium. The intermediate value of d_e illustrated in figure 4.20 d_e = 0.02m has a low frequency peak at an intermediate frequency as it represents a 'softer' surface than the thinner layer, but is still a significantly layered surface. The first lobe of the low frequency peak is narrower than those seen before, and at almost the same magnitude as the second lobe. The maximum attenuation of the low frequency peak is slightly higher for this surface than the homogeneous prediction, some values of d_e give a much larger

attenuation as a high 'sharp' peak. The high frequency peaks are the same in the homogeneous and thin layer cases

Figure 4.21 shows the variation of the attenuation function resulting from different values of α_r in the variable porosity model. Increasing the value of α_r from zero (the homogeneous model) to 100 and 200 represents a harder ground surface, since the value of σ_r given is, the value for the surface, and the flow resistivity increases with the decreasing porosity at depth. The effect of the increase in 'hardness' of the ground is similar to that of figures 4.17 and 4.20 ie. the low frequency part peaks at a higher frequency. The peaks are higher for the harder surfaces. In both variable porosity graphs the second lobe of the low frequency peak is the highest one, with the first lobe being less marked, particularly in the graph where α_r is 100. The graph with α_r equal to 200 has a very large 'sharp' peak, such a high value of α_r gives a ground which is similar to a thin rigid- backed layer. Again the high frequency part is virtually unaltered.

Figure 4.22 shows the variation of the attenuation function with different values of flow resistivity in the Delany and Bazley model. The pattern is broadly similar to that of figure 4.17 with the frequency at which the low frequency peak occurs increasing as the flow resistivity increases. The high frequency peaks occur at the same frequency for these predictions as for the predictions using the other models.

Figures 4.23 to 4.26 are predictions of the attenuation function calculated using a different test microphone location ie separation distance of 96m, and the same impedance predictions as figures 4.17 to 4.21. These figures are included to show that the conclusions reached about the dependence of the attenuation function on ground impedance hold for other experimental geometries. Figures 4.23 to 4.26 show a largely similar pattern of changing attenuation with different ground impedances; ie. the harder ground surfaces have a low frequency peak at a higher frequency. The main deviation from the descriptions of figures 4.17 to 4.22 is that the variable porosity prediction with $\alpha_r = 100$ has the first lobe as its highest peak while in that using $\alpha_r = 200$ the first and highest lobe corresponds to the second lobe of the other two graphs. Again the high frequency part is virtually unchanged in all the graphs.

Summary of the Characteristics of the Attenuation Function.

The low frequency peak is the part most affected in its location and shape by changes in impedance. The shape of this peak is dependent to some extent on the model used while its location is dependent on the location of the reference microphone as well as the ground parameters. A harder ground surface ie higher flow resistivity, lower value of d_e, or higher value of α_e gives a low frequency peak which occurs at a higher frequency; the peak can be higher, lower or of the same magnitude as a softer ground surface, depending on the experimental geometry.

The frequency at which the high frequency peaks occur is determined by the location of the test microphone (see section 4.3.1) and only slightly affected in magnitude by the impedance. The impedance of the models and measurements decreases with frequency so that at high frequencies the impedance value is small and similar. The ground wave term of the propagation equations has been shown to be very small for high frequencies at the source and receiver locations used in the experiments (see section 4.1). The attenuation calculation therefore effectively uses the plane wave reflection coefficient at high frequencies (equation 4.4), which is dependent only on $\cos\theta$ and the surface impedance. Keeping the experimental geometry constant and only changing the impedance slightly will therefore only give a slight change in the magnitude of the high frequency part of the graph.

As described above, excess attenuation can be expressed as

$$A_e = 20\log_{10}\left|1+\frac{r_1}{r_2}Qe^{ik_0(r_2-r_1)}\right| \qquad (4.21)$$

Since changes in the ground parameters have been shown to have little or no influence on the location of the high frequency peaks; the term

$$e^{ik_0(r_2-r_1)} = e^{ik_0\Delta r}$$

in this equation evidently determines the frequency at which the peak occurs. This term varies in value from a minimum of -1.0 + 0.0i to 1.0 + 0.0i. Since the reflection coefficient has a negative real part which approaches -1 at high frequencies, (corresponding to a 'pressure release' type of surface) and the ratio of r_1 and r_2 is positive, the maximum value of this expression (ie. 1.0) will minimise the excess attenuation calculation. A value of 1.0 + 0.0i is obtained when the term $k_0\Delta r = 2n\pi$ where n is a positive integer. This represents the values of k_0 at which the direct and reflected waves are 180 degrees out of phase ie. destructive interference takes place. A value of -1.0 + 0.0i is obtained when the term $k_0\Delta r = (2n-1)\pi$ This represents the values of k_0 at which the direct and reflected waves are in phase ie. constructive interference takes place causing a maximum in the excess attenuation graph. The test microphone location at high frequencies of figures 4.9 and 4.15 (source height=1.5m, receiver height=1.2m, separation distance=48m therefore Δ r = 0.076m), would be expected to give minimum values of excess attenuation (maxima of attenuation function) at frequencies of 4513 Hz and 9026 Hz, and a maximum (minimum attenuation function) at 6770 Hz. These maxima and minima can be seen in figures 4.9 and 4.15.

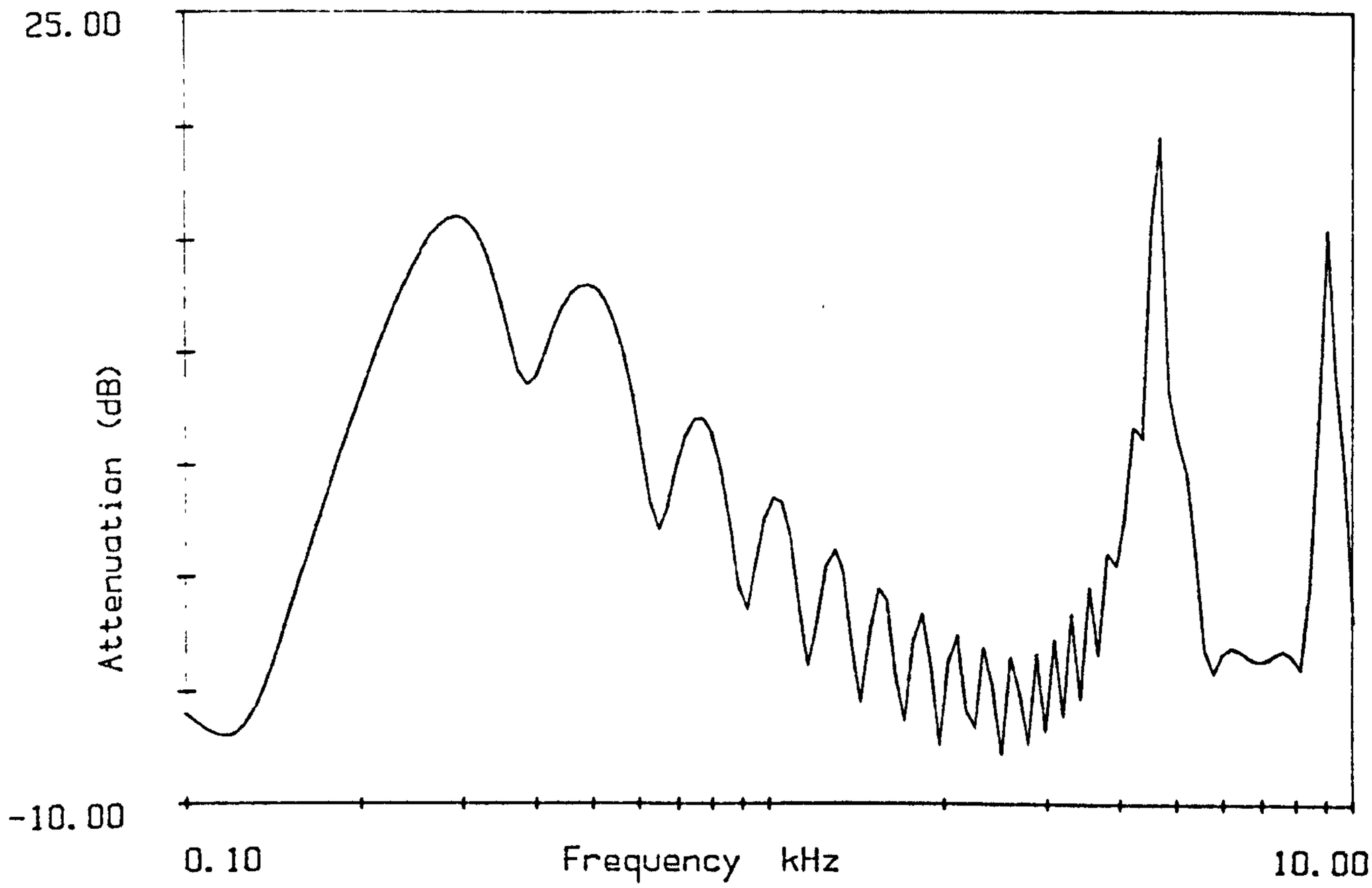

Figure 4.9. Attenuation Function.
Reference microphone:- hs=1.3m, hr=1.3m, r=2m.
Test microphone:- hs=1.3m, hr=1.2m, r=48m.
Impedance calculated from equation 4.15 or e =100,000.

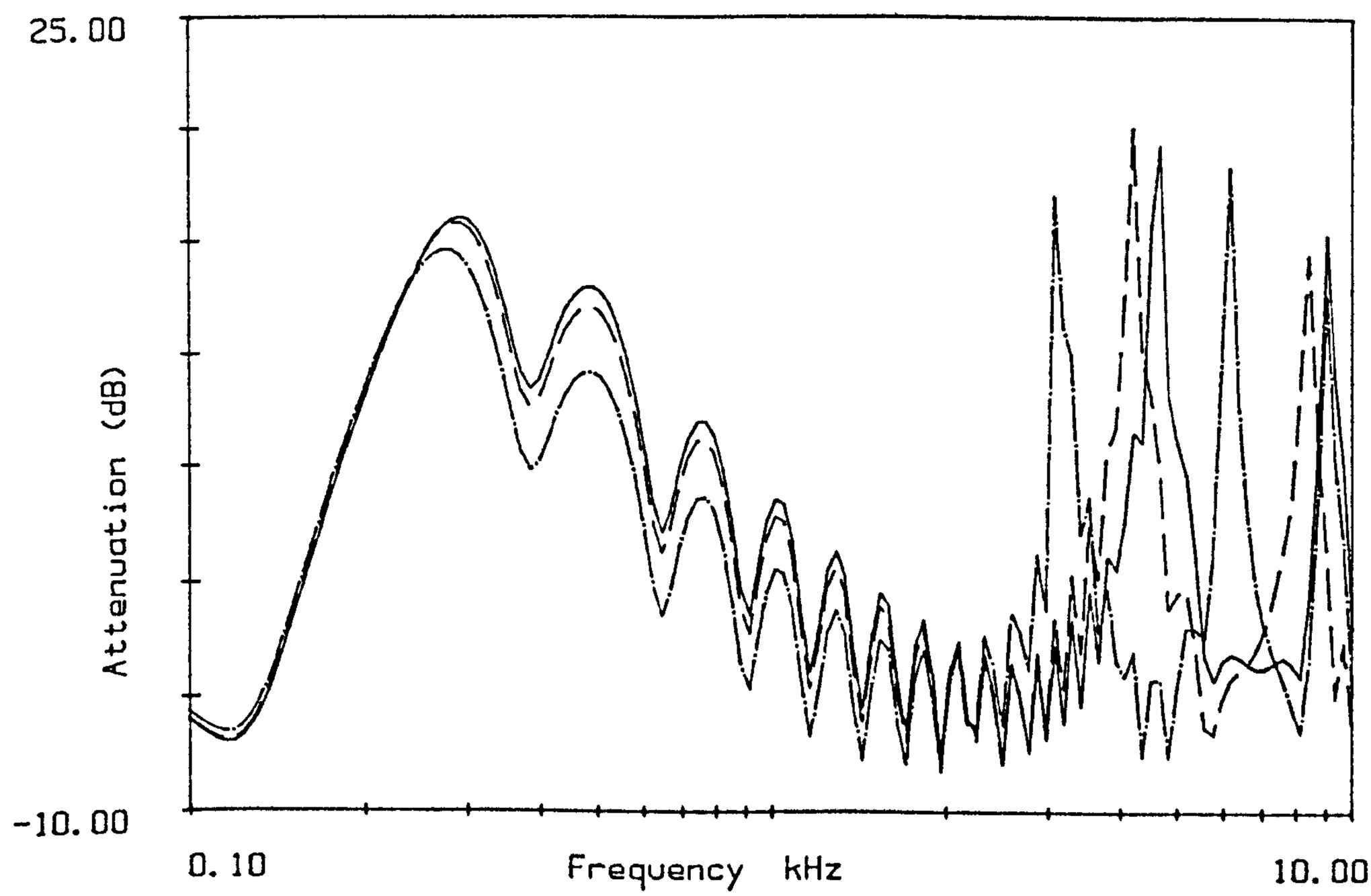

Figure 4.10
Attenuation function at 3 different test microphone heights.
hr = ———— 1.20m; — — — 1.32m; —·——·— 1.80m.
other dimensions as in figure 4.9

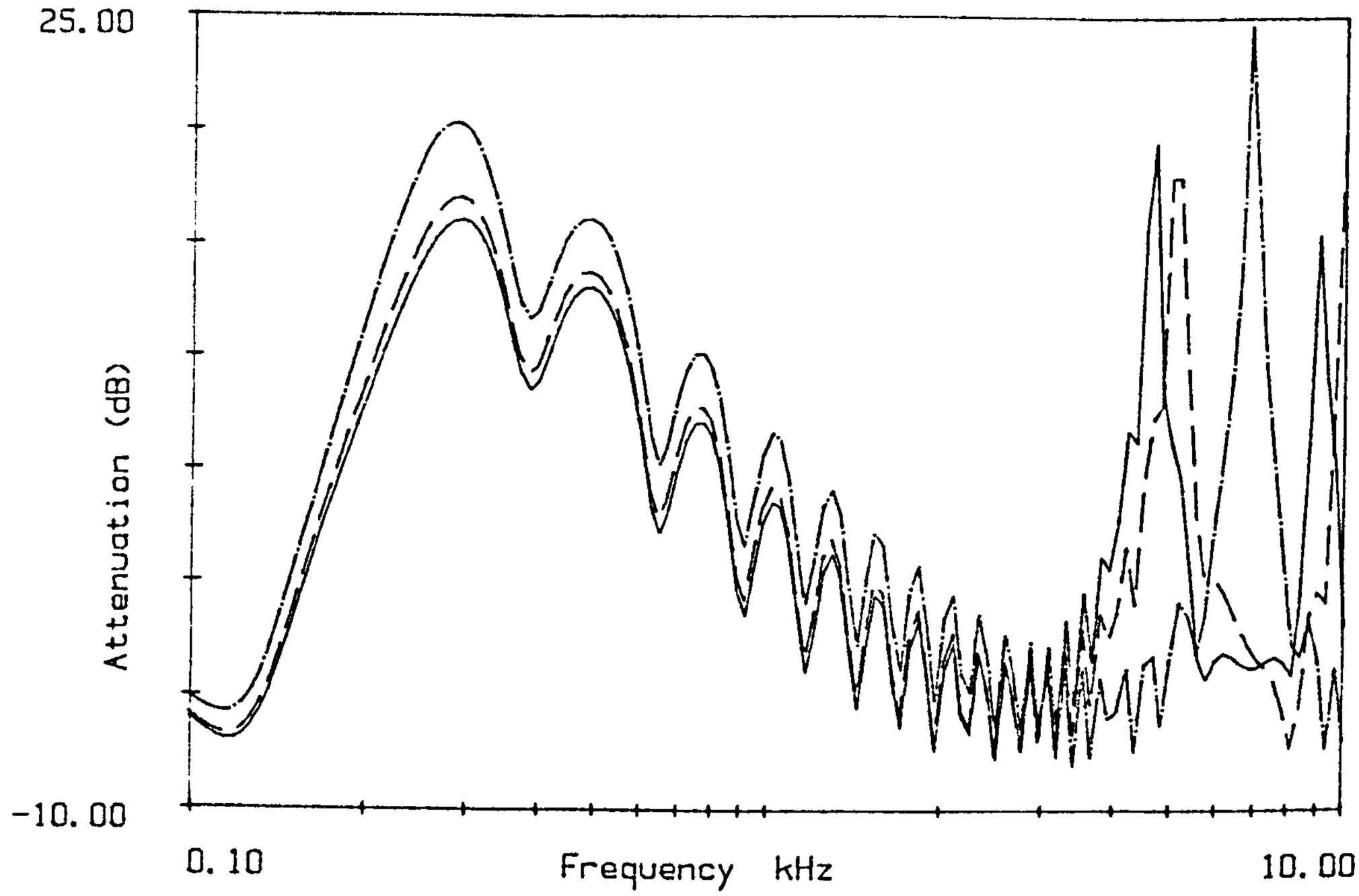

Figure 4.11
Attenuation function at 3 different test distances.
r = ———— 48.0m; — — — 52.8m; ———·——72.0m.
other dimensions as in figure 4.9

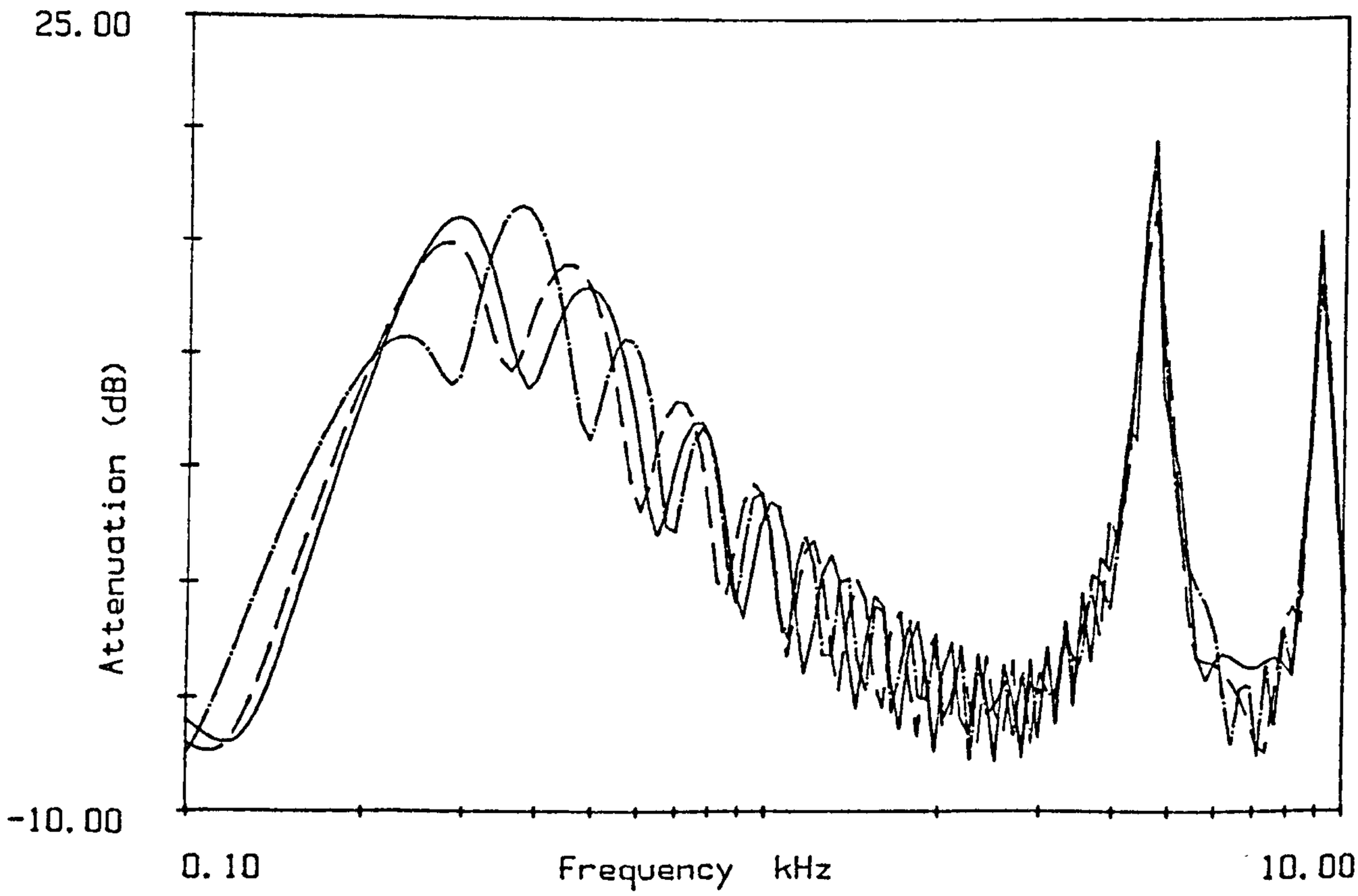

Figure 4.12
Attenuation function at 3 different reference microphone heights.
hr = ———— 1.30m; — — — 1.43m; ———·——1.95m.
other dimensions as in figure 4.9

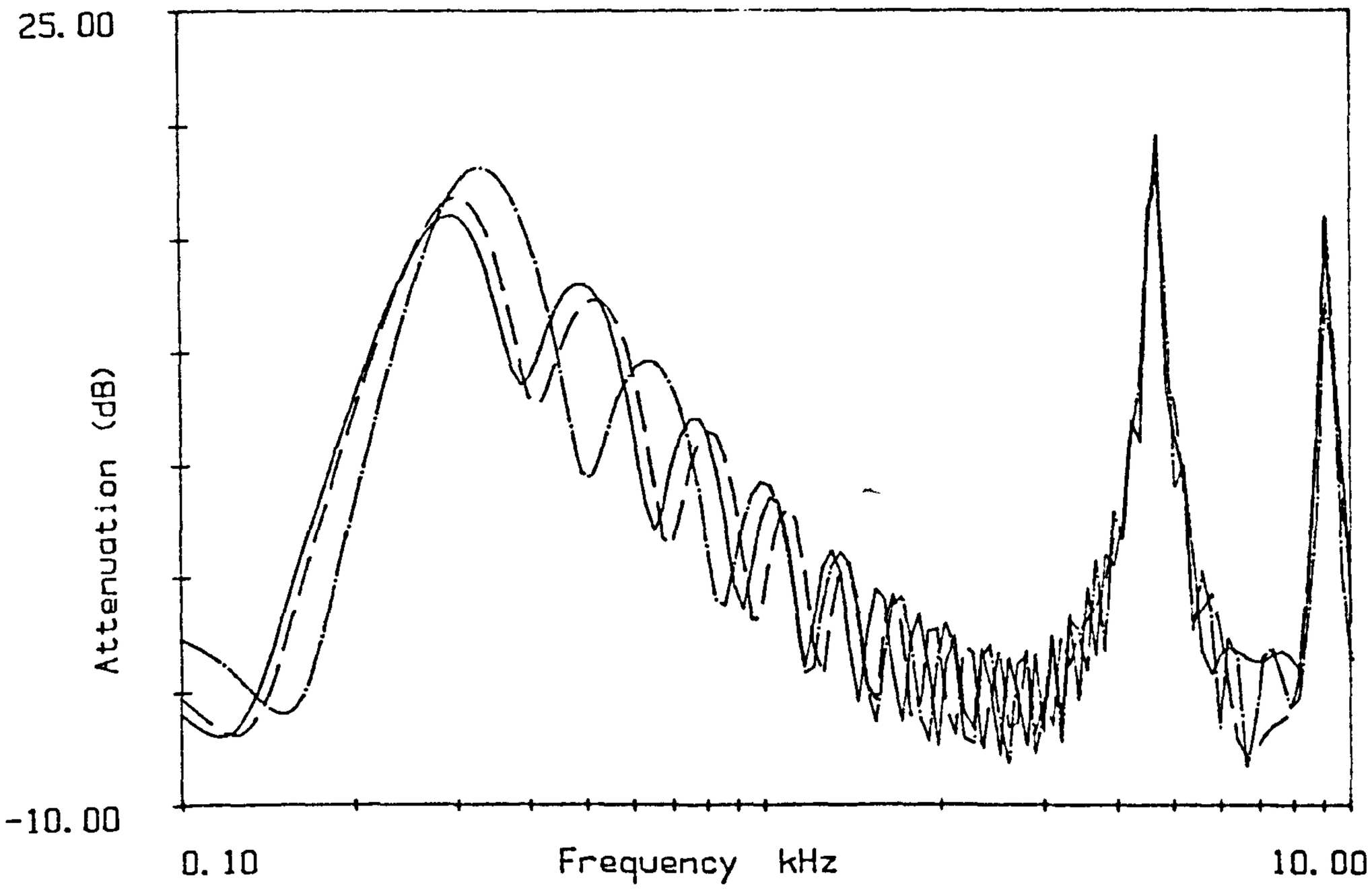

Figure 4.13
Attenuation function at 3 different reference distances.
r = ———— 2.0m; — — — 2.2m; ——·——·——3.0m.
other dimensions as in figure 4.9

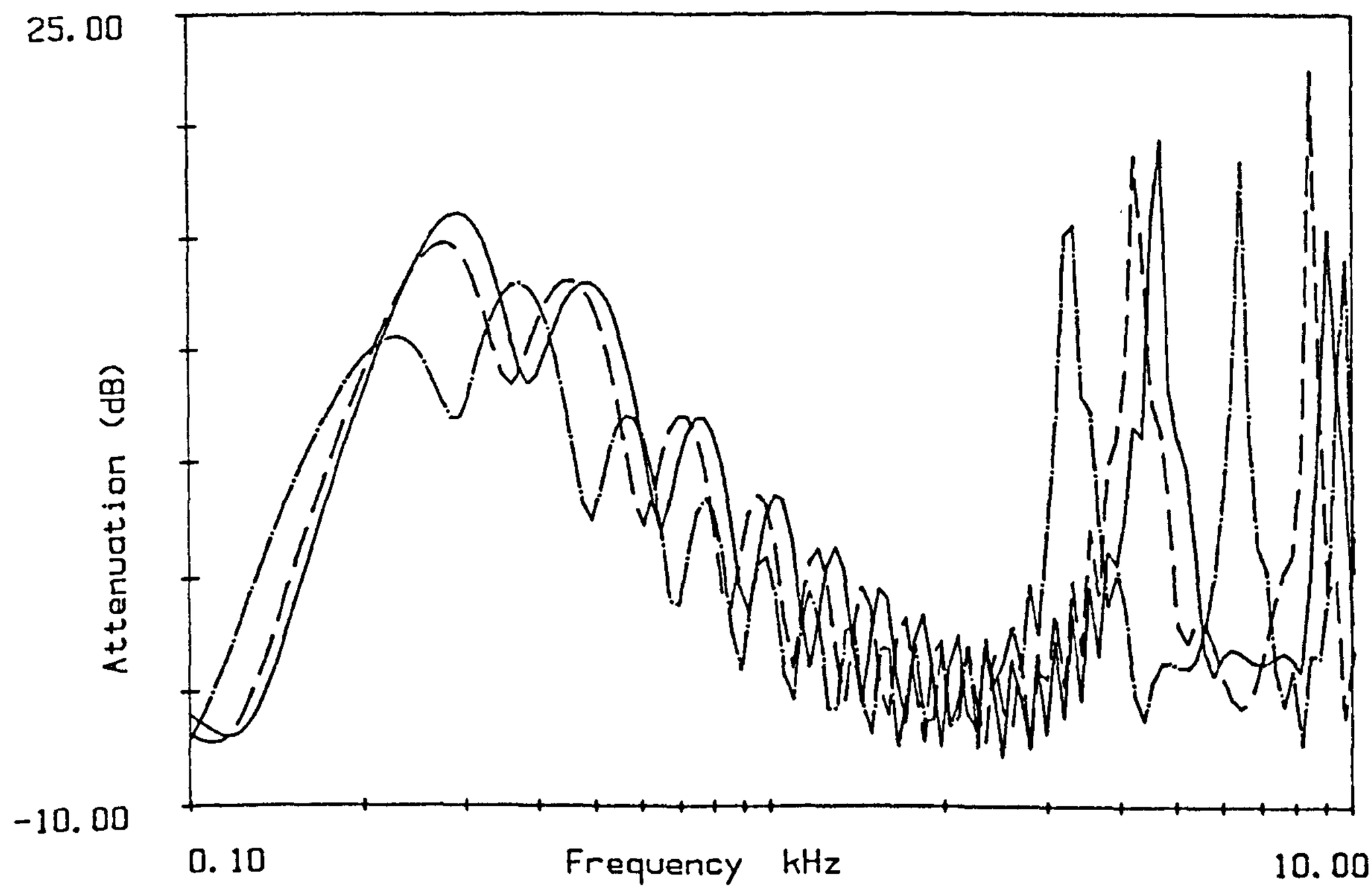

Figure 4.14
Attenuation function at 3 different source heights.
h_S = ———— 1.30m; — — — 1.43m; ——·——·——1.95m.
other dimensions as in figure 4.9

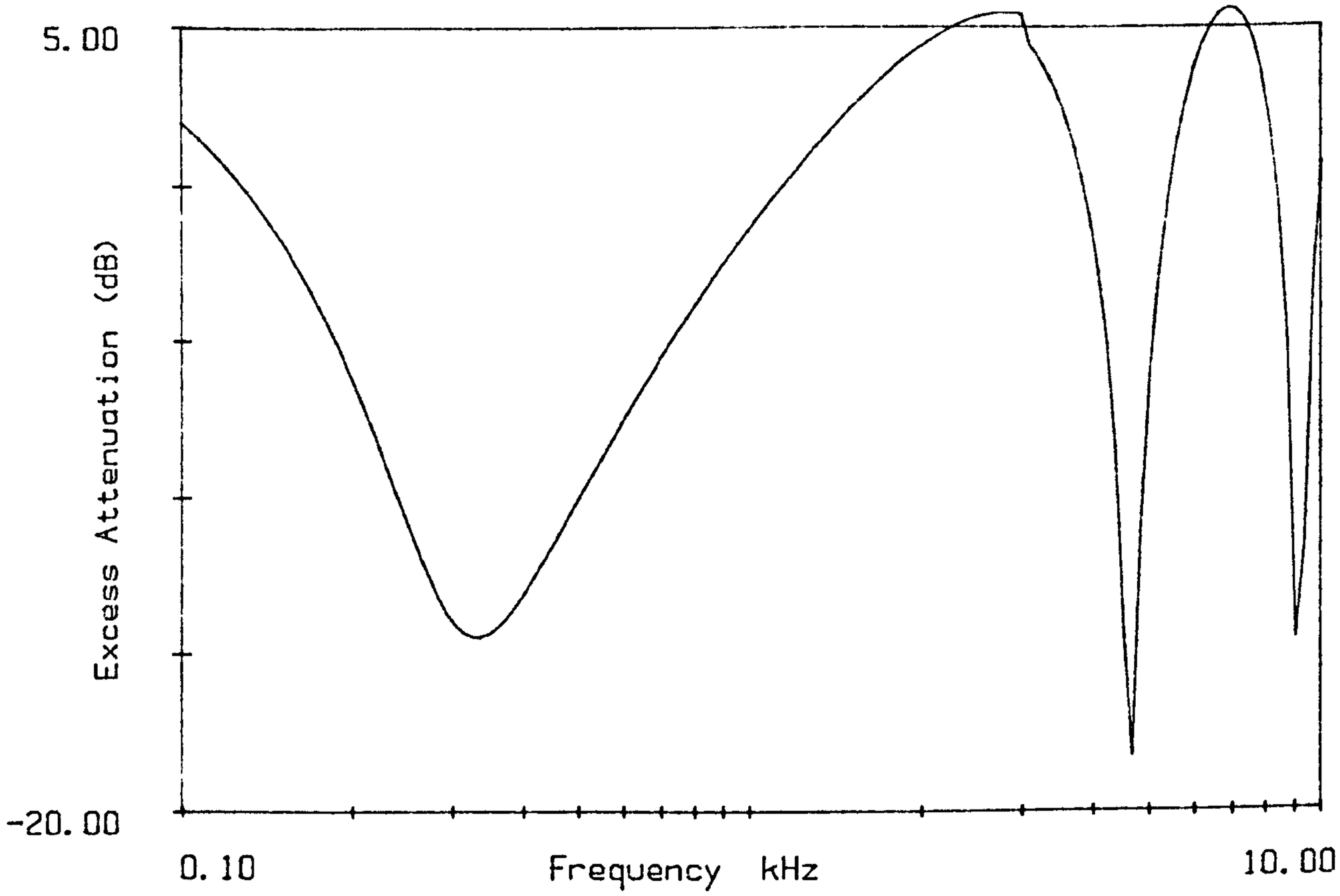

Figure 4.15.
Excess Attenuation.
Test microphone:- hs=1.3m, hr=1.2m, r=48m.
Impedance calculated from equation 4.15 σe =100,000.

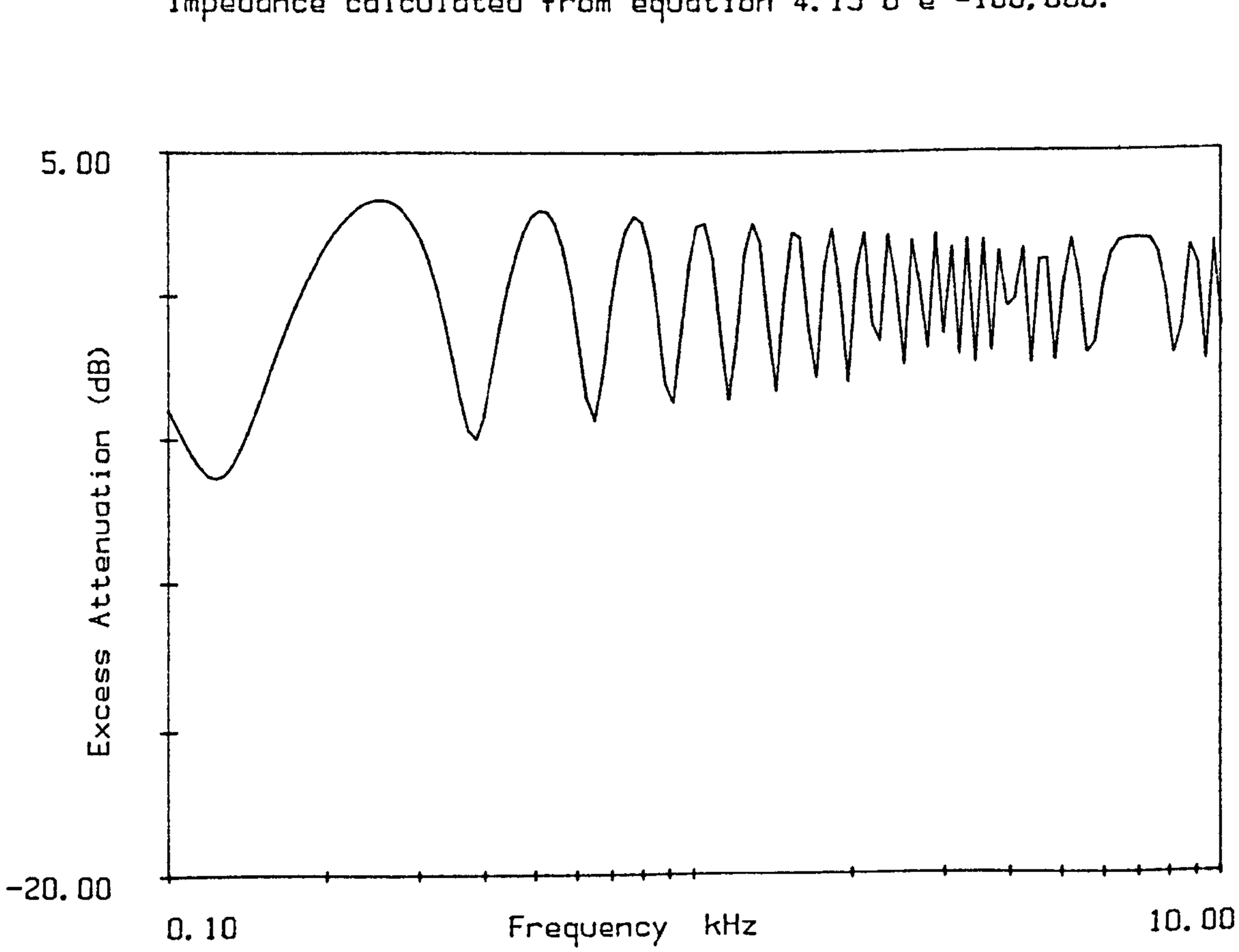

Figure 4.16.
Excess Attenuation.
Reference microphone:- hs=1.3m, hr=1.3m, r=2m.
Impedance calculated from equation 4.15 σe =100,000.

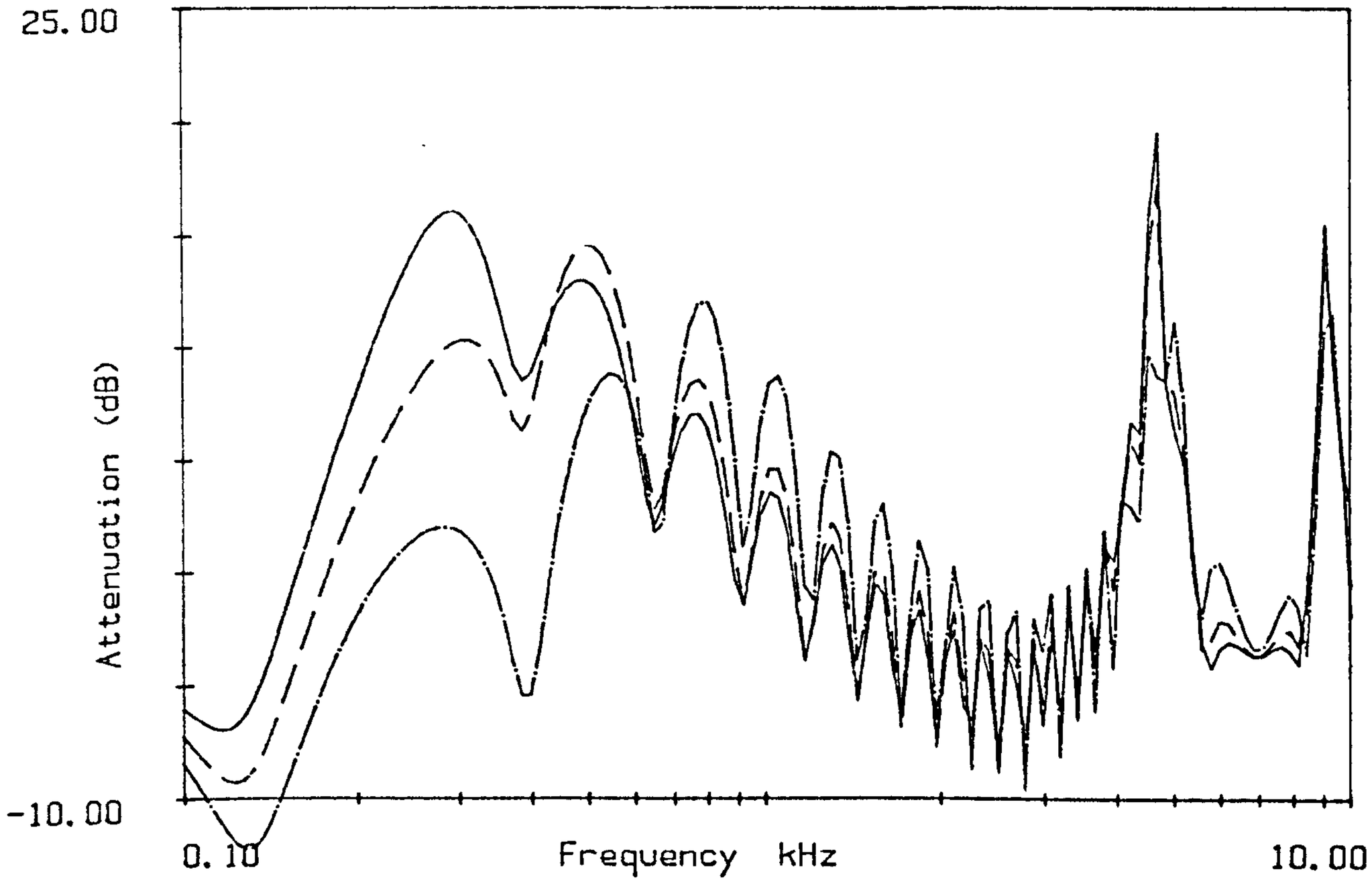

Figure 4.17
Attenuation function, using homogeneous approximation.
——————— σe = 100,000 mks rayls
— — — — σe = 200,000 mks rayls
———·——— σe =1,000,000 mks rayls
Experimental geometry as in figure 4.9

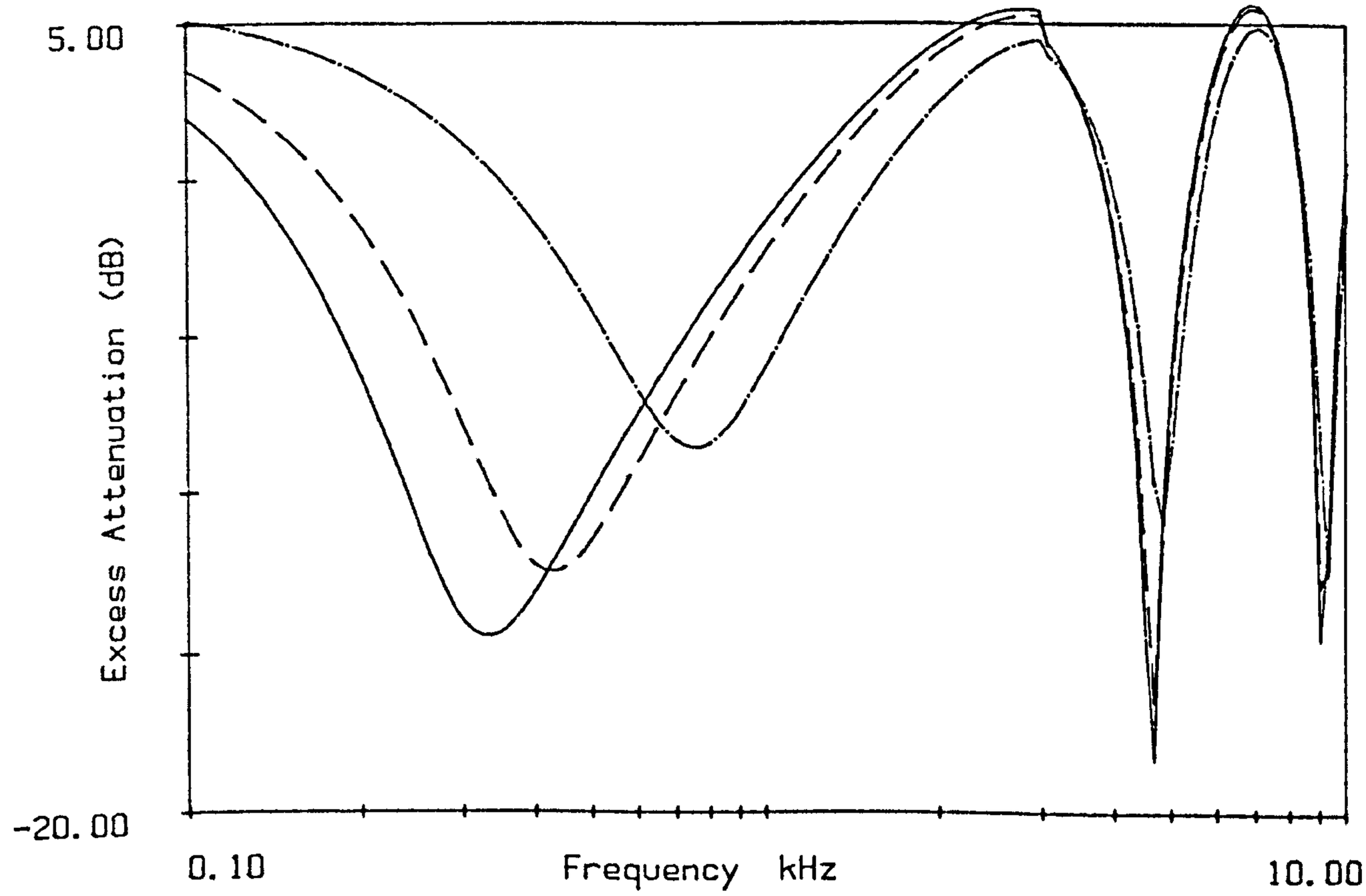

Figure 4.18.
Excess Attenuation.
Test microphone:- hs=1.3m, hr=1.2m, r=48m.
Impedance predictions as in figure 4.17

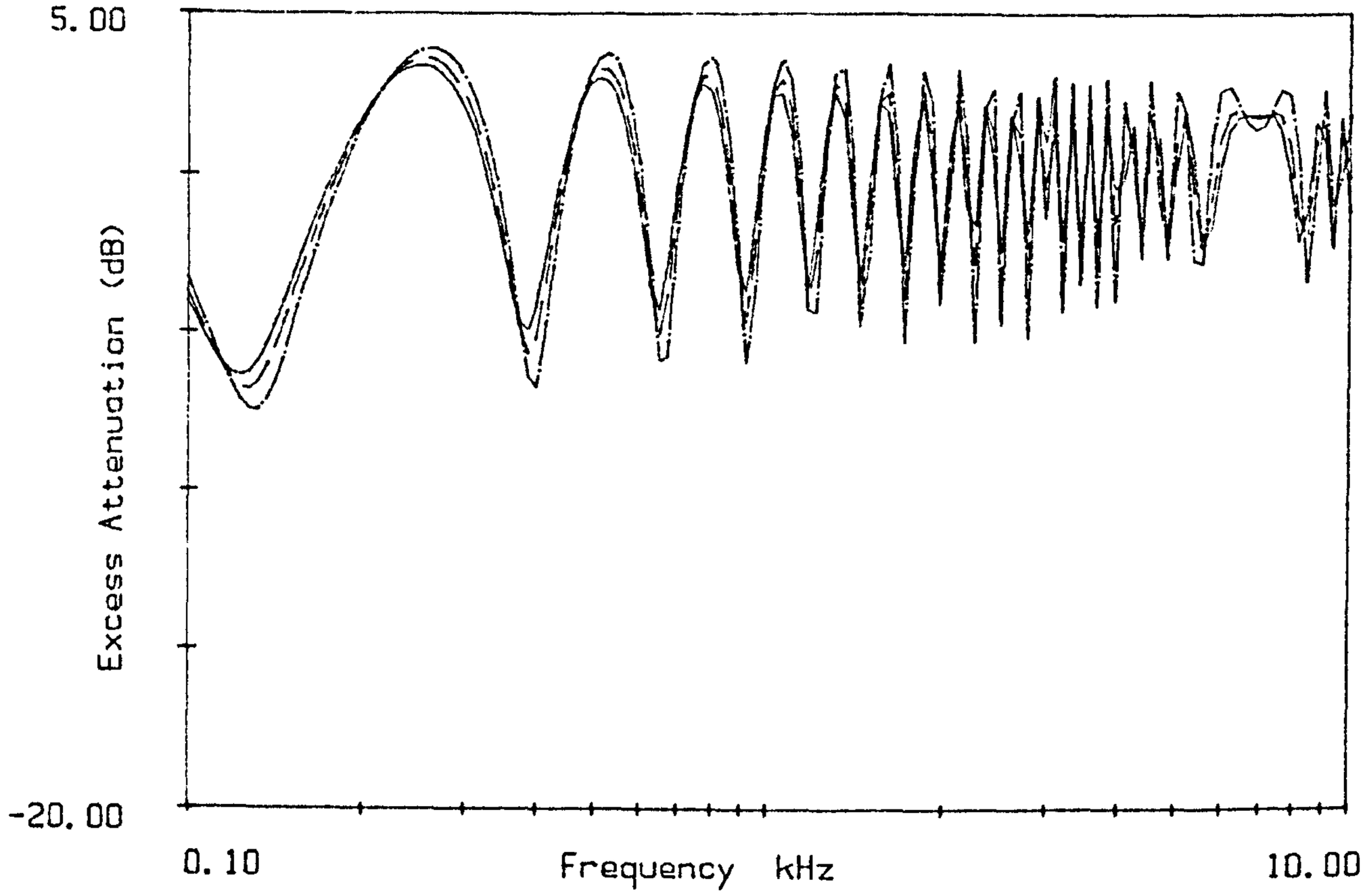

Figure 4.19.
Excess Attenuation.
Reference microphone:- hs=1.3m, hr=1.3m, r=2m.
Impedance predictions as in figure 4.17

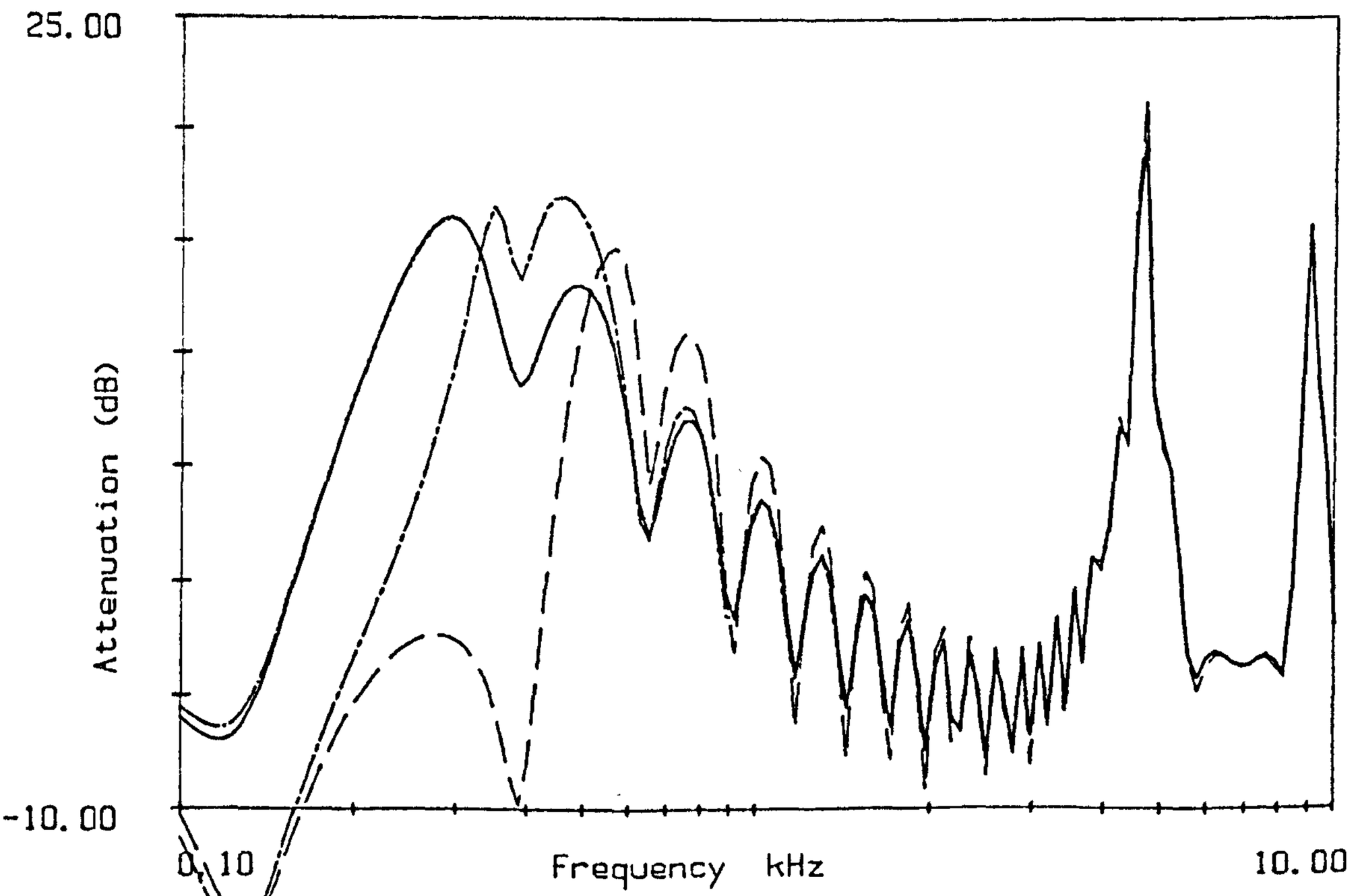

Figure 4.20
Attenuation function, using rigid-backed layer approximation.
———— σe = 100,000 mks rayls (homogeneous)
— — — σe = 100,000 mks rayls de = 0.01
—·—·— σe = 100,000 mks rayls de = 0.1
—·—·— σe = 100,000 mks rayls de = 0.02
Experimental geometry as in figure 4.9

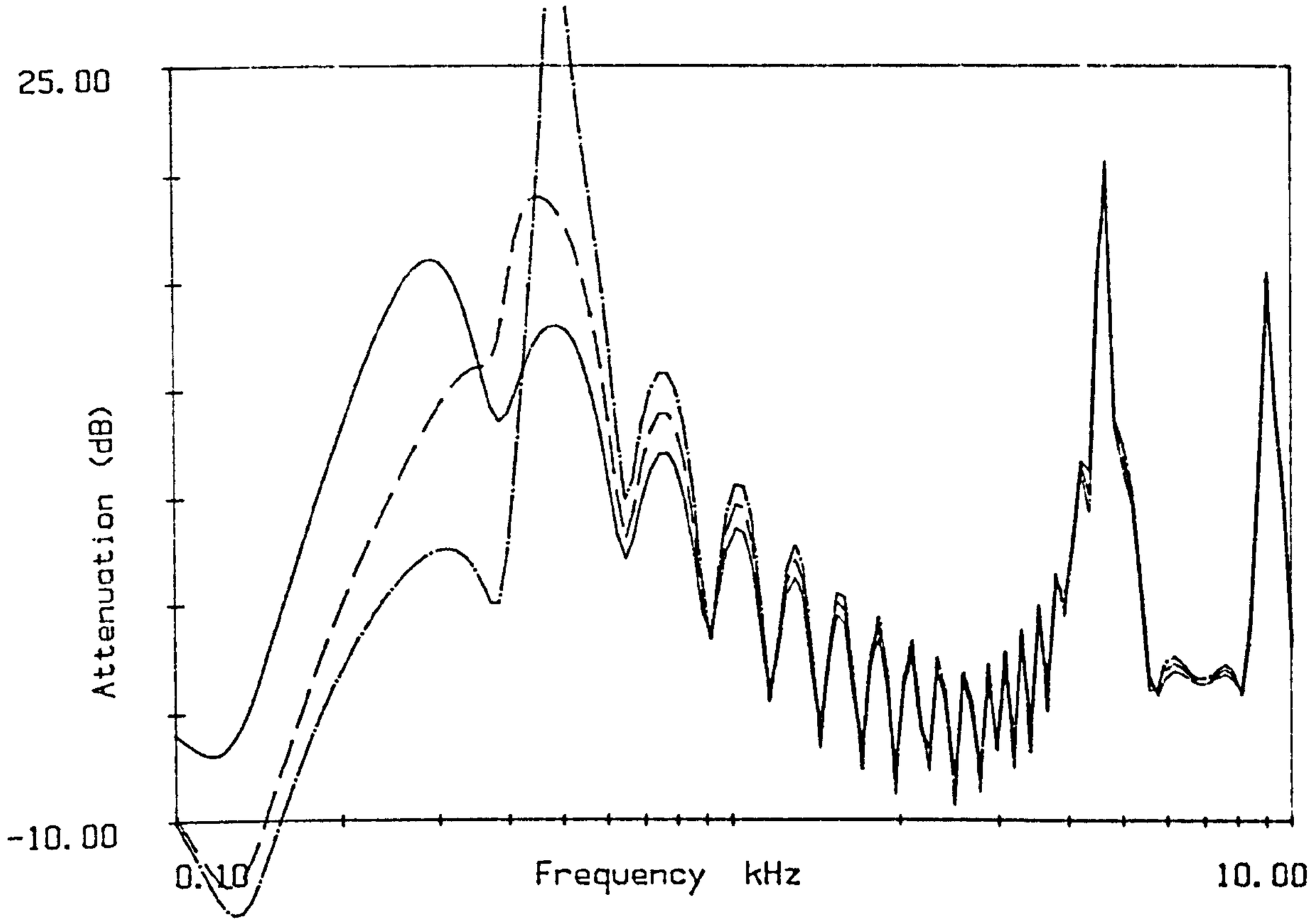

Figure 4.21
Attenuation function, using variable porosity approximation.
———— σe = 100,000 mks rayls ∝e = 0 (homogeneous)
— — — - σe = 100,000 mks rayls ∝e = 100
—·—·—·— σe = 100,000 mks rayls ∝e = 200
Experimental geometry as in figure 4.9

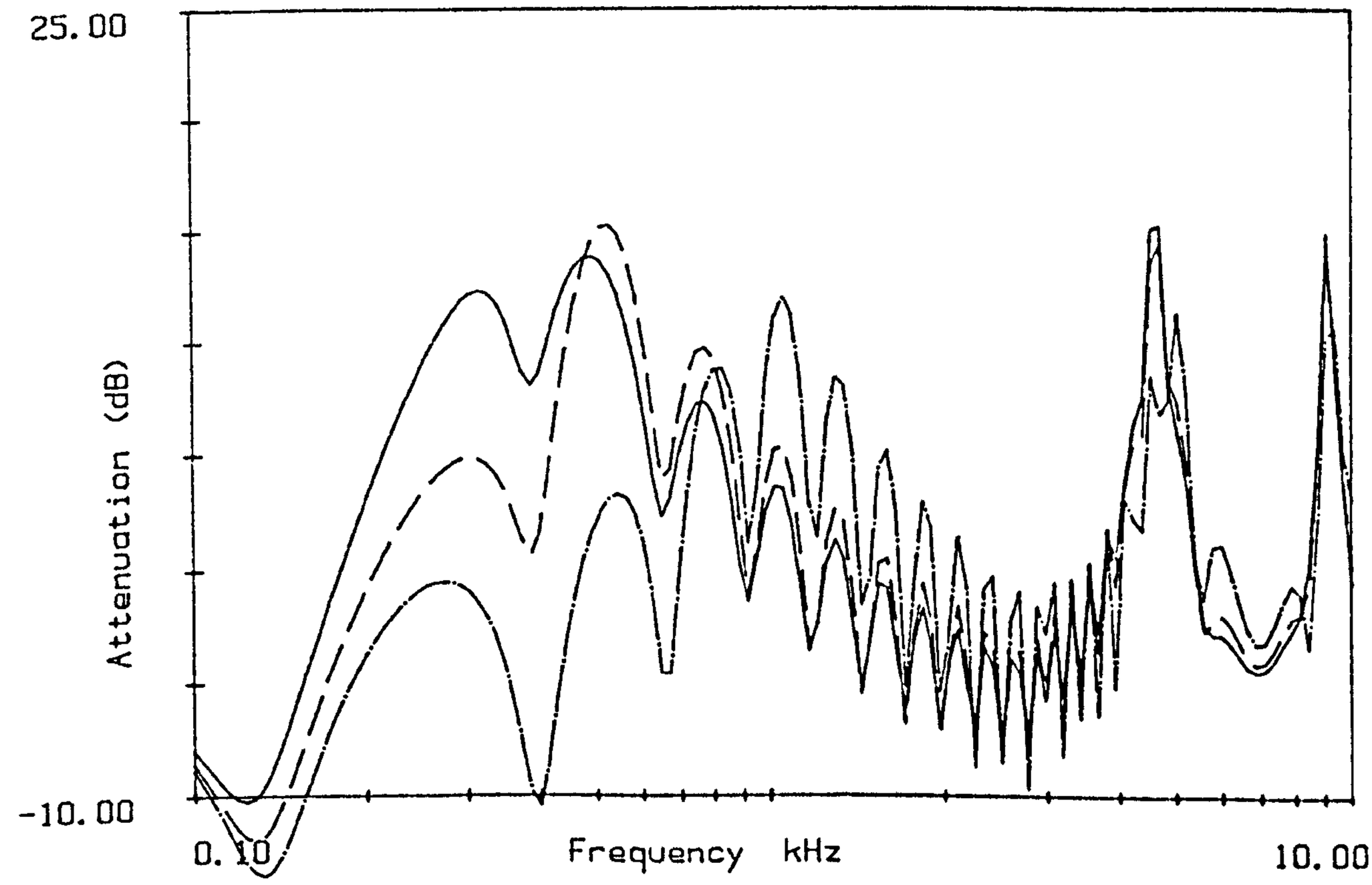

Figure 4.22
Attenuation function, using Delany and Bazley model.
———— σe = 100,000 mks rayls
— — — - σe = 200,000 mks rayls
—·—·—·— σe =1,000,000 mks rayls
Experimental geometry as in figure 4.9

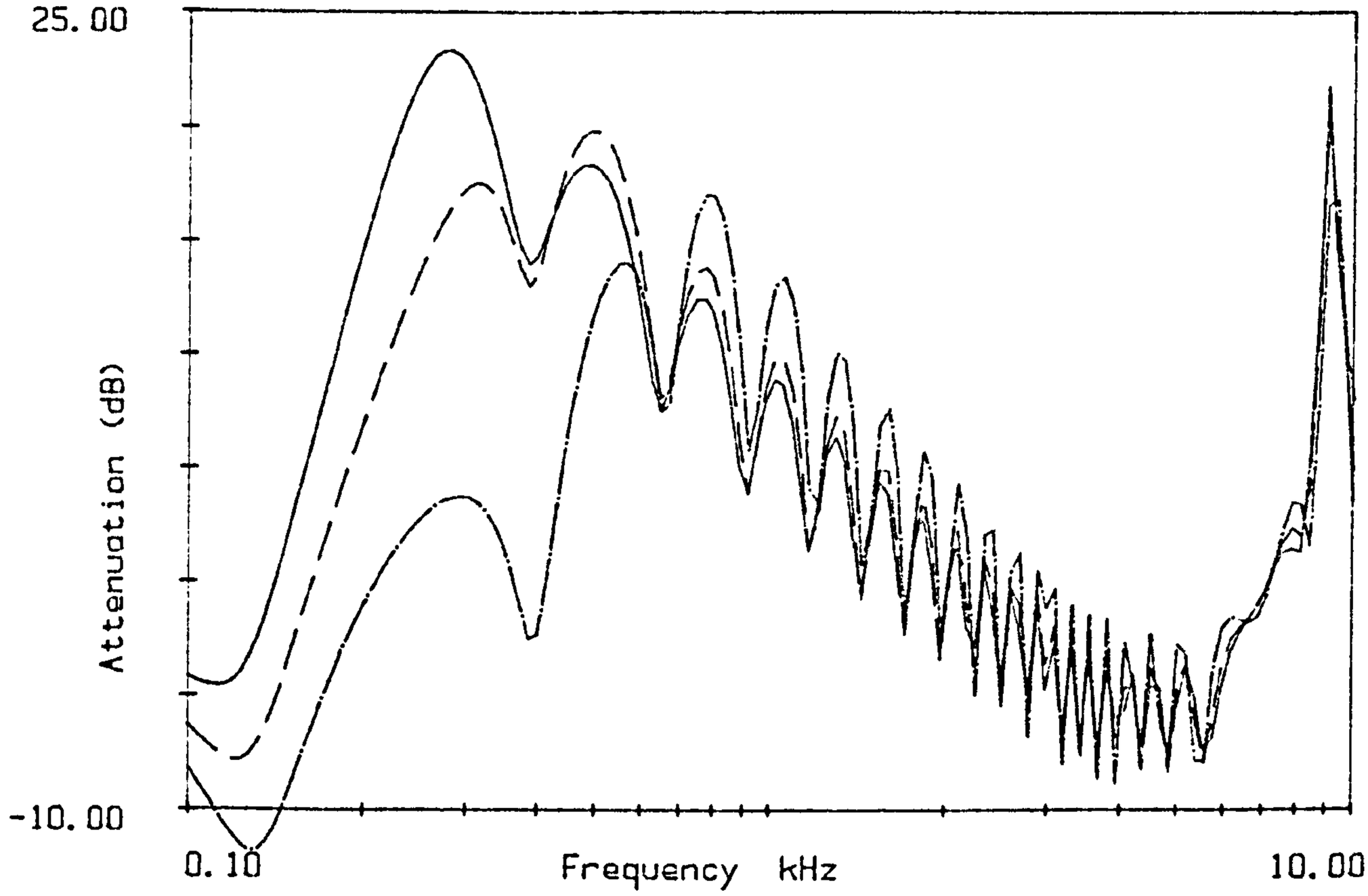

Figure 4.23
Attenuation function, using homogeneous approximation.
———— σe = 100,000 mks rayls
— — — - σe = 200,000 mks rayls
———·——— σe =1,000,000 mks rayls
Reference microphone:- hs=1.3m, hr=1.3m, r=2m.
Test microphone:- hs=1.3m, hr=1.2m, r=96m.

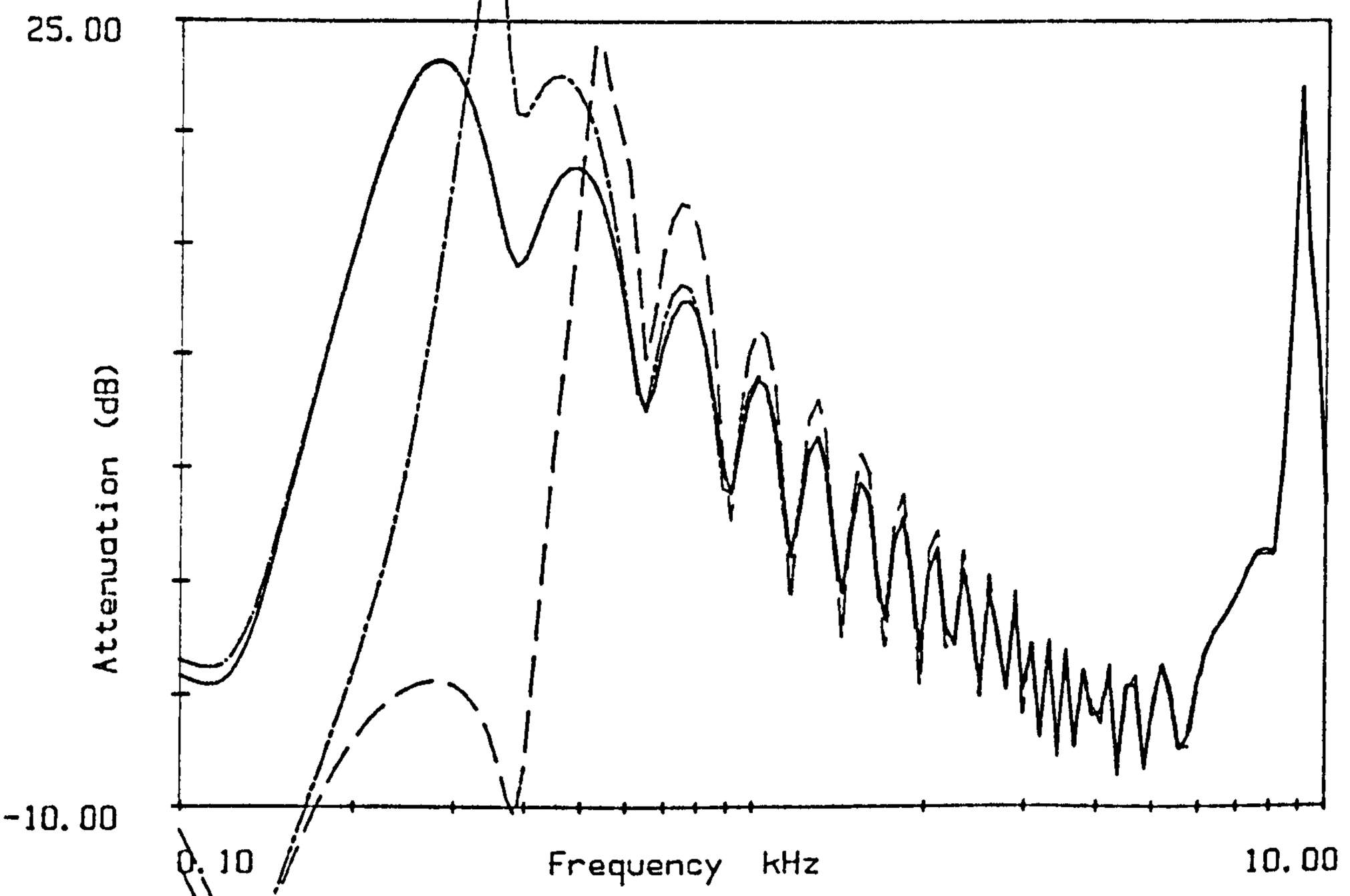

Figure 4.24
Attenuation function, using rigid-backed layer approximation.
———— σe = 100,000 mks rayls (homogeneous)
— — — - σe = 100,000 mks rayls de = 0.01
———·——— σe = 100,000 mks rayls de = 0.1
———·—·——— σe = 100,000 mks rayls de = 0.02
Experimental geometry as in figure 4.23

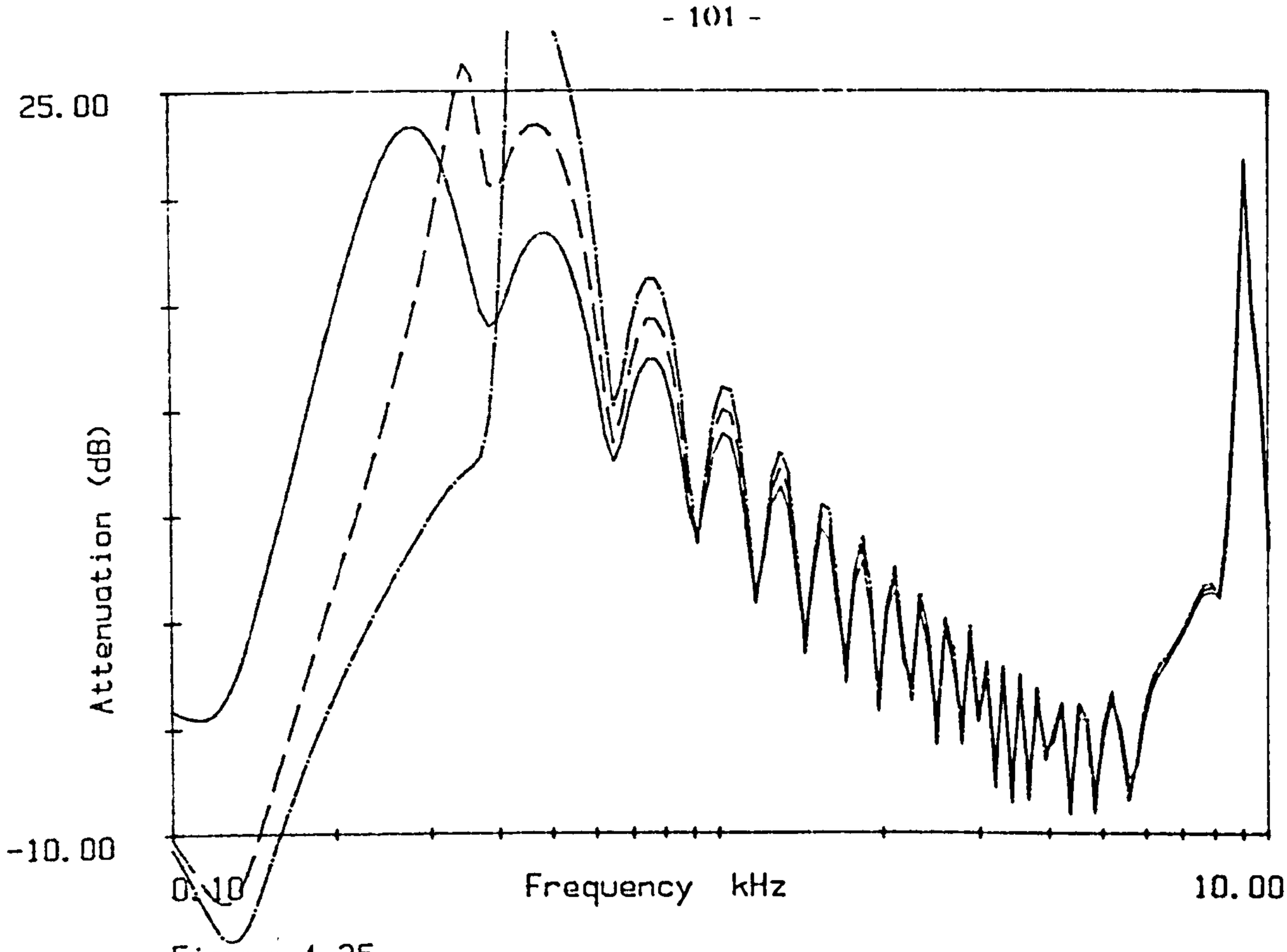

Figure 4.25
Attenuation function, using variable porosity approximation.
———— σe = 100,000 mks rayls αe = 0 (homogeneous)
— — — - σe = 100,000 mks rayls αe = 100
———·——— σe = 100,000 mks rayls αe = 200
Experimental geometry as in figure 4.23

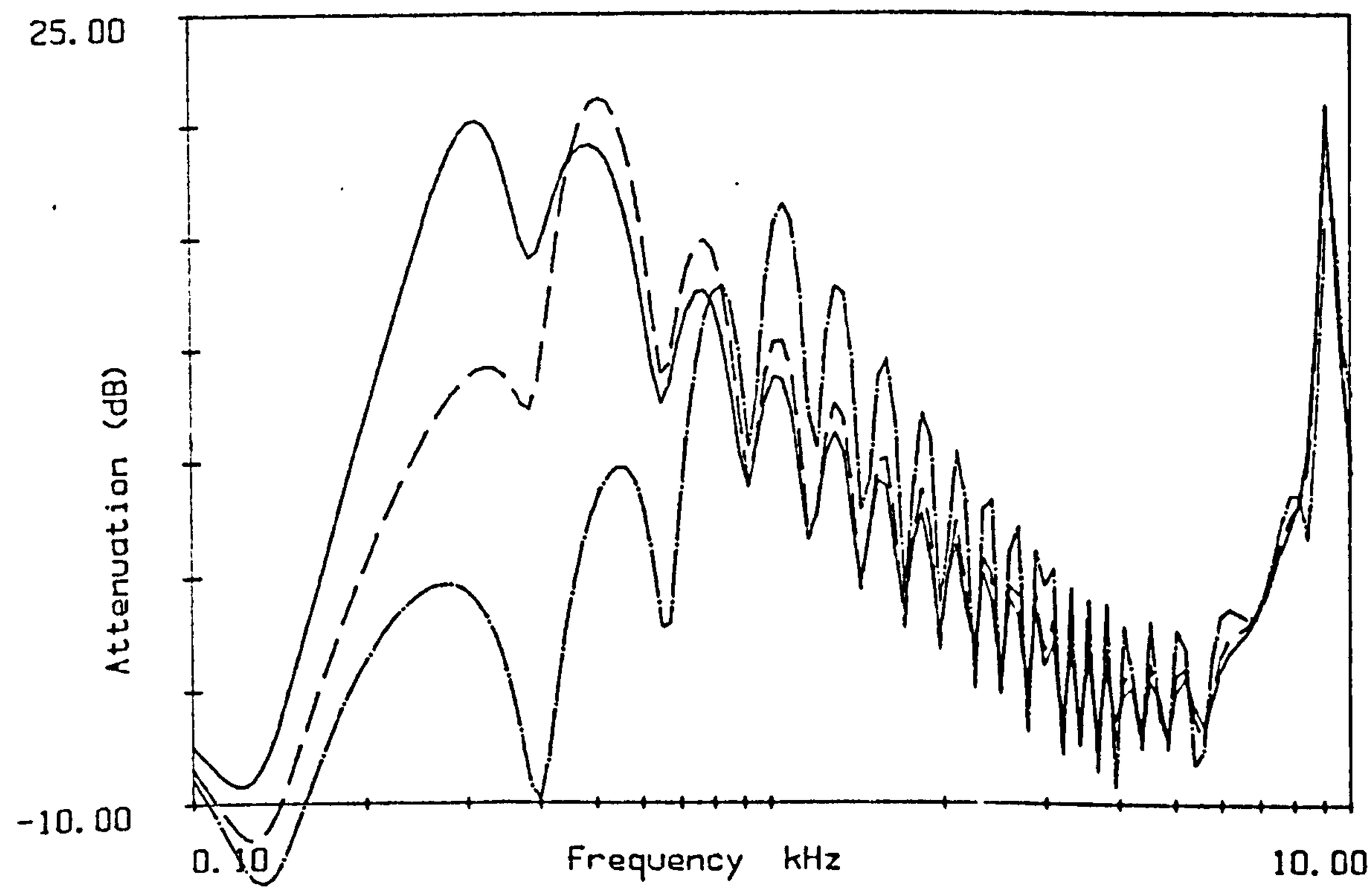

Figure 4.26
Attenuation function, using Delany and Bazley model.
———— σe = 100,000 mks rayls
— — — - σe = 200,000 mks rayls
———·——— σe =1,000,000 mks rayls
Experimental geometry as in figure 4.23

4.4 Fitting Ground Parameters to Measurements.

In order to determine which model and what input parameters will predict a measured spectrum of attenuation, most accurately, a fitting routine is used. The method used is a least squares fit: it is carried out for each of the approximation models described in section 4.2.4 and the Delany and Bazley model described in section 4.2.1. The minimum value of the mean squared difference

$$\frac{\sum_{n=1}^{n=N}\left[M_n - P_n\right]^2}{N} \qquad (4.24)$$

where : N = number of frequencies

M_n is the measured attenuation at the nth frequency,

P_n is the predicted attenuation at the nth frequency.

is calculated for a range of values of the input parameters of a model. An initial value of each of the required parameters is input to the fitting routine, with an amount by which the parameters should be incremented in each iteration of the fitting. The lowest value of the mean squared difference along with the values which are used to calculate it are output from the routine. The mean difference between the measured and predicted spectra (in decibels) is evidently the square root of this value.

The fitting is carried out in two or more stages, firstly by covering a wide range of values with large increments (e.g. 10,000 mks rayls for the flow resistivity) then by taking the best fit values from the first stage and fitting a narrower range above and below this value using smaller increments ie. 1000 mks rayls for effective flow resistivity, 0.001m for effective layer depth, and 1 unit for effective alpha. In some cases these smaller increment could give a false accuracy since the difference in the attenuation function, and therefore the mean squared difference, caused by such a small increment, is very slight. Thus it may be more relevant to only consider the results to the nearest 10,000 mks rayls particularly with high values of σ_e, and similarly only assess the value of α_e to the nearest 10 units. The low frequency part of the attenuation spectra are most affected by the ground impedance so only

the low frequency part .up to 1kHz is used in fitting the ground parameters. A listing of the FORTRAN source code of the fitting program DIF2MKFFT is included in appendix A.

References, Chapter 4.

[1] Attenborough, K. 1983. Acoustical Characteristics of Rigid Fibrous Absorbents and Granular Materials. J. ACOUST. SOC. AM. 73 785-799.

[2] Attenborough, K. 1985. Acoustical Impedance Models for Outdoor Ground Surfaces. J. SOUND AND VIBRATION 99(4) 521-544.

[3] Chien, C.F. and Soroka, W.W. 1975. Sound Propagation Along an Impedance Plane. J. SOUND AND VIBRATION 43(1) 9-20.

[4] Chien, C.F. and Soroka, W.W. 1980. A Note on the Calculation of Sound Propagation Along an Impedance Surface. J. SOUND AND VIBRATION 69 340-343.

[5] Cramond, A.J. and Don, G.C. 1984. Reflection of Impulses as a Method of Determining Acoustic Impedance. J. ACOUST. SOC. AM. 75(2) 382-389.

[6] Delany, M.E. and Bazley, E.N. 1970. Acoustical Properties of Fibrous Absorbent Materials. APPLIED ACOUSTICS 3 309 - 322.

[7] Delany, M.E. and Bazley, E.N. 1970a. Monopole Radiation in the Presence of an Absorbing Plane. J. SOUND AND VIBRATION 13 269.

[8] Don, C.G. and Cramond, A.J. 1985 Soil Impedance Measurements by an Acoustic Pulse Technique. J. ACOUST. SOC. AM. 77(4). 1601-1609.

[9] Embleton, T.F.W. Piercy, J. and Olson, N. 1976. Outdoor Sound Propagation Over Ground of Finite Impedance. J. ACOUST. SOC. AM. 59(2) 267 - 277.

[10] Rudnick, I. 1947. The Propagation of an Acoustic Wave Along A Boundary. J. ACOUST. SOC. AM. 19 348 - 356.

[11] Talaske, R. 1980. The Acoustic Impedance Of a Layered Forest Floor. USDA FOREST SERVICE AGREEMENT REPORT. PENNSYLVANIA STATE UNIVERSITY.

[12] Van der Heijden, L.A.M. 1984. The Influence of Vegetation on Acoustic Properties of Soils. PhD THESIS; UNIVERSITY OF NIJMEGEN, NETHERLANDS.

Chapter 5: Prediction of Attenuation Due To Scattering.

5.1 Calculation of Attenuation (Embleton 1966)

Embleton (1966) presents a theory describing the scattering of plane waves by a random array of cylinders of infinite length (see section 2.2), based on the multiple-scattering theory of Twersky (1953). The cylinders are characterised by their diameter and surface impedance and are defined as having a locally reacting surface. This theory has been used in comparison with the measured data from woodlands and model experiments. The implementation of the equations presented in the paper is described in this section. The FORTRAN source code for the subroutine (SCATTER) which calculates attenuation from this theoretical model is presented in Appendix A.

The model can be used to describe the attenuation caused by scattering and thermoviscous absorption by an array of cylinders. In order to physically model the thermoviscous absorption of the boundary layer of air around either a rigid or non-rigid cylinder, a complex propagation constant for air (k_0) is required. The model presented here does not, in fact, use a complex value of k_0 but the use of a non-rigid surface effectively models the thermoviscous absorption of the boundary layer as well as absorption by the cylinder itself. If a rigid cylinder assumption is used the effects of scattering alone are measured.

Calculation of bulk propagation constant.

From equations (3),(4)and (5) of Embleton's paper the bulk propagation constant of the array (k_b) is defined as:

$$k_b = \left[k_0^2 - 4iNg + \left(g_1^2 - g^2 \right) \left(\frac{2N}{k_0} \right)^2 \right]^{0.5} \qquad (5.1)$$

where k_0 = propagation constant in air $\frac{\omega}{c_0}$

N = average number of scatterers per unit area

$$g = \sum_{n=-\infty}^{n=\infty} A_n \quad \text{and} \quad g_1 = \sum_{n=-\infty}^{n=\infty} (-1)^n A_n \tag{5.2}$$

and

$$A_n = -\frac{iJ_n(ka)+Z_h J'_n(ka)}{iH_n(ka)+Z_h H'_n(ka)} \tag{5.3}$$

a = radius of the cylinders

Z_h = The normalised surface impedance of the cylinders.

In the extreme cases of infinitely soft and infinitely hard cylinders, the equations for A_n become:-

as $Z_h \rightarrow 0$

$$A_n \rightarrow -\left[\frac{J_n(ka)}{H_n(ka)}\right] \tag{5.4}$$

as $Z_h \rightarrow \infty$

$$A_n \rightarrow -\left[\frac{J'_n(ka)}{H'_n(ka)}\right] \tag{5.5}$$

Calculation of Scattering Parameters.

Subroutines S17ACF, S17ADF, S17AEF, S17AFF from the Nag10 library of subroutines: are used in a subroutine (JYH) to calculate the first and zeroth order Bessel and Hankel functions J_0, J_1, H_0 and H_1 these subroutines accept a real argument x (in this case ka) and return the values of $Y_0(x)$, $Y_1(x)$, $J_0(x)$, $J_1(x)$ Hankel functions are calculated as

$$H_0(x) = J_0(x)+iY_0(x) \tag{5.6}$$

$$H_1(x) = J_1(x) + iY_1(x) \tag{5.7}$$

The first and zeroth order derivatives of the Bessel and Hankel Functions are calculated as

$$J'_0(x) = -1 \times J_1(x) \tag{5.8}$$

$$H'_0(x) = -1 \times H_1(x) \tag{5.9}$$

$$J'_1(x) = J_0(x) - \frac{J_1(x)}{x} \tag{5.10}$$

$$H'_1(x) = H_0(x) - \frac{H_1(x)}{x} \tag{5.11}$$

The higher orders of the Bessel and Hankel functions and their derivatives were calculated using the recurrence relationships

$$R_n(x) = 2(n-2)R_{n-1}(x) - \frac{xR_{n-2}(x)}{x} \tag{5.12}$$

and

$$R'_n(x) = xR_{n-1}(x) - \frac{(n-1)R_n(x)}{x} \tag{5.13}$$

where $R = J$ or H

Since:

$$R_{-n}(x) = (-1)^n R_n(x) \tag{5.14}$$

the negative orders of A_n become

$$A_n = -\frac{i(-1)^n J_n(ka) + Z_b(-1)^n J'_n(ka)}{i(-1)^n H_n(ka) + Z_b(-1)^n H'_n(ka)} \tag{5.15}$$

Therefore $A_{-n} = A_n$ so the negative orders of the Hankel and Bessel functions need not be calculated, and

$$g = A_0 + 2\sum_{n=1}^{n=\infty} A_n \tag{5.16}$$

and

$$g_1 = A_0 + 2\sum_{n=1}^{n=\infty}(-1)^n A_n \qquad (5.17)$$

It is obviously impossible to calculate A_n for an infinite range of values of n, and not desirable to calculate many more values than necessary. In order to determine how many values of n (orders) are required to approximate to infinity, values of g and g_1 were calculated for a range of maximum values of n. Figures 5.1 and 5.2 are examples of the values of g and g_1 plotted against the maximum value of n used. It is evident, from these and graphs plotted for other values of ka, that, after a certain level increasing the number of orders used does not affect the calculated values, and that the number of orders required to reach this value depends on ka; a lower value of ka requiring fewer orders. A change in the input surface impedance was found to change the magnitudes of g and g_1 but not the number of orders required. The maximum value of n required was determined from these and other graphs (eg n = 20 in figure 5.1 and n = 5 in figure 5.2) and the results plotted against ka, as figure 5.3. The relationship between ka and the number of values of n required is approximately a straight line. The solid line shown on figure 5.3 has the equation:

$$n = 1.25ka + 7.25 \qquad (5.18)$$

this equation is used to calculate the maximum value of n used in the calculation of g and g_1. The result is assigned to an integer variable therefore the numbers after the decimal point are simply dropped. The calculated value slightly overestimates the number of orders required, this takes account of any errors in estimating n or any rounding errors.

The value of Z_b , the normalised surface impedance of the cylinders could be calculated indirectly from the results of the absorption coefficient of tree trunks measured by Frank (1976). Values of flow resistivity were put into a Delany and Bazley equation for impedance and this value of of impedance was used to calculate the absorption coefficient α_1 from

$$\alpha_1 = 1 - \left|\frac{Z-1}{Z+1}\right| \qquad (5.19)$$

The sum of squares of the differences between these values and the measured absorption coefficient was calculated. The value of flow resistivity which gives the lowest sum of squares was 5,400,000 mks rayls. This high value of flow resistivity indicates that little energy will be absorbed at the surface, as was concluded by Frank (1976), this fact also indicates that the local reaction assumption used by this model is fulfilled by the surface of tree trunks.

Calculation of Attenuation From Bulk Propagation Constant.

Embleton shows that the mean energy density approximates to e^{-2Qx} where Q is the imaginary part of the bulk propagation constant, and x is the distance from the source. The corresponding dB level is $10\log_{10}e^{-2Qx}$. At the source (or any reference point) x can be taken to be zero and at a point farther away x can be assigned d. The dB difference between the two points (the Attenuation) is therefore

$$\text{Attenuation} = 10 \log_{10} \left[\frac{e^{-2Q0}}{e^{-2Qd}} \right] \qquad (5.20)$$

$$= 20\, Qd \, \log_{10} e$$

$$= \frac{20Qd}{\log_e 10}$$

This is a familiar form for the attenuation of sound travelling through a porous medium quoted in terms of bulk propagation constant.

In order to ascertain that the calculations described above are the same as those carried out by Embleton (1966), an attenuation for hard and soft cylinders was calculated using the same parameters as figure 1 of Embleton's paper. The attenuation calculated agrees with the 'energy density loss' shown in the figure. (see figure 5.4).

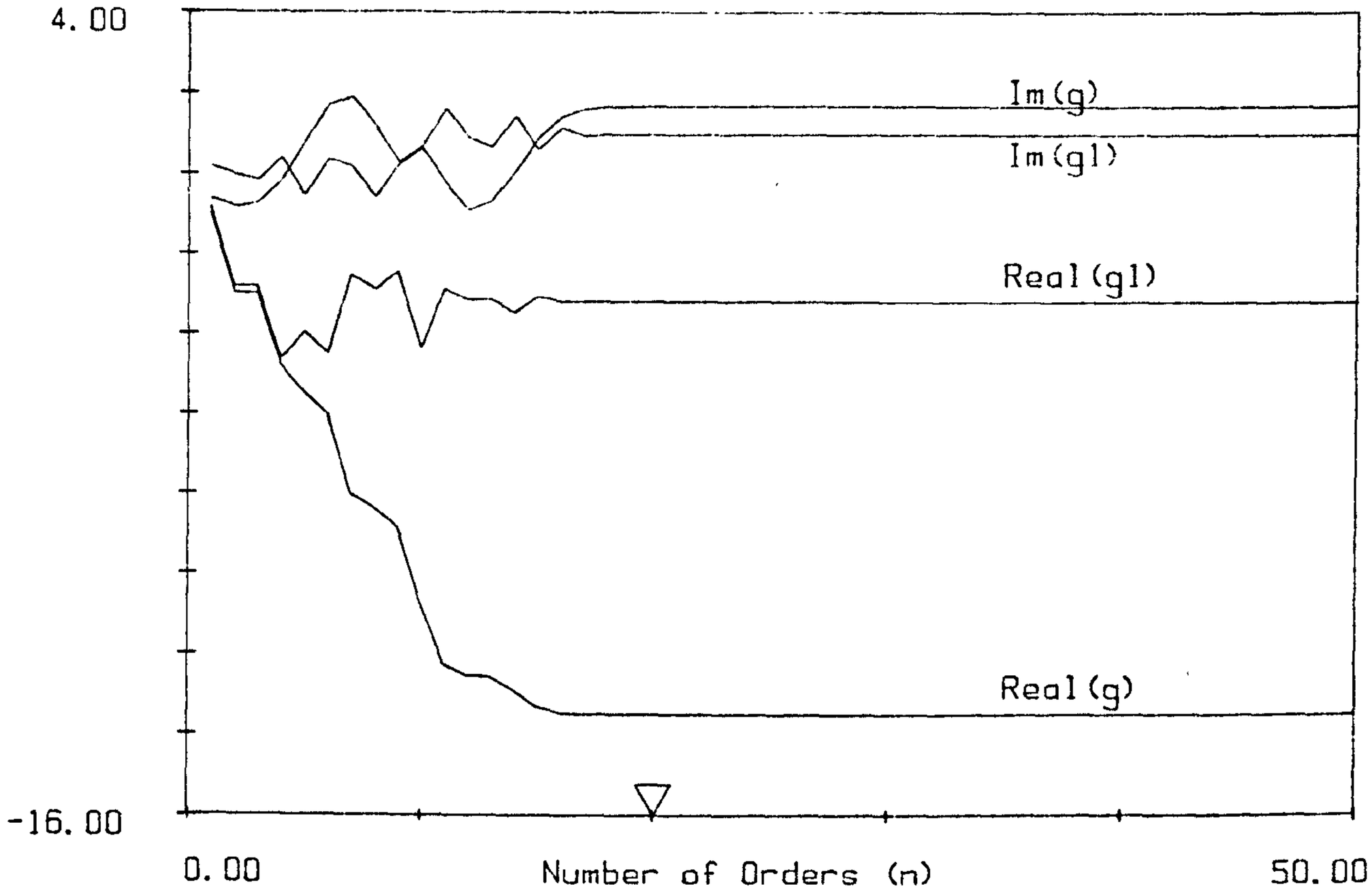

Figure 5.1
Scattering function calculated for a range of values of n.
Radius (a) = 0.1, frequency = 8kHz, ka = 14.65.

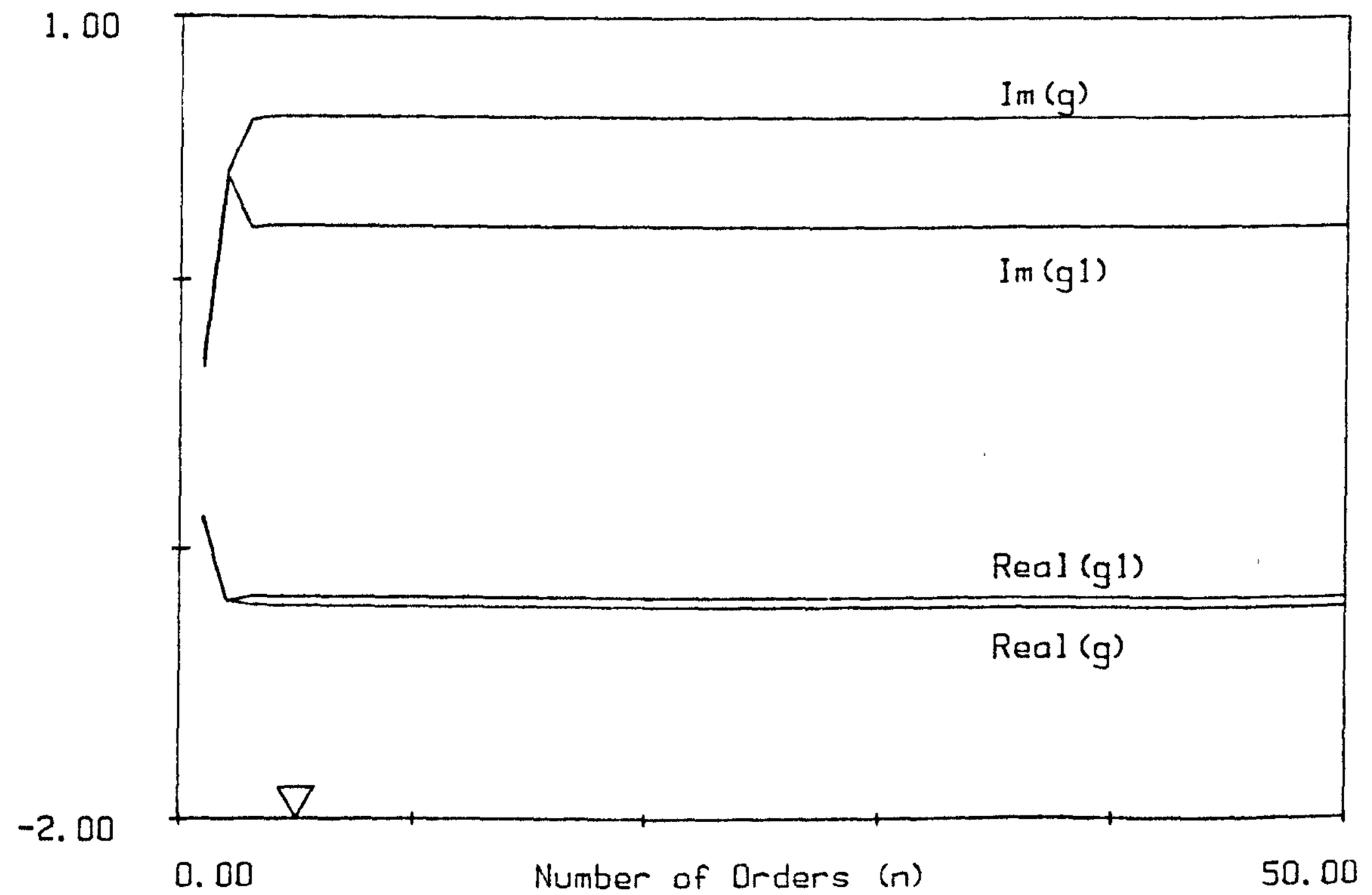

Figure 5.2
Scattering function calculated for a range of values of n.
Radius (a) = 0.1, frequency = 1kHz, ka = 14.65.

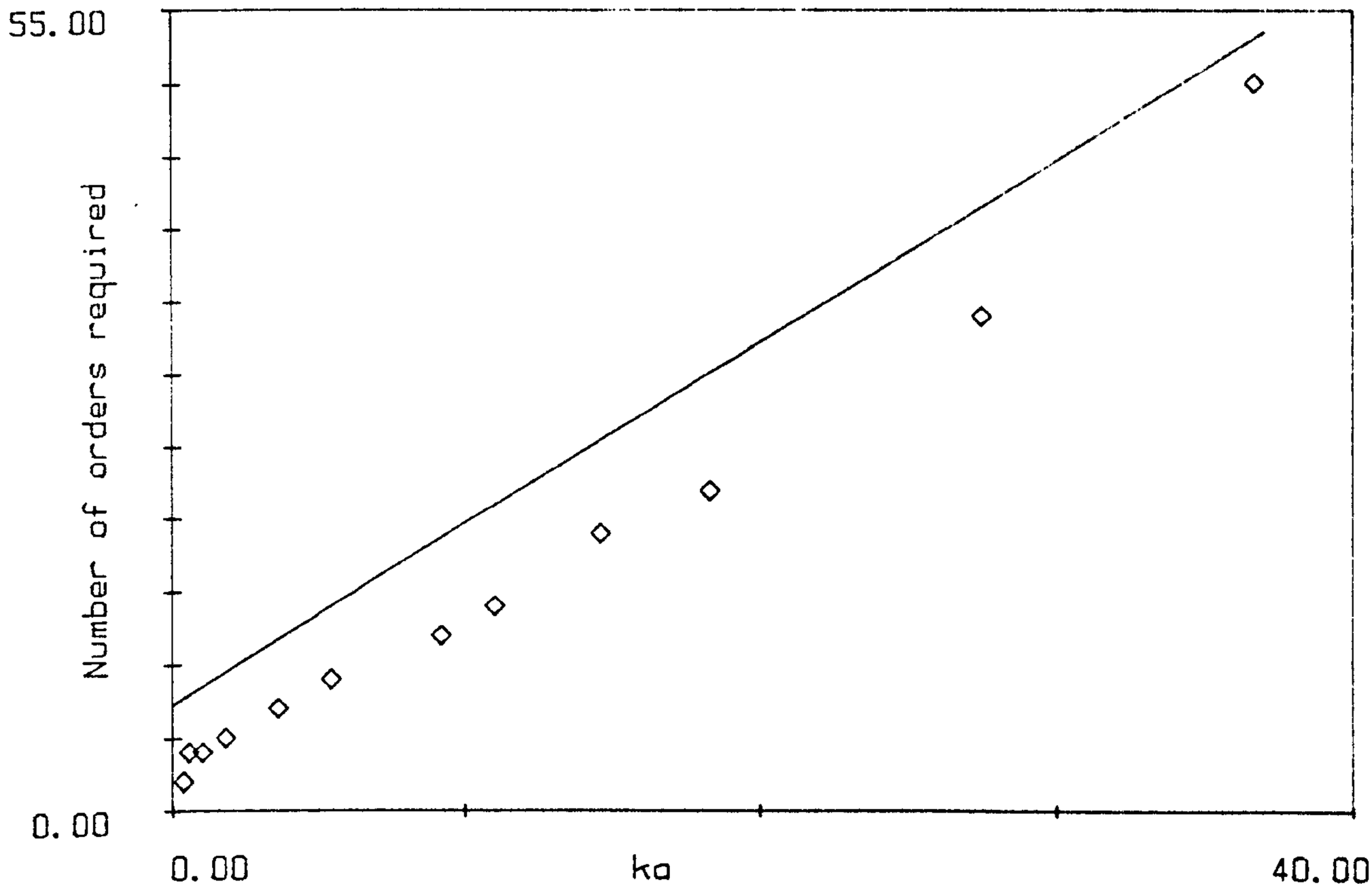

Figure 5.3 Calculation of number of orders (n) required in the calculation of An.

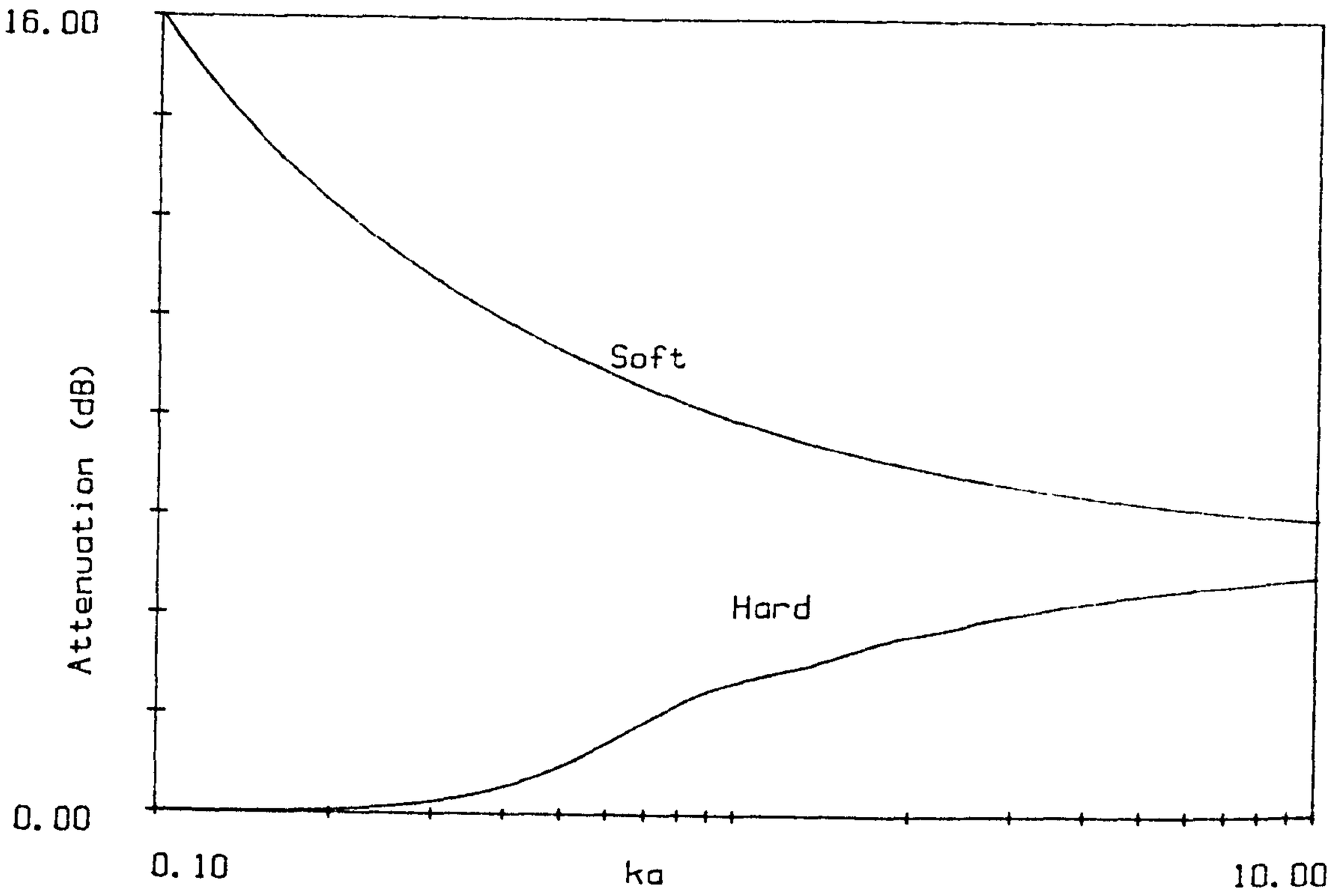

Figure 5.4
Attenuation per 100ft, radius = 1cm, density = 0.0001/cm^2
and the equivalent figure from Embleton(1966).

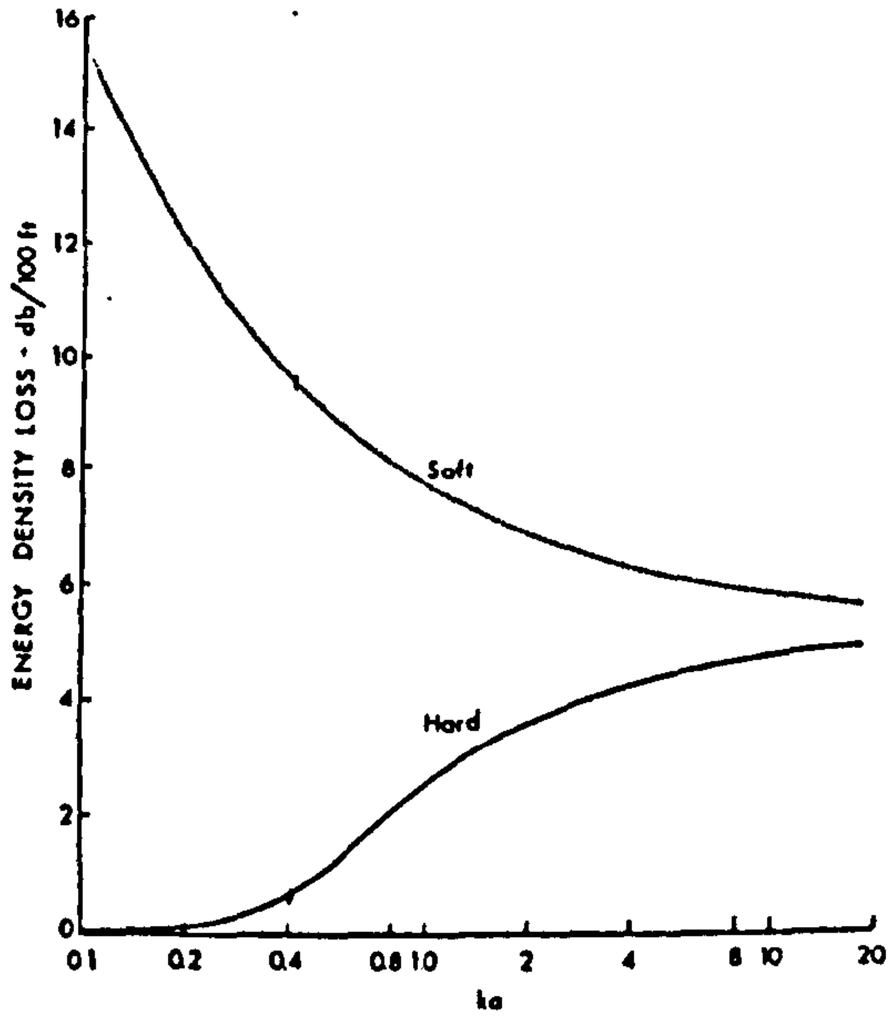

FIG. 1. Energy-density loss (dB/100 ft) as a function of ka for infinitely hard and infinitely soft cylinders. The ordinate of both curves is directly proportional to the concentration of the cylinders W and to their radius a—the ordinate is here scaled for $Wa = 10^{-4}$ cm^{-1}.

5.2 Calculation of Scattering (Aylor 1972)

Aylor (1972) calculates a value of attenuation for the stems in a woodland. The stems are assumed to be rigid cylinders. The attenuation is not frequency dependent but it is stated that the attenuation will only be significant where the wavelength is small compared to the cylinder radius. Aylor defines the frequencies at which the attenuation is significant as frequencies at which the value of ka (product of propagation constant in air k, and radius of cylinders a) is much greater than 1.

The attenuation is defined in terms of a parameter ξ which is defined as

$$\xi = 4Nad \tag{5.21}$$

where N is the number of cylinders per unit area and d is the distance.

The attenuation is defined as

$$\text{Attenuation} = 10 \log_{10} \left\{ \left| \frac{2\pi}{\xi} \right|^{0.5} e^{-\xi} \left| 1 - \frac{9}{8\xi} \right| \right\} \tag{5.22}$$

It is evident that any combination of distance, density and radius which give the same value of ξ will predict the same attenuation value. This equation cannot be calculated for ξ less than or equal to 1.125 since this would require the calculation of the logarithm of zero or a negative number.

Figure 5.5 is a graph of attenuation vs ξ, it shows that attenuation increases with increasing ξ except at the lowest values. This anomaly could be due to the fact that the equation is an approximation that is not valid at low values of ξ, therefore calculations will not be used for values of ξ of less than 1.8.

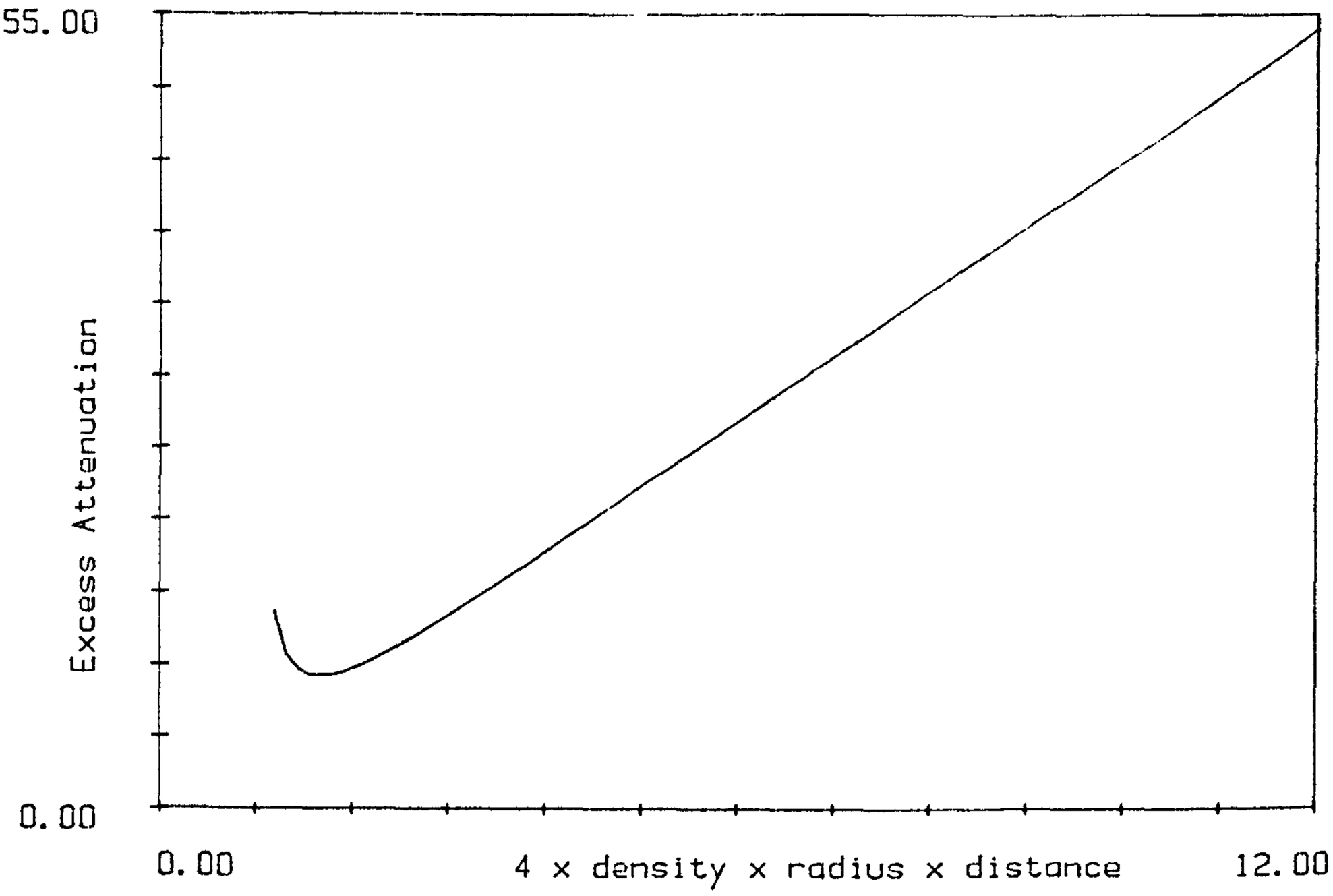

Figure 5.5
Attenuation function from Aylor(1971)

5.3 Description of Attenuation Functions.

Figures 5.6 to 5.9 show the attenuation calculated from the Embleton model plotted against frequency, the source-receiver separation distance used is 50m. The input parameters are indicated in the figure captions. The first three figures show the effect of changes in the input density and radius for the rigid cylinder case. Figure 5.9 shows the change in attenuation with changing surface impedance. The attenuation calculated from the Aylor model is indicated as a horizontal line from the frequency at which $ka = 1$ to the highest frequency. The predictions from the two models with the same input parameters (density and radius) have the same line type. The Aylor model is only shown where the value of ξ is greater than 1.8, as explained in the previous section.

The attenuation predicted by the Embleton model has an overall pattern of increasing attenuation with increasing frequency, the frequency dependence being dependent on the radius, density and surface impedance. Figures 5.6 to 5.8 show that the frequency at which the attenuation becomes significant is determined by the radius, the attenuation spectra for the larger cylinders diverging from 0 at a lower frequency than those of the smaller cylinders. All the spectra in figure 5.8 (constant radius) diverge from 0 at about the same point. At frequencies just above the point at which the spectra start to diverge, the attenuation rises rapidly and then flattens out to a smaller gradient, the gradients of the slopes being dependent on both the radius and the density.

The Aylor model predicts an attenuation value which appears to be a high frequency asymptote to the Embleton model being about 2 to 3 dB higher than the value at 10 kHz.

Increasing the flow resistivity input to the Embleton model, ie assuming a harder surface, decreases the attenuation, except where a very low value of flow resistivity is used; when the attenuation reaches a peak and then falls slightly. The 'soft' cylinder case described by Embleton, which does not have significant applications in this study, has a pattern of decreasing attenuation with increasing frequency. Predictions of attenuation calculated from these models, are compared with the measurements in chapters 7 and 8 to

determine their applicability in the calculation of sound propagation in woodland.

References, Chapter 5.

[1] Aylor 1972 Noise reduction by vegetation and ground. J ACOUST SOC AM 51(1) 197 - 205

[2] Frank. L.D. 1976 Tree Bark and the Forest Floor as Sound Absorbing elements within a forest. MS. THESIS, PENNSYLVANIA STATE UNIVERSITY.

[3] Embleton, T.F.W. 1966 Scattering by an Array of Cylinders as a Function of Surface Impedance J. ACOUST. SOC. AM 40 667-670

[4] Twersky,V. 1953. Multiple Scattering of Waves by a Volume Distribution of Parallel Cylinders. N.Y. RES. REPT. NO.EM-59 also J. MATH. PHYS. 3 700-715 (1962) and J. ACOUST. SOC. AM. 36 1314-1329 (1964).

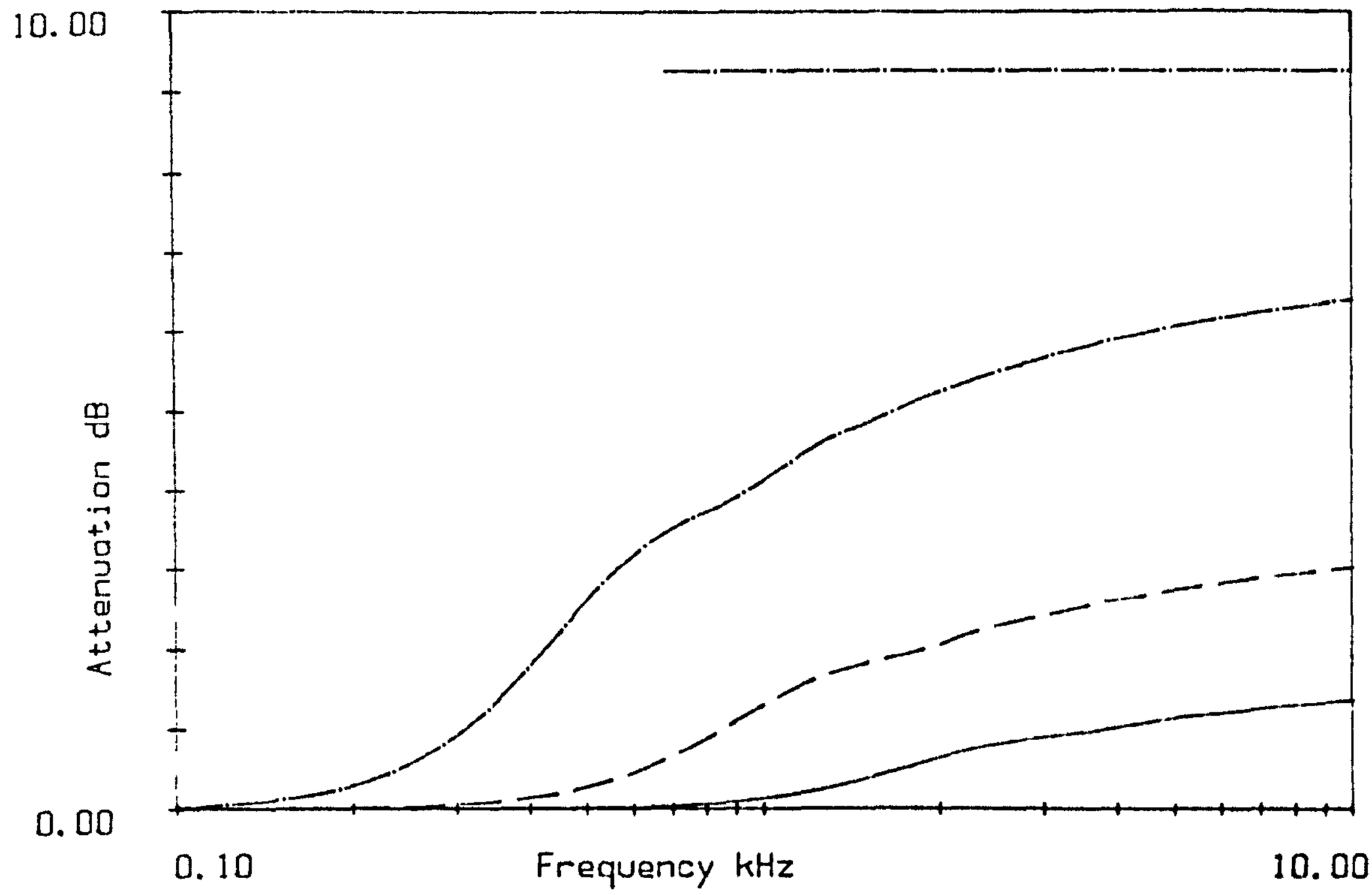

Figure 5.6
Attenuation through 50m of an array of rigid cylinders.
Radius= ———0.02, — — ·0.04, ——·—— 0.08m. Density=0.1.

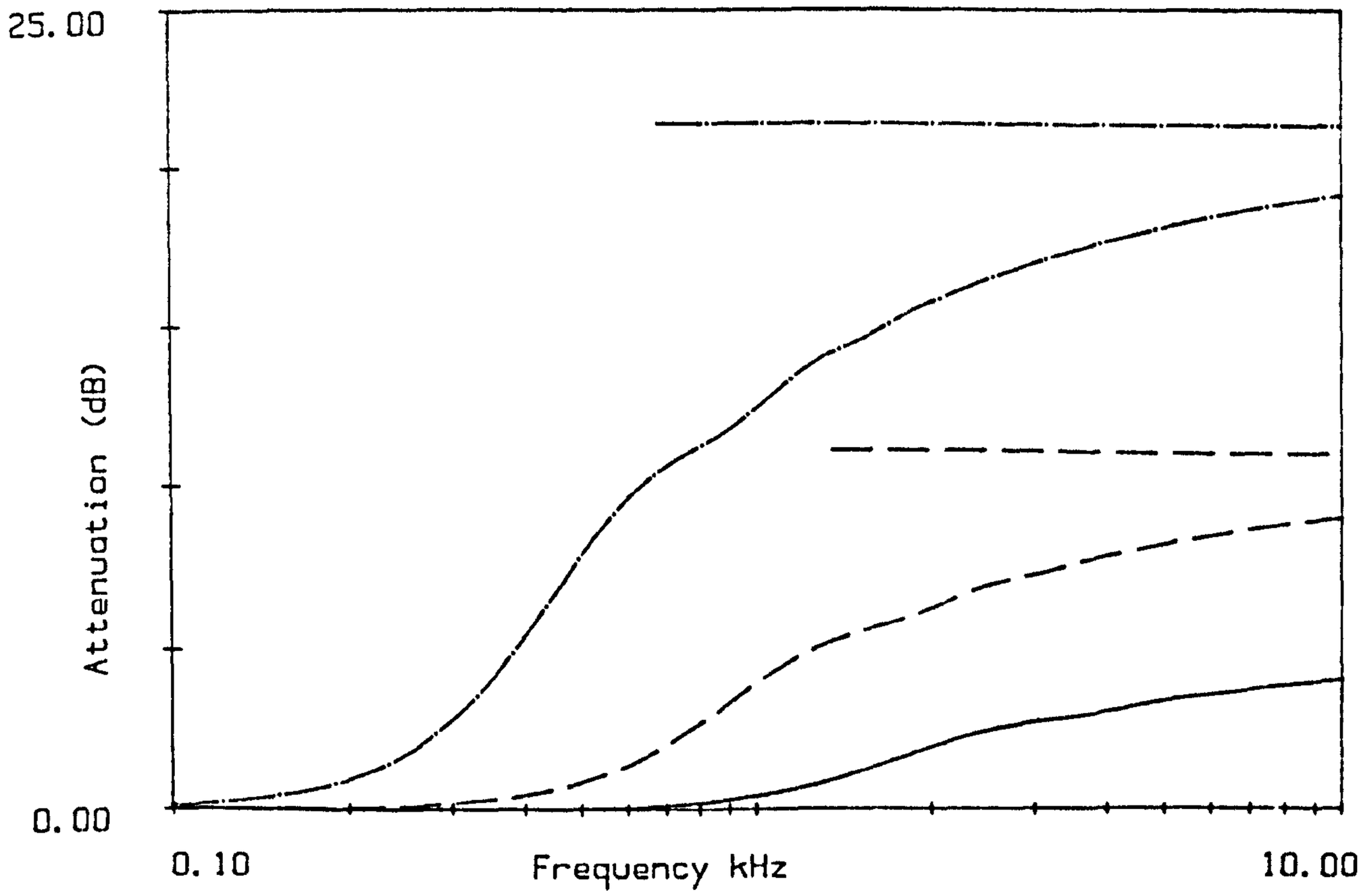

Figure 5.7
Attenuation through 50m of an array of rigid cylinders.
Radius= ———0.02, — — ·0.04, ——·—— 0.08m. Density = 0.3.

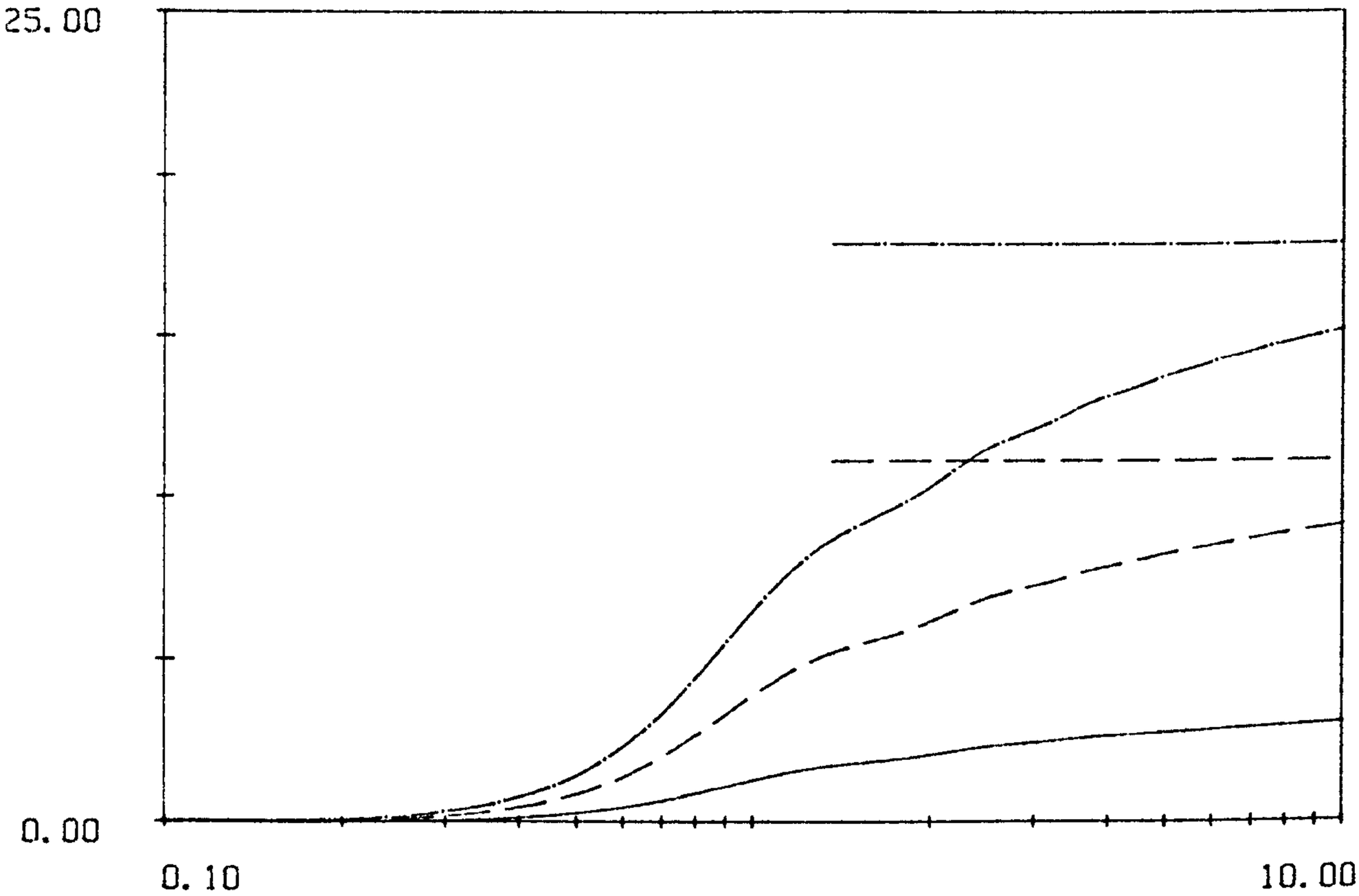

Figure 5.8
Attenuation through 50m of an array of rigid cylinders.
Density= ——— 0.1, — — · 0.3, ——·—— 0.5. Radius=0.04m.

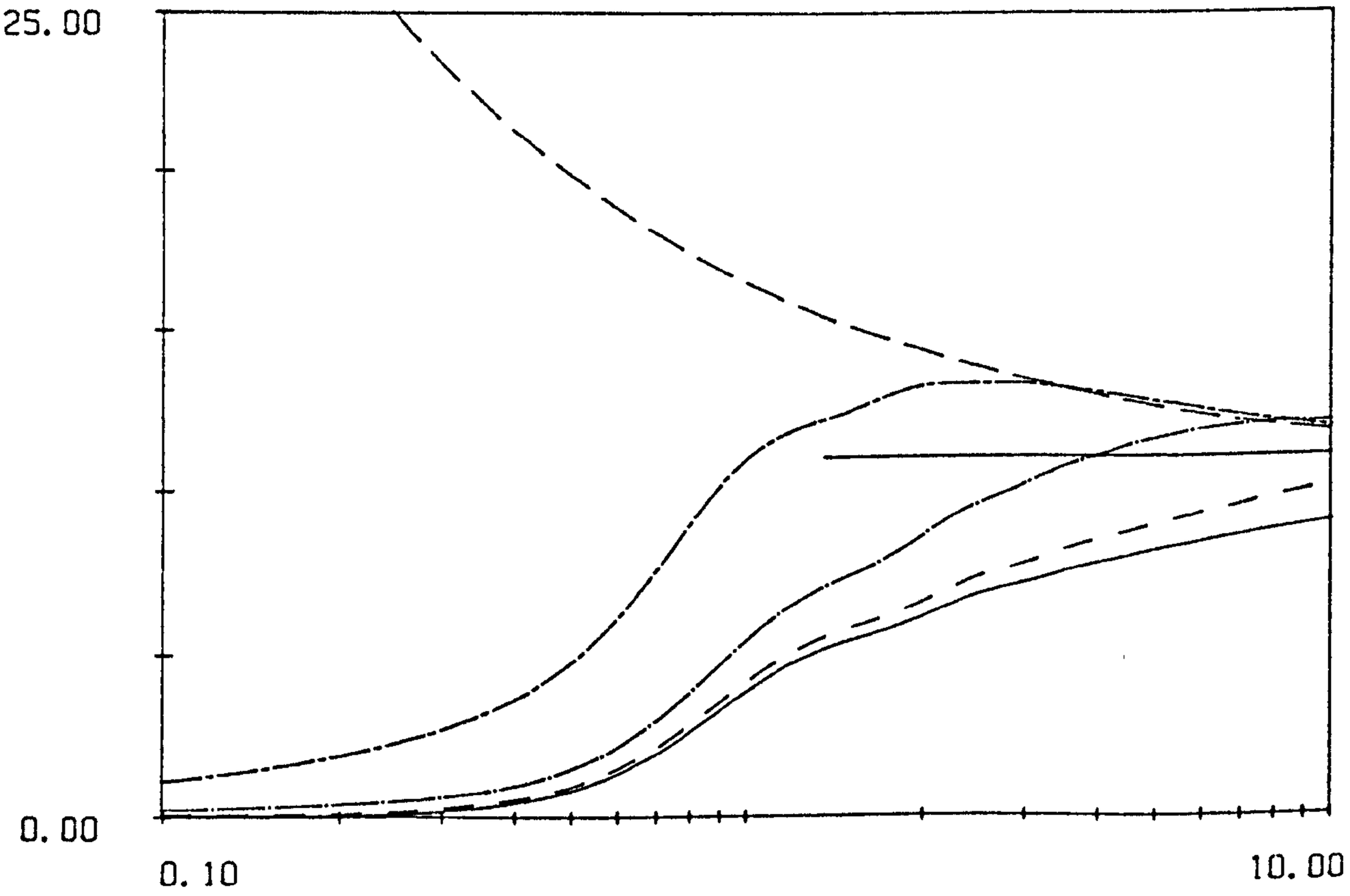

Figure 5.9
Attenuation through 50m of an array of cylinders.
Density=0.3, Radius=0.04.
Surface of cylinders : ——— hard, — — — soft,
and with impedance calculated using equation 4.11; σ·e =
— — — · 5,400,000; ——·—— 540,000; ——··—— 54,000.

Chapter 6 : Woodland Attenuation Measurements

This chapter presents the details of the propagation measurements made in wooded areas. All the sites used for this study are in the Hazelborough Forest area of Forestry Commission land near Silverstone, Northamptonshire. The stands are all on largely flat land which eliminates the need to account for the effects of topography in the experimental analysis, although there are drainage ditches, about 1m wide and 0.3 to 0.5 m deep crossing the stands at intervals. The 'compartment numbers' quoted in the site descriptions refer to the numbers of the different stands, or compartments, as marked on the Forestry Commission stock map, which also indicates planting dates. Three contrasting stands were used, each is treated individually in this chapter; presenting the characteristics of the stands, description of the main measurements made and results for each day, the results for the stand on different days are compared. A typical example of the results obtained is first analysed to assess the level of accuracy of a single measurement which can then be taken into account in the comparisons between measurements.

The diameter of the stems and the number of stems per unit area, given in the site descriptions and used in scattering predictions were ascertained by sampling the stand. The sample areas were triangles marked out within the stands with sides of 10m to 15m, chosen from within the area covered by the experimental measuring tracks. The circumference (at about 1.3 to 1.4 metres above the ground) of each tree trunk within the sample areas was measured and converted to the diameter.

The results of the measurements are presented in a variety of ways. The attenuation spectra for all the measurements made on the main experiment days are presented in full in appendix B, and certain relevant examples are included within this chapter. Since the high frequency attenuation is thought to be a linear function of distance, the results can also be presented as dB attenuation for a certain distance for comparison between measurements made over different distances. The low frequency part (up to 1kHz) of all the long range propagation measurements (mean at each location and each height) have been fitted to predictions using the models described in chapter 4. The best fit parameters are presented in full in Appendix C and summarised in this chapter.

6.1 Variability of Measurements

The description of the analysis of the tape recordings in chapter 3 states that 128 rms spectra were averaged by the Nicolet FFT Spectrum Analyser for each measurement. A set of measurements is presented to demonstrate the reasons for taking several averages and the variability within and between successive measurements. These measurements were made on 9th August 1984 at Hazelborough Wood, a full description is included in section 6.2. The measurement analysed here is that made with the test microphone 72m from the source and 1.2m above the ground. Three recordings were made at this location, one with the microphone directly above the marker post (measurement number 6) and one at about 1m to either side of it (6a and 6b). Each recording was about 2 minutes long.

The tape recording was played back into the Nicolet FFT analyser which was controlled by the Nova minicomputer which automatically restarted the averaging cycle after accepting the result of a small number of averages. Thus several short samples were taken successively from one 2 minute recording, each one the result of a small number of rms spectra averaged together. The following sample spectra were stored on the Nova disk and transmitted to the Vax for analysis:

a) 7 spectra each of only one instantaneous rms spectrum.

b) 7 spectra each the mean of 4 instantaneous rms spectra.

c) 4 spectra each the mean of 16 instantaneous rms spectra.

d) 1 spectrum of the mean of 128 instantaneous rms spectra.

taken from measurement 6, the tape was rewound before each set of samples was taken so a), b) and c) were taken from the same part of the signal. c) and d) were also carried out for measurements 6a and 6b.

The resulting spectra were converted to sound pressure levels and plotted. Figure 6.1.1 shows the maximum, minimum and mean value of the 7 instantaneous spectra. Taking only one 'snapshot' spectrum gives a wide range of levels, because there is no averaging out of the random noise. Figure 6.1.2 shows that taking the mean of 4 spectra reduces the variability considerably, there is a further reduction in the range of values when 16 spectra are

averaged as in figure 6.1.3. All electronic circuits generate noise of various types which add to and degrade the signal. Thus noise is produced by the circuitry of the Nagra and the Nicolet. Since the noise is random and therefore not correlated with the signal, and its mean value is zero, the averaging procedure increases the signal to noise ratio. The signal/noise ratio is increased as 10 $\log_{10}(m)$ where m is the number of averages. Thus taking 4 averages reduces the effect of electronic noise by 6 dB compared with the instantaneous spectrum, and 16 averages reduce it by 12 dB. Taking 128 averages reduces the relative magnitude of the noise by 21 dB, thus any random noise has little effect on the resultant signal.

Figures 6.1.3, 6.1.4 and 6.1.5 are the range of values of the four spectra obtained by averaging 16 instantaneous spectra, and the mean of 128 spectra used in the analysis of the results for each of the three recordings. The range of values are due to random variations rather than a systematic difference between the spectra of different parts of the recording. The variability within a single recording seems slight (except perhaps at low frequencies in 6a and 6b) and the value used in the analysis of the results (128 averages) lies within this range. Thus taking the average of 128 spectra for each result eliminates variations due to noise and differences within the signal, such as differences caused by small scale wind variations. The 128 averages represent a total time interval of approximately 90 seconds.

The range of values in figures 6.1.3 to 6.1.5 were compared by plotting the ranges of two of the signals on one graph, all three were compared with each of the other two. These pairwise comparisons showed that the range of values overlapped along most of the frequency range, indicating that differences in the mean spectra of the three measurements are not significant and are caused by variations within the measurements rather than significant differences between the measurements at the slightly different microphone locations. This result shows that it is valid to take the mean of the three measurements at each location to use in further analysis, but the range of values shown here should be considered. The level of accuracy of the mean values is indicated by the spread of the data (approximately ± 2.5dB).

Background noise is one factor which could possibly introduce inaccuracies into the measurements. Recordings of background noise were made at intervals between the

recordings and these were analysed to give a spectrum of the noise levels for comparison with the test recordings. In most cases the background noise was considerably below the level of the test recordings (more than 10dB lower) and was therefore ignored. Since the operator was stationed near the most distant microphone for all the recordings, major intrusive background noise such as aircraft or traffic, could normally be detected and the recording repeated when the noise had gone. Background noise is not thought to cause problems in many of the measurements except possibly at the highest frequencies, and longest distances, where the recorded levels were very low, therefore rather more prone to inaccuracy.

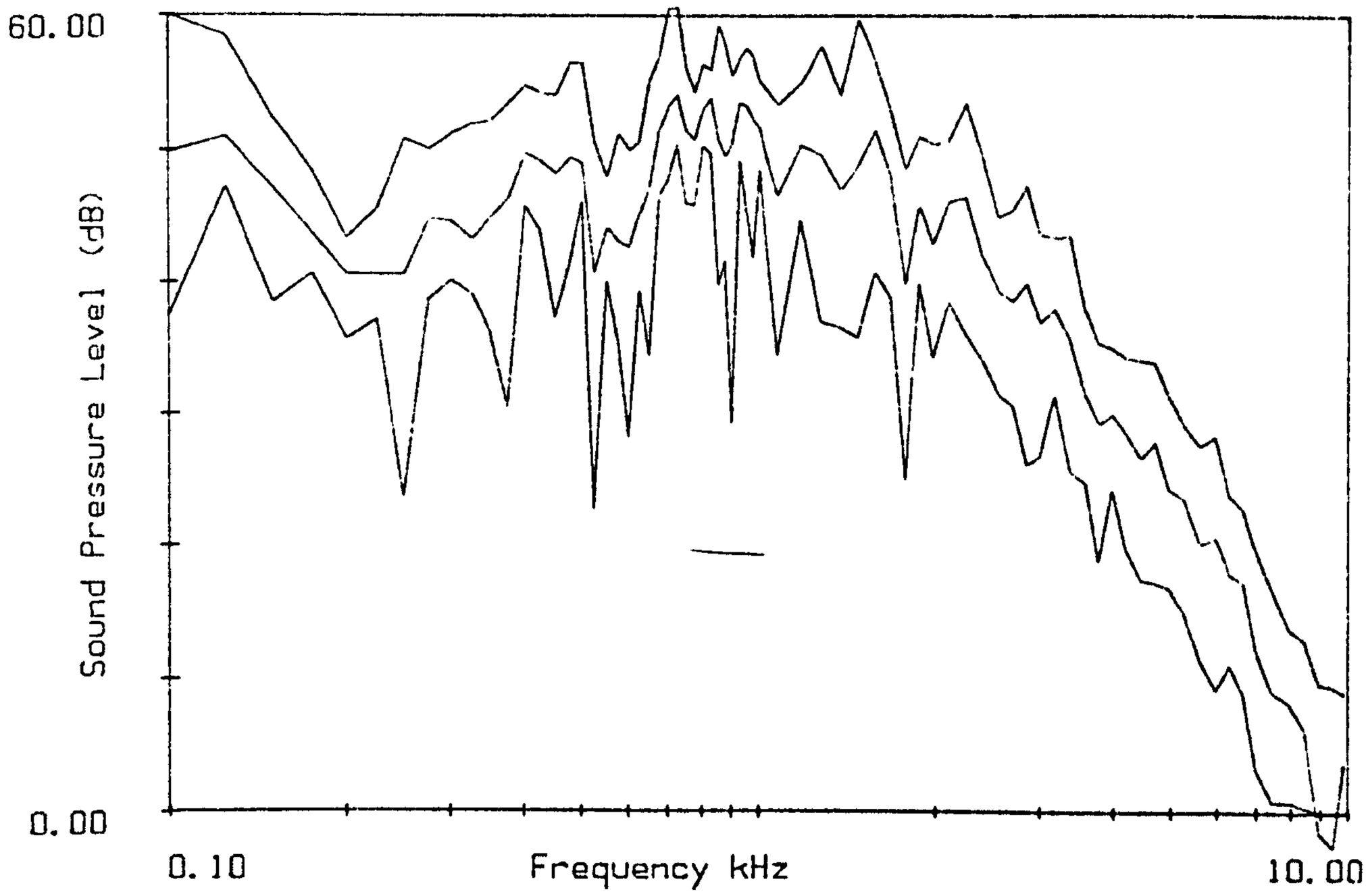

Figure 6.1.1
Maximum, minimum and mean values of Sound Pressure Level of 7 instantaneous spectra of measurement 6 on 9/8/84.

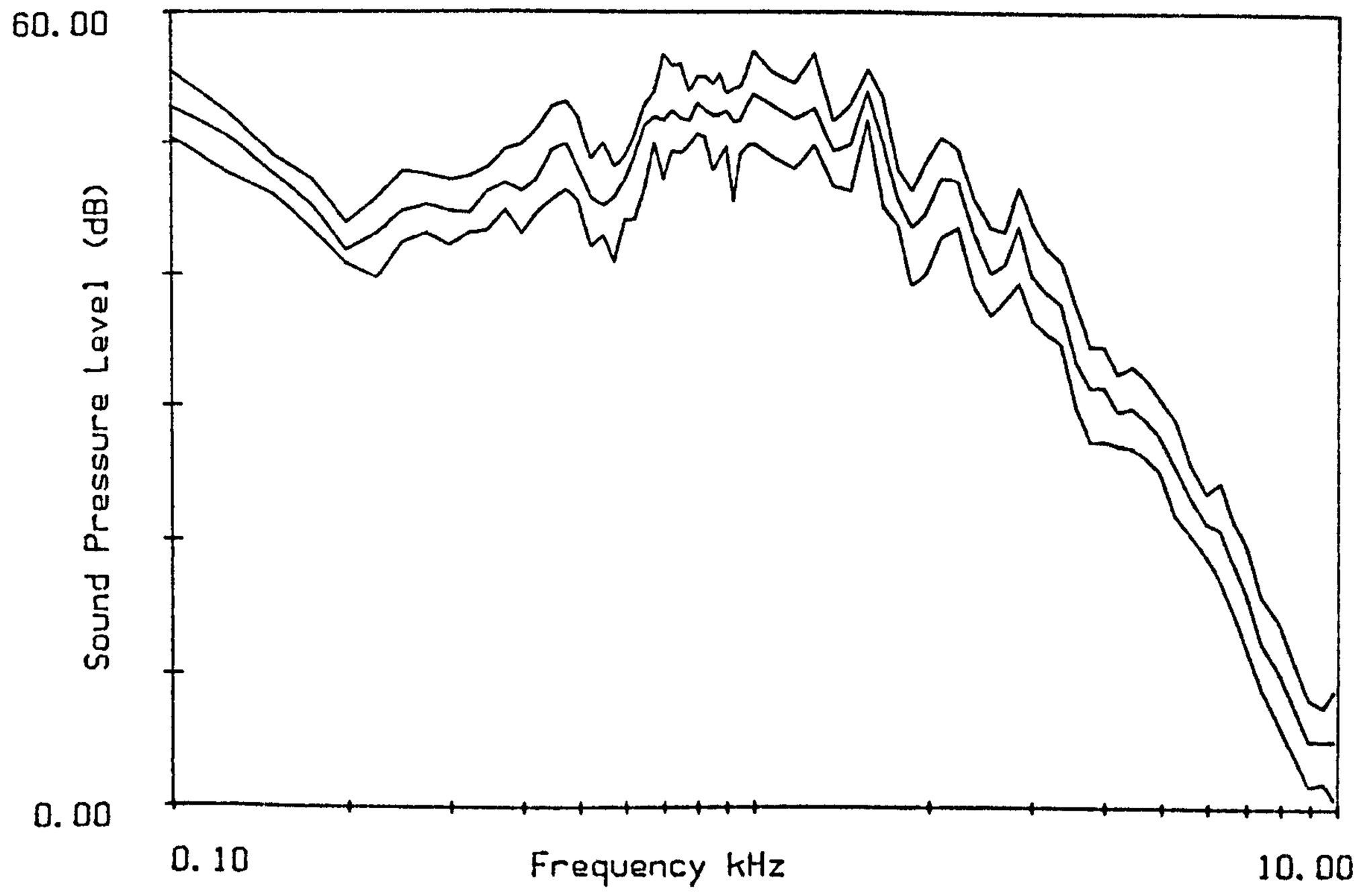

Figure 6.1.2
Maximum, minimum and mean values of Sound Pressure Level of 7 samples of the mean of 4 spectra of measurement 6 on 9/8/84.

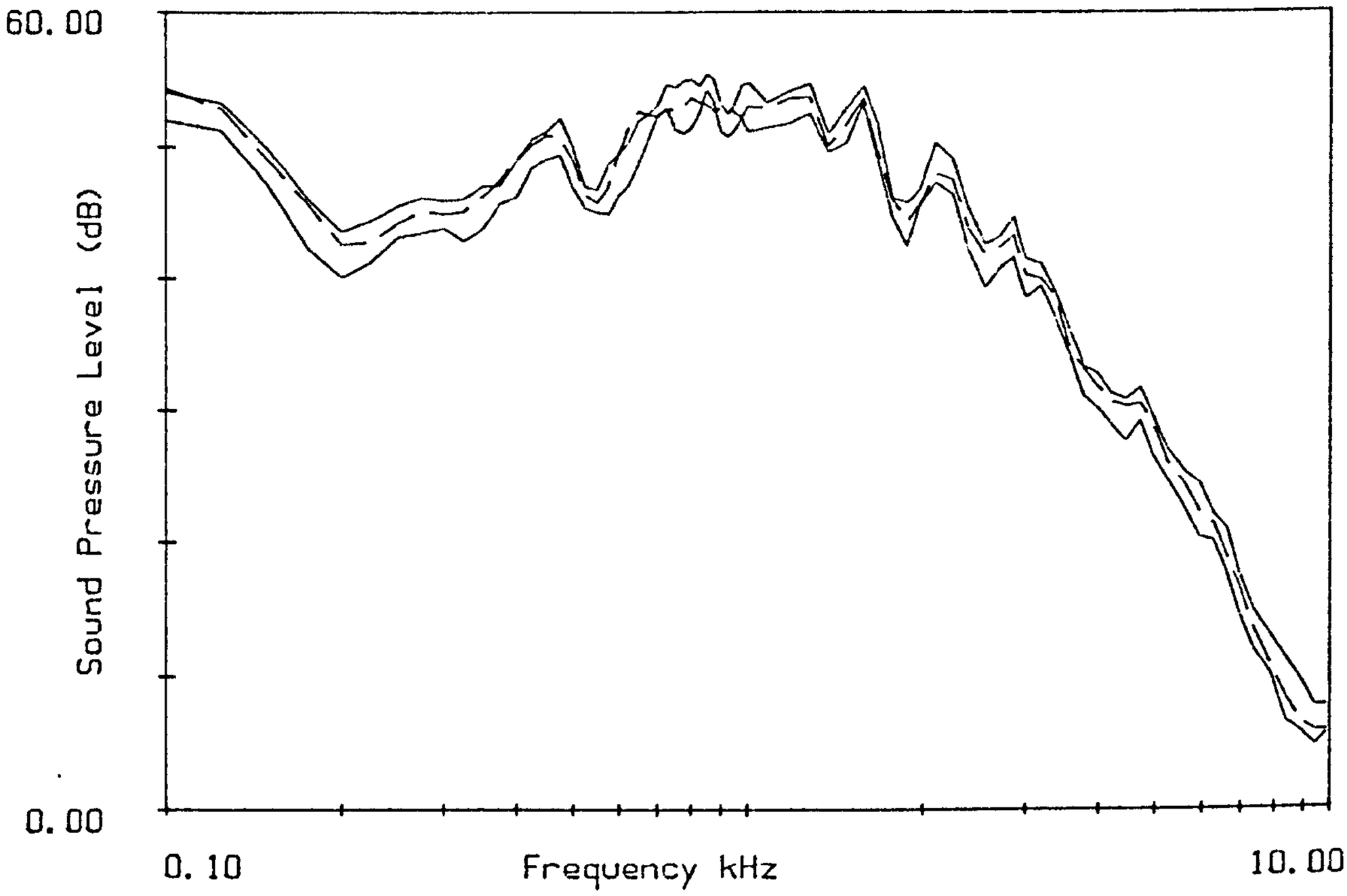

Figure 6.1.3
Maximum and minimum values of Sound Pressure Level of 4 samples of the mean of 16 spectra and the mean of 128 spectra (-----) of measurement 6 on 9/8/84 .

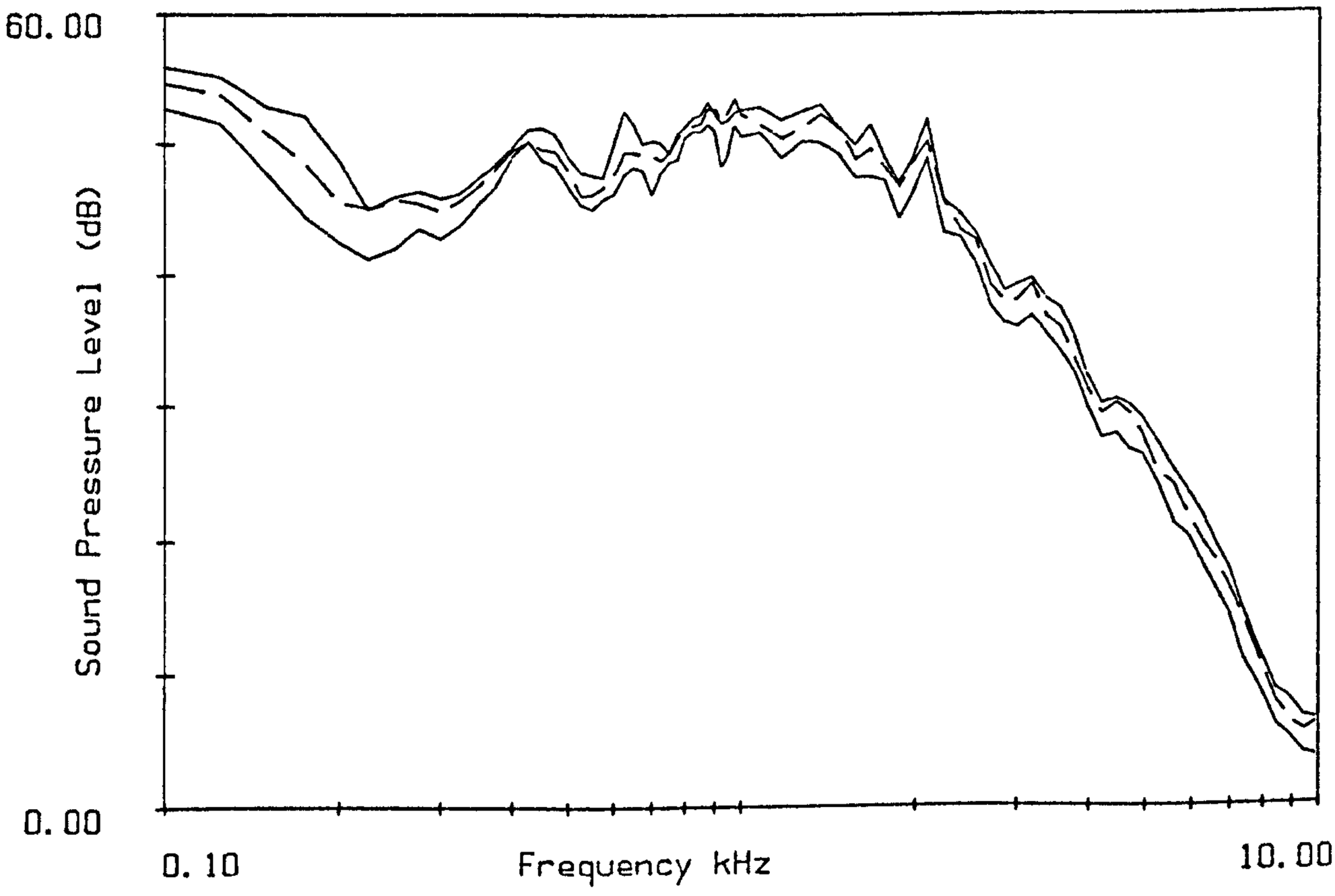

Figure 6.1.4
Maximum and minimum values of Sound Pressure Level of 4 samples of the mean of 16 spectra and the mean of 128 spectra (-----) of measurement 6a on 9/8/84 .

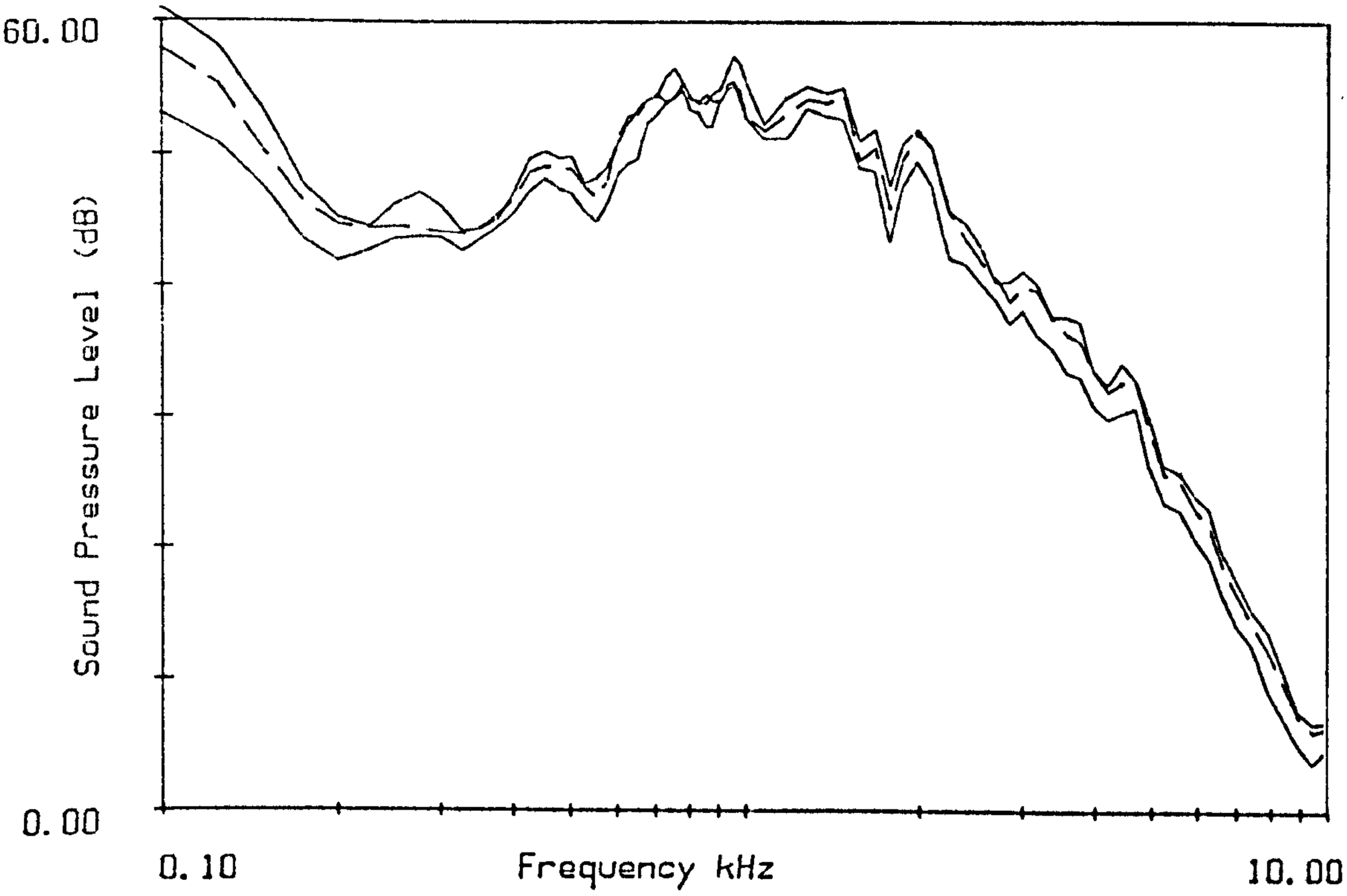

Figure 6.1.5
Maximum and minimum values of Sound Pressure Level of 4 samples of the mean of 16 spectra and the mean of 128 spectra (-----) of measurement 6ℓ on 9/8/84 .

6.2 Measurements in a Mixed Oak and Spruce Stand

Compartment 29 'Hazelborough Wood'

This compartment consists of lines of three rows of Norway Spruce with several rows of oak trees between them. The stand was planted in 1946. the spruce forms a continuous canopy over a clear area with no lower branches or undergrowth. The oak does not form a continuous canopy and has a fairly dense undergrowth mainly of hawthorn with roses, honeysuckle etc. The ground surface is covered by litter; mainly of needles under the spruce, and oak and hawthorn leaves under the oak. The distance from the edge of one spruce line to the corresponding edge of the next is about 24m. The undergrowth obscured the optical path between one marked position and the next ie the visibility is less than 24m, except in winter when there are no leaves on the shrubs of the understorey when the visibility is considerably greater. The sampled stem density of this stand is 0.267 stems per square meter (stems m^{-2}) and the mean radius 0.045m.

A measuring track was marked out in a straight line normal to the lines of trees designated "track C" the source was located at some distance from the edges of the stand in one of the lines of spruce trees for ease of access (position CS). Three microphone positions were marked out at 24m(C24), 48m(C48) and 72m(C72) all of these positions lying within one of the rows of spruce. Two positions were also marked in a line running in the opposite direction from track C (with the source at the same location) at 24m (D24) and 48m(D48). A second measuring track (track H) was marked out from a source position (HS) outside the edge of the wood alongside the forest track with the microphone positions marked out within the wood at 24m(H24), 48m(H48) and 72m(H72). Figure 6.2.1 shows the layout of the measuring positions in this stand.

Measurements made on 10/8/83

On the 10th of August 1983 measurements were made at each of the microphone sites of track C ie the source was at CS and the test microphone at C24, C48 and C72, at 1.2m and 2.5m above the ground. Two measurements were made at each location with the microphones displaced sideways slightly between each measurement.

The wind was measured in a clearing in the woodland and was found to be less than 1.5m/s. The measured relative humidity was 68% and the temperature was between 19.5° C and 20.8° C. One measurement of the temperature was made at each of three heights and was 19.5° C at the ground rising to 20.3° C at 2m and 20.8° C at about 3.7m.

Results

The results of the measurements made on this day are presented in full in Appendix B1 each spectrum is the mean of the two measurements made at each location. The best fit ground parameters are tabulated in Appendix C1, and summarised in table 6.2.1.

Table 6.2.1: Summary of best fit ground parameters 10/8/83

		Model	
	Homogeneous	Delany and Bazley	Rigid-Backed layer
σ_e			
max	59000	26000	80000
mean	39500	23833	51667
min	34000	23000	40000
mean difference			
max	4.13	3.63	3.99
mean	3.56	3.26	3.33
min	3.22	3.01	3.01
d_e			
max			0.145
mean			0.11
min			0.08

The best fit results are very similar for all the measurements using any of the models, and the flow resistivities are all low values. The rigid-backed layer approximation shows that the ground is virtually homogeneous ie. it has a large value of d_e, three of the six results correspond to the homogeneous model impedance, the variable porosity model also gives a homogeneous model best fit (ie $\alpha_e = 0$) for all measurements. The values of σ_e predicted by the rigid-backed layer model is slightly higher than those predicted by the homogeneous, and the Delany and Bazley model has a slightly lower mean difference but these differences are not significant.

Comparison between the attenuation spectra for the two microphone heights (eg figure 6.2.2) shows that in the high frequency part of the attenuation spectra, the 2.5m measurements are generally slightly lower than the 1.2m measurements; this is not a significant difference but is consistent throughout the measurements. This could indicate that the vegetation is denser at the lower levels. There was a fallen spruce tree between positions C48 and C72 which appears to give a denser structure at the lower levels.

Figure 6.2.3 shows the high frequency part of attenuation as dB per 24m from the measurements at the three separation distances, ie the 48m and 72m results have been divided by 2 and 3 respectively. Each line is the mean of the 1.2 and 2.5m measurements, at each distance. The 24m measurement is evidently influenced by interference patterns and random fluctuations, whereas the longer distances give a smoother line and a more similar value of dB per 24m, since the interference pattern is destroyed by scattering effects of turbulence and the vegetation itself, and the random fluctuations are reduced by dividing by 2 or 3. The 48m result is slightly lower than that at 72m for most of the frequency range, but the range of the data is relatively large so the means are not significantly different.

Measurements on 10/4/84

On the 10th of April 1984 measurements were made at each of the microphone sites of track C ie the source was at CS and the test microphone at C24, C48 and C72, at 1.2m and 2.5m above the ground. Two measurements were made at each location with the

microphones displaced sideways slightly between each measurement, except at C72 where only one was made.

There was no apparent wind in the wood. The temperature was about 10° C and the humidity was 60%. There were no leaves on the oak trees or the deciduous shrubs of the understorey, so the visibility in the wood was considerably greater than for the other measurements at this site. The source could be seen quite clearly from the microphone location C24 (24m from the source).

Results

The results of the measurements made on this day are presented in full in Appendix B1 with best fit ground parameters in Appendix C1, summarised in table 6.2.2.

Table 6.2.2: Summary of best fit ground parameters 10/4/84

	Model		
	Homogeneous	Delany and Bazley	Rigid-Backed layer
σ_e			
max	153000	85000	160000
mean	118833	67667	121667
min	93000	51000	90000
mean difference			
max	5.27	5.40	5.08
mean	3.61	3.57	3.59
min	2.16	2.33	2.06
d_e			
max			0.105
mean			0.071
min			0.05

The variable porosity model gives best fit values when α_e is zero for all the measurements. Two of the results of the rigid-backed layer model are homogeneous and the other results show a similar value of σ_e to the homogeneous fits with values of d_e of 0.05 to 0.07 indicating that the ground is acting to some extent as a layered surface but the layer depth

is relatively large.

Comparison of the high frequency part of the spectra for the two microphone heights shows that the 2.5m microphone gives a slightly lower attenuation in the 72m measurement only. The 48m results are very similar and the 2.5m measurement is the same or slightly higher at 24m. The denser structure at lower levels described for the 10/8/83 measurements is not apparent in this measurement suggesting that this result is due mainly to foliage, except perhaps at 72m with the fallen tree mentioned above.

Figure 6.2.4 shows the values of dB per 24m. The 24m measurement again consists of a series of peaks and dips due to interference effects and random fluctuations, which are not apparent in the longer distances due to the disruption of the interference pattern by scattering and the division of the fluctuations. The values of dB per 24m are similar for the 48m and 72m measurements.

Measurements Made on 5/7/84

On the 5 July 1984 measurements were made along both measuring tracks C and D, at 1.2m and 2.5m above the ground with the source at position CS (see figure 6.2.1). Three measurements were made at each location with the microphones displaced sideways slightly between each measurement. Measurements were first made at the three positions on track C then the speaker was turned through 180° and the reference microphone moved to an appropriate position and measurements made at the two positions of track D ie separation distances of 24m and 48m.

There was no apparent wind in the wood. The temperature was about 20° C and the humidity was 48%. There was little cloud cover.

Results

The results of the measurements made on this day are presented in full in Appendix B1. with best fit ground parameters in Appendix C1. summarised in table 6.2.3.

All the attenuation spectra measured on this day have marked peaks at about 2350 Hz which cannot be accounted for by interference patterns since it is in virtually the same place for all the measurements with different source-receiver geometries. No adjustments can be made to account for siting errors or meteorological effects which would give this result. I therefore conclude that some anomaly occurred in the measurement on this day and ignore the peak at this frequency.

Table 6.2.3: Summary of best fit ground parameters 5/7/84

	Model		
	Homogeneous	Delany and Bazley	Rigid-Backed layer
σ_e			
max	50000	30000	50000
mean	32000	20000	42000
min	20000	10000	30000
mean difference			
max	4.16	3.82	4.23
mean	3.16	2.93	3.11
min	1.93	1.75	1.81
d_e			
max			0.121
mean			0.109
min			0.100

The best fit values are very similar in all the measurements on this day. The D track has slightly lower values of best fit flow resistivity and larger values of the mean square. than the C track for all the models. The ground can again be seen to act acoustically as an homogeneous semi-infinite medium.

Figures 6.2.5 to 6.2.8 show comparisons between the two measuring tracks. The low frequency peak is at a slightly higher frequency in the C track measurements at 1.2m and

also the 2.5m measurement at 24m. The 2.5m measurement at 48m has slightly higher amplitude low frequency peak in track C than track D. The two attenuation spectra are otherwise very similar within the accuracy of the measurements as discussed in section 6.1. The similarities in the high frequency parts of the spectra indicate that there is no wind effect, since wind has a directional effect, and these two measurements were made in opposite directions but are very similar. The elements of the wood which cause the high frequency attenuation are evidently not significantly different along the two transects.

Comparison between the attenuation spectra for the two microphone heights shows that in the high frequency part of the attenuation spectra, in the C track measurements, the 2.5m measurements are generally slightly lower than the 1.2m measurements; this is not a significant difference but is consistent throughout the measurements and is similar to the results on 10/8/83. The two microphone heights give very similar high frequency attenuations in the D track measurements. This result indicates a slight difference in the structure of the vegetation of the two measuring tracks, with the D track having a more even structure and the vegetation of the C track being denser at the lower levels.

Figures 6.2.9 and 6.2.10 are the values of dB per 24m calculated as a mean value of all the measurements at each separation distance for the C and D tracks and 1.2m and 2.5m heights. The results are similar along most of the frequency range, the 24m result having a series of peaks and dips, including a very high value of attenuation at 8-10kHz. This is due to interference effects and random fluctuations which are not apparent in the longer distance measurements as discussed in previously. Above about 5kHz the 72m measurement gives a slightly lower value but this is not significant.

Measurements Made on 9/8/84

On the 9th of August 1984 measurements were made at each of the microphone sites of track 11 ie the source system was on the forestry track outside the wood (at 11S) with the microphones at locations 1124, 1148 and 1172 (see figure 6.2.1) within the wood, at 1.2m and

2.5m above the ground. Three measurements were made at each location with the microphones displaced sideways between each measurement.

There was no apparent wind. The temperature was about 21° C and the humidity was 60%. The weather was recorded as mostly sunny with some thin cloud.

Results

The results of the measurements made on this day are presented in full in Appendix B1 with best fit ground parameters in Appendix C1, summarised in Table 6.2.4.

Table 6.2.4: Summary of best fit ground parameters 9/8/84

		Model		
		Homogeneous	Delany and Bazley	Rigid-Backed layer
σ_e				
	max	40000	20000	40000
	mean	30000	20000	33333
	min	20000	20000	20000
mean difference				
	max	4.15	3.43	4.11
	mean	2.77	2.44	2.71
	min	1.90	1.65	1.90
d_e				
	max			0.185
	mean			0.145
	min			0.110

All the models give similar results for all six measurements, the Delany and Bazley model having identical results. The rigid-backed layer and variable porosity models both indicate that the ground is homogeneous.

Comparison between the attenuation spectra for the two microphone heights shows that at frequencies above 3kHz the results are very similar for the two heights, they are less

similar in the range 1kHz to 3kHz but there is no really significant difference between them. In the 72m measurements the 2.5m result is slightly lower than that at 1.2m. The part of track II between 48m and 72m is also part of track D which does not show any difference between the 1.2m and 2.5m results.

Figure 6.2.11 illustrates the values of dB per 24m calculated from all the measurements at each distance. The 24m result again shows some influence of interference patterns and random fluctuations but does not have an overall increase in attenuation above the other distances, indicating that the dense edge vegetation does not cause a significantly greater attenuation than the undergrowth within the wood. The results from the 48m and 72m measurements are not significantly different.

Measurements Made on 20/6/85

Microphones were set up at two of the microphone locations C48 and C72 with the source at CS with microphones at 1.2m and 2.5m above the ground. The microphones at C48 were Bruel and Kjaer half-inch microphones type 4130, with preamplifiers type 2642, powered by a two channel portable power supply type 2810, and the output signals from the power supply were connected to the two line inputs of the Nagra tape recorder via 50m coaxial cables. The microphones were left in place and attenuation measured at different times during the afternoon ie. 12.00, 13.00, 14.30 and 15.50. At each measurement time the lower microphone at C48 and the upper microphone at C72 were recorded simultaneously, followed by a simultaneous recording of the signal at the upper microphone at C48 and the lower at C72.

There was a cover of thin cloud for most of the day but it was bright and sunny for the 12.00 measurement. The temperature within the wood was between 16° and 17° C. There was no measurable wind within the wood.

Results

The results of the measurements made on this day are presented in full in Appendix B1 with best fit ground parameters in Appendix C1, summarised in table 6.2.5.

A first look at the results of the measurements at 48m indicate that these give much lower values of attenuation than the results from the C track on 5/7/84, whereas the 72m results are fairly similar. The 48m results give a much lower value of dB per 24m at 48m than 72m in direct contrast to the other results presented in this chapter. Since the recording equipment used at 48m was new and had not been fully tested, and similar problems were encountered with the results at Wetleys Wood on 16/5/85 using the same equipment, the results of attenuation at 48m have been ignored, although it is useful to note that the results obtained were similar for all measurement times.

Table 6.2.5: Summary of best fit ground parameters 20/6/85 (72m measurements only)

	Model		
	Homogeneous	Delany and Bazley	Rigid-Backed layer
σ_e			
max	130000	80000	130000
mean	108571	62857	117143
min	90000	50000	100000
mean difference			
max	2.74	2.93	2.61
mean	2.46	2.54	2.36
min	2.30	2.32	2.15
d_e			
max			0.080
mean			0.068
min			0.055

There is little difference between the attenuation spectra at the four different times (see figures 6.2.12 and 6.12.13). The measurement at 14.15 at the 1.2m microphone height shows some slight differences, with a slightly higher low frequency peak at a slightly higher frequency and a sharp dip at around 8kHz; but these differences are not considered to be significant since the 2.5m measurement is not different to the other times. The dip at 8kHz is

probably due to birdsong which would not necessarily occur in the 2.5m measurement since they were not recorded simultaneously. All the results have a sharp peak at about 9kHz, which has the same magnitude in all the 2.5m measurements but at 1.2m is slightly higher in the 12.00 measurement than those at the other times. Ground interference peaks would be expected to occur at about 7kHz and 14kHz for the 1.2m height and about 6.3kHz and 12.6kHz for the 2.5 measurement so it is unlikely that this peak is a result of the ground interference pattern. If a strong temperature gradient (therefore sound velocity gradient) caused a shift in these peaks they would still be expected to be at different frequencies at the two microphone heights, and also at different frequencies at the different times since a strong temperature gradient would be expected to change significantly throughout the course of a summer afternoon. The high frequency peak is probably a result of the background noise or an inaccuracy in the measurement since the sound levels recorded at such high frequencies are very low and approach the levels of the background noise.

The spread of results is greater in the 2.5m than the 1.2m result at the low frequencies, this is not reflected in the best fit ground parameters which are fairly similar for all the measurements.

The 2.5m microphone height measurement again gives a lower attenuation to that at 1.2m, the difference is small but consistent throughout the measurements.

Comparison Between Results Obtained At Hazelborough Wood On Different Days.

Comparisons of the measurements made within the wood show that the 10/8/83 measurements are very similar to those of 5/7/84 at low and mid frequencies, but have a consistently lower attenuation at high frequencies for all the measurements (eg figures 6.2.14 and 6.2.15). Thus the results obtained within the wood in the summer have a wide range of values at high frequencies. It is possible that there was a significant increase in attenuation caused by growth of the understorey shrubs between the two sets of measurements, a period of about a year. This is not, however, matched by a similar increase in attenuating

capacity of the woodland in the year between the measurements of summer 1984 and the measurement of 20/6/85 (see figure 6.2.16).

Figures 6.2.17 and 6.2.18 show examples of the comparison between the measurements made within the wood and those made at the edge ie on the 9/8/84. There is no significant difference between the measurement on this day and those made on 5/7/84 within the wood. Thus the dense vegetation at the edge of the wood does not appear to increase the high frequency attenuation significantly.

Figures 6.2.19 to 6.2.21 show the comparisons between the measurements made in this woodland in summer and 'winter' (10/4/84) when there were no leaves on the understorey. The high and mid frequency part of the winter measurement are lower than the summer measurements for both microphone heights at 72m, at 48m this difference is less marked as the winter measurement overlaps that of 10/8/83 at some frequencies, and at 24m there is no significant difference between the summer and winter measurements at high frequencies. This result suggests that the foliage of the shrub layer does have some attenuating effect but this would be difficult to quantify since it appears to only be significant at long distances, and the spread of the measurements with foliage is comparatively large.

The winter measurements of 10/4/84 have a different frequency dependence of the low frequency part at all distances, this is reflected in the different best fit values. The measurement of 20/6/85 has a frequency dependence similar to the measurement of 10/4/84. T-tests were carried out on the data using the FORTRAN program TTEST (see Appendix A) to determine whether the mean best fit effective flow resistivities obtained on different days are significantly different. The results can be divided in to two different groups, the mean values of 5/7/84, 9/8/84 and 10/8/83 are significantly lower at the 0.1% level, than both the mean values of 10/4/84 and 20/6/85. The three low means (5/7/84, 9/8/84 and 10/8/83) and the two higher means (10/4/84 and 20/6/85) are not significantly different at the 5% level. It is likely that this difference was caused by differences in the moisture content of the ground surface, which would have been higher on 10/4/84 and 20/6/85 than the other measurements which were made during long dry periods. The flow resistivity of a soil would be expected to increase with increased moisture content as indicated here.

Another explanation for the differences, especially at the high frequencies, could be differences in the meteorological effects of the different days; although the conditions on all the measurement days were similar. The measurements made on 20/6/85 suggest that the received signal does not vary significantly within the course of a summer afternoon, the time when most of the measurements were made.

Since the values of dB per 24m calculated from the 48m and 72m measurements are not significantly different, the mean values for all the 48m and 72m measurements on each day have been averaged for comparison between the different days. Figure 6.2.22 shows the results. The different days' results are similar at frequencies below about 3.5kHz with no single result being consistently higher or lower than the others, except perhaps that the 10/4/84 measurement is below the rest, above 1.6kHz. The results diverge above 3.5kHz with the results for 10/8/83 and 10/4/84 being lower than the other three. The result for 20/6/85 is consistently lower than that of 5/7/84 for frequencies above 4.3kHz, with that of 9/8/84 being close to either of these two at different frequencies. It should be noted that the three higher results come from different measuring tracks.

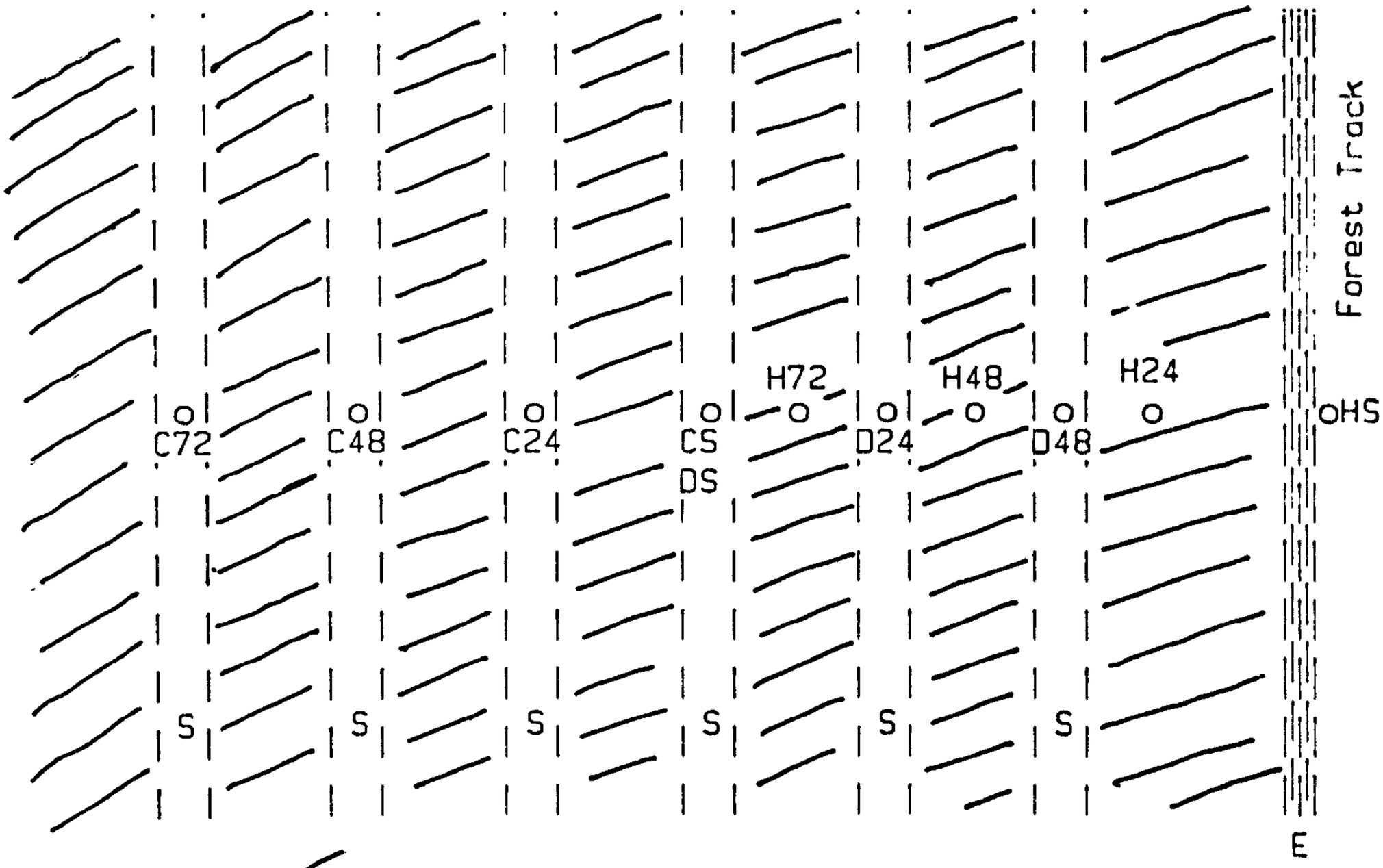

Figure 6.2.1
Layout of Marked Locations at Hazelborough Wood.

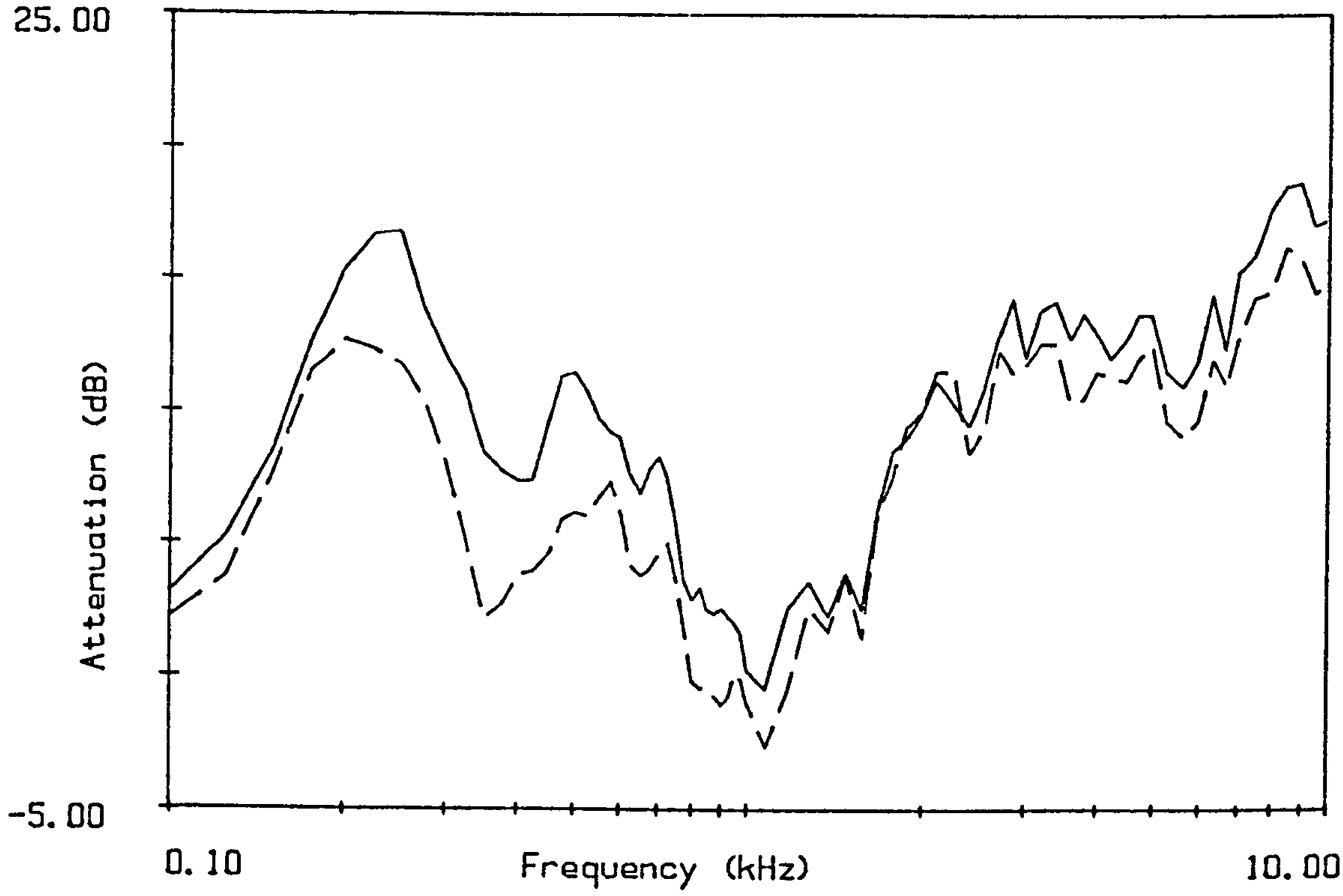

Figure 6.2.2
Attenuation at C72 on 10/8/83
Microphone heights 1.2m and 2.5m (----)

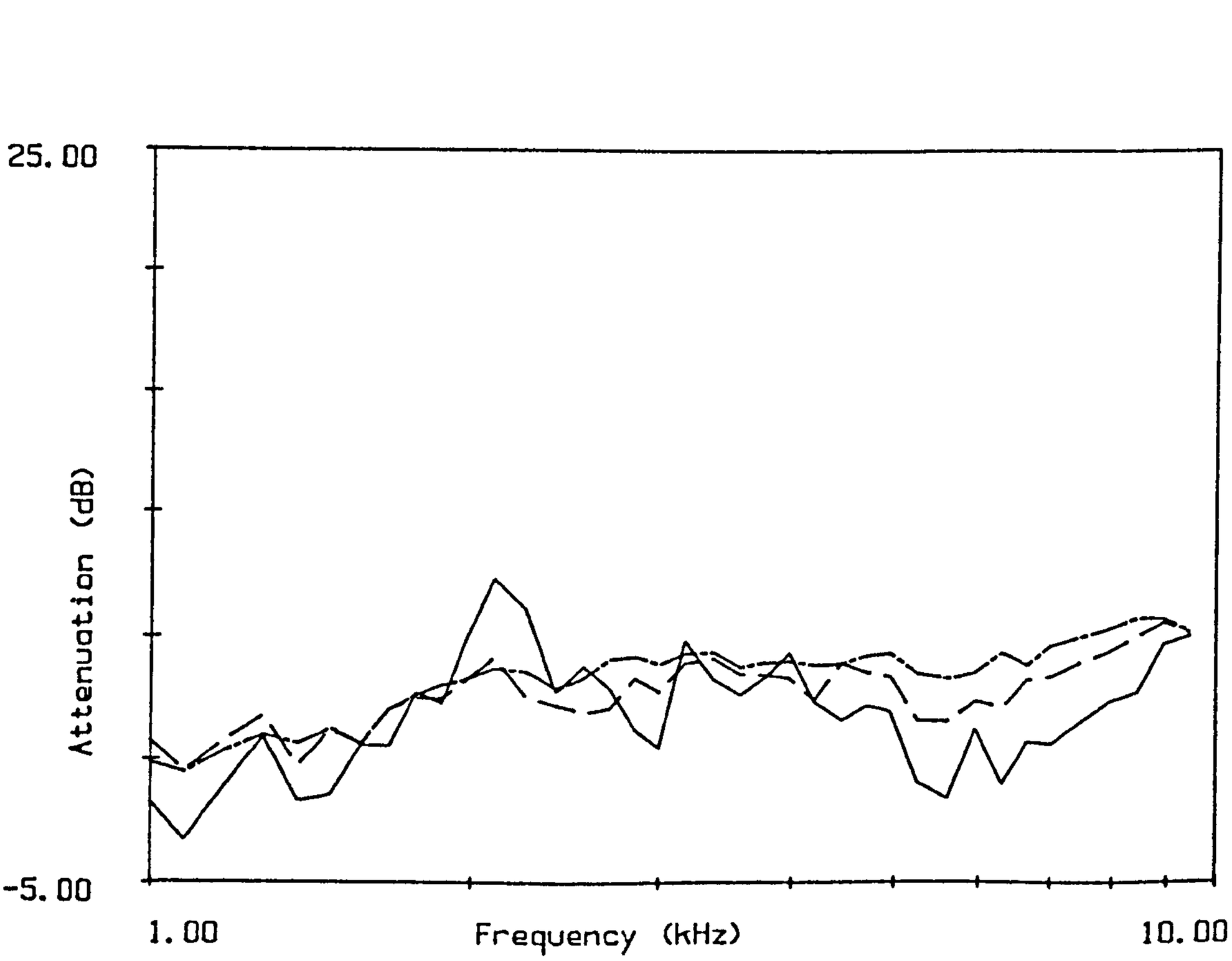

Figure 6.2.3
Mean value of dB per 24m for the measurements on 10/8/83
at ——— 24m, — — · 48m, and —·——·— 72m.

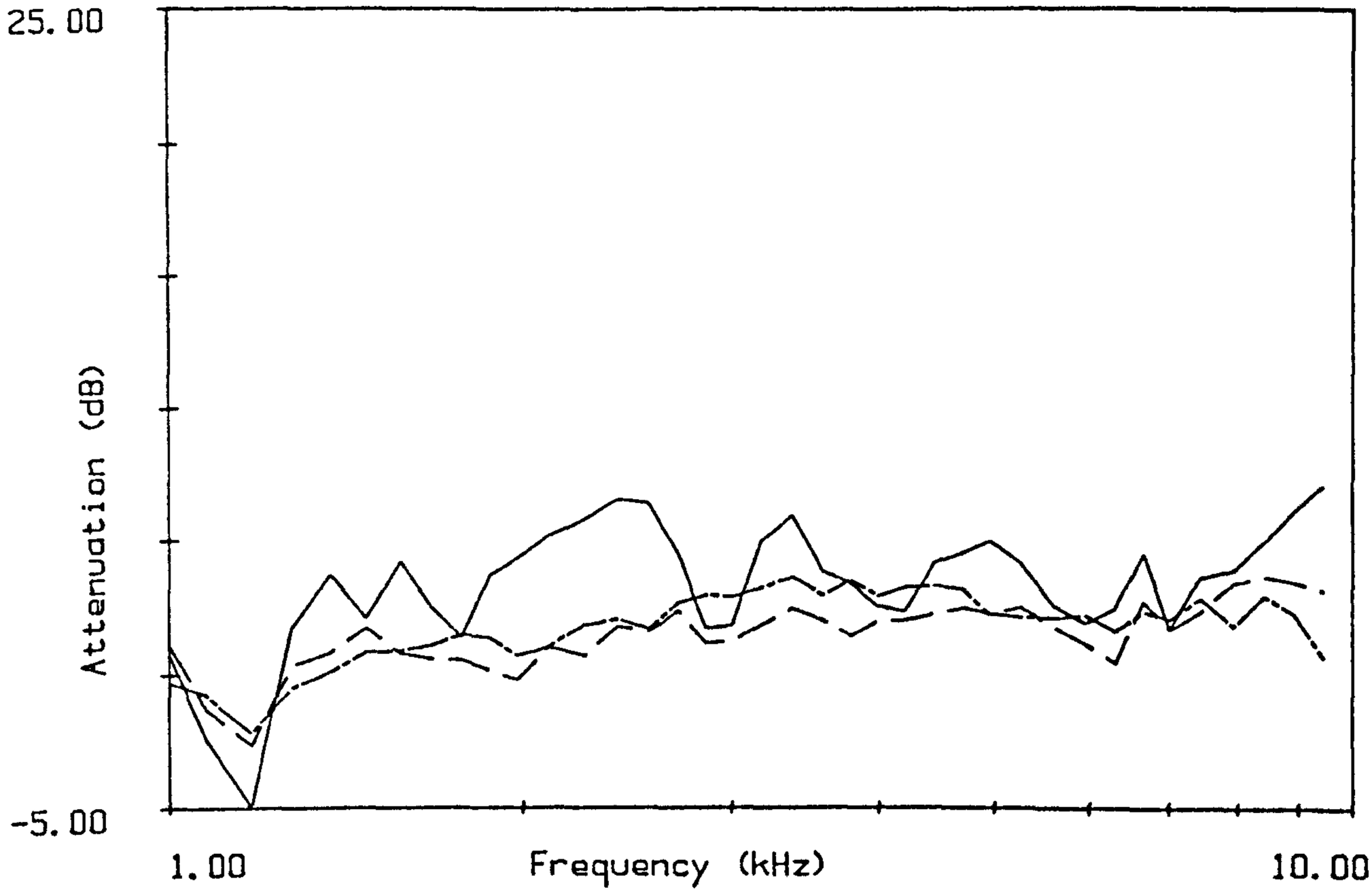

Figure 6.2.4
Mean value of dB per 24m for the measurements on 10/4/84
at ——— 24m, — — · 48m, and ——·——·— 72m.

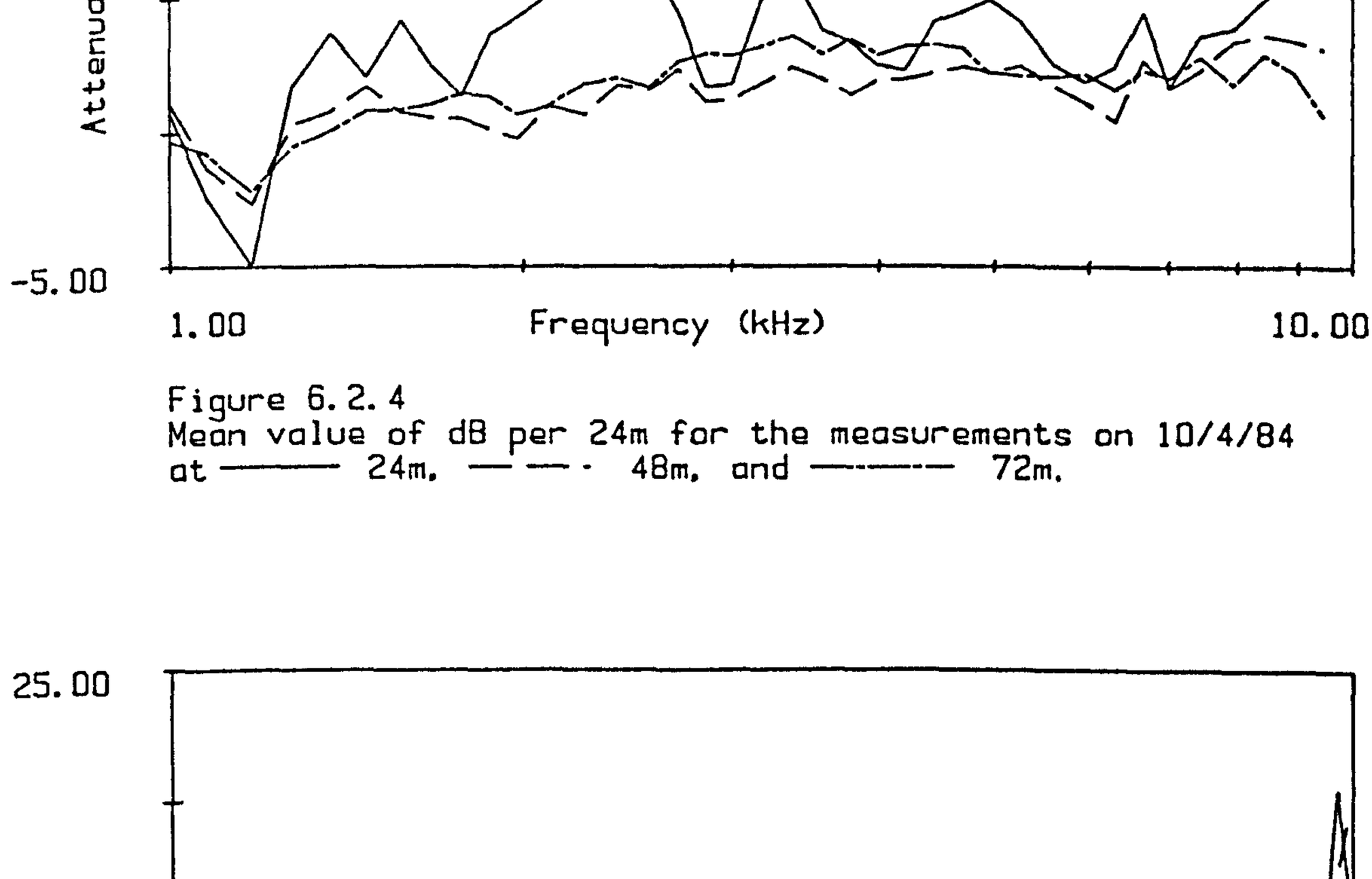

Figure 6.2.5
Attenuation at 24m, microphone height 1.2m, 5/7/84.
——— track C; — — — - track D.

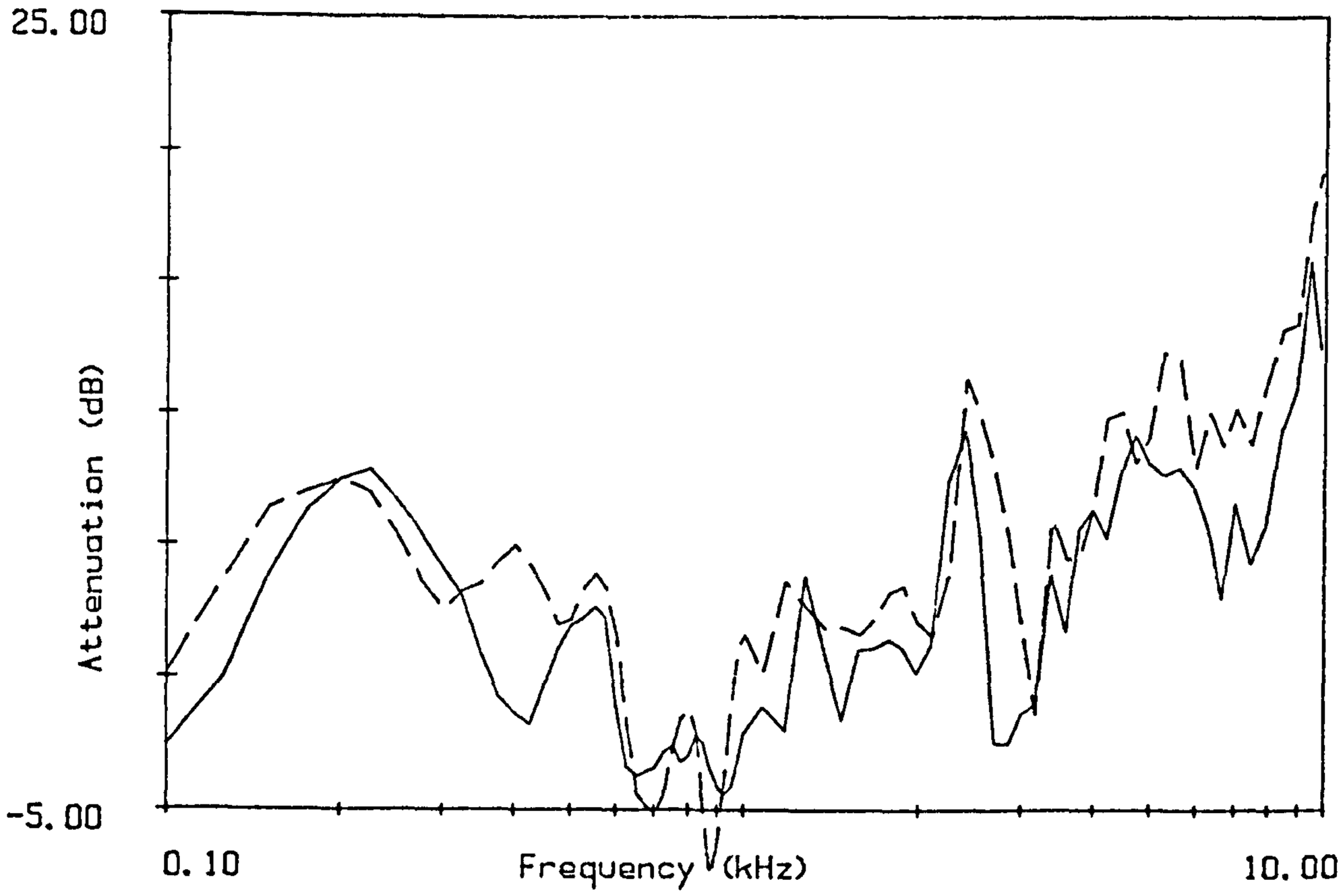

Figure 6.2.6
Attenuation at 24m, microphone height 2.5m, 5/7/84.
———— track C; — — — - track D.

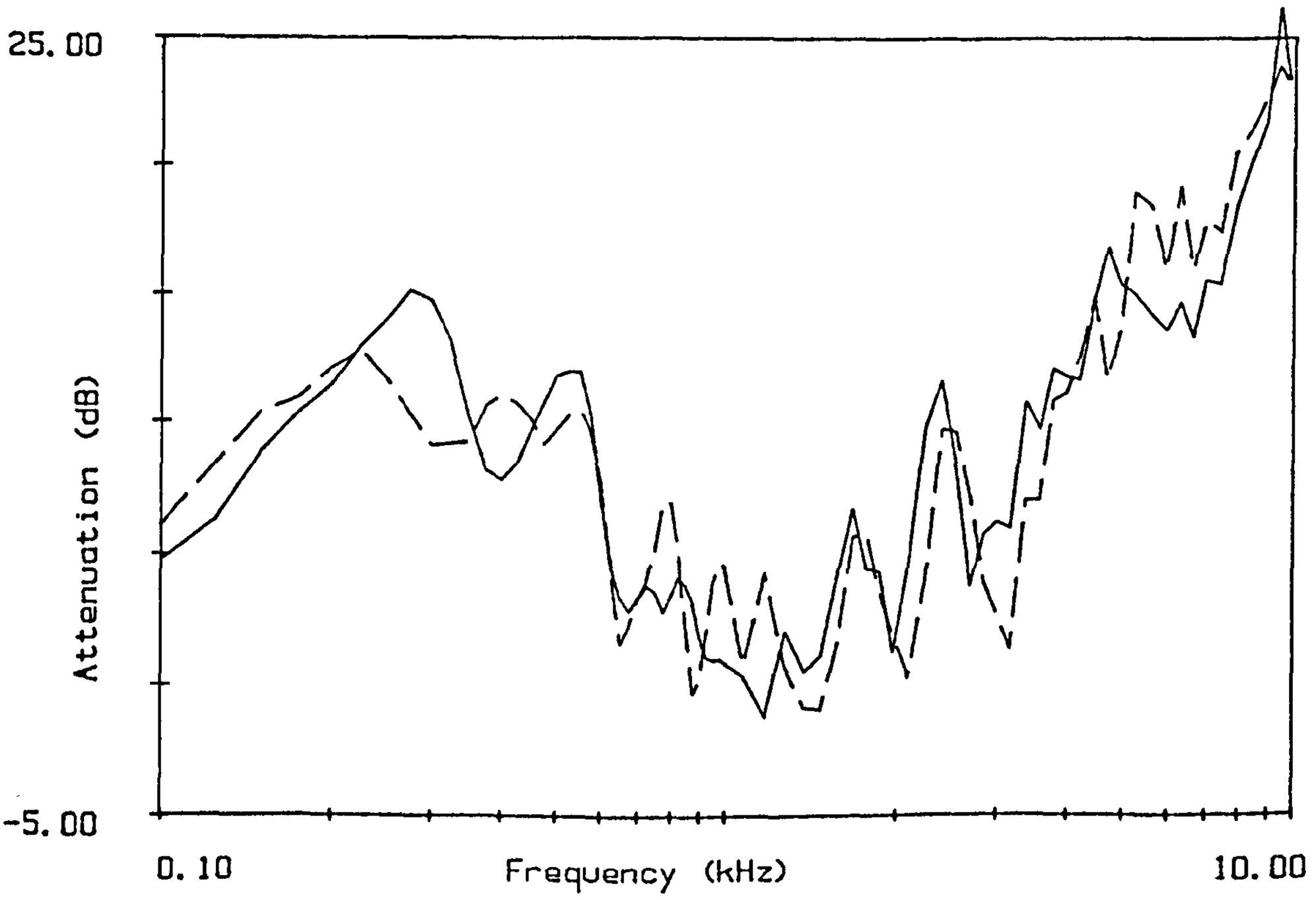

Figure 6.2.7
Attenuation at 48m, microphone height 1.2m, 5/7/84.
———— track C; — — — - track D.

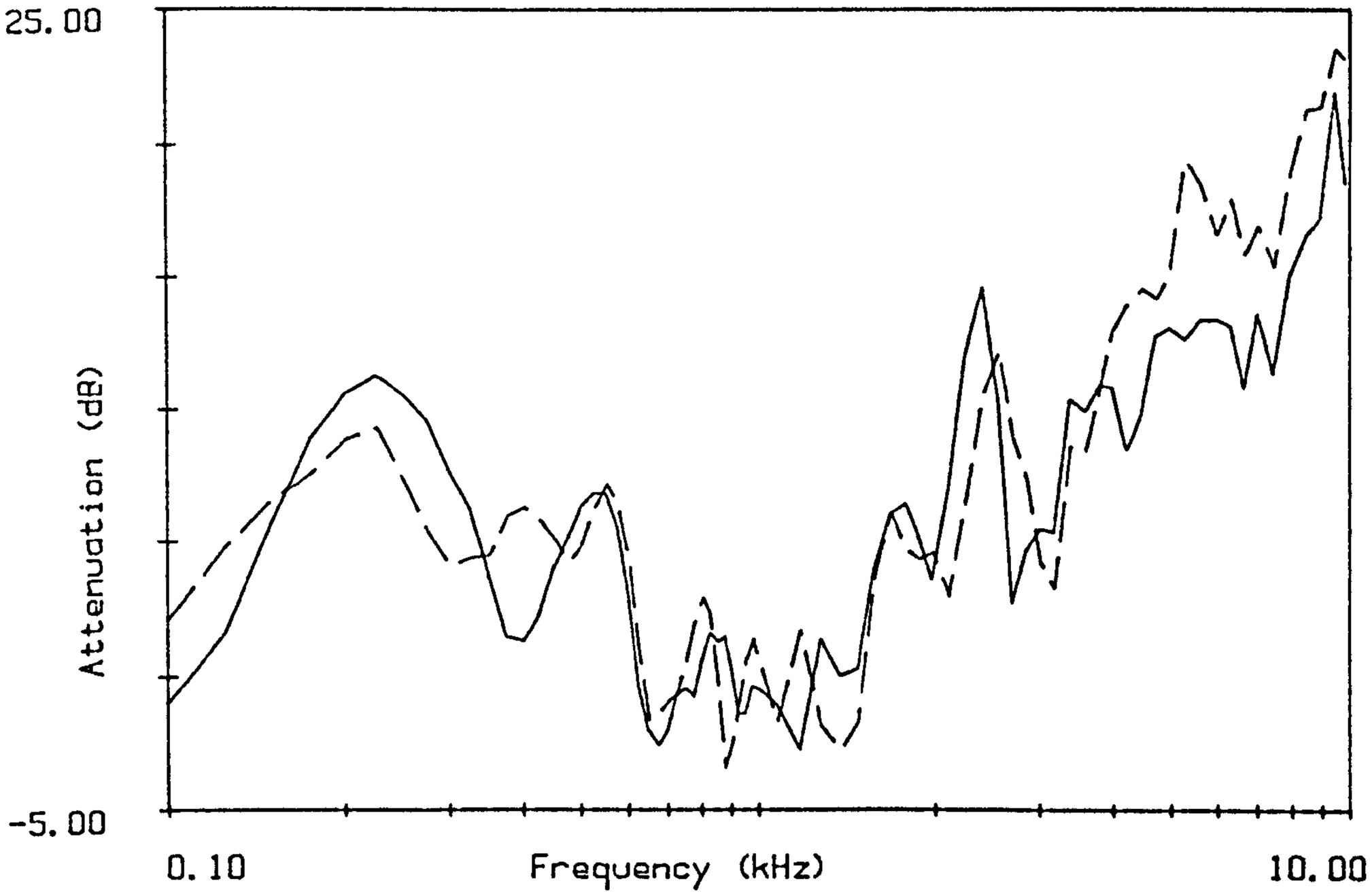

Figure 6.2.8
Attenuation at 48m, microphone height 2.5m, 5/7/84.
———— track C; — — — - track D.

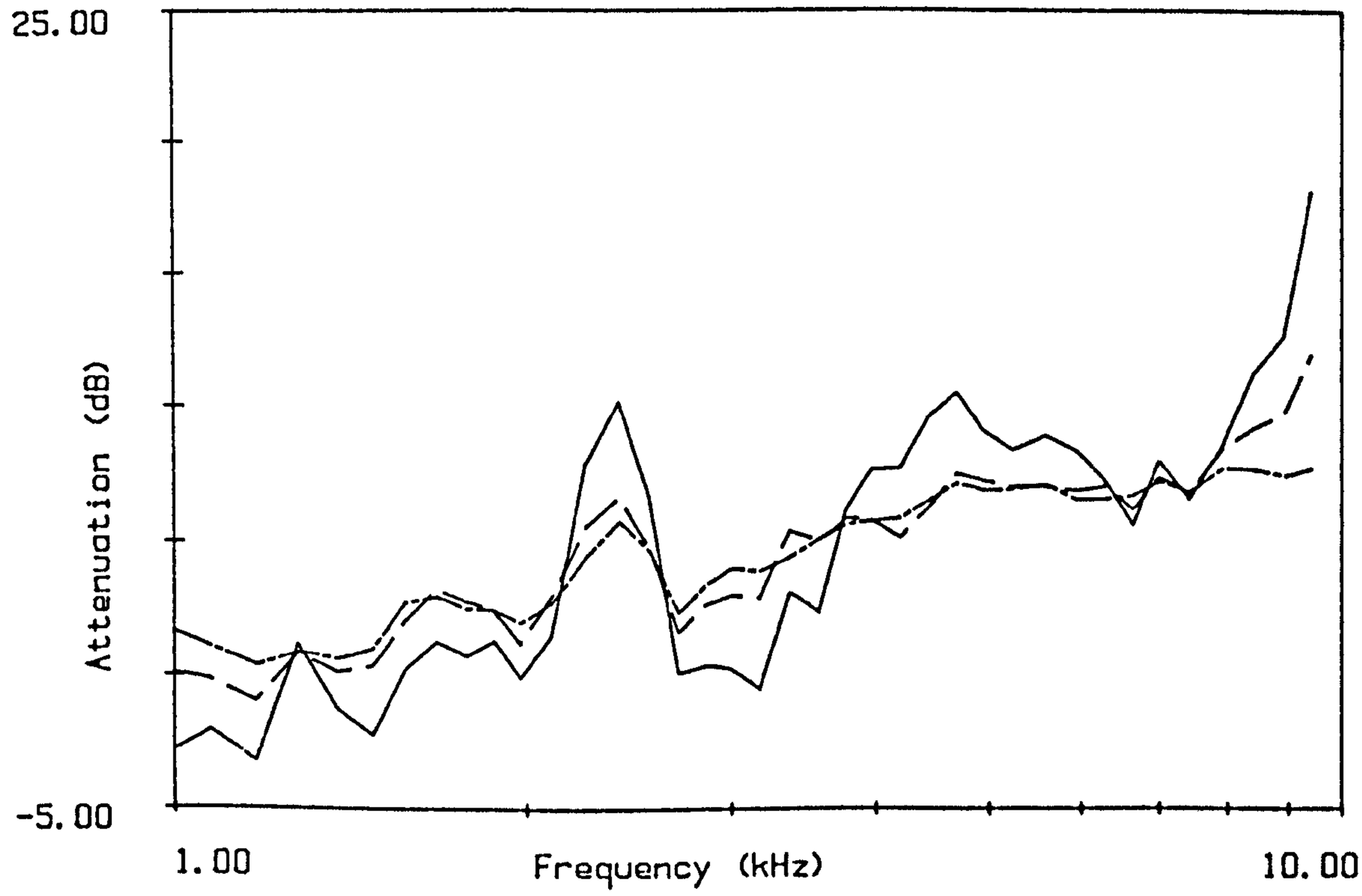

Figure 6.2.9
Mean value of dB per 24m for the C track measurements on 5/7/84
at ———— 24m, — — · 48m, and —·——·— 72m.

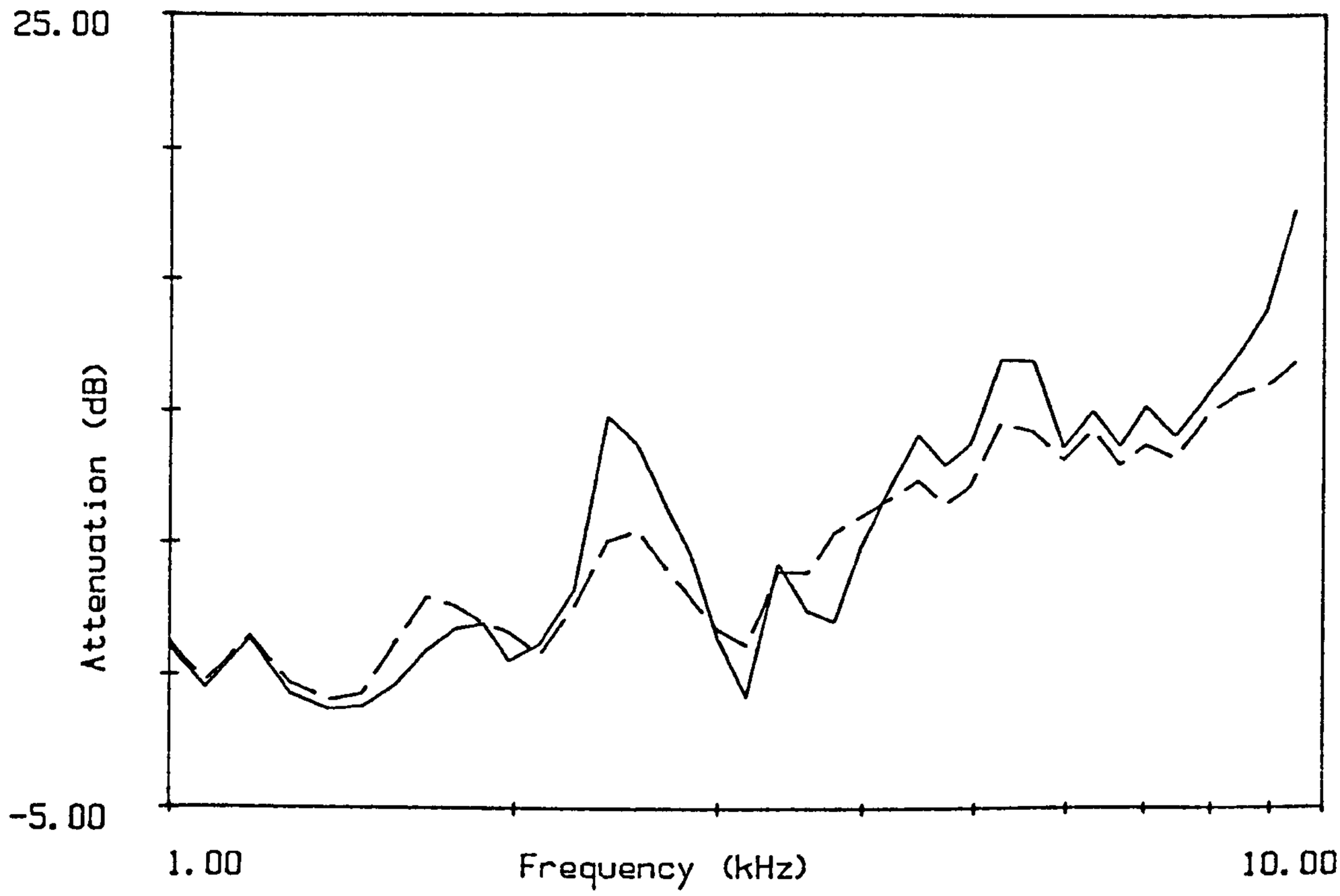

Figure 6.2.10
Mean value of dB per 24m for the D track measurements on 5/7/84
at ——— 24m, — — · 48m.

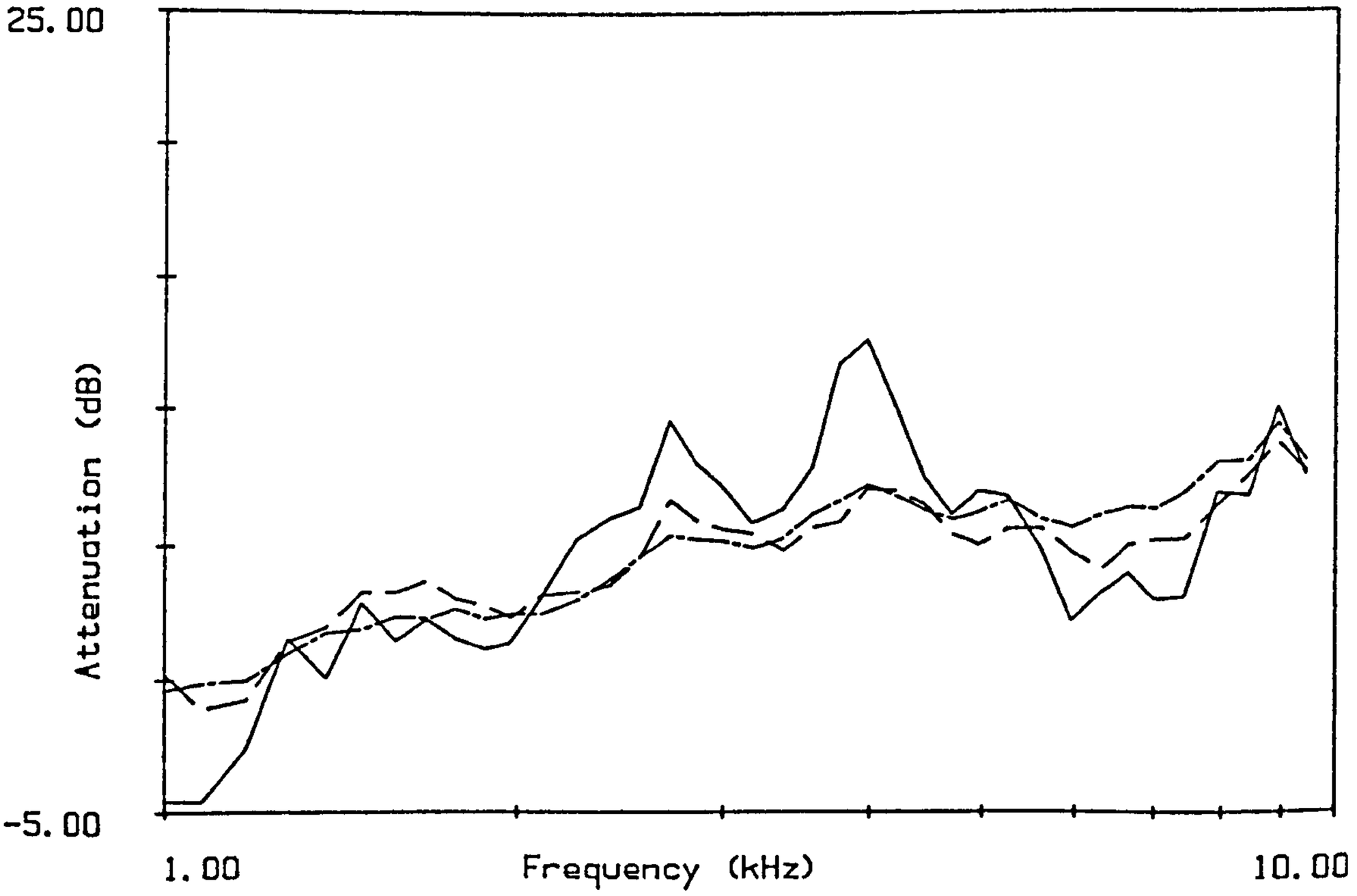

Figure 6.2.11
Mean value of dB per 24m for the measurements on 9/8/84
at ——— 24m, — — · 48m, and ——— 72m.

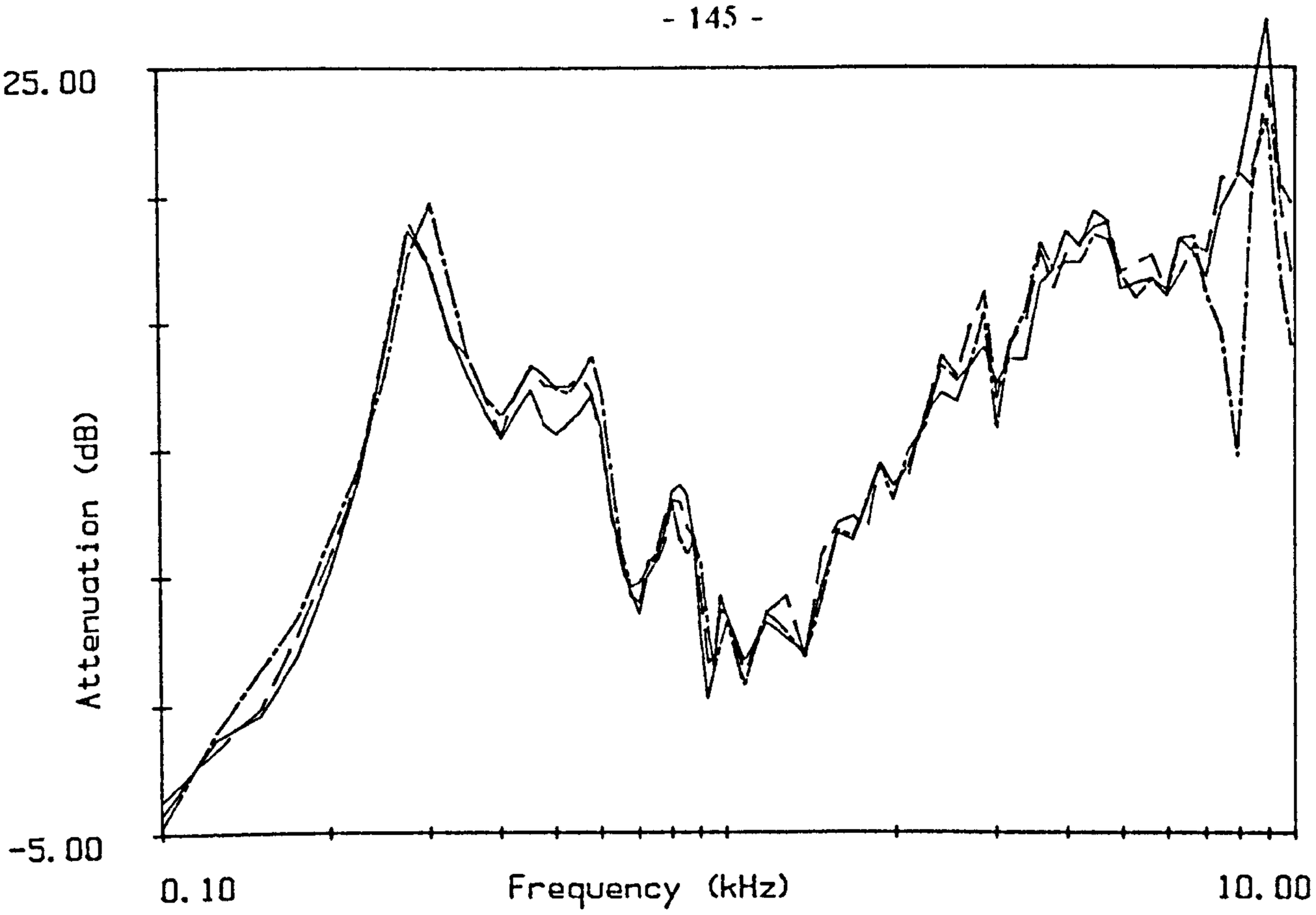

Figure 6.2.12
Measurements at C72 at different times on 20/6/85, 1.2m height.
———— 12.00, — — — 13.00, ———·——— 14.30

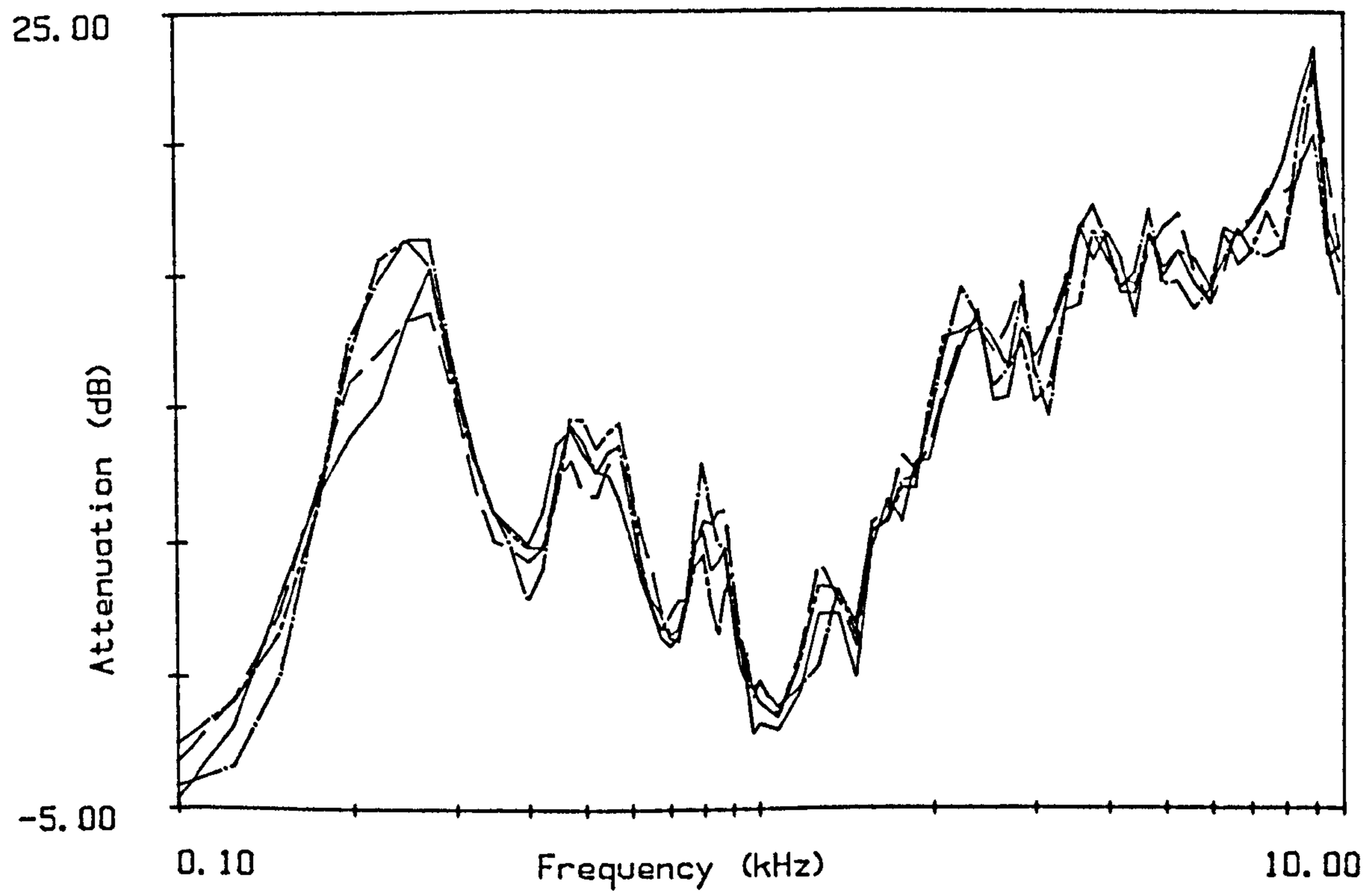

Figure 6.2.13
Measurements at C72 at different times on 20/6/85, 2.5m height.
———— 12.00, — — — 13.00, ———·——— 14.30, ———··——— 15.50

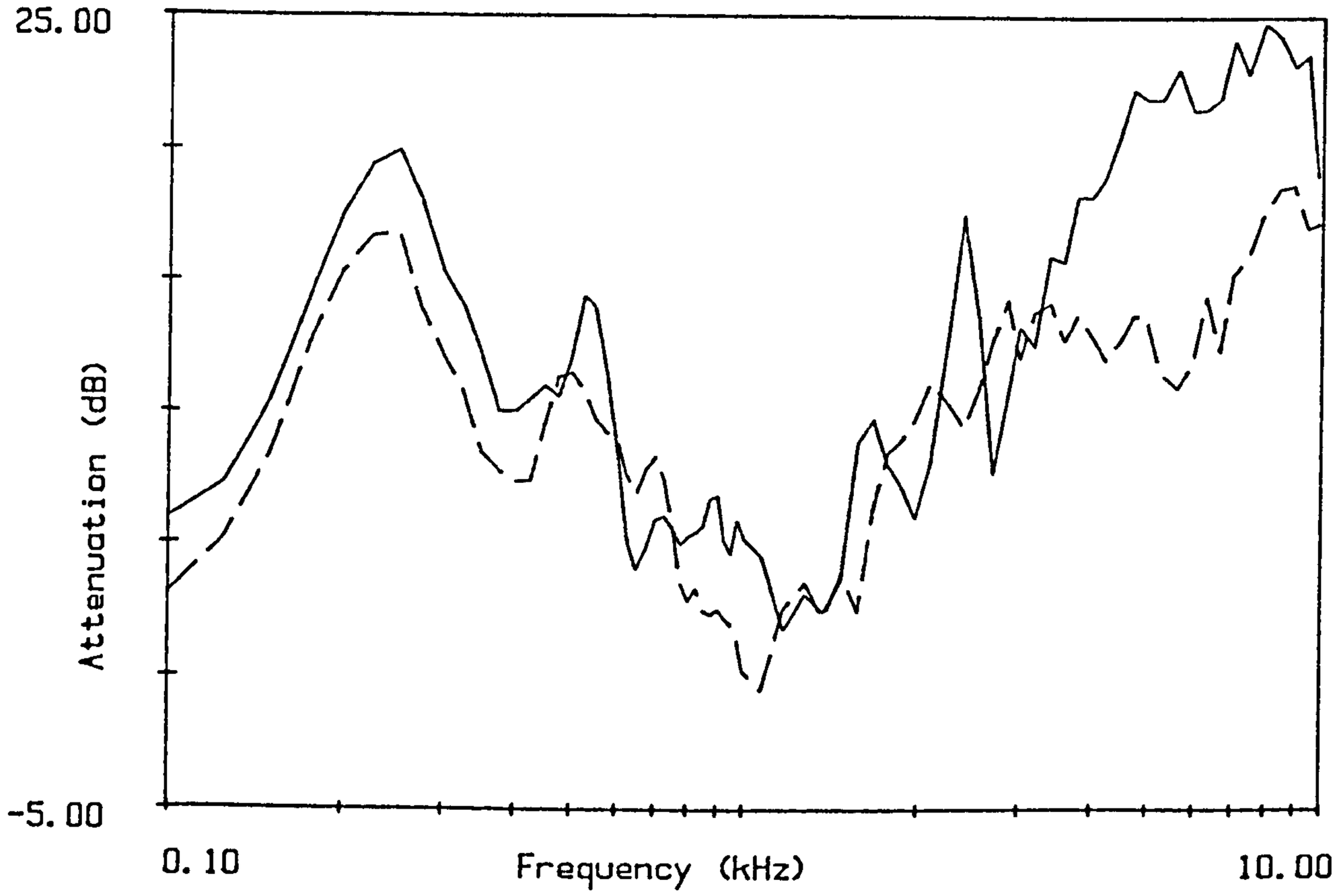

Figure 6.2.14
Measurements made at C72, 1.2m height,
on 5/7/84 and 10/8/83 (------)

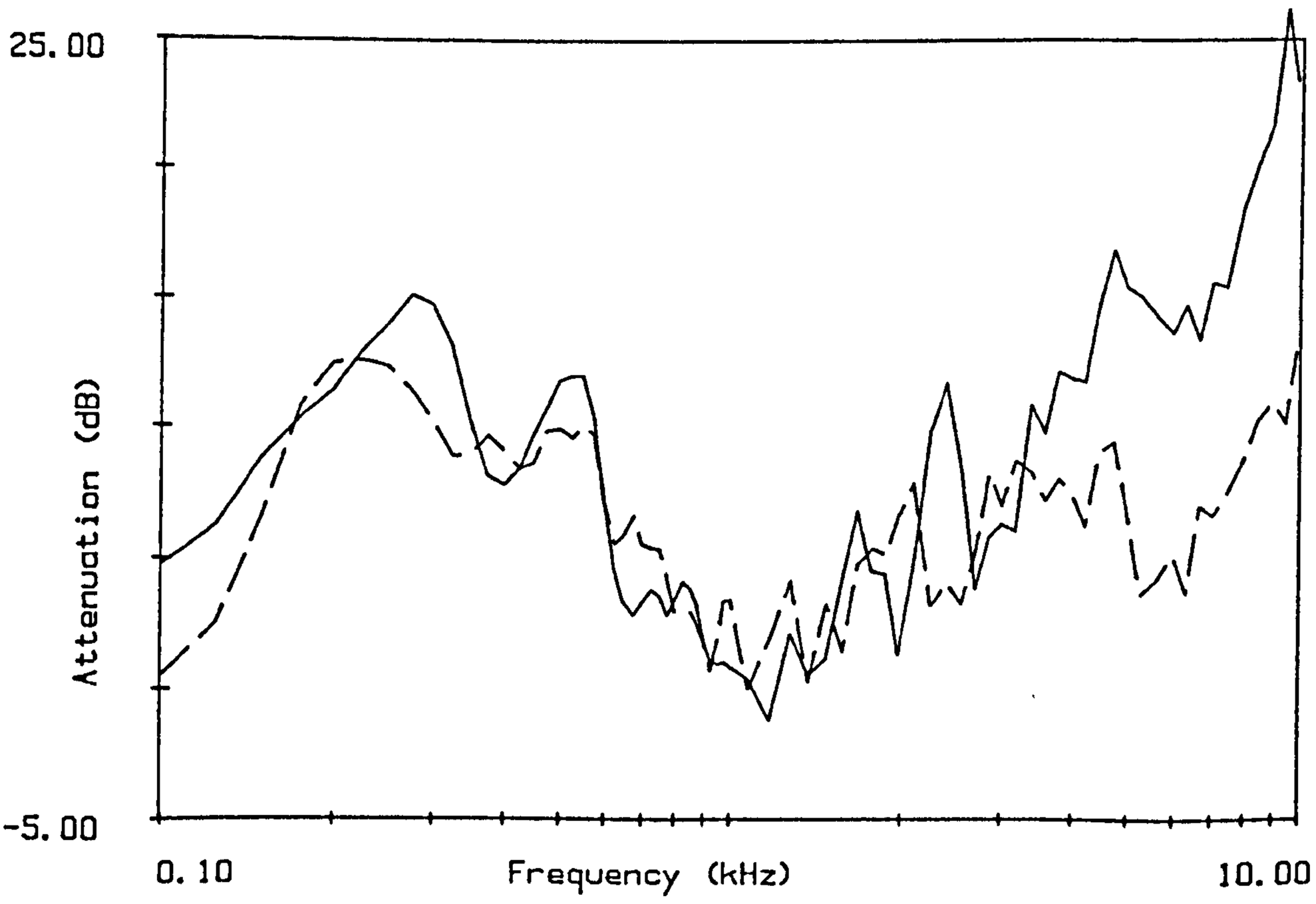

Figure 6.2.15
Measurements made at C48, 1.2m height,
on 5/7/84 and 10/8/83 (------)

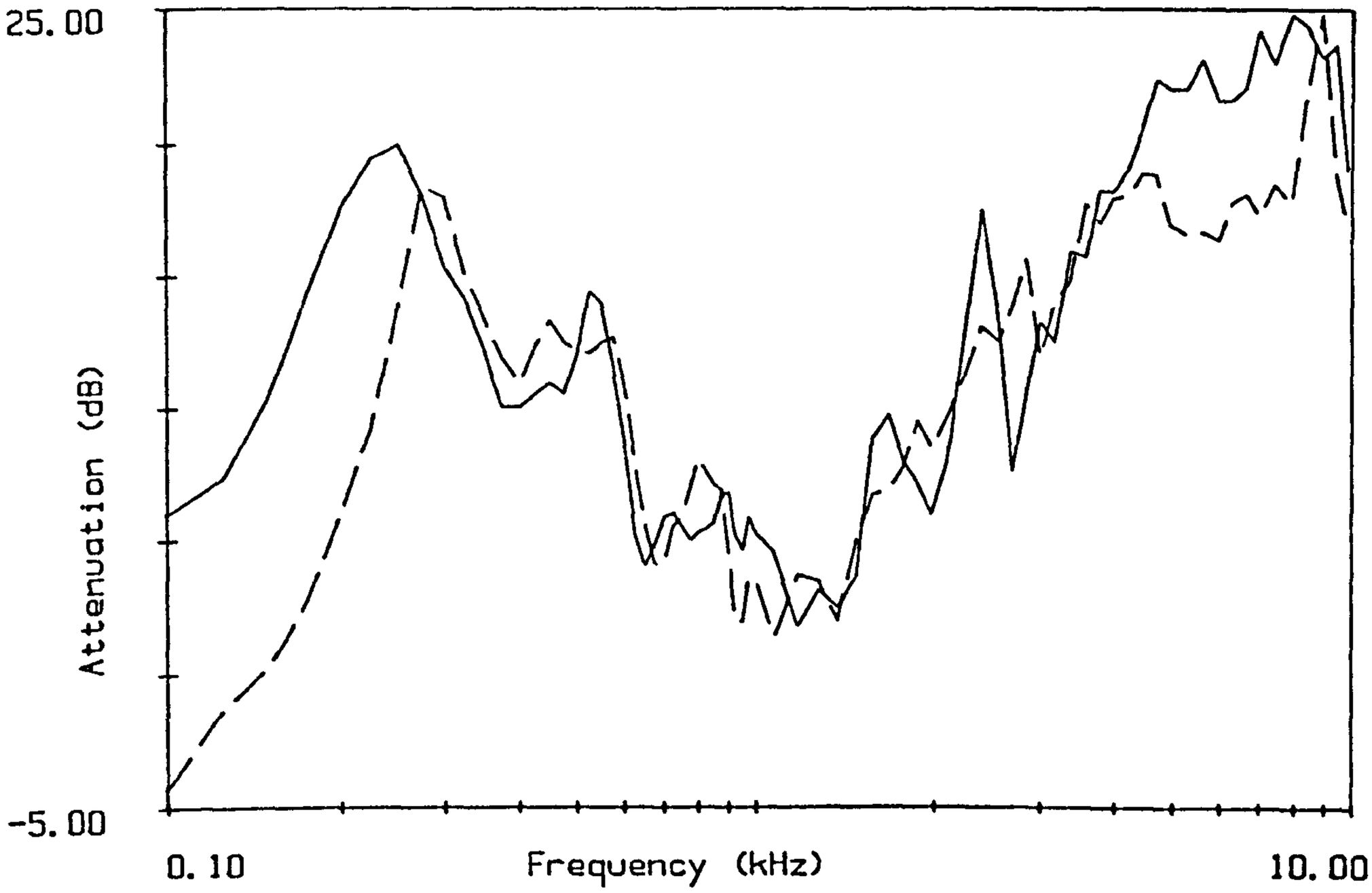

Figure 6.2.16
Measurements made at C72, 1.2m height,
on 5/7/84 and 20/6/85 (------) (mean value for all measurements).

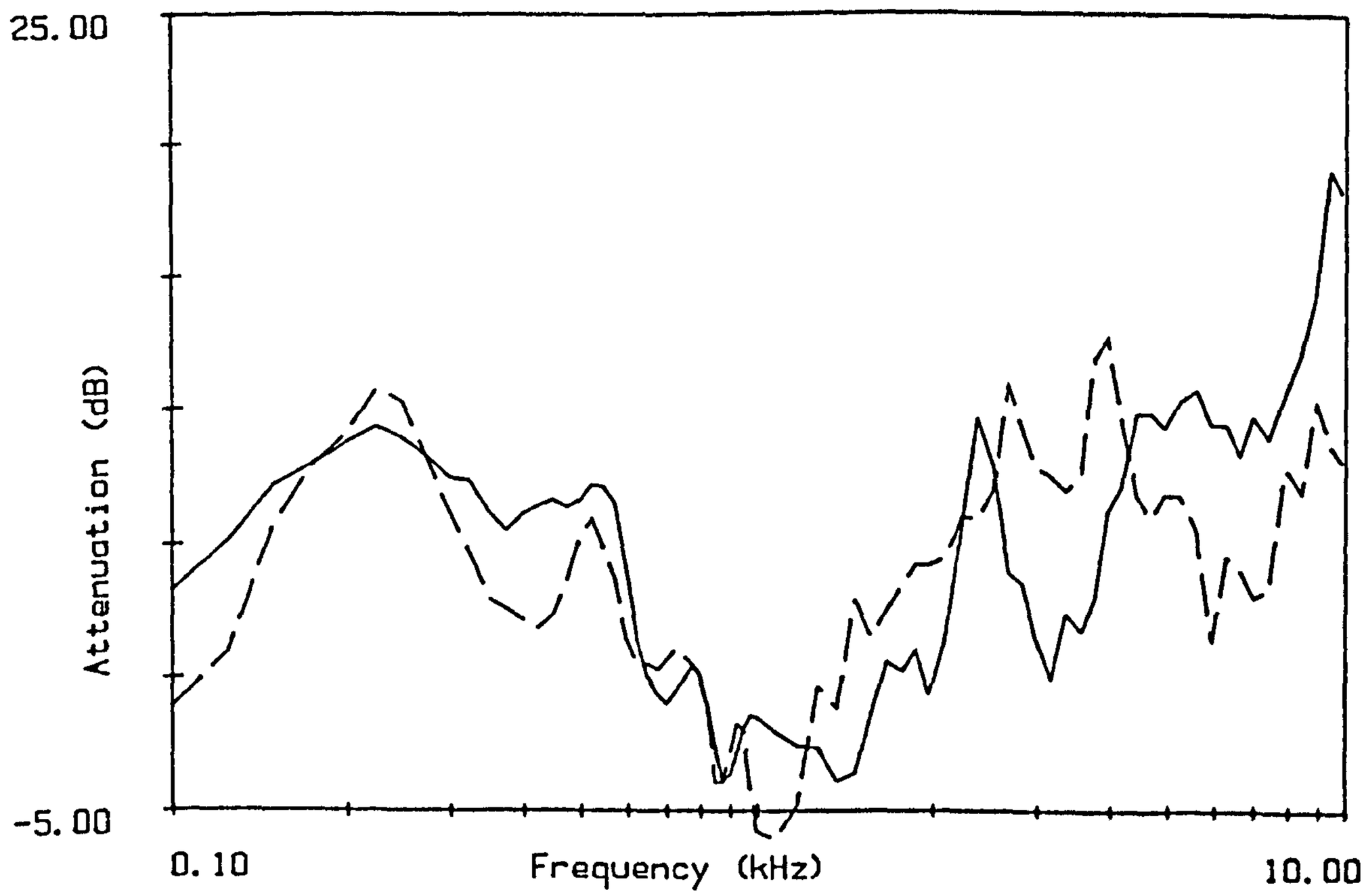

Figure 6.2.17
Measurements made at C24, 1.2m height,
on 5/7/84 and 9/8/84 (------).

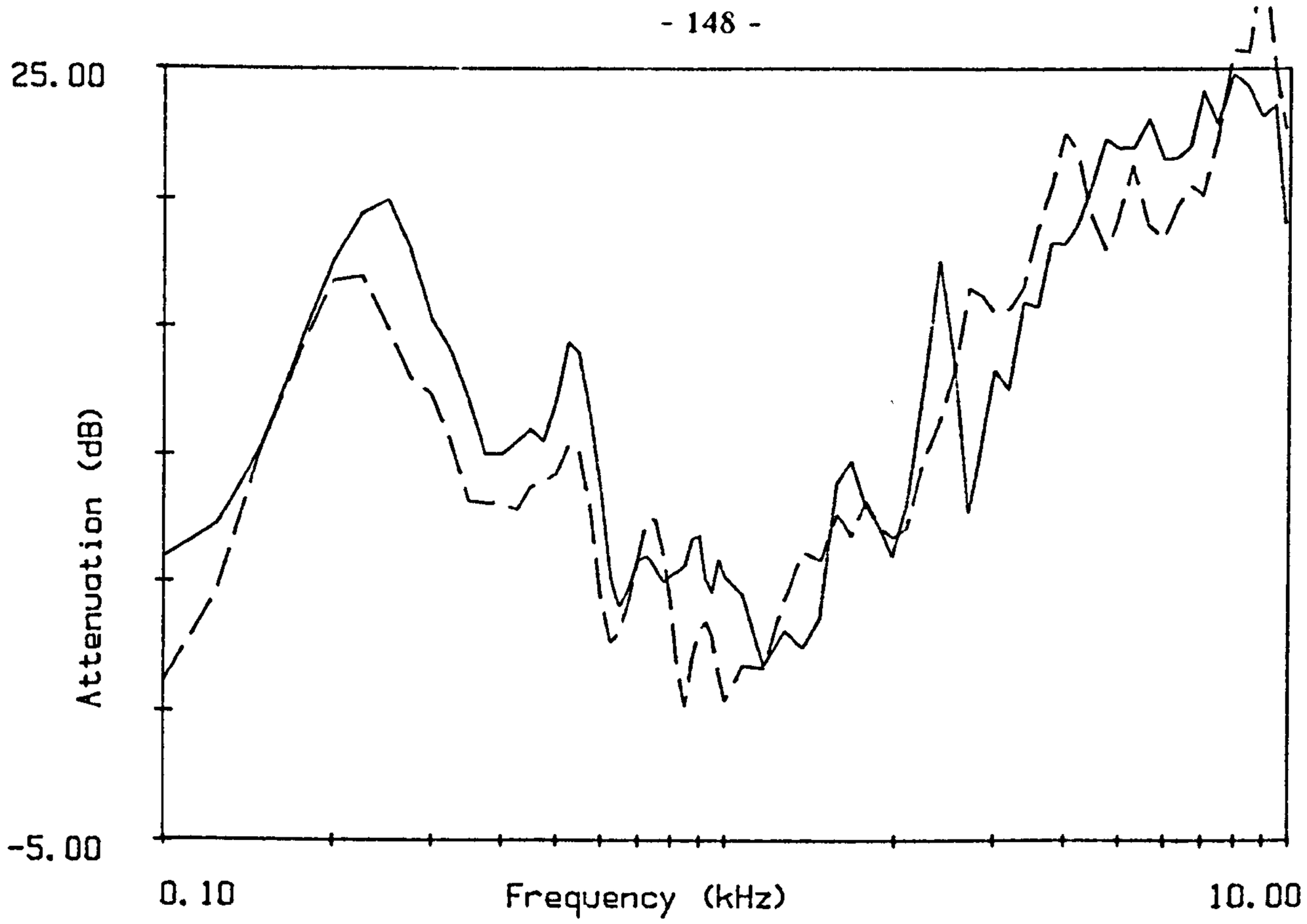

Figure 6.2.18
Measurements made at C72. 1.2m height.
on 5/7/84 and 9/8/84 (------).

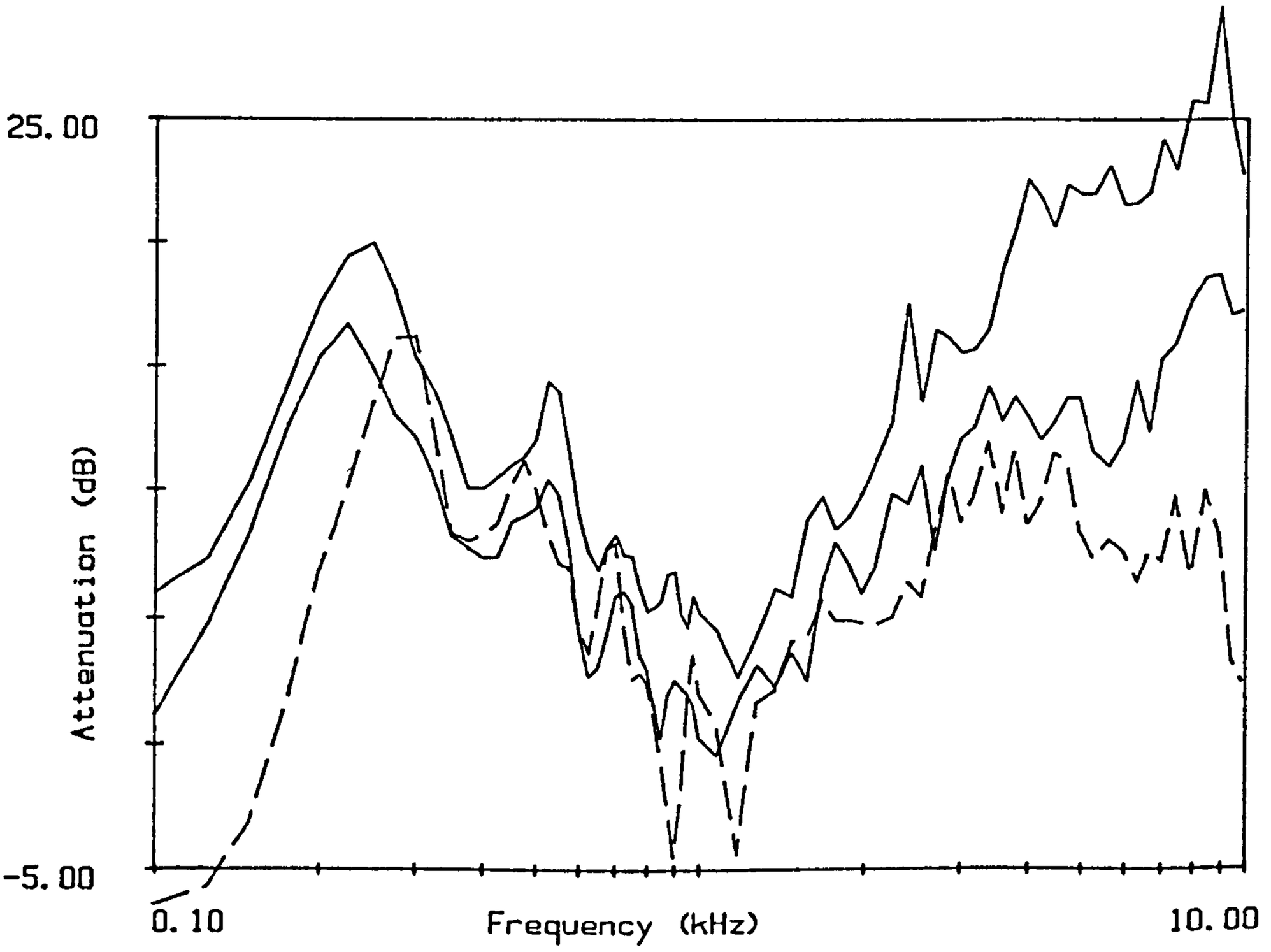

Figure 6.2.19
Maximum and minimum values of the summer measurements made on 10/8/83, 5/7/84 and 9/8/84. 72m separation, 1.2m microphone height. and winter measurement made on 10/4/84, same geometry (-----).

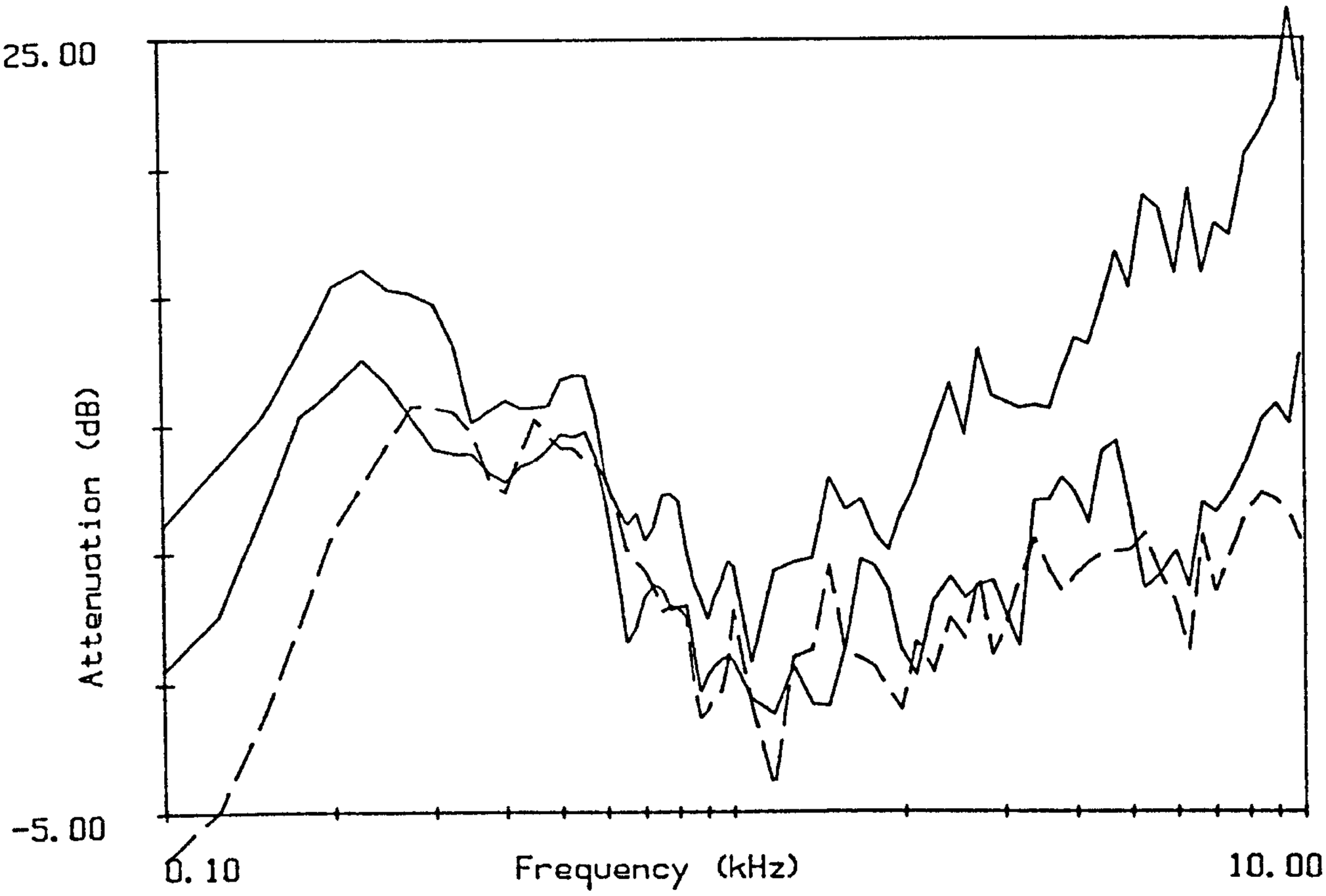

Figure 6.2.20
Maximum and minimum values of the summer measurements made on 10/8/83, 5/7/84 and 9/8/84. 48m separation, 1.2m microphone height. and winter measurement made on 10/4/84, same geometry (-----).

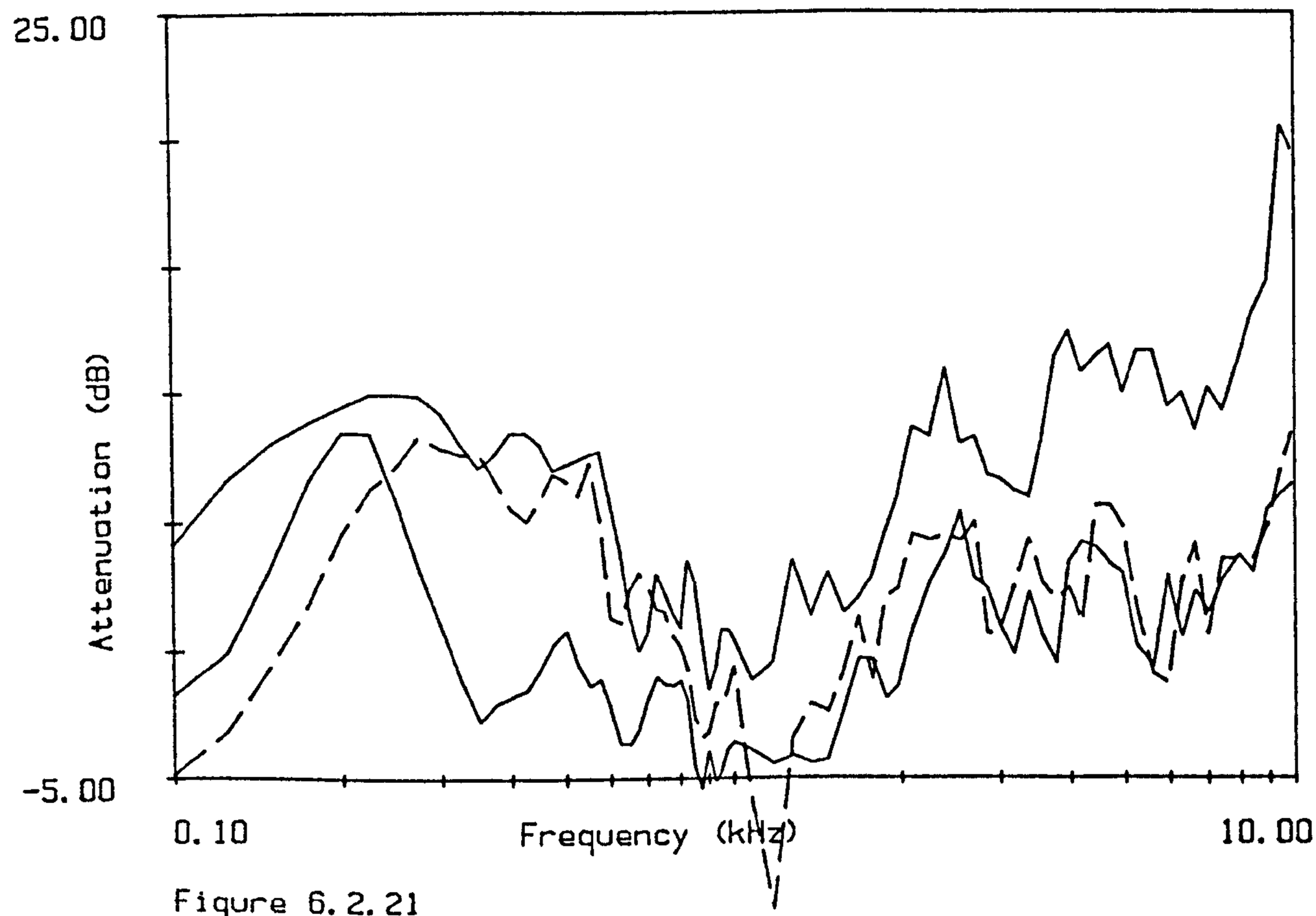

Figure 6.2.21
Maximum and minimum values of the summer measurements made on 10/8/83, 5/7/84 and 9/8/84. 24m separation, 1.2m microphone height and winter measurement made on 10/4/84, same geometry (-----).

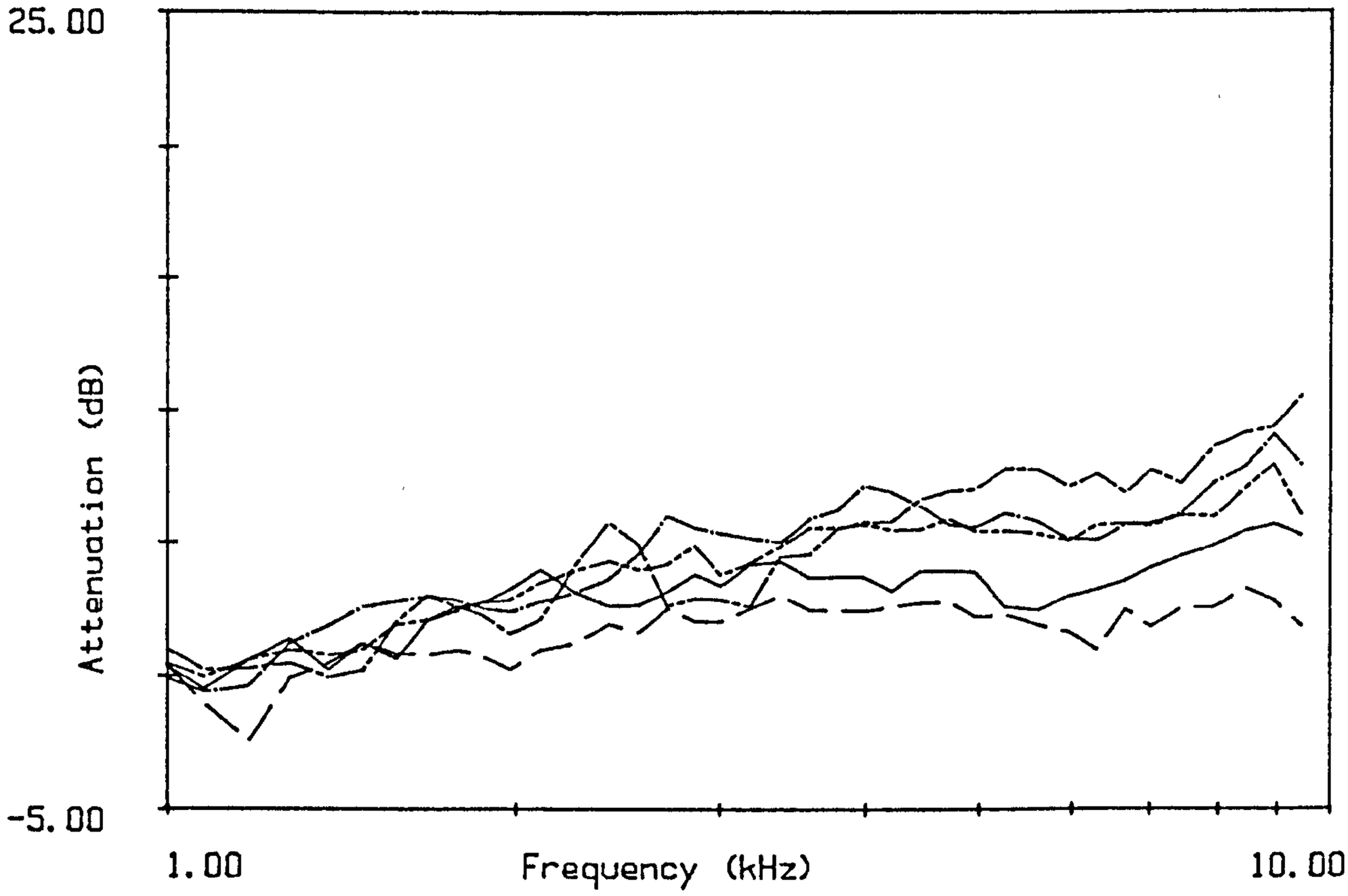

Figure 6.2.22
Mean value of dB/24m for all the measurements on:
——— 10/8/83, — — · 10/4/84, ——·—· 5/7/84
——·—·— 9/8/84, —·—·—·— 20/6/85.

6.3 Measurements made in a Spruce Monoculture Stand.

Compartment 60 'Wetleys Wood'

This compartment consists of Norway Spruce planted in 1954. The original planting was of three rows of spruce with one or two rows of oak in between. The oak trees were, however, sprayed to kill them off while still small and only remnants of these rows remain as a few small spindly trees within a spruce stand. The trees are about 11-13m tall (trees measured are at the edge but the height of the trees appears to be fairly uniform throughout the stand). The sampled stem density is 0.303 stems m^{-2} and the mean radius 0.059m. The spruce trees have no living branches below about 4m but the dead branches are still attached to the trunk giving a dense layer of dead branches which impede visibility. There are gaps between the rows of spruce where the oak used to be with little or no vegetation, living or dead, at the lower levels; the living spruce branches do, however, spread over the top of these gaps excluding light from the ground, thereby preventing the development of any undergrowth. The ground surface is covered in a thick layer of spruce needles in various stages of decomposition. This compartment was thinned during the winter of 1983-84.

Two 'measuring tracks' were laid out within Wetleys Wood these are designated track A and track B, as illustrated in figure 6.3.1. The source position was the same for both tracks being situated within one of the cleared (formerly oak) rows for ease of access. Microphone positions were marked with wooden posts at various distances from the source position i.e. 12m (positions A12 and B12), 24m(A24 and B24), 48m(A48 and B48) and 96m(A96 and B96). All the A positions were in a straight line running diagonally across the line of the tree rows at an angle of about 60° and the B track in a straight line at an angle of approximately 30° from it i.e. approximately 90° to the line of the trees.

Three main sets of measurements were made at this site; on 28/7/83, 26/6/84 and 16/5/85.

Measurements made on 28/7/83.

On the 28th of July 1983 two measurements were made at each of the measuring positions of the A track displacing the microphones slightly to one side between the measurements. The weather was warm (21° C) with a relative humidity of 64%. The wind, measured in a slight clearing in the wood did not exceed 1.5m/s. There were a few drifting clouds but it was mostly sunny. The ground was dry.

The results of the measurements made on this day are presented in Appendix B2 with the best fit ground parameters in Appendix C2 and summarised in table 6.3.1.

Table 6.3.1: Summary of best fit ground parameters 28/7/83

	Model		
	Homogeneous	Delany and Bazley	Rigid-Backed layer
σ_e			
max	58000	35000	60000
mean	38125	26125	45000
min	29000	20000	30000
mean difference			
max	4.82	3.99	5.05
mean	2.92	2.66	2.87
min	1.73	1.35	1.77
d_e			
max			0.175
mean			0.116
min			0.080

The 12m measurements give rather higher effective flow resistivities than the measurements at the other distances which all give similar, low, values of σ_e. Five of the eight measurements made indicate that the best fit parameters for the rigid-backed layer model are semi-infinite cases, and the other three have large values of d_e, and values of σ_e similar to the homogeneous model best fits indicating a homogeneous medium. The variable porosity model also indicates a homogeneous medium ie $\alpha_e = 0$

The 1.2m and 2.5m measurements are generally similar at high frequencies apart from the differences caused by the interference patterns, which are apparent in the 12, 24 and 48m measurements. The location of the peaks of the interference patterns in the two shorter distances coincide fairly closely with those expected from the propagation prediction model but some adjustment would be required to accurately locate the peaks for the 48m measurements. The peaks can be matched with the prediction by adding 0.65m to the receiver heights, as illustrated in figures 6.3.2 and 6.3.3. This suggests an inaccuracy in the location of the measuring position, either because of the way the separation distance was measured or a dip in the ground surface between the source and receiver. The fact that both spectra exhibit the interference pattern of the same corrected geometry demonstrates that some of the high frequency peaks and dips can be attributed to the ground interference pattern. Interference patterns cannot be detected in the 96m measurements.

Figure 6.3.4 shows the high frequency attenuation corrected to dB per 24m for the 24m, 48m and 96m measurements. Each line being the mean of the values for the 1.2m and 2.5m microphone heights. The 12m measurement is not corrected in this way since all the observed attenuation can be accounted for by ground interference effects, which do not have a linear relationship with distance. Apart from the peaks caused by the interference patterns the values of dB per 24m are similar.

Measurements made on 26/6/84

On the 26th of June 1984 three measurements were made at each measuring position in both track A and B, with the source at position AS. Measurements were first made at the four positions on track A then the speaker was turned through 30° and the reference microphone moved to an appropriate position and measurements made at the four positions of track B. Three measurements were again made at each location except that only two measurements were made at position B12. The weather was warm (22° C) with little or no wind, described at the time as 'close'; with a relative humidity of 64%. The sky was mainly overcast for most of the measuring period.

Results

The results of the measurements made on this day are presented in Appendix B2 with the best fit ground parameters in Appendix C2 and summarised in table 6.3.2.

All the attenuation spectra measured on this day have a marked peak at about 2550Hz. This is not thought to be a significant attenuation effect, as discussed in section 6.2 for the measurements of 5/7/84, and is therefore ignored in the analysis of the results.

Table 6.3.2: Summary of best fit ground parameters 26/6/84 (excluding measurement at B12/2.5m)

	Model		
	Homogeneous	Delany and Bazley	Rigid-Backed layer
σ_e			
max	107000	62000	110000
mean	83467	52733	88000
min	69000	44000	70000
mean difference			
max	5.04	4.98	4.99
mean	3.89	4.03	3.76
min	2.87	2.94	2.59
d_e			
max			0.10
mean			0.076
min			0.050

The similarities in the values of σ_e obtained using the variable porosity, rigid backed layer and homogeneous approximation models and the large values of d_e, again indicate that the ground acts as a homogeneous medium.

In order to assess the similarities, and differences, between the results from the two measuring tracks, A and B, the attenuation spectra at each distance from the two tracks were compared. Figures 6.3.5 and 6.3.6 show the comparisons for the 96m measurements. The two measuring positions show the same overall pattern of attenuation. The 1.2m

microphone at A96 has a consistently higher attenuation, but the actual difference is small, and the ranges of values for each microphone position overlap. The first 'lobe' of the low frequency peak is similar in the two spectra but the second lobe is at a slightly higher frequency and narrower in the B track. This difference is consistent throughout all three measurements at each location.

The other three separation distances follow a largely similar pattern to the 96m measurements, showing no significant differences between the two measuring tracks at high frequencies. The second lobe of the low frequency peak is at a slightly higher frequency and narrower in the B track. The spectra are otherwise similar. The second lobe difference is probably due to a slight difference in the reference microphone location as discussed in chapter 4. The similarities in the high frequencies indicate that the elements of the woodland which cause the attenuation are not significantly different along the two transects. The results show that there are no directional wind effects on the measurement, since the results are similar although the propagation was in different directions.

The first lobe of the low frequency peak spectra are very similar in the two tracks for all the measurements (except for the 2.5m microphone at 12m) This is reflected in the best fit values, the results for the two measurements at the same distance being similar. All the best fit results are, in fact, very similar except for the 2.5m measurement at B12 which has a much higher value, this is probably due to a small scale difference in the ground surface close to the source, or some experimental error. This result has been ignored in the analysis of the ground surface data since it is so different from the other results.

Figures 6.3.7 and 6.3.8 show a comparison between the high frequency attenuation from the different distances, again normalised to the attenuation per 24m. Apart from the spurious peak mentioned above the pattern is an increase in attenuation with frequency. The 12m measurement is not shown since the attenuation can largely be accounted for by interference effects, which are also visible to some extent in the 24m measurements. The mean attenuation is similar for the 48m and 96m measurements.

Measurements made on 16/5/85.

On the 16th May 1985 measurements were made at two of the microphone positions A48 and A96. The microphones were left in place and measurements made at different times during the afternoon i.e. 13.00, 14.00, 15.00, 16.00, 16.30, in order to investigate the variability of measurements taken on a bright sunny day. At each measurement time the lower microphone at A48 and the upper microphone at A96 were recorded simultaneously, followed by a simultaneous recording of the signal at the upper microphone at A48 and the lower at A96. Each signal was used to obtain two spectra of attenuation, one from the first half of the signal and one from the second half. In most cases the two spectra were very similar, so the mean value was used. The exception being the lower 48m microphone and the upper 96m one of the 14.00 recordings where the first half of the signal was significantly lower than the second half in the low frequencies. Since these two were recorded simultaneously and some background noise (a light aircraft) was observed in the first part of the signal, only the second half was used in the analyses, (including the plotted spectra in Appendix B2).

The weather was bright and sunny with some patchy cloud increasing slightly for the measurements at 16.00 and 16.30. The temperature was about 22° C for most of the measurements, a little lower for the earlier measurements. The relative humidity was 64%. There was little or no detectable wind within the wood and only intermittent slight breezes outside the wood. The ground was quite damp after recent rain.

The results of the measurements made on this day are presented in full in Appendix B2. with best fit ground parameters in Appendix C2.

The 48m measurements have a very low value of attenuation, especially in the high frequencies, compared to other measurements made at this site. It is thought that this was due to problems with the equipment as discussed in the results for 20/6/85 at Hazelborough Wood. It is, however, useful to look at the frequency dependence of the results and differences between the results at different times, since it is unlikely that the fault in the

equipment would have altered significantly throughout the time of the experiments. The attenuation spectra of the 1.2m microphone height at 48m have a marked peak at around 3khz and further peaks at 5-6khz and at about 9kHz. The first of these three peaks is at a different frequency and height for each of the measurements and there are also small changes in the other peaks. The 48m/2.5m attenuation spectra do not show such a definite pattern of peaks but do have 2 dips which occur at similar frequencies and the region between these could be interpreted as a broad peak although it consists of 2 or 3 small peaks. Similarly the region between 1kHz and about 2.5kHz could be a small peak. The patterns of peaks and dips are a result of the ground interference effects. Comparison between the measurements and the predicted interference patterns is used to elucidate the changes in the spectra at the different times.

Figures 6.3.9 and 6.3.10 show examples of the attenuation spectra compared with a prediction using the nominal separation distance and height and an adjusted geometry where one parameter, the test microphone height is altered to give a better fit to the measurement. Adjusting the microphone height simply has the effect of altering the pathlength difference (Δ r) between the direct and reflected paths, which shifts the interference peaks, as discussed in chapter 4. The amount of adjustment required to give a good fit to the measured data for each measurement is given in table 6.3.3.

Table 6.3.3
Best fit microphone heights for 48m measurements at Wetleys Wood on 16/5/85.

	'Predicted Height' (predicted-actual)	
Time	lower microphone	upper microphone
13.00	1.9m (0.7)	3.2m (0.7)
14.00	1.8m (0.6)	3.2m (0.7)
15.00	2.0m (0.8)	3.6m (1.1)
16.00	2.4m (1.2)	3.6m (1.1)
16.30	1.9m (0.7)	3.0m (0.5)

Although the difference between the actual and best fit height is not precisely the same for the higher and lower microphone heights they do follow a similar pattern with the

15.00 and 16.00 measurements requiring a greater adjustment than the other three. The only factor which could have caused the differences between the different times is the micrometeorological conditions. The bright sunshine heating the top of the canopy more than the shaded ground surface causes a positive gradient under the canopy which has the effect of refracting the sound rays. Differences in the temperature profile cause differences in the curvature of the refraction. It is uncertain what effect such a refraction would have on the location of the interference peaks but it seems logical that an effective change in Δ r could result. In this case it seems that the increasing temperature gradient which would be expected during the afternoon of a bright sunny day causes an increase in Δ r. The refraction of the sound is another explanation for the difference between the measured and predicted microphone height for the 48m measurements of the 28/7/83 measurements. It has been suggested that calculating the predicted excess attenuation assuming a curved ground surface may be the best way to predict the influence of vertical velocity gradients. It is possible that frequency shifts in the interference patterns could be useful in analysing temperature gradients in outdoor sound propagation, but the application in woodland is obviously limited because the interference patterns are interrupted by scattering and are therefore not apparent at long distances.

No interference patterns which could be analysed in a similar way can be seen in the attenuation spectra of the 96m measurements. Figure 6.3.11 is an example of the measured and predicted attenuation at 96m. The 96m spectra are very similar for each of the measurements. Figures 6.3.12 and 6.3.13 are the range of values obtained, excluding the lower microphone of the measurement made at 16.00 which has a lower attenuation at low frequencies than the other measurements. The two spectra from this recording were also rather different at low frequencies. The difference is due to the presence of a light aircraft which was unnoticed at the time of the recording and the low frequency part of this measurement was therefore ignored in the analysis of the data.

Table 6.3.4 summarises the results of fitting the models to the 96m measurements. The results are all similar and again indicate that the homogeneous case is appropriate for both the variable porosity and rigid-backed layer approximations.

Table 6.3.4 :Summary of best fit ground parameters 16/5/85 (96m)

	Model		
	Homogeneous	Delany and Bazley	Rigid-Backed layer
σ_e			
max	130000	60000	140000
mean	68000	44000	81000
min	50000	40000	70000
mean difference			
max	5.18	4.60	5.25
mean	2.78	2.47	2.77
min	1.65	1.35	1.75
d_e			
max			0.095
mean			0.070
min			0.055

Comparisons Between Results Obtained At Wetleys Wood On Different Days.

The spread of mean best fit values is relatively large, with the best fit values of σ_e from 26/6/84 being higher than that for 16/5/85 and the result from 28/7/83 having the 'softest' ground. The differences are all significant at the 5% level of the studentised T-test, using the best fit parameters from all the measurements. The significance levels of the differences are summarised in table 6.3.5.

Table 6.3.5 Levels of Significance (T-test)

Date	mean	28/7/83	26/6/84	16/5/85
Homogeneous Approximation				
28/7/83	38,000	*	0.1%	1%
26/6/84	83,000		*	5%
16/5/85	61,000			*
Delany and Bazley Model				
28/7/83	26,000	*	0.1%	0.1%
26/6/84	53,000		*	1%
16/5/85	42,000			*

These results show that the most significant difference is between the measurement of 28/7/83, and the results from the other days; this is probably due to the fact that some thinning was carried out during the winter of 1983/84 and vehicles, used to remove the felled trees, churned up the ground surface and probably also compacted it causing an increase in the effective flow resistivity. The lower value in the measurement from summer 1985 could be caused by some 'recovery' of the ground surface with the deposition of more needles in the litter layer and weathering effects on the soil.

Figure 6.3.14 shows a comparison between the mean values of attenuation per 24m calculated from all the 48m and 96m measurements on the different days (96m only for 16/5/85). It is evident that there is very little difference between them. This result indicates the repeatability of the measurements between different days. The repeatability suggests either that the meteorological conditions were the same on all the days or that the meteorological conditions had little effect on the measurements. Some measurements were done on overcast days and some on sunny days in which the temperature gradients could be expected to change during the course of the measurement period, suggesting that the measured attenuation is not altered to a great extent by meteorological conditions.

The similarity between the results on different days indicate that the small amount of thinning carried out in the winter of 1983/84 does not have a significant effect on the attenuation; in fact the measurement made in 1983 has a slightly lower attenuation at high frequencies. Any reduction in high frequency attenuation caused by the thinning is less than the variation between similar measurements.

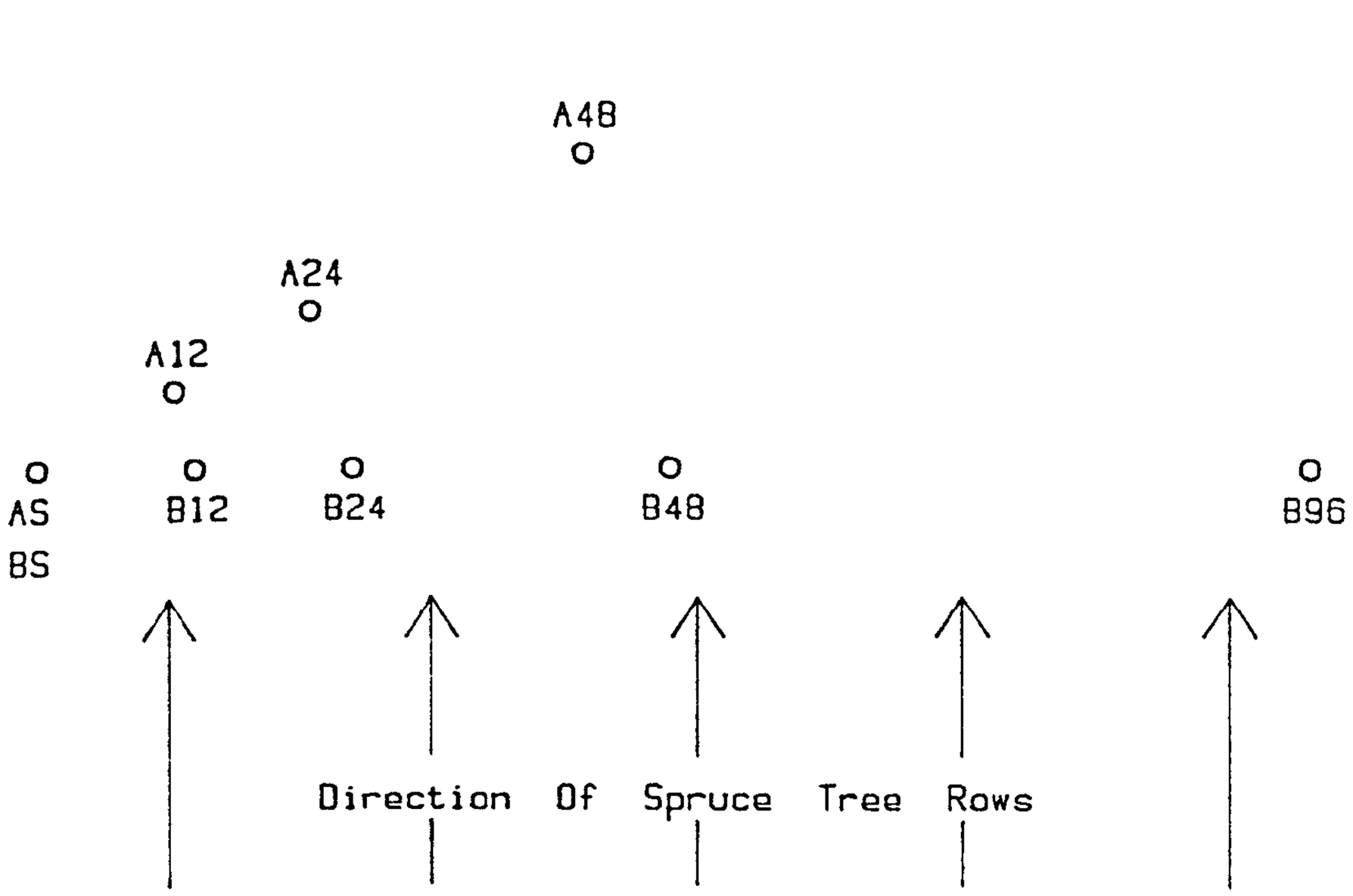

Figure 6.3.1
Layout of Marked Locations at Wetleys Wood.

Scale
⊢——————⊣ = approximately 24m

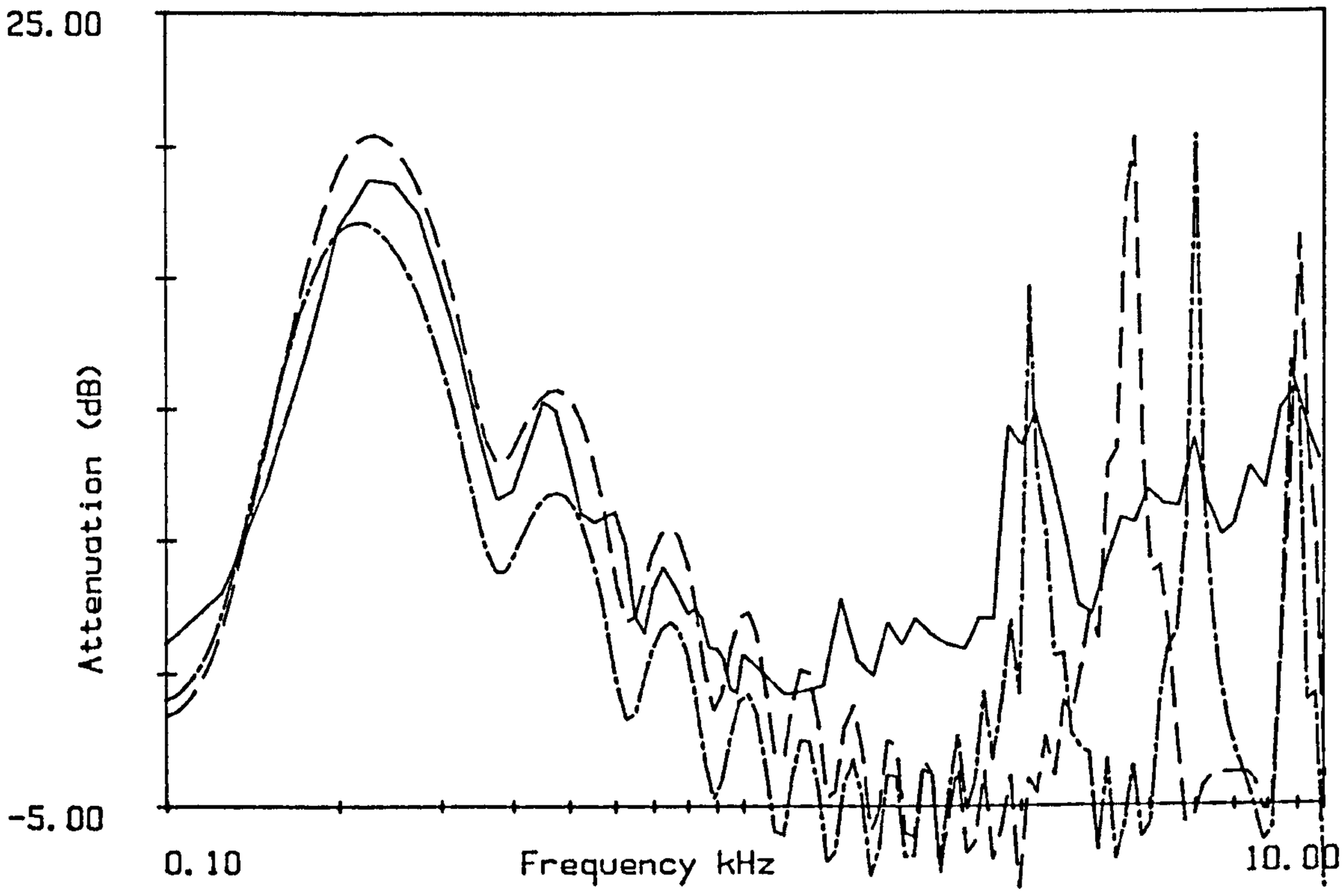

Figure 6.3.2
Attenuation at 48m 28/7/83 microphone height 1.2m.
Predictions using Homogeneous approximation o e=34.000.
and test microphone height 1.2m — — — , and ——·——·——1.85.

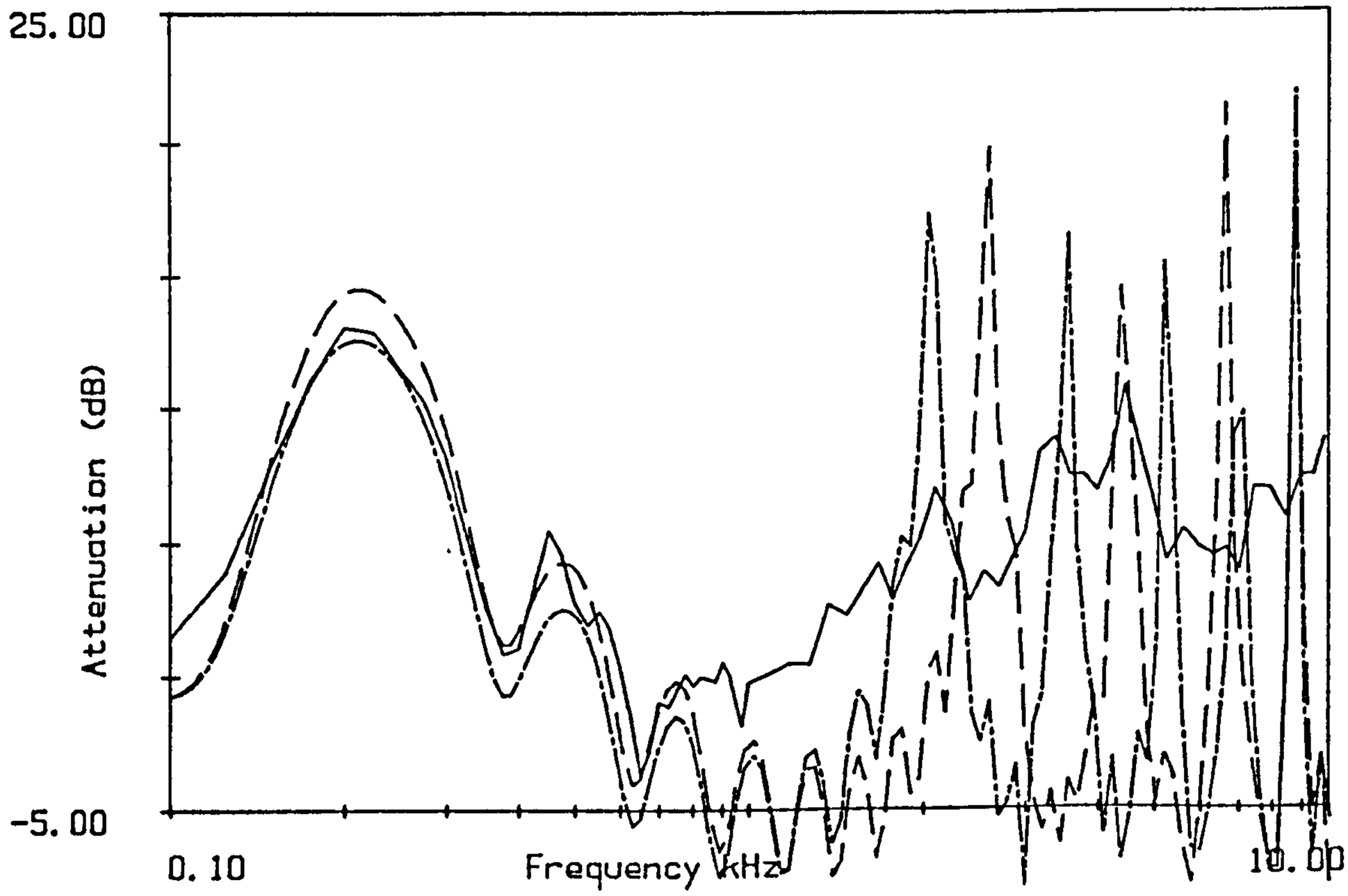

Figure 6.3.3
Attenuation at 48m 28/7/83 microphone height 2.5m.
Predictions using Homogeneous approximation o e=34.000.
and test microphone height 2.5m — — — , and ——·——·——3.15.

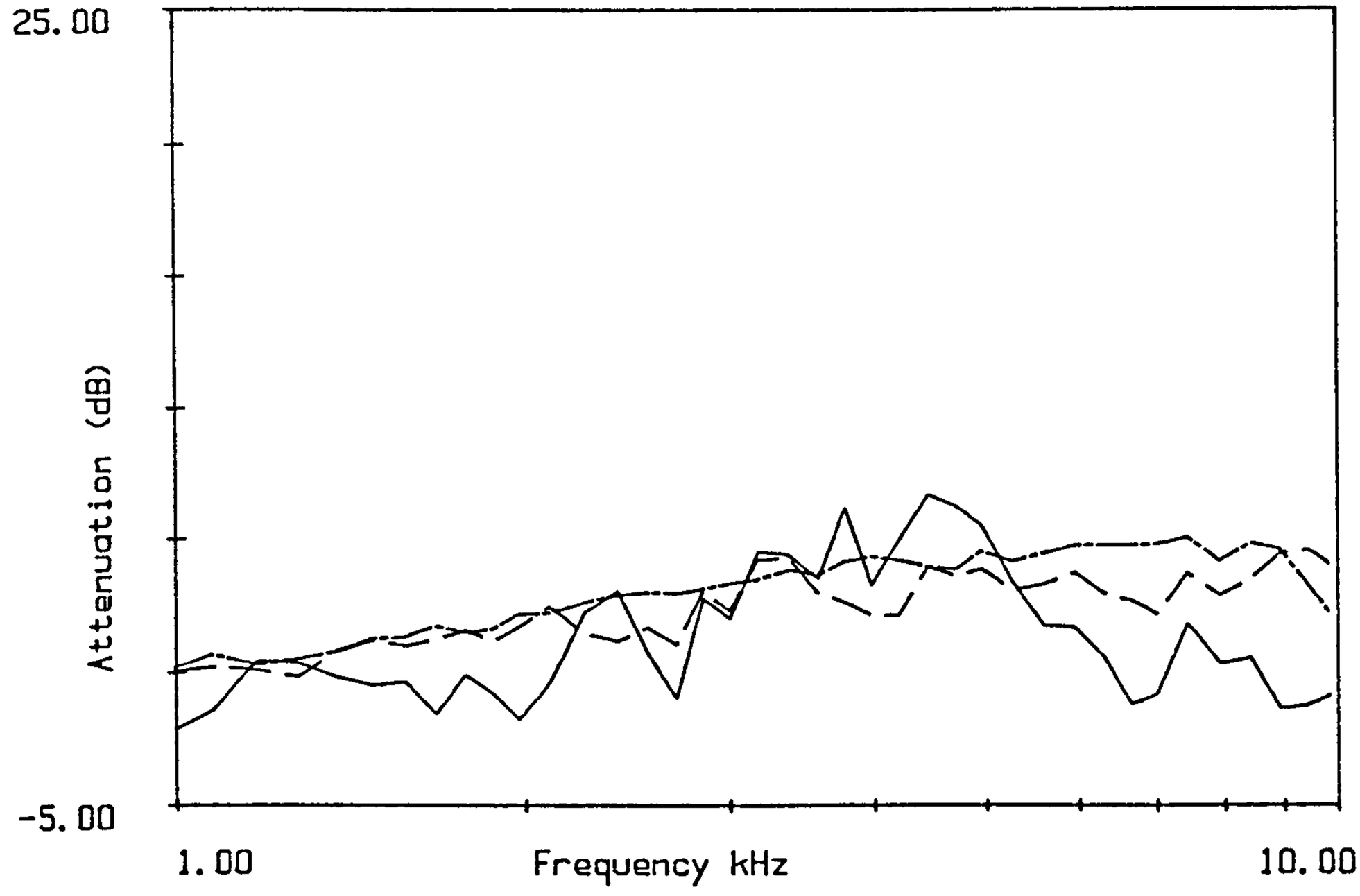

Figure 6.3.4
Mean attenuation (dB per 24m) for the measurements on 28/7/83 at ——— 24m, — — — · 48m, and ——·——·—— 96m .

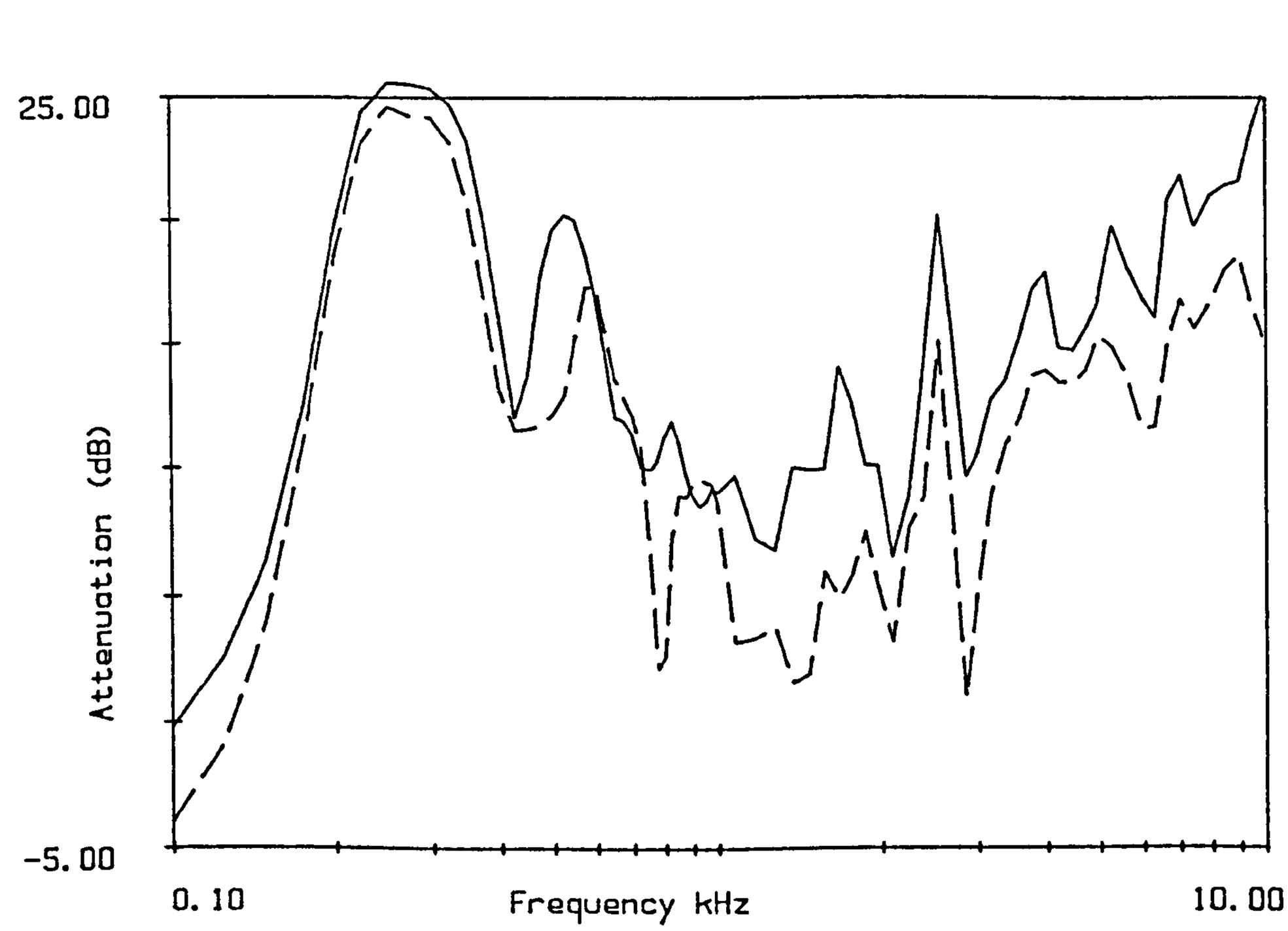

Figure 6.3.5
Attenuation at A96 and B96 (----) on 26/6/84
microphone height = 1.2m.

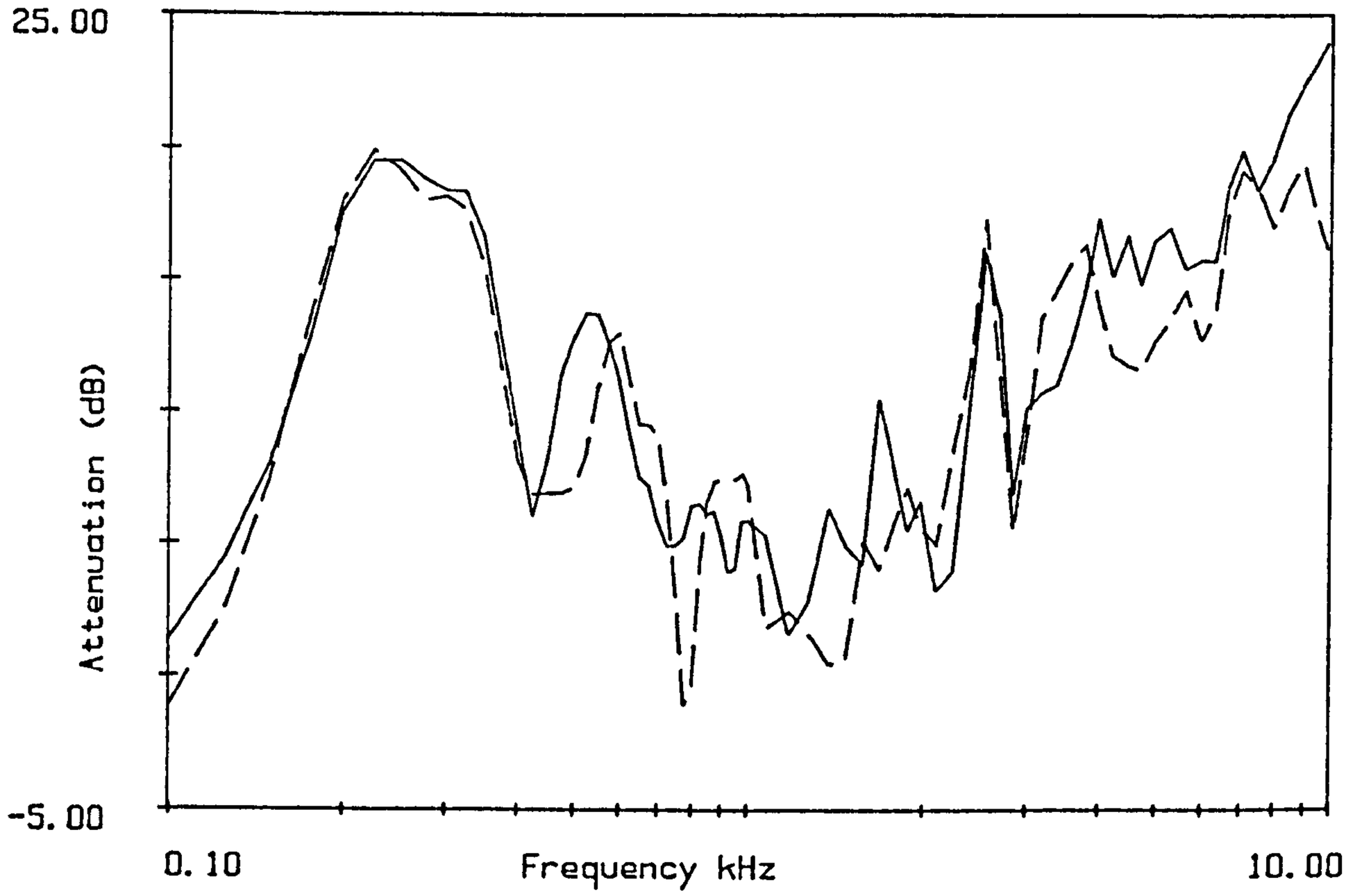

Figure 6.3.6
Attenuation at A96 and B96 (----) on 26/6/84
microphone height = 2.5m.

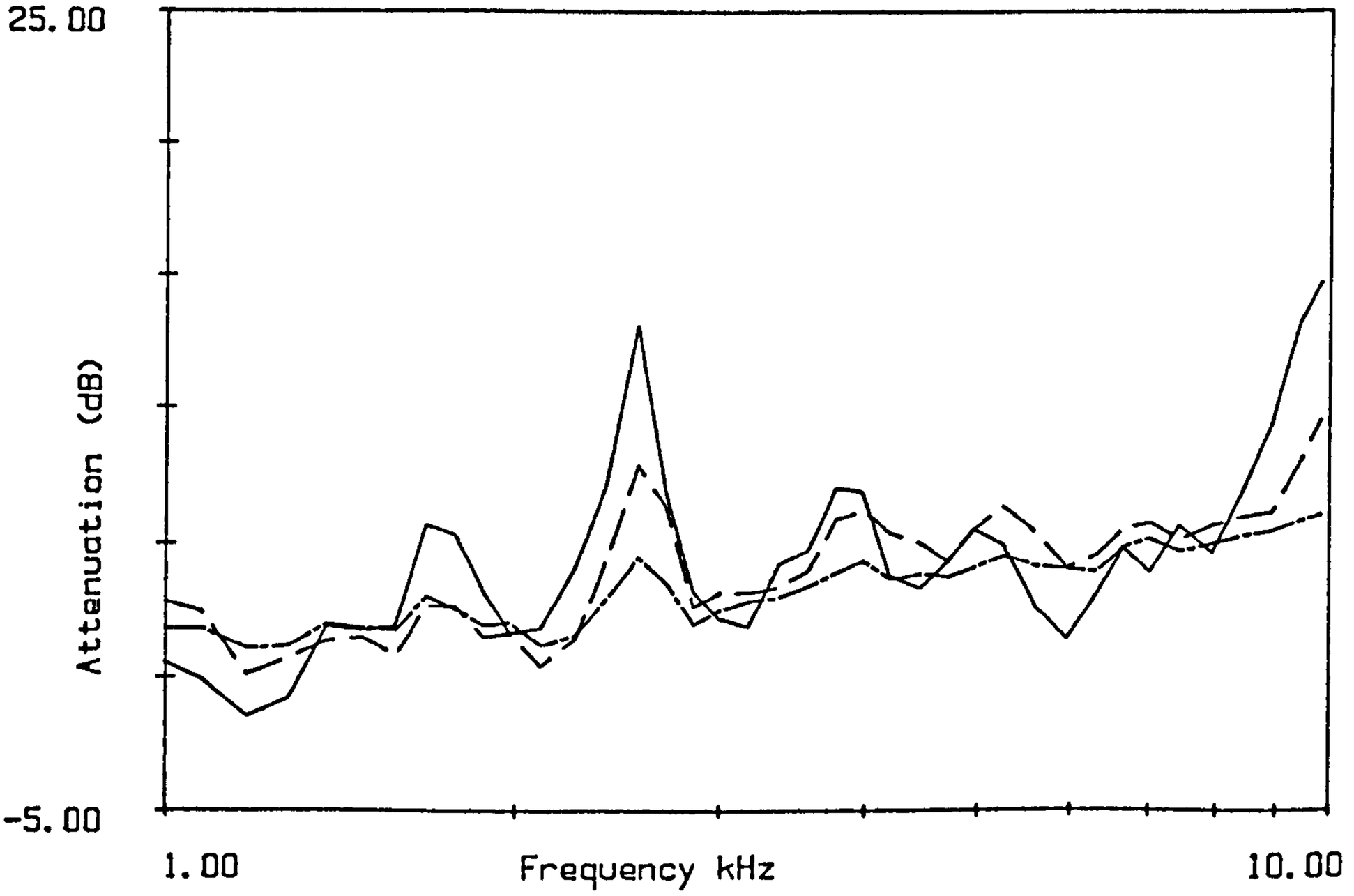

Figure 6.3.7
Mean attenuation (dB per 24m) for track A on 26/6/84
at ——— 24m, — — — · 48m, and ——·——·—— 96m .

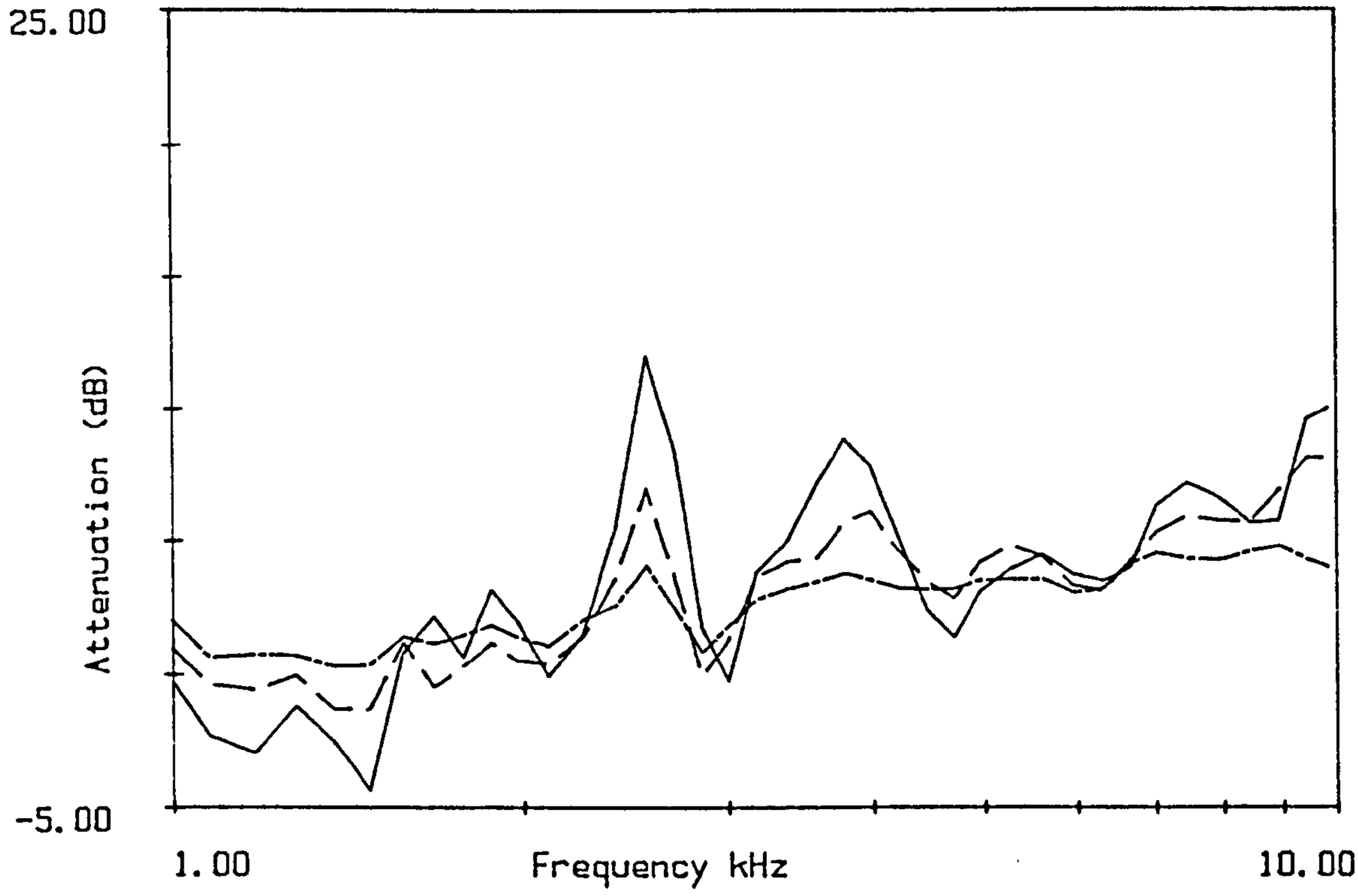

Figure 6.3.8
Mean attenuation (dB per 24m) for track B on 26/6/84
at ——— 24m, — — — · 48m, and —·—·—·— 96m .

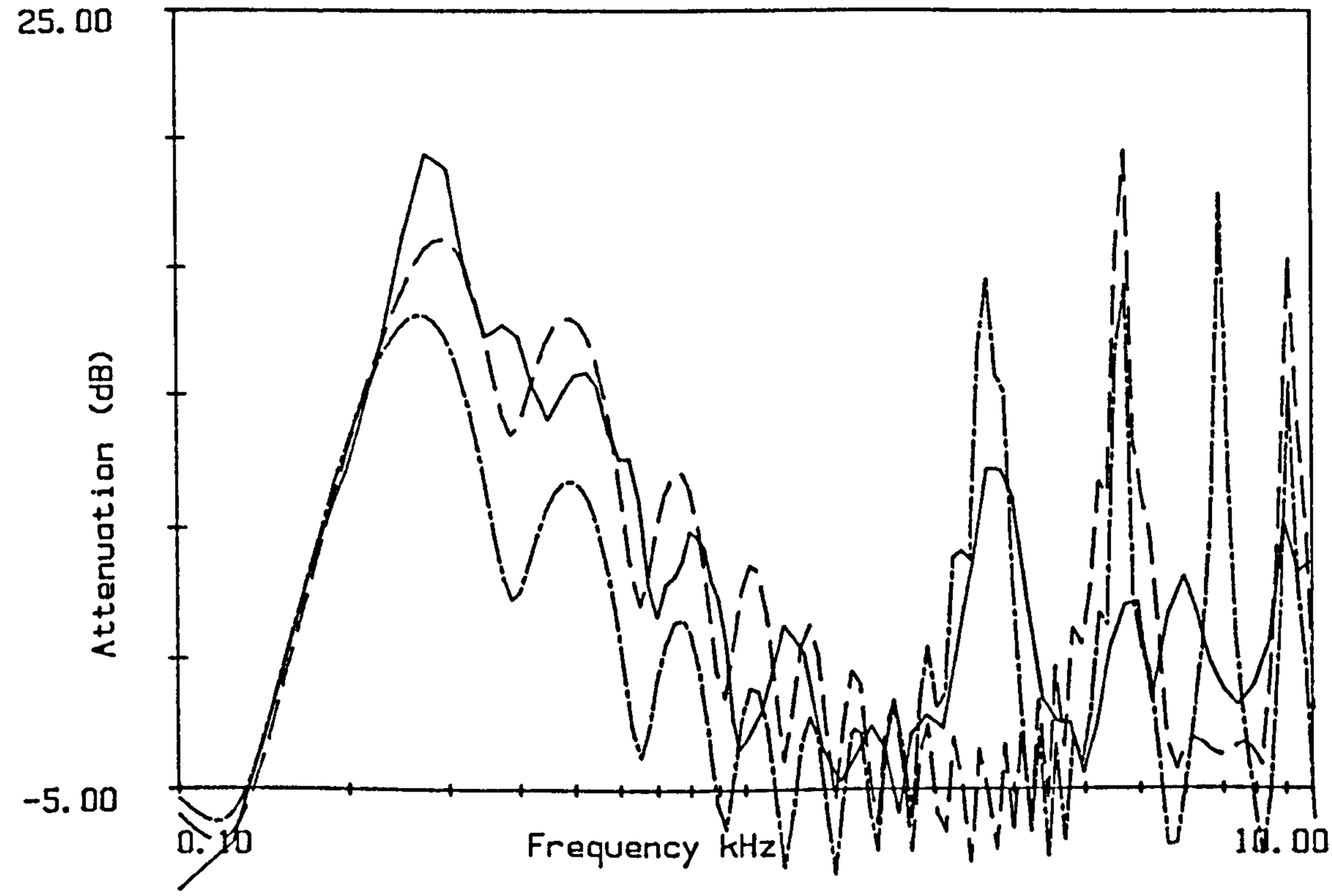

Figure 6.3.9
Attenuation at A48 at 16.00 16/5/85 microphone height = 1.2m. ———
Predictions using nominal height (1.2m) — — —
and altered height (2.4m) —·—·—

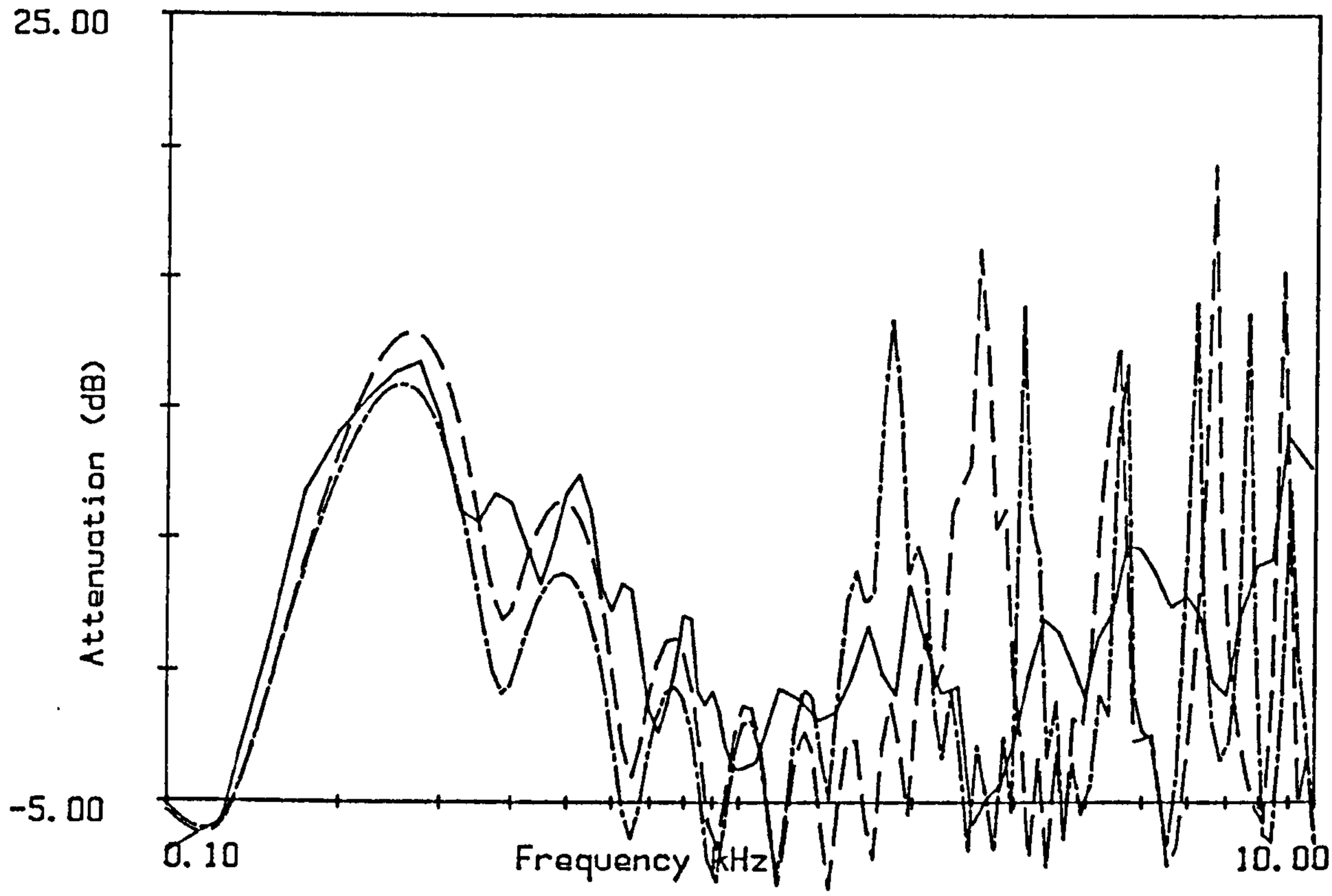

Figure 6.3.10
Attenuation at A48 at 16.00 16/5/85 microphone height = 2.5m. ————
Predictions using nominal height (2.5m) — — —
and altered height (3.6m) ————·——

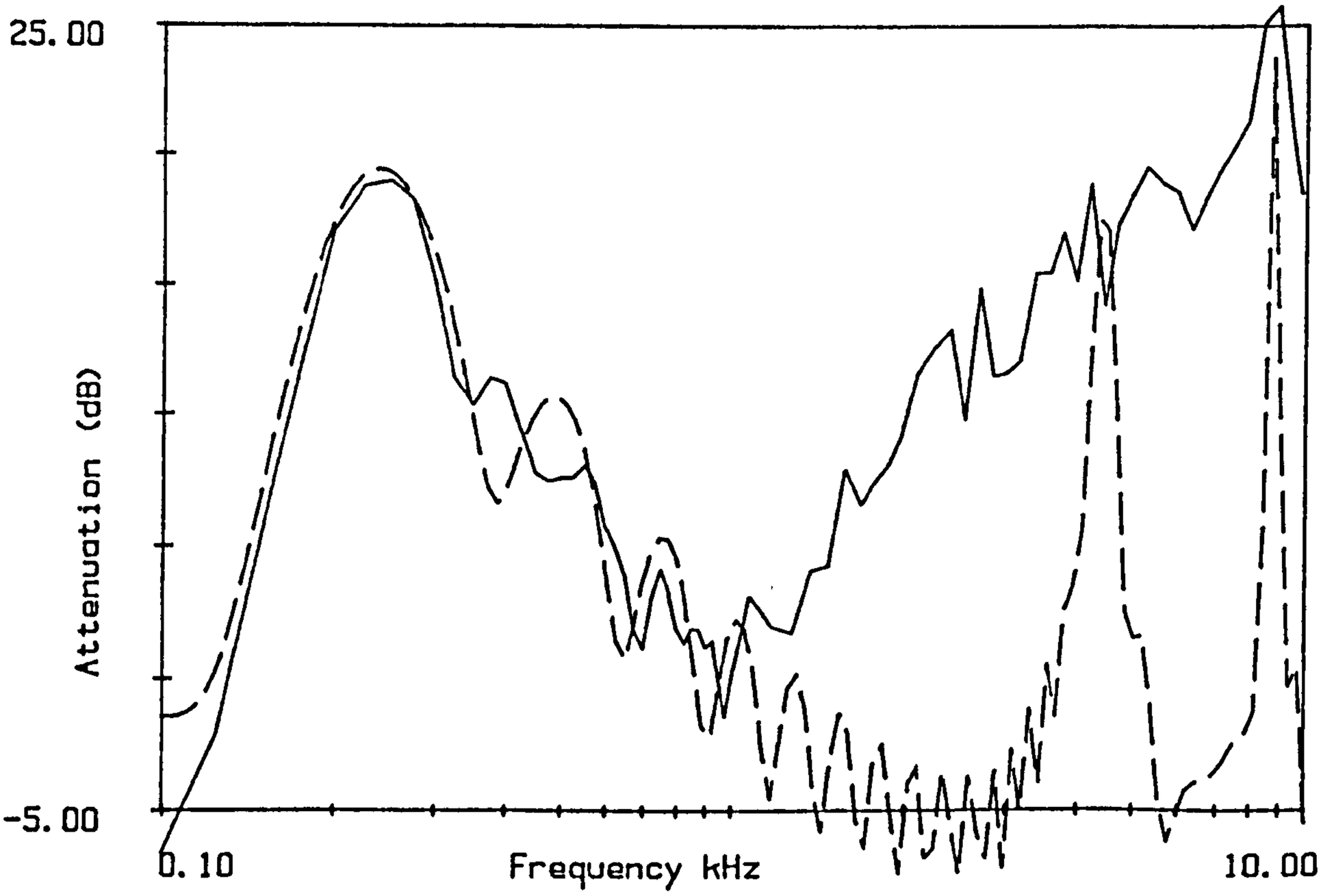

Figure 6.3.11
Attenuation at A96 16/5/85 microphone height = 2.5m.
Predictions using nominal height (2.5m -----)

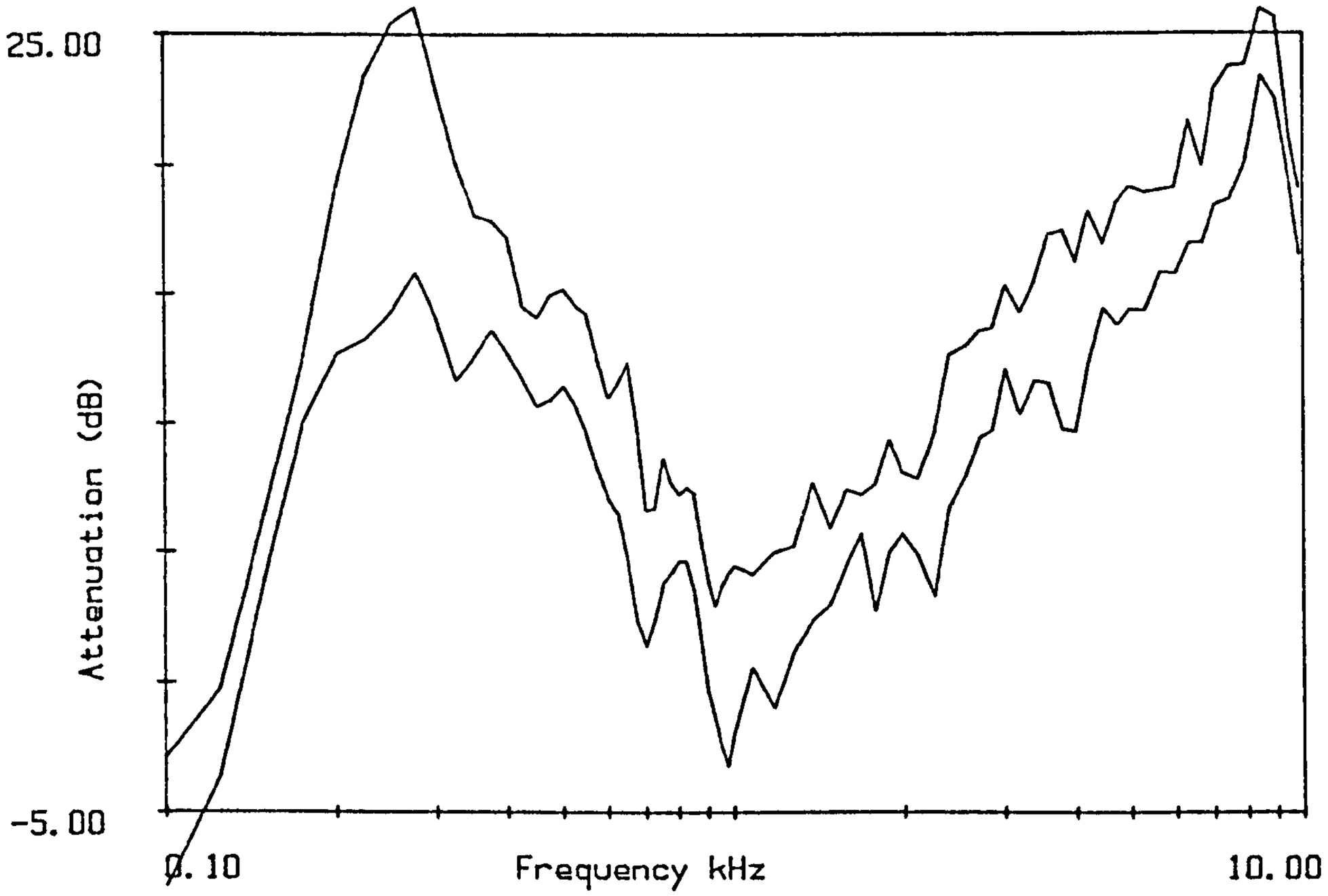

Figure 6.3.12
Range of attenuation at A96 16/5/85 microphone height = 1.2m.

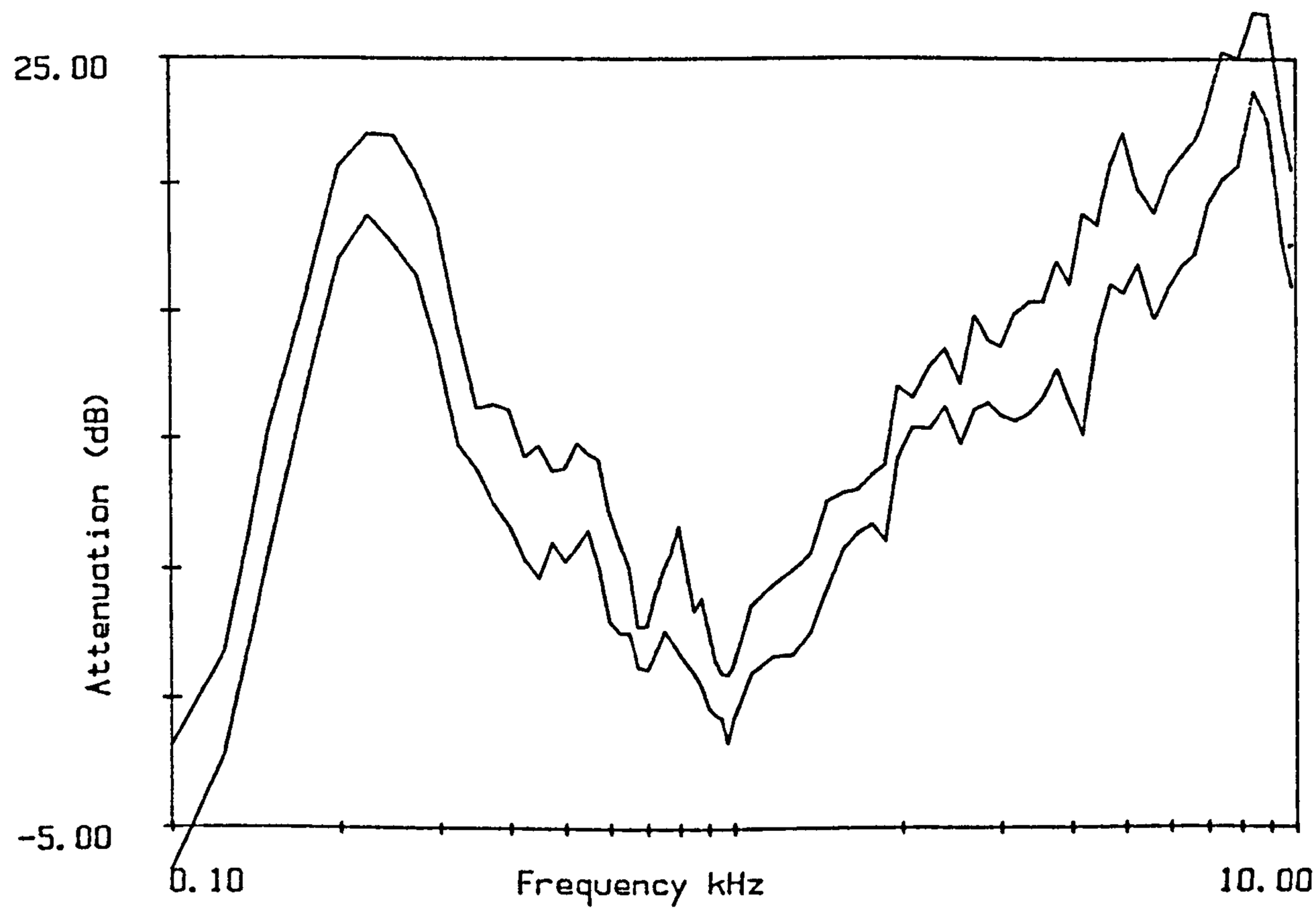

Figure 6.3.13
Range of attenuation at A96 16/5/85 microphone height = 2.5m.

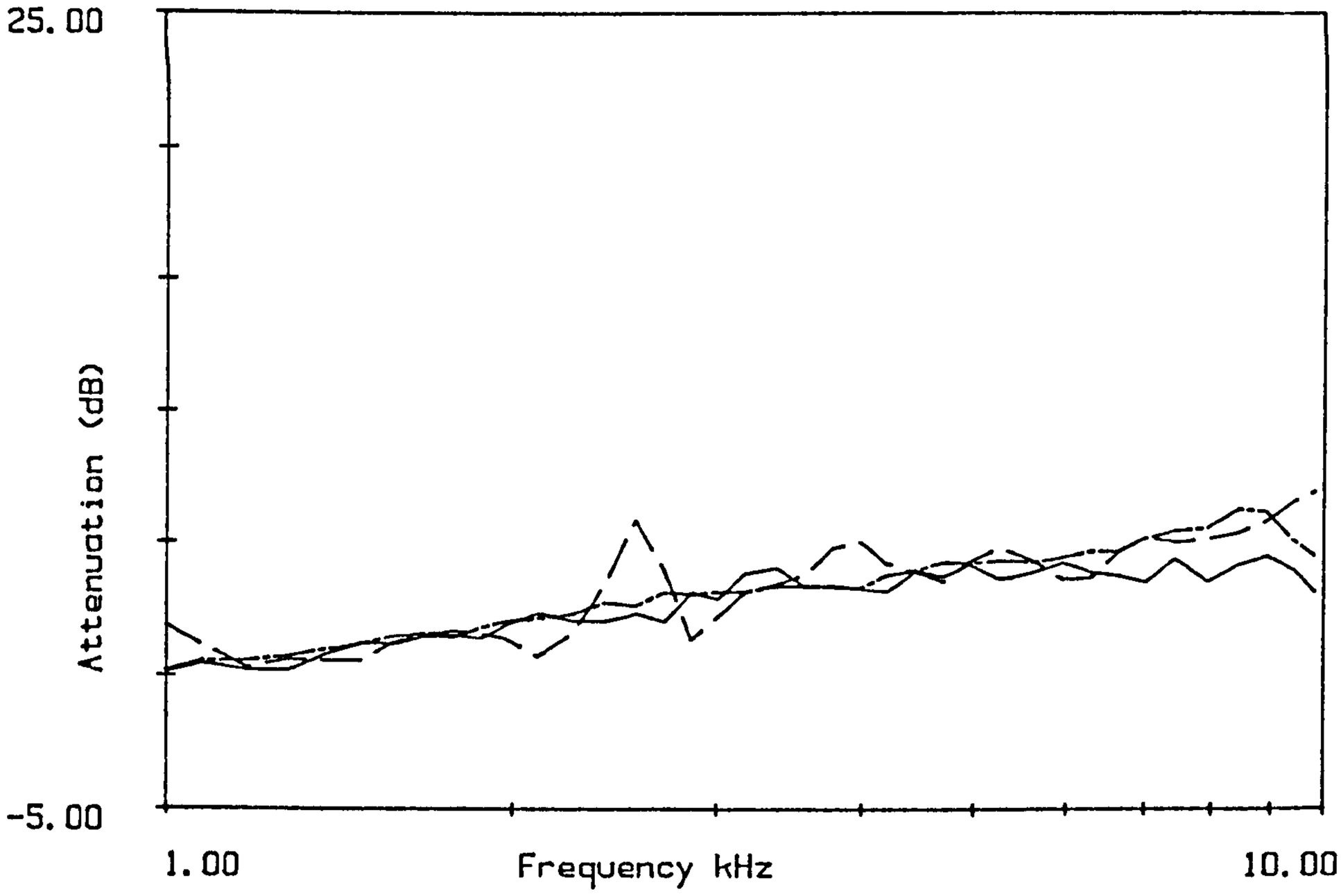

Figure 6.3.14
Mean attenuation (dB per 24m) for the different days.
———— 28/7/83, — — - 26/6/84, and —·——·— 16/5/85.

6.4 Measurements made in a Young Mixed Coniferous Stand.

Compartment 9a 'Bucknell Wood'

This compartment consists of rows of Red Cedar, Norway Spruce and Corsican Pine planted in 1962 and 1969. The Red Cedar forms a continuous barrier of vegetation with neighbouring trees touching or overlapping. There are some gaps between the spruce and pine with long grass and undergrowth among them. The sampled stem density is 0.181 stems m^{-2} and the mean radius 0.066m.

Two measuring tracks were marked out in this stand; tracks F and G as shown in figure 6.4.1. Track F was marked out diagonally across the line of the trees at an angle of about 80°. The source position (FS) was located about 60m from the edge of the stand in a gap between a spruce row and a red cedar row, two microphone positions were marked at 12m (F12) and 26m(F26) from it . Track G has the source position (GS) at position (F26) and the measuring track is at an angle of about 50° from track F ie at an angle of about 30° from the line of the trees. Two microphone positions were marked out along this line at 24m (G24) and 40m (G40) from the source position.

Measurements Made 9/7/84

The source and reference microphone were set up at position F26, the reference microphone was not placed directly in the line of the measuring track but to one side of the speaker, because the speaker position was very close to a dense red cedar row and the reference position would therefore lie within this row. The reference recordings were made between test recordings, turning the speaker face the reference microphone. Test recordings were made with the two microphones (heights 1.2m and 2.5m) at positions F12, G24, G40 and FS (ie separation distances of 14m, 24m, 40m, 26m respectively). Three recordings were made at each location, moving the microphones sideways between the measurements.

There was a full cover of cloud for most of the day. The wind was mostly below 1.5m/s but occasionally gusting to about 2.5m/s. The temperature was about 19.5° C and the relative humidity was 70%.

Measurements Made 8/8/84

The source and reference microphone were set up at position F26 the reference microphone placed to one side of the speaker, as explained above. The reference recordings were made between test recordings, turning the speaker face the reference microphone. Test recordings were made with the two microphones (heights 1.2m and 2.5m) at positions F12, G24, G40 and FS (ie separation distances of 14m, 24m, 40m, 26m, respectively). The source and reference microphone were moved to position FS and test recordings made at F26 and F12, in this case the reference microphone was located in line with the measuring track, (only one microphone was used at F12, at 1.2m height). The measurements at each location were again repeated with the microphones moved to either side of the marked post.

The weather was recorded as mostly sunny with some thin cloud and no apparent wind. The temperature was about 16.5° C at the beginning of the experiments rising to about 19.5° C later in the day. The relative humidity was 60%.

9/7/84 and 8/8/84 results.

The results of the measurements made on these two days are presented in full in appendix B3, with best fit ground parameters in appendix C3, summarised in tables 6.4.1 and 6.4.2.

Table 6.4.1 Summary of best fit ground parameters 9/7/84.

		Model		
		Homogeneous	Delany and Bazley	Rigid-Backed layer
σ_e				
	max	110000	60000	110000
	mean	73750	41250	77500
	min	50000	30000	50000
mean difference				
	max	6.95	7.39	6.98
	mean	5.41	5.63	5.42
	min	3.21	3.38	3.10
d_e				
	max			0.090
	mean			0.073
	min			0.060

Table 6.4.2 Summary of best fit ground parameters 8/8/84.

		Model		
		Homogeneous	Delany and Bazley	Rigid-Backed layer
σ_e				
	max	110000	60000	110000
	mean	64545	36364	69091
	min	40000	30000	50000
mean difference				
	max	7.91	8.25	7.81
	mean	4.98	5.01	4.89
	min	3.49	3.32	3.39
d_e				
	max			0.109
	mean			0.083
	min			0.056

The relatively large spread of the best fit results and high values of least mean square, for both sets of measurements, indicate that the simplified model of a flat, uniform ground surface does not adequately represent the ground effect in this stand. The ground can be seen to be uneven and non-uniform as there is a covering of tussocky grass below the pine and spruce rows. This ground covering may affect the sound propagation. The results indicate a homogeneous ground surface rather than one with a layered structure or increasing porosity with depth. The results obtained on 9/7/84 and 8/8/84 are very similar, and there

is no significant difference between the best fit results for the two measuring tracks.

The high frequency part of the attenuation measured in this woodland on the two days are also very similar within the limits of the accuracy of the experimental techniques. Figures 6.4.2 and 6.4.3 are examples of comparisons between the measurements made on the two days.

The shorter distance measurements (12m and 14m figures B3.1, B3.5, B3.10 appendix B3) show large scale variations due to interference patterns which are less evident in the longer distance measurements. The peaks and dips do not match those of the predictions, this is again likely to be due to the unevenness of the ground. There could also be some meteorological effects; a slight wind or a velocity gradient would cause interference peaks to be broadened or shifted in frequency, respectively.

When the source is at F26 the attenuation at F5 and G24 can be compared directly over the whole frequency range since the separation distances are approximately the same (26m and 24m respectively). Figure 6.4.4 shows the mean of the measurements made on 8/8/84 and 9/7/84 at each of these measuring positions compared for the two microphone heights. The two attenuation spectra are similar but the G track generally has a higher attenuation at most frequencies. This difference is slight but is consistent throughout the data. A further comparison can be made between the two tracks and different parts of the same track, at high frequencies by converting all the attenuation data to the attenuation per 24m.

Figures 6.4.5 to 6.4.8 show the results of converting the results to attenuation per 24m. The shorter range measurements (12m and 14m) are evidently affected by interference effects and other fluctuations, the measurements made at 24m or more show the overall pattern of increasing attenuation with frequency with only relatively small peaks and dips ie. a fairly smooth line.

The overall structure of the stand is evidently not homogeneous as it consists of areas of particularly dense foliage and branches in the red cedar rows and a much more open structure in the spruce and pine rows. The attenuation spectra indicate that the high frequency attenuation does reflect the density of the vegetation. The G track passes through a longer distance of the dense red cedar stand; since it crosses the rows at an oblique angle whereas the F track is approximately normal to the rows. Figure 6.4.9 shows that the attenuation rate is greater in the G track.

Two of the measurements made at Bucknell Wood on the 8th August 1984 were made along the same measuring track but the source and microphones were reversed. The measurements were made over a measuring track of 26m, the source and microphones were located at sites FS and F26. The resulting attenuation graphs are illustrated in figures 6.4.10 and 6.4.11. It is evident that the attenuation spectra are very similar. When the range of attenuation values are plotted for each of these attenuation spectra, the ranges overlap along practically their whole length except for frequencies above 7kHz for both microphone heights. Exchanging the source and receiver positions does not represent an exact reversal of the source-receiver geometry since the microphones are not located at exactly the same height as the speaker. In the high frequencies the source height can be assumed to be 1.5m whereas the receivers are at 1.2m and 2.5m. Differences in the vegetation structure at the different heights close to the source or receivers, could have caused a real difference between the signals propagating in the different directions, this suggests that such vegetation effects are high frequency phenomena such as scattering and absorption by branches and foliage. The other cause of the difference could be reflections from the trees, particularly the dense red cedar rows, the source at F26 is very close to a belt of red cedar which could therefore be reflecting sound back towards the speaker, decreasing the test signal and increasing the reference signal, thus increasing the attenuation.

Measurements Made 2/7/85

Measurements were made on 2nd July to assess the extent to which the high frequency attenuation in this woodland can be attributed to the red cedar belts. Figure 6.4.12 shows the layout of the experiment designed to assess the attenuation rates from different parts of the stand. the three locations of track F are included along with some extra locations: the measurements made are summarised in table 6.4.3. Microphones were located at 1.2. and 2.5m heights for each measurement location.

Table 6.4.3 : Measurements made 2/7/85

Measurement number	Source location	Source height	Microphone location	Separation distance
1	FS	1.3	a	2 (reference)
2	FS	1.3	b	7 (no trees in path)
3	FS	1.3	c	7
4	FS	1.75	c	7
5	FS	1.75	F12	12
6	FS	1.3	F12	12
7	FS	1.3	d	16.8
8	FS	1.75	d	16.8
9	FS	1.75	F26	26
10	FS	1.3	F26	26
11	FS	1.3	F26	26
12	F12	1.3	F26	14
13	F12	1.75	F26	14

If the red cedar rows cause significantly more attenuation than the other species and the wider row has a greater effect than the narrower, the magnitude of the attenuation rates in dB per 24m should be ranked according to the proportion of the propagation path which passed through the red cedar belt. Table 6.4.4 shows this ranking as determined from figure 6.4.12.

Table 6.4.4

Position	measurement number
highest	12.13
|	9.10
|	5.6
|	7.8
|	3.4
lowest	2

Comparison between the attenuation values of the measurements is shown in figures 6.4.13 to 6.4.15. The values illustrated are mean values for all the measurements at each of the microphone locations, at the two different microphone heights and source heights. The attenuation spectra are illustrated in full in Appendix B3.

Figure 6.4.13 shows the comparison between the 2 measurements at the shortest separation distance. Measurement 2 was made along an open space between the trees with a clear path between the source and receiver. There were only a few spruce and pine branches in the measuring path of measurements 3 and 4 but no dense vegetation so it is unlikely that the small increase in attenuation at high frequencies is significant. The spectrum for the two 7m measurements are evidently dominated by the interference patterns and are therefore not very useful in the comparisons of the attenuation attributable to the trees themselves. The only useful comparisons that can be made are therefore the differences between the attenuation through the thick belt and the thinner belt of red cedar, since these measurements were made at a rather longer distance and are less affected by the interference patterns although some interference effects can still be seen as the distances range from only 12m to 26m.

Figure 6.4.14 compares the measurement made through the wider red cedar belt only and that made through both belts, thus the red cedar made up a greater proportion of the propagation path in the former(measurements 9 and 10). The result for measurements 9 and 10 are slightly higher for most of the range although the large peak in the data appears to be due to an interference maximum. At the highest frequencies the values are more similar

although this is the part where the greatest differences would be expected.

Figure 6.4.15 shows that the results from the measurements with both the red cedar belts are indeed higher than those made with two belts of the spruce and pine but only one of red cedar. The relatively smooth spectra are due to the slightly longer distance causing a greater disruption of the interference pattern by scattering and turbulence. The differences between the two measurements are mainly in the higher frequencies as would be expected if an increase in attenuation with frequency is assumed. It seems that a more detailed analysis of the differences between the propagation paths is not possible since the ground interference effects have so great an influence.

The influence of the ground effect has been discussed in this chapter to describe some of the similarities and differences between the results from different days in the same stand. Similar comparisons can be made for the high frequency part by using the scattering model described in chapter 5. Such comparisons with predictive models are also, of course, useful in comparing the different stands. In order to assess the applicability of this model, particularly in the presence of a ground surface, some model experiments were carried out which are described in the following chapter. To avoid unnecessary repetition, therefore, further discussion of the results and comparison between the stands have been left until Chapter 8, following the results of the model experiments.

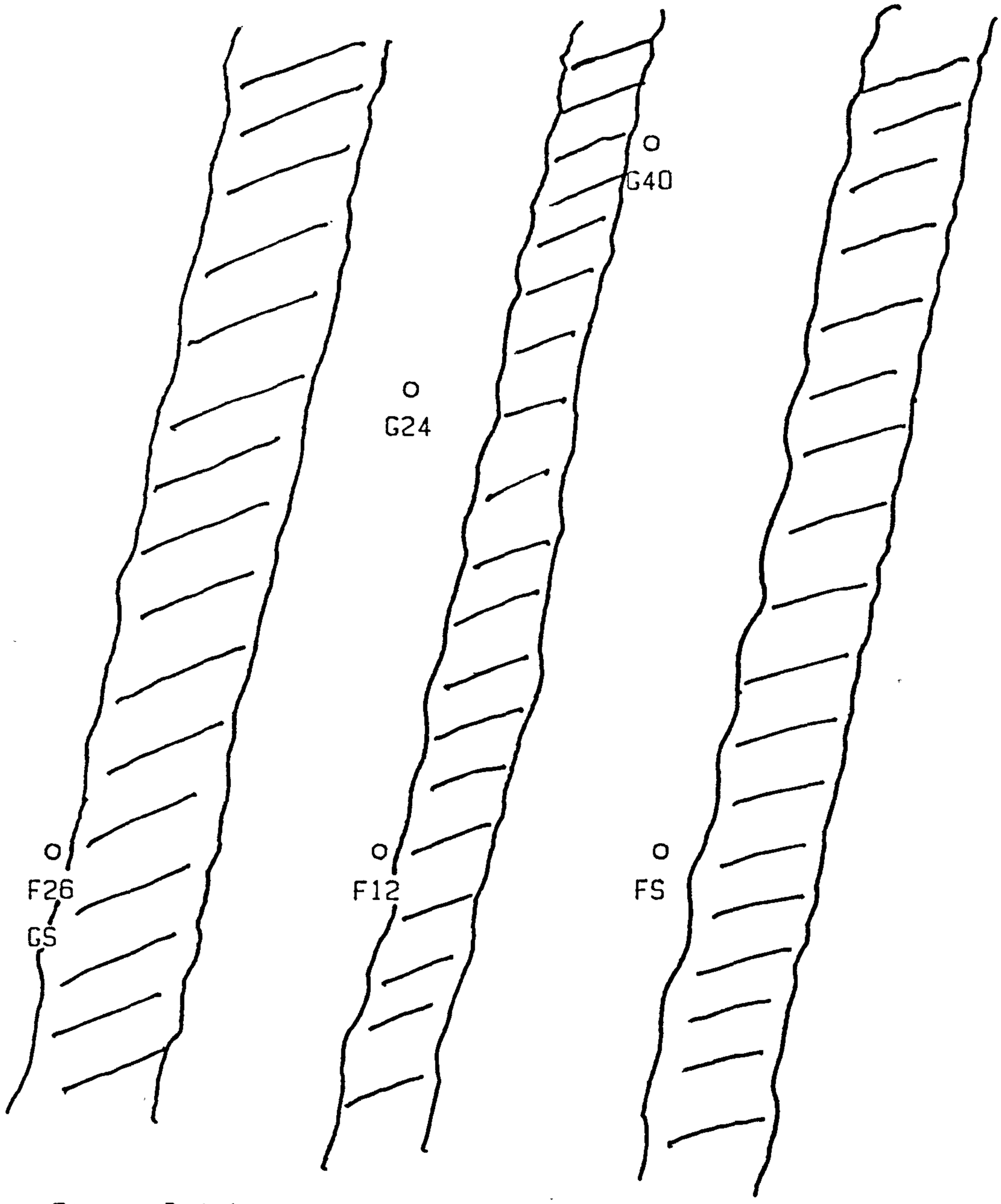

Figure 6.4.1
Layout of Marked Locations at Bucknell Wood.

Scale

├──────────┤ = approximately 12m.

//// = Red cedar rows.

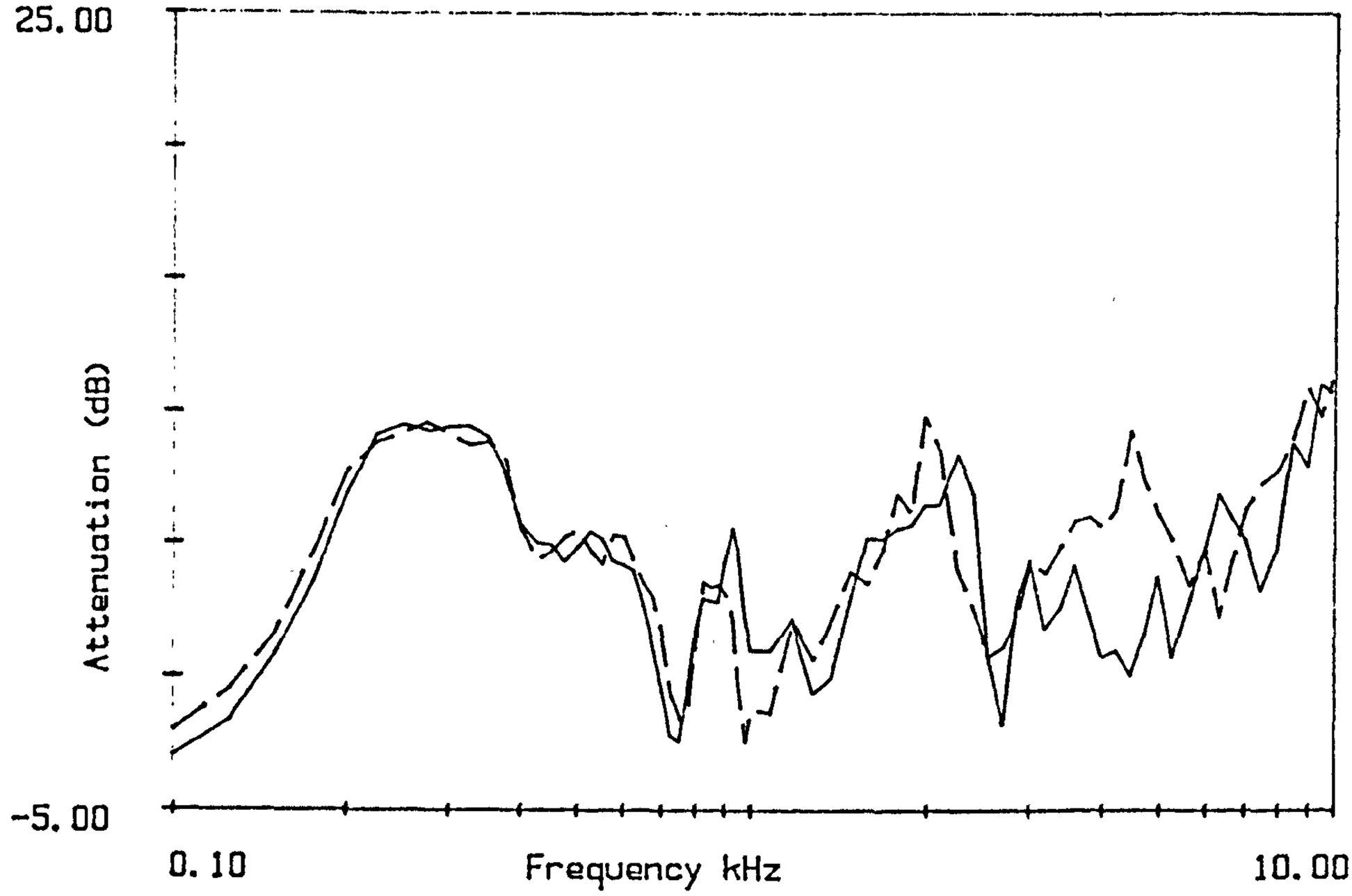

Figure 6.4.2
Measurements made at the same location on different days.
Source at F26, receiver at F12. on 9/7/84 and 8/8/84 (--r--).

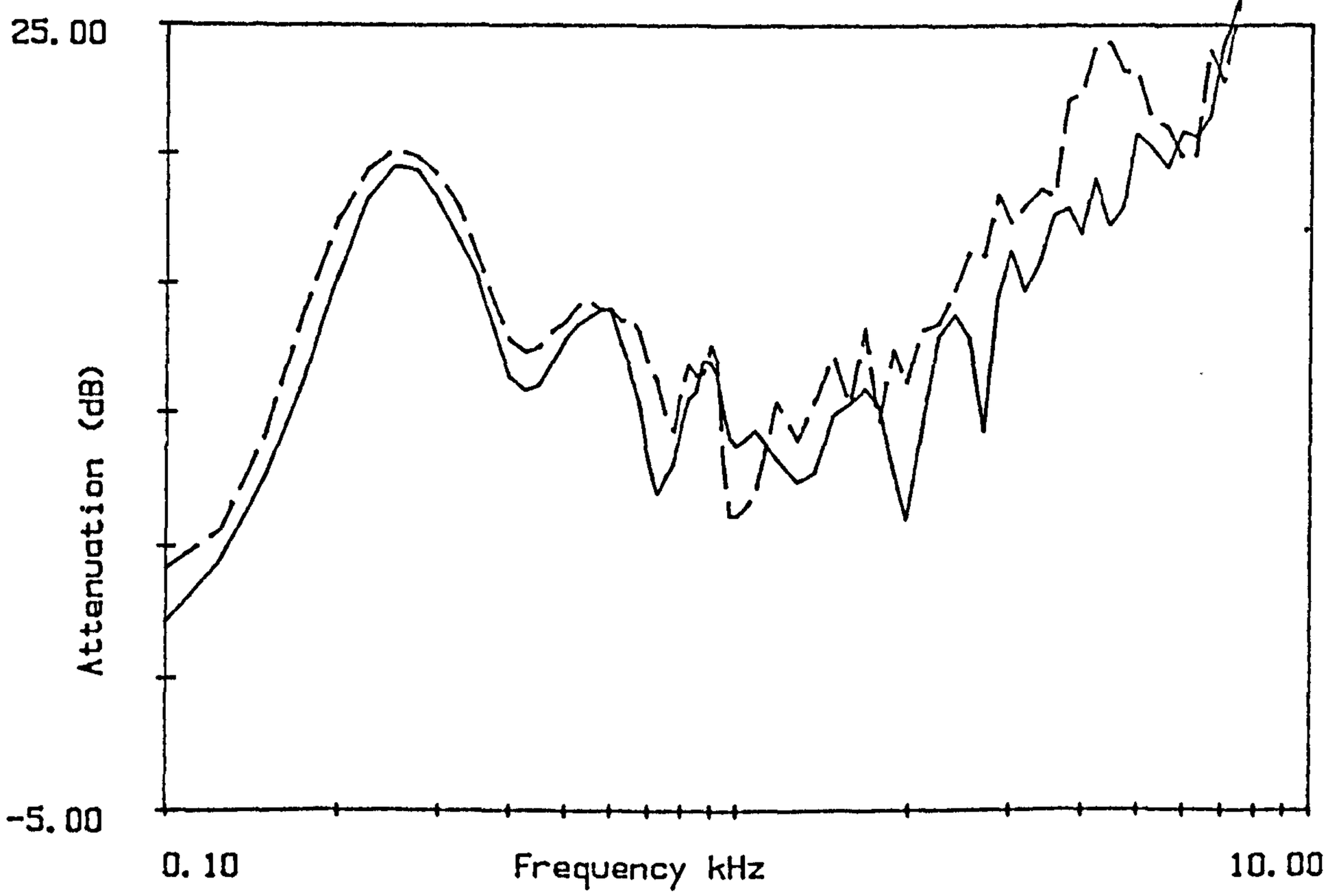

Figure 6.4.3
Measurements made at the same location on different days.
Source at F26, receiver at G40. on 9/7/84 and 8/8/84 (-----).

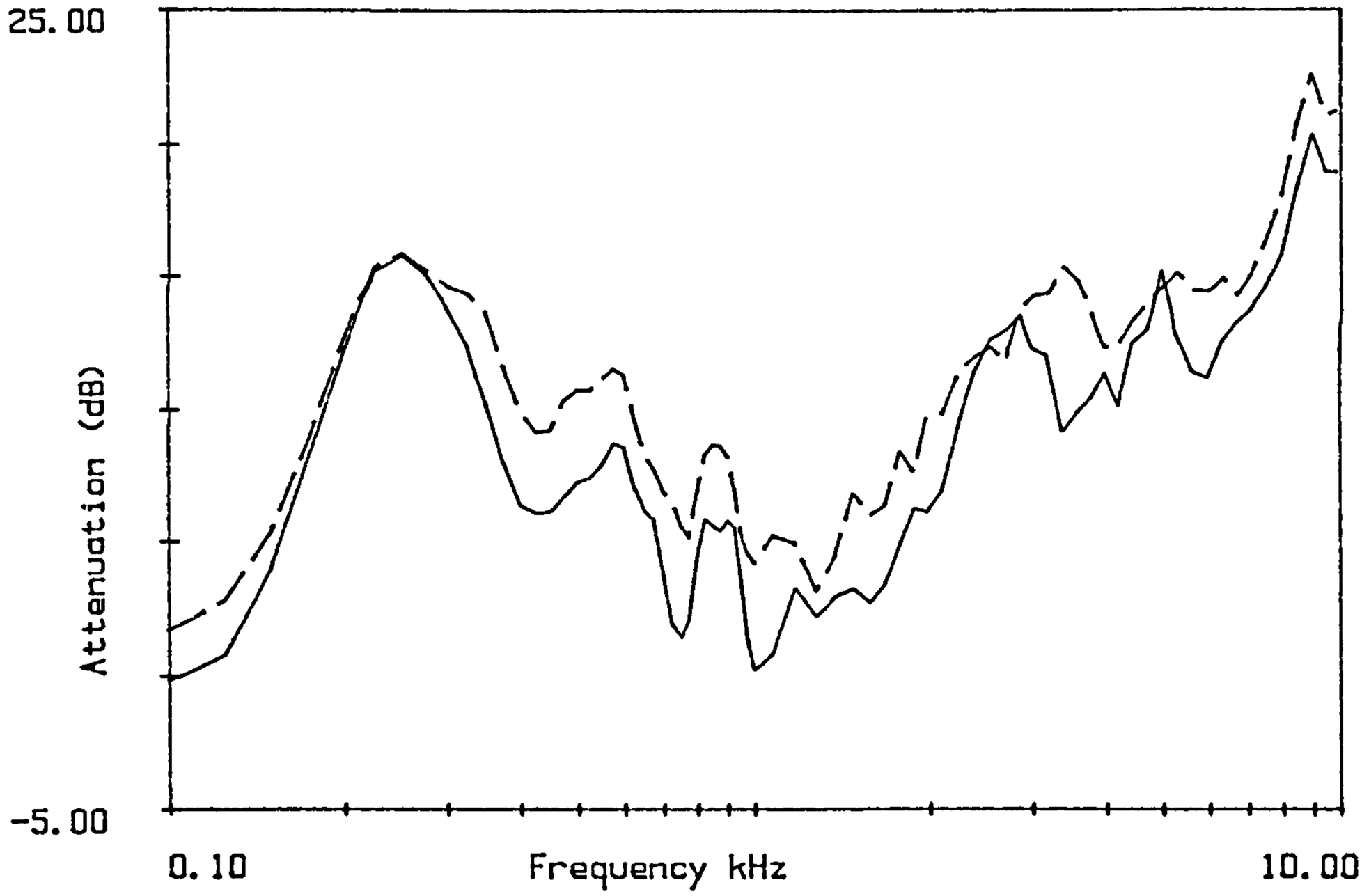

Figure 6.4.4
Measurements made at the same distance along different tracks.
Each spectrum is the mean of the values on 9/7/84 and 8/8/84 at 1.2
Source at F26, receiver at F26 and G24(------).

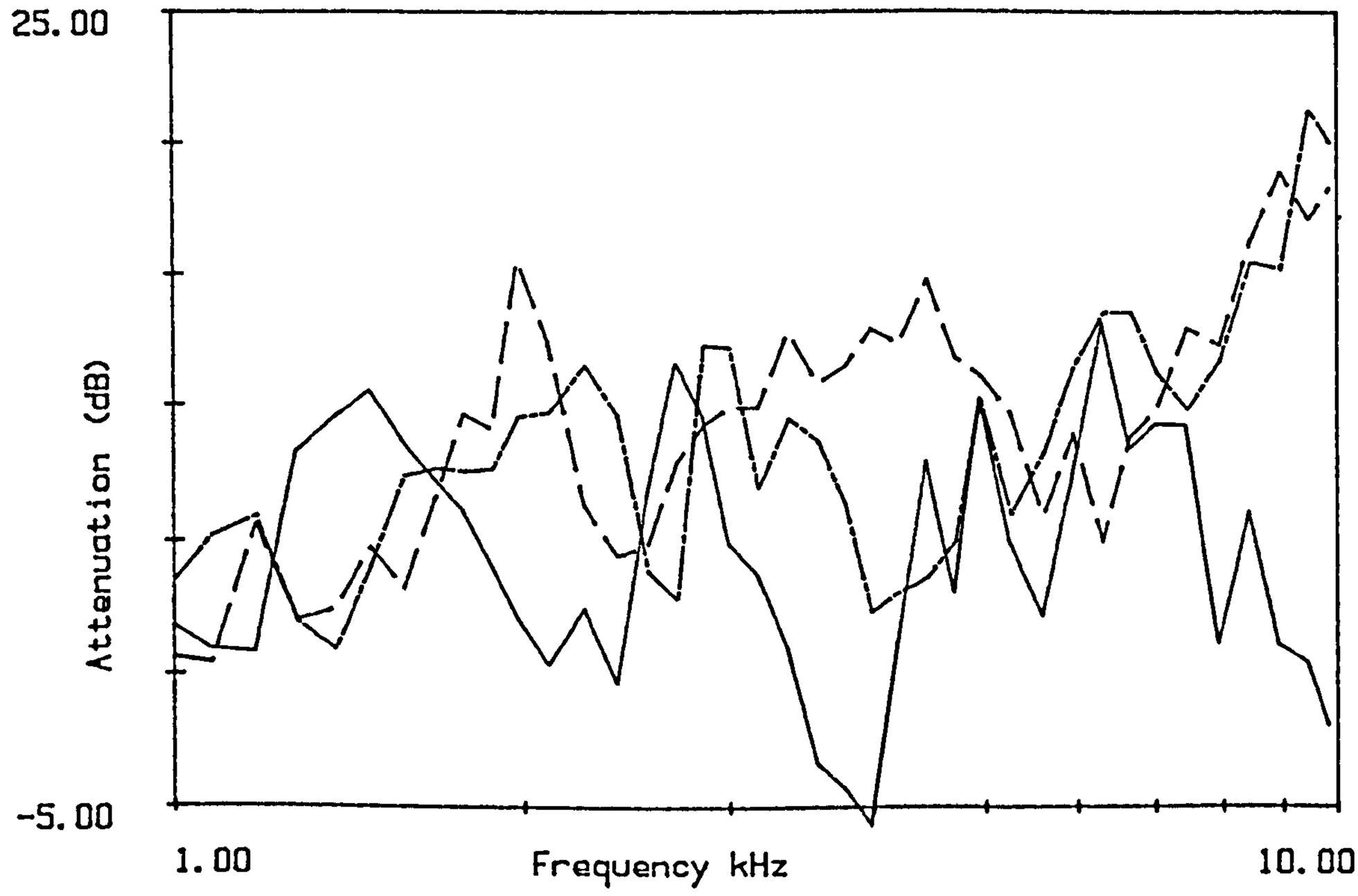

Figure 6.4.5
Attenuation per 24m for shorter distance measurements at Bucknell.
———— source at FS receiver at F12 8/8/84 1.2m height.
— — — source at F26 receiver at F12 8/8/84 mean of 2 heights.
———— source at F26 receiver at F12 9/7/84 mean of 2 heights.

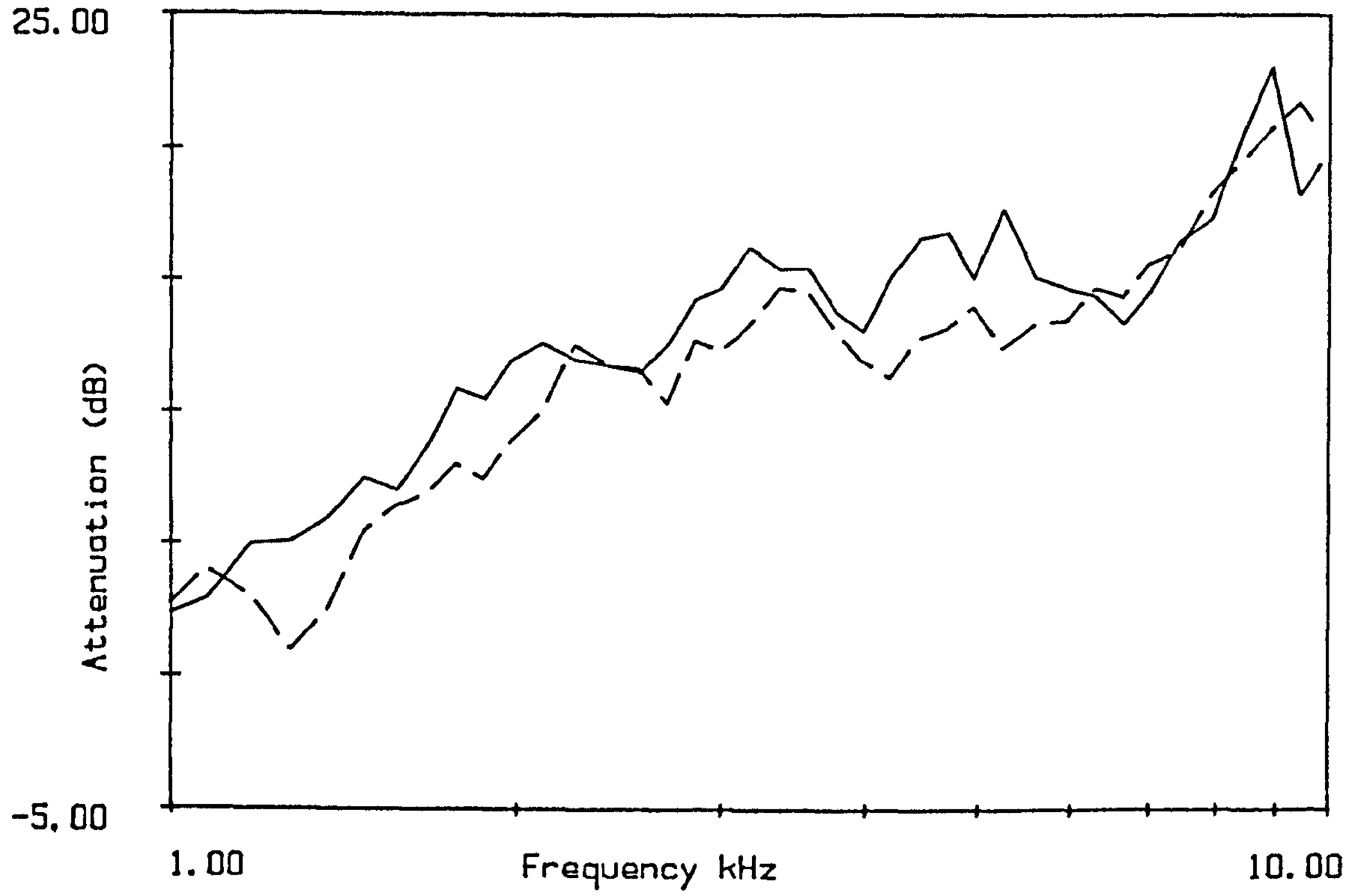

Figure 6.4.6
Attenuation per 24m for 24m measurements at Bucknell. (G track)
——————— source at F26 receiver at G24 8/8/84 mean of 2 heights.
— — — source at F26 receiver at G24 9/7/84 mean of 2 heights.

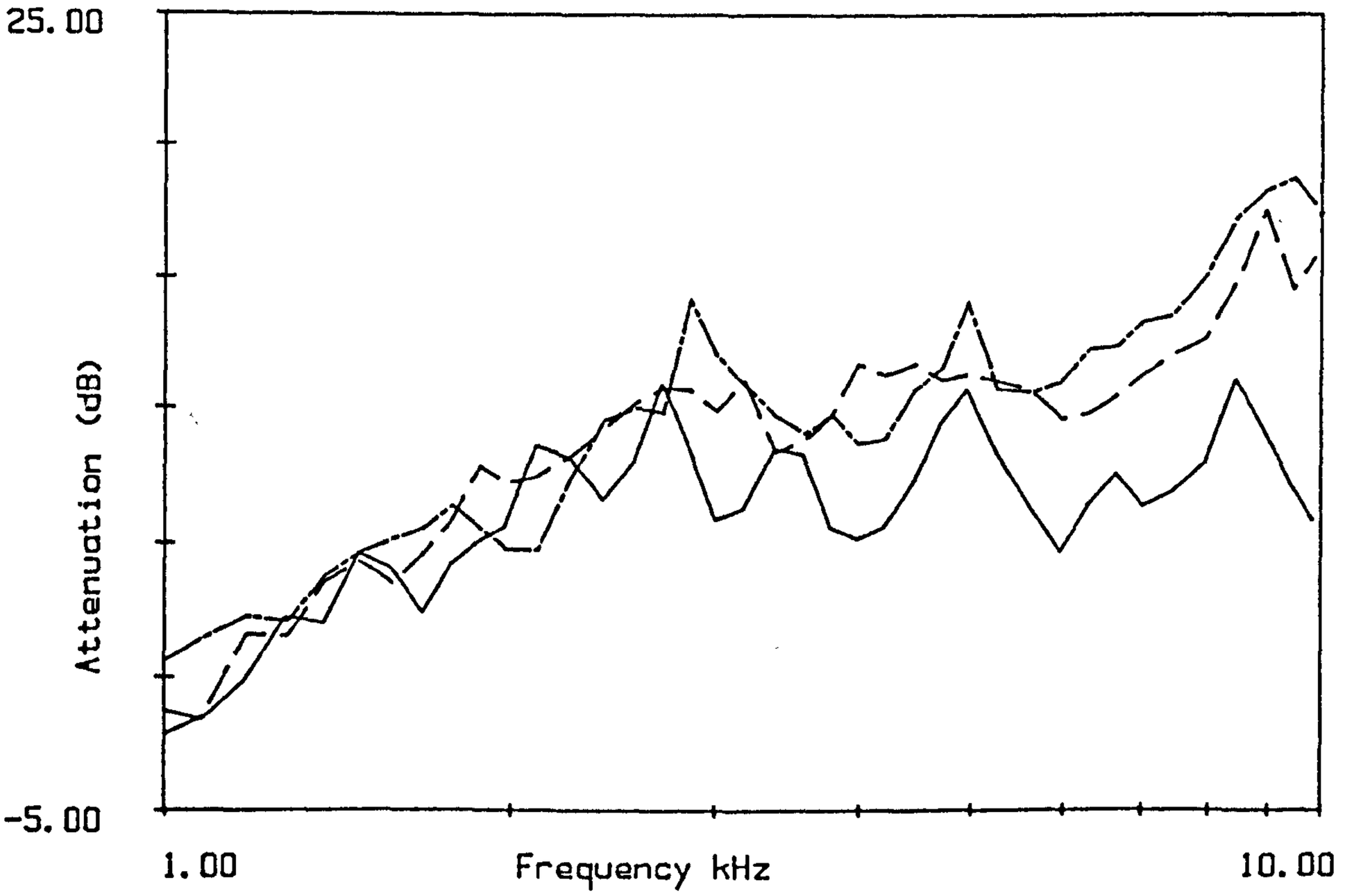

Figure 6.4.7
Attenuation per 24m for 26m measurements at Bucknell (track F).
——————— source at FS receiver at F26 8/8/84 mean of 2 heights.
— — — source at F26 receiver at FS 8/8/84 mean of 2 heights.
—·—·— source at F26 receiver at FS 9/7/84 mean of 2 heights.

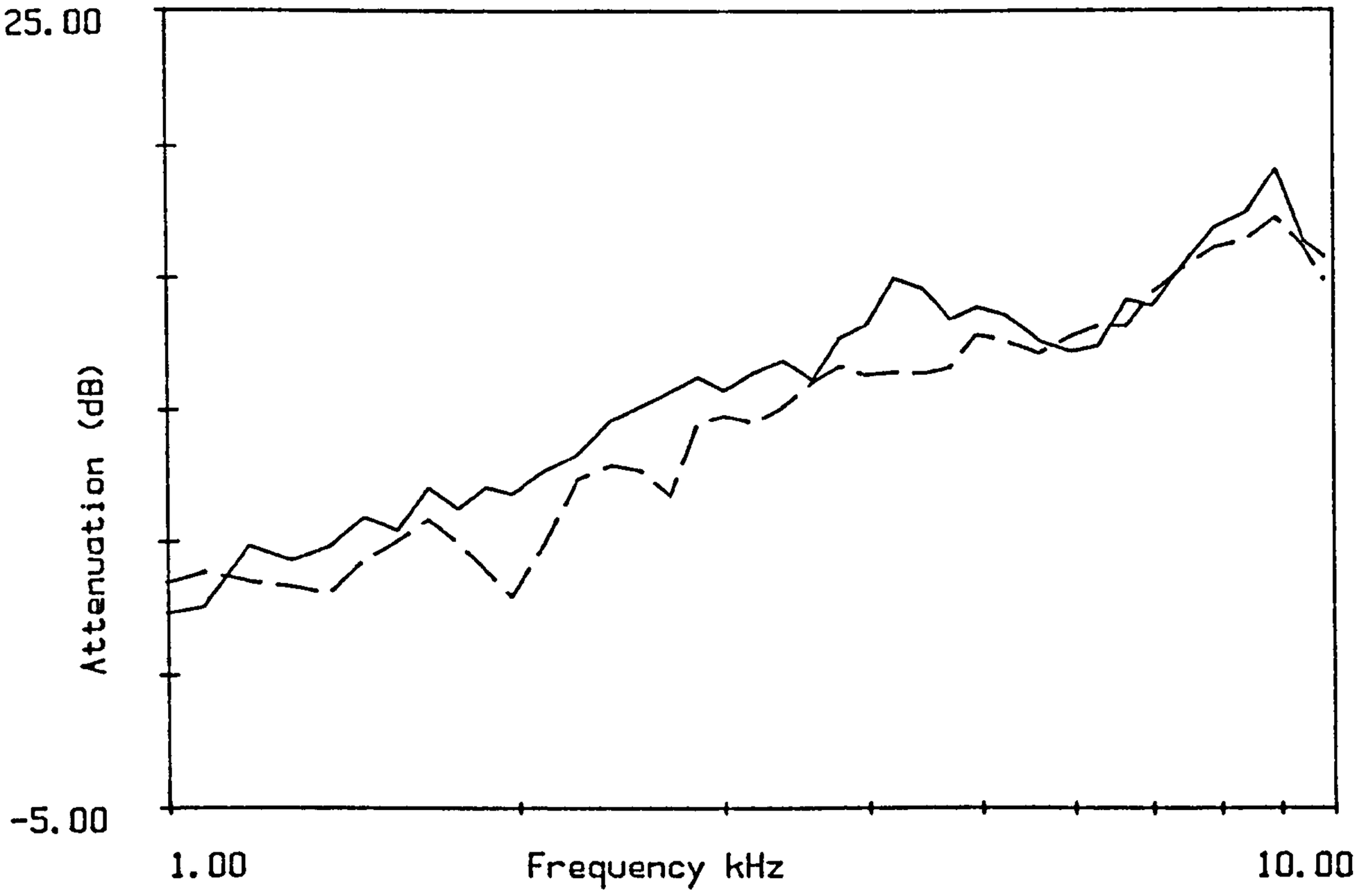

Figure 6.4.8
Attenuation per 24m for 40m measurements at Bucknell. (G track)
——— source at F26 receiver at G40 8/8/84 mean of 2 heights.
— — — source at F26 receiver at G40 9/7/84 mean of 2 heights.

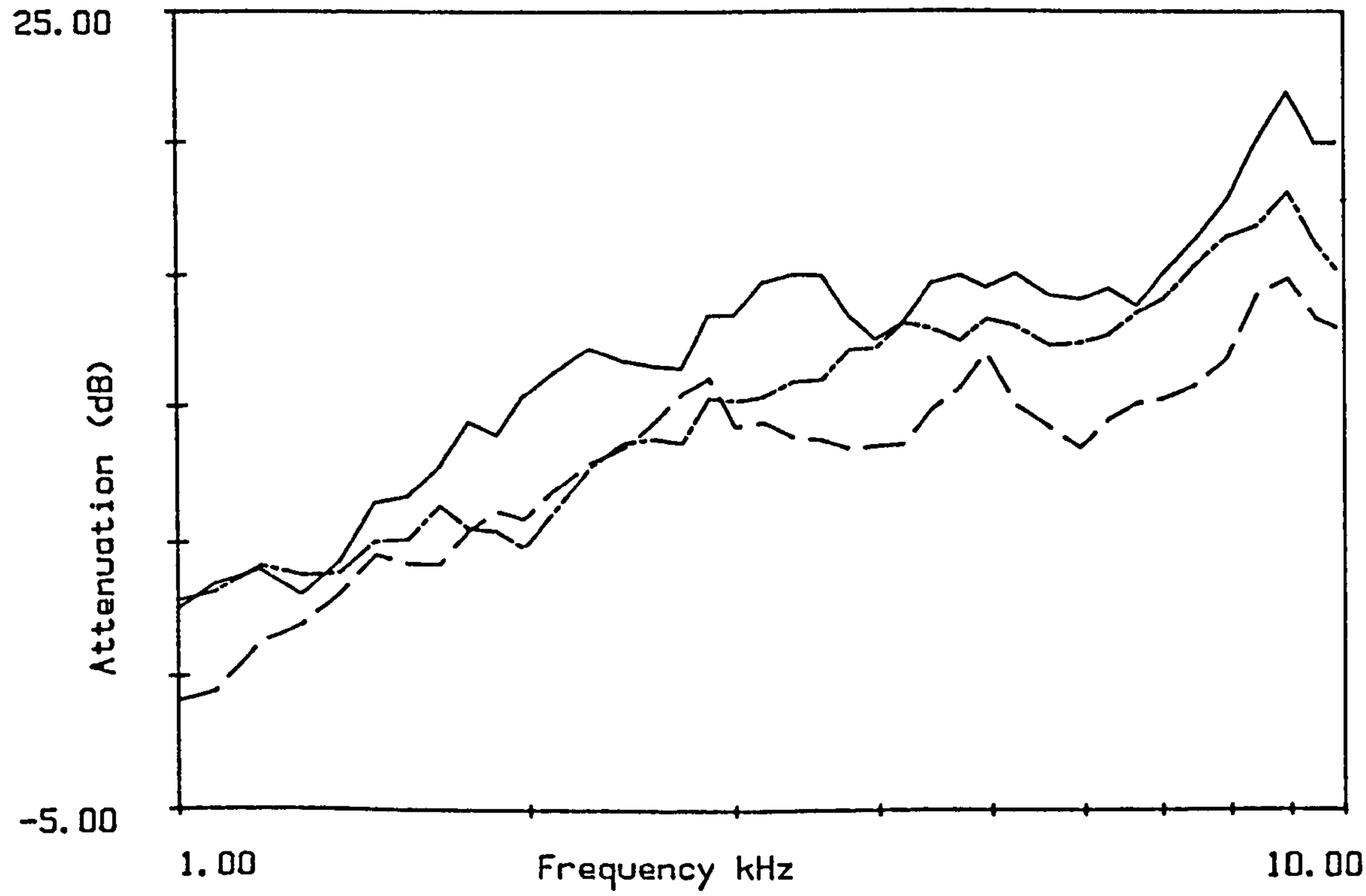

Figure 6.4.9
Attenuation per 24m for 26m, 24m and 40m measurements at Bucknell.
——— 24m along G track mean of both days.
— — — 26m along F track mean of both days.
——·—·— 40m along G track mean of both days.

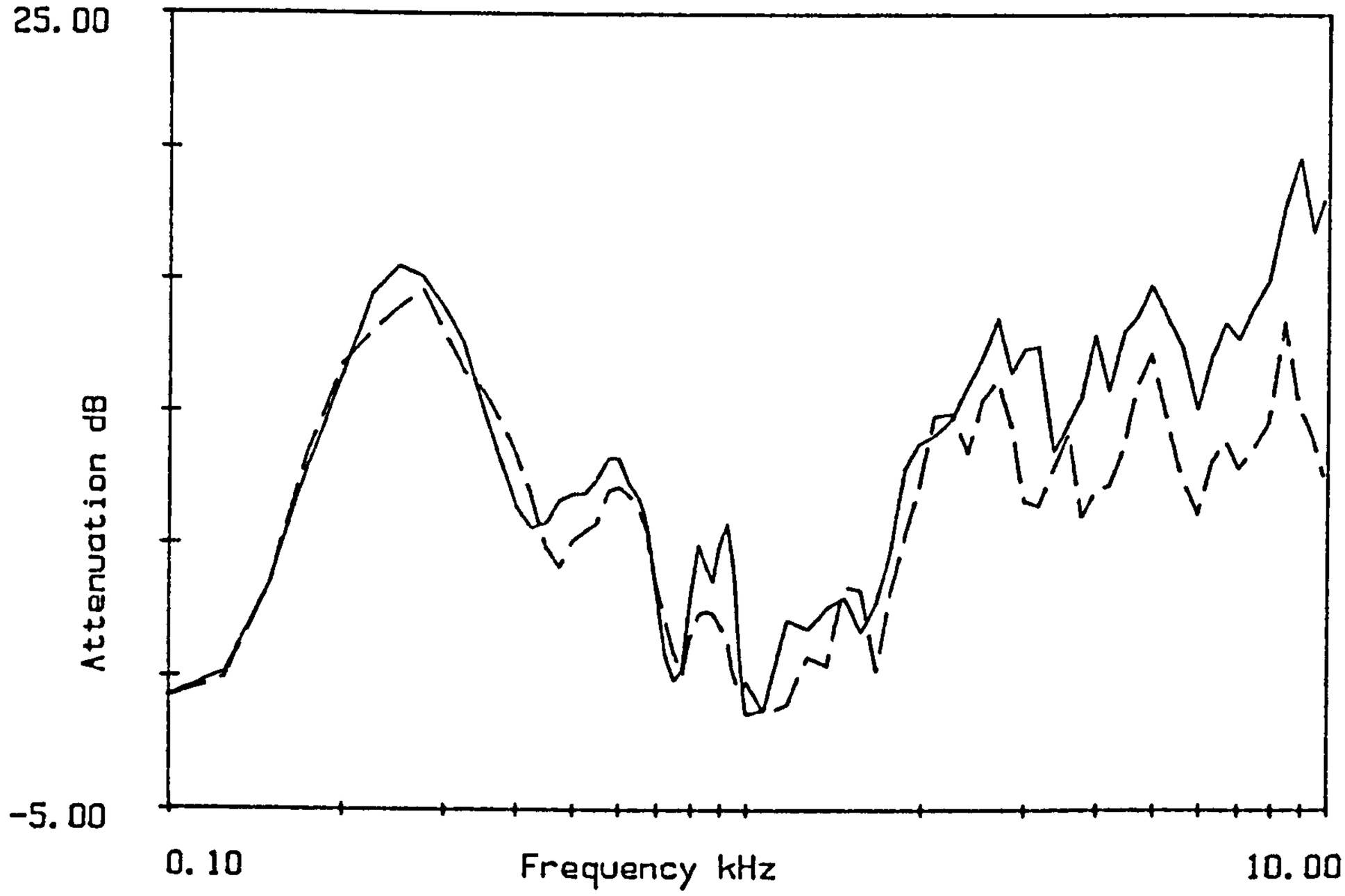

Figure 6.4.10
Measurements made along the same path in opposite directions.
measurements made 8/8/84. Path is between F26 and FS.
Microphones at FS, and microphones at F26(-----). 1.2m height.

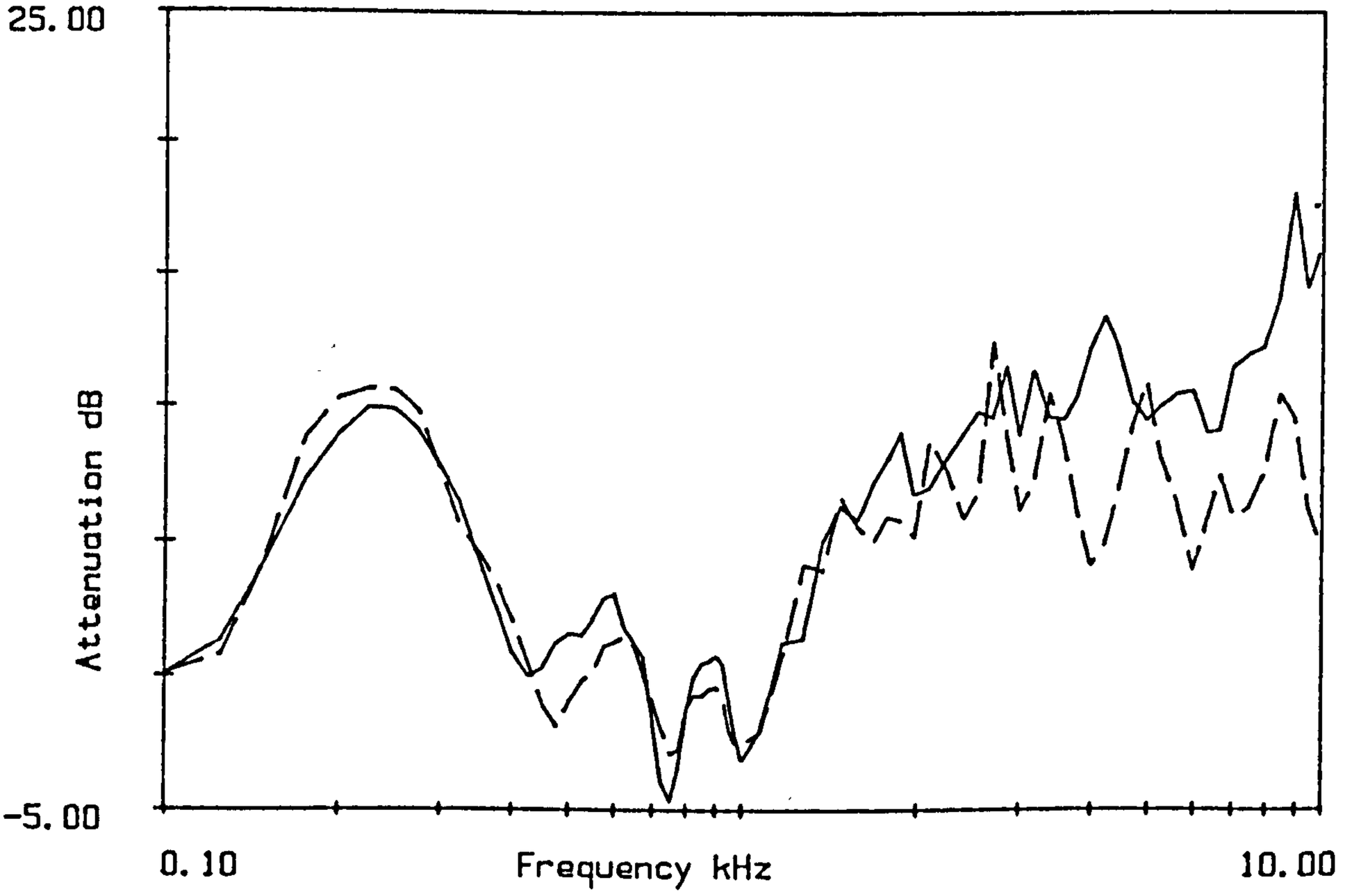

Figure 6.4.11
Measurements made along the same path in opposite directions.
measurements made 8/8/84. Path is between F26 and FS.
Microphones at FS, and microphones at F26(-----). 2.5m height.

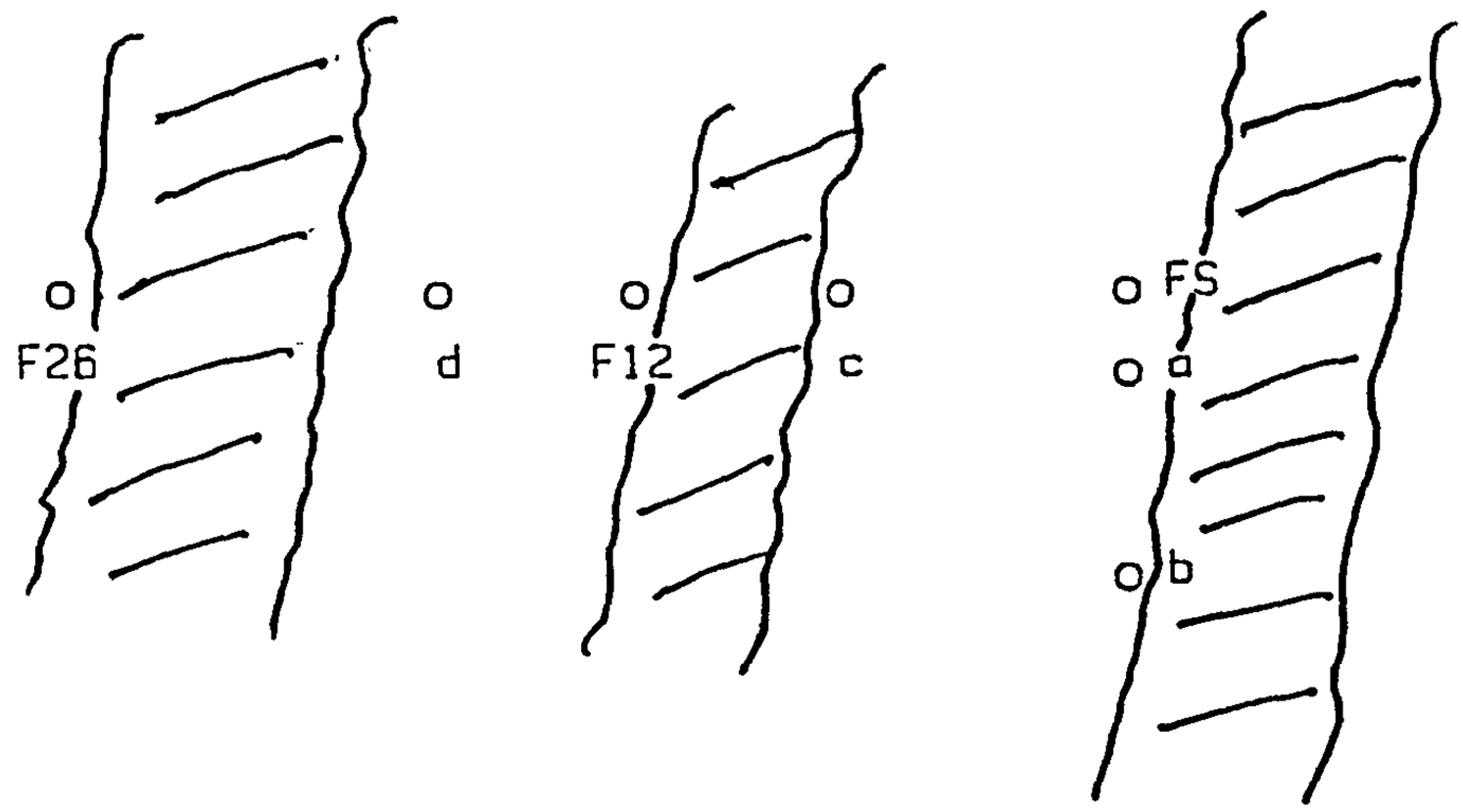

Figure 6.4.12
Layout of Experiment on 2/7/85.

Scale
|——————————| = approximately 12m

= Red cedar rows.

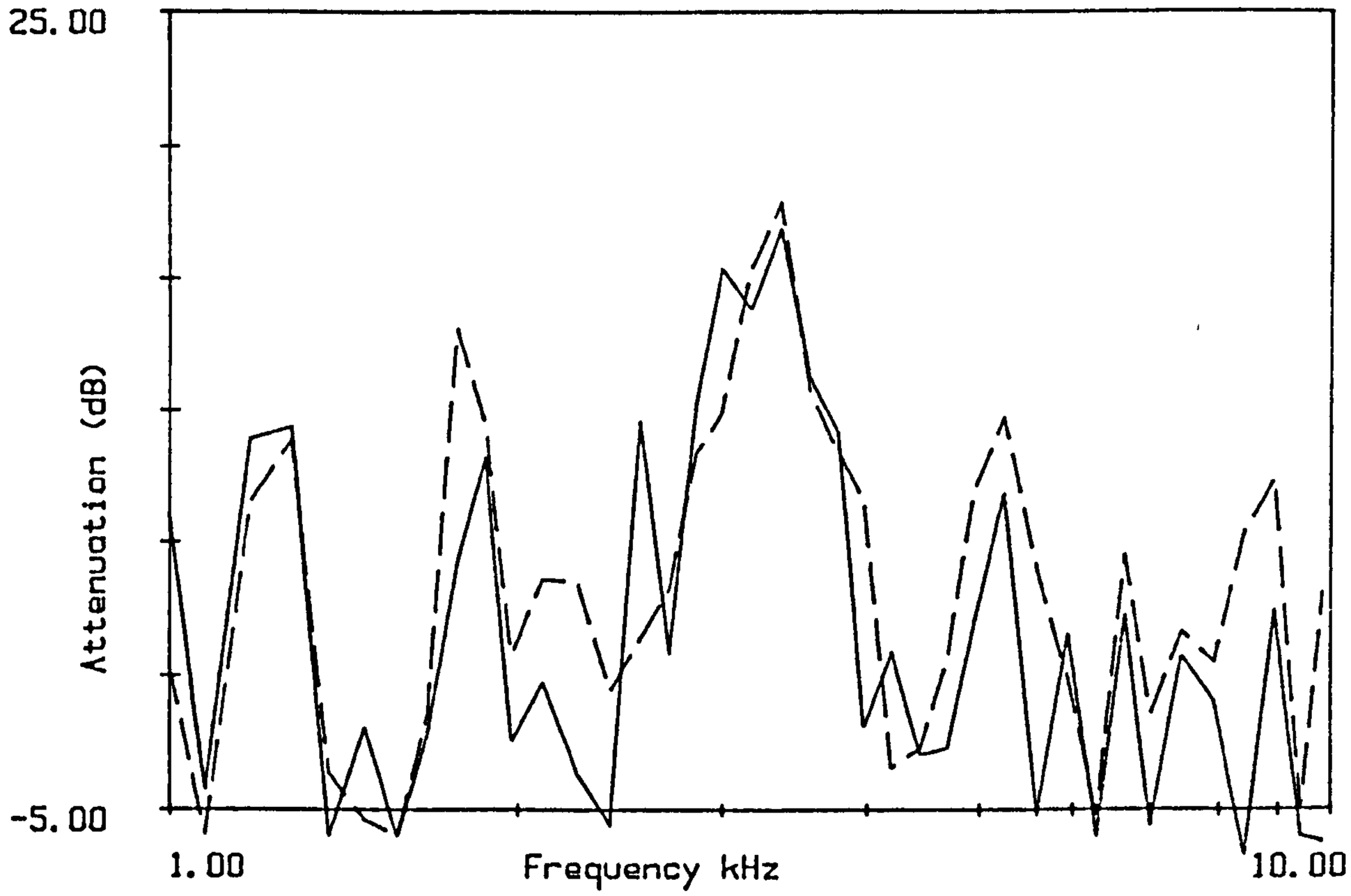

Figure 6.4.13
2/7/85 mean of attenuation at 7m separation distance.
Measurement 1 (no trees in path), and 2 (-----)

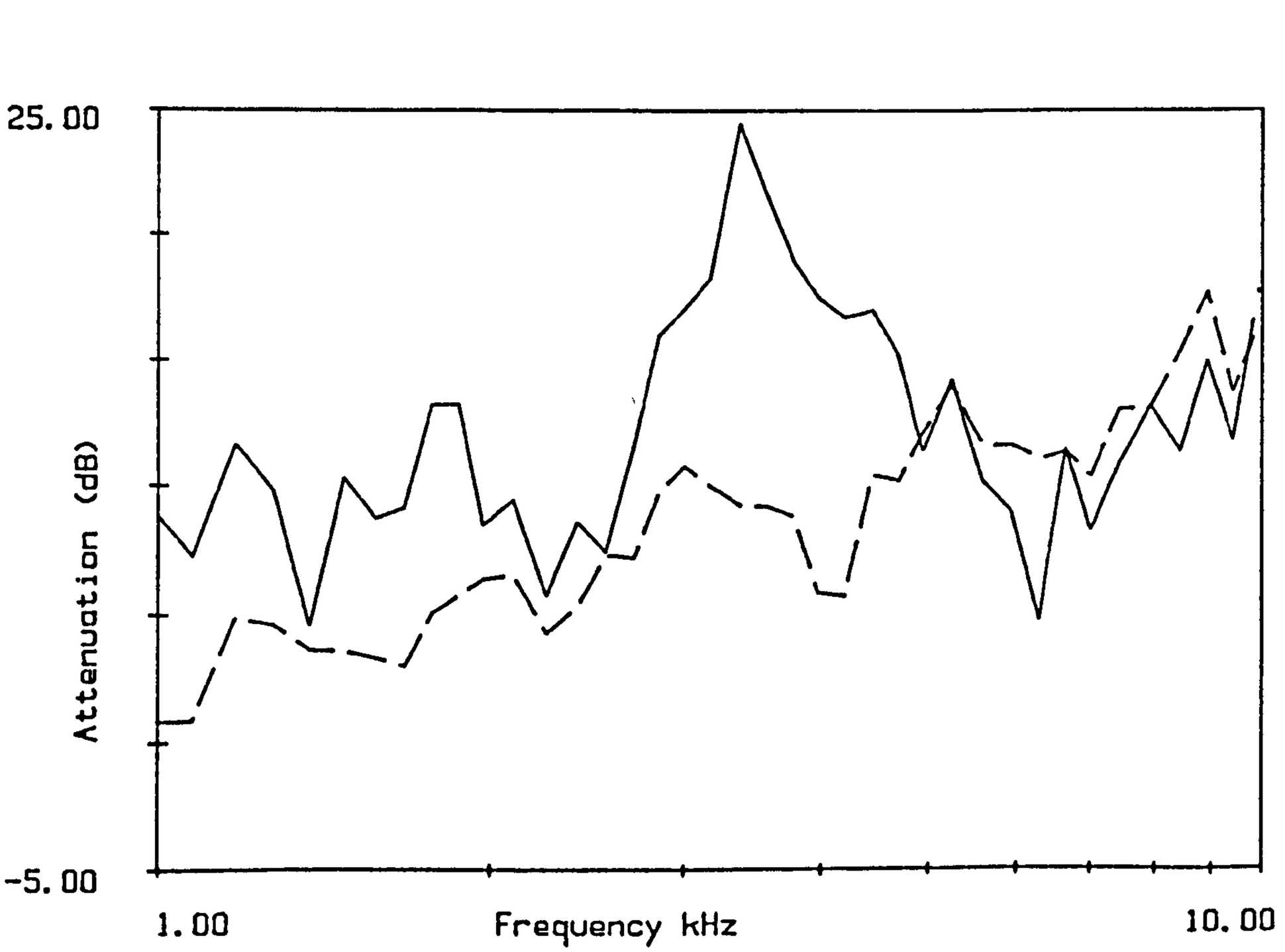

Figure 6.4.14
2/7/85 mean of 4 attenuation measurements, microphone at F26, source at FS and at F12(-----).

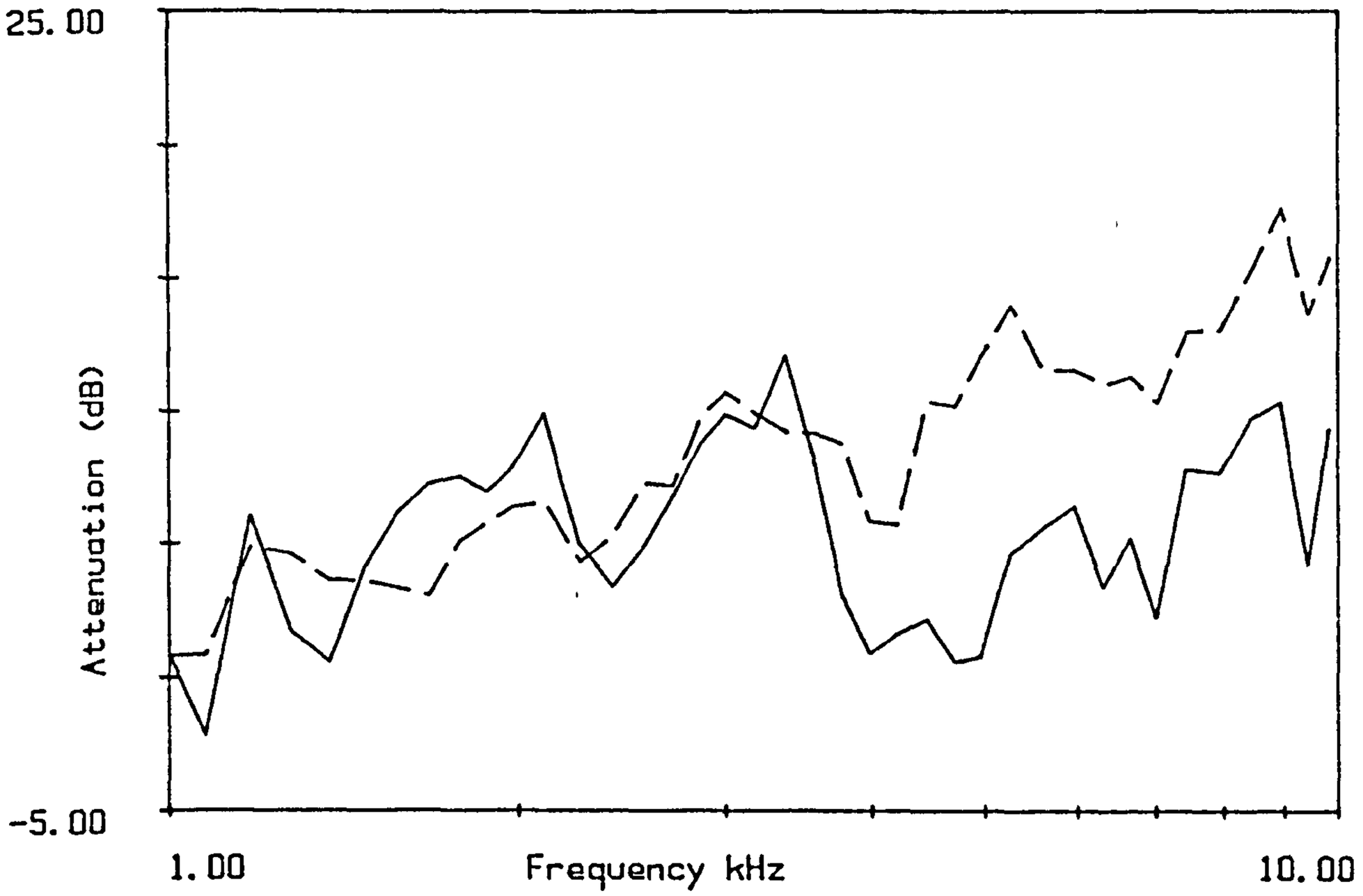

Figure 6.4.15
2/7/85 mean of 4 attenuation measurements, microphone at F26, source at FS and source at FS microphone at d (16.8m). (-----)

Chapter 7: Experiment to Investigate Scattering by an Array of Cylinders.

Experiments were carried out to assess the magnitude and frequency dependence of attenuation caused by an array of cylindrical scatterers. The Embleton model described in chapter 5 defines the attenuation by an array of infinitely long cylindrical scatterers so the first experiment was designed to determine the validity of this model in scale model experiments. The second experiment assesses the attenuation by an array of scatterers near to a ground surface, a situation more comparable to the field measurements described in chapter 6. Both parts of the experiment were carried out using the apparatus illustrated in figure 7.1.

7.1 The infinite length cylinder case.

Method

An array of long, cylindrical scatterers was constructed in a small anechoic chamber. The cylinders used were wooden dowel rods of 6mm or 12mm diameter, there were 160 rods of each diameter. A piece of welded wire mesh with parallel wires 12mm apart was attached to the ceiling of the anechoic chamber, below the foam lining of the chamber. The wire mesh was marked with a grid so that each hole of the mesh could be identified by x and y coordinates. A FORTRAN routine using a system subroutine for generating random numbers, was used to generate a series of random locations (x and y coordinates) for the rods in an array of given density and length. The distance between the top of the foam and the wire mesh was a few centimeters less than the length of the rods (ie about 1.8 meters). Each rod was located in the square of the mesh corresponding to the x,y coordinates of the random array. The bottom of the rod was located on the foam so that it was supported in a near vertical position. The rods were evidently not exactly vertical since they were simply judged by eye and could move around within the squares of the mesh. Some measurements were made comparing the array with the cylinders judged to be near vertical and the same array with the rods deliberately moved away from the vertical position.

The sound source used was the air jet described in detail by Heap (1982) which gives a broad band random noise signal with much energy in the high frequencies. The air jet behaves as a spherical source with the actual position of the origin of the sound between 2 and 4 mm above the top of the air jet (Heap 1982). The air jet was located within the array, clamped to a retort stand.

An array of four microphones were used, to give a spatial average of attenuation. The microphones were attached to a horizontal rod in the chamber. The microphones were thus oriented with the diaphragms approximately normal to the wave front. Details of the microphones and preamplifiers used are given in figure 7.2. These microphones systems were chosen as they were the only small diameter microphones available. Half inch microphones were considered to have insufficient response at high frequencies for this experiment since the experiment relied on recording high frequencies, up to 100kHz. The x and y coordinates of the source and microphones were determined by suspending a plumb-line from the wire mesh, at a known x,y location so that it was just touching the end of the microphone or slightly above the centre of the top of the air jet. The separation distance between the source and each of the microphones was 0.6m to 0.7m.

The experimental set up was assumed to approximate to the case of infinitely long cylinders, since the propagation path is shorter than the distance between the source or receivers and the end of the cylinders, or the floor, ceiling or grid. The pathlength difference is therefore sufficiently large to reduce the level of any reflections from the floor or ceiling to 8 to 10 dB less than the direct signal, even if a rigid surface is assumed (there is no hard surface so the level of reflections is likely to be considerably lower).

Attenuation measurements were carried out as follows:

i) The array of rods were installed in the anechoic chamber and the compressed air source to the air jet turned on. The air jet was left on throughout the experiment to avoid any changes in pressure and therefore sound level, between the different measurements.

ii) The signal from two microphones was fed into two measuring amplifiers (type 2607 or 2608) and the attenuators set to give a suitable output level to the Nicolet FFT spectrum

analyser. The rms spectra from the two microphones was averaged over 128 .004 ms samples giving an rms spectrum of the signal up to 100kHz - the maximum range of the instrument. The rms spectra were transmitted to the computer.

iii) The other two microphones were then plugged into the measuring amplifier and similarly analysed. Various measurements were made with the rods in place eg. they may have been moved out of the vertical position or a portion or the array removed.

iv) All the rods were then removed from the chamber, taking care not to move the microphones or air jet, and the free field sound of the air jet measured at each of the microphones.

v) The air jet was then switched off and the noise from the system measured, ie the same procedure carried out as for the experimental measurements, with the same attenuator settings on the measuring amplifiers.

The attenuation is calculated as the difference between the free field sound pressure level and the level with the scatterers in place. In practice this was actually the ratio between the output voltages from the measuring amplifier for the two cases: corrected for any difference in measuring amplifier gain, this was not generally required since the 'with' and 'without' measurements were made using the same attenuator settings. Since the whole system is the same for both measurements ie. the same microphones, cables, preamplifiers and amplifiers, no other calculation or correction is required. The data was again smoothed before plotting.

Arrays Constructed

Figures D.1 to D.13 in appendix D illustrate the measurements made. The sizes of the array, the rods and the source are approximately to scale. Brief descriptions of the arrays are given in table 7.1. Five arrays were created using the same locations, first with the 6mm rods and then the 12mm rods; the locations of the source and microphones were also approximately the same. Two of these arrays are random with densities of 240 (measurements A-6 and A-12), and 360 rods / m^2 (measurements B-6 and B-12). The regular arrays of measurements C to E were used because the density is more uniform and can easily be

altered by removing each alternate row (D-6 and D-12) and then each alternate column (E-6 and E-12). this gives arrays with densities of approximately 400, 200 and 100 rods / m^2 respectively. Measurement F is a mixed array in which the array from A-12 is used and another random array with the same density (240 rods / m^2) created within it using the 6mm rods. Measurements A-6, B-6 and B-12 were repeated with the rods deliberately moved so they were located in the same grid square at the top but were no longer vertical or near vertical, to investigate how much influence the orientation of the rods has on the overall attenuation.

Table 7.1: Description of arrays (illustrated in Appendix D)

Measurement number	radius	density	arrangement
A-6	0.003	240	random
B-6	0.003	360	random
C-6	0.003	400	regular
D-6	0.003	200	regular
E-6	0.003	100	regular
A-12	0.006	240	random
B-12	0.006	360	random
C-12	0.006	400	regular
D-12	0.006	200	regular
E-12	0.006	100	regular
F	0.003/0.006	480	random

Results

In this section the conclusions to be drawn from the results will be disussed with reference to some examples of attenuation measurements from individual measurements and mean values.

Air Jet Free Field Spectra.

Figures 7.3a to 7.3d show the spectra of the air jet measured at each of the four microphones, from measurement B-6, for the without scatterers ('free field') case, the scattering case and background noise. The separation distance was about .65m and the array was of 6mm rods with a density of 360. The spectra are the Voltage levels output from the measuring amplifiers in decibels relative to 1 Volt. The attenuator was set at a different setting for the 1/8 inch microphone (microphone 3) ie. the gain was 20dB greater than that for the 1/4 inch microphones because of the lower microphone sensitivity of the 1/8 inch microphone, but the Voltage output from the measuring amplifier is of a similar level.

It is evident that the 'without scatterers' spectrum is dependent on the free field spectrum of the air jet, air absorption, the frequency response of the microphone, background noise and any reflected sound energy. The air jet has been shown (Heap 1982) to approximate to a spherical source, therefore the free field level is the same at all the microphones, with only very small differences in level due to the slightly different separation distances. The 1/8 inch microphone has a flatter frequency response to higher frequencies than the 1/4 inch ones as can be seen in figure 7.3d. The spectrum shape from the three 1/4 inch microphones is very similar, ie. the graphs of the spectra are approximately parallel with small differences in magnitude due to differences in the sensitivity and gain of the different systems. The 1/8 inch microphone spectrum is also very similar in shape up to about 50 kHz, the difference at the higher frequencies being due to the better response for the 1/8 inch than the 1/4 inch microphones. This suggests that the spectrum measured is very close to the actual free field spectrum of the air jet, since any reflections from elements of the chamber would affect the microphones differently due to their different locations.

Signal to Noise Ratio

Figures 7.3a to 7.3d also illustrate a comparison between the received spectra with the air jet turned on (both with and without scatterers cases) measurements and the 'noise' for the measuring systems ie. the measuring set up was the same with the same attenuator settings, but the air jet was switched off. For most frequencies the signal is considerably higher (40 to 50 dB) than the noise, the difference being lower at both ends of the frequency scale. The signal is always at least 10dB above the noise therefore the signal level is assumed to be high enough to give a reliable result at all frequencies. A similar check was carried out for all the measurements with and without the arrays in place to ensure an adequate signal to noise ratio for each experiment. In a few cases the signal to noise ratio was less than 10 dB for the 1kHz point but no correction is made for this. It is possible that the noise introduced some inaccuracies into the low and high frequency parts of the measurements.

Attenuation Spectra

Figures 7.4a to 7.4d show typical examples of the measured attenuation spectra from each of four microphones. The attenuation spectra were calculated from measurement A-6; ie a separation distance of about 0.65m and an array of 6mm rods with a density of 240 rods / m^2. The solid lines are the first set of measurements and the broken lines the measurements made after the rods had been moved slightly. The series of sharp peaks and dips at different frequencies in the different measurements suggests that some interference effects occurred; that is, two or more paths between the source and receiver exist causing cancelling and enhancing effects related to phase differences. The geometry of the system relative to the floor and walls of the anechoic chamber was unchanged between the free field and scattering cases so that the peaks and dips caused by interferences were unlikely to have been caused by reflections from elements of the chamber or measurement system. The interferences can therefore be assumed to result from reflection by the cylinders. This assumption is supported by the fact that the measurements with the cylinders in slightly different positions have different patterns of attenuation. Similar conclusions can be drawn from the data of the 12mm arrays where the cylinders were moved out of the vertical. (see figures D.20 to

D.23)

The low frequency parts of the attenuation spectra are generally close to zero with only small scale peaks and dips. This suggests that little scattering occurred, the small scale deviations being within the accuracy of the measuring system. Scattering effects are obvious above these frequencies, both as interference patterns and as a positive attenuation. The lowest frequency at which the scattering effects are obvious are between 5 and 10 kHz for the 6mm rods and between 2 and 6 kHz for the arrays containing 12mm rods, indicating that the diameter determines the frequencies that are scattered, as would be expected. The frequency at which the wavelength is equal to the diameter of the rods is 57.17 kHz and 28.58 kHz for the 6mm and 12mm rods respectively, but there is significant scattering at frequencies well below this, as low as frequencies at which the wavelength is ten times the diameter of the rods. Theories predicting the scattering by a single scatterer suggest that there is little or no scattering effect when the wavelength is much larger than the scatterer. In multiple scattering theory, ie where the density of scatterers is sufficiently large, the single scatterers interact to give an effect which is greater than the sum of the effects of the same number of single scatterers. These results, therefore, demonstrate that multiple scattering occurred in the experiment.

At higher frequencies the attenuation increases with increasing frequency. Many of the spectra flatten or drop at the top end of the frequency range. The marked high frequency dip in some of the data (eg figure 7.4a) may simply be a result in the drop in sensitivity of the microphones at high frequencies introducing an inaccuracy into the measurement.

The differences between the attenuation spectra with the rods in slightly different positions is not very great in most of the attenuation spectra examined. This suggests that the attenuation is not greatly affected by the fact that the rods are not located exactly in the same place or exactly vertically; certainly this will not significantly affect the average attenuation values. The source - receiver separation distance was virtually the same for all the microphones, the differences between attenuation at the different microphones is therefore due to the fact that the array was random rather than regular, so the propagation paths had a different arrangement of scatterers which would evidently cause differences in

attenuation.

Measurements were carried out with array A-12 then repeated with the rods behind the microphones removed (see figure D.13), thus the microphones were at the edge of the array rather than within it. Figures 7.5a to 7.5d show the comparisons between the two cases (ie microphones at the edge of, or within the array) at each microphone for these measurements. There is some evidence of a slightly smaller attenuation with the rods removed, but the differences do not seem to be significant therefore the other measurements made with the microphones at the edge of the array are assumed to approximate to the case of receivers within a semi-infinite array, as is defined for the predictive model. A similar result was obtained by removing all the rods behind the microphones in the array of experiment F, and comparing the attenuation with that of the whole array, figure 7.6 is an example of such a comparison; again showing that removing the rods behind the microphones has little effect on the attenuation.

Paired Comparisons Between Mean Spectra.

The overall attenuation should be assessed as a mean from many locations to eradicate the effects of interferences in the comparisons between different arrays and between the measured and predicted values. In the following sections the mean values of different measurements are compared to investigate various factors involved in the attenuation of sound by the arrays. The comparisons are made by plotting the mean values of all the attenuation spectra (from the four microphones) for two particular measurements on one graph, and comparing the spectra visually. The maximum and minimum attenuation values (the 'range' of values) obtained from the four microphones are plotted on a second graph in order to assess whether any differences in the mean values can be considered to be significant ie whether the range of values obtained overlaps.

6mm vs 12mm rods.

Figures 7.7 and 7.8 compare the mean attenuation values from measurements A-6 and A-12 and B-6 and B-12. The arrays of 12mm rods generally give a higher attenuation than those of 6mm rods. The range of values only overlap slightly for array A (figure 7.7a) but overlap considerably more in the more dense array B, (figure 7.8a) ie the difference between the two diameters is less marked. The difference between the 12mm and 6mm arrays for the regular arrays (C,D,E) is negligible (see figures 7.9). The attenuation appears to be lower for array E-12 than for E-6, which is rather unexpected, the attenuation values for this array are, however very small.

Random vs Regular Arrays.

The array density and source and receiver positions were approximately the same for measurements B-6 and C-6 (6mm rods) and for B-12 and C-12 (12mm rods) but the distribution of the rods is different. B-6 and B-12 being random arrays and C-6 and C-12 arranged in regular rows. Figures 7.10 and 7.11 show the mean values of the attenuation measured for the two arrays and Figures 7.10a and 7.11a show the range of attenuation values obtained at each frequency. Figures 7.11 and 7.11a show that the random array gives a slightly higher mean attenuation than the regular array for the 12mm rods, although the density is slightly lower, this difference is not significant since the ranges overlap over most of the spectrum. The regular array appears to have a rather smaller spread of data than array B-12. Figures 7.10 and 7.10a show even less difference for the 6mm rods except at frequencies between 10 and 20 kHz and at the highest frequencies, where the random array gives a slightly higher attenuation. The regular array again has a slightly smaller range of attenuation values. There does seem to be some difference between the random and regular arrays which cannot easily be defined from the limited results here. The smaller range of values observed suggests that the four propagation paths for the regular array were more similar than those for the random array as might be expected eg. from figures D.3 and D.8 in Appendix D. The differences in the conclusions of the previous section concerning the differences between 6mm and 12mm diameter rods also point to differences between the

regular and random arrays. It is possible that some form of multiple reflections between the rods arranged in regular rows cause the differences in the patterns of attenuation. The differences are, however, small.

Two densities of random arrays.

Figures 7.12 and 7.12a show the comparison between the mean attenuation spectra for the two different densities of random arrays. There is little difference in the attenuation obtained with the two arrays; with a more marked difference between those constructed with 6mm rods than the 12mm arrays. This shows that the attenuation is not much affected by changes in the density of the arrays.

Regular Arrays With Half and Quarter Densities.

The regular arrays D and E are formed by removing parts of array C so that D has half the density of C, and E has half the density of D (see figures D.3 to D.5). Figures 7.13a to 7.13d show some comparisons between the mean attenuations for these arrays, comparing the different densities of arrays. The mean attenuation for array C is greater than that of arrays D and E for both the 12mm and 6mm rod measurements. The difference between arrays D and E is less marked. The attenuation measured for array E is very low, it is negligible for the 6mm rods but generally above zero for the 12mm rods. Array D gives slightly greater attenuation than array E for the 6mm rods but arrays D-12 and E-12 give very similar results. Again, these results show that the attenuation is relatively insensitive to changes in density. The very small values for arrays E perhaps indicate that the attenuation is only similar above a certain density which is sufficient to give a measurable attenuation. The wide ranges of attenuation values obtained makes interpretation of the differences uncertain.

Mixed 480 array vs pure 240 array.

Figure 7.14 demonstrates that adding an array of 6mm cylinders within the array of 12mm cylinders did not give a significantly greater attenuation. There is also no significant difference between the results from array B-12 and the mixed array F. (figure 7.14a)

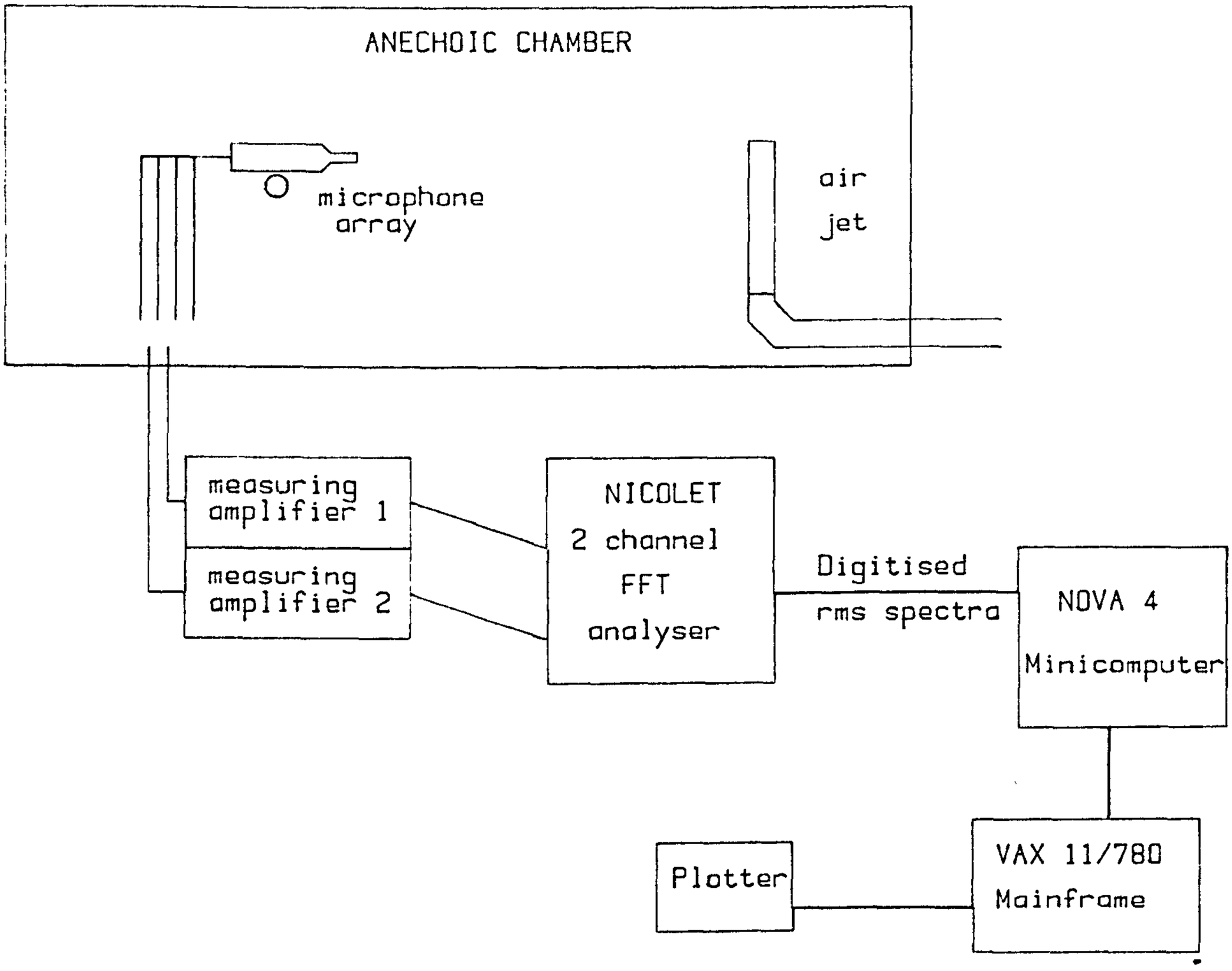

FIGURE 7.1 APPARATUS FOR MODEL EXPERIMENTS.

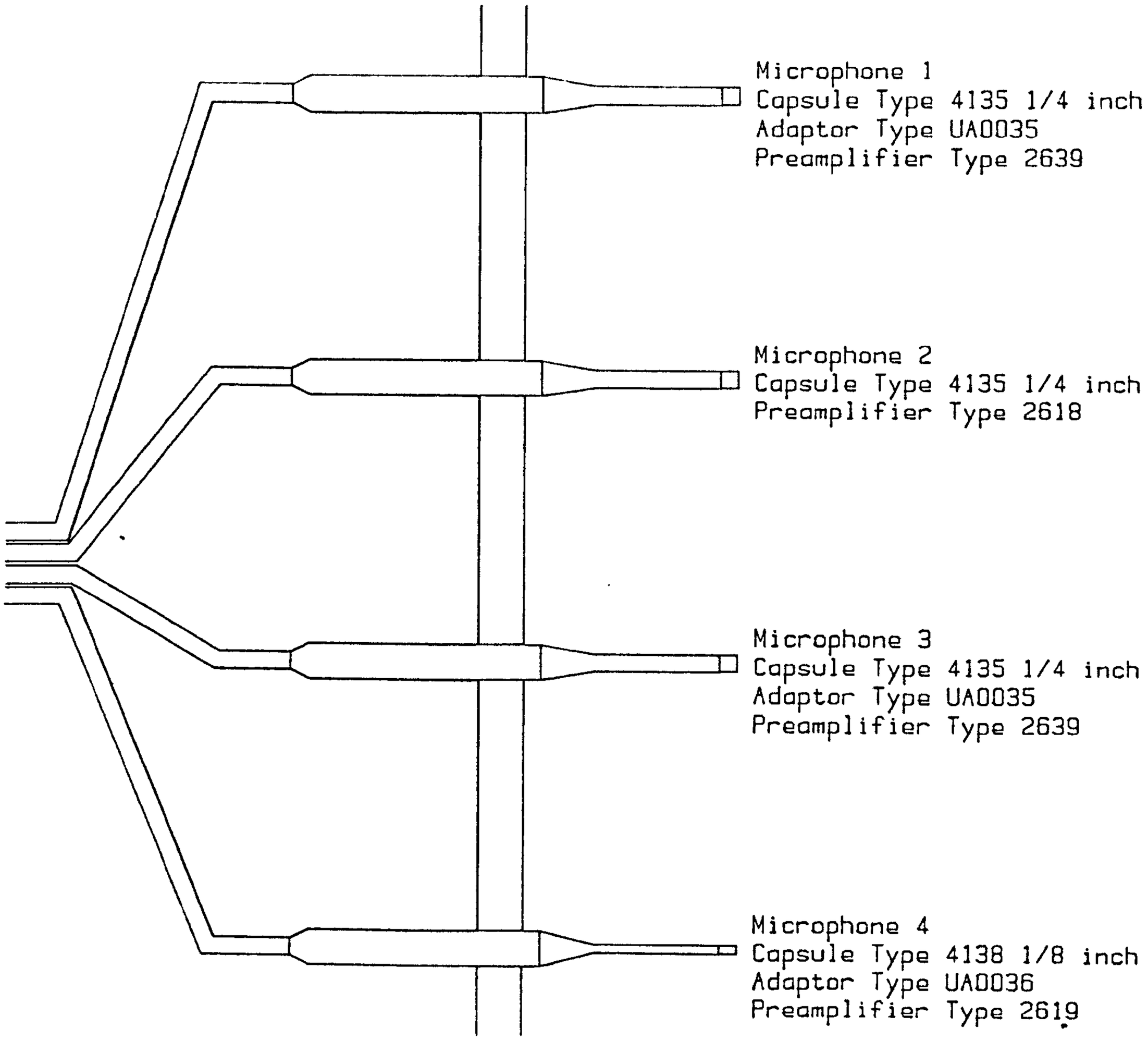

FIGURE 7.2
MICROPHONE ARRAY USED IN MODEL EXPERIMENTS.
With Bruel and Kjaer Type Numbers.

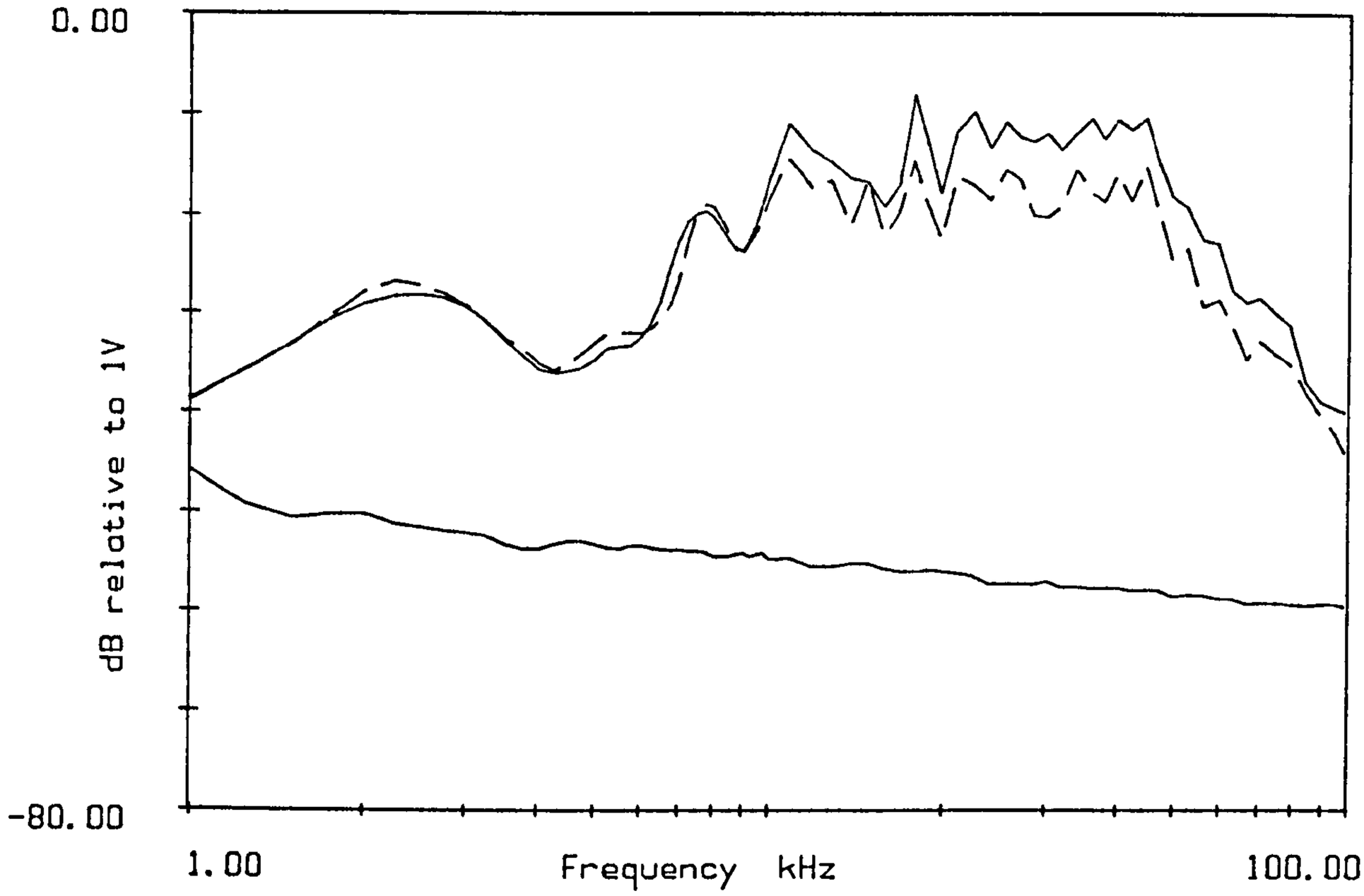

Figure 7.3a
Measurement B-6 microphone 1
Signal level from the measuring amplifier for free field.
with array (----), and noise. (array density 360)

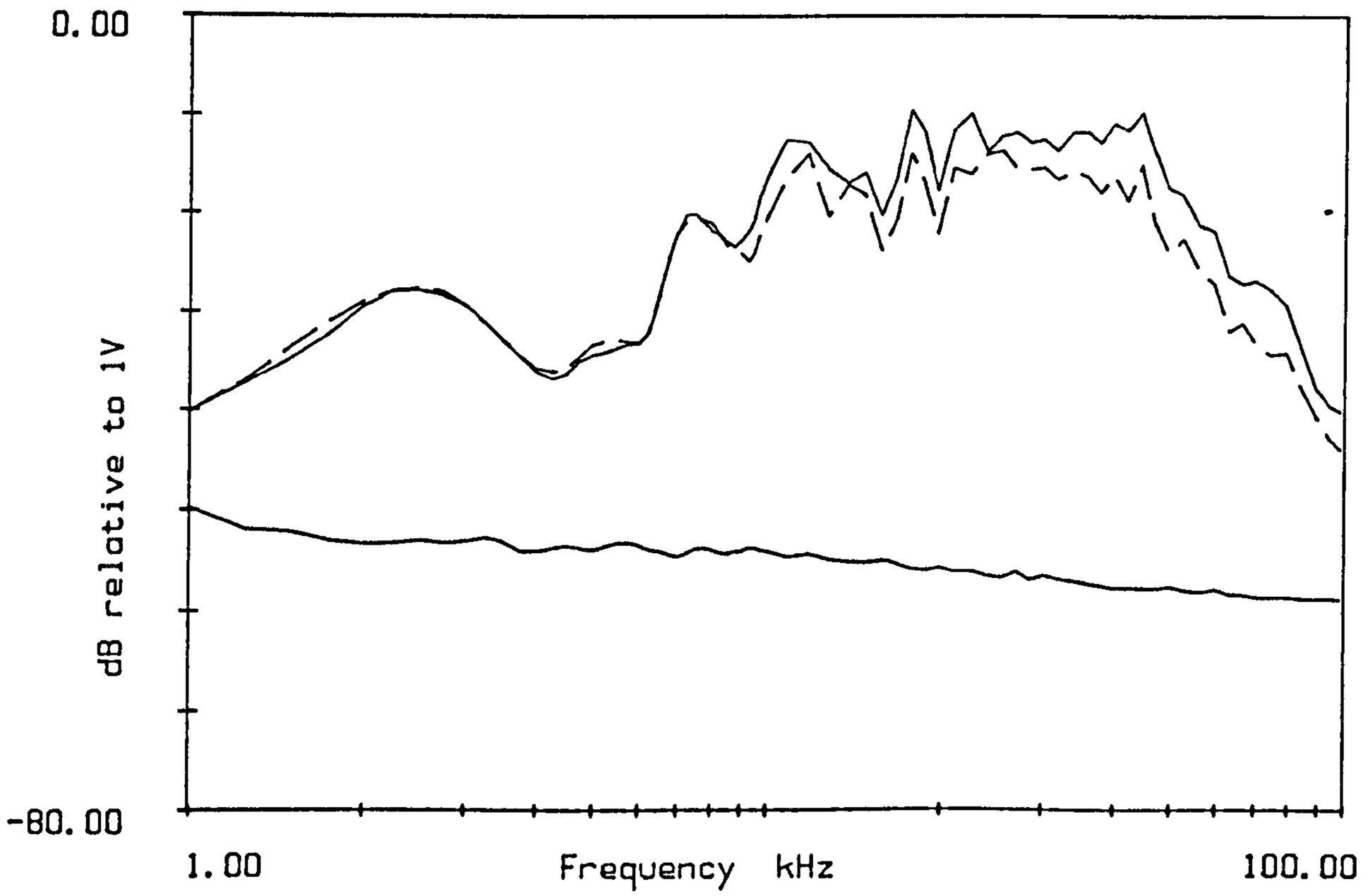

Figure 7.3b
Measurement B-6 microphone 2
Signal level from the measuring amplifier for free field.
with array (----), and noise. (array density 360)

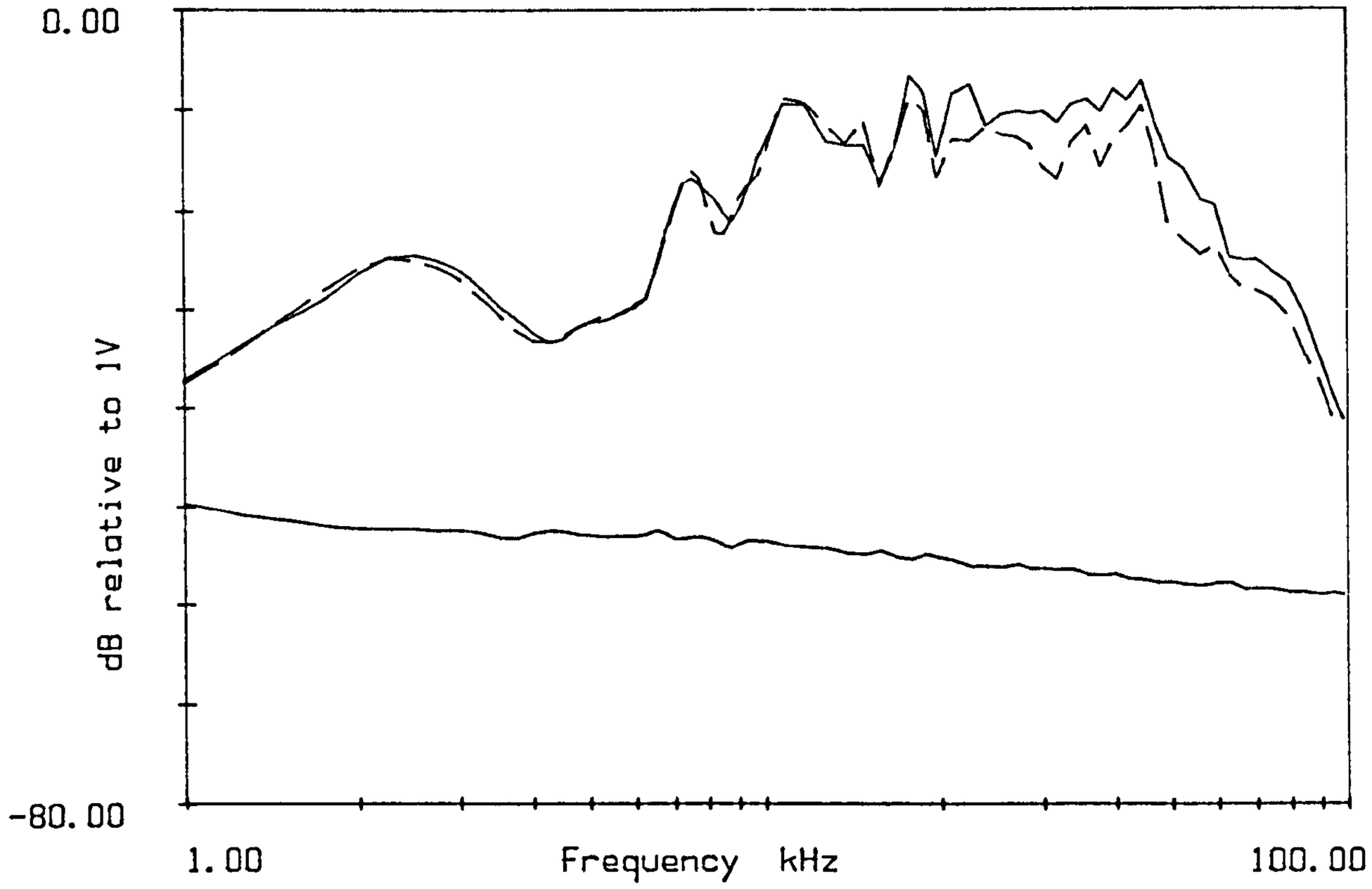

Figure 7.3c
Measurement B-6 microphone 3
Signal level from the measuring amplifier for free field,
with array (----) and noise. (array density 360)

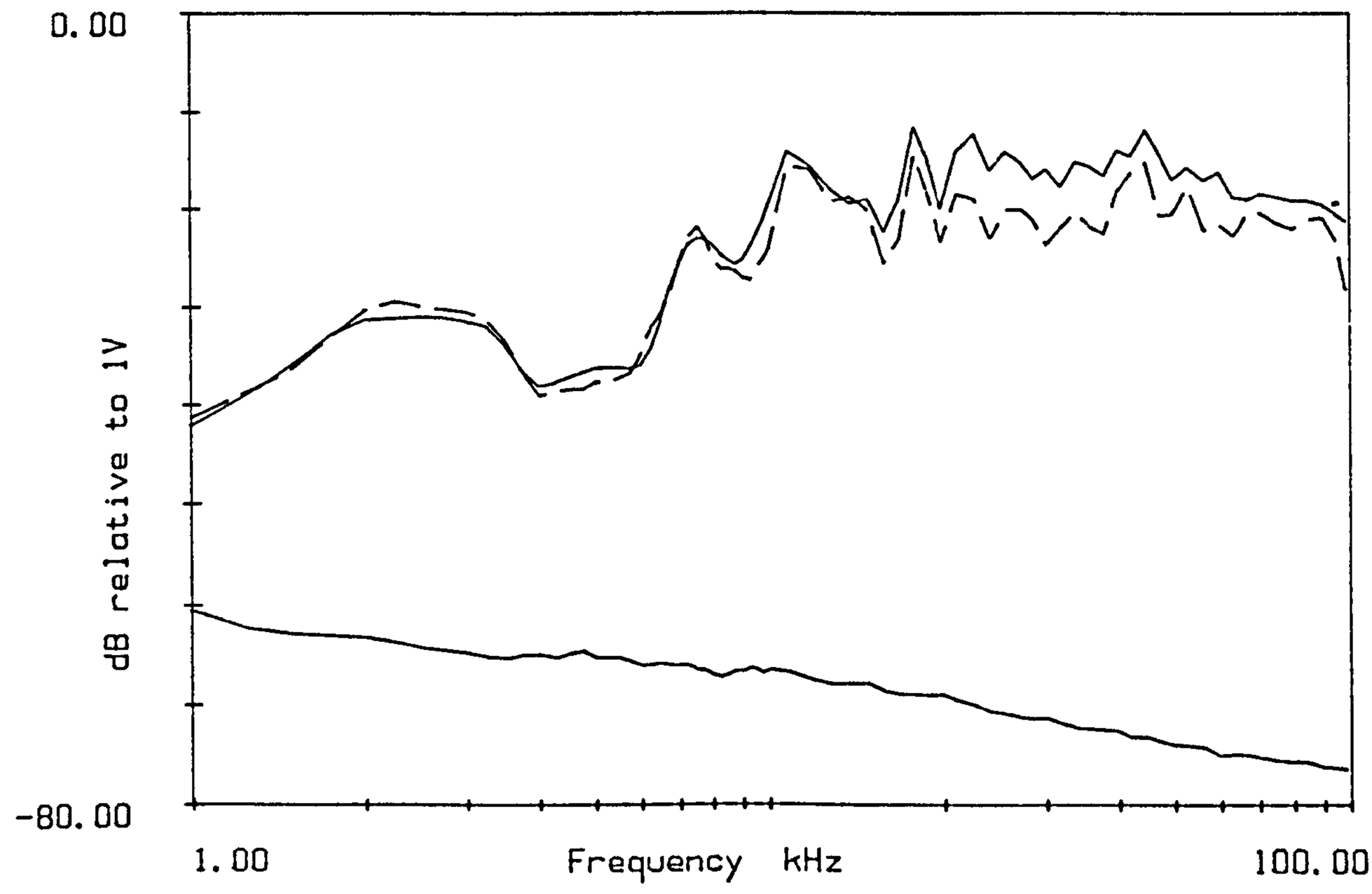

Figure 7.3d
Measurement B-6 microphone 4
Signal level from the measuring amplifier for free field,
with array (----) and noise. (array density 360)

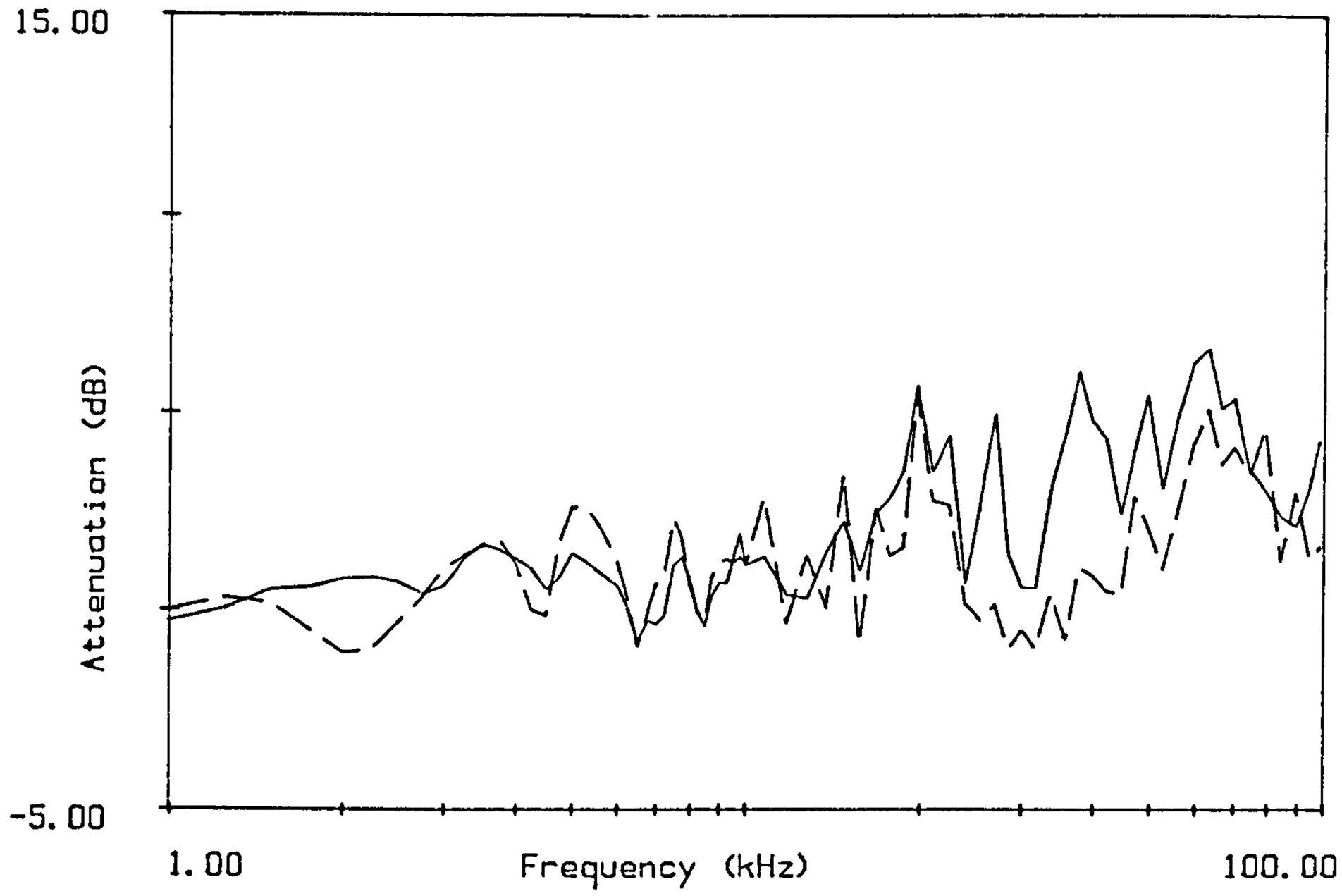

Figure 7.4a microphone 1
Attenuation through array A-6 with the rods displaced slightly between measurements (array density 240)

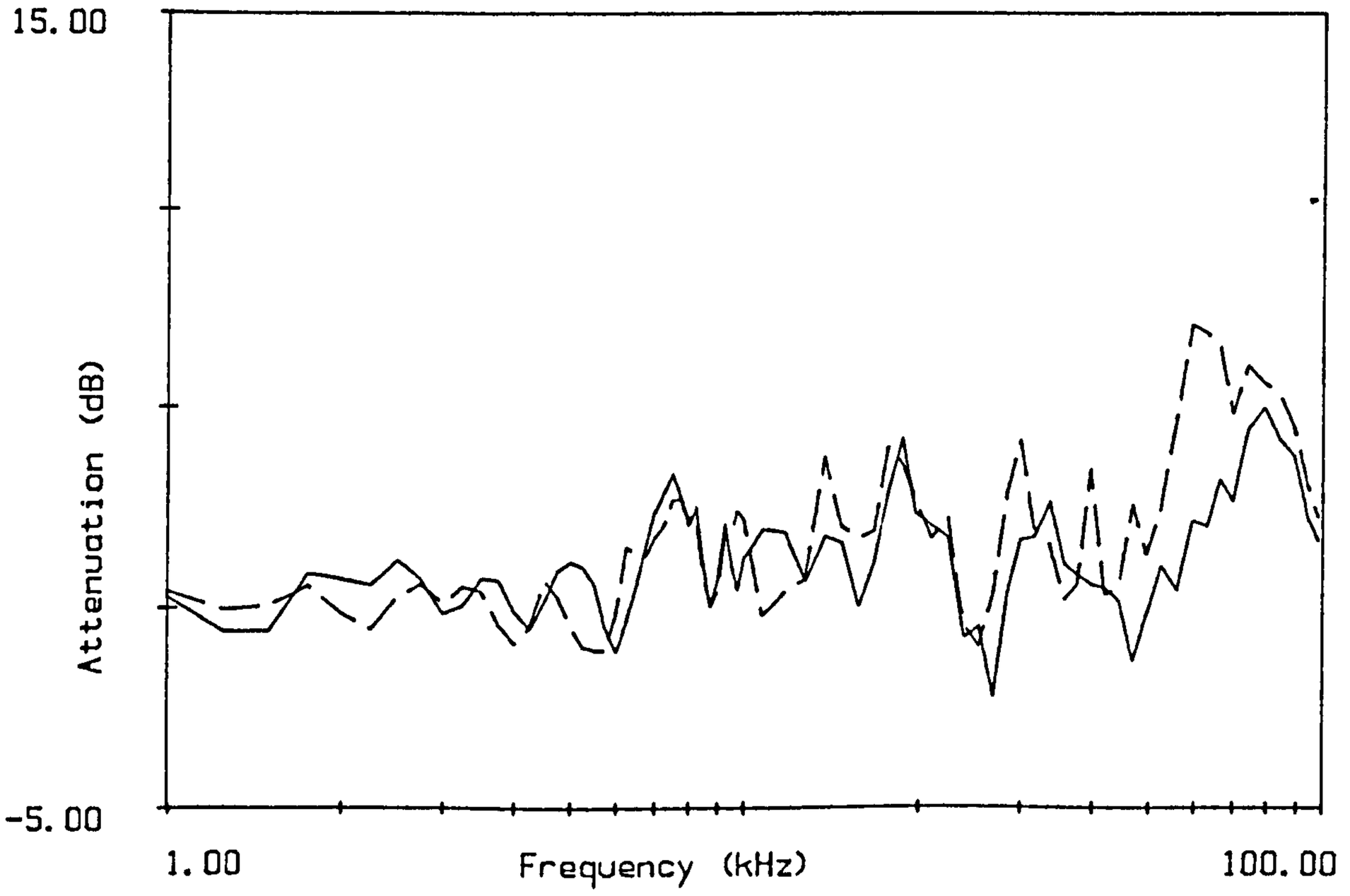

Figure 7.4b microphone 2
Attenuation through array A-6 with the rods displaced slightly between measurements (array density 240)

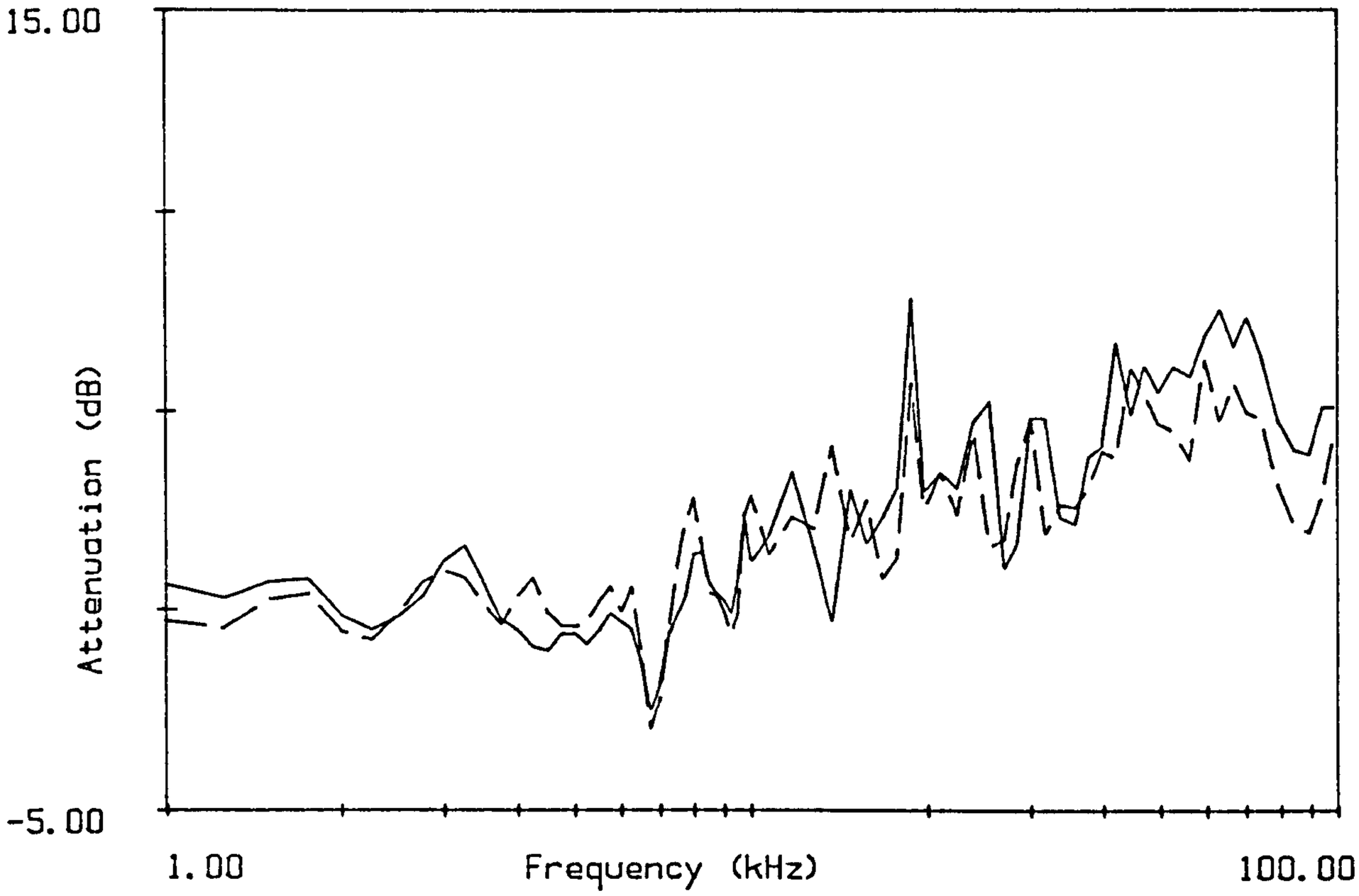

Figure 7.4c microphone 3
Attenuation through array A-6 with the rods displaced slightly between measurements (array density 240)

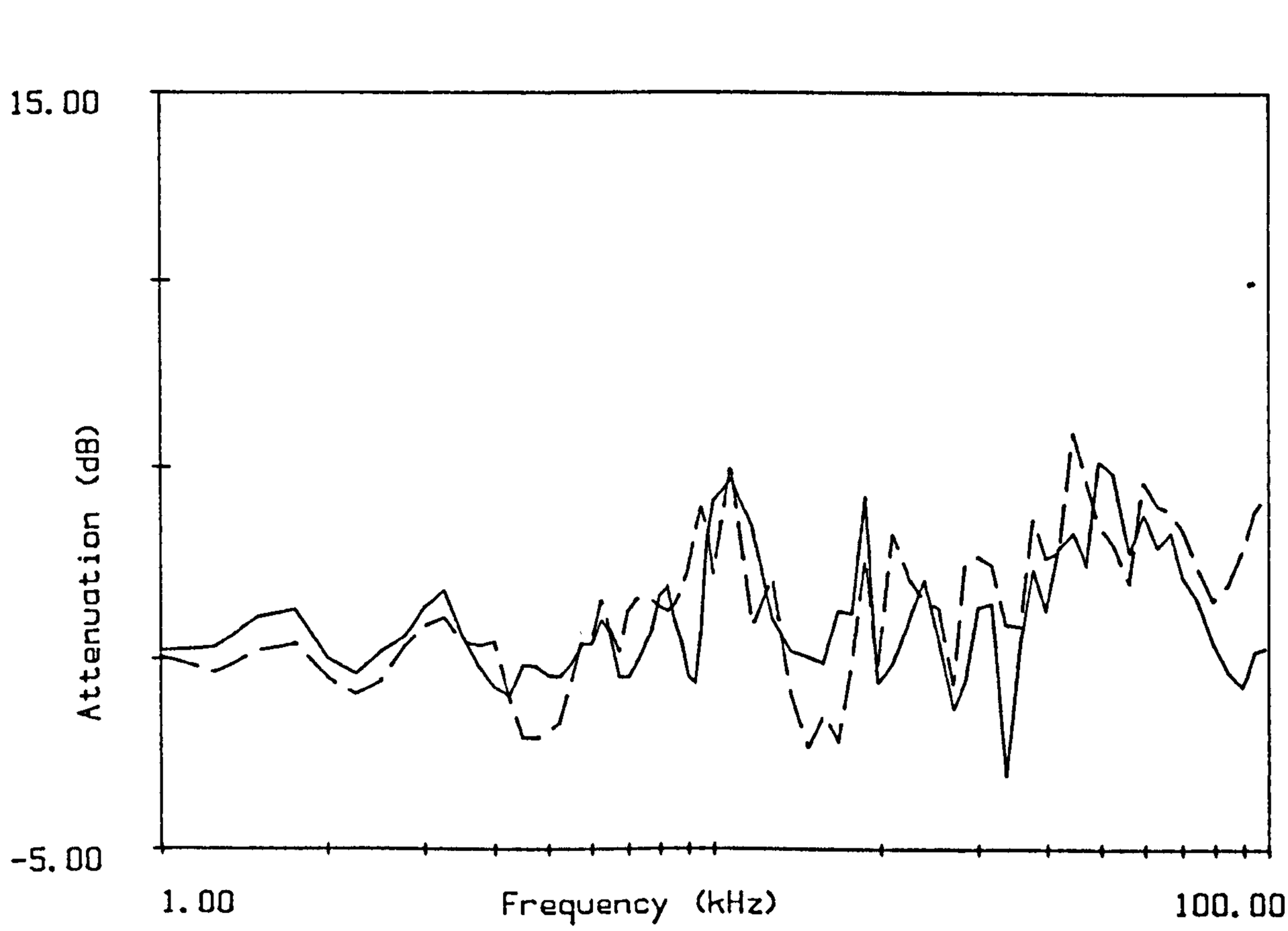

Figure 7.4d microphone 4
Attenuation through array A-6 with the rods displaced slightly between measurements (array density 240)

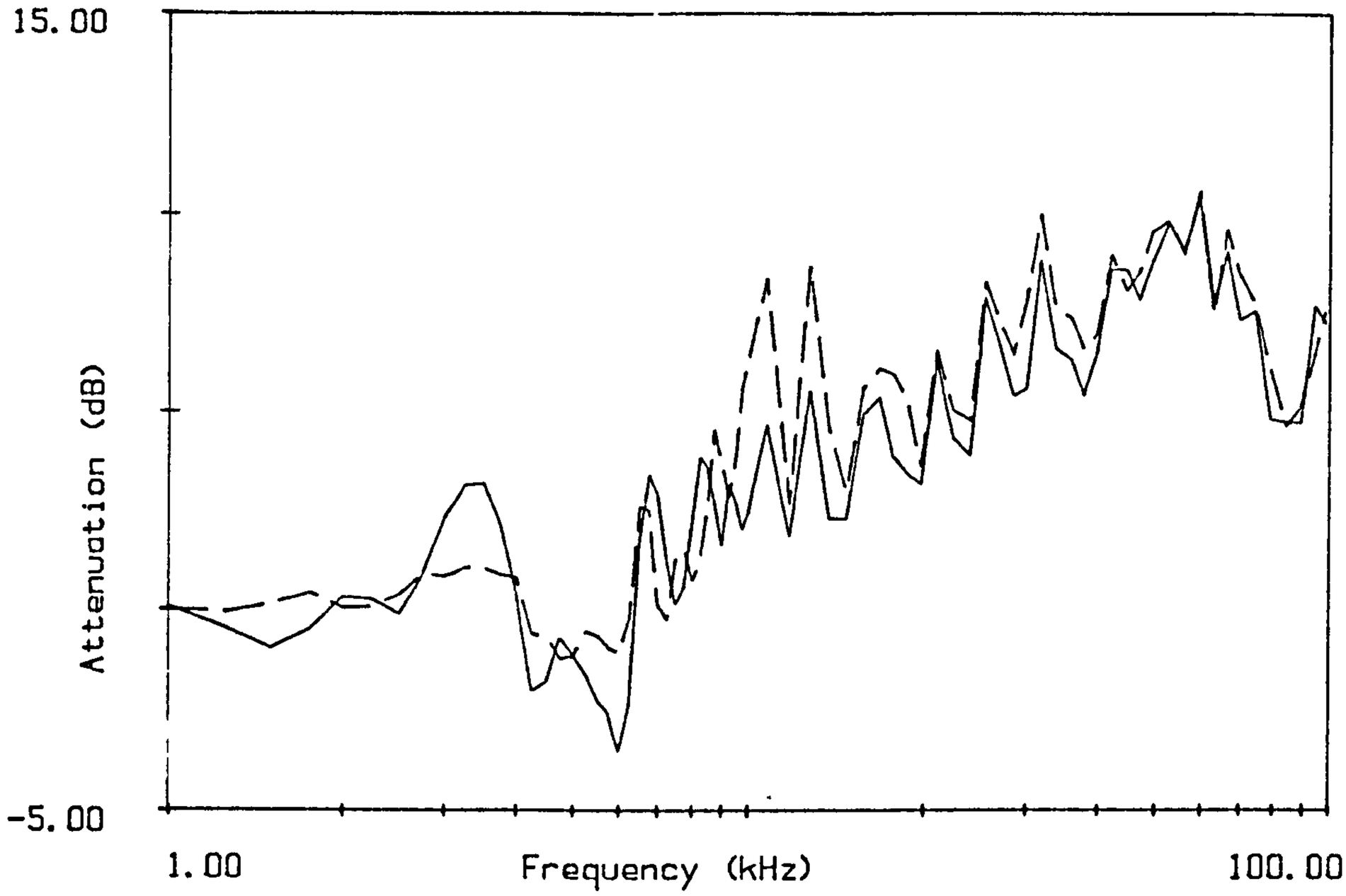

Figure 7.5a microphone 1.
Attenuation through array A-12 with all the rods in place and (-----) with the rods behind the microphones removed. (array density 240)

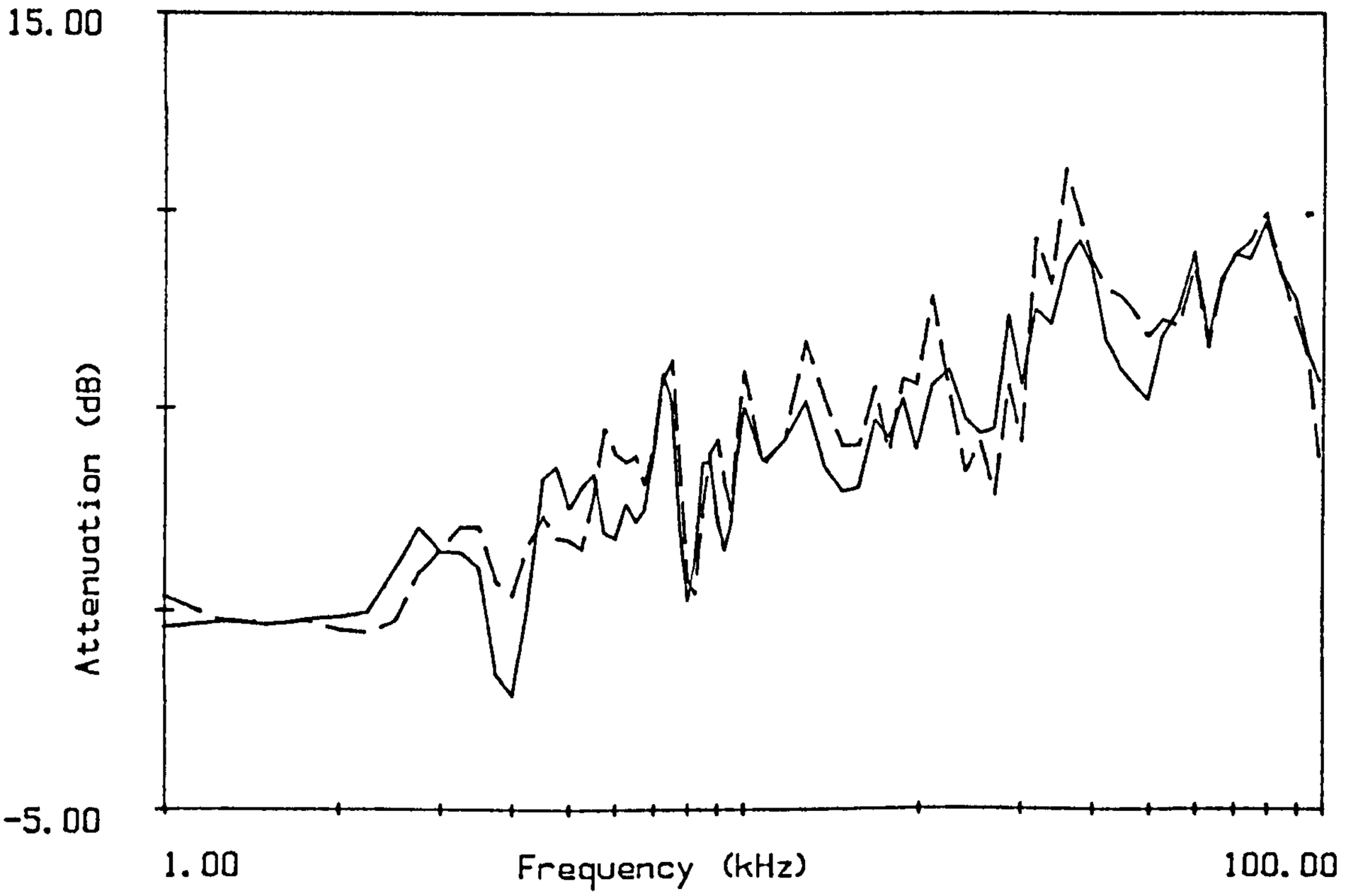

Figure 7.5b microphone 2.
Attenuation through array A-12 with all the rods in place and (-----) with the rods behind the microphones removed. (array density 240)

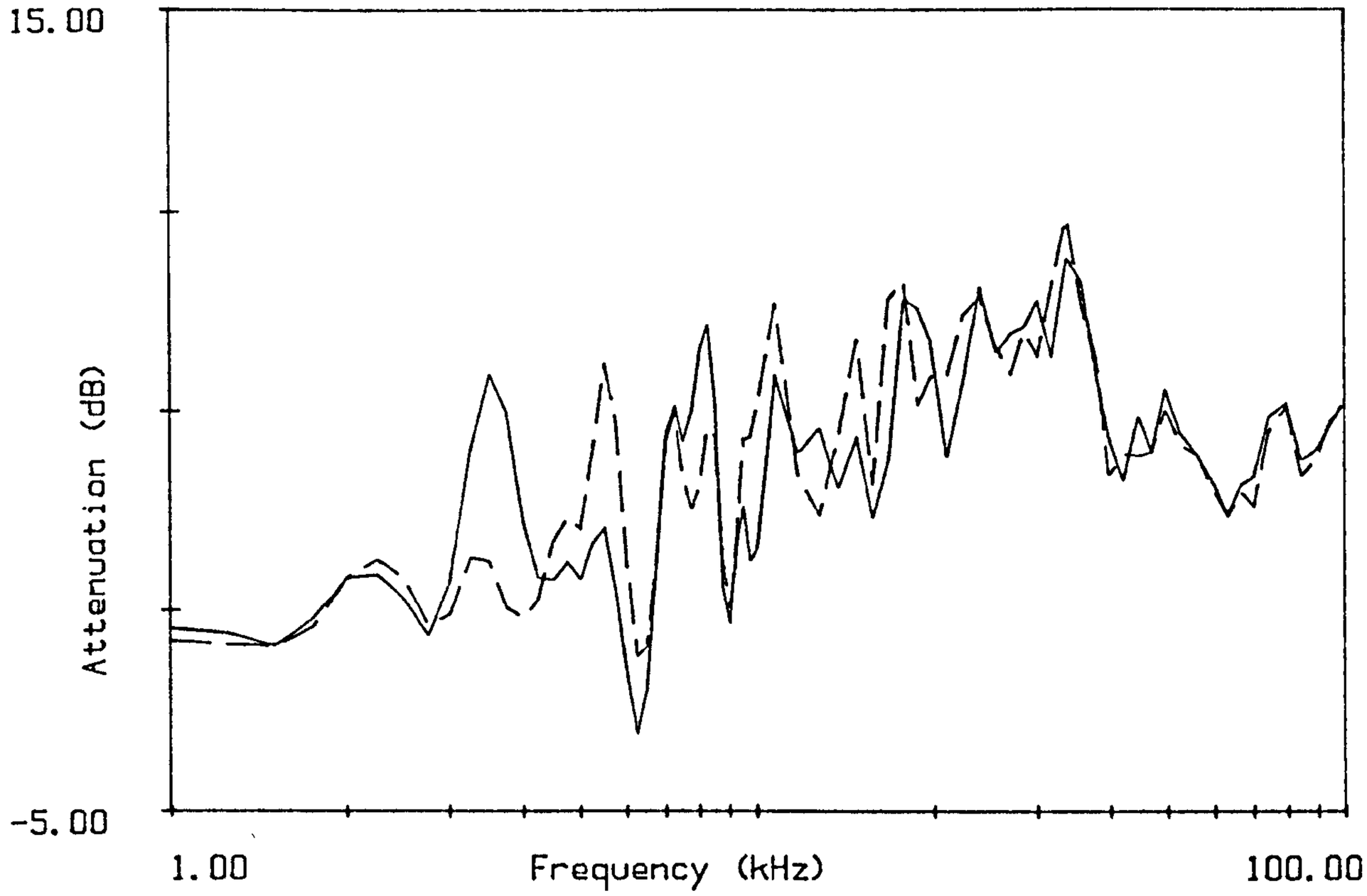

Figure 7.5c microphone 3.
Attenuation through array A-12 with all the rods in place and (-----) with the rods behind the microphones removed. (array density 240)

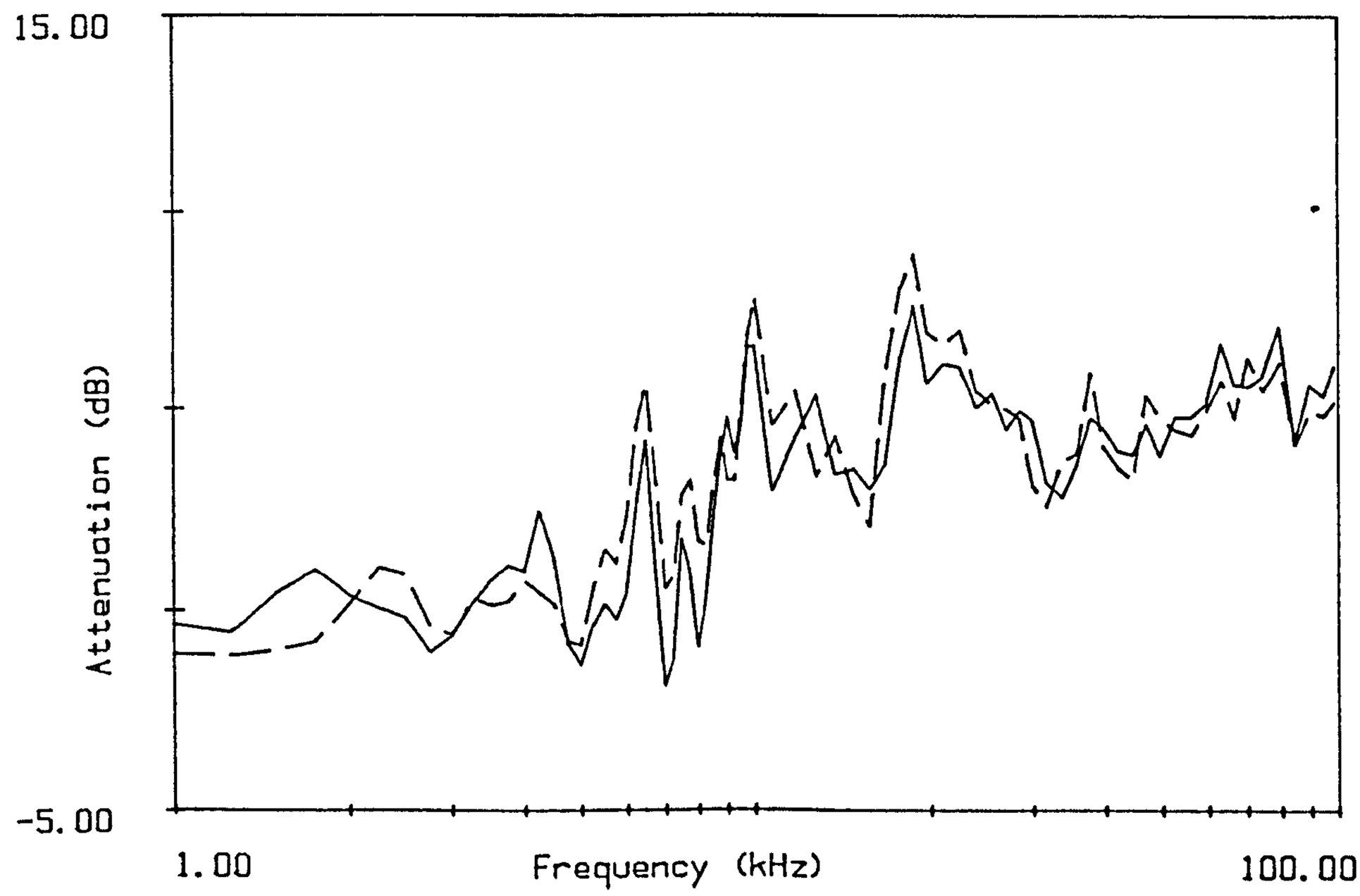

Figure 7.5d microphone 4.
Attenuation through array A-12 with all the rods in place and (-----) with the rods behind the microphones removed. (array density 240)

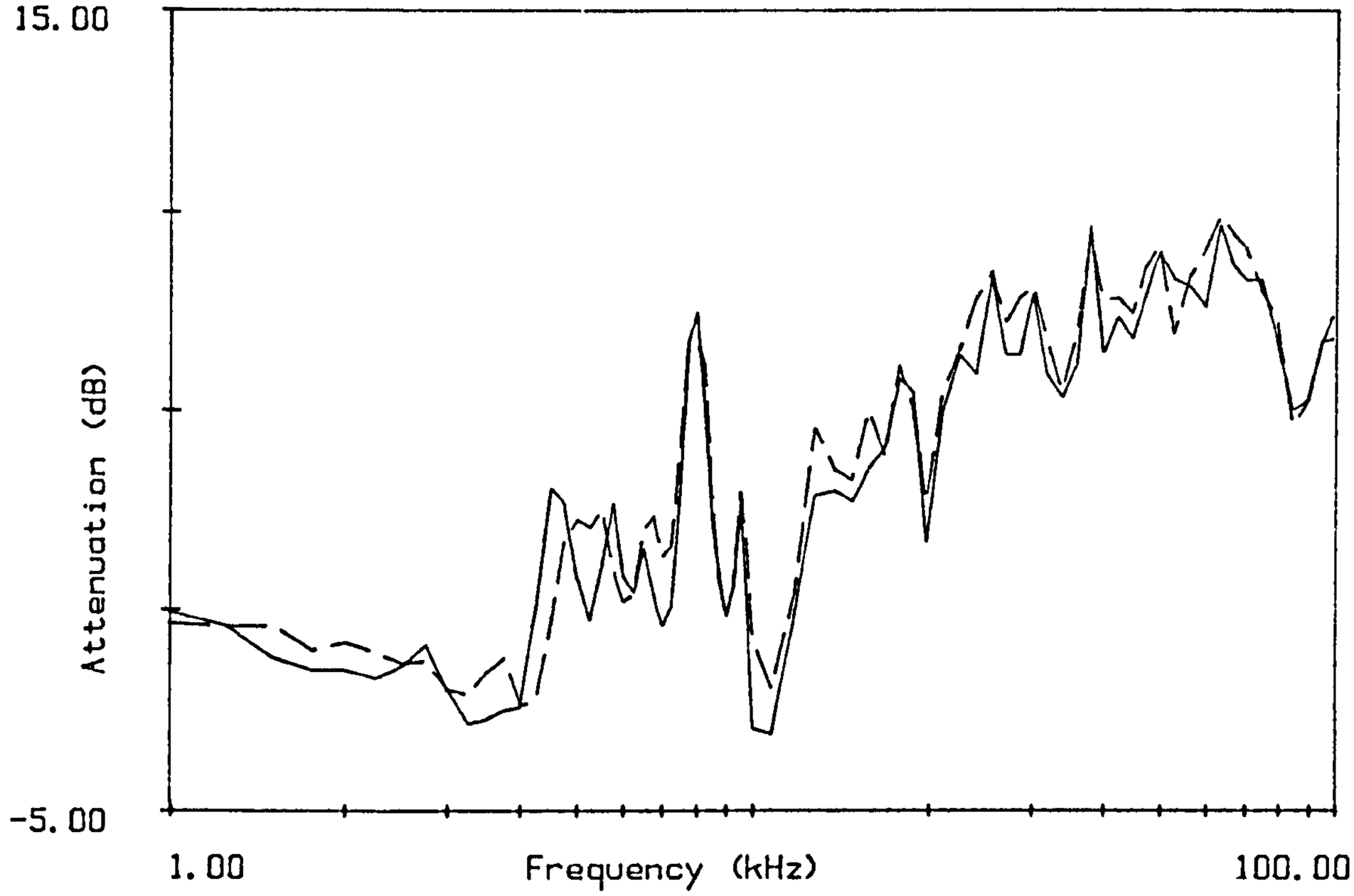

Figure 7.6 microphone 1.
Attenuation through array F with all the rods in place and (-----) with the rods behind the microphones removed.
(mixed array of 6mm and 12mm rods; total density 480)

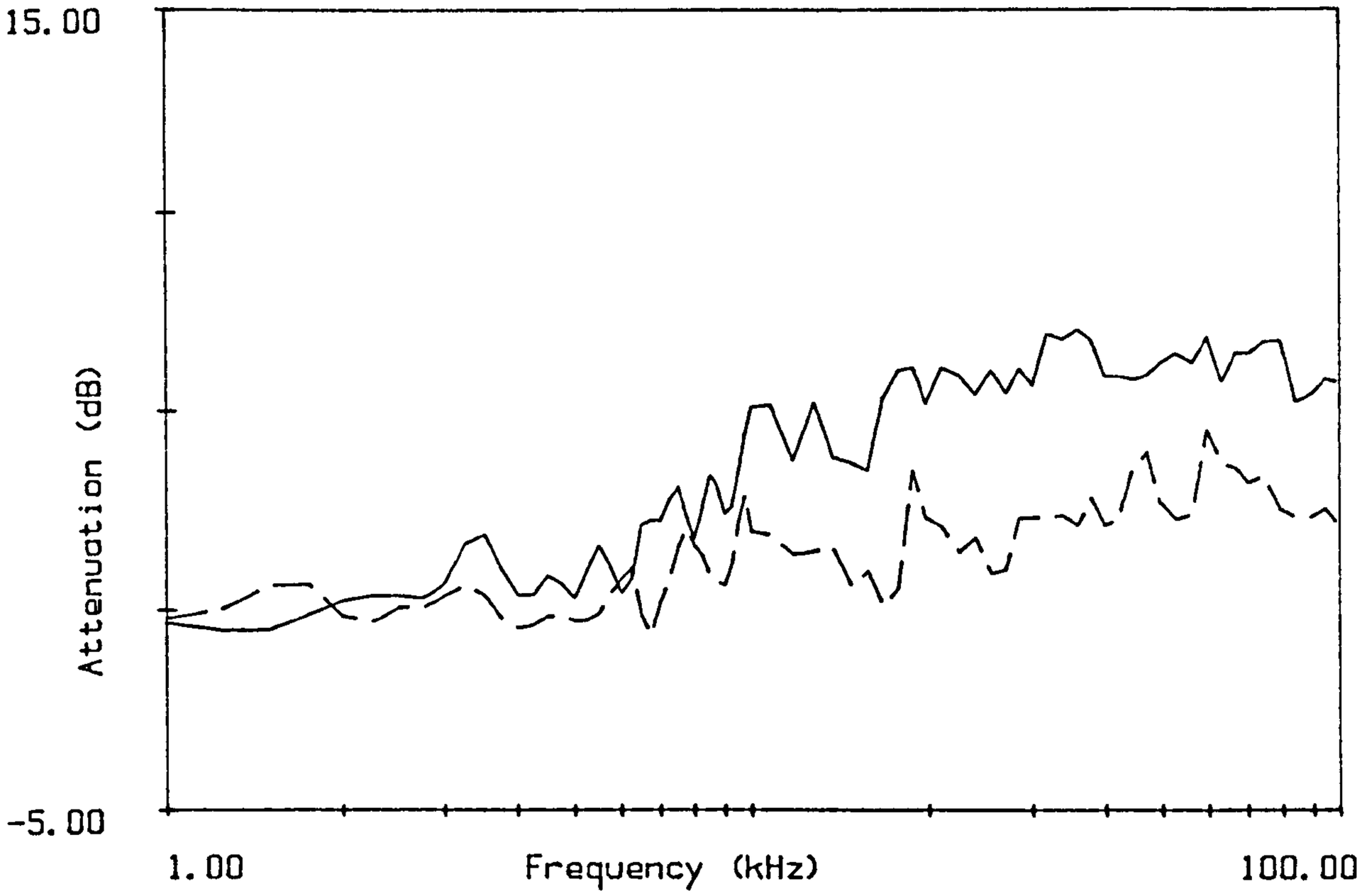

Figure 7.7
Attenuation through array A-12 and array A-6 (----).
Mean value for the 4 microphones. (array density 240)

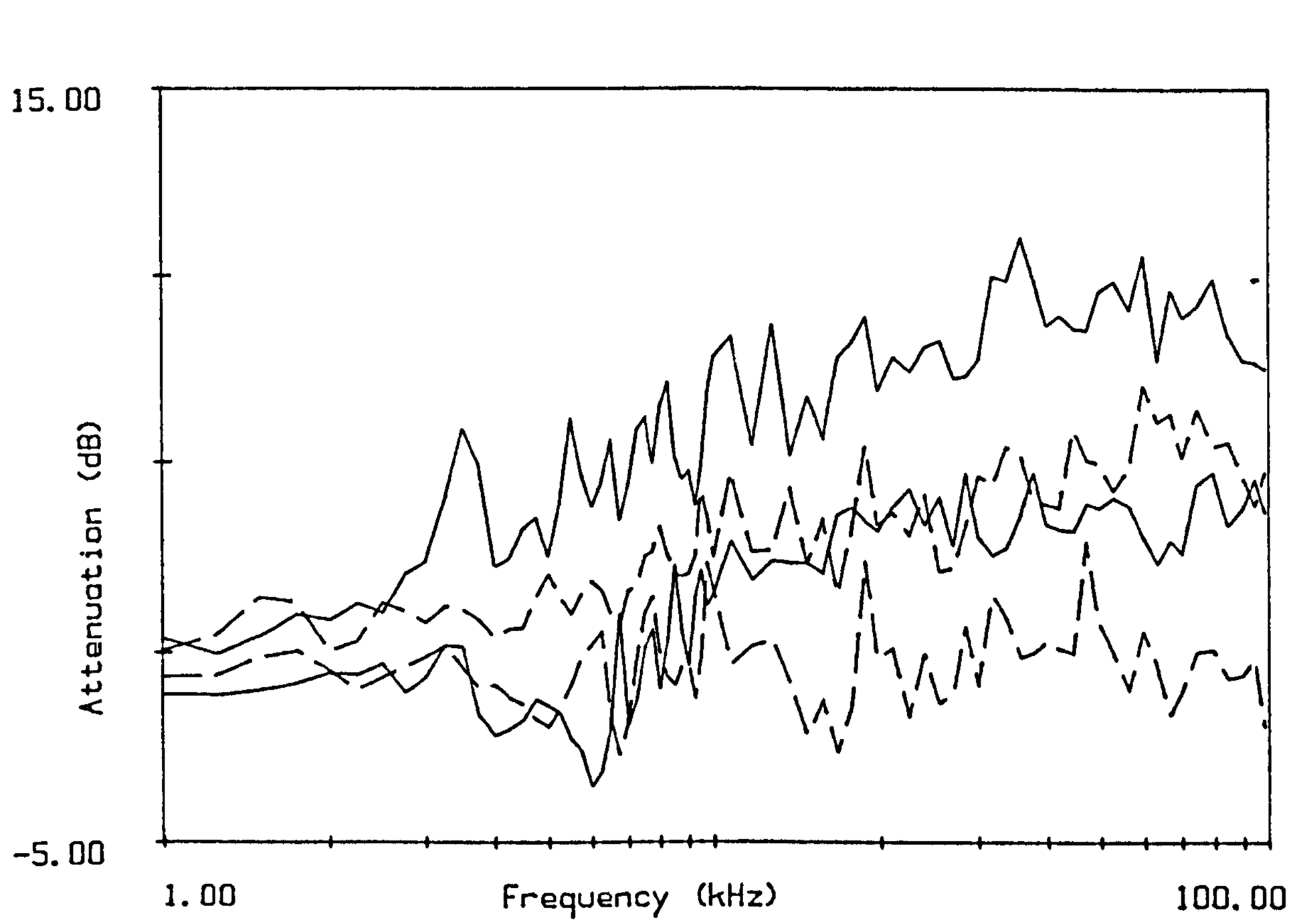

Figure 7.7a
Attenuation through array A-12 and array A-6 (----).
Range of values from the 4 microphones.

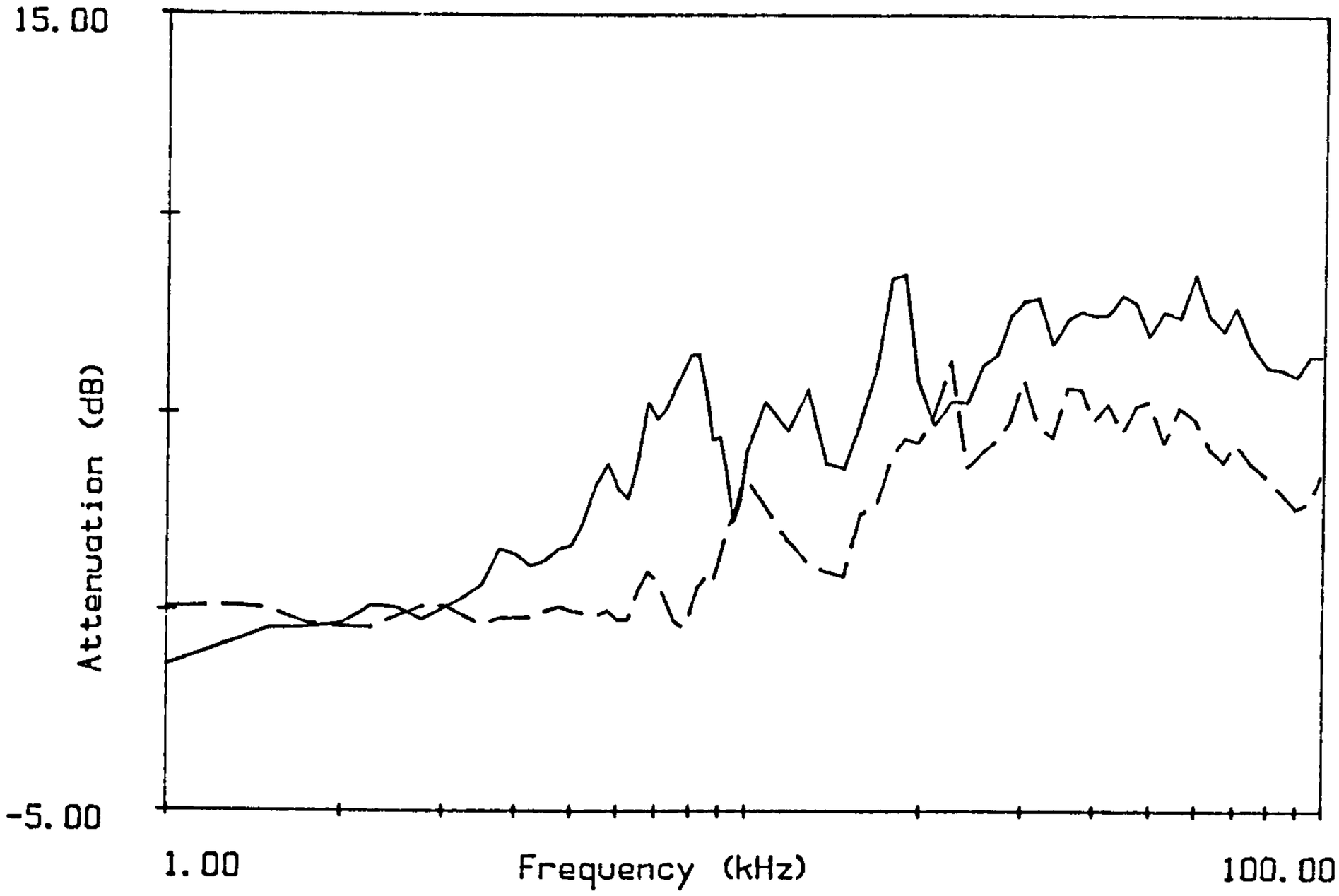

Figure 7.8
Attenuation through array B-12 and array B-6 (----).
Mean value for the 4 microphones. (array density 360)

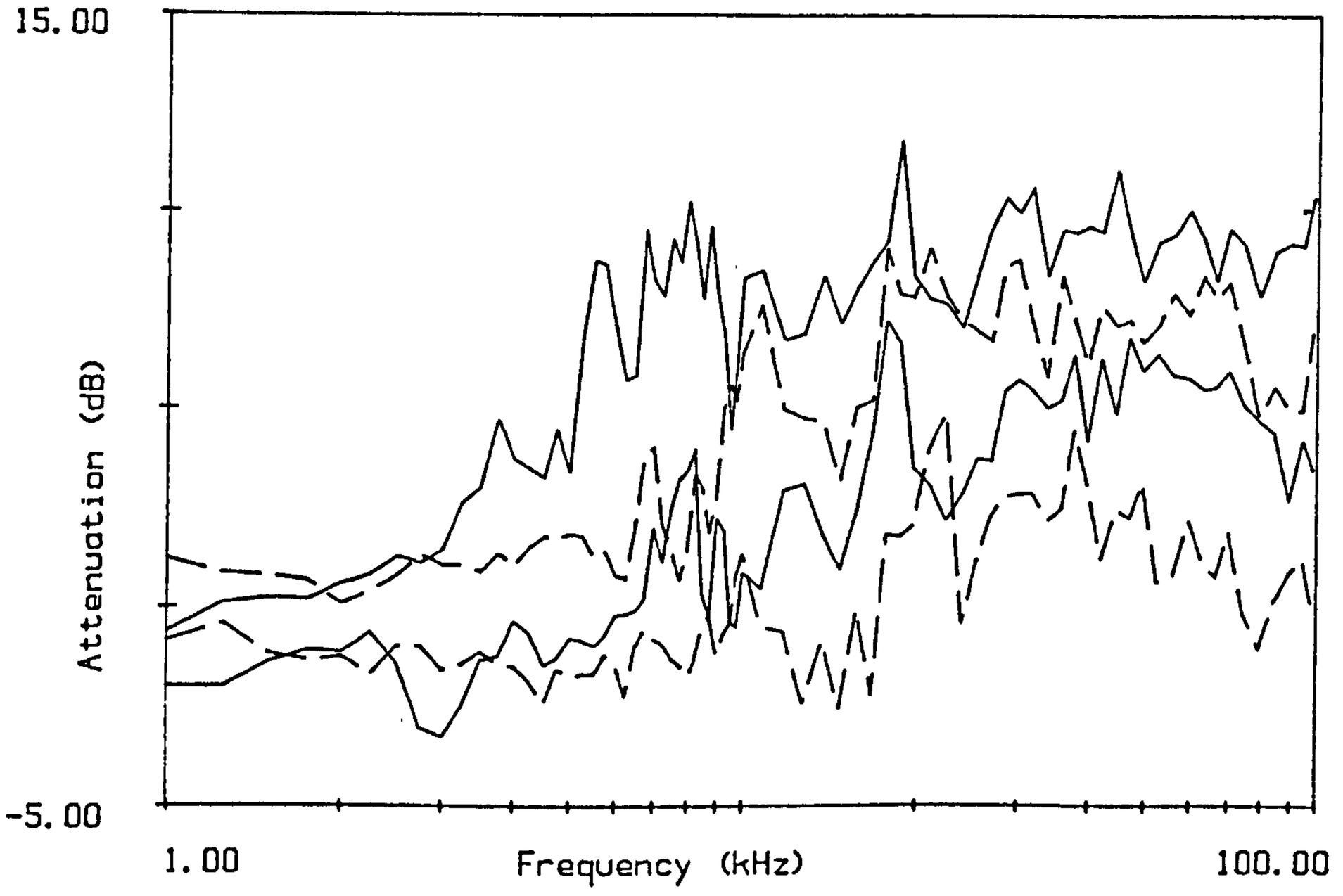

Figure 7.8a
Attenuation through array B-12 and array B-6 (----).
Range of values from the 4 microphones.

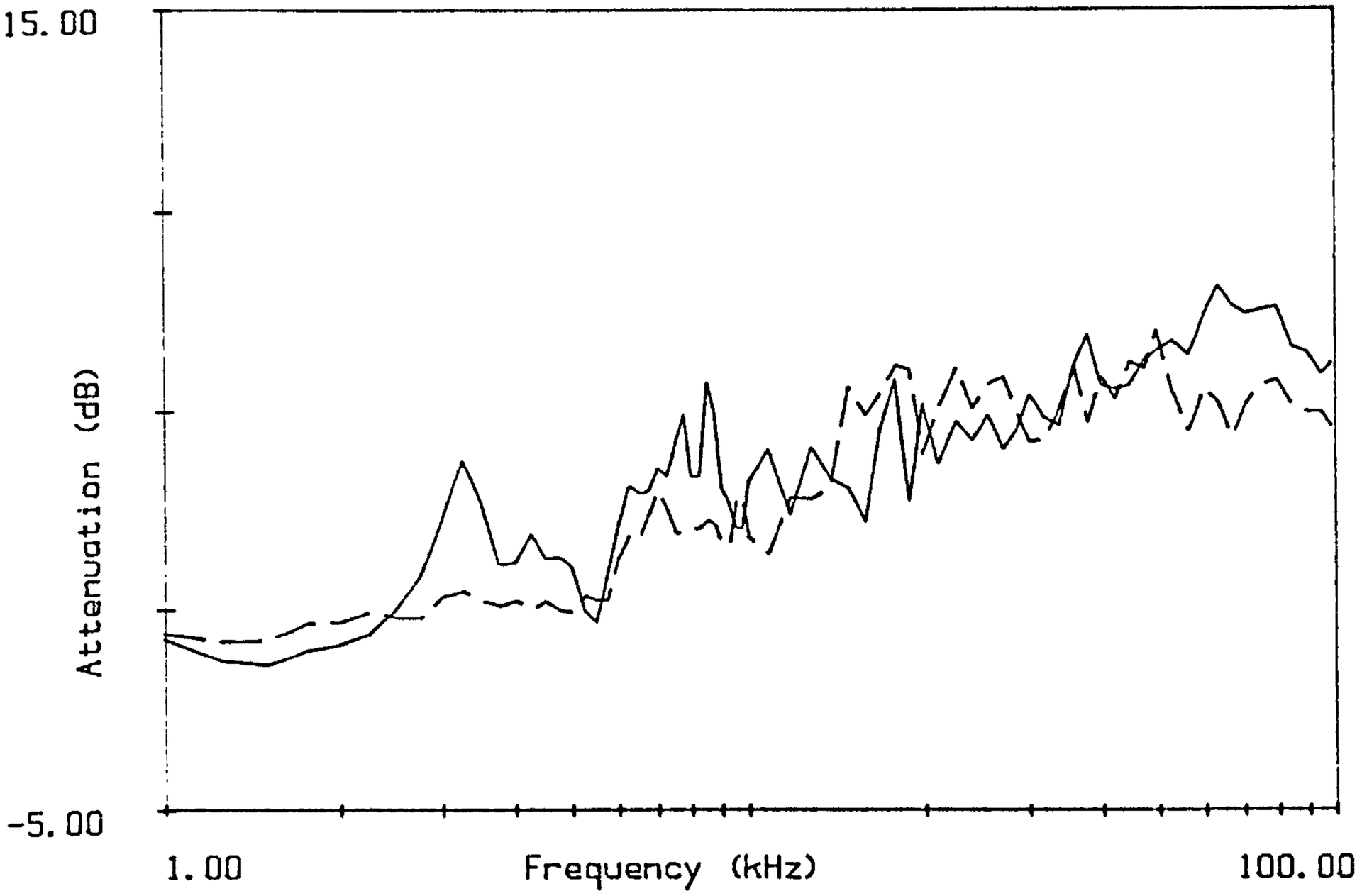

Figure 7.9a
Attenuation through array C-12 and array C-6 (----).
Mean value for the 4 microphones. (array density 400)

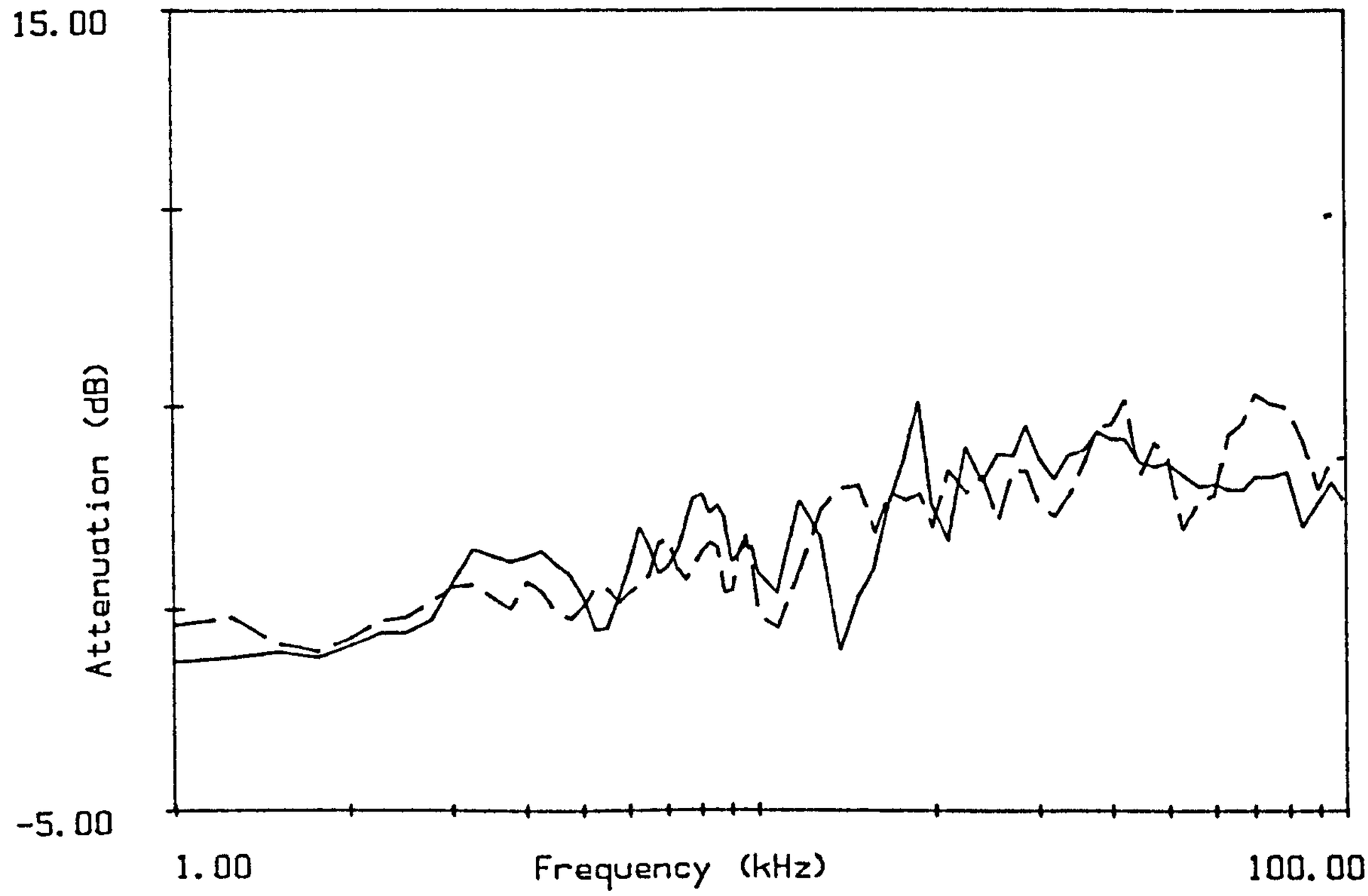

Figure 7.9b
Attenuation through array D-12 and array D-6 (----).
Mean value for the 4 microphones. (array density 200)

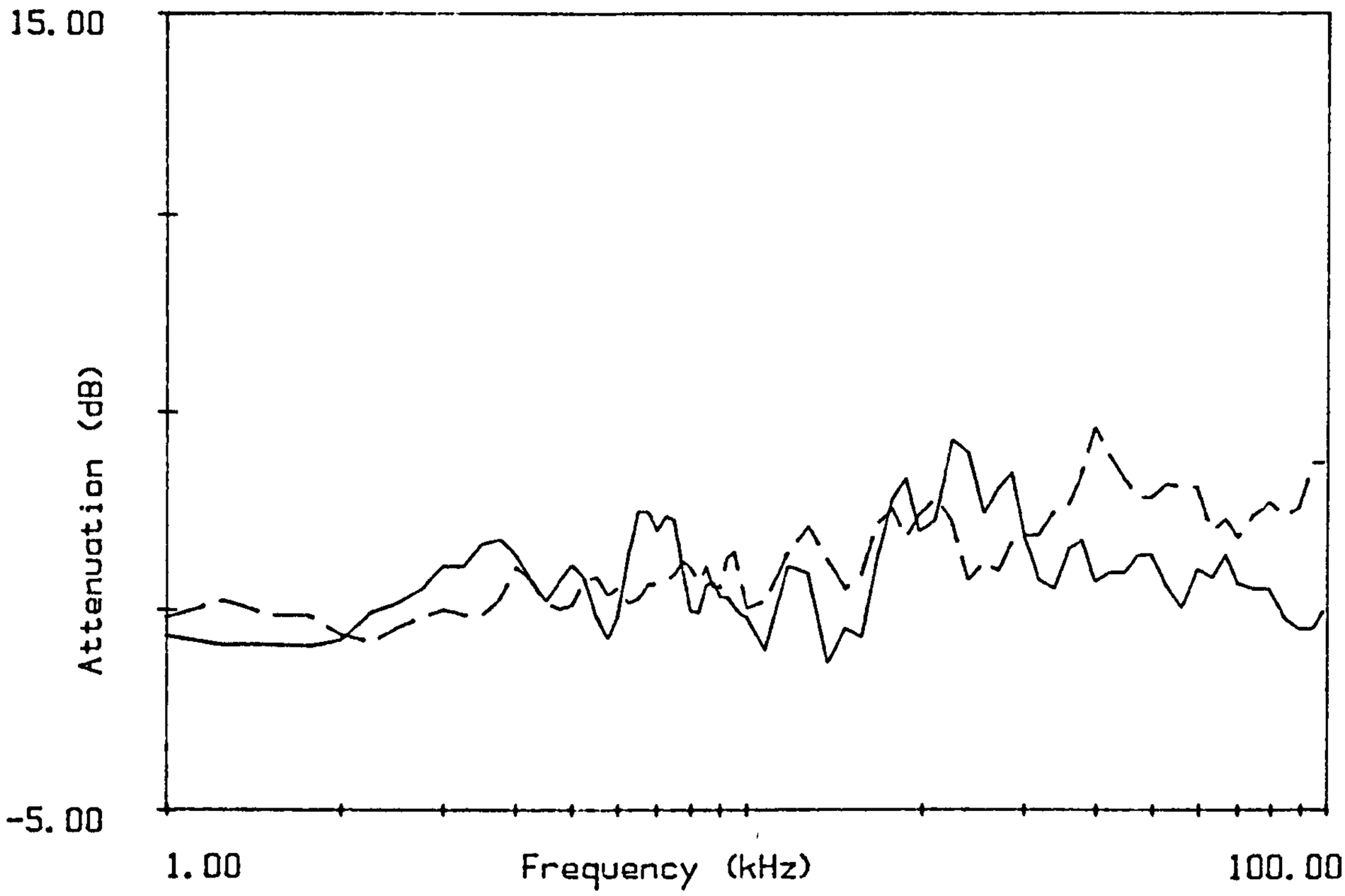

Figure 7.9c
Attenuation through array E-12 and array E-6 (----).
Mean value for the 4 microphones.

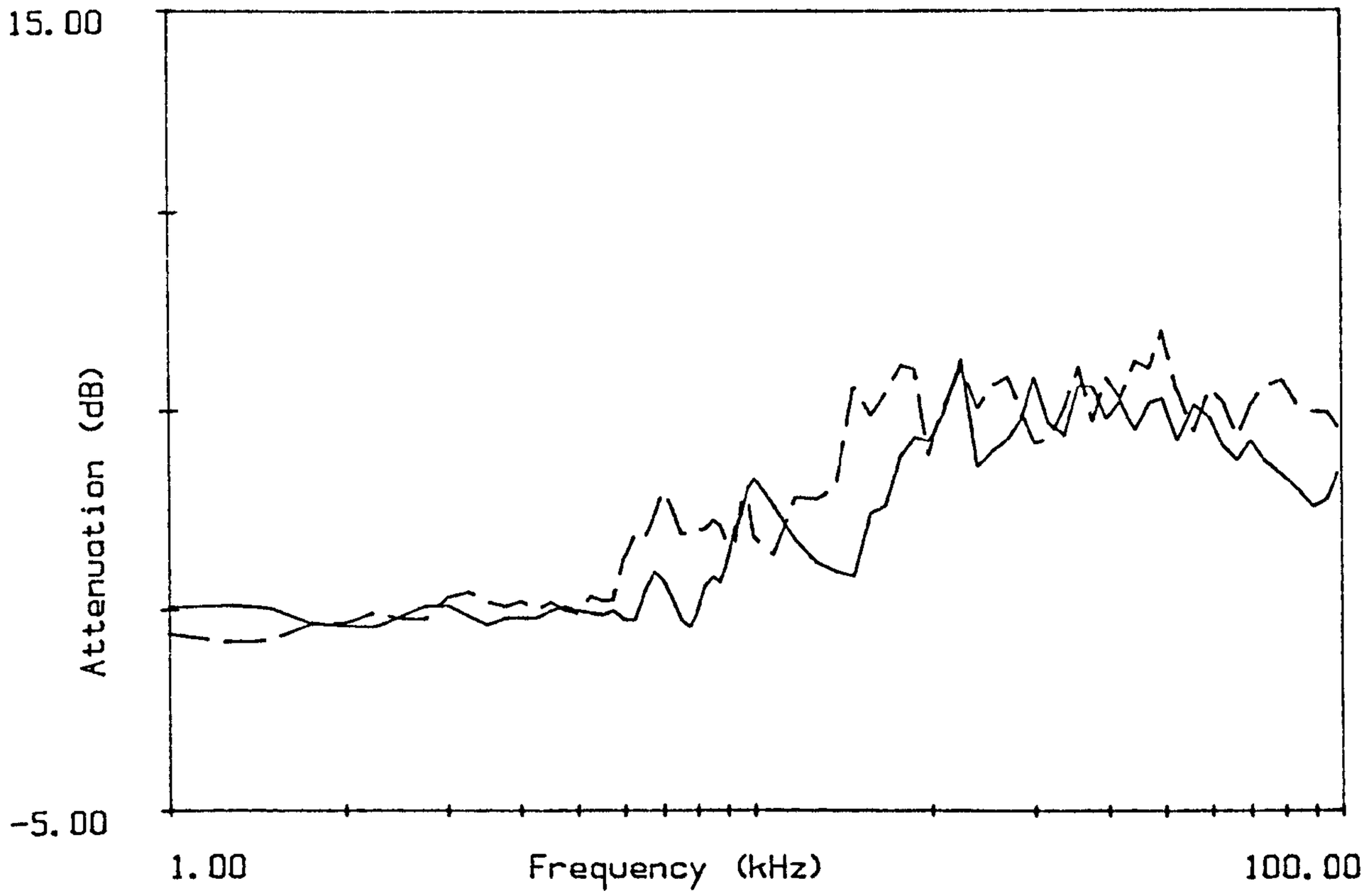

Figure 7.10
Attenuation through array B-6 and array C-6 (----).
Mean value for the 4 microphones.
(array densities: B = 360, C = 400)

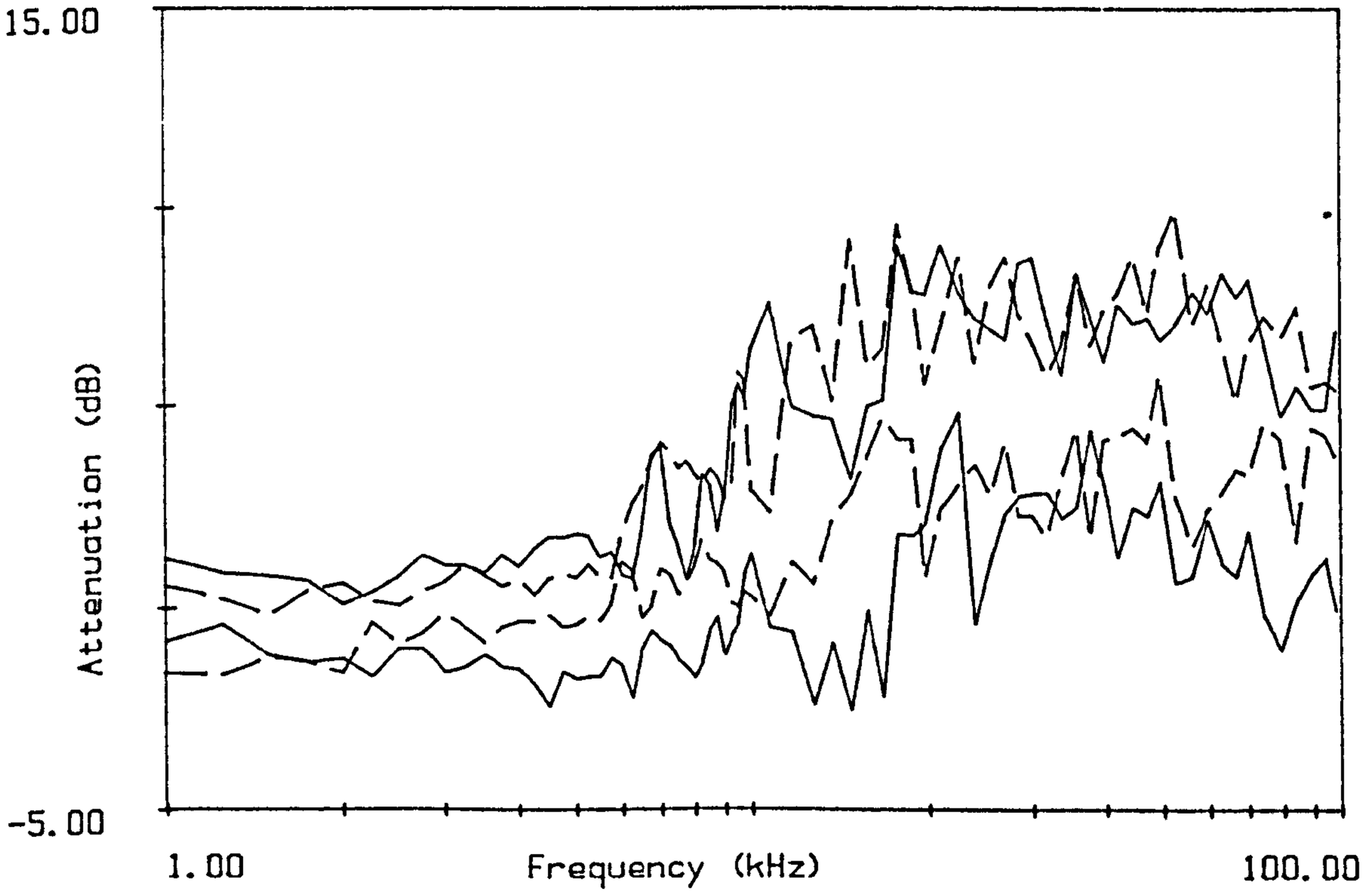

Figure 7.10a
Attenuation through array B-6 and array C-6 (----).
Range of values from the 4 microphones.

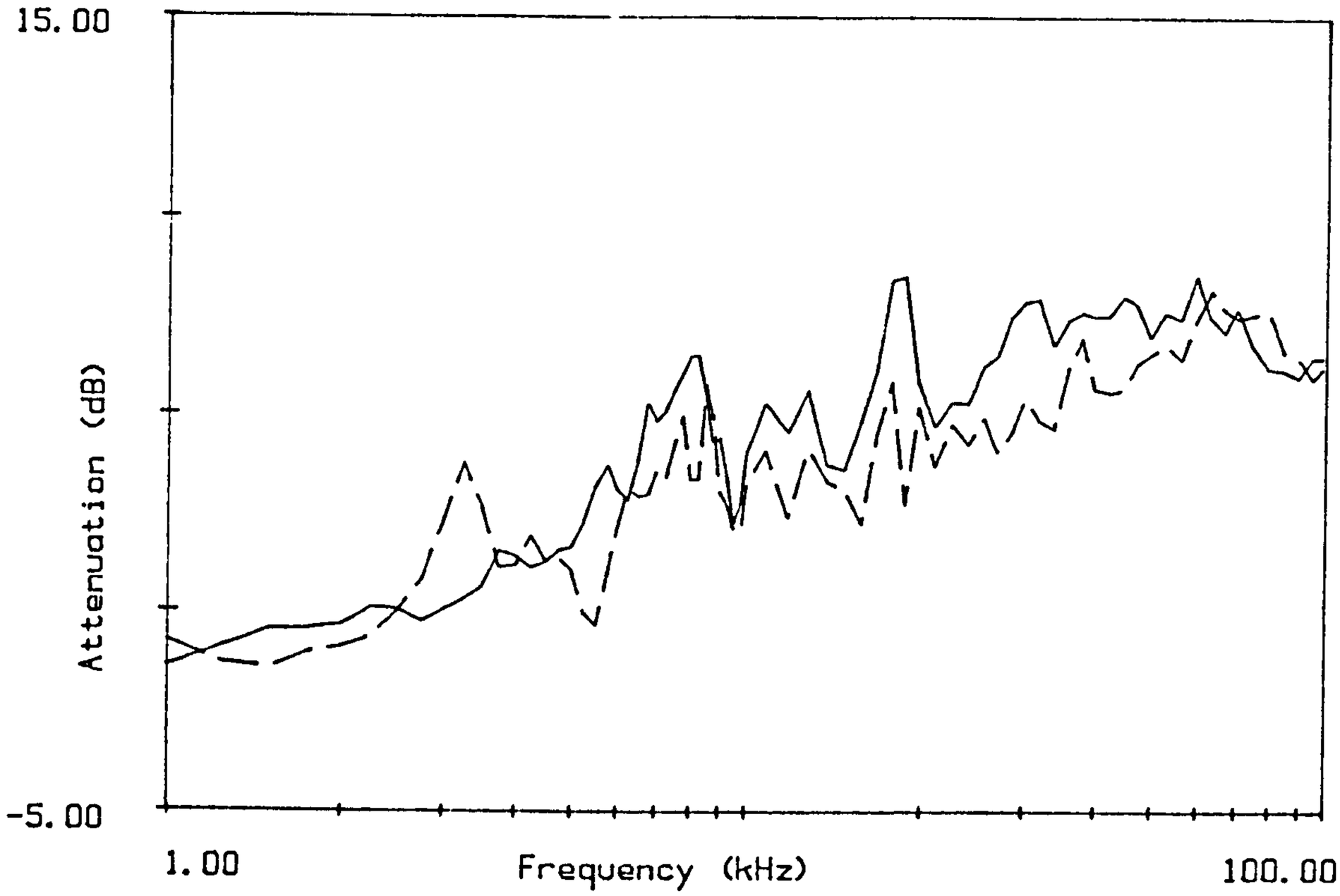

Figure 7.11
Attenuation through array B-12 and array C-12 (----).
Mean value for the 4 microphones.
(array densities: B = 360, C = 400)

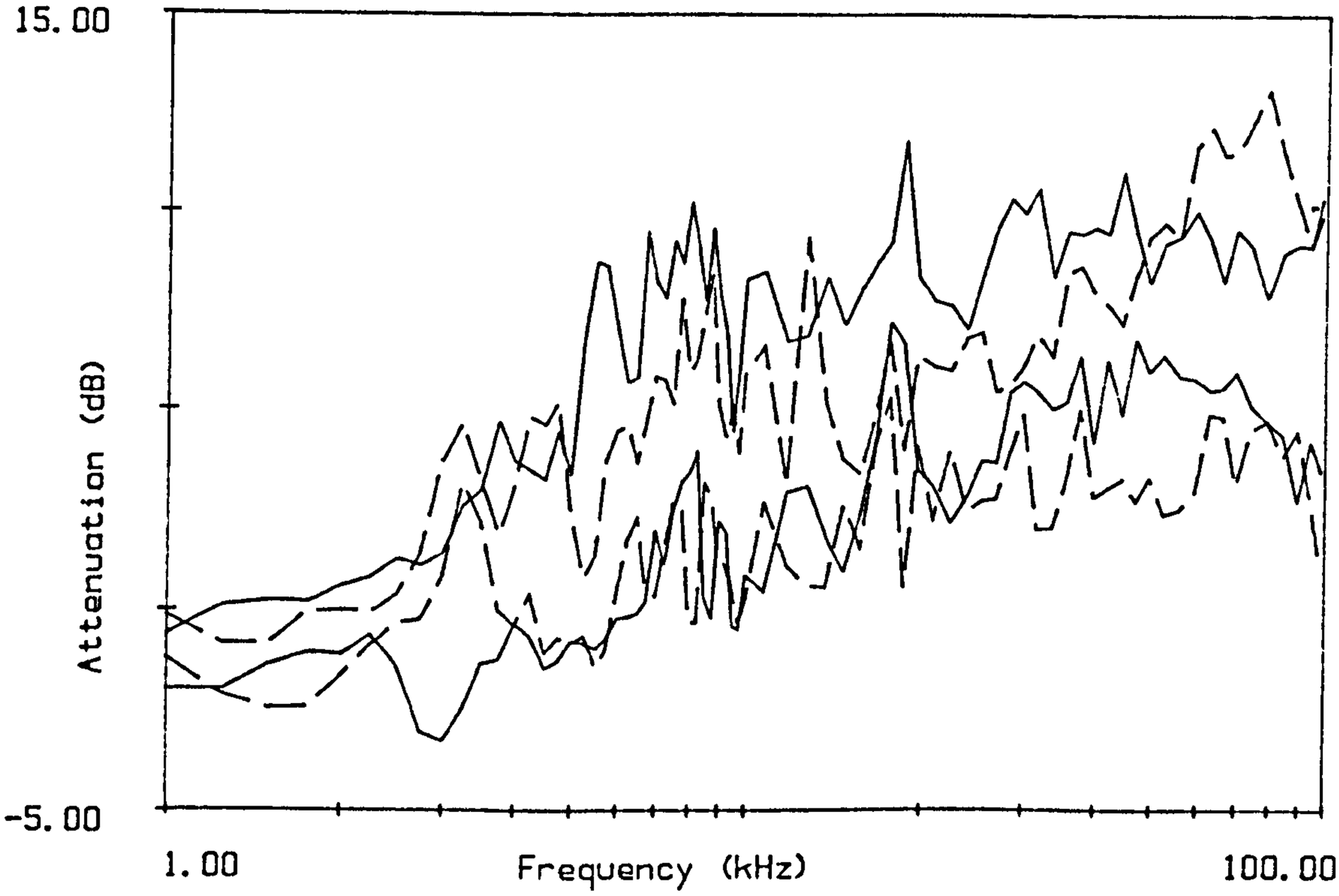

Figure 7.11a
Attenuation through array B-12 and array C-12 (----).
Range of values from the 4 microphones.

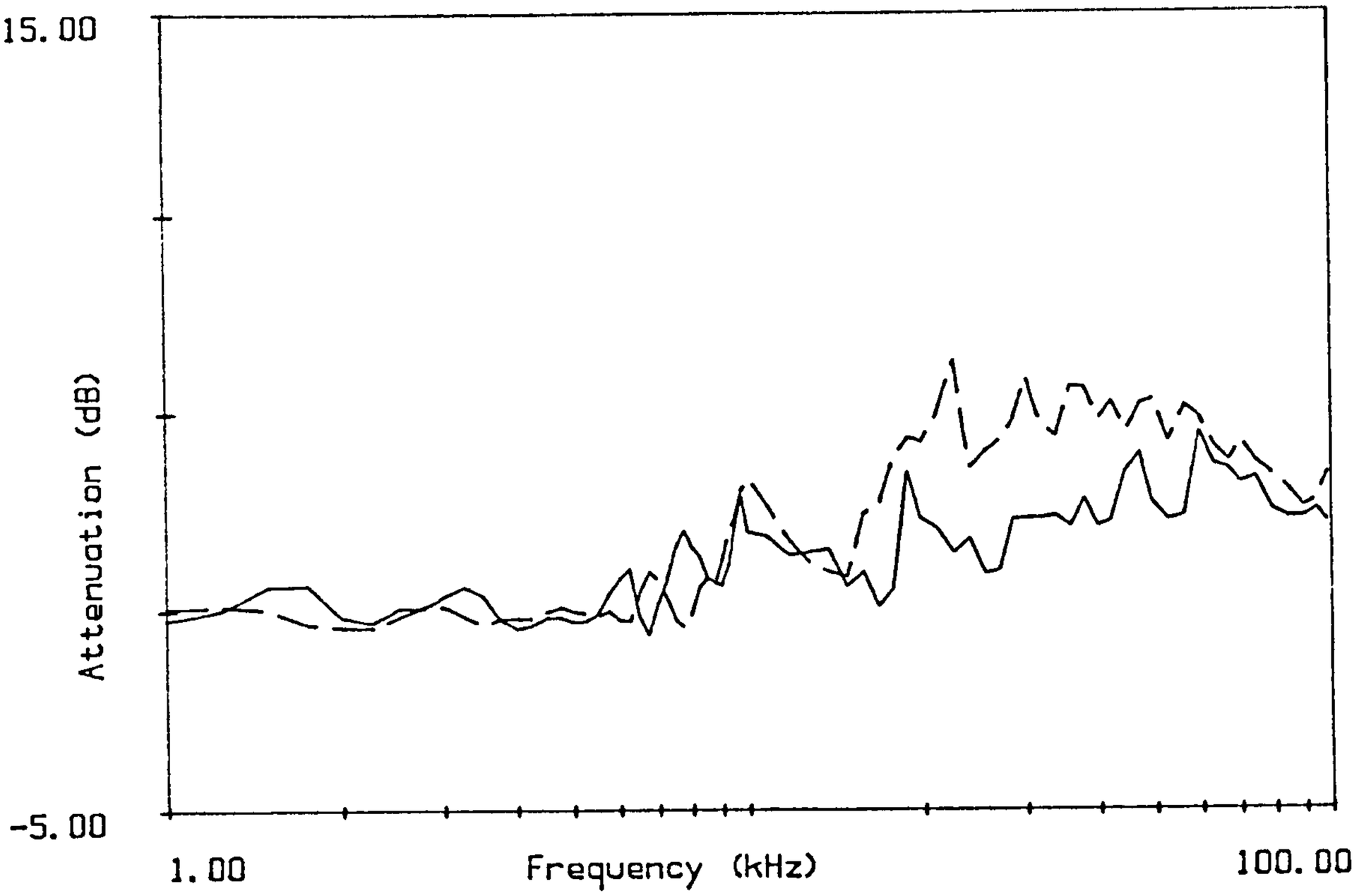

Figure 7.12
Attenuation through array A-6 and array B-6 (----).
Mean value for the 4 microphones.
(array densities; A = 240, B = 360)

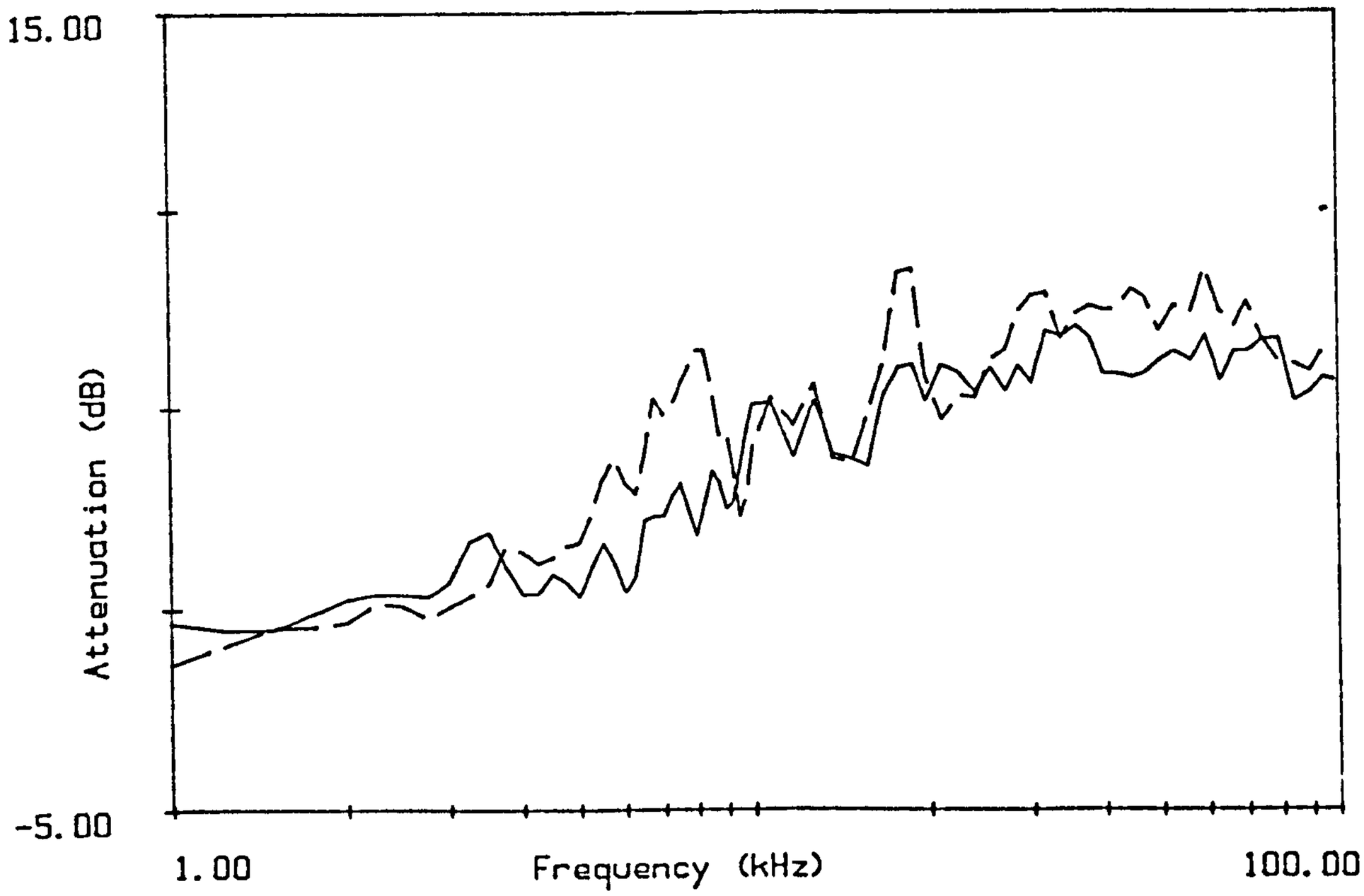

Figure 7.12a
Attenuation through array A-12 and array B-12 (----).
Mean value for the 4 microphones.
(array densities; A = 240, B = 360)

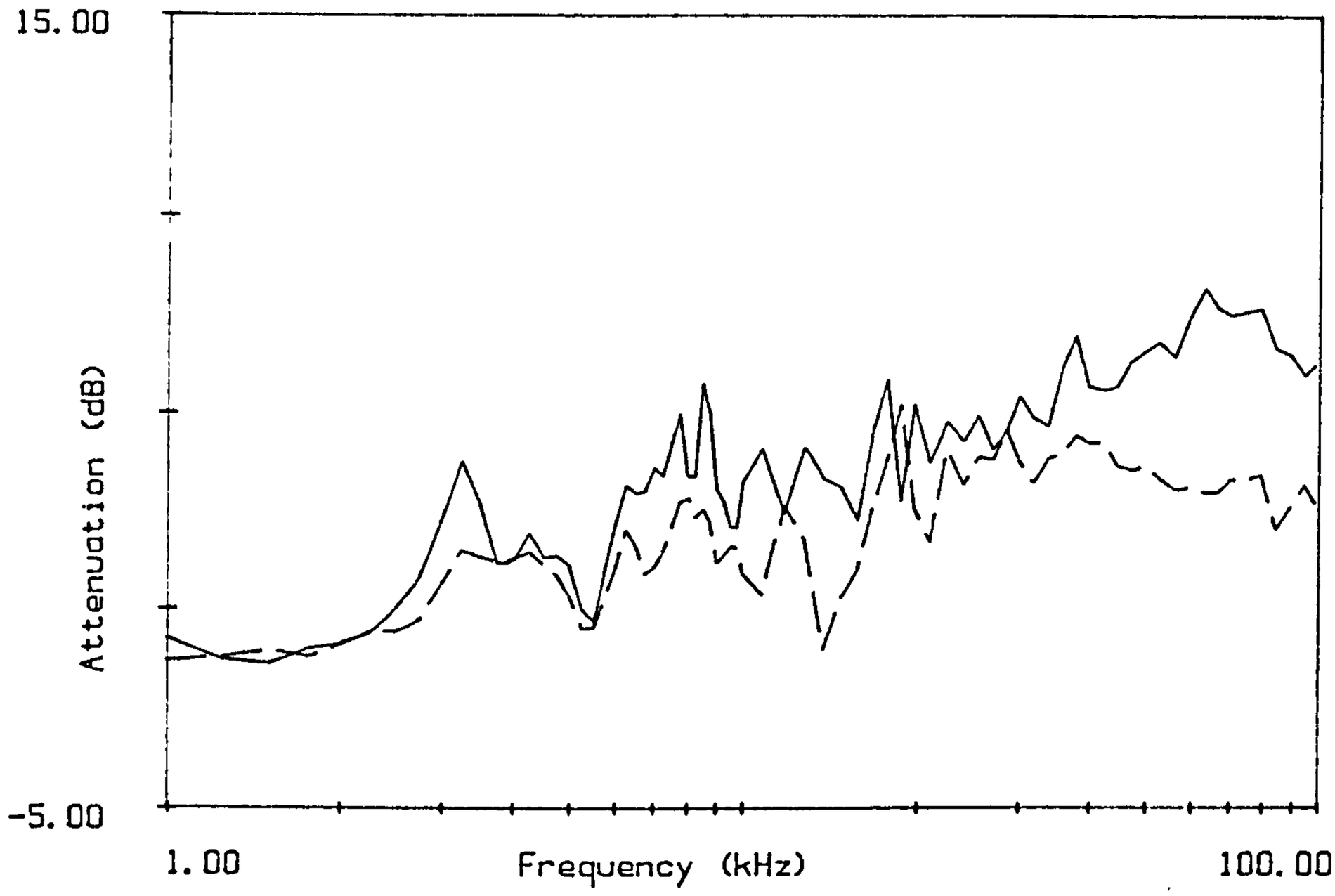

Figure 7.13a
Attenuation through array C-12 and array D-12 (----).
Mean value for the 4 microphones.
(array densities: C = 400. D = 200)

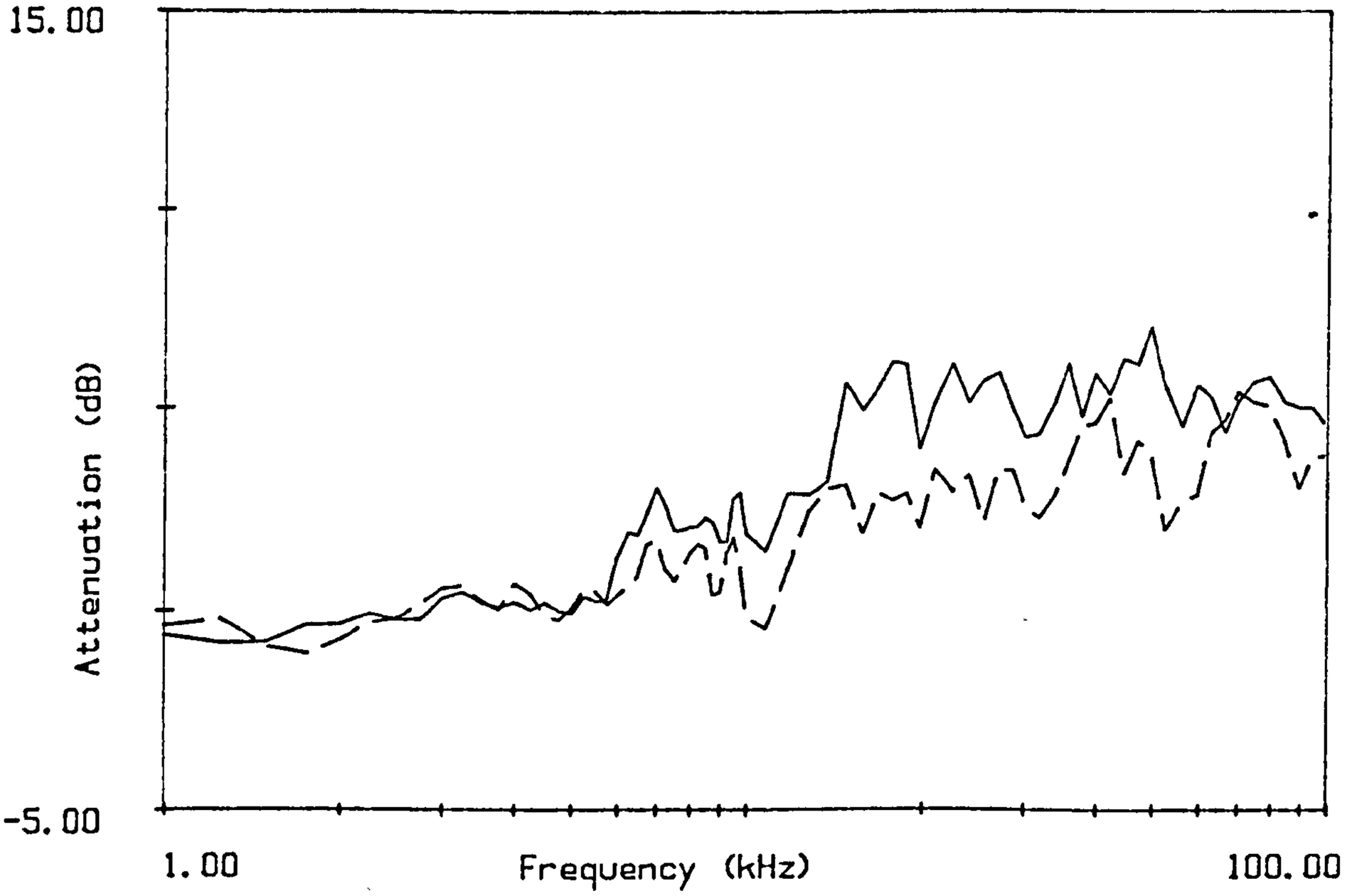

Figure 7.13b
Attenuation through array C-6 and array D-6 (----).
Mean value for the 4 microphones.
(array densities: C = 400. D = 200)

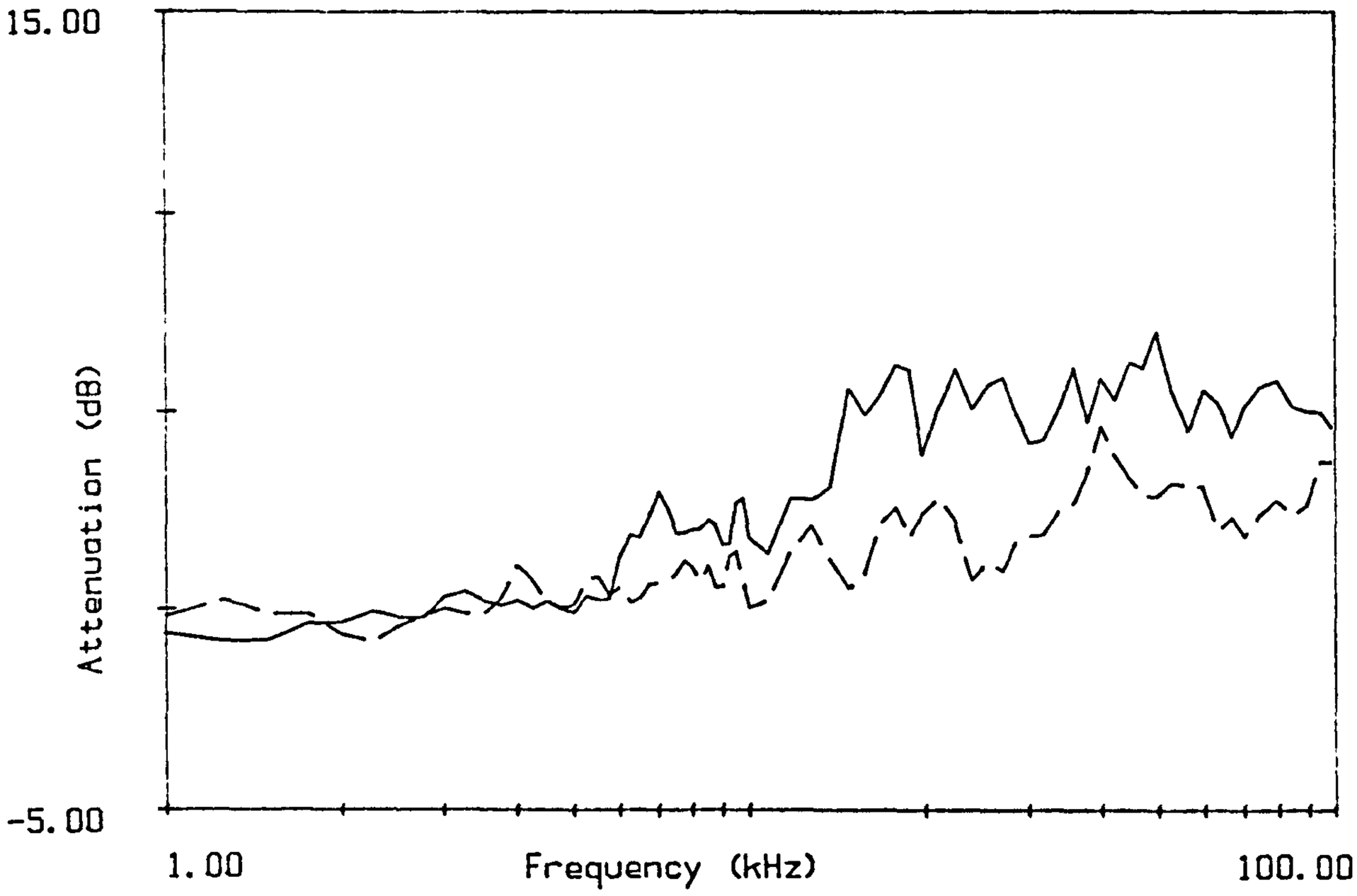

Figure 7.13c
Attenuation through array C-6 and array E-6 (----).
Mean value for the 4 microphones.
(array densities; C = 400, E = 100)

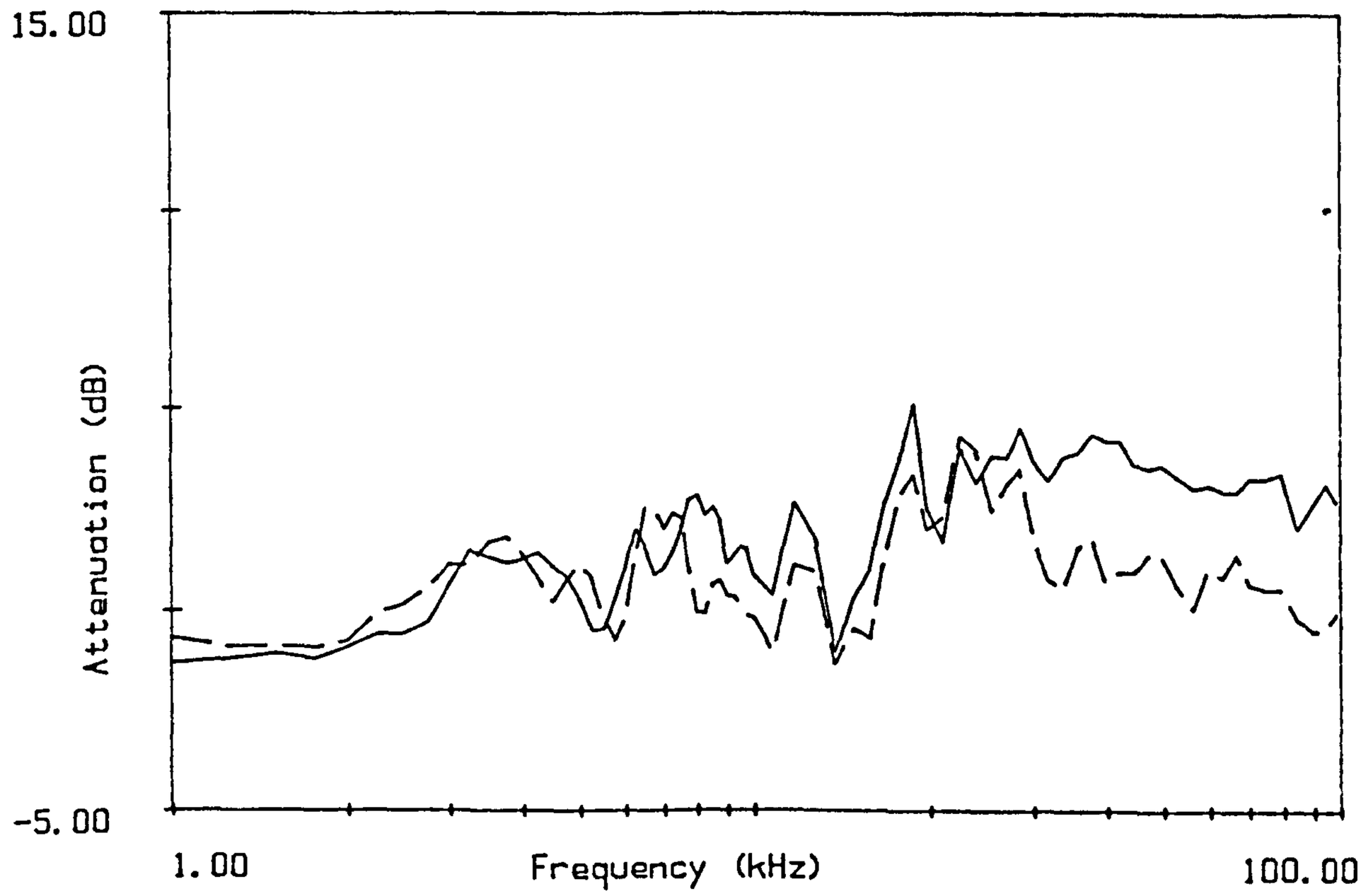

Figure 7.13d
Attenuation through array D-12 and array E-12 (----).
Mean value for the 4 microphones.
(array densities; D = 200, E = 100)

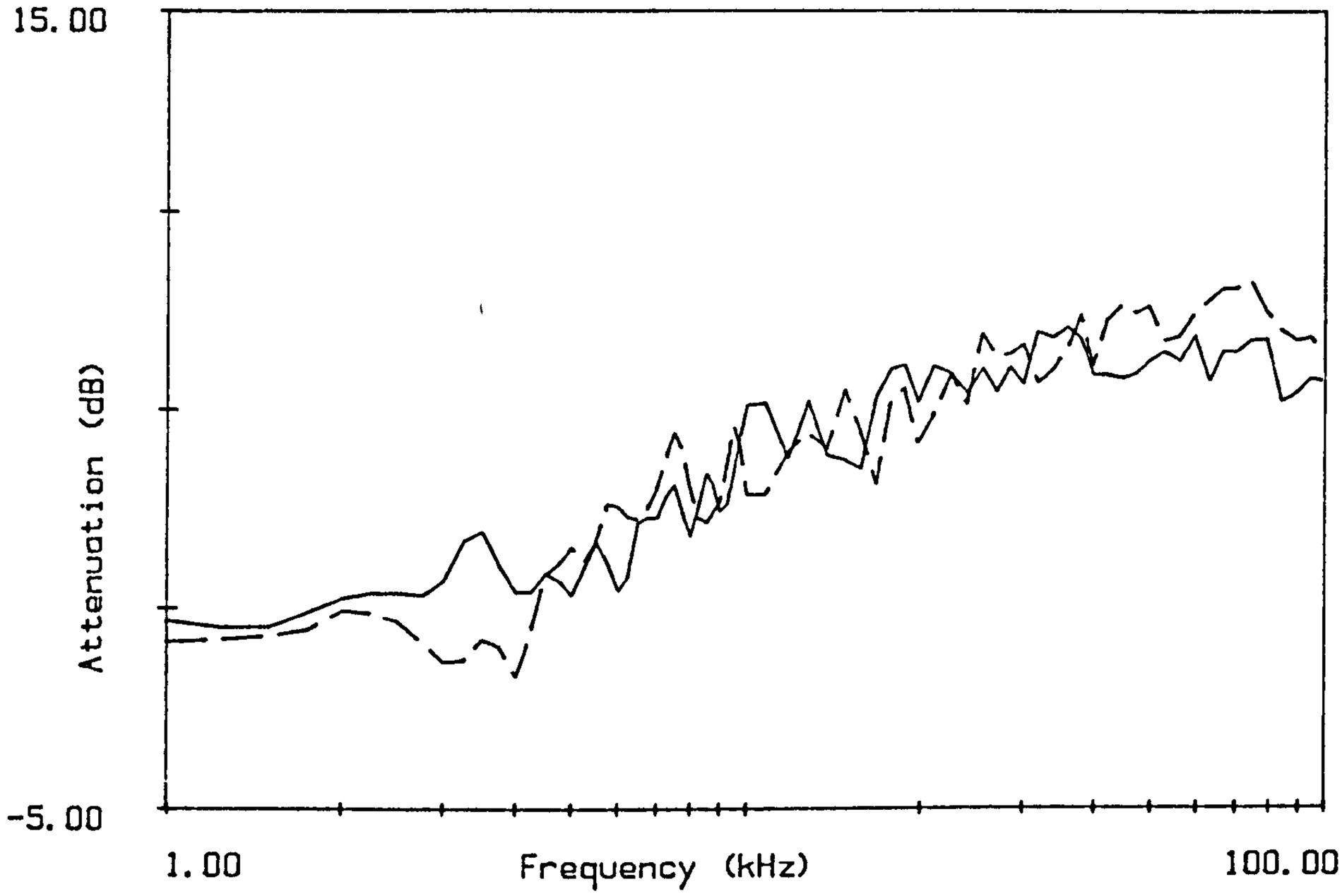

Figure 7.14
Attenuation through array A-12 and array F (----).
Mean value for the 4 microphones.
(array densities; A = 240, F = 480 - mixed radii)

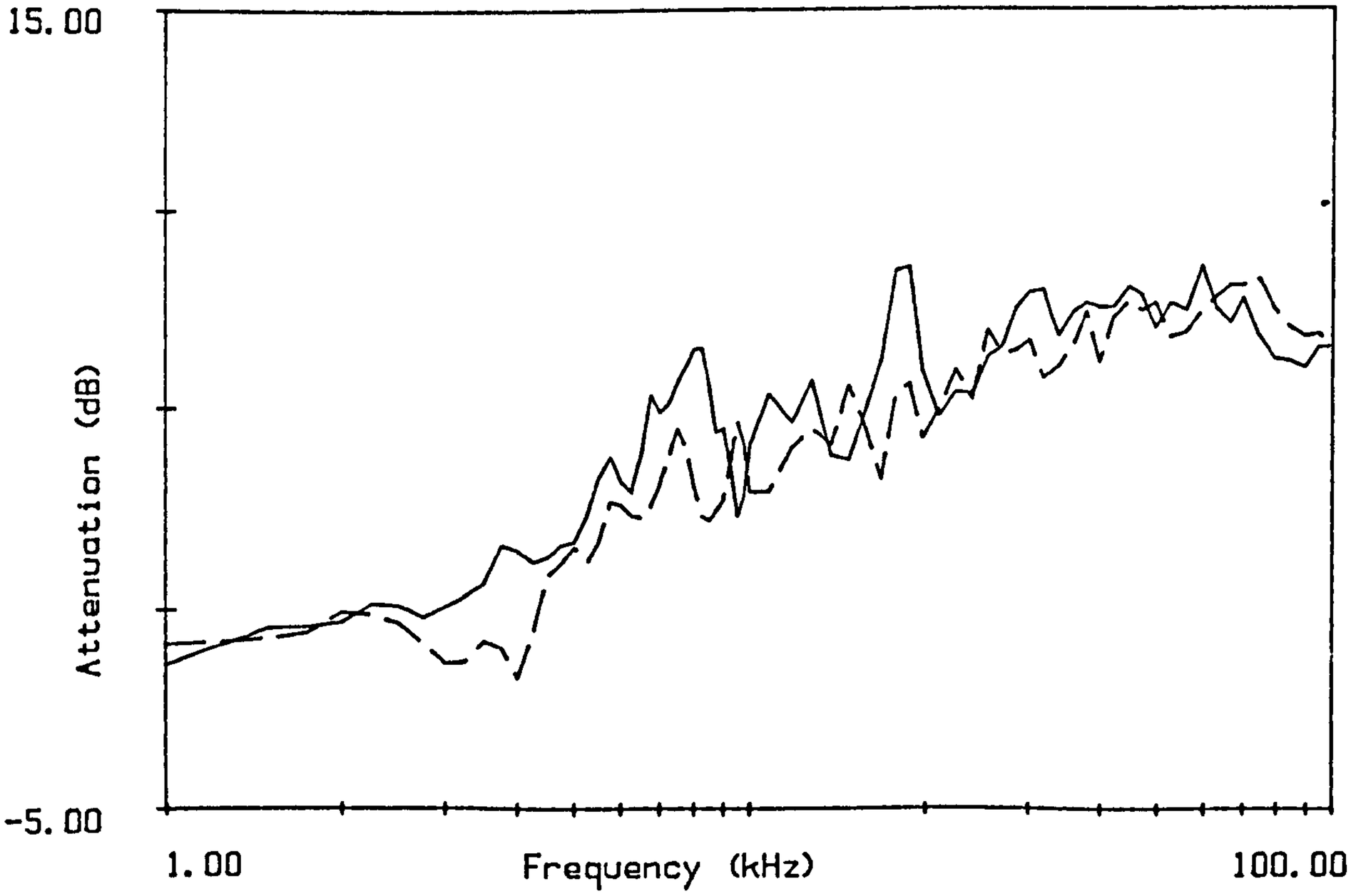

Figure 7.14a
Attenuation through array B-12 and array F (----).
Mean value for the 4 microphones.
(array densities; B = 360, F = 480 - mixed radii)

7.2 Comparison with Predictive Model

The solid lines of Figure 7.15a and 7.15b are the mean attenuation spectra of measurements A-6 and A-12 compared with the prediction of attenuation from the scattering model presented by Embleton (1966), described in chapter 5. The predictions use the measured input parameters and assume the surface of the cylinders to be rigid. It is evident that the model over-predicts the attenuation observed in the experiments, particularly for the 12mm rods. Reducing the input density considerably gave a much better correlation between the predicted and measured spectra, as did using a much smaller input radius. The model was therefore incorporated into a least mean squares fitting routine. Any two of the parameters, radius, density, separation distance and surface impedance of the cylinders; could be altered in incremental steps within a given range of values. The values of the two parameters which gave the smallest mean difference, over the whole of the frequency range 1kHz to 10kHz (ie 'the best fit' parameters) were output by the program, together with the lowest mean difference value which is calculated from these parameters.

Table 7.2 Results of Fitting the Predictive Model to the Measured Attenuation.

The mean difference (md) is calculated for the actual values of radius (rad) and density (den) using the measured separation distance and assuming hard cylinders (column 4). Fitting is then carried out by changing both the radius and density (columns 5-7), or the density (columns 8 and 9) or radius (10 and 11) alone, maintaining the measured values for the other parameters and assuming hard cylinders. A lower md value indicates a better fit to the data.

Actual Values				Fitting both radius and density			Fitting density only		Fitting radius only	
array	rad	den	md	rad	den	md	den	md	rad	md
A-6	0.003	240	2.21	0.0042	70	0.70	110	0.75	0.0017	0.88
B-6	0.003	360	3.02	0.0036	140	0.99	180	1.00	0.0019	1.25
C-6	0.003	400	2.88	0.0046	130	0.82	230	1.02	0.0021	1.43
D-6	0.003	200	1.06	0.0032	140	0.73	150	0.73	0.0025	0.77
E-6	0.003	100	0.64	0.0035	90	0.62	110	0.62	0.0032	0.62
A-12	0.006	240	4.95	0.0051	140	0.71	110	0.78	0.0035	0.99
B-12	0.006	360	8.69	0.0063	130	1.09	140	1.12	0.0030	2.09
C-12	0.006	400	11.16	0.0060	110	1.13	110	1.13	0.0024	1.75
D-12	0.006	200	5.46	0.0054	70	0.97	60	0.97	0.0025	1.17
E-12	0.006	100	3.17	0.0125	10	1.16	20	1.20	0.0021	1.3
F	0.0045	480	7.96	0.0048	160	0.84	170	0.85	0.0022	1.58

Table 7.2 presents the results of fitting the model to the attenuation data for the results described in section 7.1. The separation distance was maintained as the mean

measured source to receiver distance, and the cylinders assumed to be rigid, since the surface impedance of wood is high The results of fitting the radius and density together and separately are given, as well as the mean difference for the actual measured radius and density. The radius was fitted in increments of 0.0001m and the density in increments of 10 rods / m^2. The radius used for array F is 4.5mm, the mean radius for the rods, since an equal number of the 6mm and 12mm rods was used.

The best fit, altering the radius and density simultaneously, was achieved by altering the density considerably more than the radius. The mean for all the results indicates a best fit where the density is reduced by 50% and the radius increased by 5%. The change in radius is different for the two sizes of rods ie for the 3mm radius rods the radius is increased by about 30% and for the 6mm radius rods the radius is reduced by about 80% this would be expected from the result noted in section 7.1 that there is not a very large difference in the attenuation spectra for the arrays with different densities and radii. The main exception to this result was the comparison between arrays A-6 and A- 12 (figure 7.7). The best fit radii for these arrays (maintaining the measured density) are 0.0017m and 0.0035m ie both achieve a best fit by reducing the radii by 42 to 43%, similarly both give the same best fit density when the measured radii are used ie. 110 a reduction of 54% from the actual value. These are the sort of results which would be expected from this experiment if the dependence of the attenuation on radius size and density is correctly described by this model.

The lowest mean difference values are smallest for the simultaneous fitting of both parameters, as would be expected. The value obtained by maintaining the measured radius and altering the density only is consistently lower than that obtained when altering the radii; this leads to the conclusion that reducing the input density is likely to give a more accurate prediction of the attenuation. The conclusions reached in section 7.1 that the attenuation is relatively insensitive to changes in density is supported by the fact that the reductions in density required are large. The mean adjustments made for the 3mm radius rods and the 6mm radius rods (from column 8) were 32% and 68% respectively. In table 7.3 the overall mean of the mean squared difference values obtained by reducing the density by 30, 40, 50, 60 and 70% are compared. The mean value of mean squared difference

obtained indicates that the best simple stratagem to improve the prediction by this model over all the measurements would be to reduce the density input to the model by approximately 60%. Figures 7.15a to 7.15f are examples of the comparisons of the mean values with predictions using the actual, best fit (from column 8 of table 7.2), and modified (reduced by 60%) densities. These figures show that the modified model gives a fairly good fit to most of the data, obviously the prediction is not as good as that from the best fit densities. The modified model does not give such a good fit to the attenuation spectra of C-12.

Figure 7.16 shows that the prediction using the mean radius and total density is virtually the same as that for sum of the attenuations from the two individual arrays, one with a radius of 3mm and one of 6mm. This illustrates the validity of using the mean radius of a mixed array in the modified prediction model,in this experiment.

Table 7.3. Mean effect of altering the input density by a given percentage.

% by which density is reduced	0	30	40	50	60	70
mean of all MS values	31.97	10.10	5.76	2.97	1.74	2.23
standard deviation of all MS values	39.72	13.30	7.62	3.56	1.13	1.04

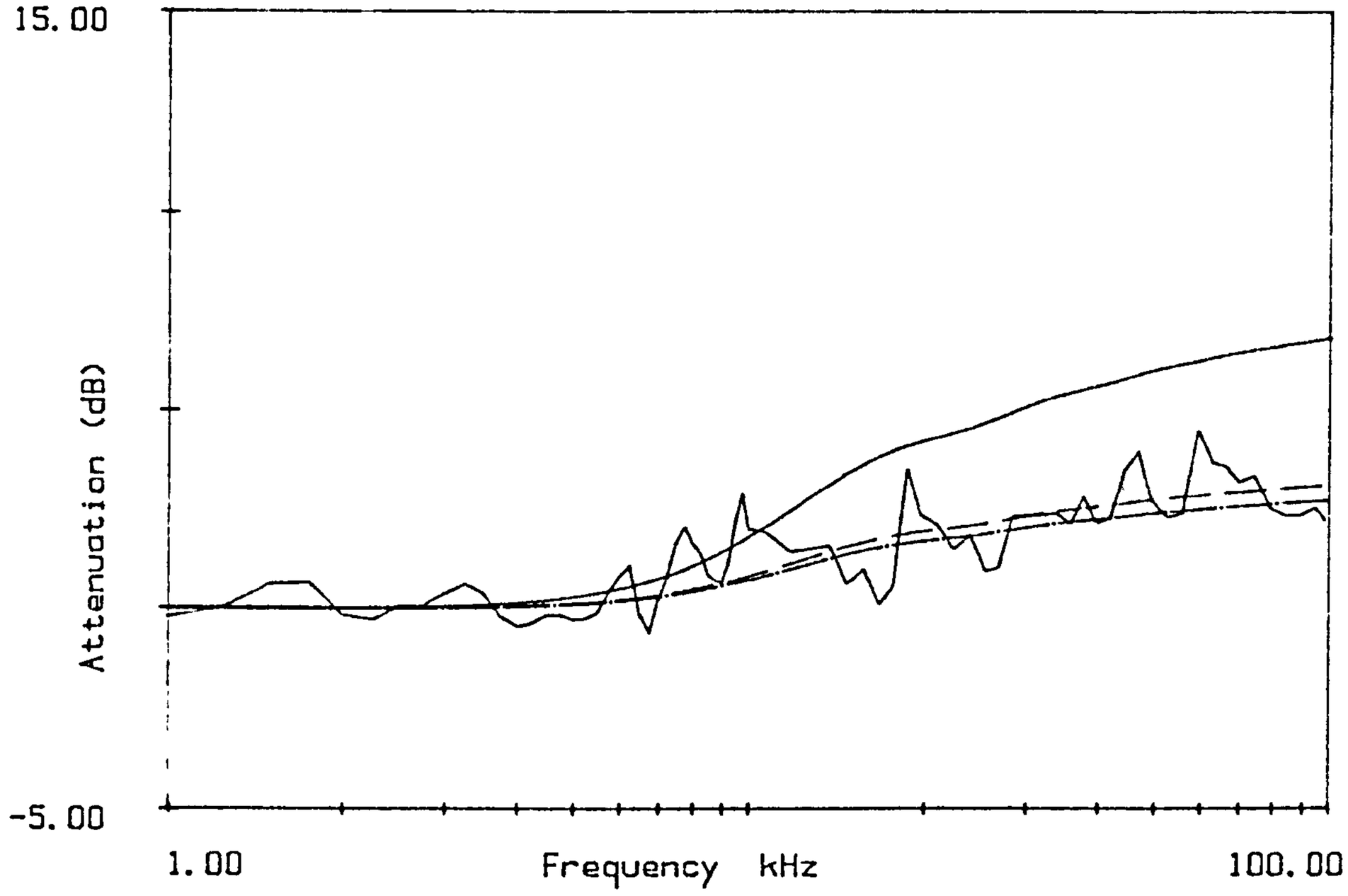

Figure 7.15a
Measured and Predicted Attenuation for Measurement A-6.
Density = ——— 240. — — — 110. —·—·— 96.

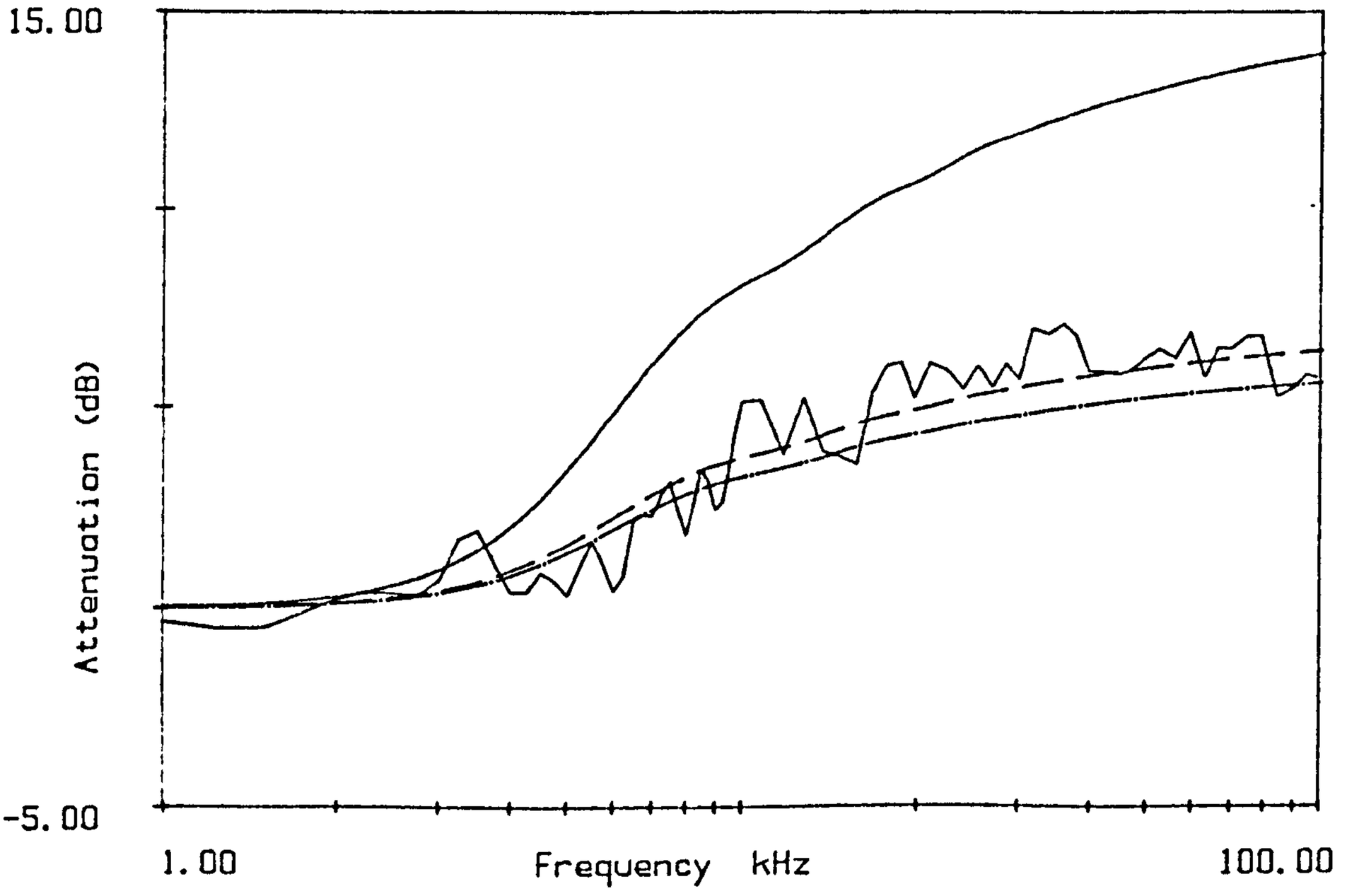

Figure 7.15b
Measured and Predicted Attenuation for Measurement A-12.
Density = ——— 240. — — — 110. —·—·— 96.

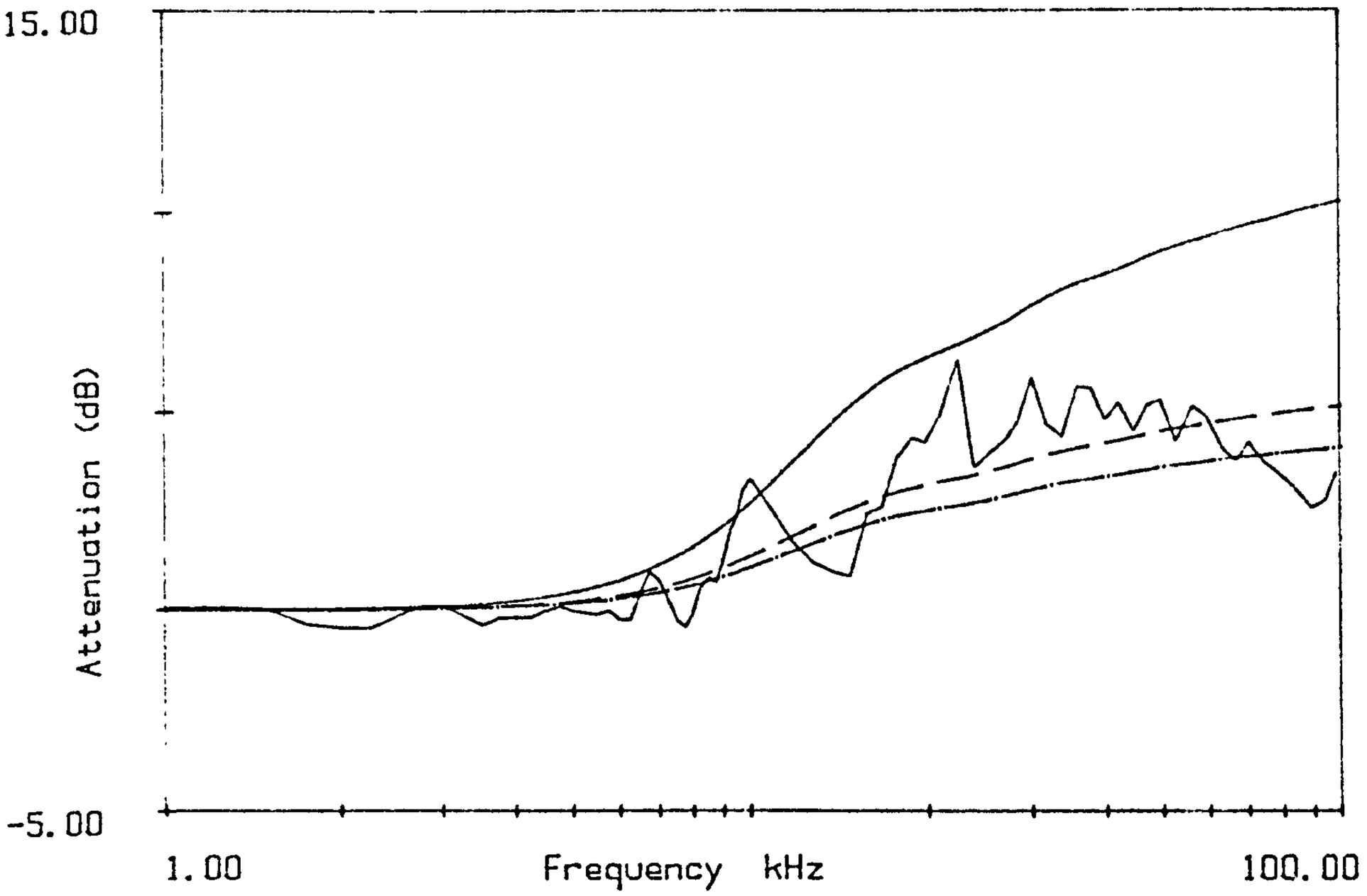

FIGURE 7.15c
Measured and Predicted Attenuation for Measurement B-6.
Density = ———— 360. — — — 180. —·—·— 144.

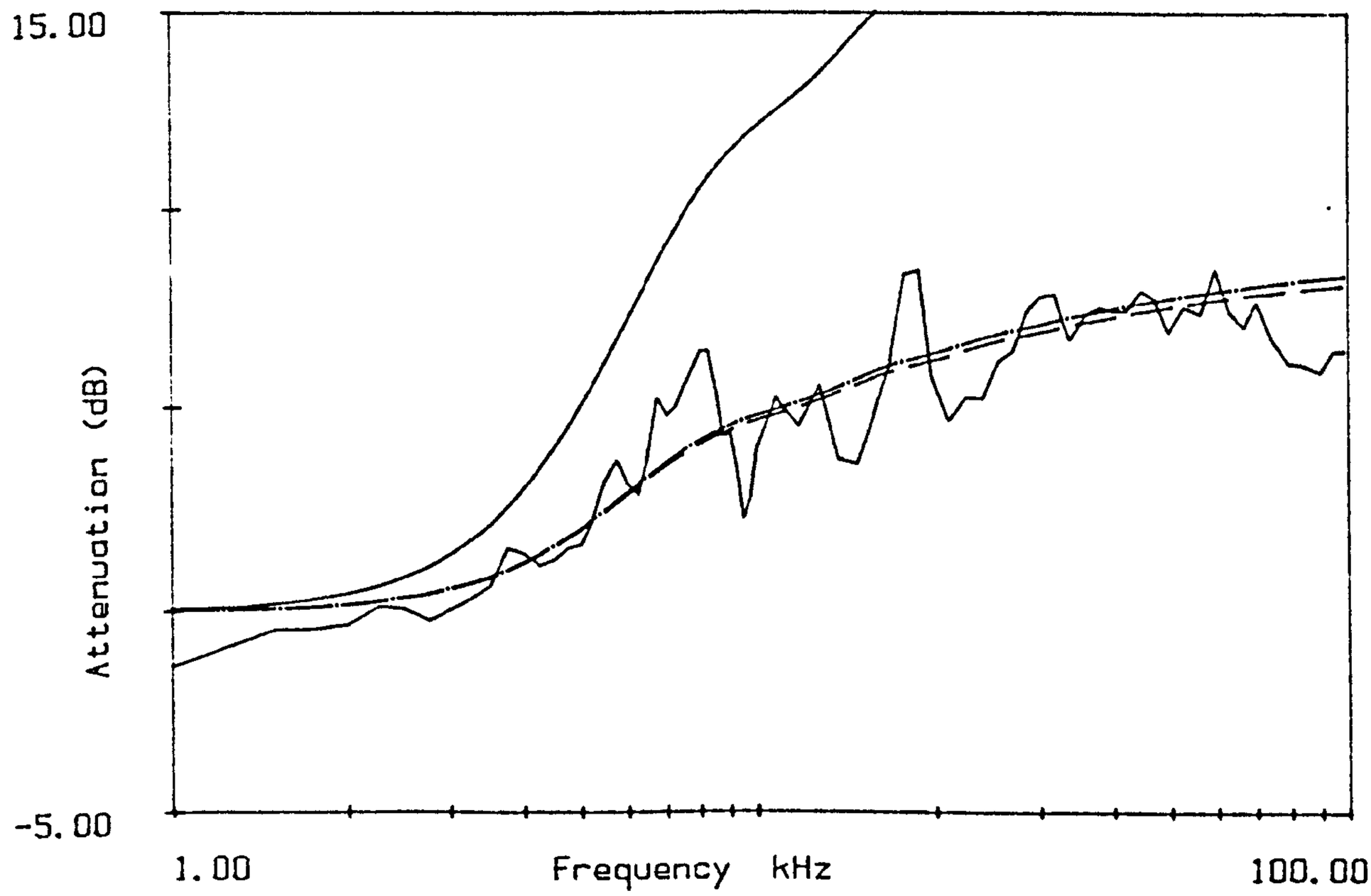

Figure 7.15d
Measured and Predicted Attenuation for Measurement B-12.
Density = ———— 360. — — — 140. —·—·— 144.

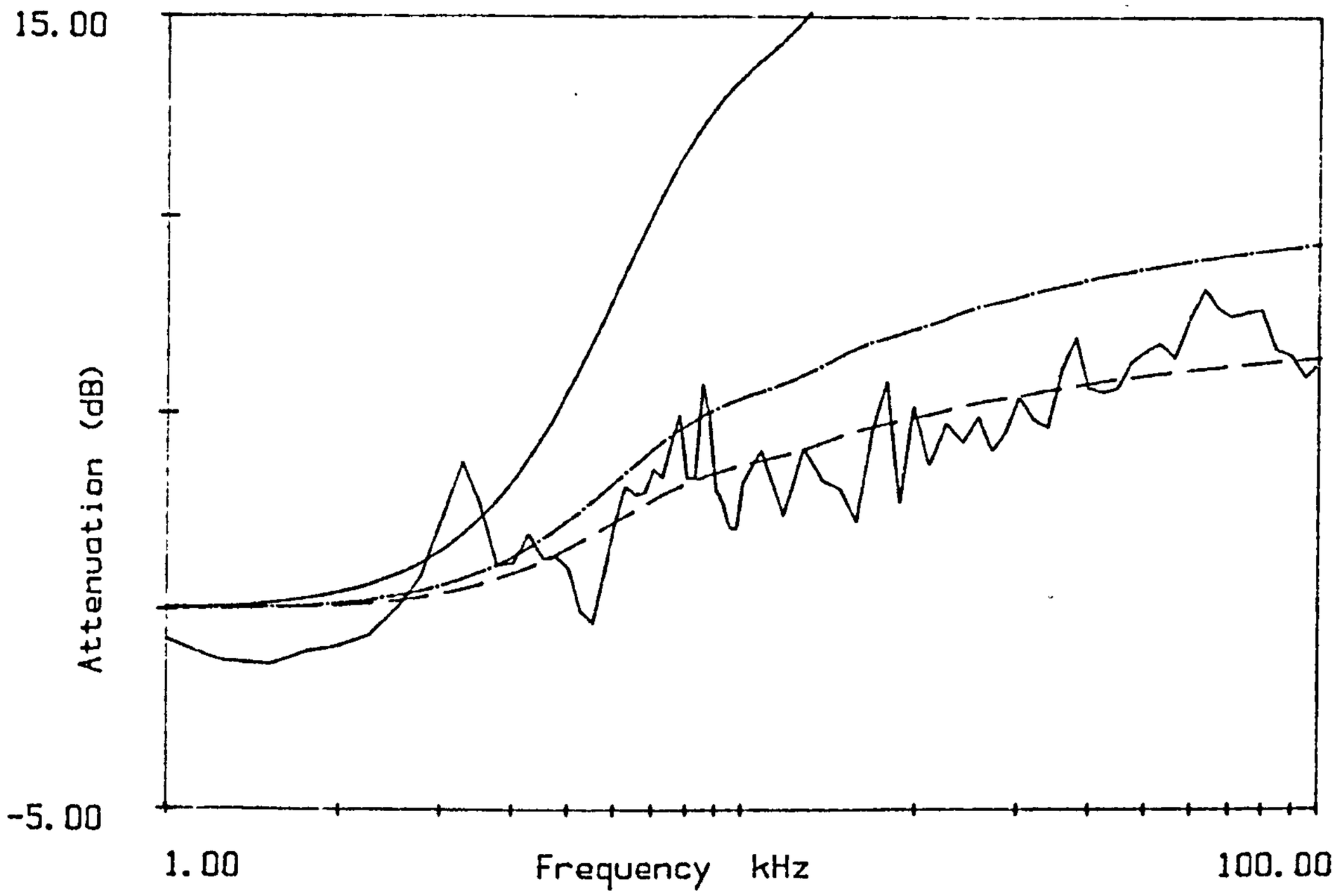

Figure 7.15e
Measured and Predicted Attenuation for Measurement C-12.
Density = ——— 400, — — — 110, ——·——— 160.

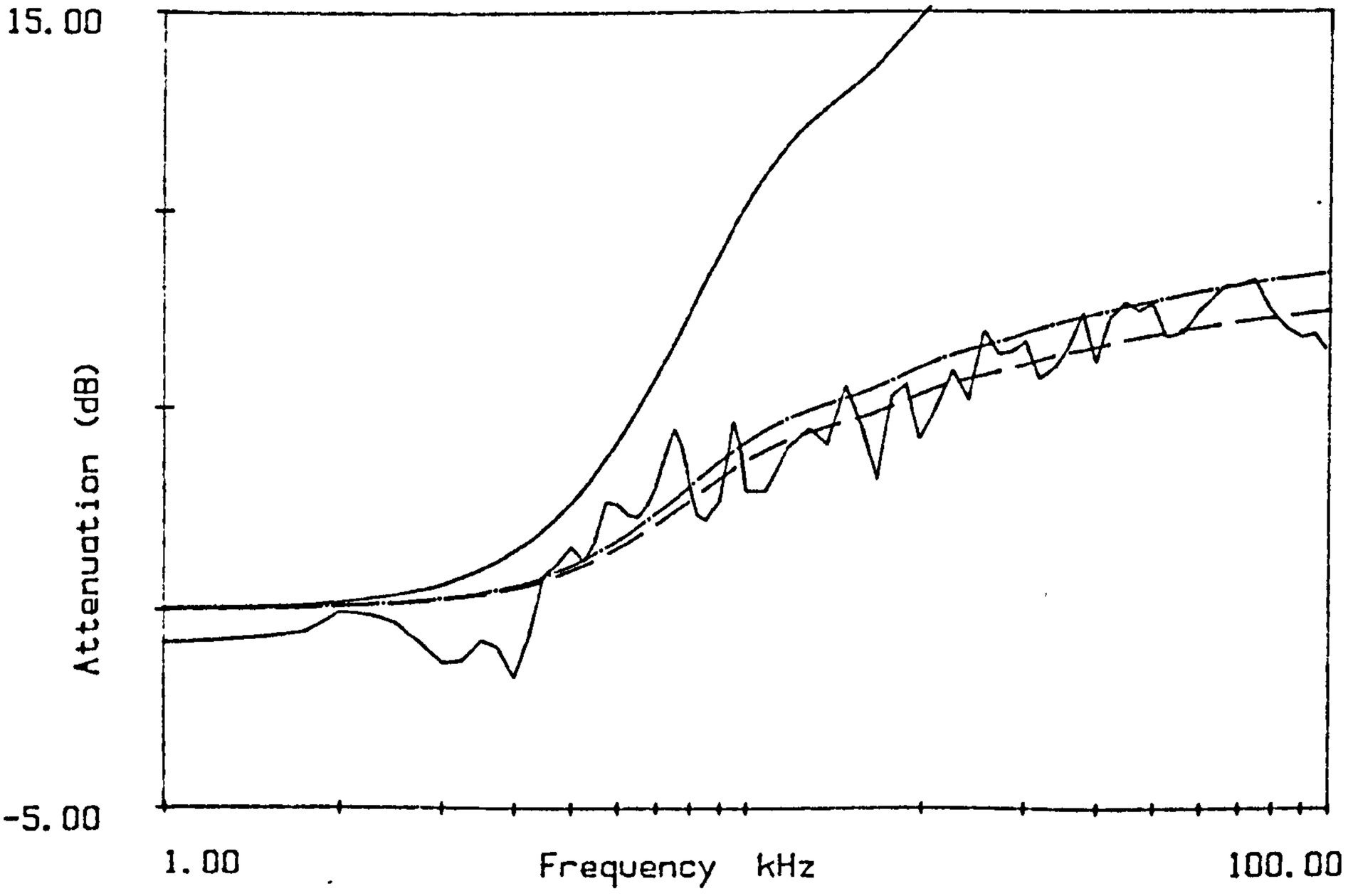

Figure 7.15f
Measured and Predicted Attenuation for Measurement F.
Density = ——— 480, — — — 170, ——·——— 192.

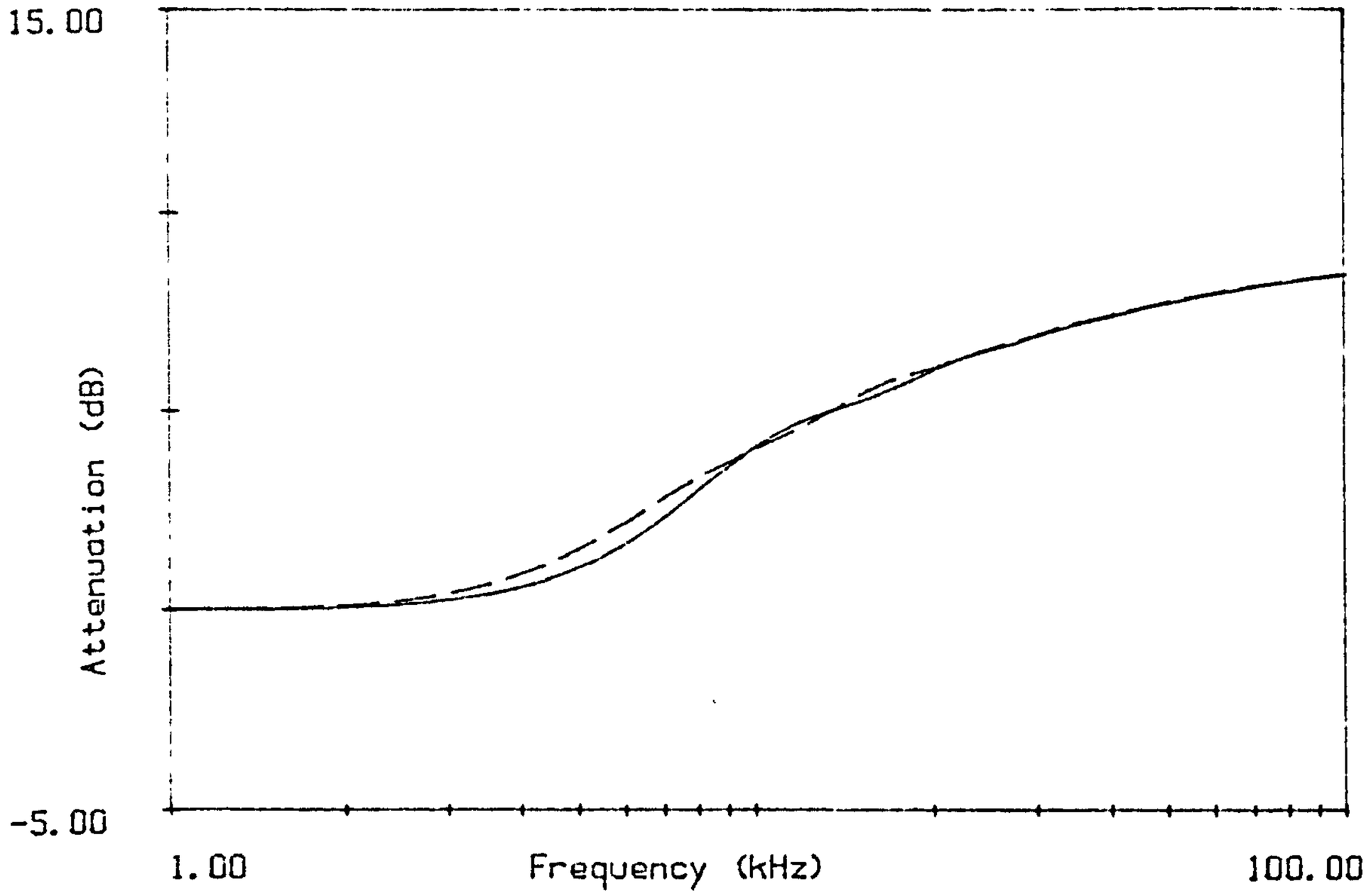

Figure 7.16
Sum of attenuations from two arrays of rigid cylinders with density 96; radii 0.003 and 0.006
and (-----) single array radius=0.0045, density=192

7.3 Measurements with a 'ground' surface.

The second set of measurements carried out was designed to investigate the effects of an array of cylinders in the presence of a ground surface. The aim was to find out whether it is acceptable to simply add the attenuation due to scattering to the ground interference effects. The insertion loss of an array was calculated as the difference between the propagation across a surface without and with an array of scatterers 'planted' in it. It follows that if the total attenuation is the sum of the ground and scattering attenuations, the insertion loss should be the same as the attenuation calculated in the previous, 'infinite case' measurements.

The 12mm rods used in the previous experiment were cut to fit between the grid on the ceiling and a tray of sand on a table in the anechoic chamber. There were then 160 rods approximately 1.52m long and 160 short rods 0.28m long. The tray of sand was 1.2m wide, 2.4m long and about 0.075m deep, the air jet protruding vertically through the bottom of the tray and the sand so the open end was about 0.065 cm above the sand surface. The microphones were in the same array (see figure 7.2), and were located at approximately the same x,y coordinates as in the previous experiments, about 7cm above the surface of the sand.

The longer 12mm rods were used to construct the arrays A-12 and B-12 in the same way as the first set of measurements ie. the tops of the rods were located in the grid squares and the bottom ends were pushed into the sand. The signal from the air jet was analysed and stored and the long rods replaced with the short rods, ie the 28cm rods were pushed into the holes left in the sand when the long rods were removed. Approximately 20cm of the rods protruded above the sand. The rods were then removed and the signal from the air jet analysed and stored before and after filling in the holes and smoothing the surface. The air jet was again left on throughout the experiment to avoid fluctuations in air flow, and the same situation repeated at intervals to check that the source is constant ie the 'no rods, unsmoothed ground surface' measurement was carried out before, in the middle and at the end of the regular array measurements; the results were all very similar.

Figure 7.17 (and 7.17a) shows a comparison between the mean of the results from array B-12 constructed long and short rods. There was little difference between the two cases. Short rods were therefore used to construct arrays C-12, D-12 and E-12 and the smaller arrays, since the shorter rods were easier to work with. The 'strips' of scatterers were constructed by inserting short rods into some of the holes left in the sand when array C-12 was removed. These were used to investigate whether a narrower strip of scatterers of the same radius and density will give a proportionately smaller attenuation and whether the location of such a strip has any influence on the result.

The stored spectra were transferred to the VAX mainframe where the insertion loss was calculated by subtracting the level recorded with the array in place from that recorded over the flattened sand surface. The excess attenuation was also calculated for some of the data, particularly for the measurements without the rods. Since it was not possible to measure the free field at the time of this experiment, stored free field spectra from the experiments described in section 7.1 were used. The excess attenuation is calculated as the level recorded in this experiment minus the stored free field level, corrected for any differences in measuring amplifier gain setting.

Results

Figure 7.18 shows the excess attenuation at one of the microphones of some preliminary measurements over the flattened sand carried out before the scatterers were introduced into the sand. The prediction illustrated is calculated from the propagation model described in chapter 4 using the best fit flow resistivity from the Delany and Bazley model of ground impedance. This show a fairly good level of agreement in the location of the peaks and dips, if not in their magnitude; indicating that ground interference effects occurred and could be detected.

Unfortunately the excess attenuation measured from the rest of the measurements in this experiment indicated that the spectrum of the air jet had changed significantly. For

example the excess attenuation illustrated in figure 7.18a is from the same experimental set-up as that of figure 7.18 but is quite different in frequency dependence and magnitude. The differences cannot be accounted for by inaccuracies in the location of the microphones or differences in the ground surface, therefore I conclude that the source spectrum had altered.

The spectra measured from the propagation over the smoothed and unsmoothed sand surfaces alone are generally very similar, (see figures D.24 to D.27) therefore the ground effect from the measurements carried out using parts of C-12 with the remaining holes left in the sand can be assumed to be the same as that for a smoothed surface; and either the smoothed or unsmoothed measurements used in the calculation of insertion loss.

Figures 7.19a to 7.19d are examples of the comparisons between the mean attenuation from the 'infinite length' measurements and the mean insertion loss using the same array. The ranges of values obtained for the four microphones overlap considerably over most of the frequency range ie the means are not significantly different. Thus the conclusion can be drawn that an infinite length prediction could be added to the attenuation expected from the ground surface alone, to predict the attenuation due to an array of vertical cylinders over a ground surface. The conclusions obtained for the infinite length case will therefore also hold for the situation investigated in the sand-box, including the conclusion that the scattering model has to be modified considerably to predict the attenuation accurately.

Figures 7.20 and 7.20a show comparisons between the insertion loss results for the experiments using parts of array C-12, as illustrated in figures D.14 to D.19. The differences in the means are small but both the 6 row and 4 row measurements do give a consistently greater attenuation with the rods closer to the receiver, at frequencies around 30 to 70 kHz. Table 7.4 gives the same results for these measurements as table 7.2 does for the attenuation data. The depth of the array is calculated as a proportion of the separation distance for the measurements of array C-12 (ie 4/13 or 6/13 times the total separation distance;) and is used as the separation distance in the fitting routine. The results are similar to those for the attenuation data ie the density has to be reduced considerably to give a good fit to the data. The increase in attenuation with the rods close to the receiver is reflected as an increase in best fit density for both the 4 row and 6 row measurements, which give very similar best fit

densities. The results indicate that, where only part of the propagation path is through an array of scatterers, it is valid to input the depth of the array as the separation distance in the prediction model.

Table 7.4

Results of fitting the predictive model to the measured insertion loss for parts of array C 12. The mean difference (md) is calculated for the actual values of radius (rad) and density (den) using the measured separation distance and assuming hard cylinders (column 4). Fitting is then carried out by changing both the radius and density (columns 5 7), or the density (columns 8 and 9) or radius (10 and 11) alone, maintaining the measured values for the other parameters and assuming hard cylinders.

Actual Values				Fitting both radius and density			Fitting density only		Fitting radius only	
Rows	rad	depth	md	rad	den	md	den	md	rad	md
1 6	0.006	0.324	5.98	0.0076	90	1.85	120	1.87	0.0025	2.29
4 9	0.006	0.324	4.83	0.0093	100	1.51	170	1.57	0.0034	2.03
7 12	0.006	0.324	4.14	0.0073	160	1.31	210	1.34	0.0038	1.73
1 4	0.006	0.210	3.77	0.0066	110	1.09	120	1.10	0.0026	1.32
5 8	0.006	0.210	3.17	0.0097	100	1.37	180	1.40	0.0035	1.58
9 12	0.006	0.210	2.73	0.0062	200	1.10	210	1.10	0.0038	1.28
whole	0.006	0.648	11.05	0.0074	100	1.61	130	1.68	0.0027	2.77
whole	0.006	0.648	10.85	0.0077	100	1.58	130	1.71	0.0027	2.87

References, Chapter 7.

[1] Embleton, T.F.W 1966. Scattering by an Array of Cylinders as a Function of Surface Impedance. J. ACOUST. SOC. AM. 40(3). 667-670.

[2] Frank, L.D. 1976. Tree Bark and the Forest Floor as Sound Absorbing Elements Within a Forest. MSc THESIS PENNSYLVANIA STATE UNIVERSITY.

[3] Heap, N.W. 1982. Sound Propagation over Mixed Impedances. PhD THESIS. OPEN UNIVERSITY.

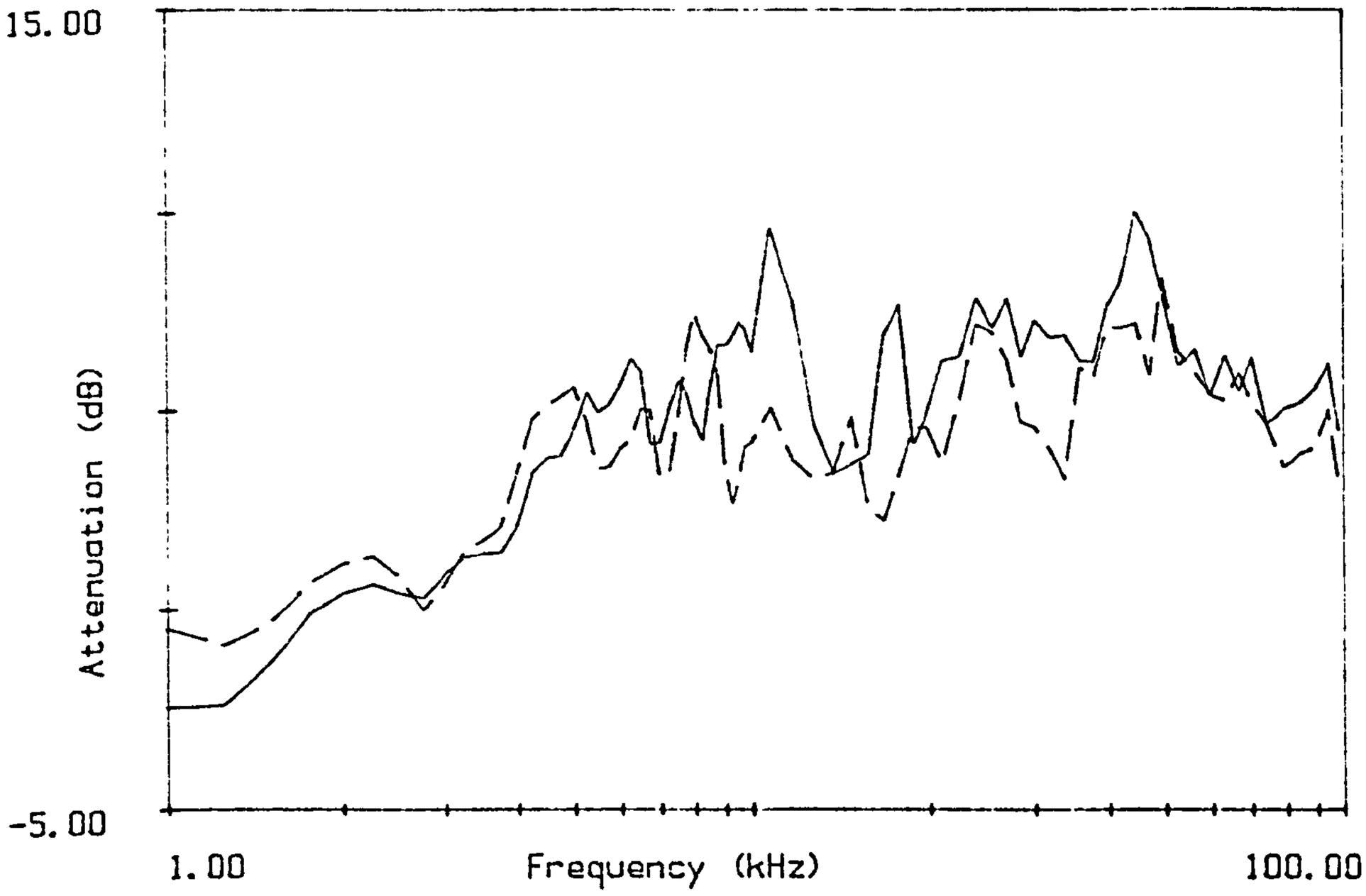

Figure 7.17
Mean insertion loss spectra for array B-12 constructed in the sand box from long and short(---) rods.

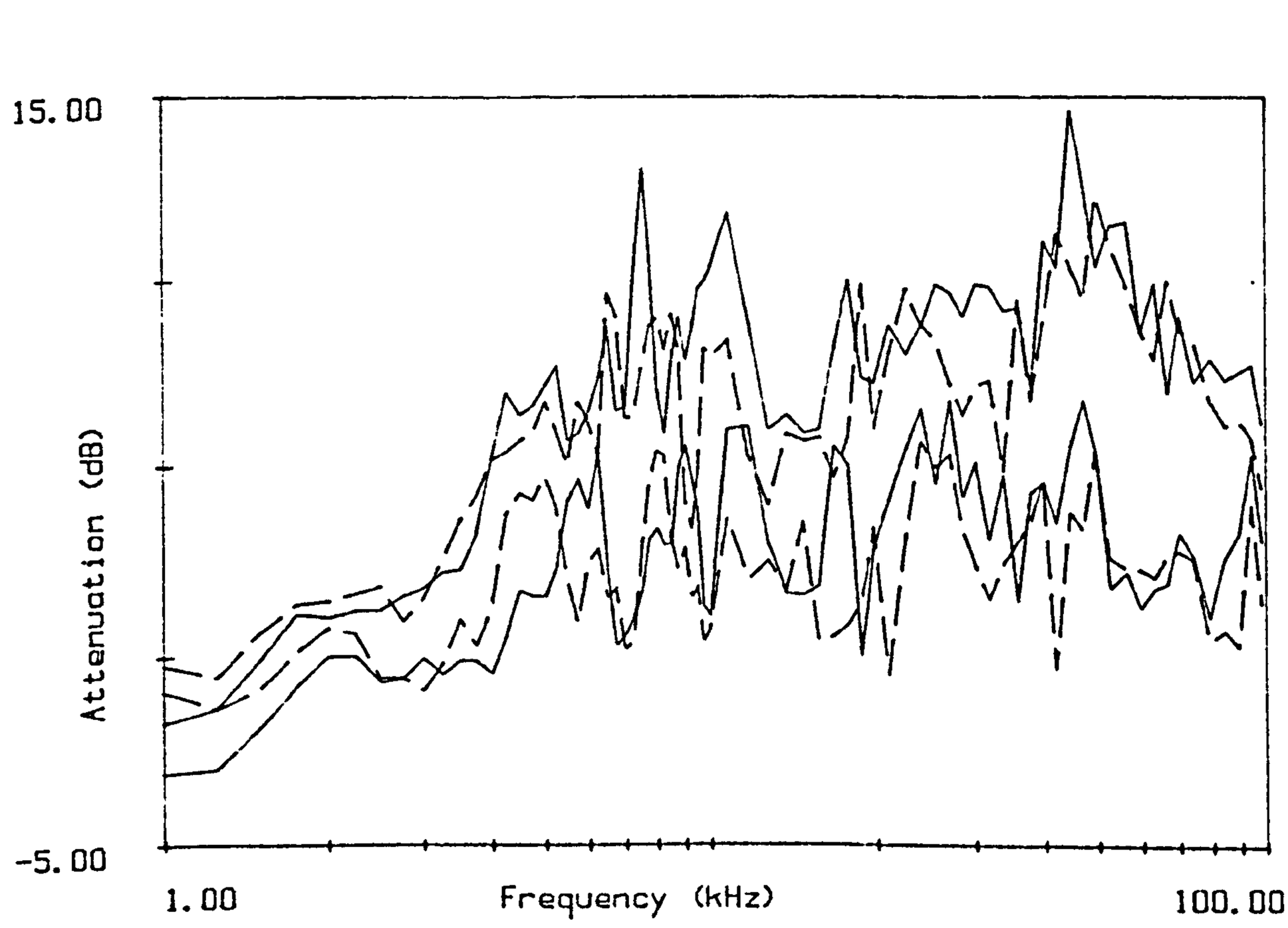

Figure 7.17a
Range of insertion loss spectra for array B-12 constructed in the sand box from long and short(---) rods.

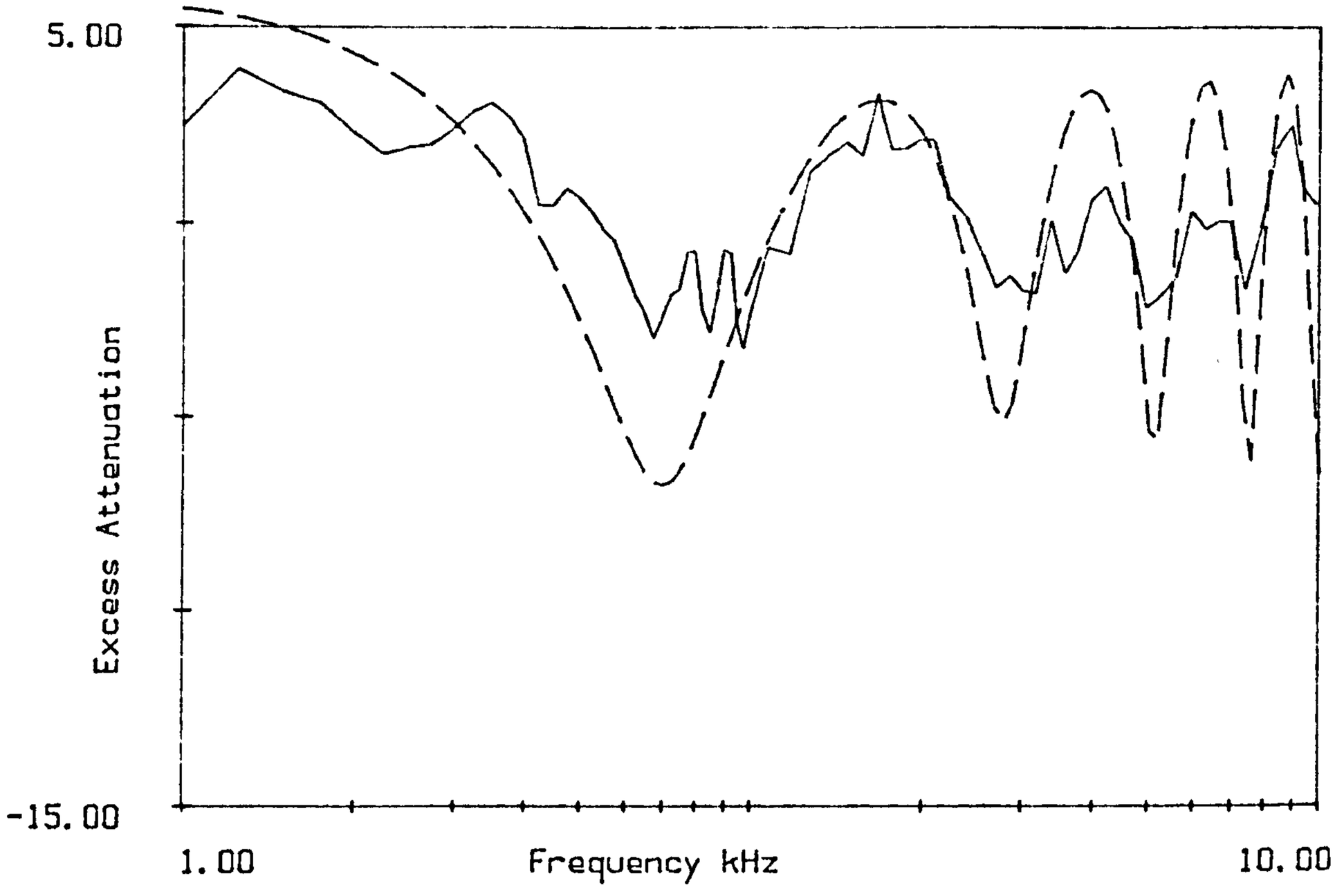

Figure 7.18 Microphone 1
Measured vs Predicted Excess Attenuation over Sand.
hs=hr=0.07, r=0.7 σe =2,000,000

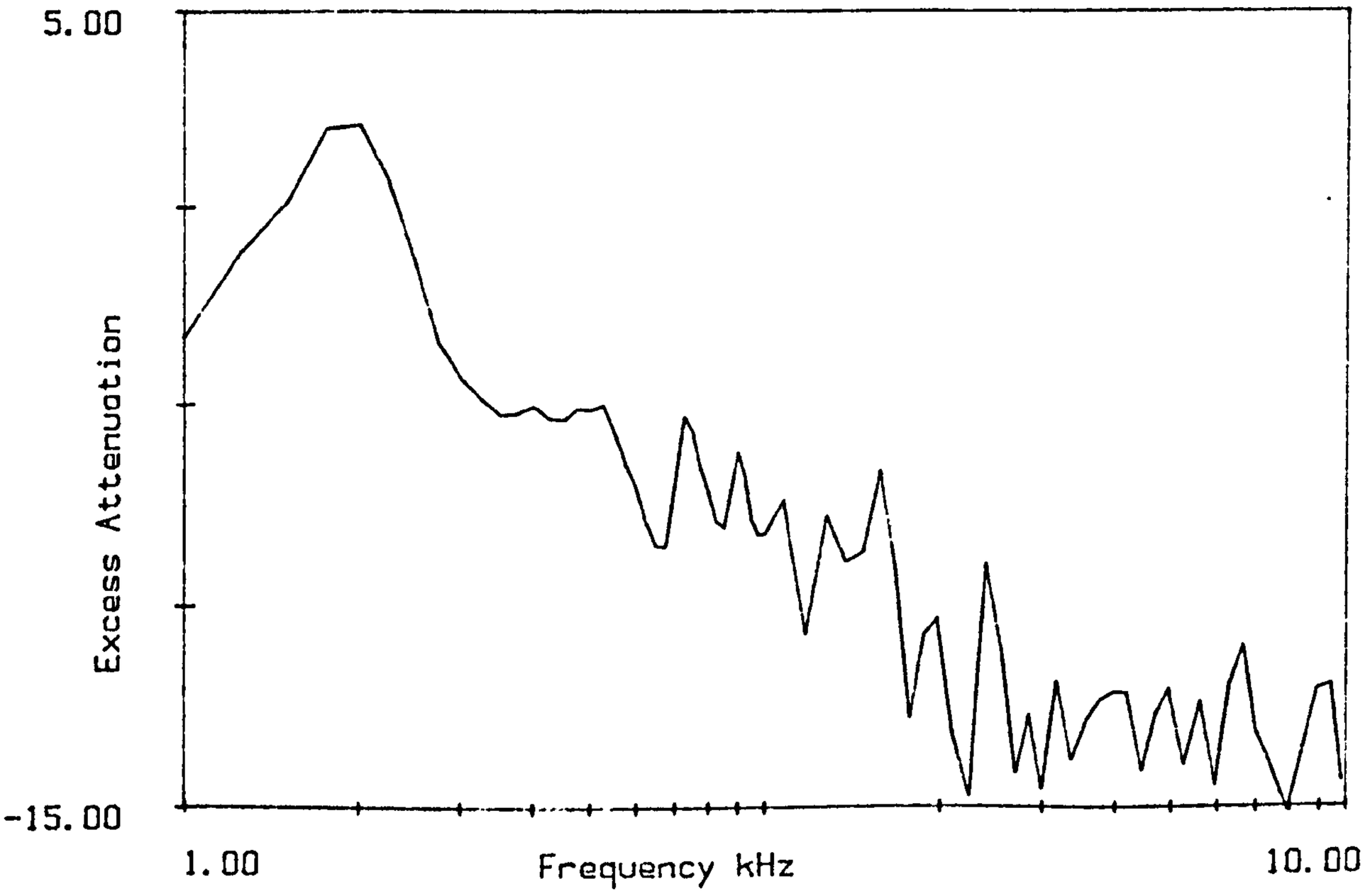

Figure 7.18a
Microphone 1. Measured Excess Attenuation over Sand.

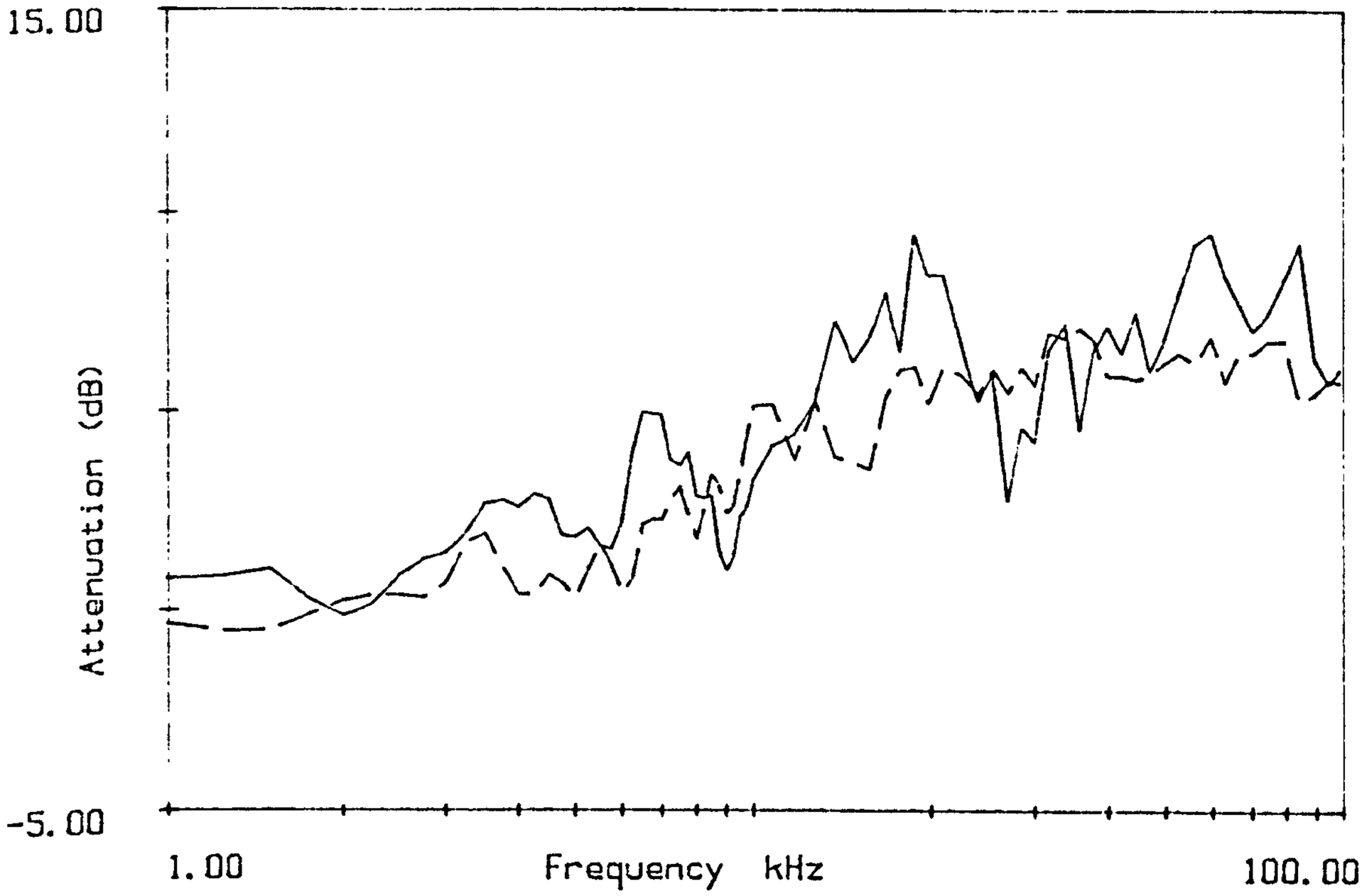

Figure 7.19a
Array A-12 mean Insertion Loss and Attenuation (----).

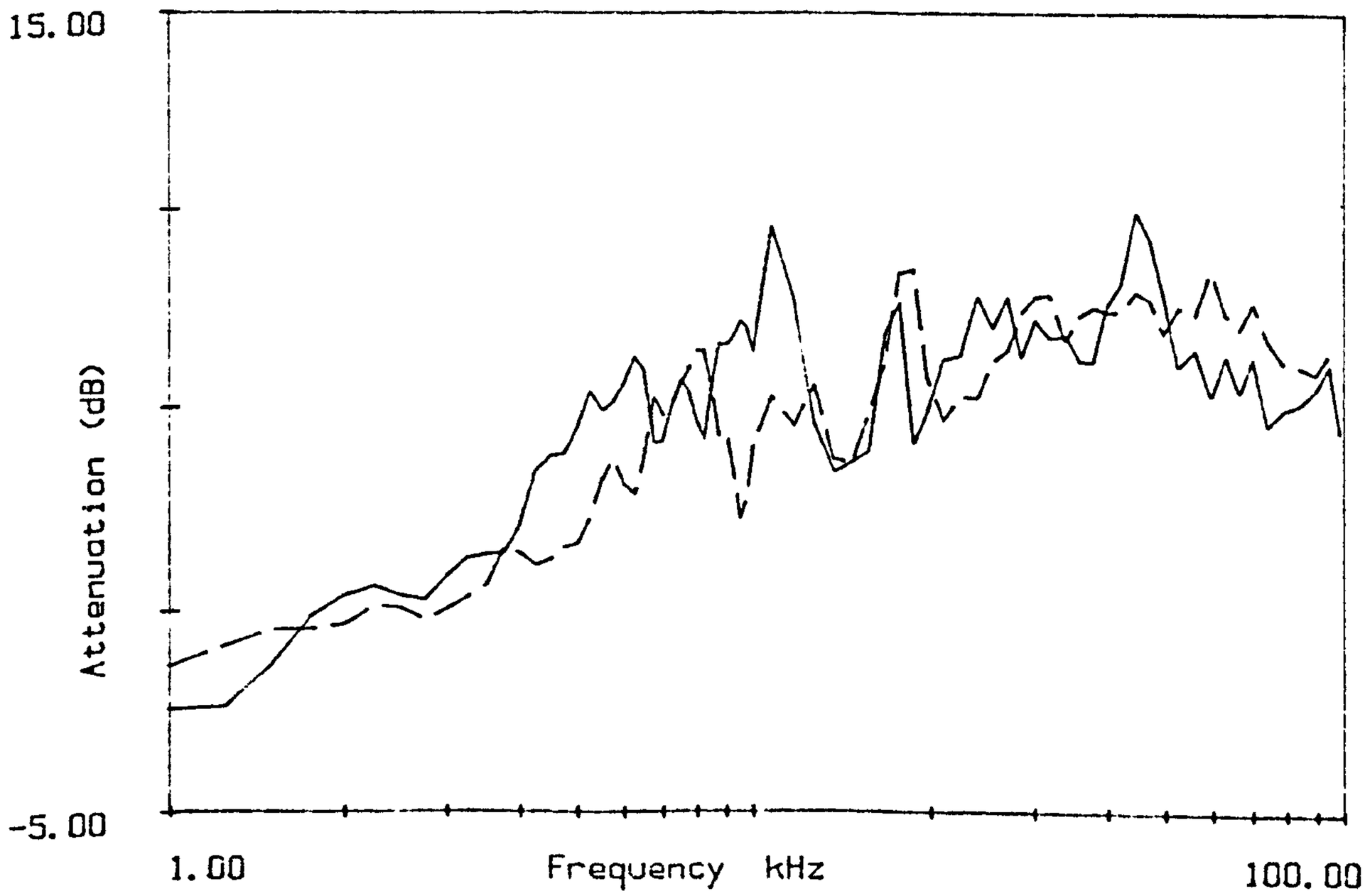

Figure 7.19b
Array B-12 mean Insertion Loss and Attenuation (----).

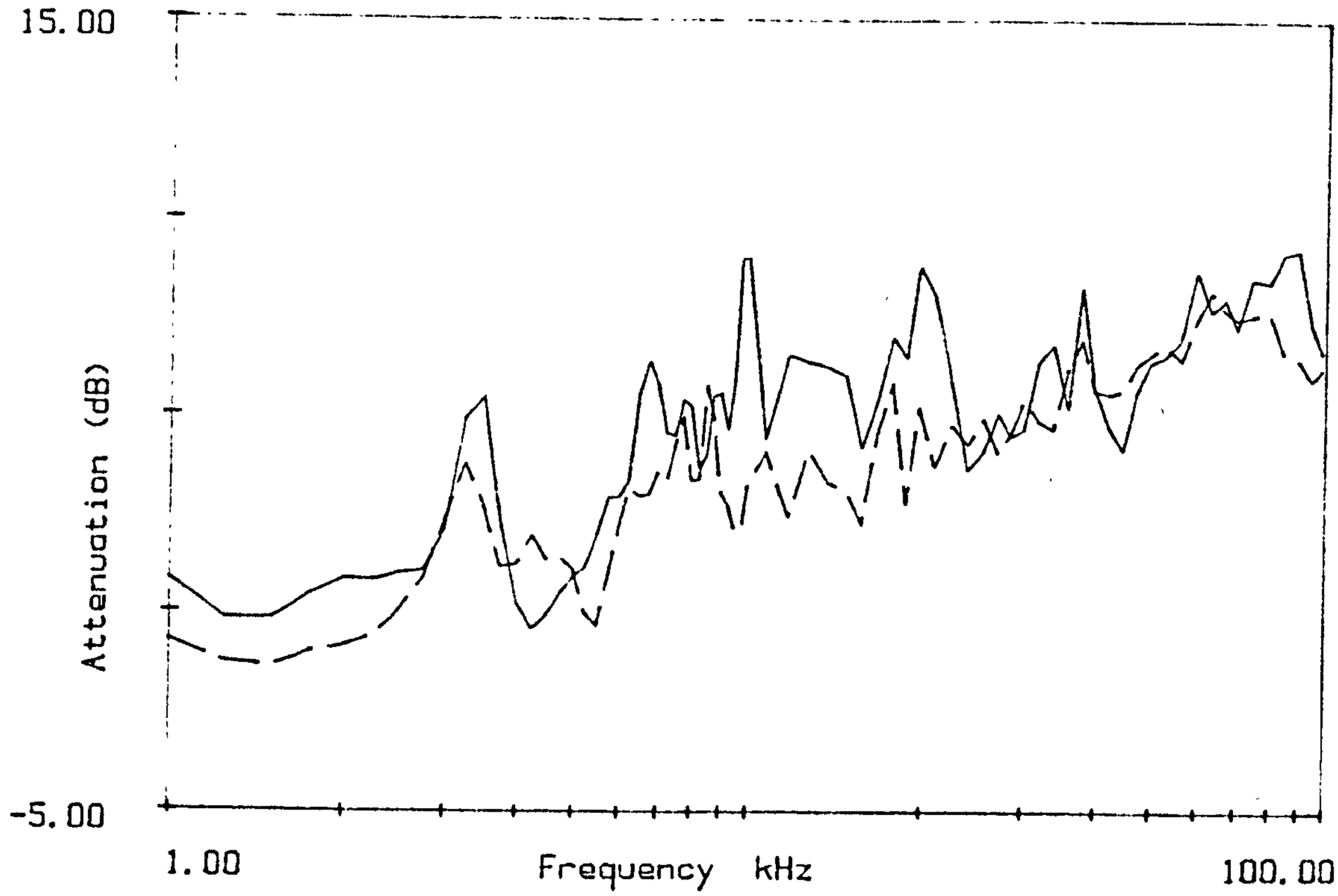

Figure 7.19c
Array C-12 mean Insertion Loss and Attenuation (----).

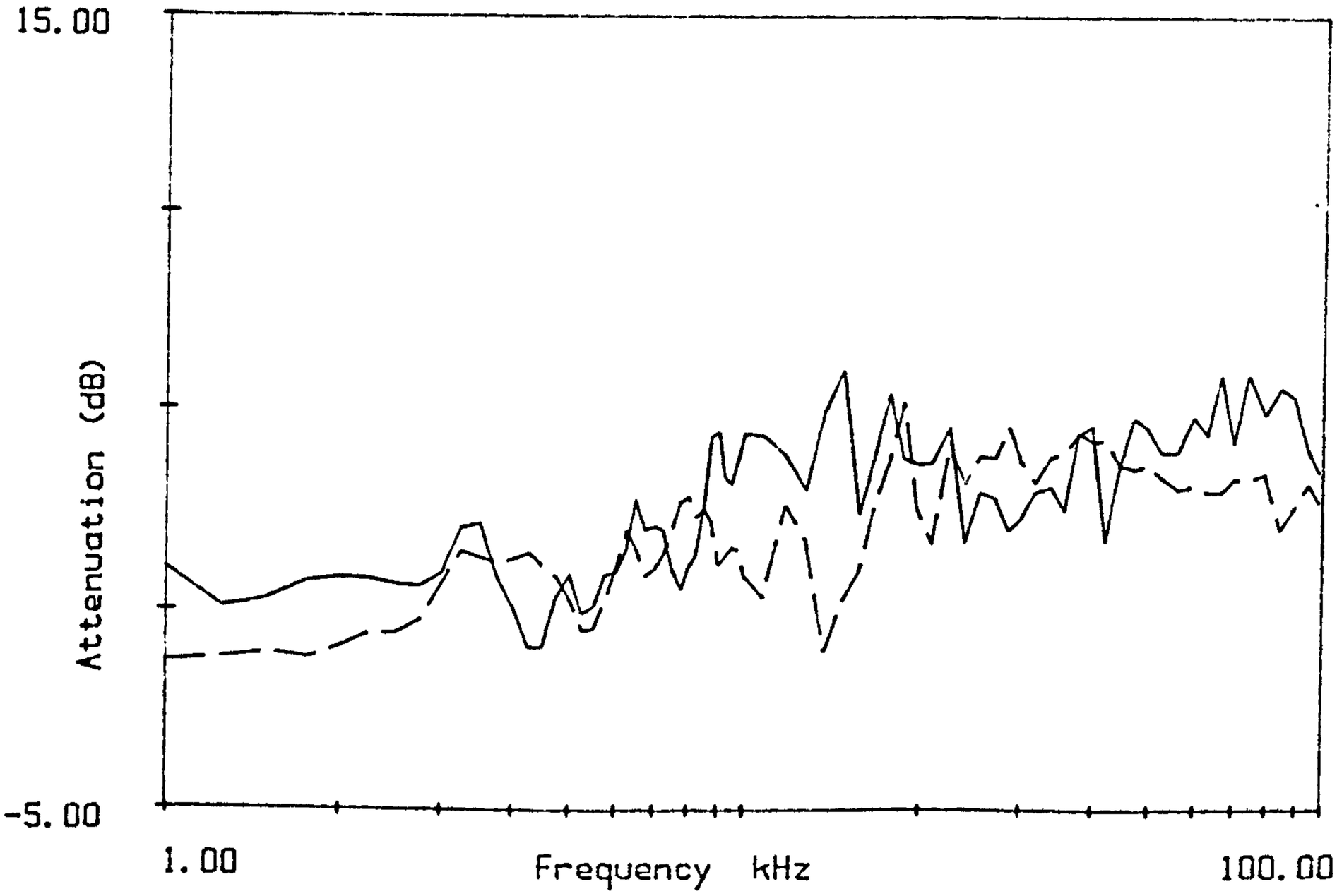

Figure 7.19d
Array D-12 mean Insertion Loss and Attenuation (----).

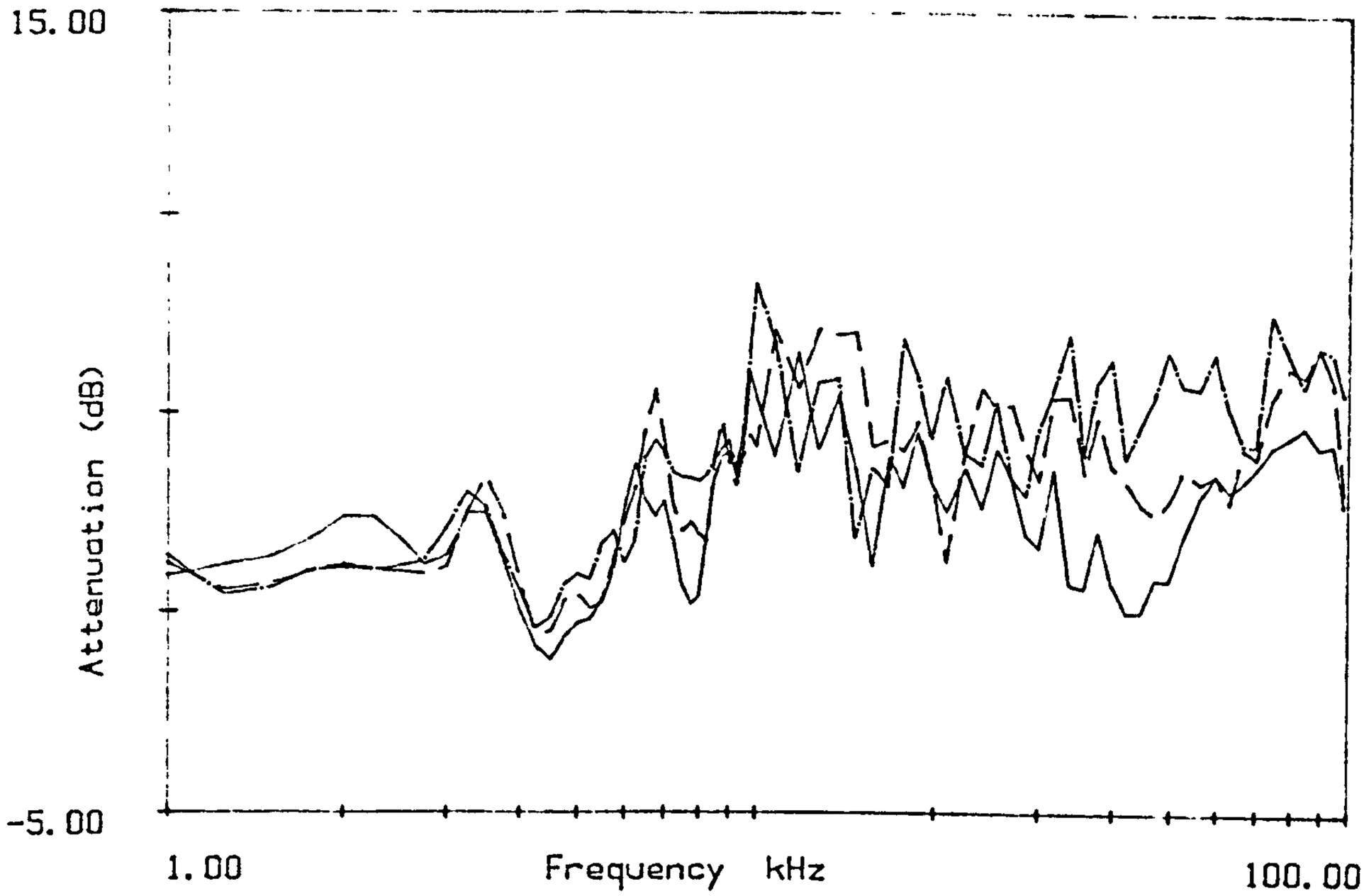

FIGURE 7.20
Mean insertion loss for 6 rows of array C-12
rows used : ——— 1-6 — — — 4-9 —·—·— 7-12.

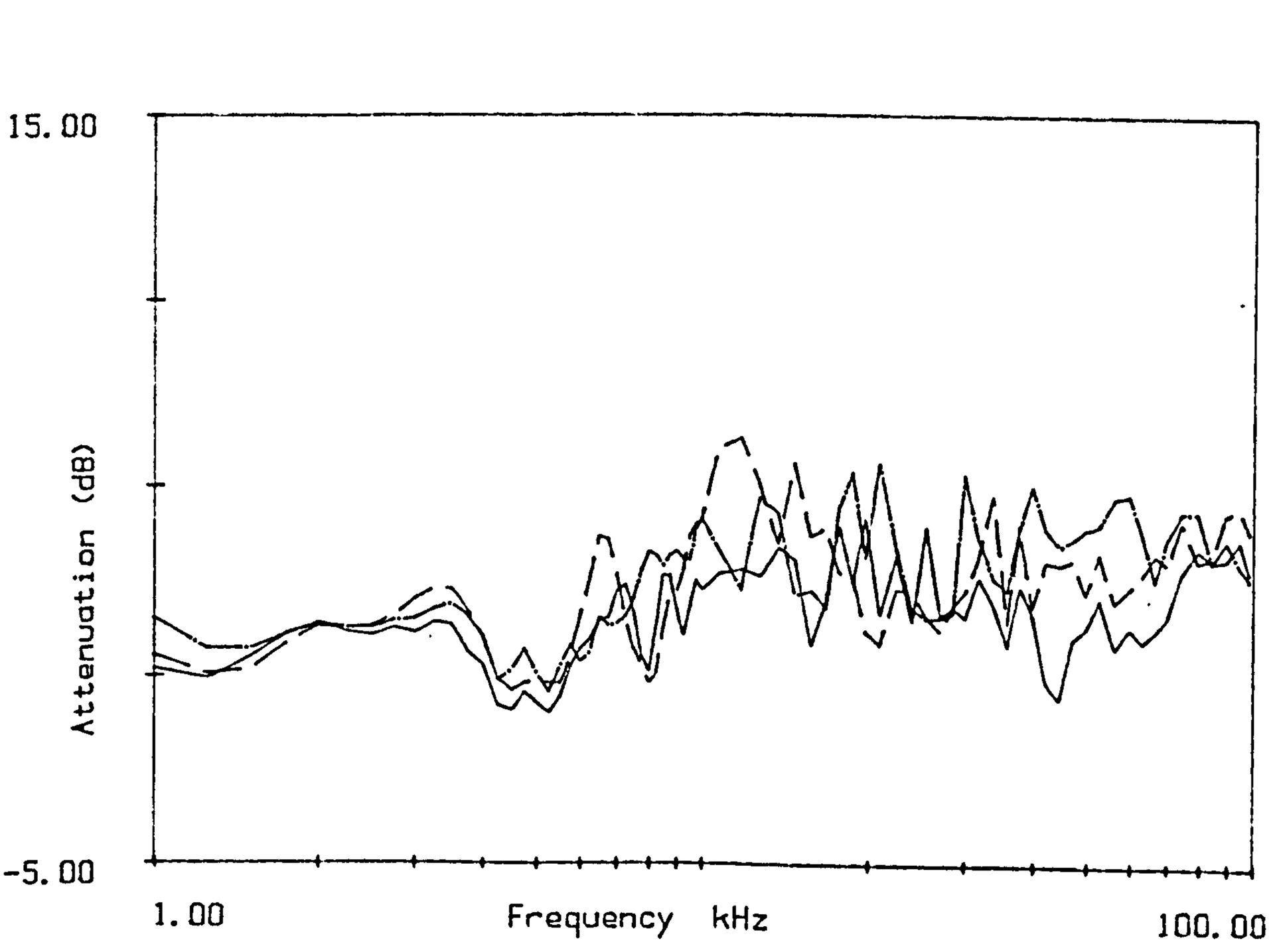

FIGURE 7.20a
Mean insertion loss for 4 rows of array C-12
rows used : ——— 1-4 — — — 5-8 —·—·— 9-12.

Chapter 8 : Comparisons Between Woodlands, and Conclusions.

The results presented in Chapters 6 and 7 show that the scattering and ground predictive models provide a useful means of quantifying and explaining differences within and between different stands and measurements made at different distances. In this, concluding, chapter therefore the results of comparing the models with the various predictions will be used to make such comparisons. The possible applications of the knowledge gained from this study will be discussed and useful further work suggested.

8.1 Ground Effect.

The mean difference between the measured and predicted attenuation spectra for ground effect, have been used extensively in chapter 6 to describe the low frequency attenuation results in terms of one or two variables. A complete set of best fit results from all the measurements presented in chapter 6 are given in appendix C and analysis of these results will be used in this section to draw conclusions concerning the fitting of the ground effect models to the measurements. The mean difference value indicates the 'goodness of fit' as it is a calculation of the mean value of the difference (in decibels) between the measured and predicted spectra at each of the frequencies. Figures 8.1 to 8.8 are examples of comparisons between measured and predicted spectra using best fit parameters giving a range of mean difference values (details in the figure captions). The predictions giving the lowest mean difference value can be seen to give a better fit to the measurement. In all these figures the location of the low frequency peak is well represented by the prediction, particularly the first, major, peak. The location of the smaller 'lobes' of this peak do not coincide in all the graphs (eg. figure 8.3) but are generally only slightly different, this is due to slight differences in the location of the reference microphone, as discussed in section 4.3.

In the more distant of the measurements illustrated here the magnitude of the first peak tends to be overpredicted, the results presented in appendix C do not, however, show any clear relationship between the mean difference or best fit parameters, and distance ie. the result of fitting to a measurement at 96m is as likely to give a particular value of

effective flow resistivity or of mean square as one at 12m. This indicates that effects such as scattering by vegetation or turbulence or the refraction of the sound waves are unlikely to have influenced the low frequency propagation significantly since any of these effects would be expected to have a greater influence at longer distances. This observation also has implications for the deduction of the ground parameters from measurements over the ground. Glaretas (1981) and Attenborough and Hess (1985) have suggested that measurements of propagation over short distances, (3 to 15m) expressed as a level difference between two vertically separated microphones could be used to deduce the acoustic impedance of a ground surface. The results of this study show that a wider range of distances could be employed to give a measurement of the impedance. Measurements made over longer distances would appear to be more relevant in the deduction of ground parameters for predicting long range propagation, as they are likely to give a mean value over the relatively large area of ground reflection. Small scale sampling employed in techniques such as the inclined track and impedance tube methods of measuring impedance are likely to vary somewhat from place to place within an area, so a large number of measurements would be required to gain such an average. The mixed stand at Hazelborough Wood, for example, has two distinct soil types, under the oak and and under the spruce trees, the best fit results do not vary greatly so the results obtained appear to represent a mean value of effective flow resistivity for the stand as a whole.

Figures 8.1 and 8.2 illustrate the degradation of the interference patterns with distance, in the high frequencies. The 12m measurement has a series of small peaks and dips, some of which coincide in location with the predicted pattern, the longer distance measurements, however, do not reflect the peaks and dips of the predicted interference patterns. This indicates that scattering by turbulence and vegetation removes the interference effects, at high frequencies. The fitting procedure was carried out at frequencies from 100Hz to 1kHz in recognition of the fact that observed ground interference effects are a low frequency phenomenon only.

The discrepancy in the magnitude of the first peak in the longer distance measurements cannot be accounted for solely by the ground prediction models used in this study, since the predictions illustrated are the best fit values for all four models, and the best fit values

from all the models give very similar predicted spectra (see figures 8.2 and 8.6) and therefore similar values of mean difference. Fitting the spectrum of figure 8.2 over a more limited frequency range (up to only 400Hz) was carried out to investigate whether this would produce a better fit but this did not give a significantly different result, demonstrating that the low frequency peak is adequately fitted by using the frequency range up to 1kHz despite the fact that the mean difference is affected more by the second part of the low frequency peak (about 400Hz to 1000Hz) than the main peak since there are more points in this region. For example the layered model prediction of figure 8.6 is closer to the measured spectra than the other two predictions in the main low frequency peak, but it gives a higher mean difference value when fitted up to 1kHz.

Since the location of the peak, rather than its magnitude, is altered by altering the input parameters, and the rigid backed layer and variable porosity models tend to increase the height of the peak over that of the homogeneous model at a given location, it seems unlikely that an improved fit could be found, for the data which is over-predicted, using any of these one- and two-parameter approximations. It is possible that more accurate impedance models such as those outlined in chapter 4 would give a better fit to some of the data. The local reaction assumption is generally less valid for surfaces with a low impedance and at grazing incidence, so it is likely that the local reaction inherent in the propagation model is not appropriate at longer distances over the soft surface of the woodland floors. The propagation model used has not been rigorously tested for soft surfaces such as woodland floors since most studies of outdoor ground propagation in which the model has been used have been concerned with grassland or harder surfaces.

Figures 8.9 and 8.10 are the result of using the extended reaction assumption (as implemented by subroutine EXTEND in Appendix A) for the prediction of attenuation over a ground surface, compared with the measurements illustrated in figures 8.2 and 8.4, and the best fit local reaction prediction for the Delany and Bazley model. The best fit flow resistivity for the extended reaction is considerably lower than that for the local reaction. It is evident that the extended reaction gives a considerably better fit to the measurement of figure 8.9 by reducing the magnitude of the low frequency peak. The local reaction prediction of figure 8.10 also overpredicts the attenuation but the extended reaction underpredicts

the attenuation of the low frequency peak. It is possible, therefore, that the extended reaction assumption may give an improved prediction of the impedance of woodland soils, in some cases.

The best fit results such as those illustrated in figures 8.1 to 8.8 are simply individual results for single measurements. The most common value obtained in a set of measurements, or the mean value could give an appropriate overall description the woodland soil in terms of the ground parameters. The mean value and scatter about the mean are used in analysis in this chapter, and chapter 6, because most sets of results from a single day have a relatively small scatter about the mean, so the mean values are generally not very different to the individual results, also an effective statistical test (T-test) can be used to compare mean values.

Table 8.1 shows the results of pairwise t-test comparisons between the mean best-fit ground parameters of measurements of each of the days described in detail in chapter 6. It is evident that if all the values for all the days from each wood are compared there is no significant difference between the means. The overall mean values of effective flow resistivity from each wood, for the homogeneous approximation, are all between 63,000 and 69,000 mks rayls and for the Delany and Bazley Model between 37,000 and 44,000 mks rayls. There are, however, significant differences between certain of the sets of data. All the reported mean values for the Delany and Bazley model in table 8.1 are between 20,000 and 68,000 mks rayls, this is within the range of previously published results as quoted in table 2.2.

The results from Hazelborough wood were shown in Chapter 6.2 to separate into two groups, with different ground parameters, these are thought to represent 'wet' and 'dry' ground conditions. As indicated in table 8.1 the means from both of these groups were significantly different (at the 0.1% level) from the mean values at the other two sites. The mean for the dry days being significantly lower and the wet days significantly higher, than those of the other two woods. This result is also shown in the levels of significance for the individual days. Most of the days' data from Hazelborough Wood is statistically

Table 8.1: T-test comparisons between best fit values of effective flow resistivity from all the experimental days.

The percentage levels of significance of the difference between the two means, are given for the best fit parameters to the homogeneous approximation and where the level of significance is different for the Delany and Bazley model a footnote is made to this effect. NS indicates that the means are not significantly different at the 5% level. The mean values are given in column 2, that for the homogeneous approximation above that for the Delany and Bazley model.

		Hazelborough								Wetleys				Bucknell		
Date	mean σ_e	10/8	10/4	5/7	9/8	20/6	dry	wet	all	28/7	26/6	16/5	all	9/7	8/8	all
Hazelborough Wood Data																
10/8/83	39500 23833	×	0.1	NS	NS	0.1	NS	0.1	NS	NS	0.1	5@	1@	1	5†	1
10/4/84	118833 67667		×	0.1	0.1	NS	0.1	NS	1	0.1	0.1†	0.1	0.1	1	0.1	0.1
5/7/84	32000 20000			×	NS	0.1	NS	0.1	5	NS‡	0.1	0.1	0.1	0.1	0.1	0.1
9/8/84*	30000 20000				×	0.1	NS	0.1	NS	NS	0.1	1@	0.1	0.1	1@	0.1
20/6/85	108571 62857					×	0.1	NS	1	0.1	0.1‡	1@	0.1	1	0.1	0.1
dry days	33500 21045						×	0.1	1	NS‡	0.1	0.1	0.1	0.1	0.1	0.1
wet days	113308 65077							×	0.1	0.1	0.1†	0.1	0.1	0.1	0.1	0.1
All days	63143 37500								×	NS	NS‡	NS	NS	NS	NS	NS
Wetleys Wood Data																
28/7/83	38125 26125									×	0.1	1@	1@	1	5	1
26/6/84	83467 52733										×	5†	5	NS‡	5@	5@
16/5/85	68000 44000											×	NS	NS	NS	NS
All days	68303 43636												×	NS	NS	NS
Bucknell Wood Data																
9/7/84	73750 41250													×	NS	NS
8/8/84	64545 36364														×	NS
All days	67895 39474															×

Footnotes:

* for the Delany and Bazley model all the values of σ_e are 20000 ie. there is no deviation from the mean.

‡ Delany and Bazley result is 5%

† Delany and Bazley result is 1%

@ Delany and Bazley result is 0.1%

significantly different from most of the days from other woods; the main exception being the values from Wetleys Wood on 28/7/83. The values from 28/7/83 are similar to the values obtained on each of the dry days (10/8/83, 5/7/84 and 9/8/84). This is the measurement of 'undisturbed' mature forest floor made during the same dry spell as those of 10/8/83. This result suggests that there is, in fact, little difference in the acoustic properties of the two soils in the same, undisturbed, dry condition. The other two measurements from Wetleys Wood have a higher value than the dry measurements but a significantly lower value than the wet measurements at Hazelborough Wood. As discussed in chapter 6.3, the difference between days at Wetleys Wood is probably due to the disturbance of the soil by logging operations and also to moisture content.

The values of mean difference given in the summary tables in chapter 6 are generally higher in the measurements from Bucknell Wood than the other two woodlands. Taking the mean values of all the values of mean difference from these tables the overall mean difference (homogeneous model) for Hazelborough Wood is 3.11, for Wetleys Wood 3.20, and for Bucknell Wood this value is 5.19. There does, however, appear to be some difference between the results from the two measuring tracks. From appendix C3 the mean of the mean difference value is 6.51 for track G but only 4.21 for track F. Figures 8.7 and 8.8 show typical examples of the difference between the measured and predicted attenuation for this stand. In the low frequency part (400Hz to 1000Hz) of figures 8.7 and 8.8 the predictions are consistently lower than the measured spectra, especially for the measurement at G40, this is due to the trees absorbing or scattering sound within this frequency range. This stand is alone, among those measured, in having the ground-fitting, up to 1kHz, significantly corrupted by the presence of the trees. The fitting routine does, however give a best fit value which predicts a peak in attenuation at the same frequency as the measurement, this indicates that the best fit value is appropriate for the ground surface even with a high value of mean difference. The magnitude of the difference betwen the measurement and prediction generally increases with frequency. The discussion, in chapter 6, of the results of attenuation from Bucknell Wood indicated that the dense belts of Red Cedar caused considerable attenuation, this being greater in track G in which the sound passed through a greater distance of this type of material than track F, this is reflected even in the low frequency part of the measurements.

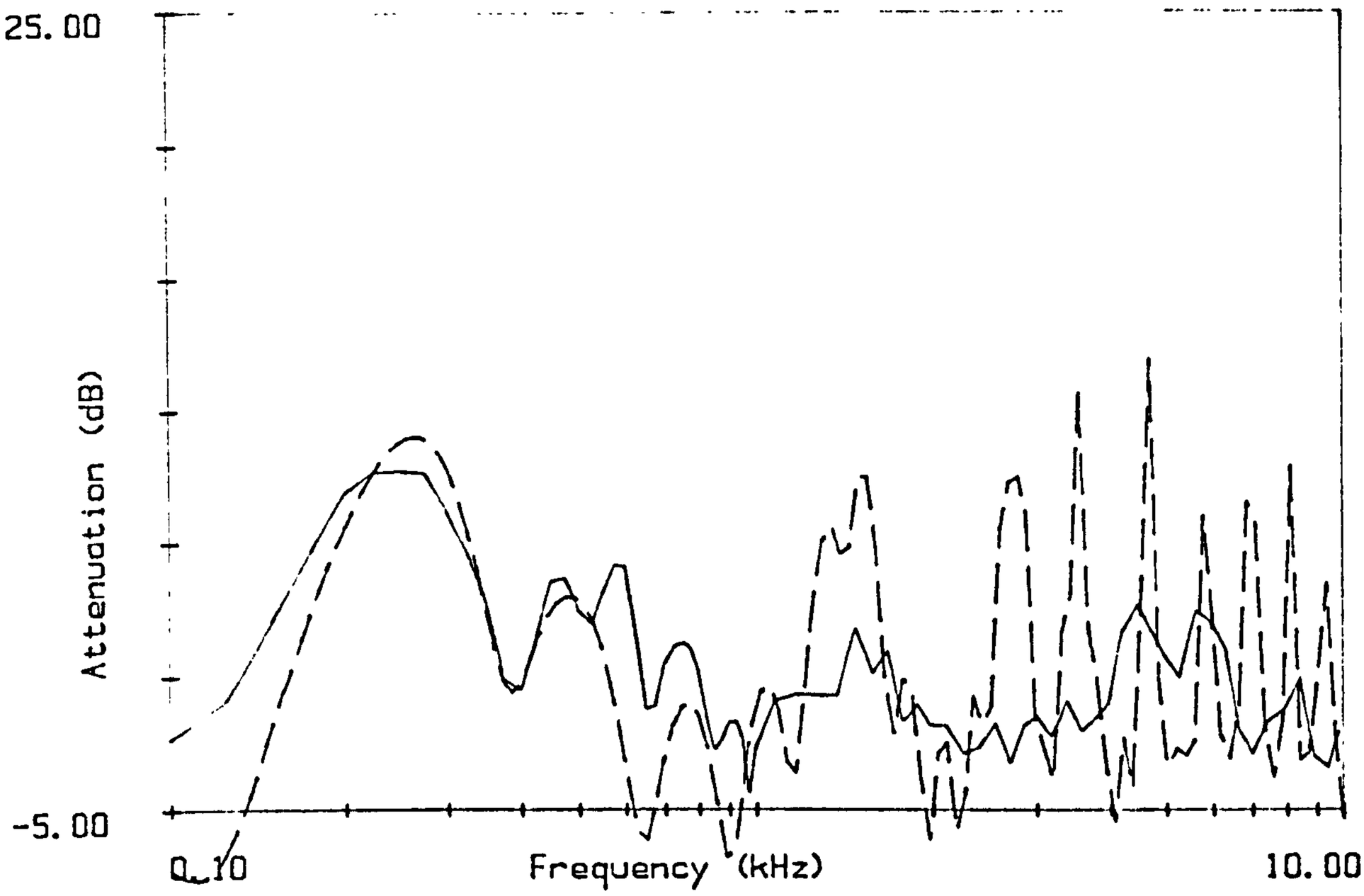

Figure 8.1
Measured attenuation from Wetleys Wood 28/7/83;
Separation distance 12m A track. 1.2m microphone height.
with best fit prediction for Rigid-backed Layer model
σe = 60.000 mks rayls, de = 0.085 mean difference = 3.13 dB.

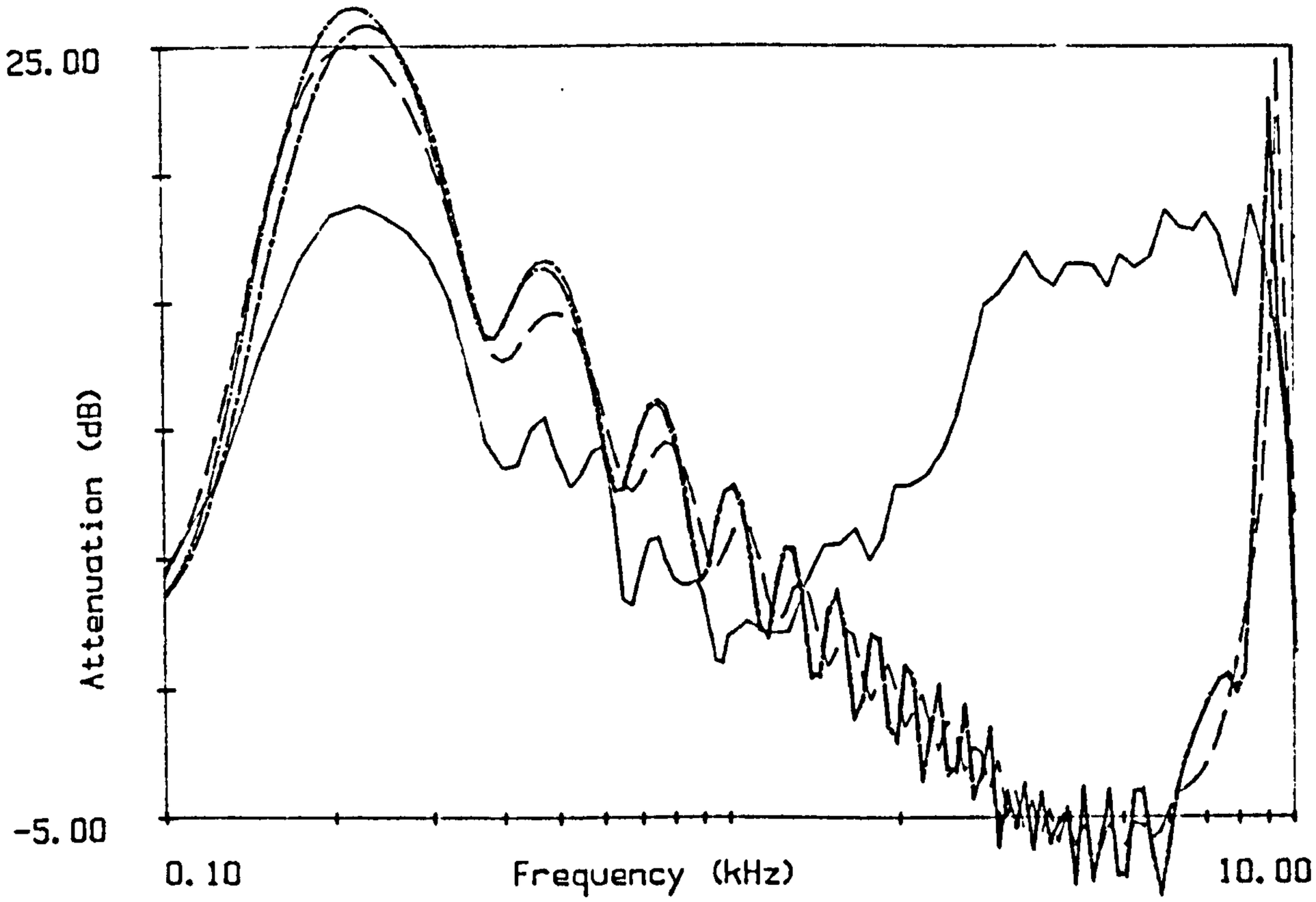

Figure 8.2
Measured attenuation from Wetleys Wood 28/7/83:
Separation distance 96m, A track, 1.2m microphone height.
with best fit predictions:
— — · Delany and Bazley σe = 22.000 mks rayls, md = 3.99 dB.
——·—·— Homogeneous σe = 33.000 mks rayls, md = 4.82 dB.
——··—·— Layer de = 0.135, σe = 40.000 mks rayls, md = 4.82 dB.

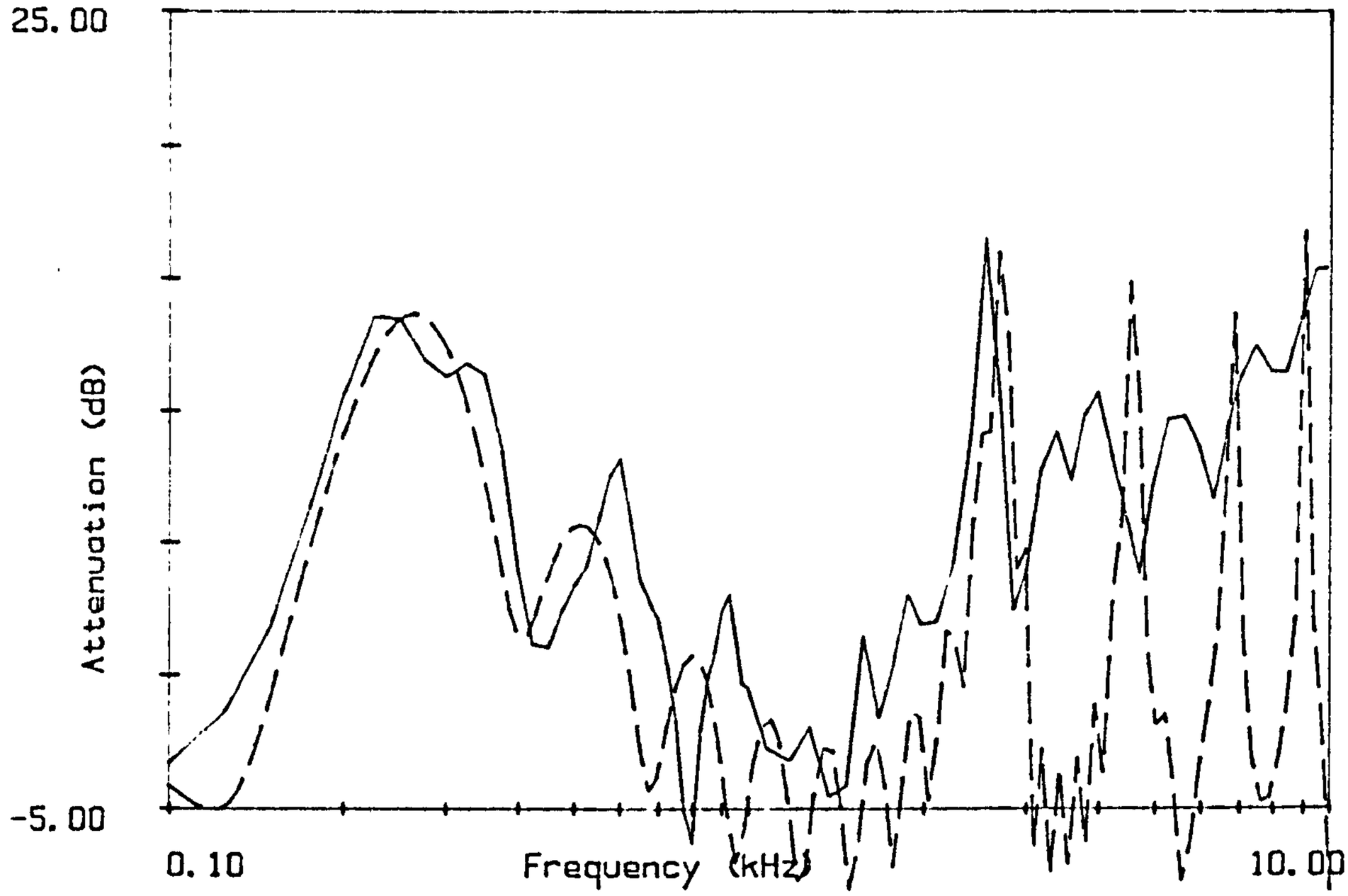

Figure 8.3
Measured attenuation from Wetleys Wood 26/6/84;
Separation distance 48m B track. 2.5m microphone height.
with best fit prediction for Homogeneous approximation
σe = 82.000 mks rayls. mean difference = 4.19 dB.

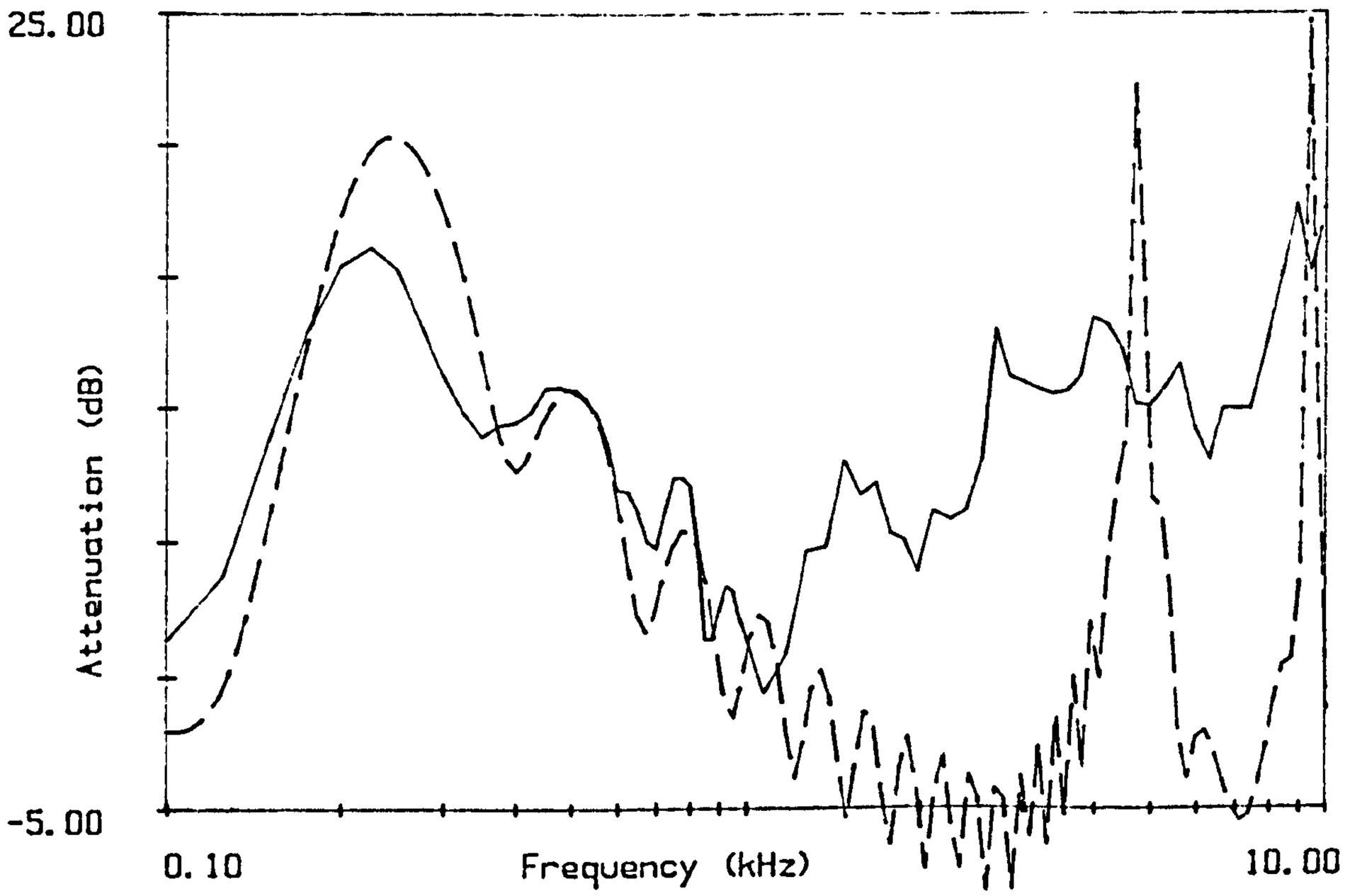

Figure 8.4
Measured attenuation from Hazelborough Wood 9/8/84;
Separation distance 48m. H track. 1.2m microphone height.
with best fit prediction for Homogeneous approximation.
σe = 40.000 mks rayls. mean difference = 2.69 dB.

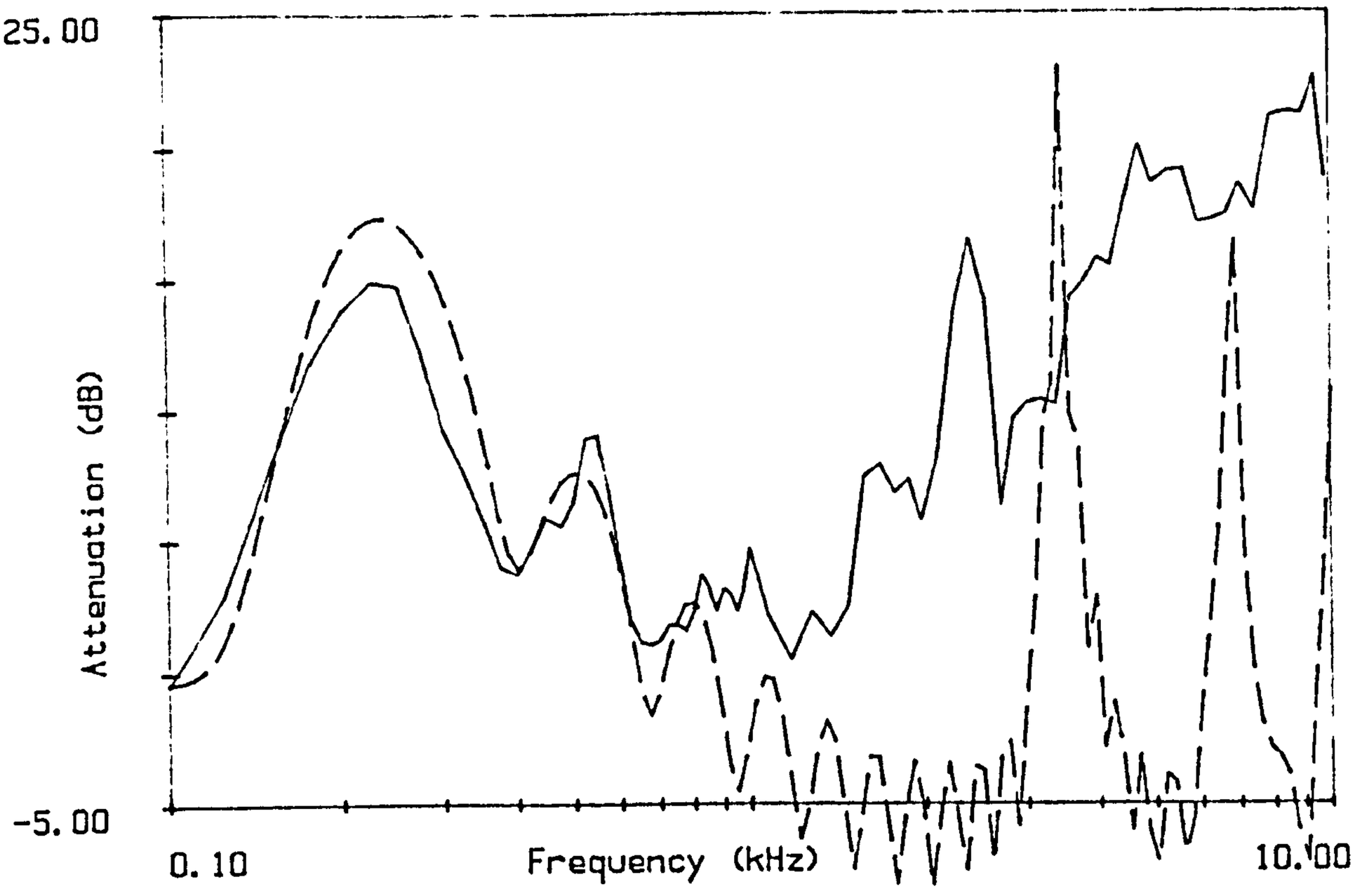

Figure 8.5
Measured attenuation from Hazelborough Wood 5/7/84;
Separation distance 72m, C track, 2.5m microphone height,
with best fit prediction for Homogeneous approximation.
σ e = 50,000 mks rayls, mean difference = 3.08 dB.

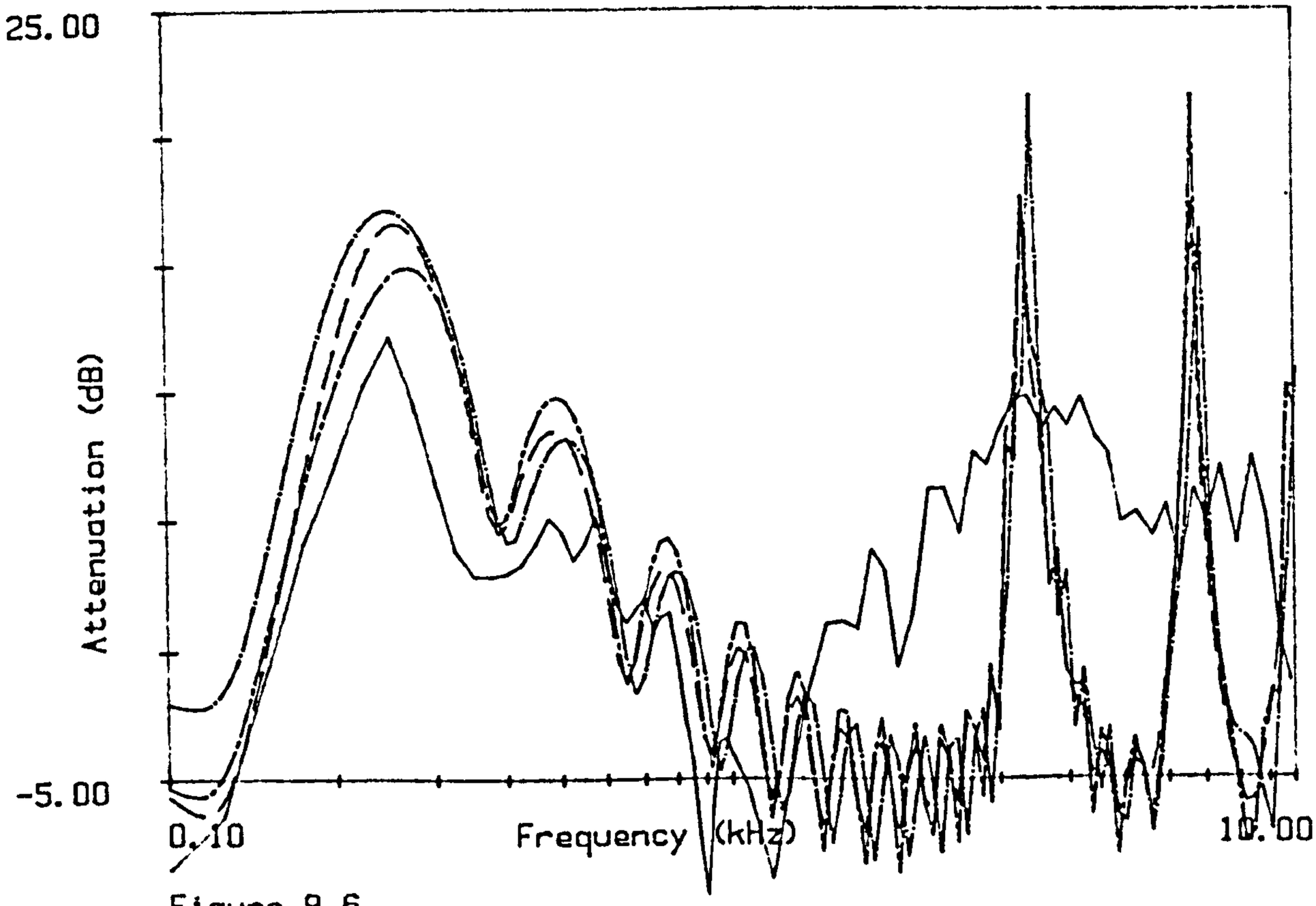

Figure 8.6
Measured attenuation from Hazelborough Wood 10/4/84:
Separation distance 72m, C track, 2.5m microphone height,
with best fit predictions:
— — · Delany and Bazley σ e = 62,000 mks rayls, md = 3.99 dB.
———— Homogeneous σ e = 113,000 mks rayls, md = 3.84 dB.
———— Layer de = 0.060, σ e = 130,000 mks rayls, md = 4.82 dB.

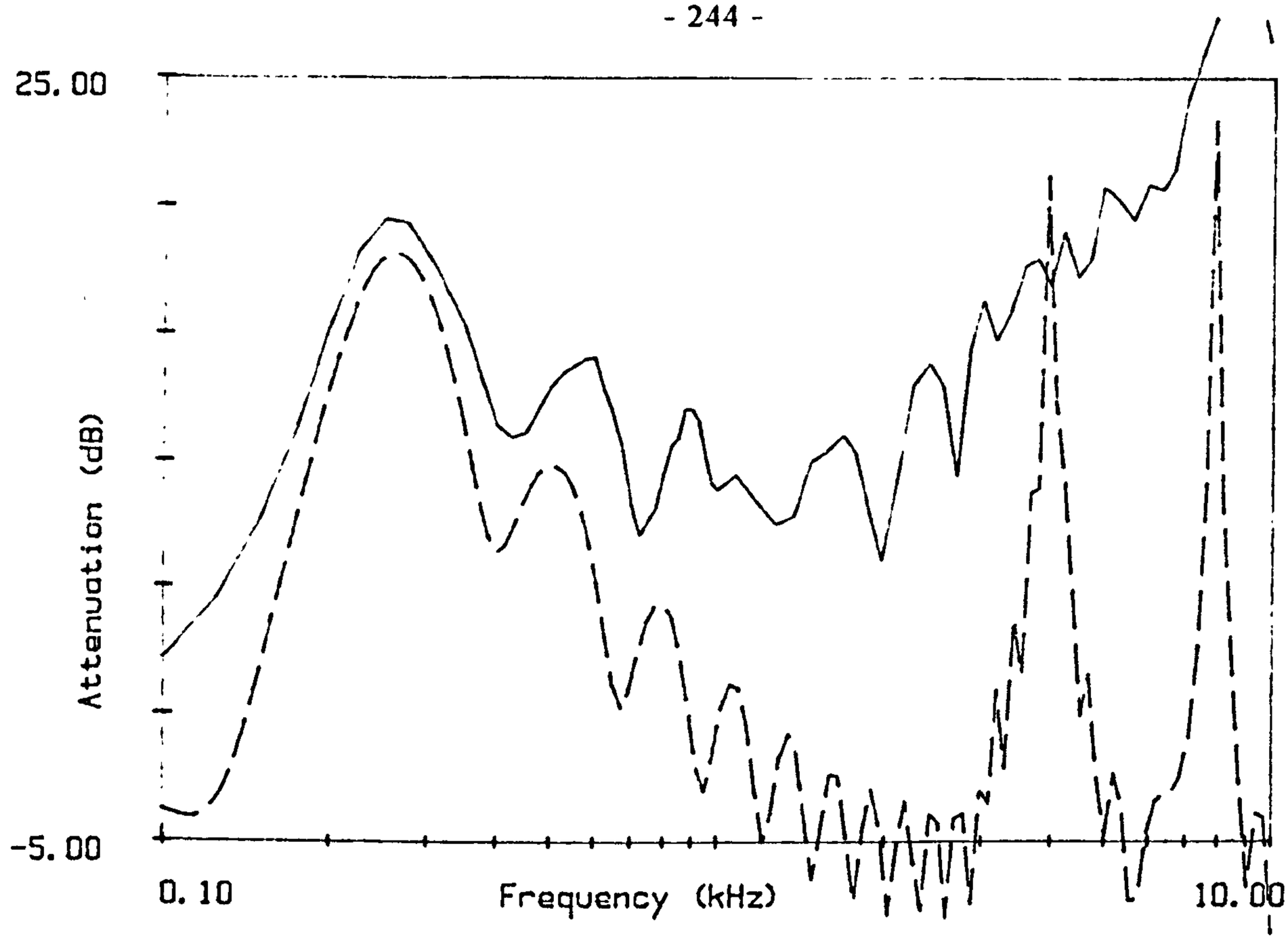

Figure 8.7
Measured attenuation from Bucknell Wood 9/7/84:
Separation distance 40m G track. 1.2m microphone height.
with best fit prediction for Homogeneous approximation.
σ e = 50.000 mks rayls. mean difference = 6.95 dB.

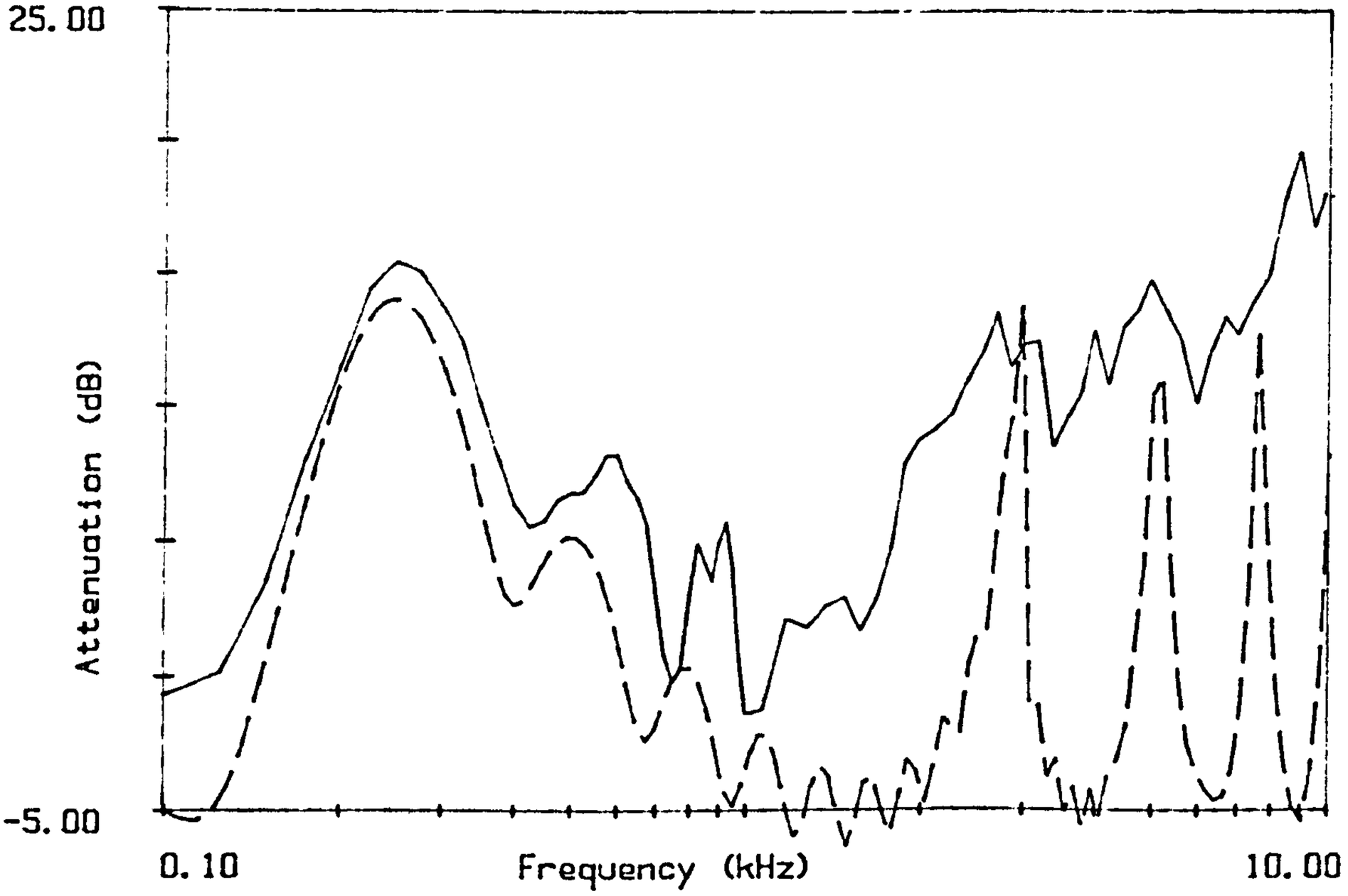

Figure 8.8
Measured attenuation from Bucknell Wood 8/8/84:
Separation distance 26m F track. 1.2m microphone height.
with best fit prediction for Delany and Bazley model
σ e = 30.000 mks rayls. mean difference = 4.64 dB.

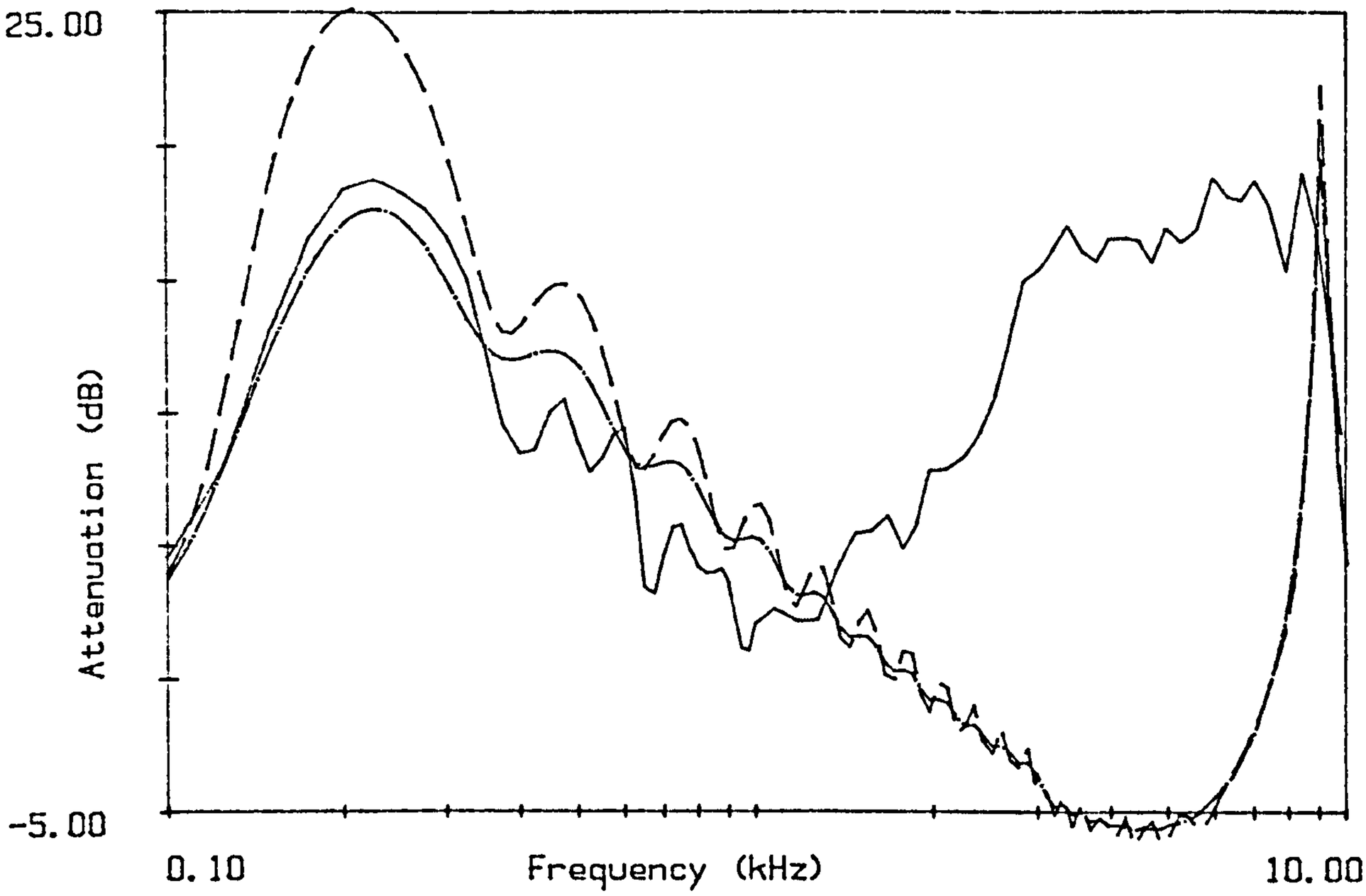

Figure 8.9
Measured attenuation from Wetleys Wood 28/7/83;
Separation distance 96m, A track, 1.2m microphone height.
— — Delany and Bazley σe = 22.000 mks rayls, Local reaction.
—— Delany and Bazley σe = 6.000 mks rayls, Extended reaction.

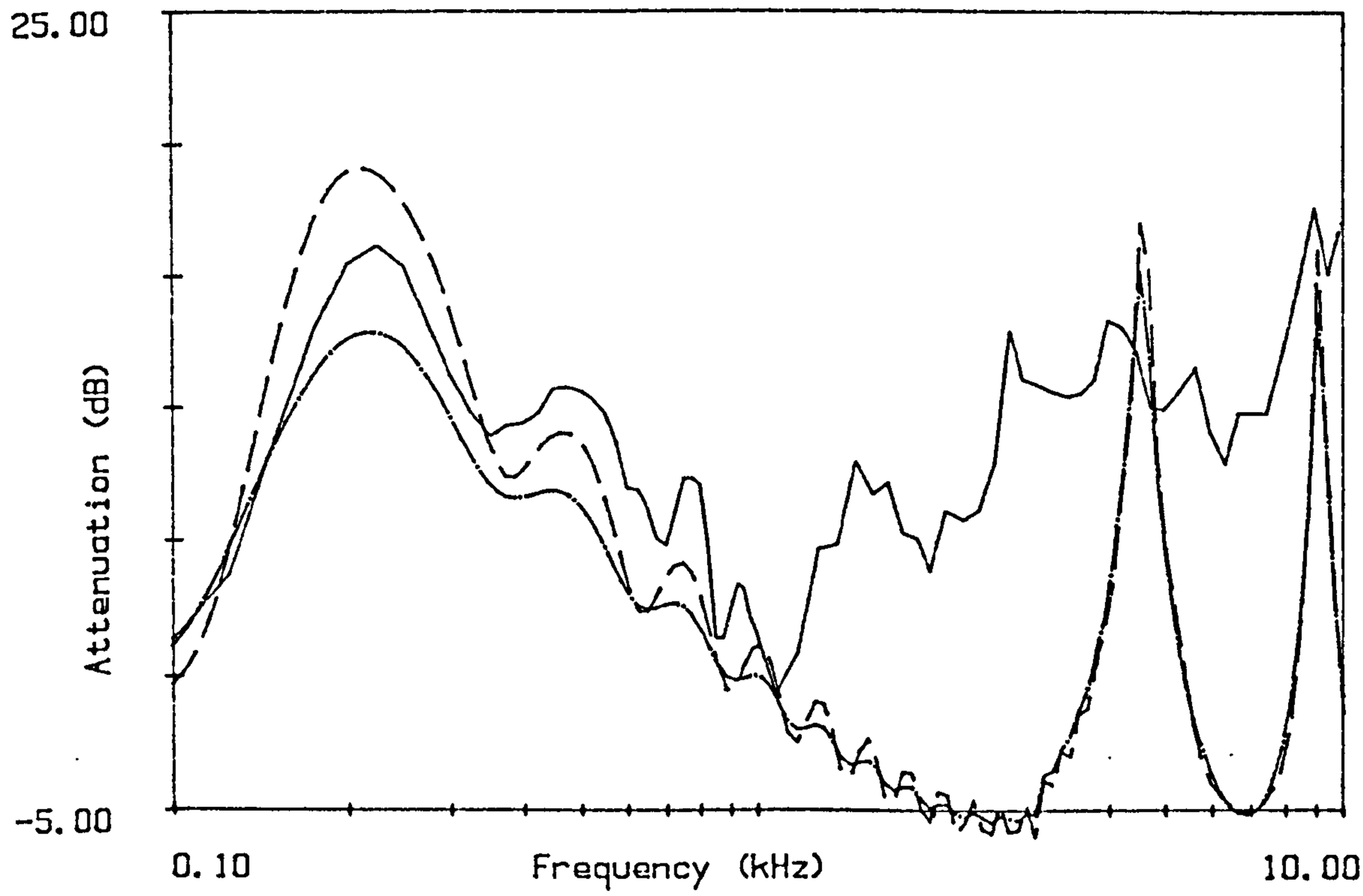

Figure 8.10
Measured attenuation from Hazelborough Wood 9/8/84;
Separation distance 48m, H track, 1.2m microphone height.
— — Delany and Bazley σe = 20.000 mks rayls, Local reaction.
—— Delany and Bazley σe = 6.000 mks rayls, Extended Reaction.

8.2 High Frequency Attenuation.

Various models were introduced in chapters 2 and 5 which have been suggested as appropriate formulae for predicting attenuation through woodland. It is evident from the above discussions that these are only required for prediction in the high frequency part of the attenuation measurements presented in chapter 6. The mean high frequency attenuation of the various woodlands, in terms of dB per 24m, will therefore be used in comparison with these models. (the summer measurement for Hazelborough Wood excludes the data from 10/8/83 since this is rather different from the other summer measurements) these attenuation spectra are illustrated in figure 8.11. It is evident that the high frequency attenuation is considerably greater in Bucknell Wood than the other two woodlands with the result from Wetleys Wood being between the winter and summer measurements of Hazelborough Wood.

The paper by Aylor (1972) proposes two models to account for the attenuation of sound by foliage. The first is also described by Yamada et al (1977) and gives an attenuation which is proportional to the square root of frequency; while in the second the attenuation increases by 6dB per doubling of frequency ie attenuation is proportional to 20 $\log_{10}(f)$. Aylor states that the measured data has the frequency dependence of the latter, and therefore that this is the more appropriate. Figures 8.12 to 8.14 show that this frequency dependence is only shown in part of the frequency range of one of the woodlands studied, ie that at Bucknell Wood. Aylor proposes a model for attenuation by a single thin wall of surface area density S (equation 2.7) which can be written as:

$$A_e = 20 \log_{10}(f) - 20 \log_{10}\left|\frac{41.5}{\pi S}\right| \qquad (8.1)$$

Thus, from figure 8.12, S for 24m of the transmission path at Bucknell Wood is 0.015; the corresponding value of S for 100ft (to compare with Aylor's measurements) is 0.019; this is approximately one-third of that suggested by Aylor to give the correct value of attenuation at 100Hz for a cornfield. Therefore, using S as a measure of 'foliage density', this stand could be considered as one-third of the density of a corn field. It is uncertain how this relates to the physical parameters of the vegetation. Since the other woodlands do not have

the correct frequency dependence for this model it is not particularly useful in predicting the attenuation of woodland in general.

The model proposed by Aylor and Yamada et al gives an attenuation which is proportional to the square-root of frequency (equation 2.6) thus:

$$A_e = 2.16A\left[\frac{\pi\nu f}{\rho c^2}\right]^{1/2} FL \qquad (8.2)$$

where

f = frequency

A = a constant describing the dimensions and shape of the leaf,

ν = the viscosity of air (0.018 kg m^{-1} s^{-1})

ρ = the density of air (1.2 kg m^{-3})

c = the speed of sound in air (343 ms^{-1})

L = the distance through the woodland m

F = the average leaf area density m^{-1}

A value of A = 2.2 gives Aylor's version of this model, which is described for corn leaves. Since the leaves in the woodlands are very different to corn leaves it seems appropriate to use the parameter FA to describe a woodland for this model. Thus, using the air parameters given in brackets above, equation 8.2 for 24m propagation path (L) reduces to

$$A_e = 0.0328\ FA\ \sqrt{f} \qquad (8.3)$$

Figures 8.15 to 8.17 show that the measured data does show a similar frequency dependence to this model. Table 8.2 gives the equivalent values of FA from these figures.

This gives a single parameter by which the attenuation from different stands can be compared, for example, it shows that on average, the attenuation in the summer at Hazelborough Wood is 3.2 times that in the winter so that three-quarters of the observed summer attenuation can be attributed to the foliage. The young, dense coniferous stand at Bucknell Wood is shown to be twice as effective in attenuating high frequency sound as the hawthorn

Table 8.2. Approximate values of FA.

Stand	value of X where $A_e = X\sqrt{f}$	FA
Bucknell Wood	0.17	5.18
Wetleys Wood	0.05	1.52
Hazelborough Wood (summer)	0.08	2.44
Hazelborough Wood (winter)	0.025	0.76

brush and oak and spruce trees at Hazelborough Wood in summer and nearly 3.5 times as effective as the older, 'hollower' coniferous stand at Wetleys Wood. This model is, however, defined as being for the foliage effect and does not account for attenuation caused by the trunks and branches. The scattering model described by Embleton (1966) as discussed in detail in chapter 5 and assessed in the model experiments of chapter 7 will be compared with the measured data in the following section.

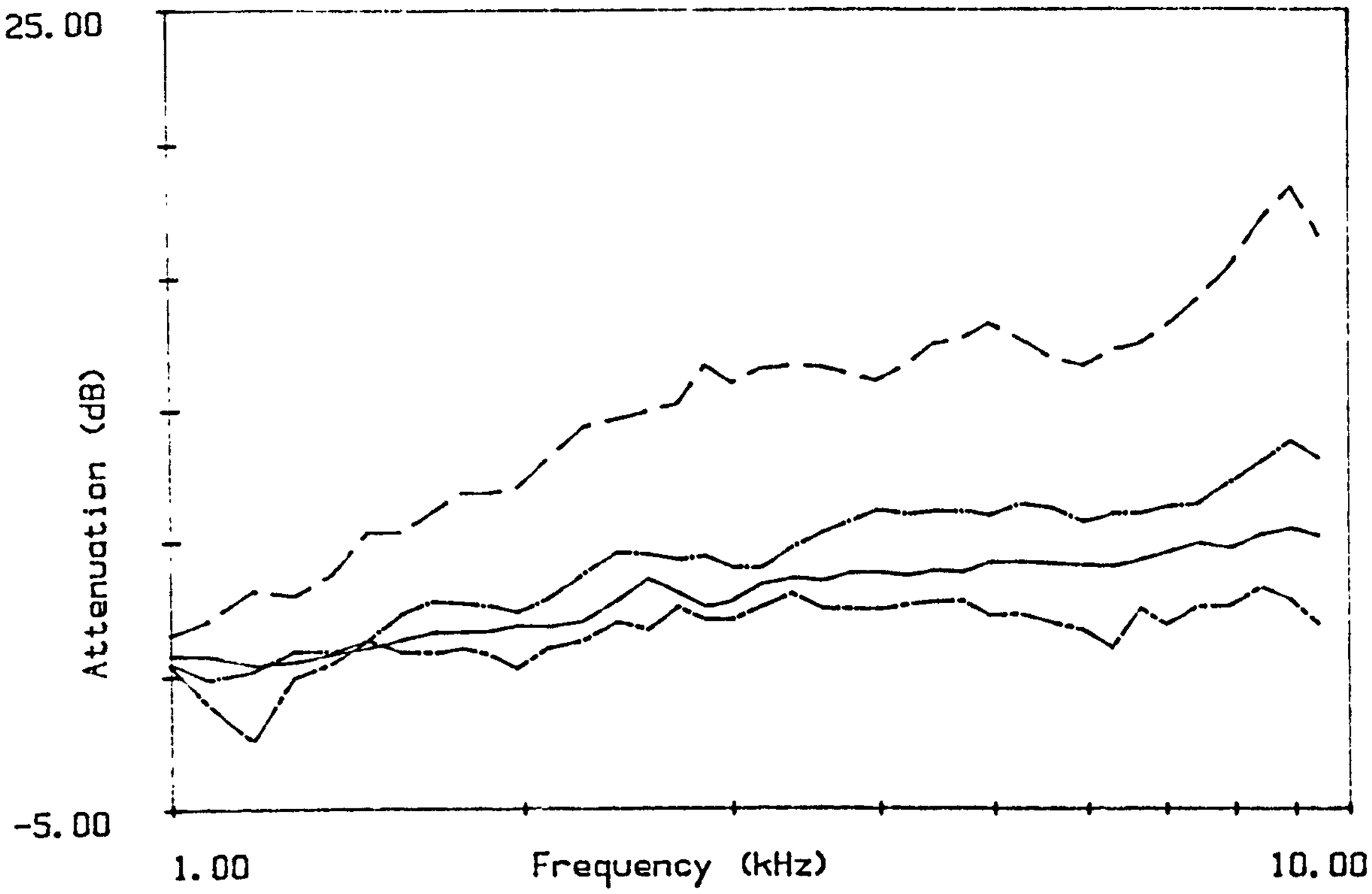

Figure 8.11
Mean measured attenuation (dB per 24m) for the three woodlands.
——— Wetleys Wood
— — · Bucknell Wood
—·—·— Hazelborough Wood summer measurements (excluding 10/8/83)
—·—·— Hazelborough Wood winter measurements

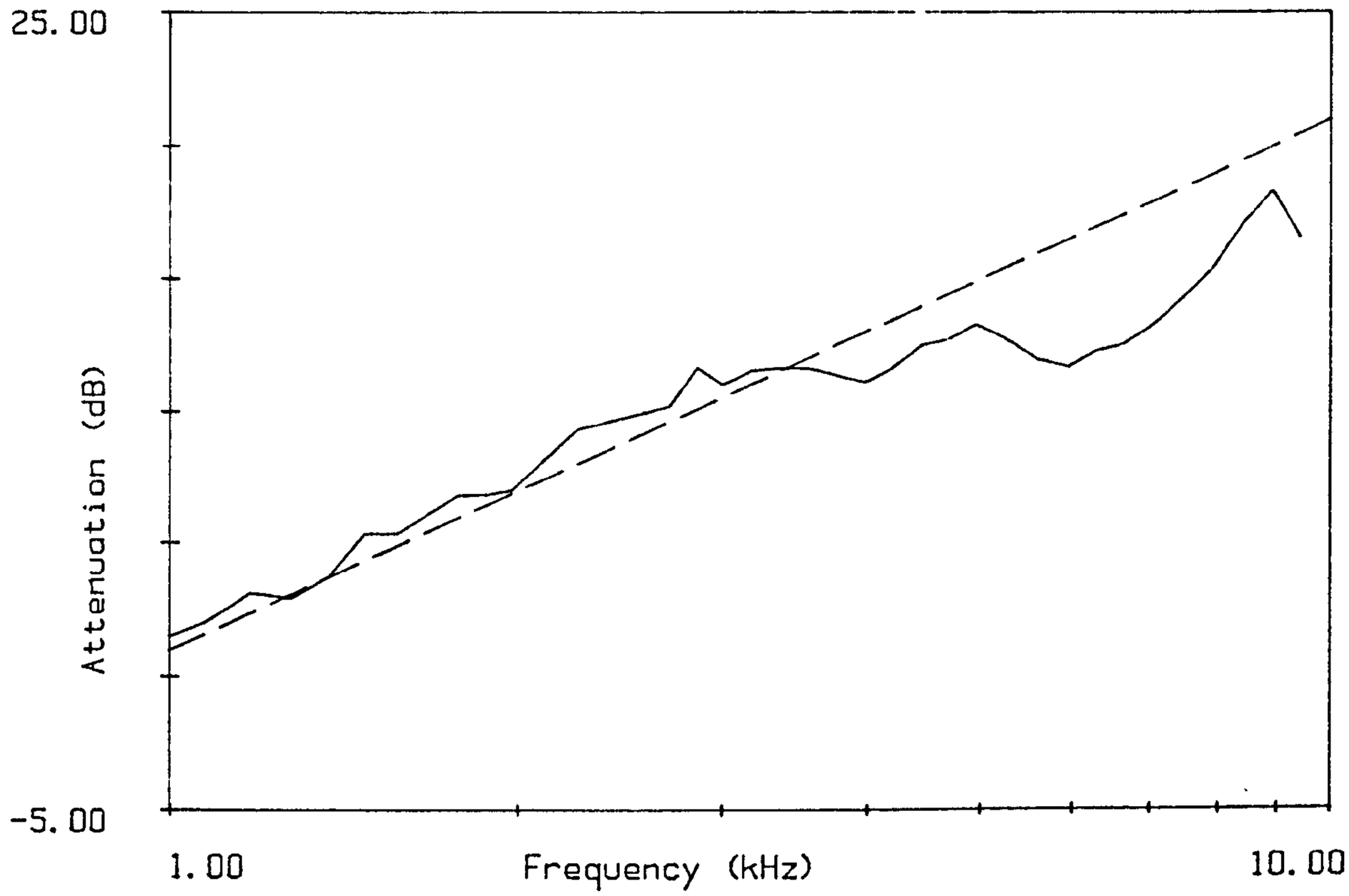

Figure 8.12
Mean measured attenuation (dB per 24m) for Bucknell Wood.
---- is 20*log(frequency)-59.0.

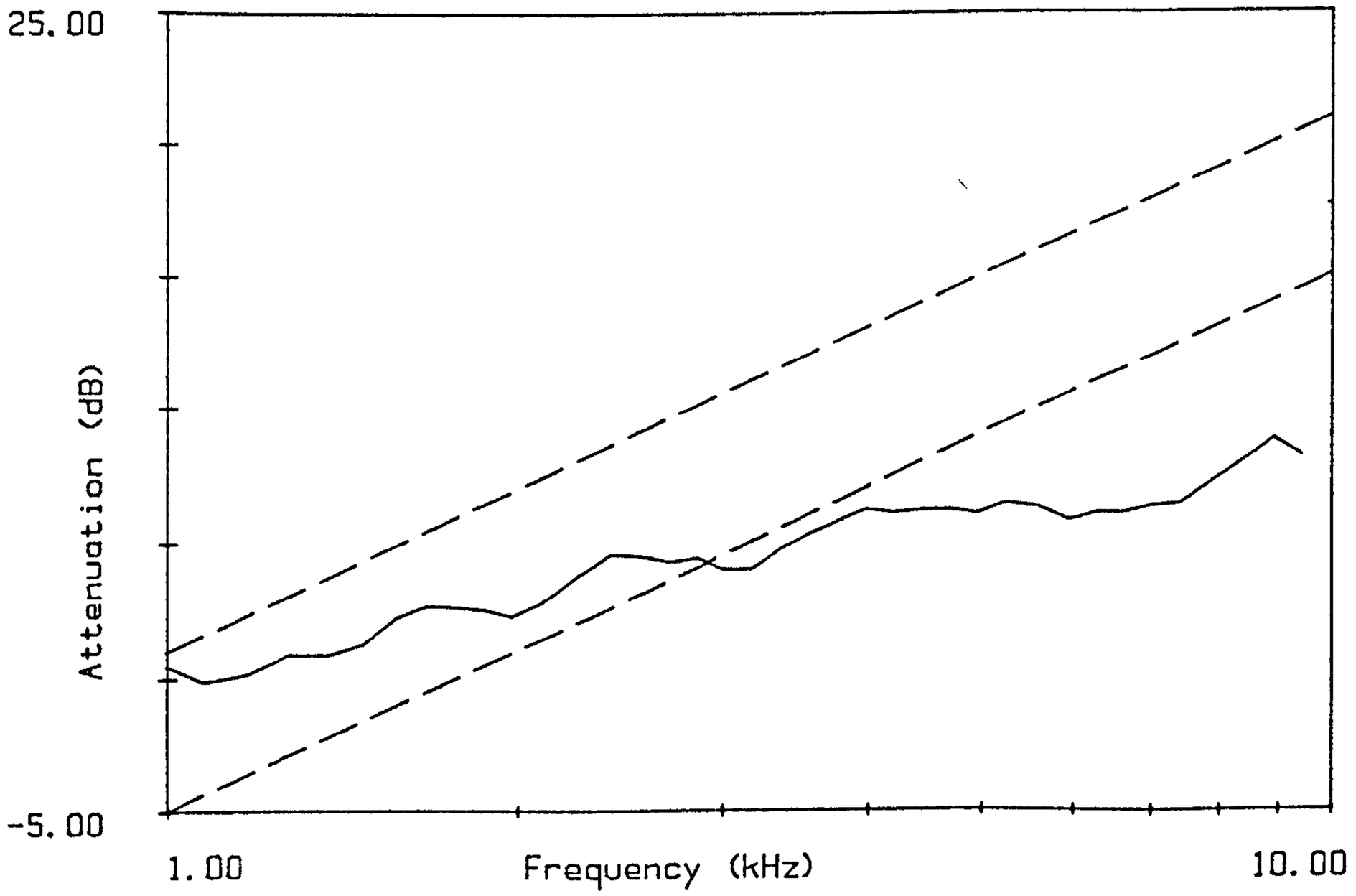

Figure 8.13
Mean measured attenuation (dB per 24m) for Hazelborough Wood.
(all summer measurements except 10/8/83)
---- are 20*log(frequency)-59.0 and 20*log(frequency)-65.0.

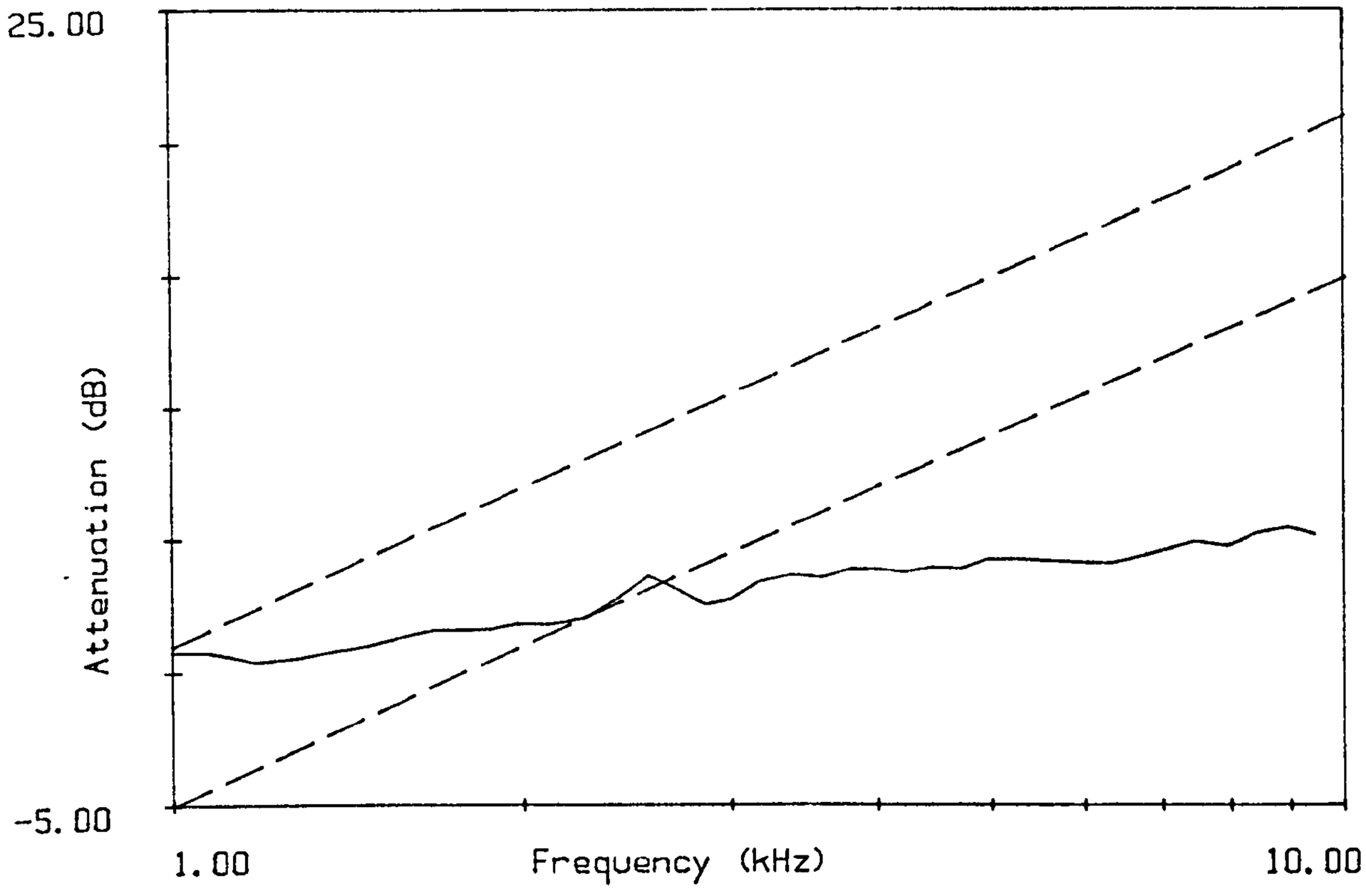

Figure 8.14
Mean measured attenuation (dB per 24m) for Wetleys Wood.
---- are 20*log(frequency)-59.0 and 20*log(frequency)-65.0.

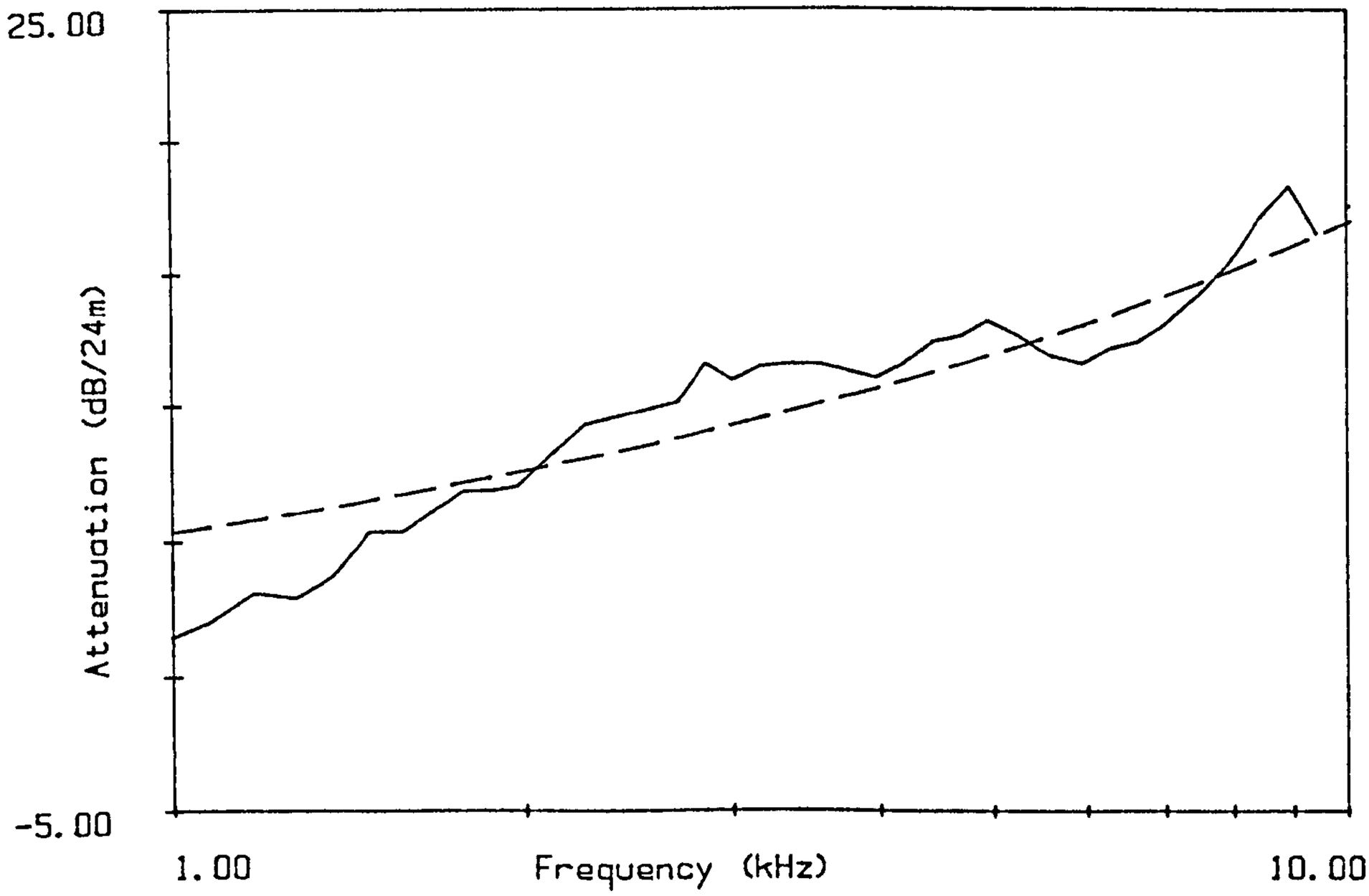

Figure 8.15
Mean measured attenuation (dB per 24m) for Bucknell Wood.
---- is sqrt(frequency)*0.17

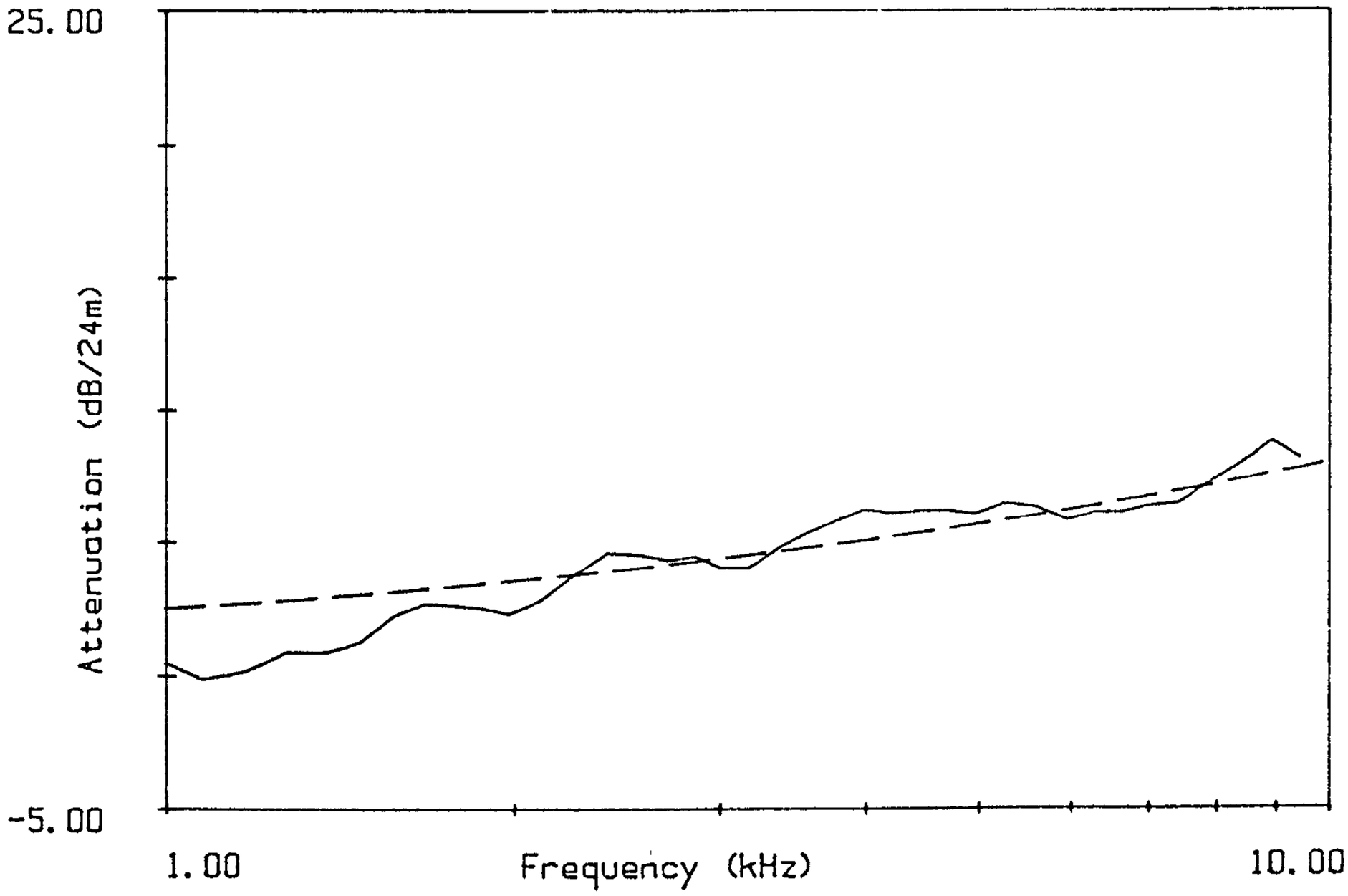

Figure 8.16
Mean measured attenuation (dB per 24m) for Hazelborough Wood.
(all summer measurements except 10/8/83)
---- is sqrt(frequency)*0.08

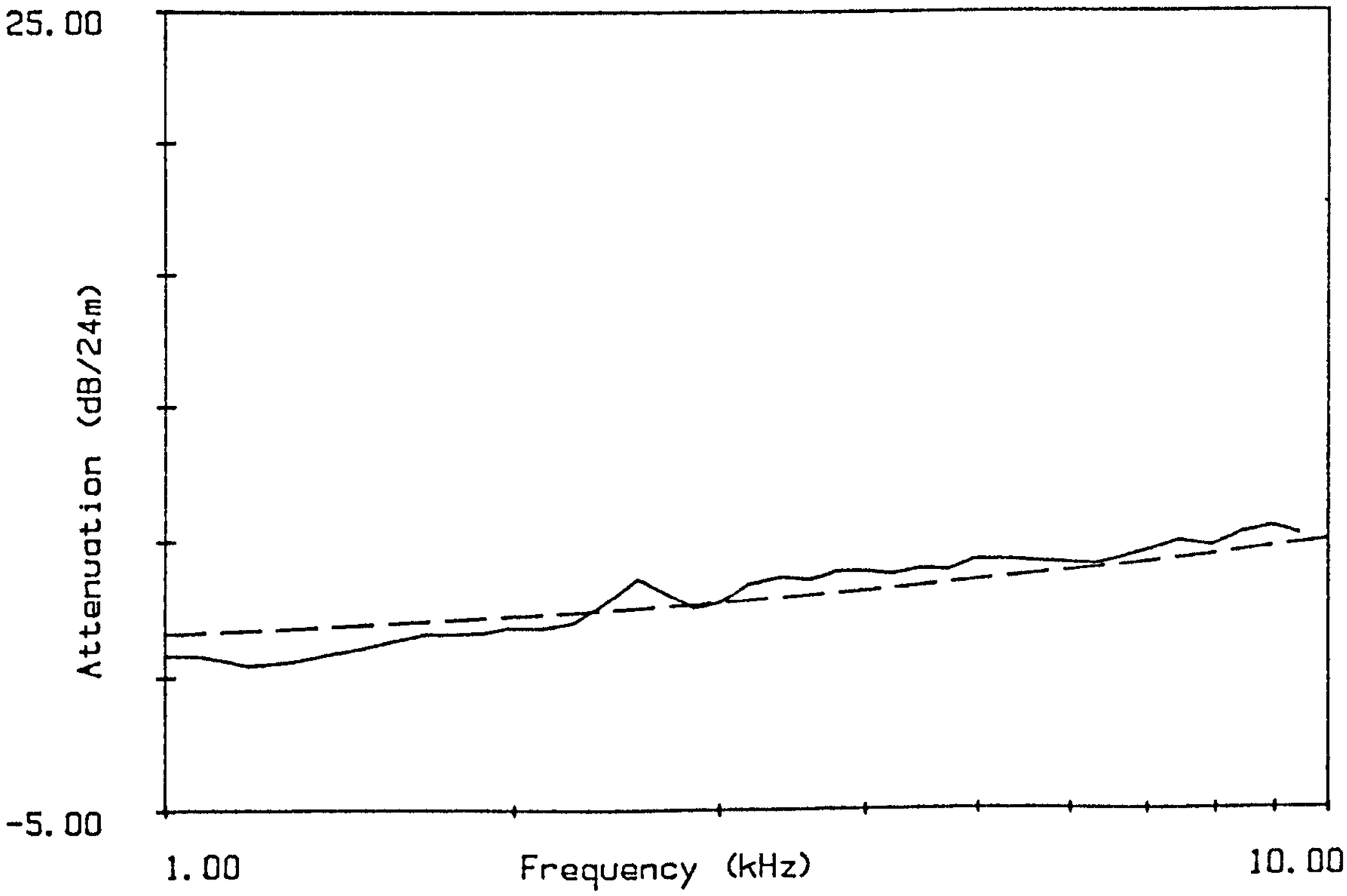

Figure 8.17
Mean measured attenuation (dB per 24m) for Wetleys Wood.
---- is sqrt(frequency)*0.05

8.3 Implications of the Model Experiments for Sound Propagation in Woodland.

The spread of the results from the experiments described in chapter 7 makes detailed conclusions uncertain. However, in general terms the results and modification to the scattering model are useful in a discussion of woodland sound propagation. Figures 8.18 and 8.19 illustrate the validity of using the mean radius of a mixed array in the modified prediction model using radii of the range of trunk radii observed in the woodland. This is the stratagem employed in the calculation of the predictions for the woodland data. The actual sizes of the tree trunks were fairly similar as the experimental sites were even-aged forestry stands.

The predictive model evidently has implications for the interpretation of the outdoor experiment results. Figures 8.20 to 8.23 show the range of values of attenuation per 24m obtained from each of the woodlands, compared with the original and modified scattering models. The range of measured values illustrated is the maximum and minimum value at each frequency of the mean attenuations for each day as illustrated in figures 6.2.22, 6.3.14 and 6.4.9. The predictions use the radius and density obtained from measurements made on sample areas. As described in Chapter 5.1, Frank (1976) concluded, from impedance tube measurements, that the surface impedance of trees is high, therefore the rigid cylinder case is used in the predictive model.

It is evident that the modified model under-predicts the observed attenuation at high frequencies. The conclusion can therefore be drawn that trunk scattering is not the only factor involved in the high frequency attenuation, even for the spruce monoculture, but that branches and leaves also contribute. Comparison between the measurements and the predictions may also elucidate the proportion of attenuation which can be attributed to scattering by the trunks. The attenuation from the mixed coniferous stand illustrated in figure 8.23 is considerably greater than either of the predictions while some of the attenuation spectra from the mixed woodland (particularly the winter measurement) and virtually all the spectra from the spruce monoculture lie between the two predictions. These results imply that the trunk attenuation accounts for a considerably larger proportion of the attenuation for the spruce monoculture and mixed woodland in winter than for the mixed woodland in

summer and that only a very small proportion of the attenuation for the mixed coniferous stand can be attributed to scattering by the trunks. This reflects the actual differences between the stands since the mixed stand has considerably more undergrowth and foliage than the spruce monoculture and the mixed coniferous stand forms an altogether denser barrier of branches and foliage than the other two.

The model studies also demonstrate that scattering effects may be significant at frequencies well below the frequency at which the wavelength is the same as the diameter of the scatterers. This implies that the mid-frequency attenuation could be caused by scattering by trunks and that much high frequency attenuation could be due simply to scattering by the smaller twigs and branches.

Although the smaller elements of the woods cannot, physically, be considered as consisting entirely of cylinders, it seems that the model of scattering proposed by Embleton (1966) could also be used to account for the attenuation observed above that predicted by the trunk scattering. The model describes attenuation due to both scattering and viscous absorption, the absorption being described in terms of a finite surface impedance of the cylinders, as discussed in chapter 5. A version of the fitting routine described in chapter 7 has been used to fit the sum of the attenuation due to the 'trunk array' and a variable array varying two of the parameters; radius, density and the surface impedance (by varying the assumed flow resistivity) to the measured mean attenuation spectra (dB per 24m) illustrated in figure 8.11.

The assumption illustrated in figures 8.18 and 8.19 that a 'mean array' (using the mean radius and total density of two arrays) rather than the sum of two arrays can be used to model an array of mixed radii, only holds for arrays with fairly similar radii and densities. Figure 8.24 shows the result of taking a mean array where the radii and densities are not similar. The two predictions are significantly different, thus to account for attenuation by two such different arrays, the arrays must be added together.

The fitting routine was first carried out maintaining the rigid cylinder assumption and varying the radius and density to obtain the best possible fit. In figures 8.25 to 8.28 the measured data are compared with the attenuation calculated from the best fit results from this fitting procedure, the input parameters used and mean difference are given in the figure captions. The two predictions from the individual arrays are shown in figures 8.25a to 8.28a to illustrate the attenuation contributed to the total from each. The best fit radius for the Wetleys Wood data is small, the density relatively large and the prediction gives a close fit to the data. The Bucknell Wood data cannot be fitted well to the model using an assumption of rigid cylinders. figure 8.28 shows the best fit attainable by adjusting the radius and density. The predictions for the two arrays are shown in figure 8.28a. It is evident that a high density of small rigid scatterers gives the wrong frequency dependence to fit the data, with little attenuation in the lower frequencies and a sharp rise at frequencies above about 5kHz. Figures 8.25 and and 8.26 indicate that the rigid assumption predictions can give a good fit to both the summer and winter measurements from Hazelborough Wood. The summer measurement requiring a larger radius than the winter measurement to account for the higher attenuation.

It is evident that the prediction of scattering alone described by the rigid cylinder case is not adequate for explaining the attenuation in the stand at Bucknell Wood, therefore a further fitting procedure has been carried out using a small input radius (0.001m) and varying the density and surface impedance of the second array (the 'trunk array' is again taken as the measured mean radius and 'adjusted density'). Figure 8.29 shows that this procedure does produce a considerably better fit to the data for Bucknell Wood since the predicted attenuation for the less dense array of softer cylinders is significant at the lower part of the frequency range. This result shows that the attenuation at Bucknell Wood can only be modelled in this way if the effects of both thermo-viscous absorption and scattering are included by assuming non-rigid cylinders. Figures 8.30 to 8.32 show that the data from the other stands can also be fitted using an assumed radius of 1mm and a non-rigid surface, there is, however, little difference in the mean difference value obtained using the rigid or non-rigid fitting procedures.

Comparison of the attenuation caused by the two arrays shows that in the Bucknell Wood and summer Hazelborough Wood measurements the 'trunk attenuation' contributes less than the 'small scatterers' attenuation to the whole, and in the Bucknell Wood result the trunk scattering is insignificant compared to the measured attenuation. The lower attenuation of the winter and Wetleys Wood measurements is, however, significantly affected by the attenuation due to the trunks, these conclusions are broadly similar to those reached from figures 8.20 to 8.23.

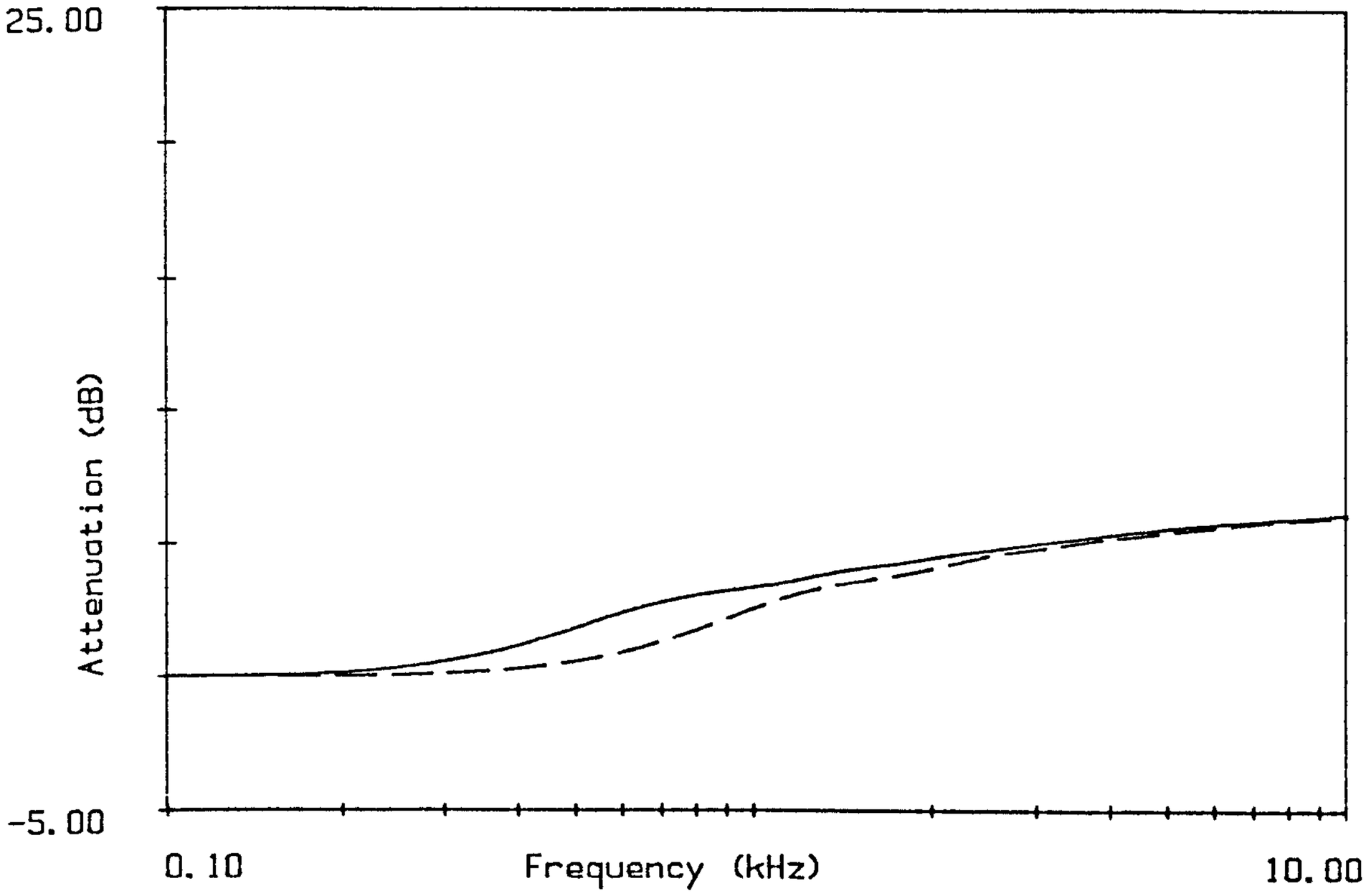

Figure 8.18
Sum of two arrays of rigid cylinders with densities 0.1
radii 0.01 and 0.07
and (-----) single array radius=0.04, density=0.2
separation distance = 50m

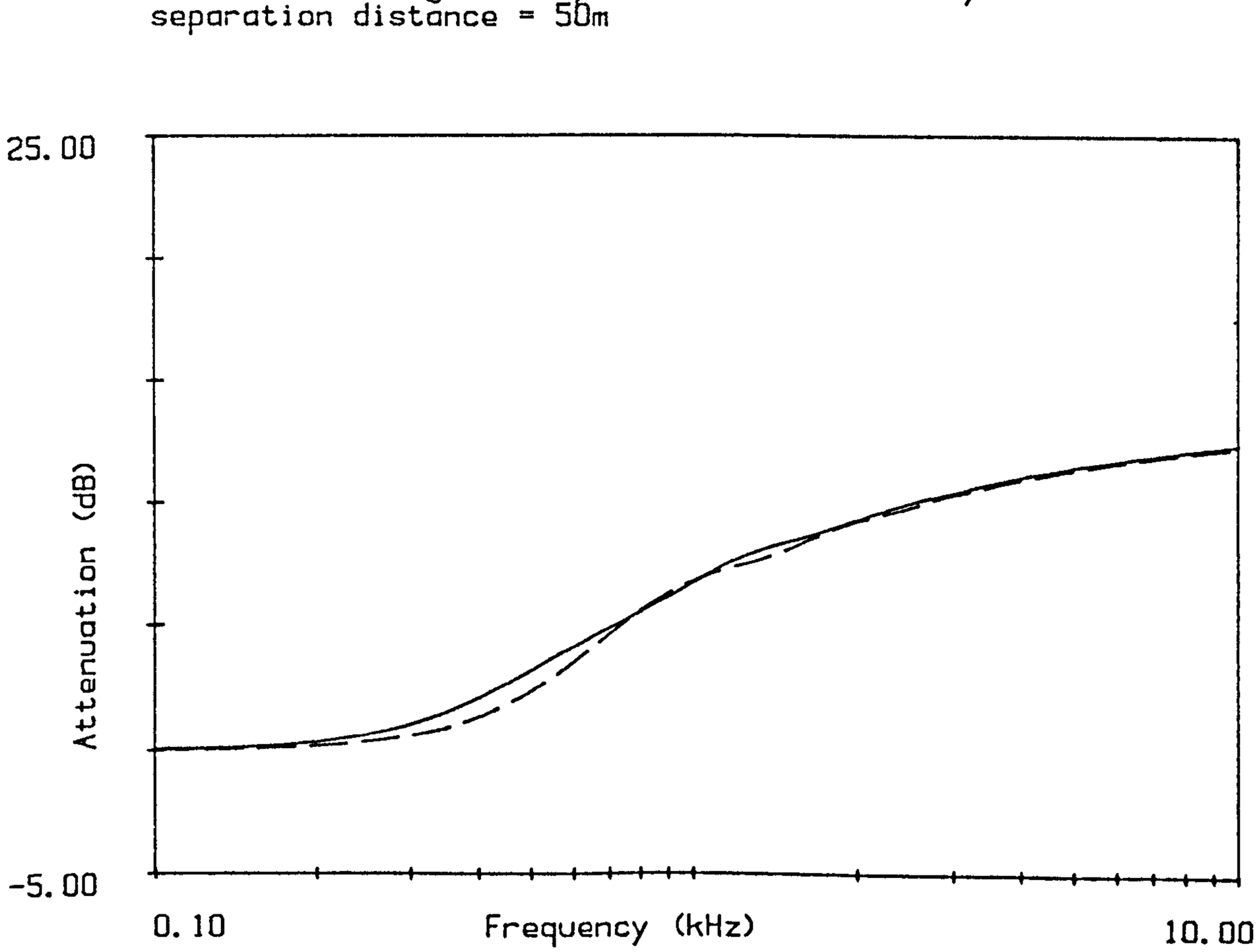

Figure 8.19
Sum of two arrays of rigid cylinders
a) density 0.2 radius 0.04
b) density 0.1 radius 0.08
and (-----) single array radius=0.053, density=0.3
separation distance = 50m

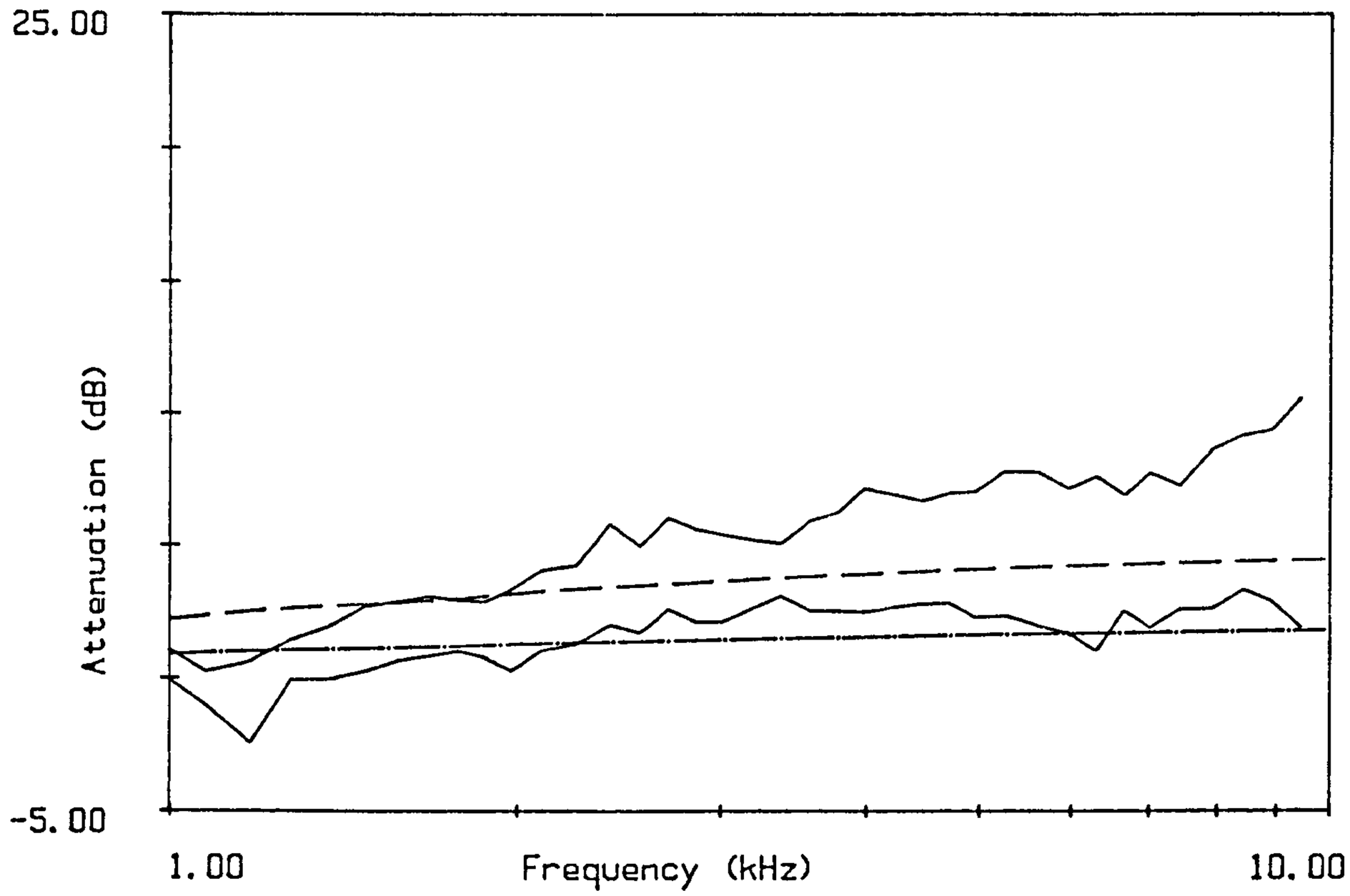

Figure 8.20
Range of attenuation (dB per 24m) for all Hazelborough Wood measurements. With 'trunk scattering' predictions.
— — · radius=0.045, density=0.267 (measured).
——·—· radius=0.045, density=0.1068 (-60%).

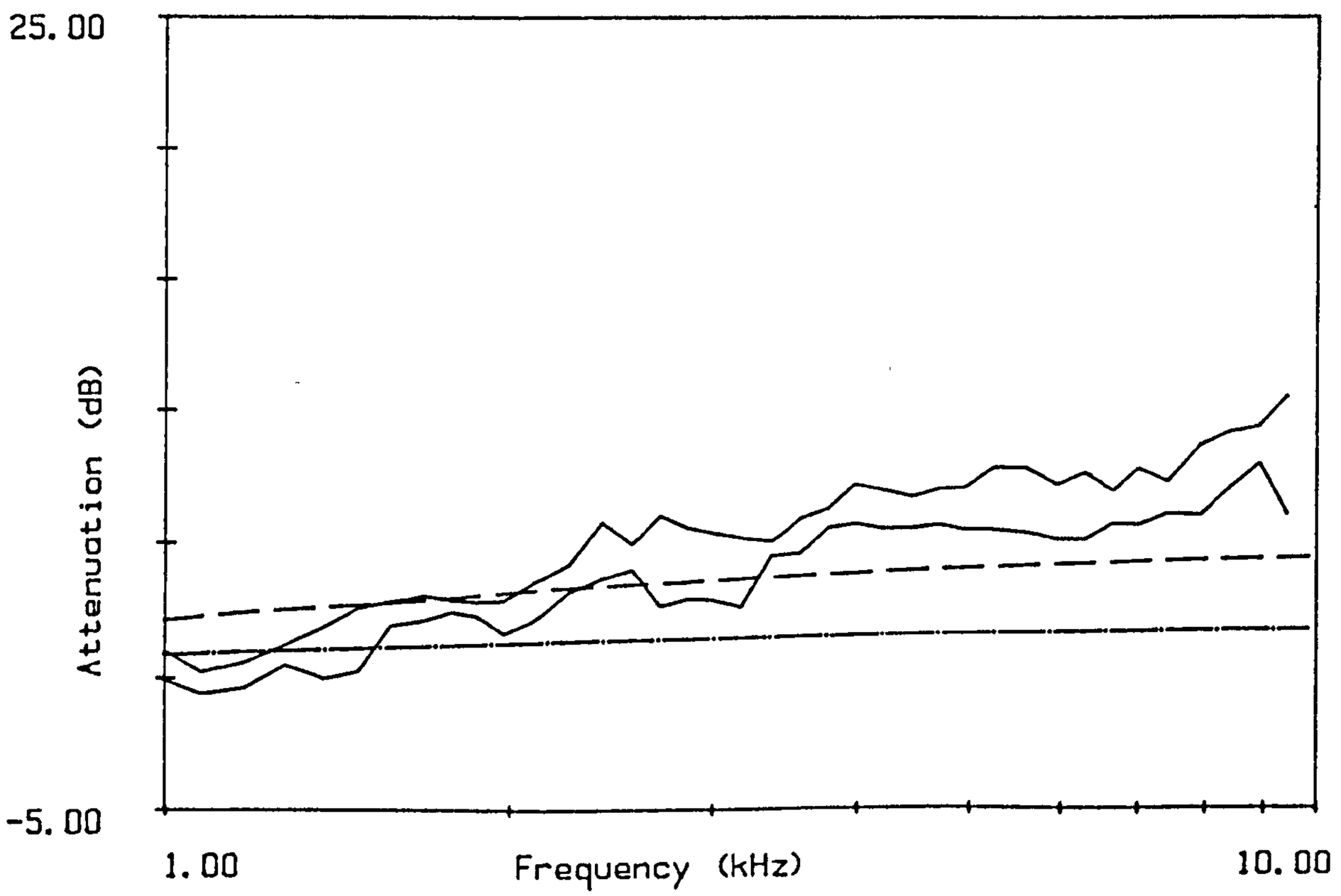

Figure 8.21
Range of attenuation (dB per 24m) for Hazelborough Wood excluding winter and 10/8/83 measurements.
With 'trunk scattering' predictions.
— — · radius=0.045, density=0.267 (measured).
——·—· radius=0.045, density=0.1068 (-60%).

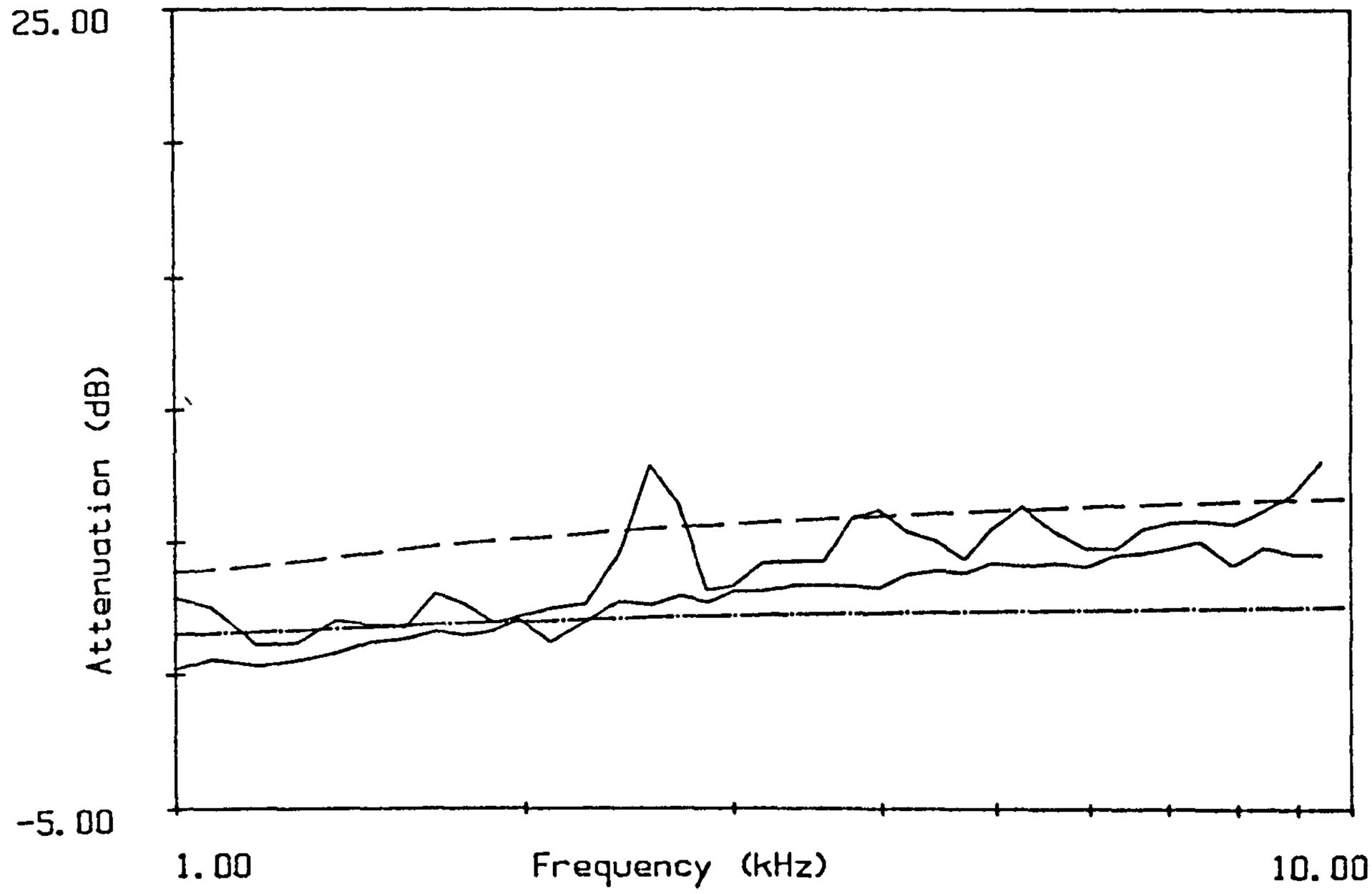

Figure 8.22
Range of attenuation (dB per 24m) for all Wetleys Wood measurements. With 'trunk scattering' predictions.
— — · radius=0.059, density=0.303 (measured).
——·—·— radius=0.059, density=0.1212 (-60%).

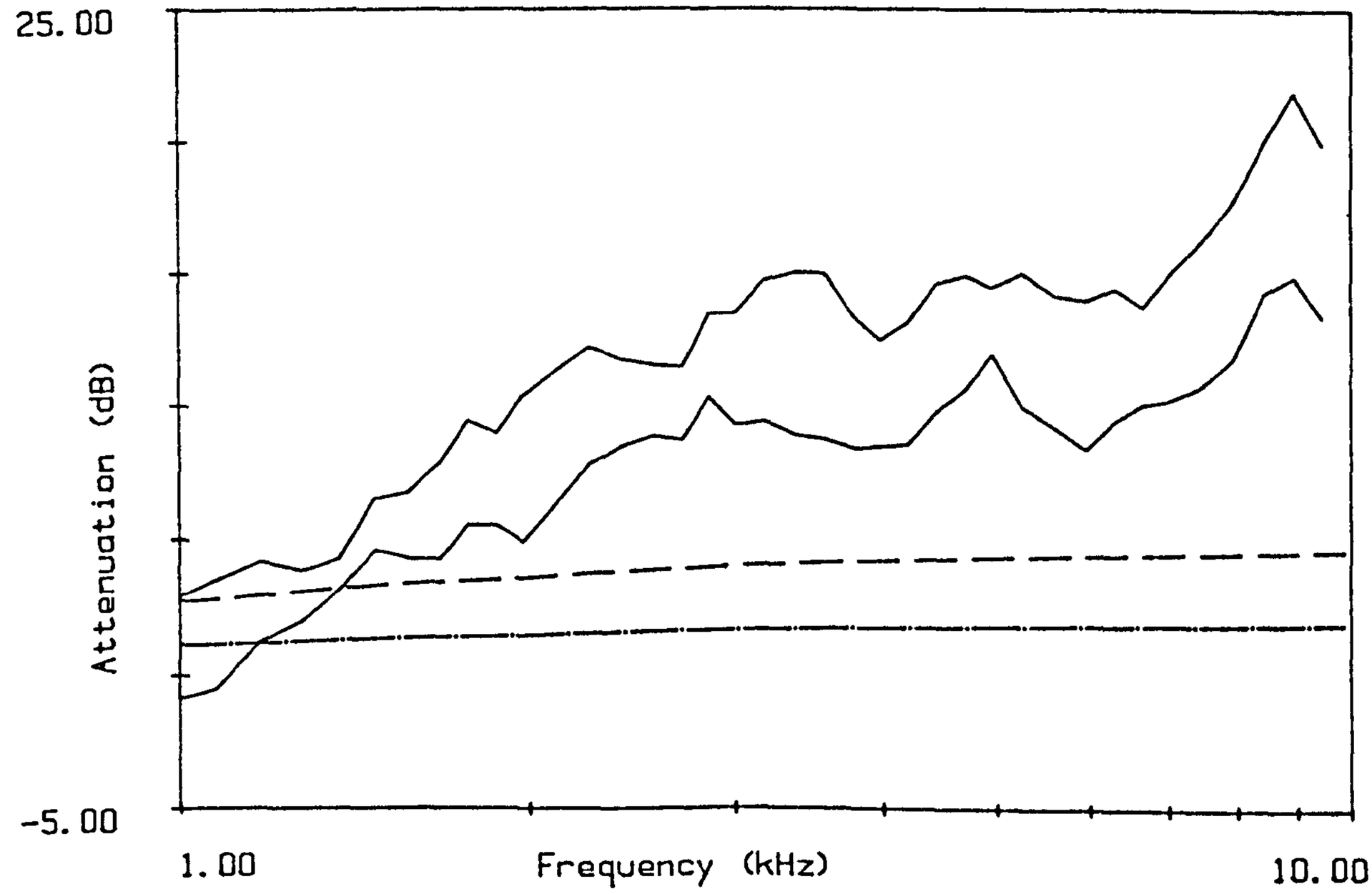

Figure 8.23
Range of attenuation (dB per 24m) for all Bucknell Wood measurements. With 'trunk scattering' predictions.
— — · radius=0.066, density=0.181 (measured).
——·—·— radius=0.066, density=0.0724 (-60%).

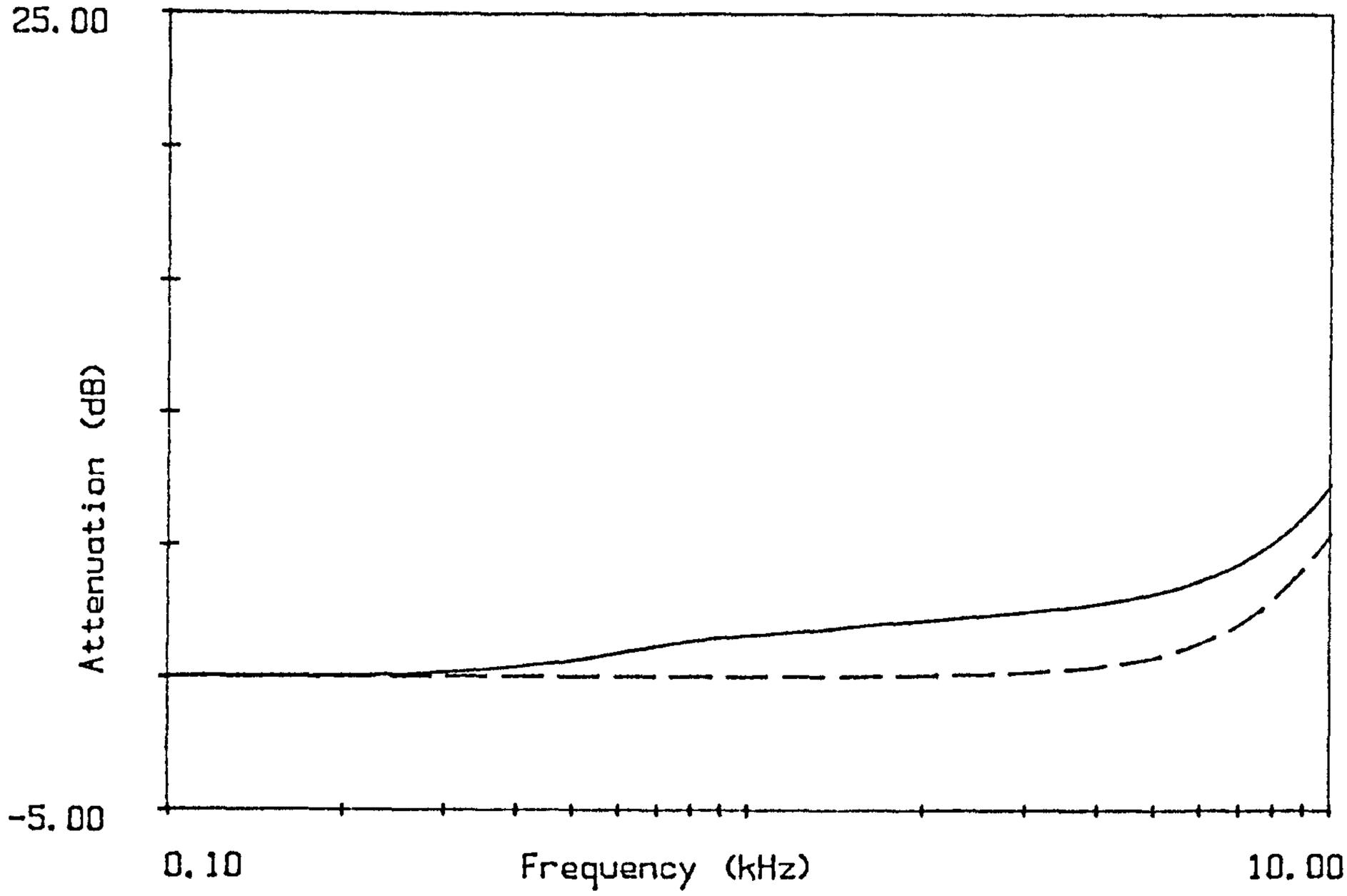

Figure 8.24
Predicted attenuation over 24m using:
———— sum of 2 arrays of rigid cylinders
a) radius 0.059m, density 0.1212.
b) radius 0.0019m, density 80.0. and
— — — — 'mean array' radius 0.00199 density 80.1212.

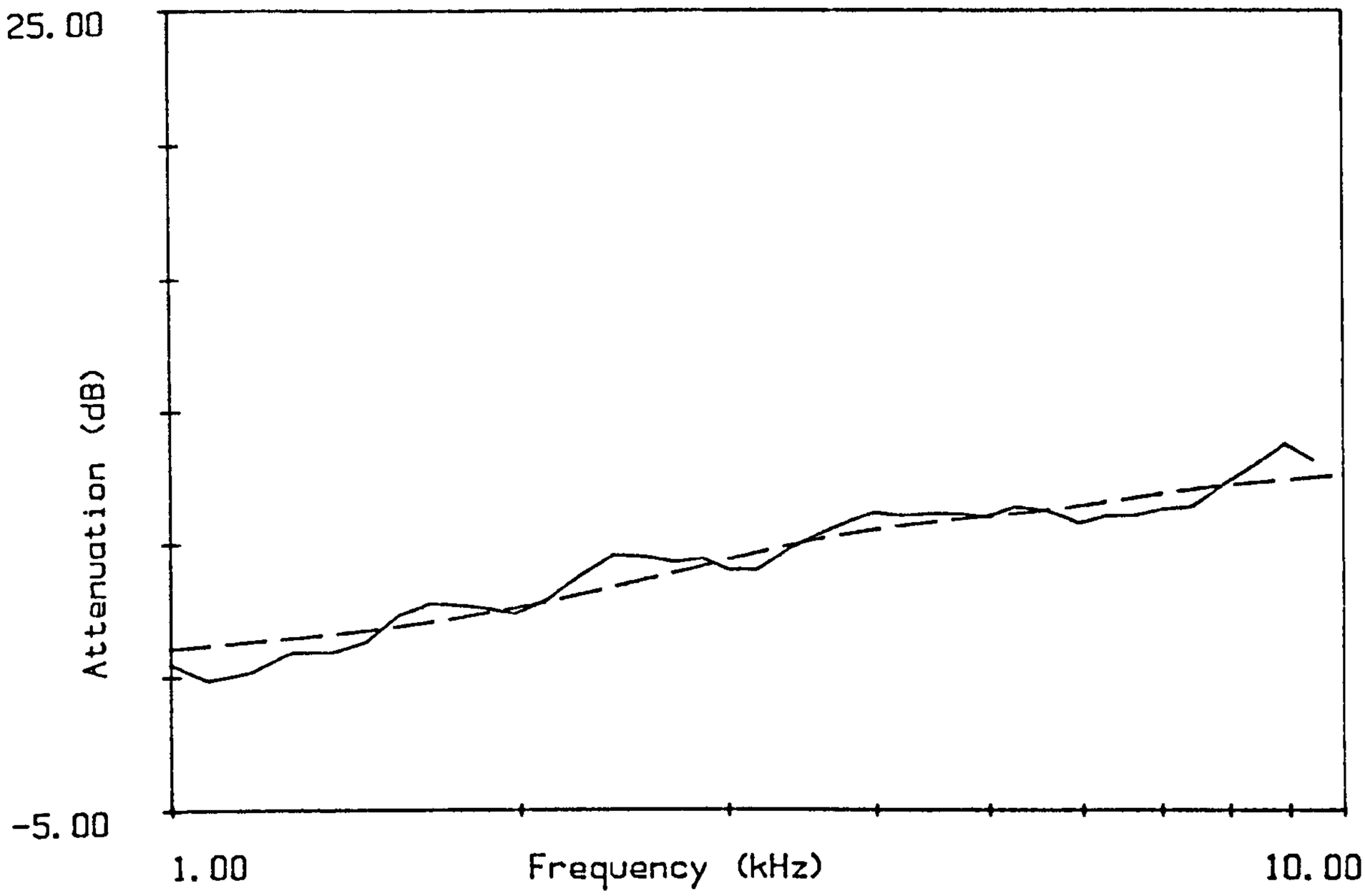

Figure 8.25
Mean measured attenuation (dB per 24m) for Hazelborough Wood. summer measurements.
---- is sum of predictions for 2 arrays. Mean difference=0.62dB.
a) radius=0.045, density=0.1068 rigid cylinders and
b) radius=0.0131, density=1.5, rigid cylinders.

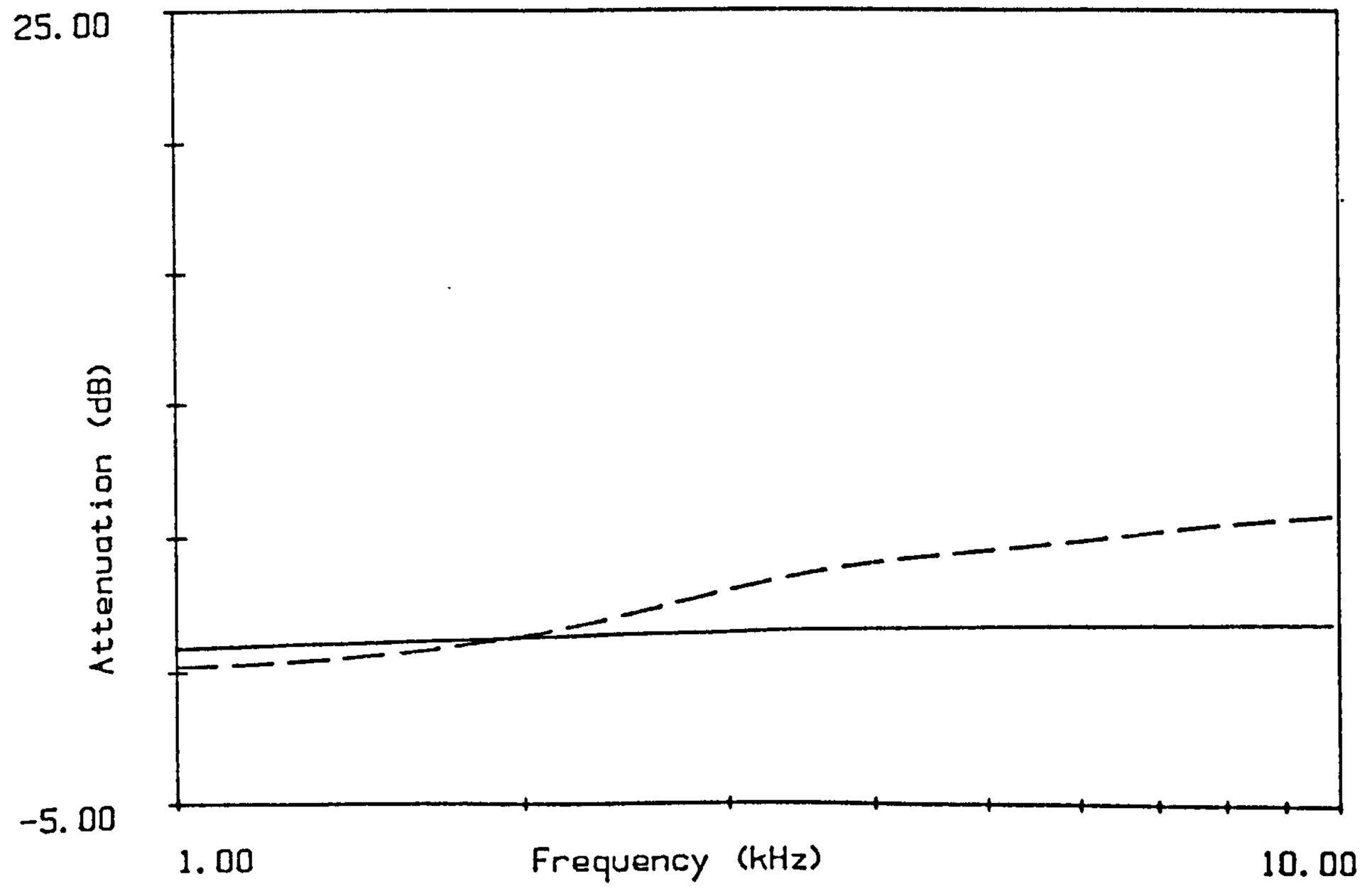

Figure 8.25a. Prediction for 2 arrays
radius=0.045, density=.1068 rigid cylinders
and (-----) radius=0.0131, density=1.5, rigid cylinders.

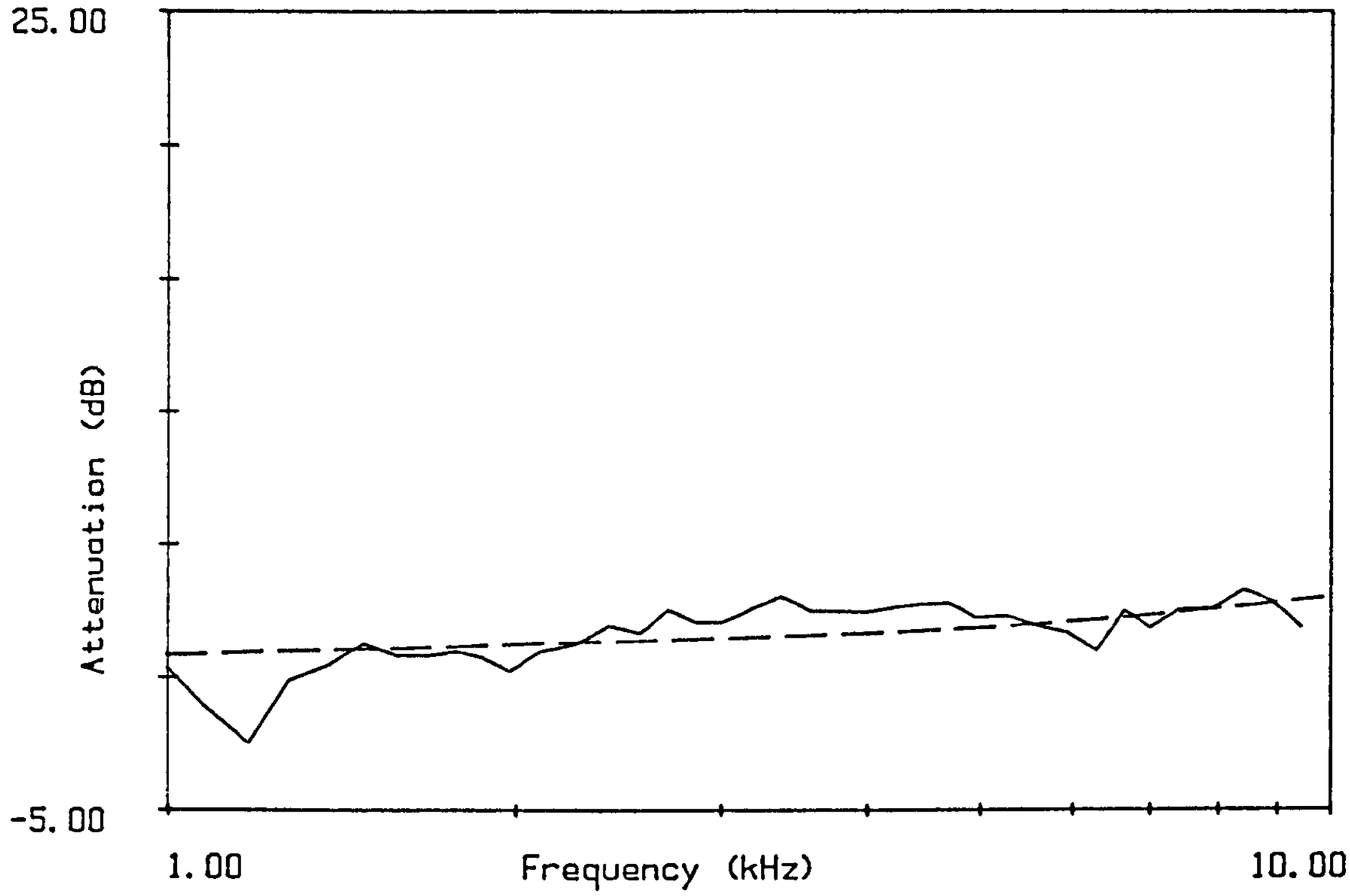

Figure 8.26
Mean measured attenuation (dB per 24m) for Hazelborough Wood. winter measurements.
---- is prediction for sum of 2 arrays, mean difference=0.89.
2 arrays a) radius=0.045, density=0.1068 rigid cylinders and
b) radius=0.001, density=2, rigid cylinders.

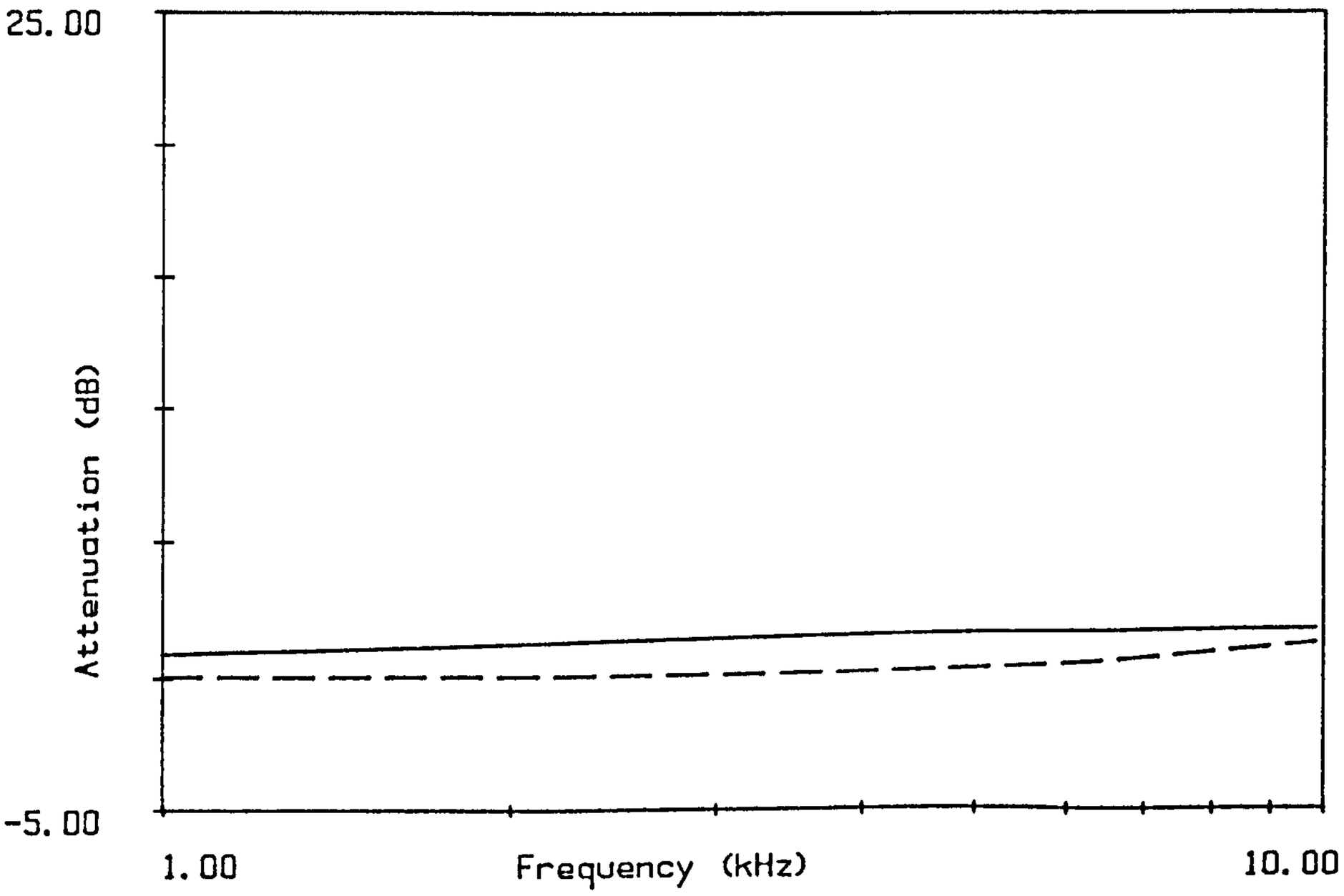

Figure 8.26a Prediction for 2 arrays
radius=0.045, density=0.1068 rigid cylinders
and (-----) radius=0.001, density=2, rigid cylinders

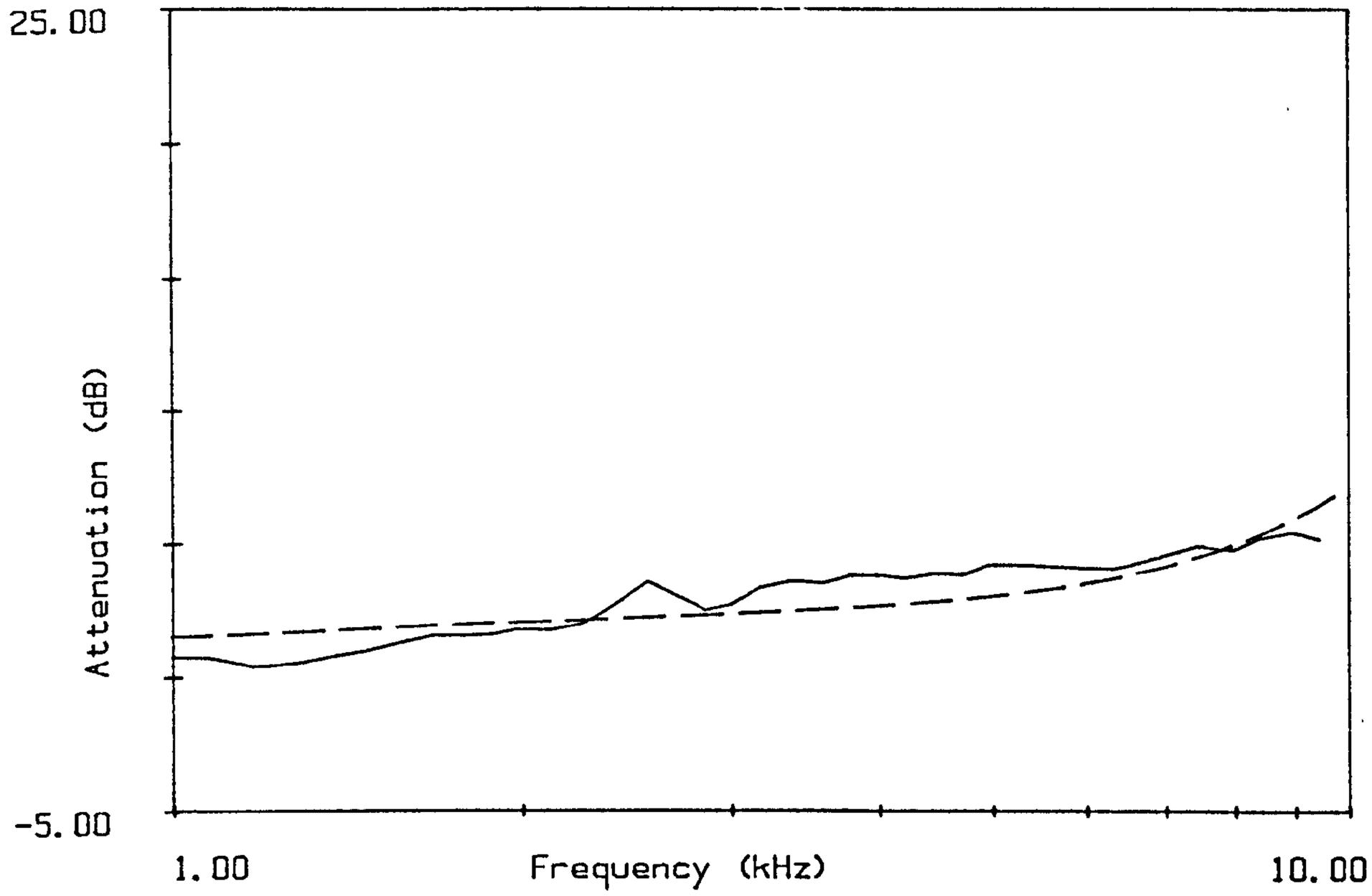

Figure 8.27
Mean measured attenuation (dB per 24m) for Wetleys Wood.
---- is sum of predictions for 2 arrays. Mean difference=0.80dB.
a) radius=0.059, density=0.1212 rigid cylinders and
b) radius=0.0019, density=80, rigid cylinders

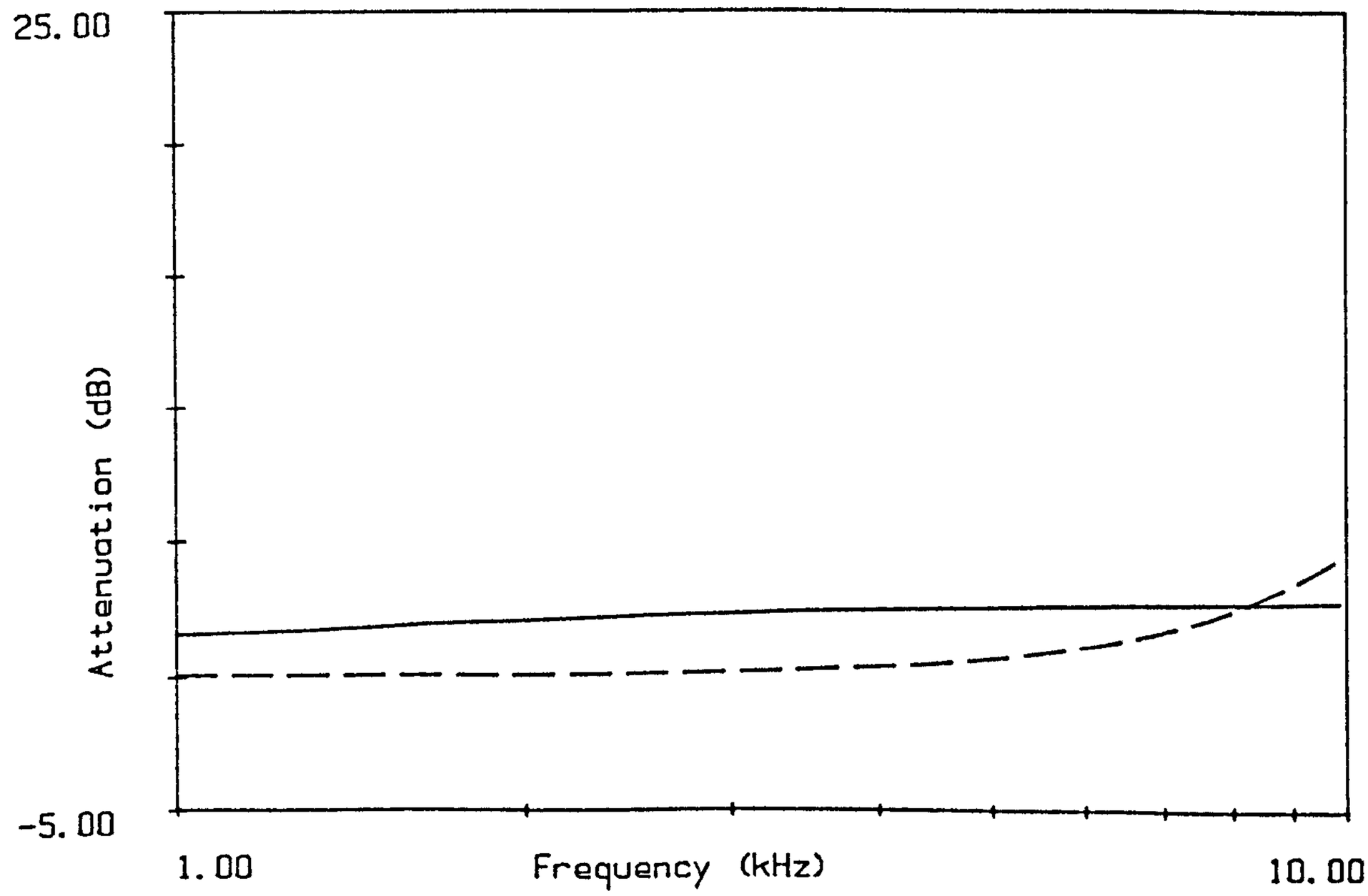

Figure 8.27a Prediction for 2 arrays
radius=0.059, density=0.1212, rigid cylinders
and (-----) radius=0.0019, density=80, rigid cylinders.

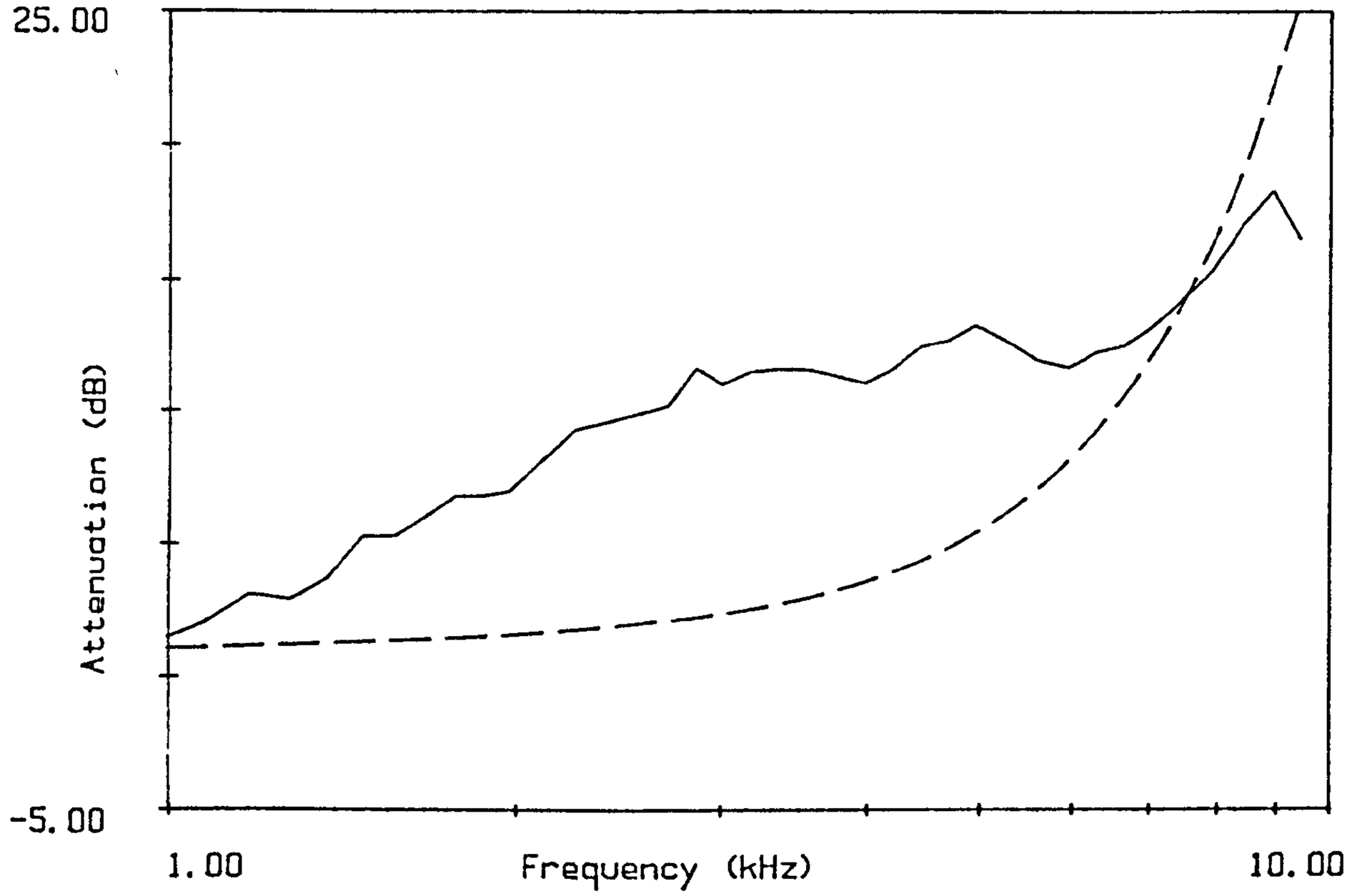

Figure 8.28
Mean measured attenuation (dB per 24m) for Bucknell Wood.
---- is sum of predictions for 2 arrays. Mean difference=6.04dB.
a) radius=0.066, density=0.0724 rigid cylinders and
b) radius=0.0021, density=340. rigid cylinders

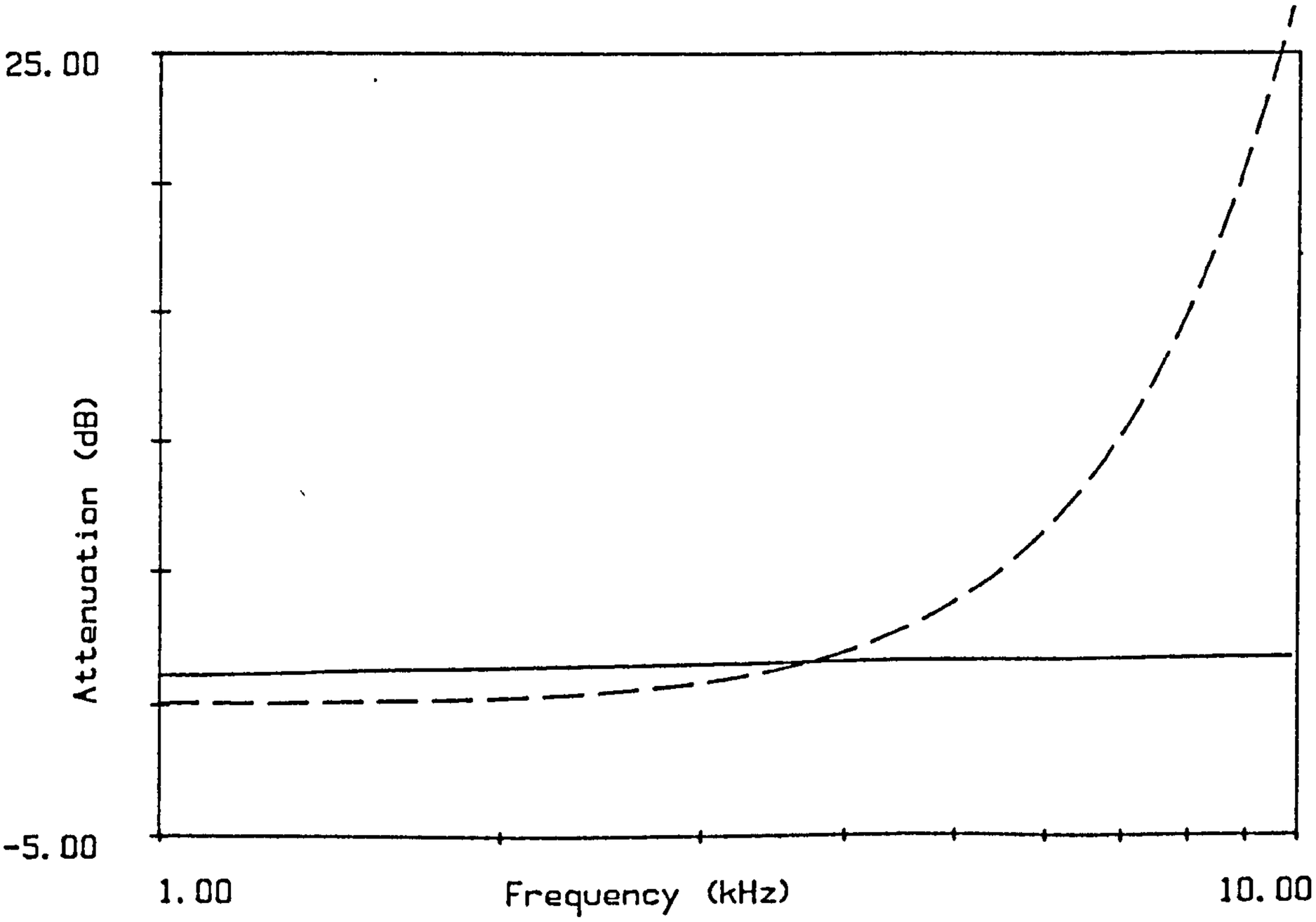

Figure 8.28a Prediction for 2 arrays
radius=0.066, density=.0724 rigid cylinders
and (-----) radius=0.0021, density=340. rigid cylinders.

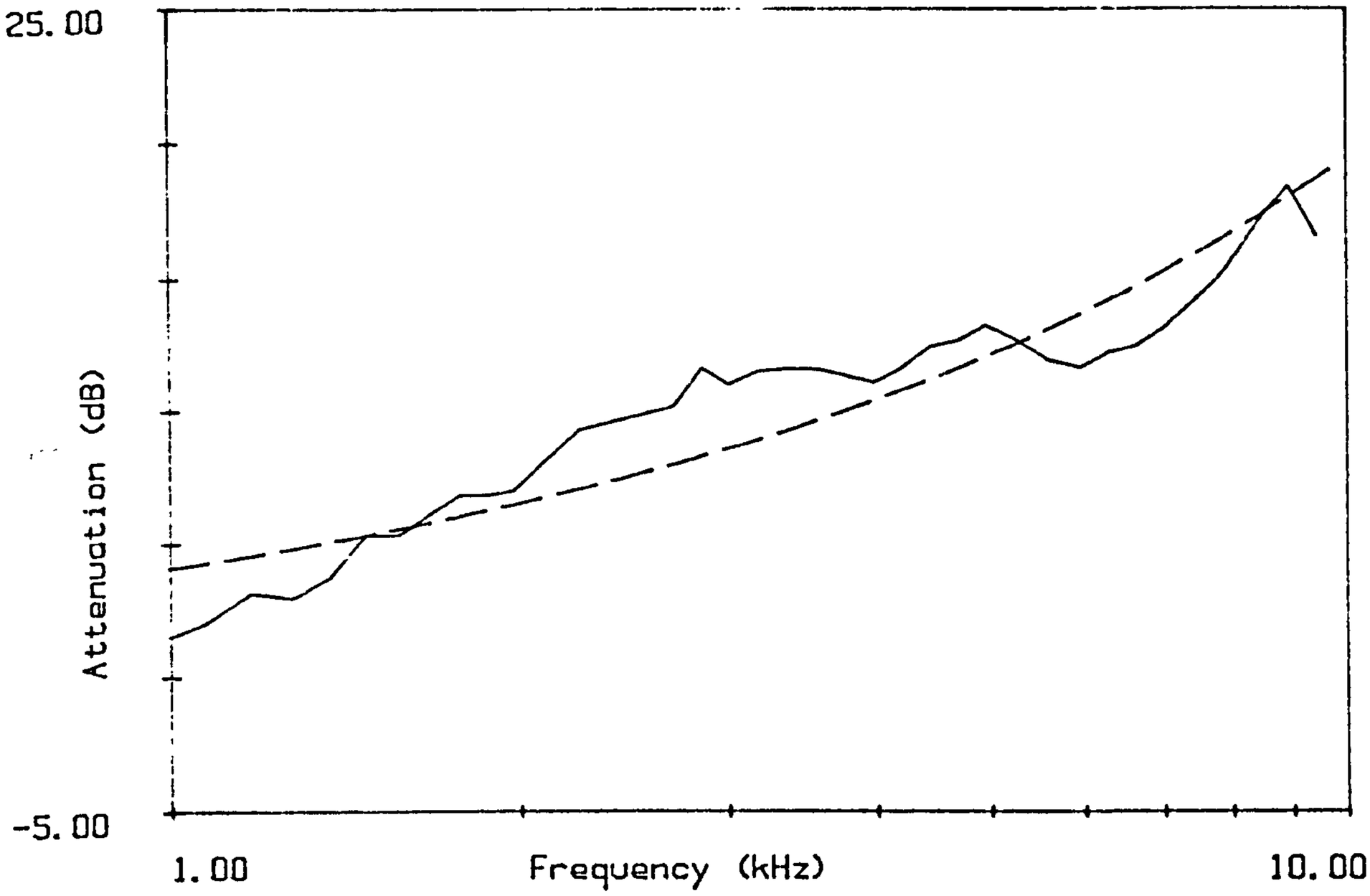

Figure 8.29
Mean measured attenuation (dB per 24m) for Bucknall Wood.
---- is sum of predictions for 2 arrays. Mean difference=1.69dB.
a) radius=0.066. density=0.0724 rigid cylinders and
b) radius=0.001. density=100. σe = 860.000

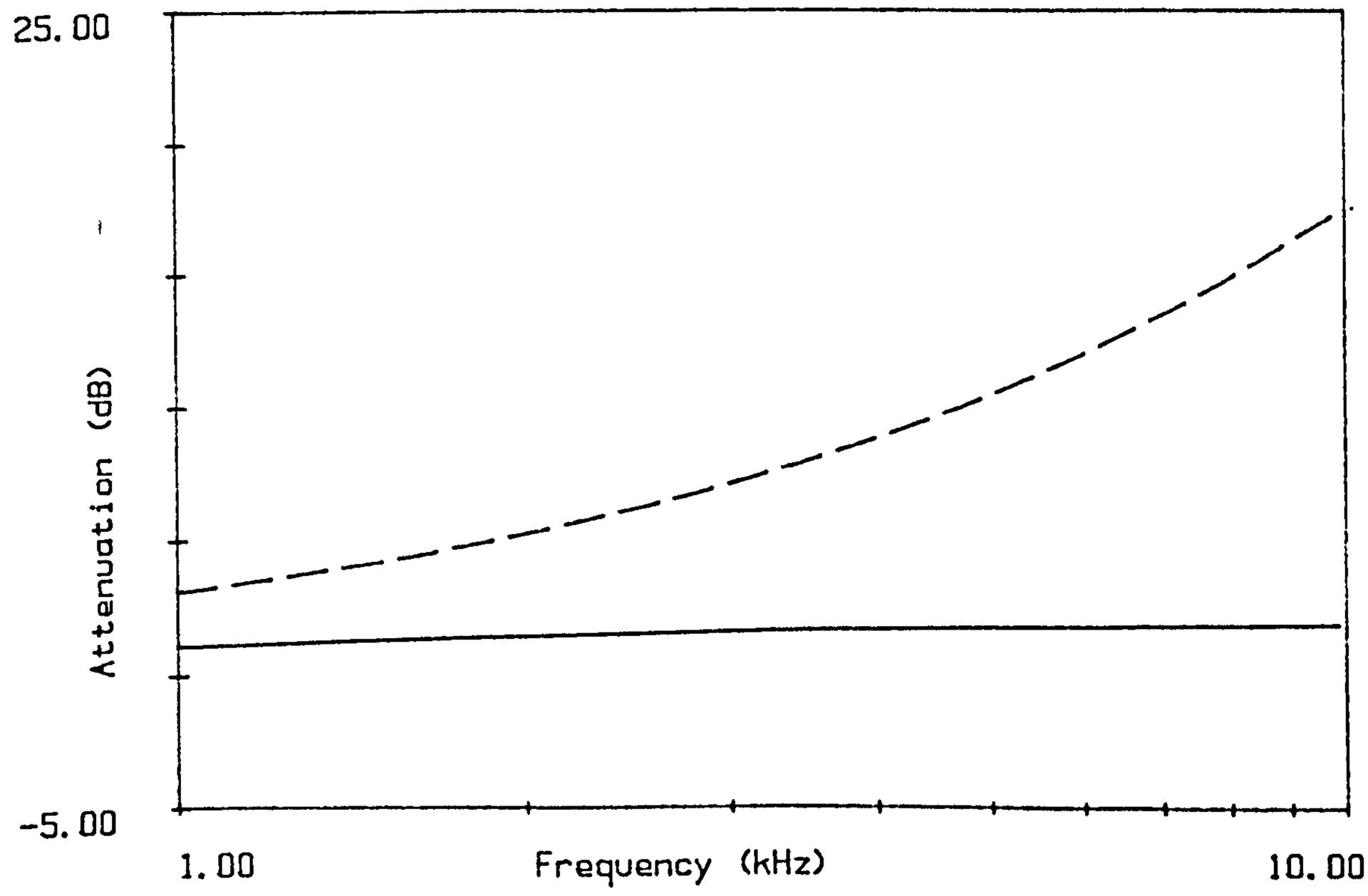

Figure 8.29a Prediction for 2 arrays
radius=0.066. density=.0724 rigid cylinders
and (-----) radius=0.001. density=100. σe = 860.000

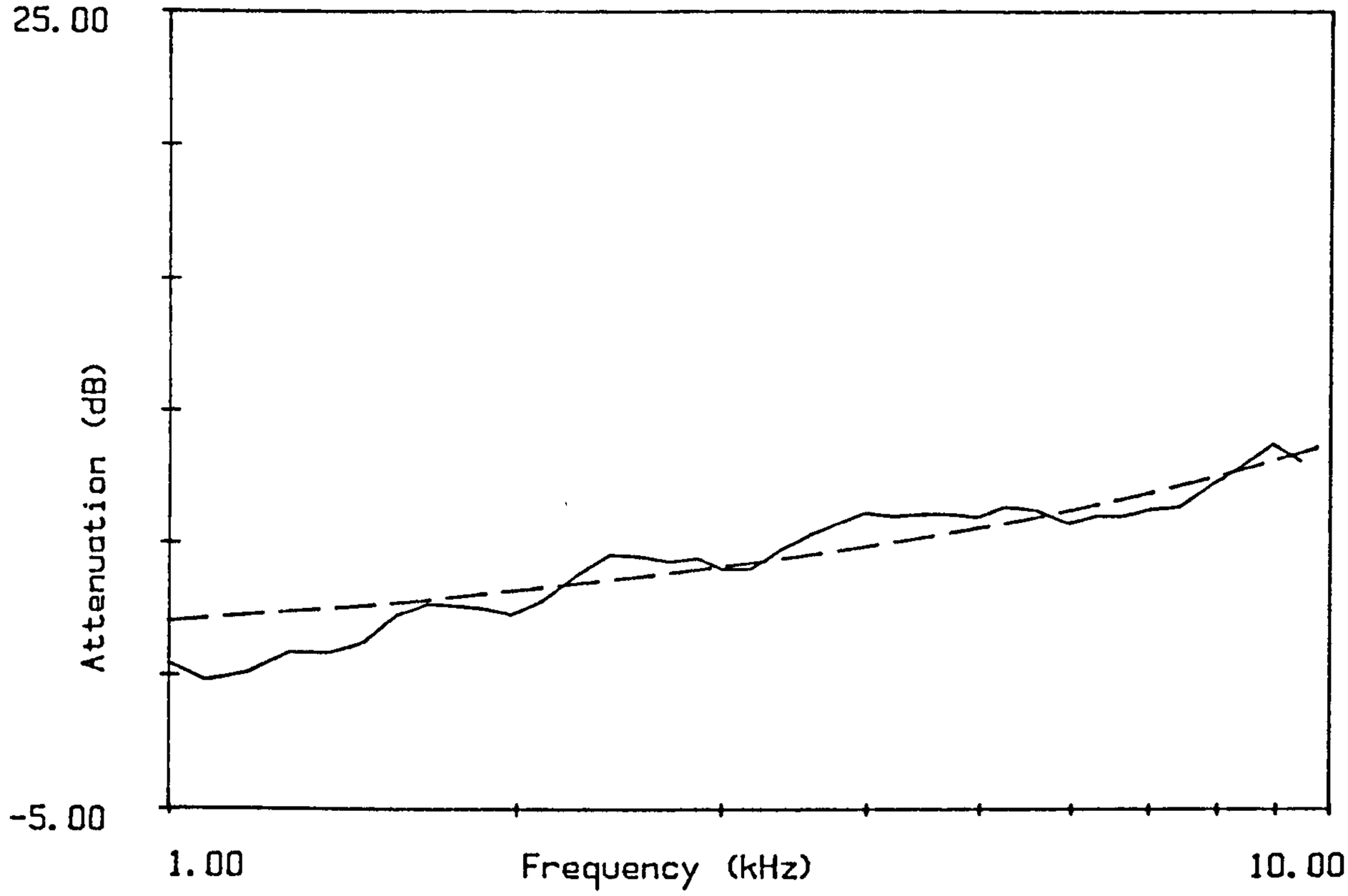

Figure 8.30
Mean measured attenuation (dB per 24m) for Hazelborough Wood. summer measurements.
---- is sum of predictions for 2 arrays. Mean difference=0.92dB.
a) radius=0.045, density=0.1068 rigid cylinders and
b) radius=0.001, density=70, σe = 1,900,000

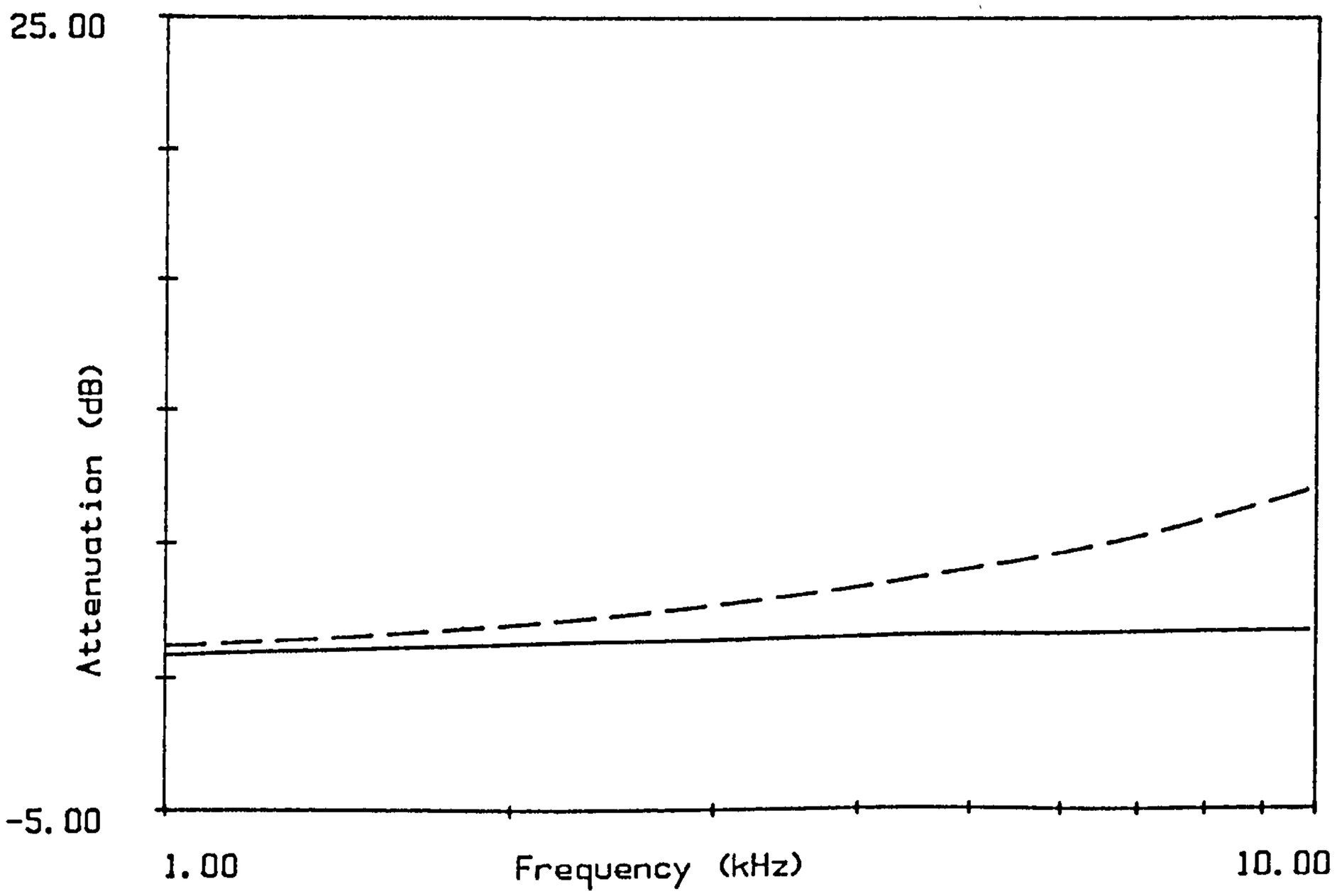

Figure 8.30a Prediction for 2 arrays
radius=0.045, density=.1068 rigid cylinders
and (-----) radius=0.001, density=70, σe = 1,900,000

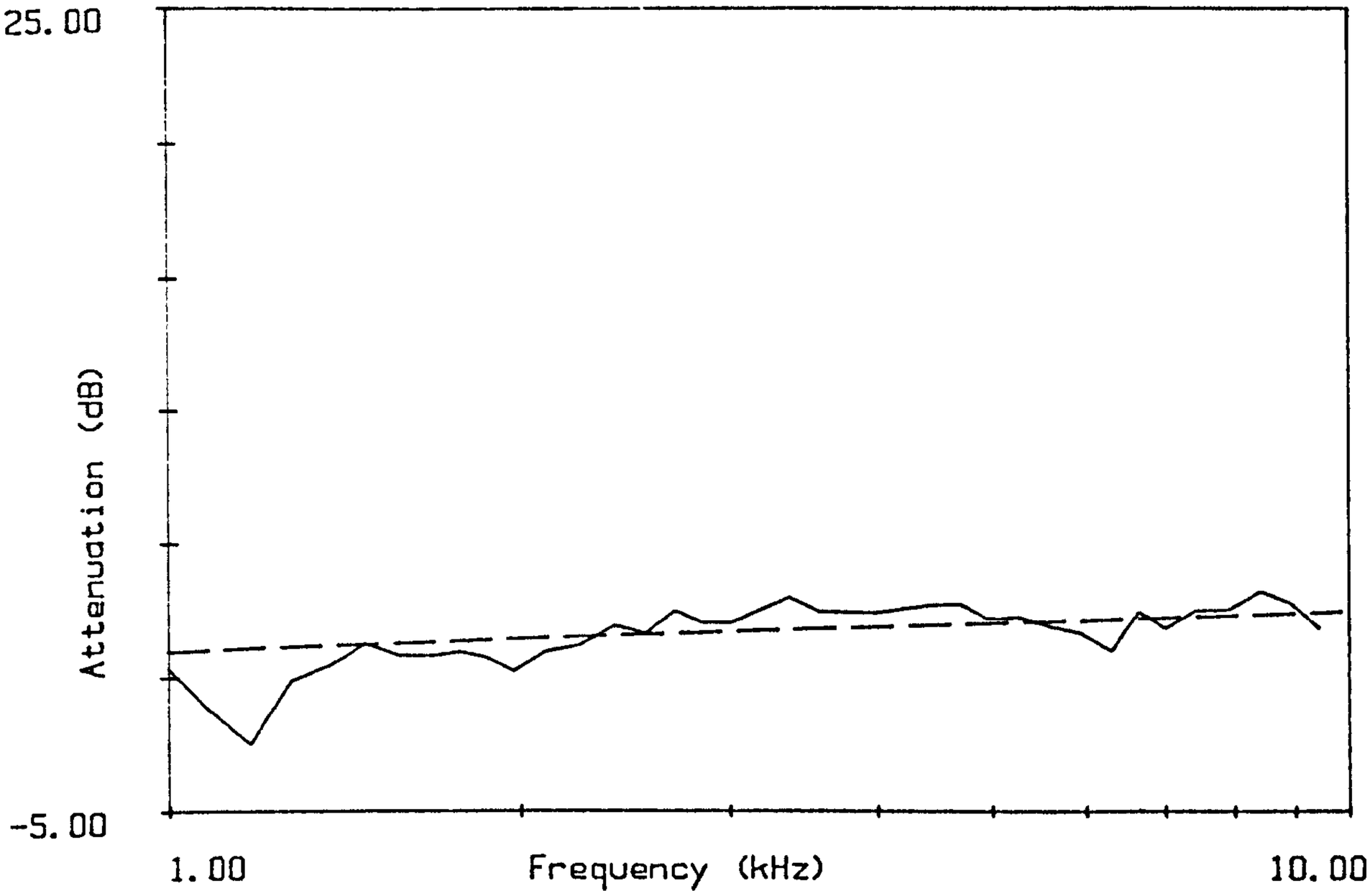

Figure 8.31
Mean measured attenuation (dB per 24m) for Hazelborough Wood. winter measurements.
---- is prediction for sum of 2 arrays, mean difference=0.92.
2 arrays a) radius=0.045, density=0.1068 rigid cylinders and
b) radius=0.001, density=4, σe = 800,000

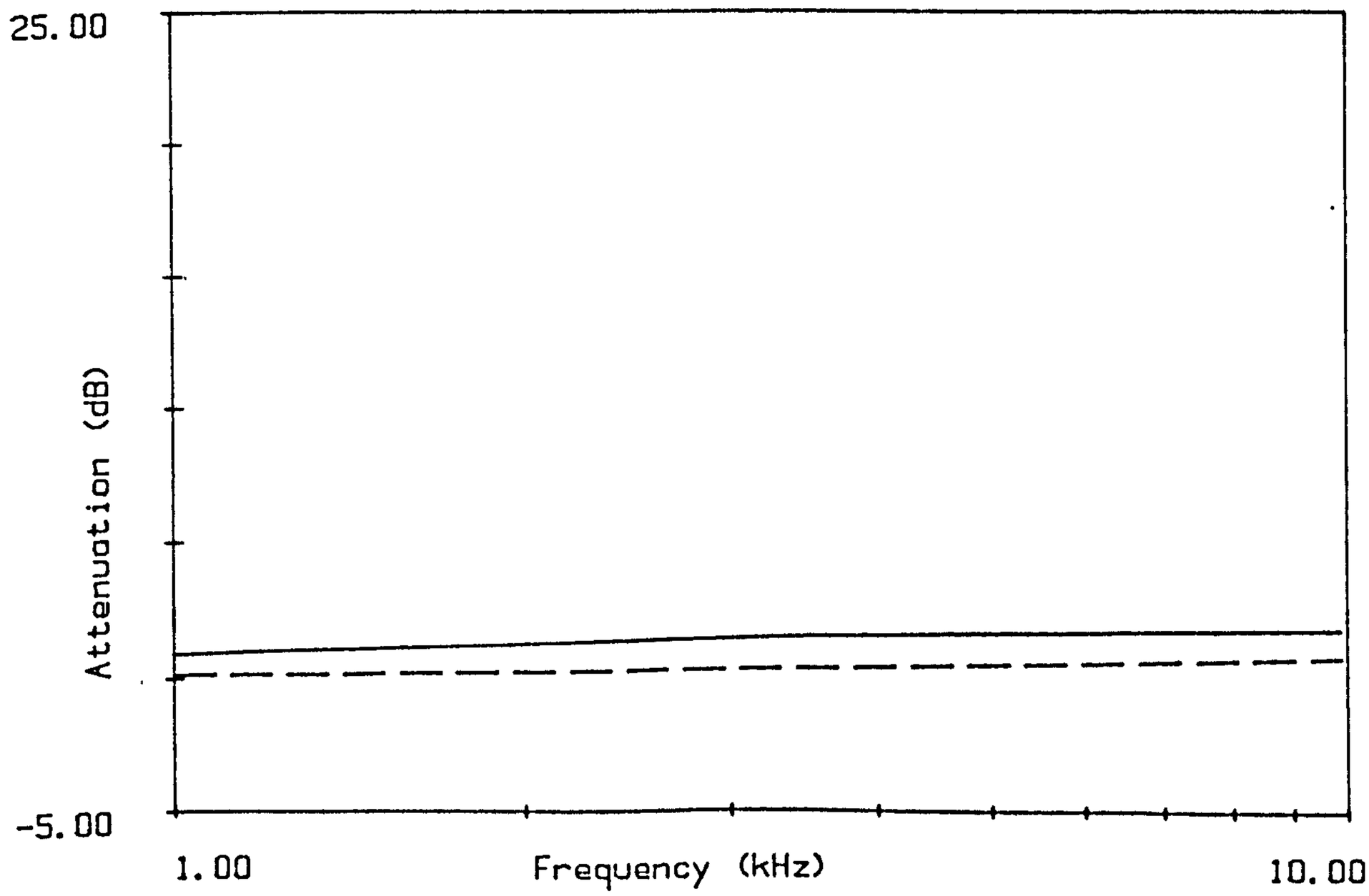

Figure 8.31a Prediction for 2 arrays
radius=0.045, density=.1068 rigid cylinders
and (-----) radius=0.001, density=4, σe = 800,000

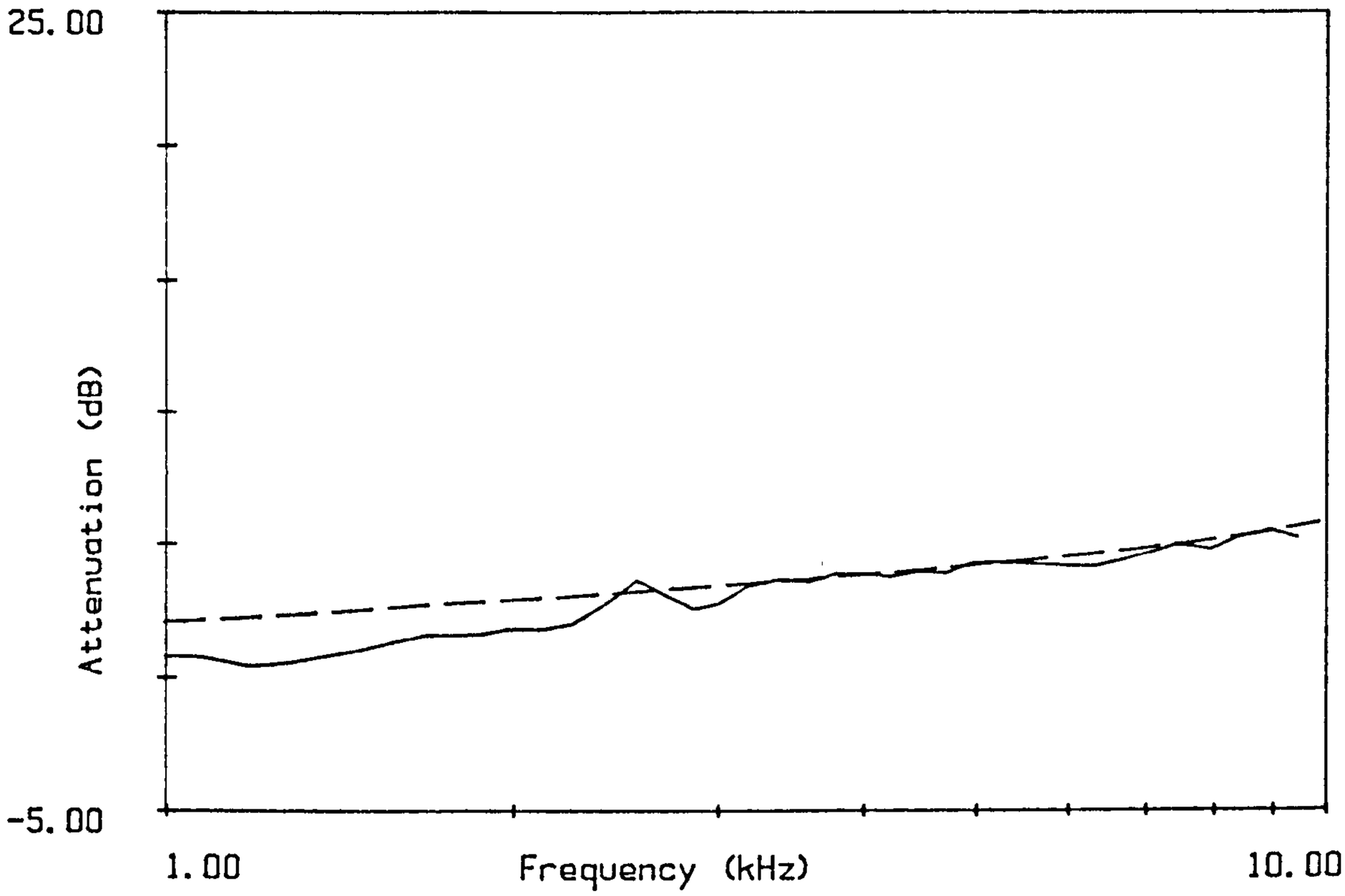

Figure 8.32
Mean measured attenuation (dB per 24m) for Wetleys Wood.
---- is sum of predictions for 2 arrays. Mean difference=0.84dB.
a) radius=0.059, density=0.1212 rigid cylinders and
b) radius=0.001, density=100, σe = 10,000,000.

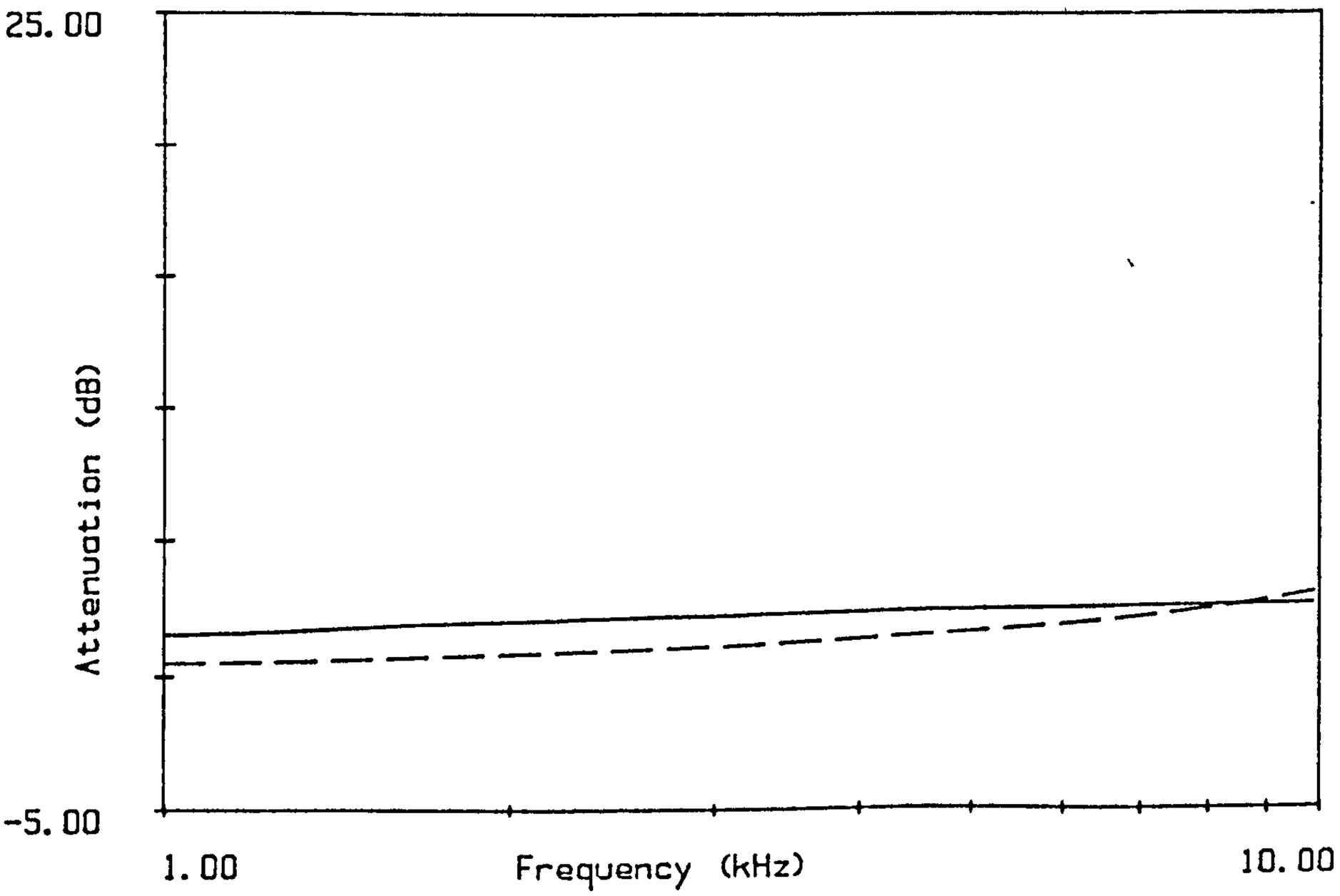

Figure 8.32a Prediction for 2 arrays
radius=0.059 density=0.1212 rigid cylinders
and (-----) radius=0.001, density=100, σe = 10,000,000.

8.4 A Combined Prediction of Attenuation in Woodland.

The two attenuation mechanisms of ground interference and scattering have been shown to predict the attenuation of sound in woodland in the low and high frequency ranges, respectively. However, to give a useful prediction model for the whole frequency range, the two mechanisms must be combined in some way. The ground interference effects have been shown to have little influence at high frequencies at distances of over 30 to 40m or more due to the disruption of the interference patterns by scattering. There is, however, no reason to assume, that the scattering effect is not present at low frequencies. The stratagem employed to combine the two models is, therefore, to add the ground effect attenuation to that of the scattering model in the low frequencies (up to 2000Hz) while using the scattering predictions alone for the higher frequencies. Since the scattering predictions generally give a small attenuation at low frequencies such an addition may be effective even when the ground prediction alone gives a good fit to the low frequency data. In some experimental results (for example in figure 8.7) the ground prediction under-predicts the attenuation at low and mid frequencies so an addition of some low frequency attenuation may improve the agreement between the prediction and the measurement.

Figure 8.33 illustrates the prediction obtained using this 'combined model' in comparison with the measurement of figure 8.7. The same best fit ground parameters are used as in figure 8.7 and the scattering parameters used are the best fit parameters for the sum of the trunk scattering and the non-rigid small scatterers (as in figure 8.29). The prediction obviously gives a much better fit to the measured data than the ground prediction alone in the low and mid frequencies, since the difference noted between the prediction and measurement of figure 8.7 is compensated for by the scattering prediction. Figure 8.34 shows a similar comparison for the data of figure 8.4 at 48m separation in Hazelborough Wood, the prediction is again similar to the measured spectrum. Since the scattering prediction is a linear function of distance, the addition of the scattering model has a greater effect at longer distances giving rise to a possible over-prediction of the low and mid-frequencies at longer distances (as in figure 8.41).

Comparisons between the combined prediction model and all the measured data have been made by plotting the range of values at each of the separation distances (1.2m microphone height) with the combined predictions using the mean effective flow resistivity (homogeneous approximation) for all the data from a woodland (from appendix C) and the best fit scattering parameters, using an input radius of 0.001m and varying the density and surface (see figure captions), these comparisons are shown in figures 8.35 to 8.44.

In general the prediction is within the range of the measured data. The exceptions being mainly at the longer distances (72m and 96m) where the model tends to over-predict the low and mid frequency parts, this is due to the fact that at longer distances even the low frequency attenuation is significant for the scattering prediction, and this is, in some cases, added to an over-prediction by the ground model. The longer distance would, perhaps be fitted better by simply using the ground prediction at lower frequencies and the scattering prediction for the higher frequencies, but there is little physical justification for this. Figures 8.25 and 8.27 show that the data for Hazelborough Wood and Wetleys Wood can be effectively fitted with a prediction using the rigid cylinder assumption for both arrays, and that the two best fit arrays give a lower value of attenuation at 1kHz than those using non-rigid small cylinders as used above. The parameters from figures 8.25 and 8.27 have therefore been compared to the longer distance measurements in figures 8.45 and 8.46 and can be seen to improve the agreement, in the mid-frequencies, over that of figures 8.41 and 8.44. Although the high frequency part of figure 8.41 is in better agreement with the measurement than that of figure 8.45 which gives a markedly concave curve in the high frequencies tending to underpredict the result. It could be argued that the cut-off frequency should be lower for the longer distances since there is more likelihood of the waves being scattered and therefore the interference patterns being disrupted to a greater extent. Figures 8.47 and 8.48 show the same comparisons as figures 8.41 and 8.44 but the ground effect model is only added up to 800Hz, these can be seen to give a good agreement with the measurements.

The combined model does give the typical spectrum shape of woodland noted in this study, and others, with a low frequency peak, a mid-frequency dip, increasing with frequency in the high frequency part. In most of the predictions illustrated in figures 8.33 to 8.48 the mid-frequency dip occurs in approximately the same frequency range as in the

measurements, this being due to the combined effects of the interference pattern and the increasing scattering attenuation. The longer distances, however, require the use of a lower 'cutoff frequency' to obtain a dip in approximately the correct location. The sharp cutoff shown in the combined model is not a physical phenomenon but the simplest numerical means of combining the ground and scattering models. Physically, it is more likely that there is a gradual transition from the region at which the ground effect can be clearly seen and the region at which the scattering is dominant, but it is not, at present, possible to define such a transition. The sharp cutoff does, however, seem to give a good agreement with the data.

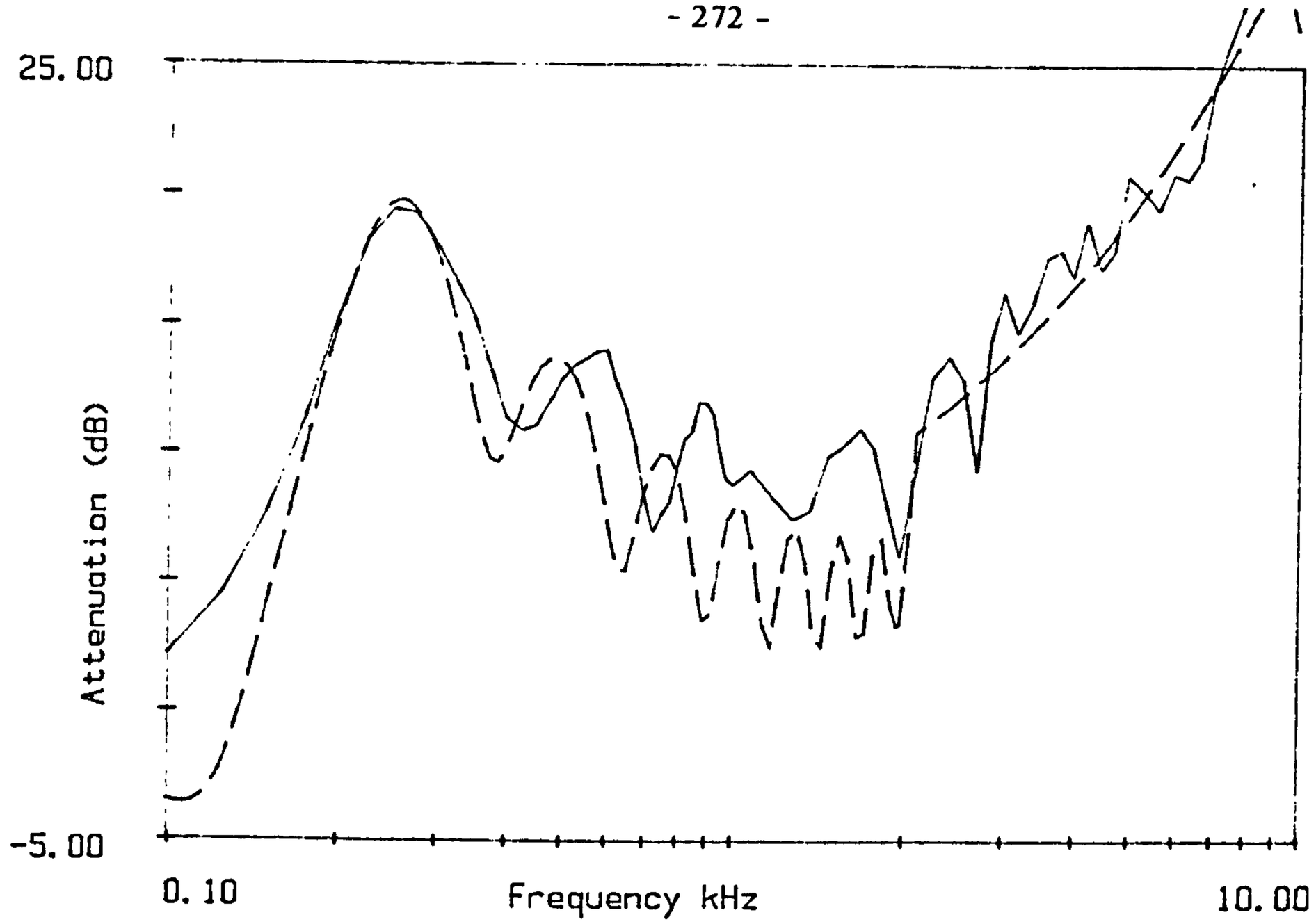

Figure 8.33
Measured attenuation from Bucknell Wood 9/7/84;
Separation distance 40m G track, 1.2m microphone height,
Prediction using homogeneous approximation σ e = 50,000; to 2kHz.
+ scattering radius= 0.066, density = 0.0724, rigid cylinders
+ radius= 0.001, density = 100 , σ e = 860,000

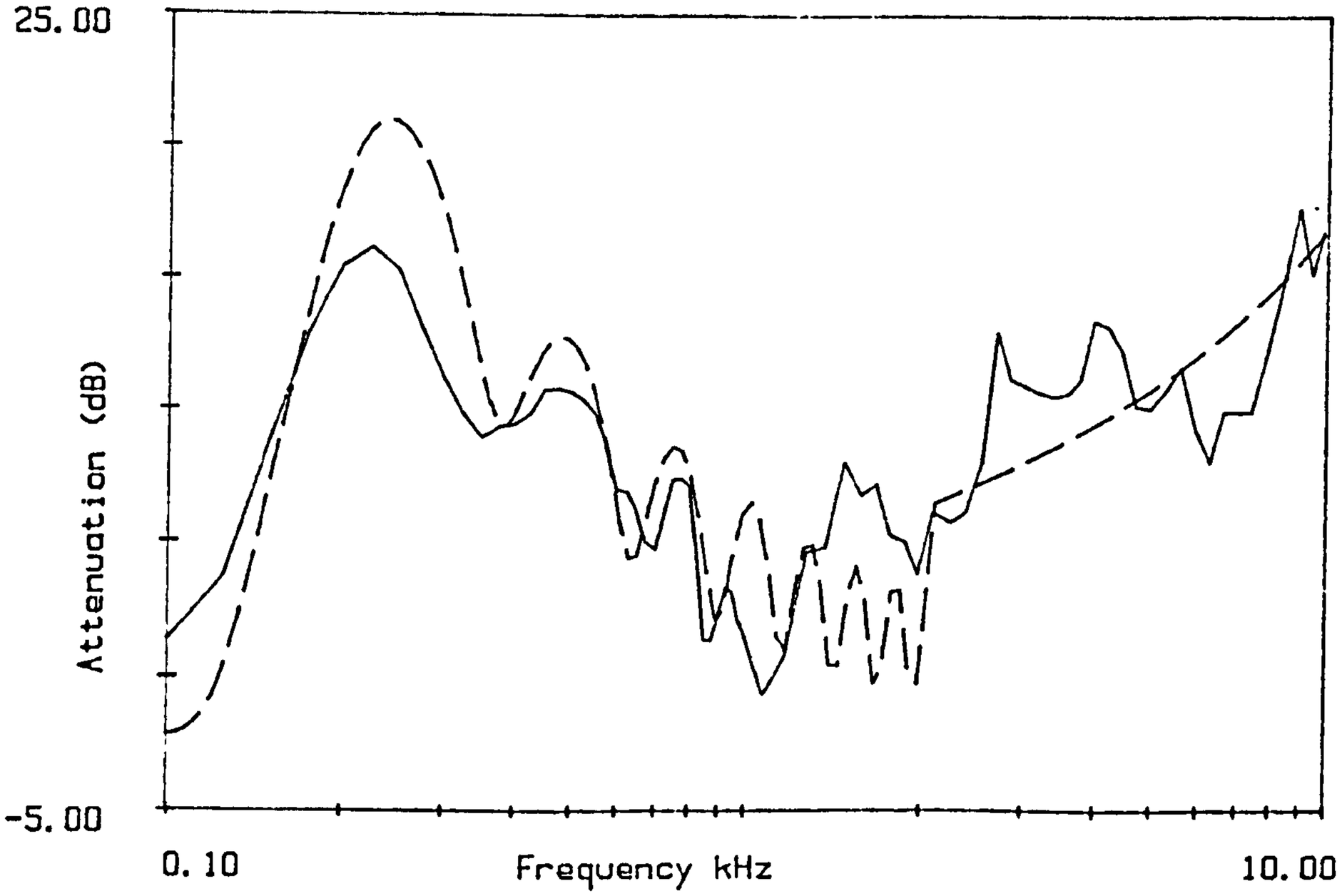

Figure 8.34
Measured attenuation from Hazelborough Wood 9/8/84;
Separation distance 48m, H track, 1.2m microphone height,
Prediction using homogeneous approximation σ e = 40,000; to 2kHz.
+ scattering radius= 0.045, density = 0.1068, rigid cylinders
+ radius= 0.001, density = 70 . σ e = 1,900,000

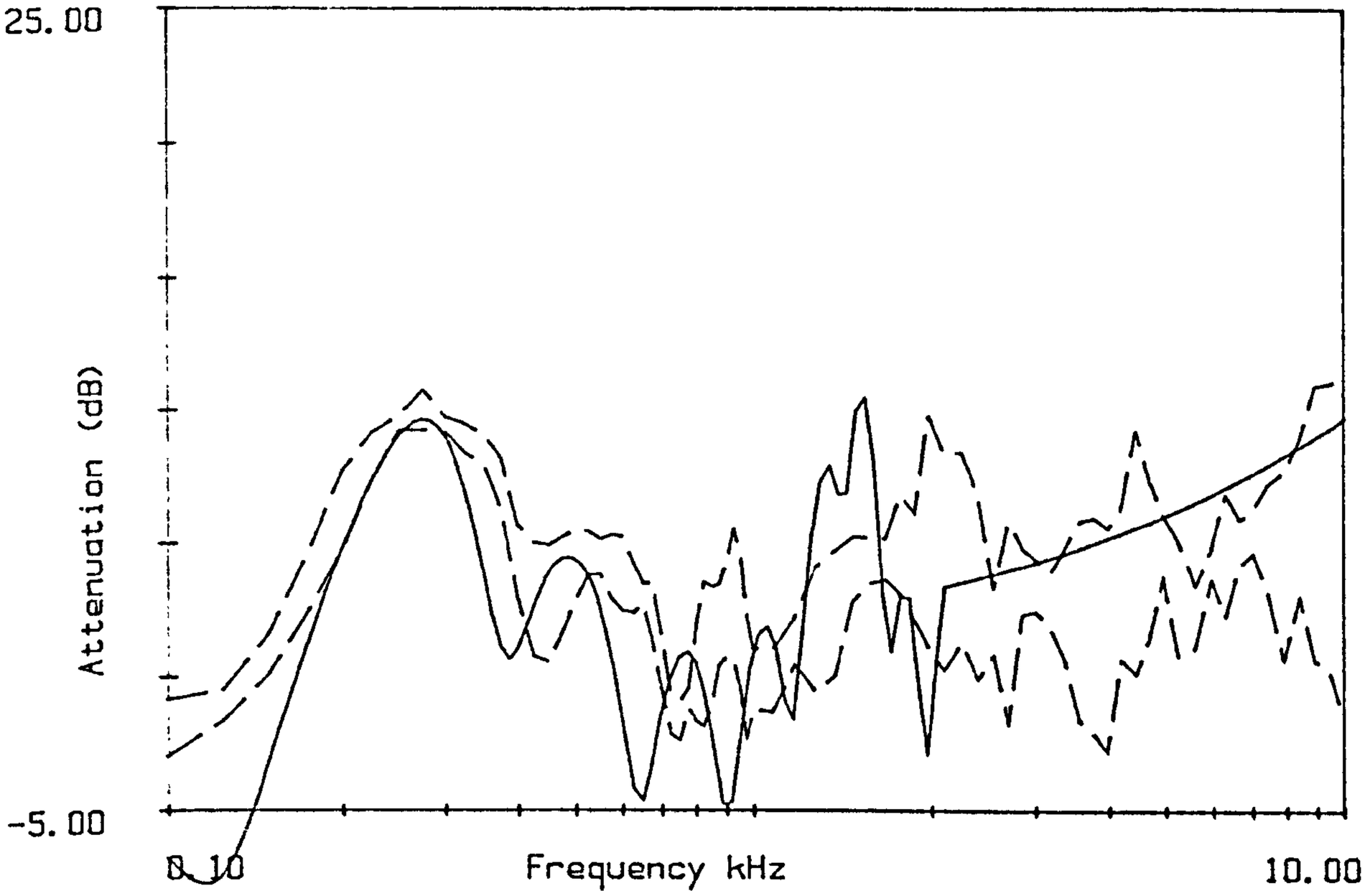

Figure 8.35
Range of values for Bucknell Wood 12m separation.
Prediction using homogeneous approximation σe = 68.000; to 2kHz.
+ scattering radius= 0.066, density = 0.0724, rigid cylinders
+ radius= 0.001, density = 100 . σe = 860.000

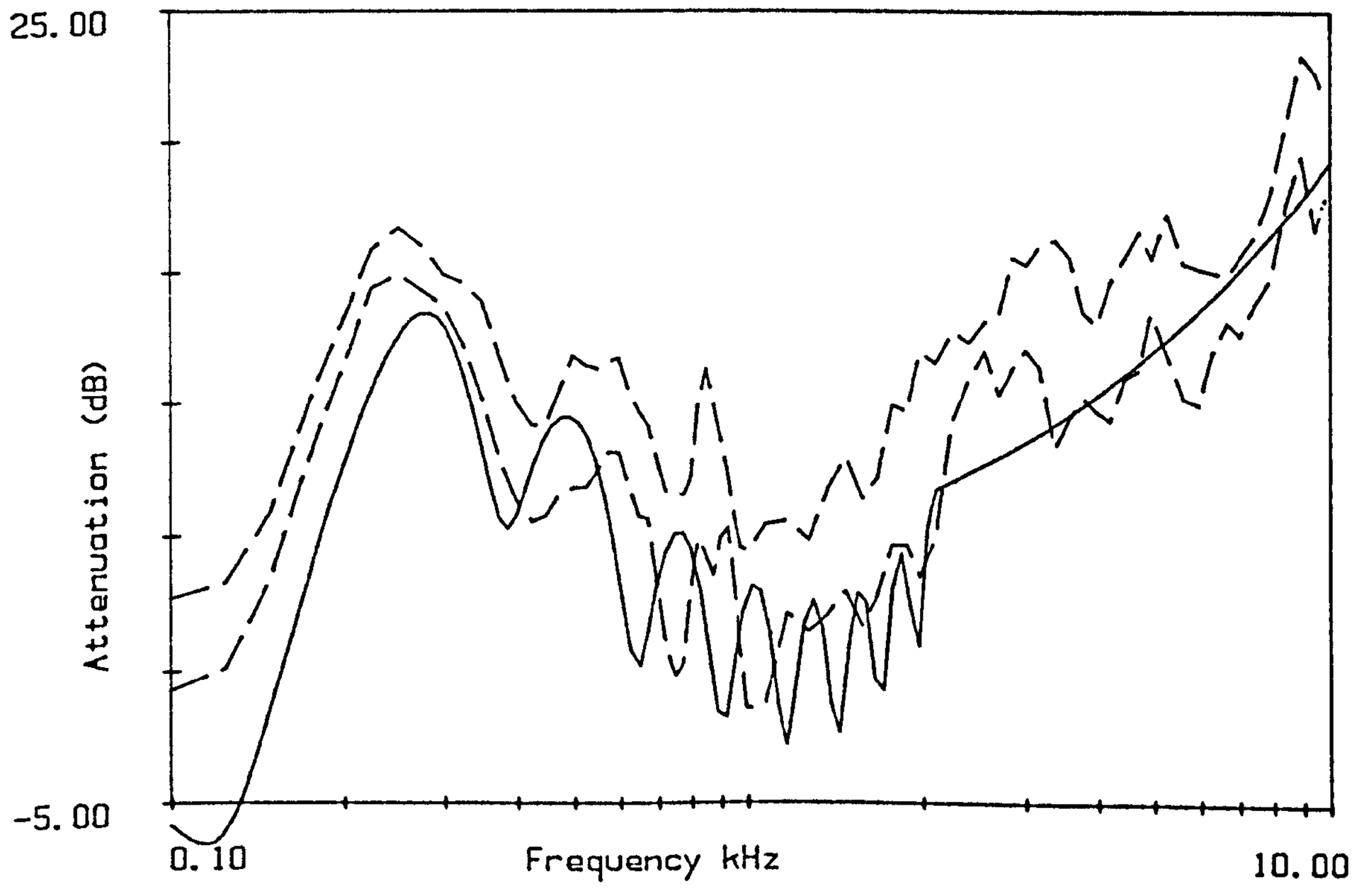

Figure 8.36
Range of values for Bucknell Wood 24m separation.
Prediction using homogeneous approximation σe = 68.000; to 2kHz.
+ scattering radius= 0.066, density = 0.0724, rigid cylinders
+ radius= 0.001, density = 100 . σe = 860.000

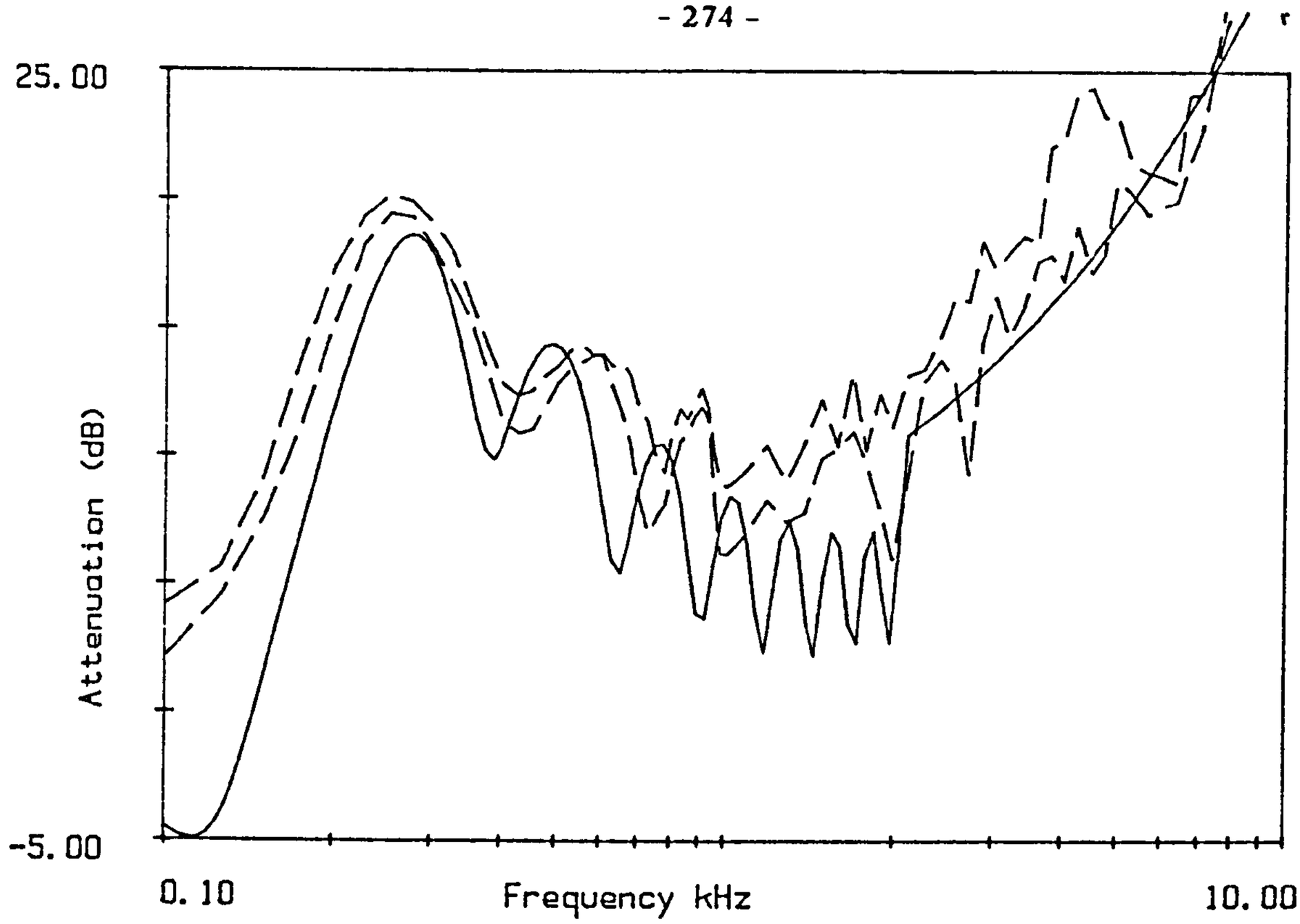

Figure 8.37
Range of values for Bucknell Wood 40m separation.
Prediction using homogeneous approximation σ_e = 68,000; to 2kHz.
+ scattering radius= 0.066, density = 0.0724, rigid cylinders
+ radius= 0.001, density = 100 , σ_e = 860,000

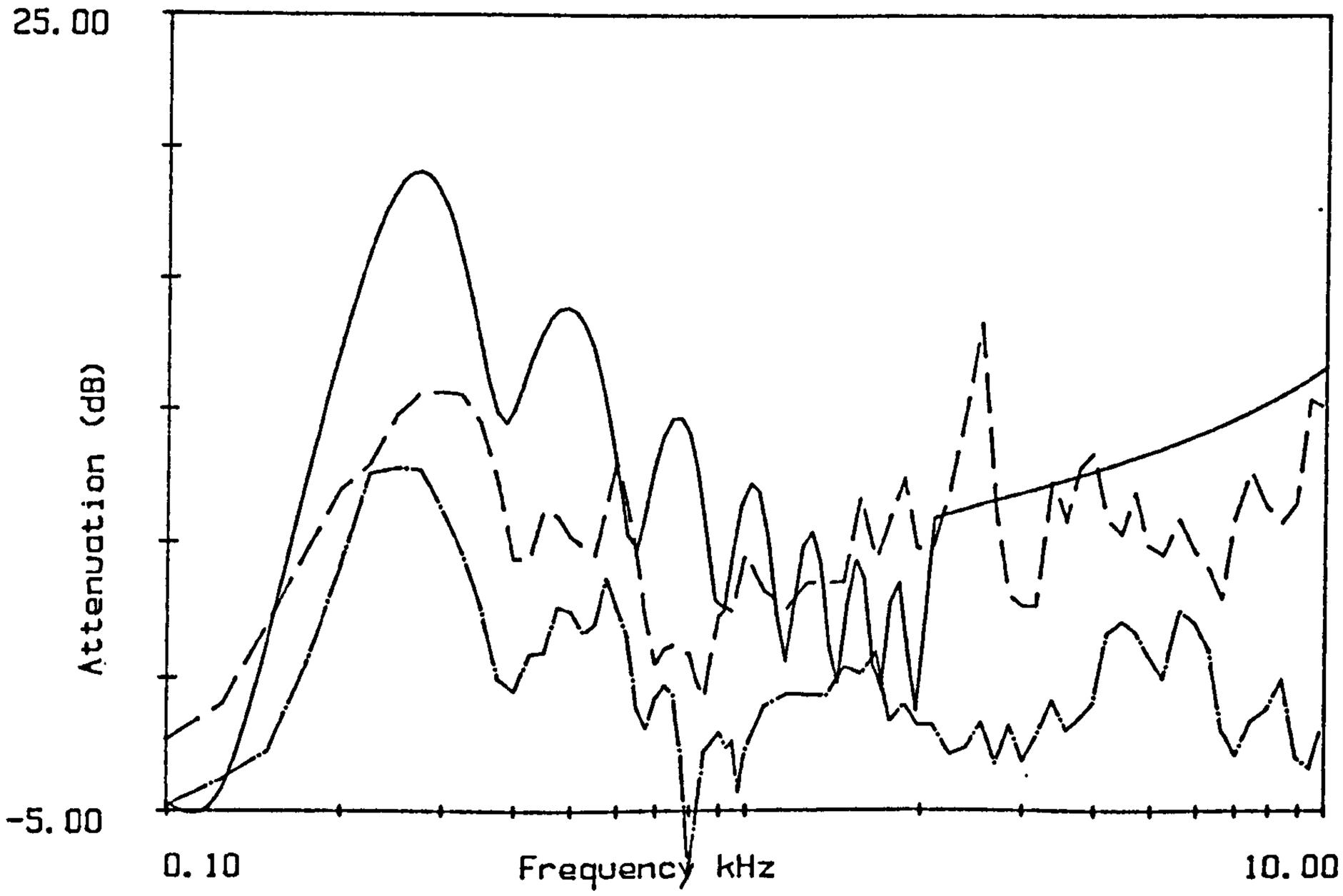

Figure 8.38
Range of values for Wetleys Wood 12m separation.
Prediction using homogeneous approximation σ_e = 68,000; to 2kHz.
+ scattering radius= 0.059, density = 0.1212, rigid cylinders
+ radius= 0.001, density = 100 , σ_e = 10,000,000

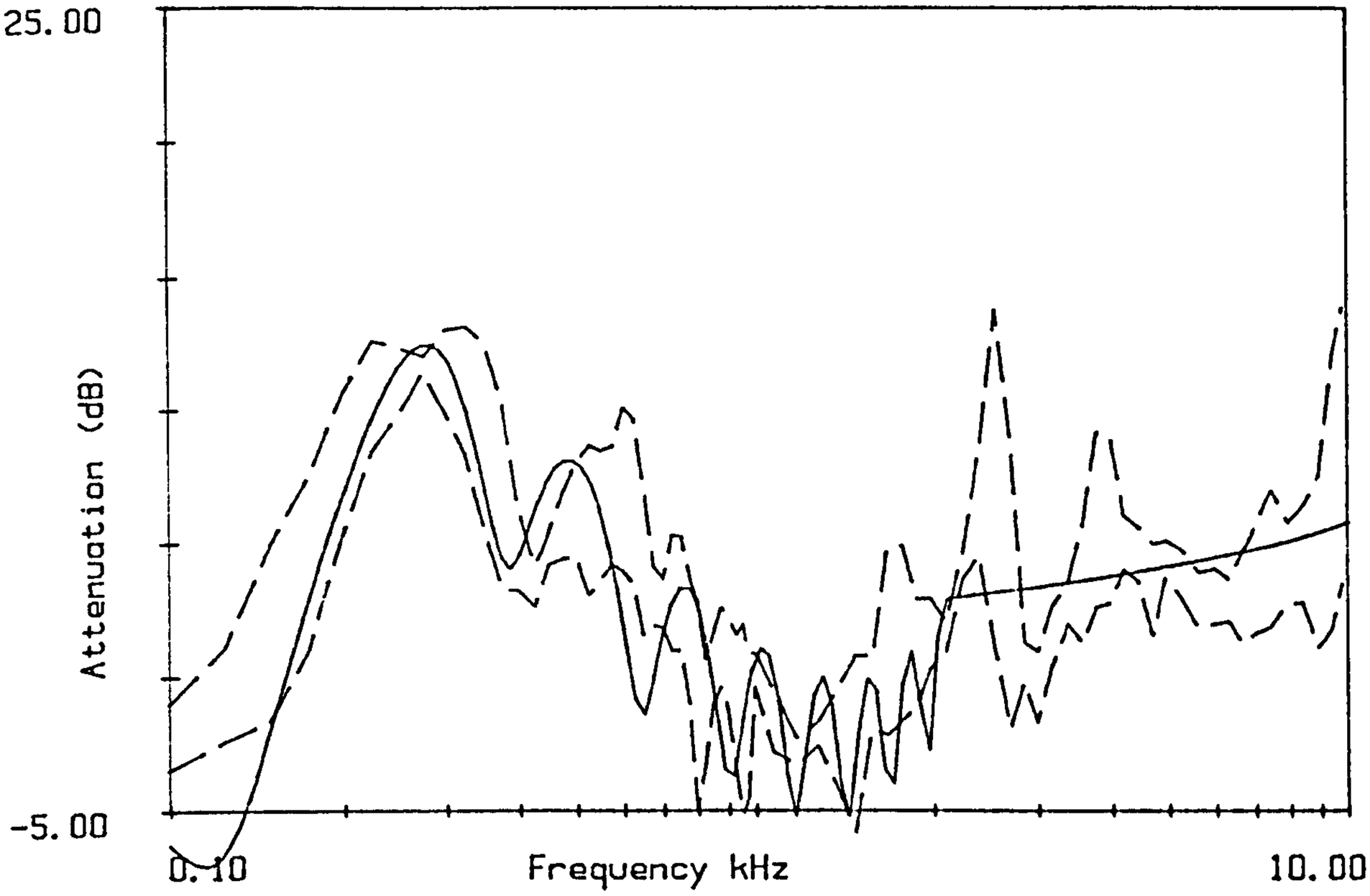

Figure 8.39
Range of values for Wetleys Wood 24m separation.
Prediction using homogeneous approximation σe = 68,000; to 2kHz.
+ scattering radius= 0.059, density = 0.1212, rigid cylinders
+ radius= 0.001, density = 100 , σe = 10,000,000

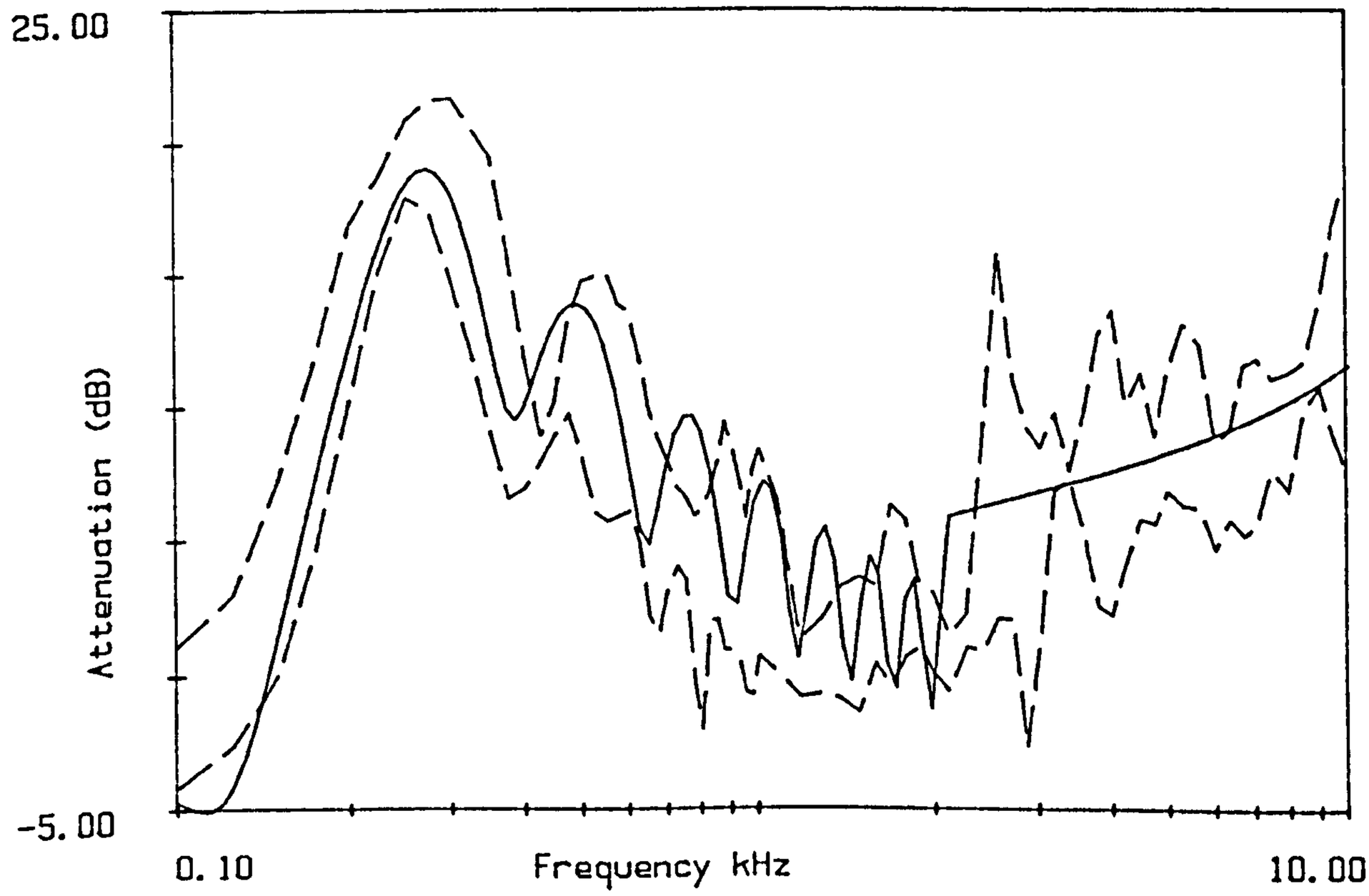

Figure 8.40
Range of values for Wetleys Wood 48m separation.
Prediction using homogeneous approximation σe = 68,000; to 2kHz.
+ scattering radius= 0.059, density = 0.1212, rigid cylinders
+ radius= 0.001, density = 100 , σe = 10,000,000

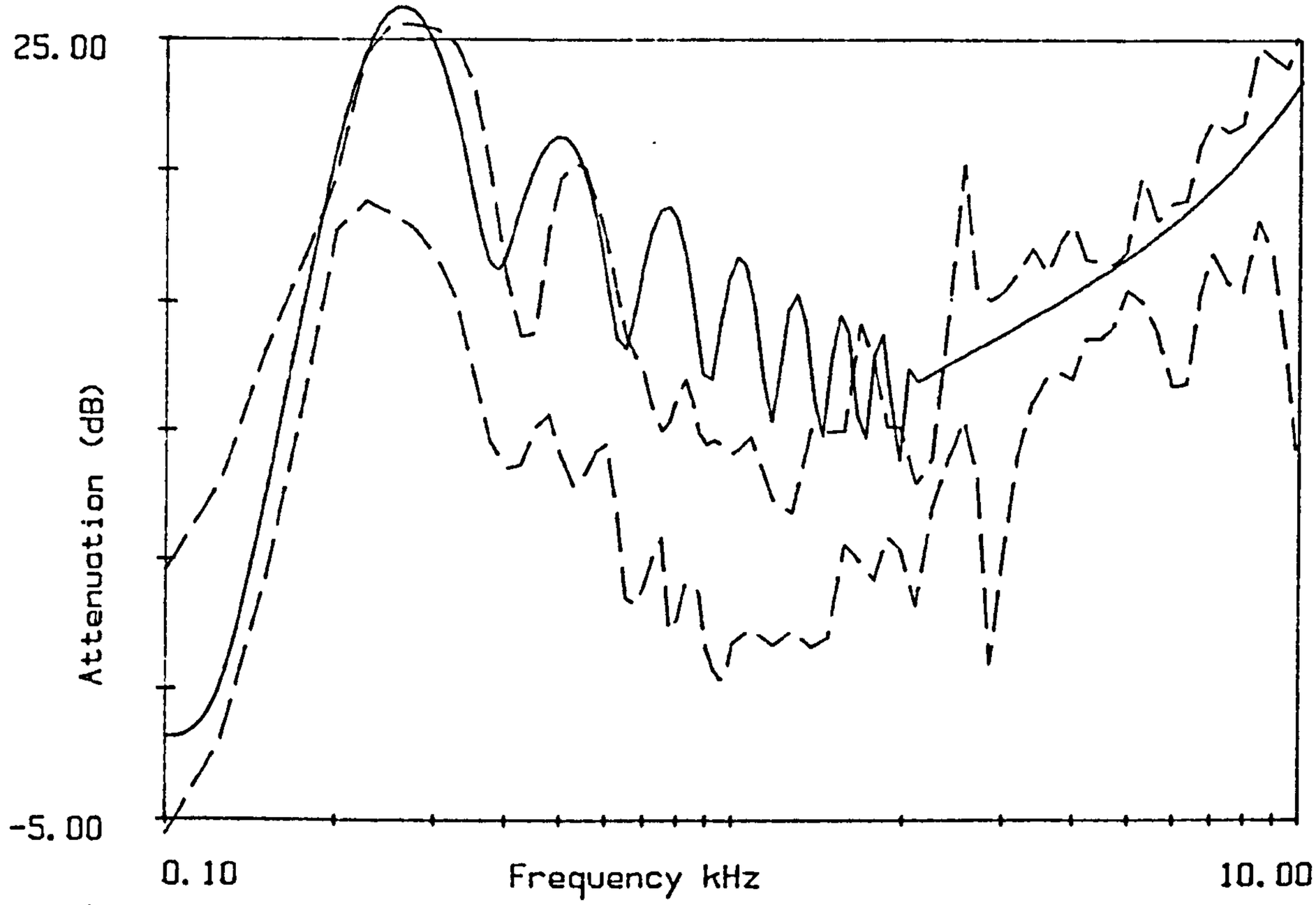

Figure 8.41
Range of values for Wetleys Wood 96m separation.
Prediction using homogeneous approximation σe = 68,000; to 2kHz.
+ scattering radius= 0.059, density = 0.1212, rigid cylinders
+ radius= 0.001, density = 100 . σe = 10,000,000

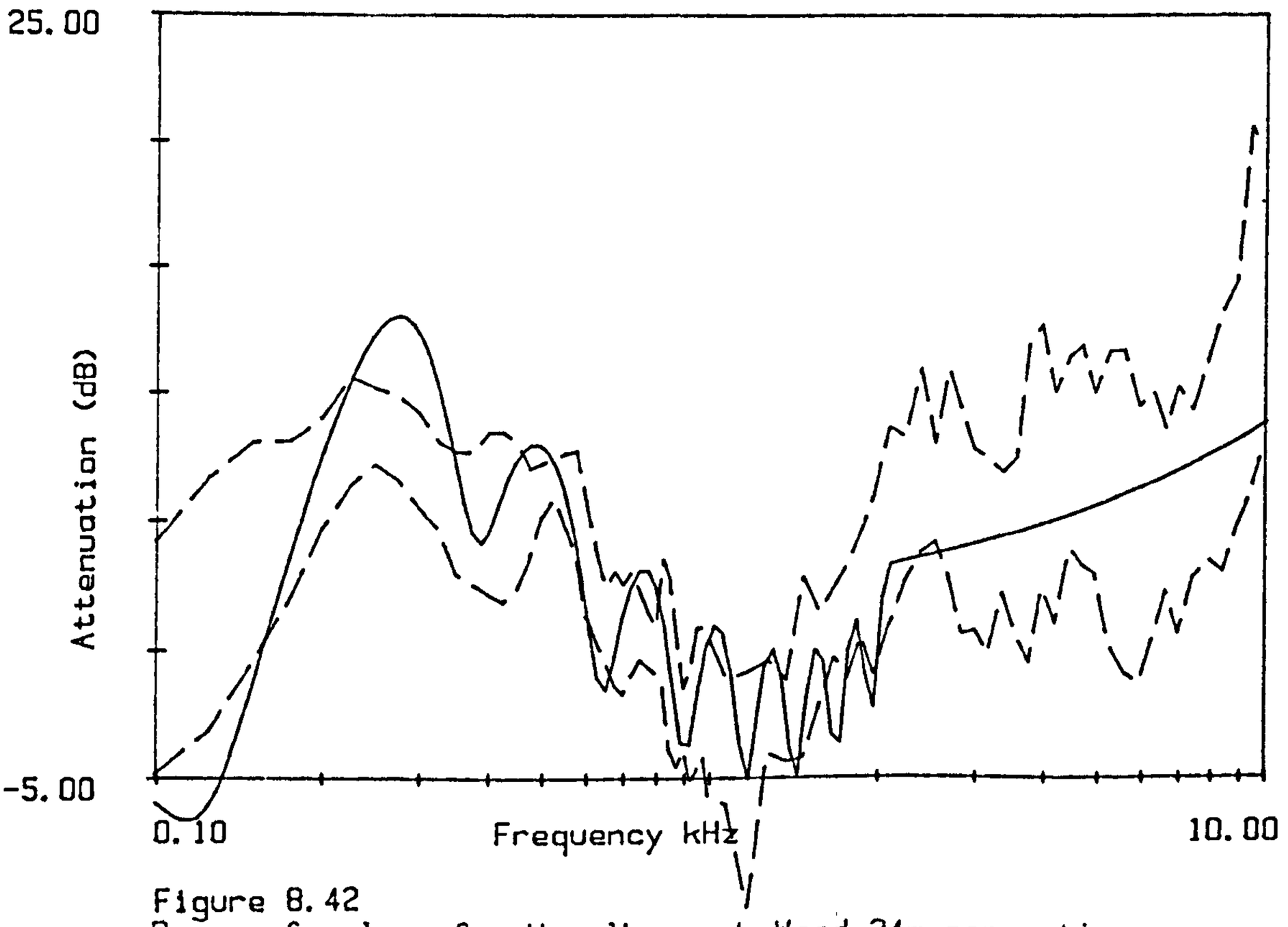

Figure 8.42
Range of values for Hazelborough Wood 24m separation.
Prediction using homogeneous approximation σe = 63,000; to 2kHz.
+ scattering radius= 0.045, density = 0.1068, rigid cylinders
+ radius= 0.001, density = 70 . σe = 1,900,000

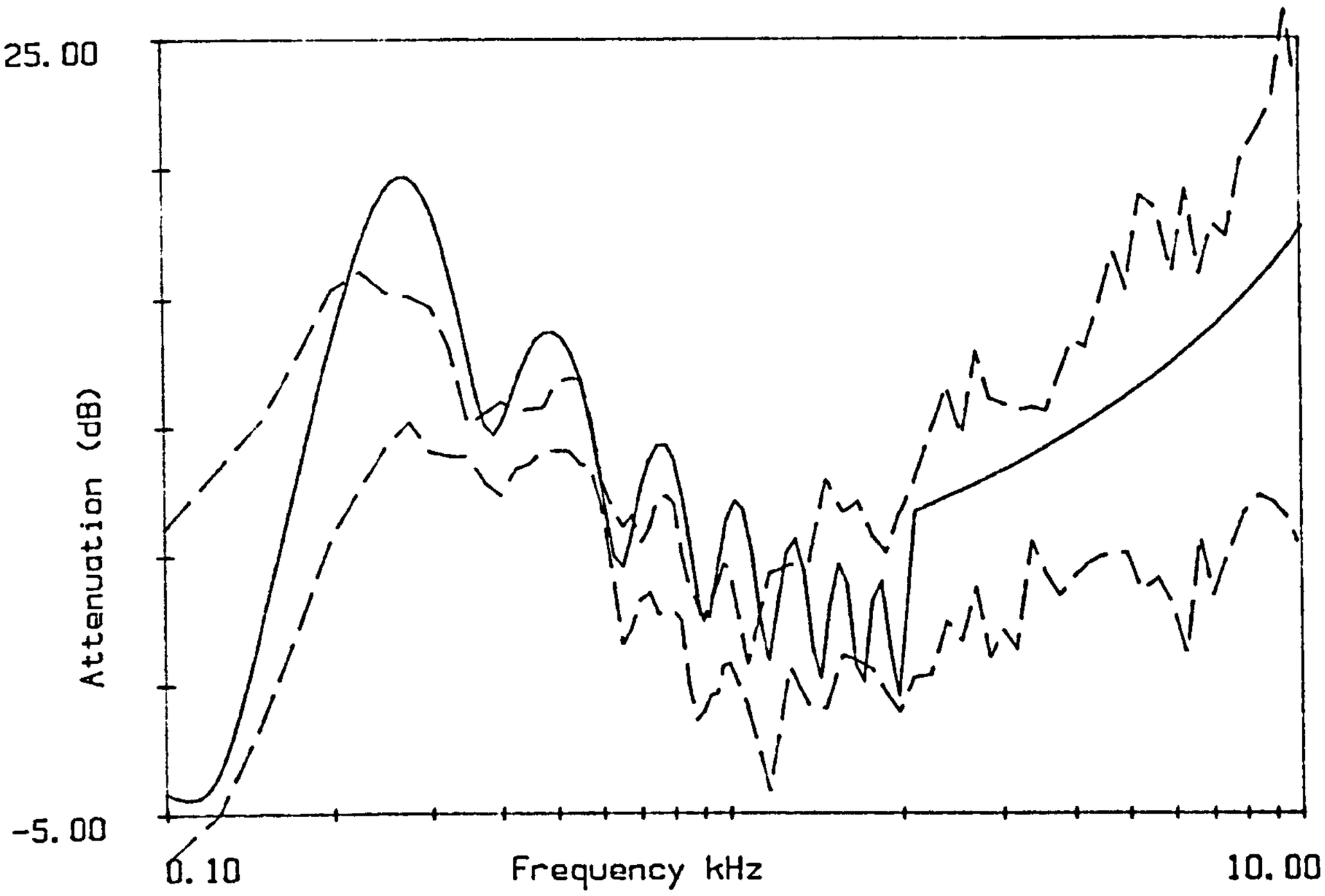

Figure 8.43
Range of values for Hazelborough Wood 48m separation.
Prediction using homogeneous approximation σ_e = 63,000; to 2kHz.
+ scattering radius= 0.045, density = 0.1068, rigid cylinders
\+ radius= 0.001, density = 70 , σ_e = 1,900,000

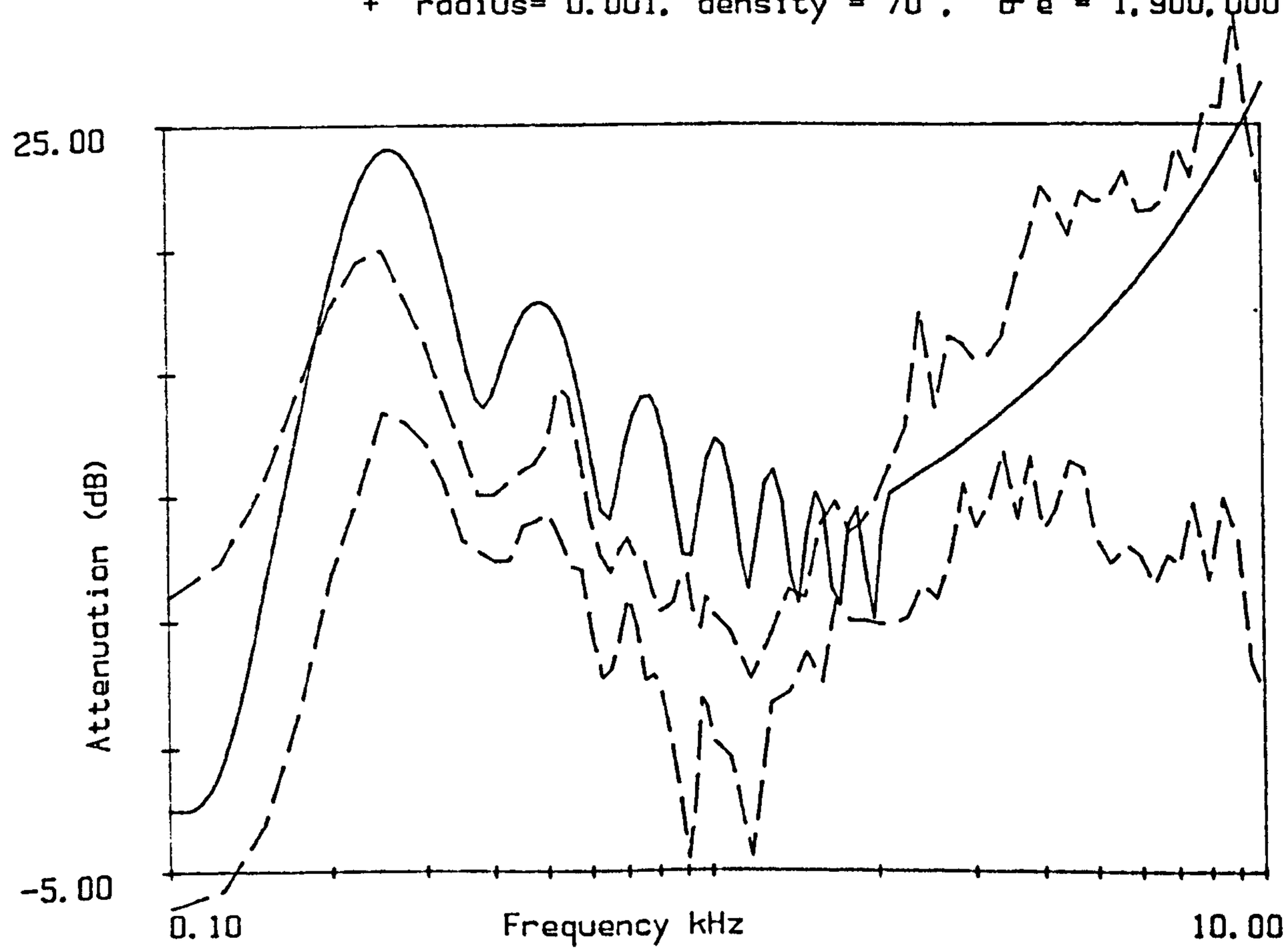

Figure 8.44
Range of values for Hazelborough Wood 72m separation.
Prediction using homogeneous approximation σ_e = 63,000; to 2kHz.
+ scattering radius= 0.045, density = 0.1068, rigid cylinders
\+ radius= 0.001, density = 70 , σ_e = 1,900,000

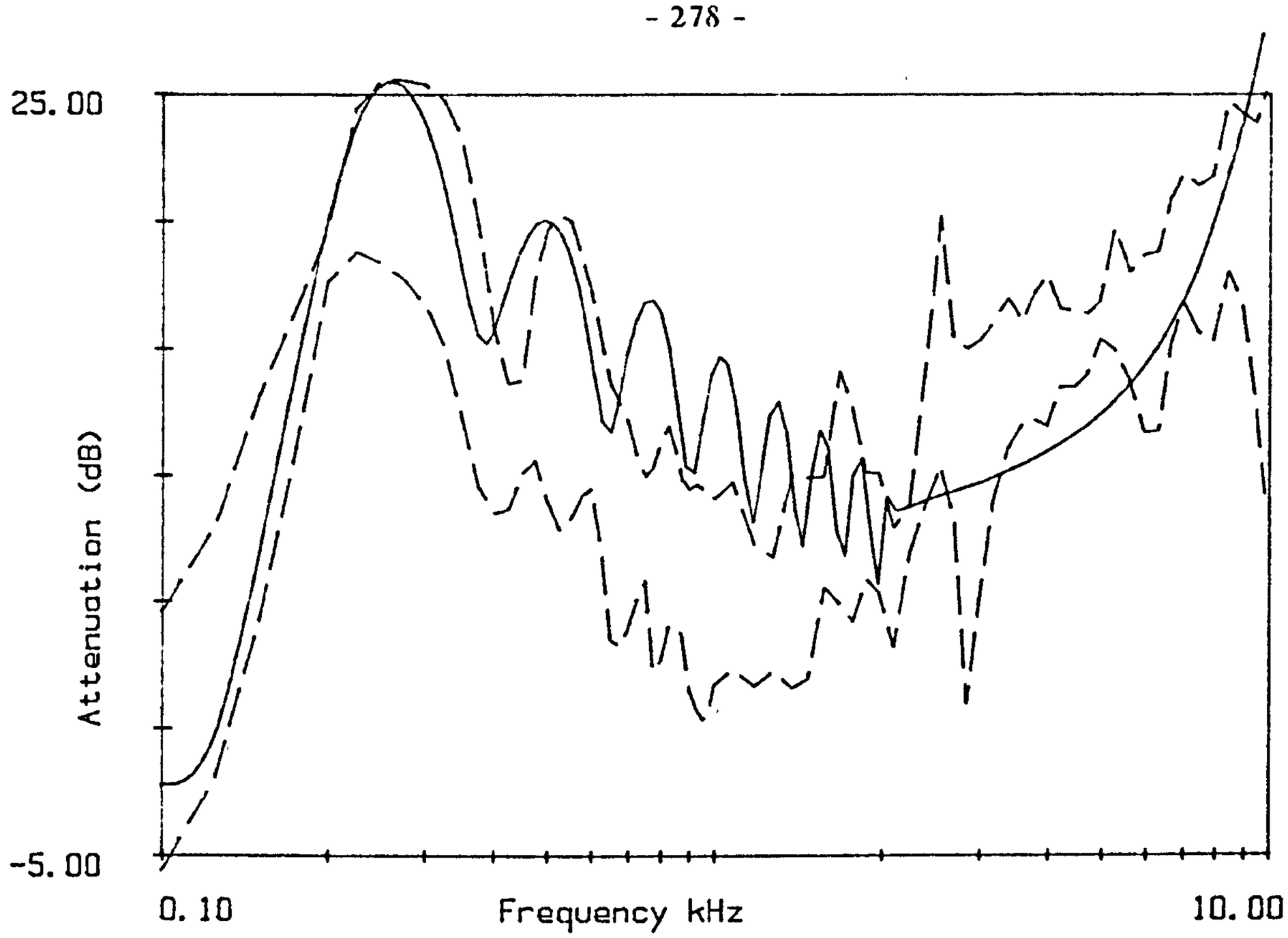

Figure 8.45
Range of values for Wetleys Wood 96m separation.
Prediction using homogeneous approximation σe = 68,000; to 2kHz.
+ scattering radius= 0.059, density = 0.1212, rigid cylinders
+ radius= 0.0019, density = 80 , rigid cylinders

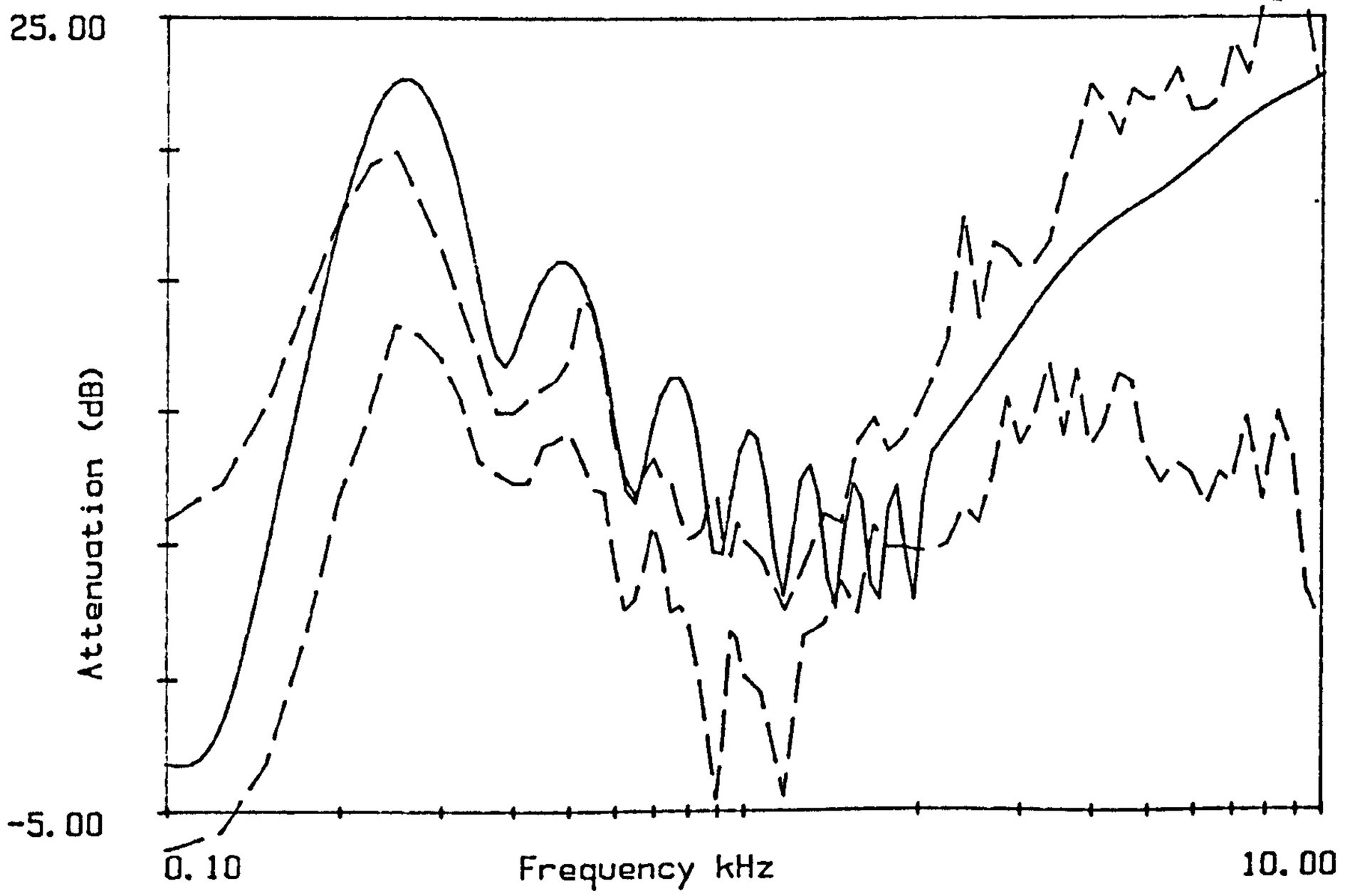

Figure 8.46
Range of values for Hazelborough Wood 72m separation.
Prediction using homogeneous approximation σe = 63,000; to 2kHz.
+ scattering radius= 0.045, density = 0.1068, rigid cylinders
+ radius= 0.0131, density = 1.5 , rigid cylinders.

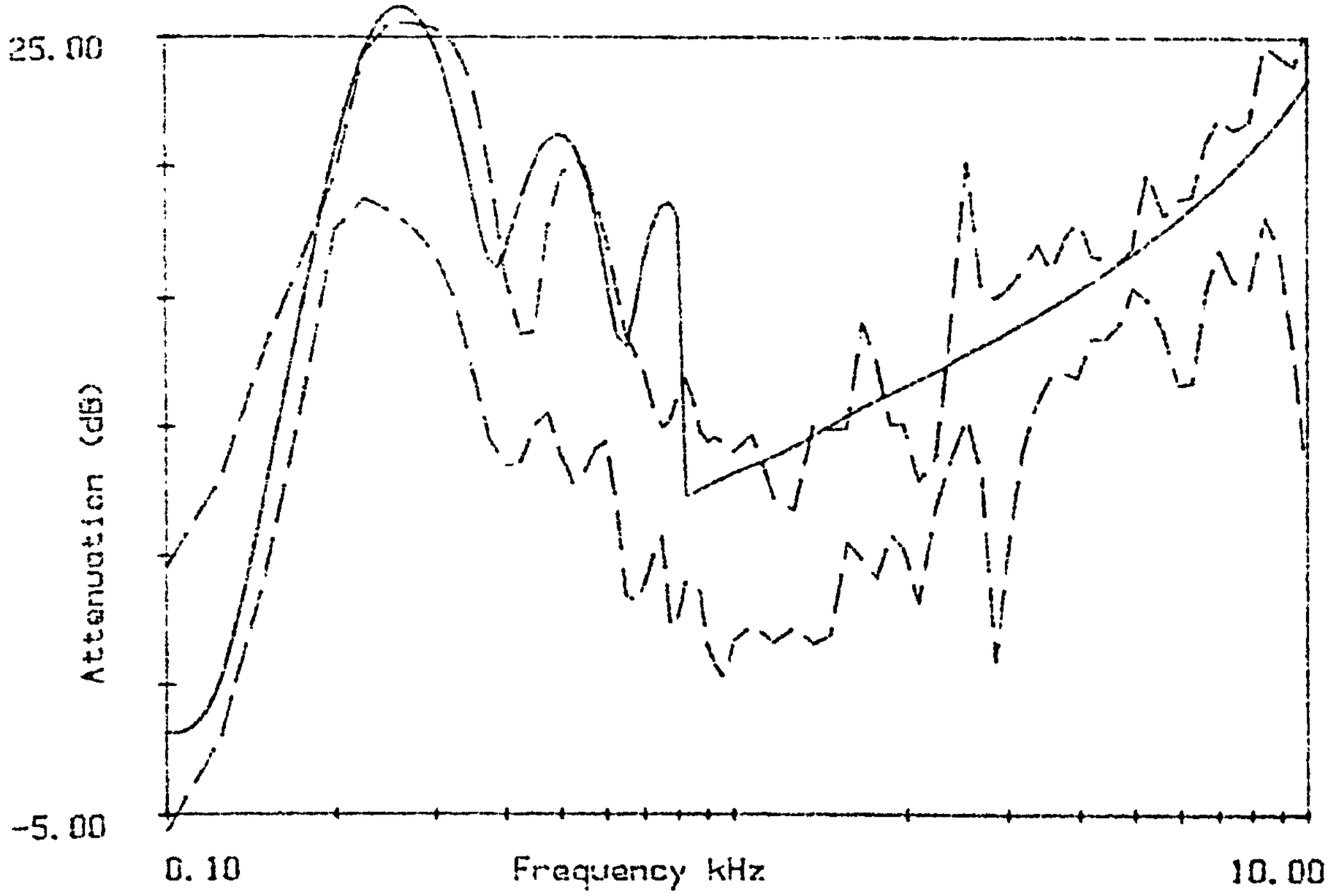

Figure 8.47
Range of values for Wetleys Wood 96m separation.
Prediction using homogeneous approximation σ_e = 68.000; to 800Hz.
+ scattering radius= 0.059. density = 0.1212. rigid cylinders
+ radius= 0.0019. density = 80 . rigid cylinders

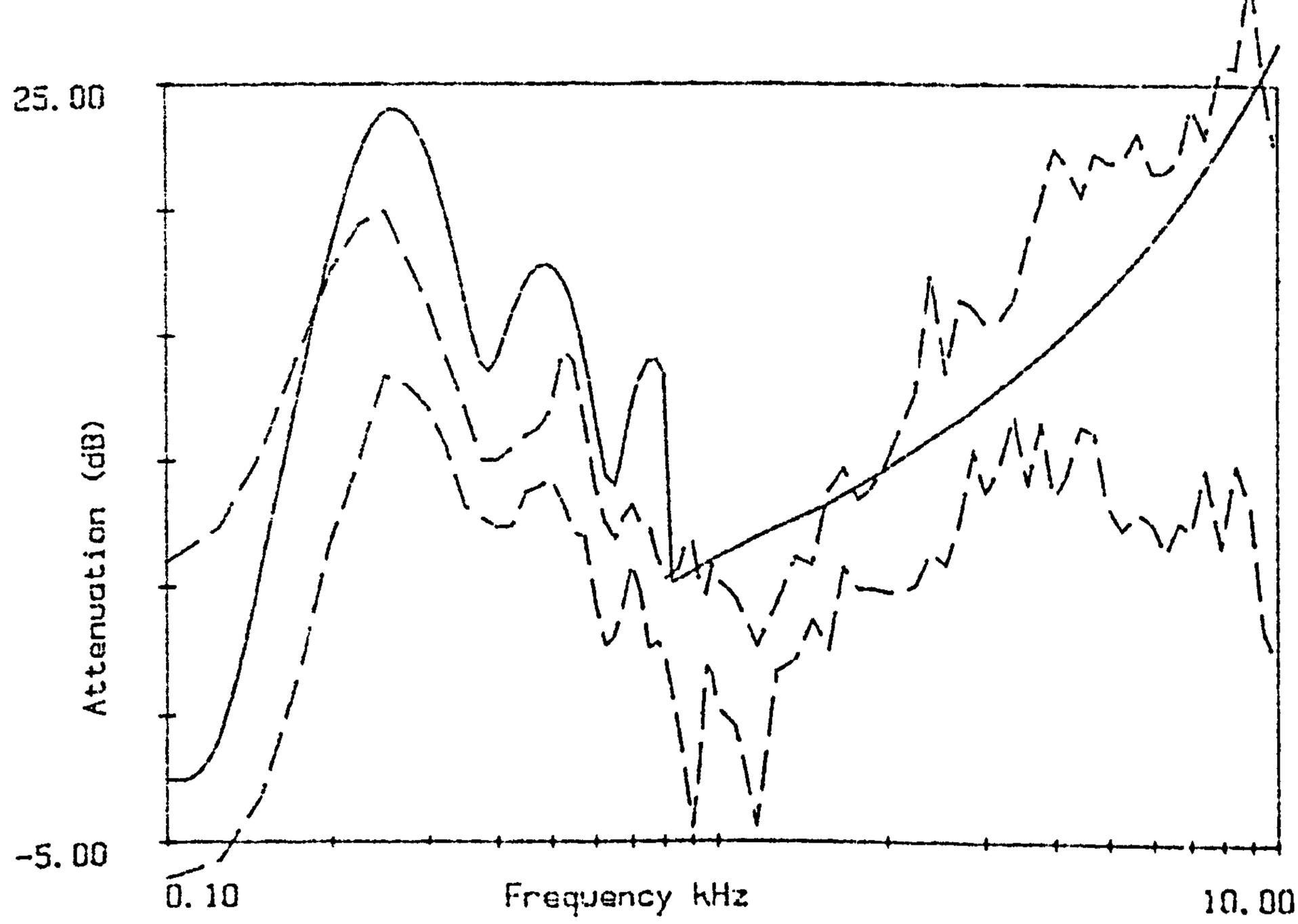

Figure 8.48
Range of values for Hazelborough Wood 72m separation.
Prediction using homogeneous approximation σ_e = 63.000; to 800Hz.
+ scattering radius= 0.045. density = 0.1068. rigid cylinders
+ radius= 0.0131. density = 1.5 . rigid cylinders.

8.5 Practical Applications of the Results of This Study.

The combination of the ground and scattering models as described above provides the basis of a prediction scheme which could be used to determine the likely effect of an existing, or planned, area of woodland on the transmission of sound with any frequency distribution, for planning purposes, acoustic ranging etc. The model illustrated in comparison with the attenuation measurements can easily be adapted to give predictions of excess attenuation, the measurement most often used in studies of outdoor sound propagation. All three parameters of the second array were altered in section 8.3 to obtain a good fit to the attenuation data but it seems that a good fit to all of the data could be obtained by maintaining a radius of 0.001m and a density of 100 stems/m^2 and altering the input surface impedance according to the foliage density. Figures 8.49 and 8.50 illustrate model predictions of excess attenuation using the range of values of surface impedance (σ_e), of the small arrays, obtained in the fitting routines. The ground model uses the mean value of σ_e for all the woodlands (68,000 mks rayls). Graphs such as these could be used directly to estimate excess attenuation by classifying the woodland as 'dense' (zone a), 'less dense' (zone b) and 'open' (zone c). A requirement for the use of this prediction would be that the floor of the woodland is of an undisturbed woodland floor type, ie. with a litter layer of uncompacted leaves.

Kragh et al. (1982) described a prediction scheme which accounts for the attenuation of sound by woodland (see chapter 2) and also that caused by a soft ground. The result of calculating the sum of these two factors for 50m and 100m of woodland is illustrated in figures 8.51 and 8.52. The ISO working group number 24 (ISO 1986) propose a similar model, the result of this scheme is also illustrated. The two schemes apply the same correction factor for woodland attenuation for each third-octave above 250Hz, but the ISO scheme allows only one such correction for each belt of woodland whereas the Kragh et al. scheme adds this factor for each 50m of woodland present. The ISO scheme, however, has an additional factor of 1dB/100m at 4kHz and 5dB/100m at 8kHz, thus the two schemes account for increased attenuation with distance, but in different ways. Both schemes state that the vegetation should be dense but do not distinguish between woodlands of different densities. Both prediction schemes underestimate the attenuation measured in this study, even that in

the least dense woodlands.

To predict the attenuation through a substantial belt of trees with a well-developed structure of dense undergrowth, the scattering model calculated for the width of the belt could be added in the same way to a prediction of attenuation calculated either using the ground parameters appropriate to the surrounding terrain, or, perhaps, a model of sound propagation over mixed impedances such as those presented by Heap(1982) to account for the different ground impedances under the trees and on the surrounding terrain.

The use of sound to determine vegetation density is an attractive idea since it could be a convenient, non-destructive means of sampling woodland density. The analysis of the results at Bucknell Wood on 2nd July 1985 illustrates some of the limitations to using broad-band attenuation measurements for such a purpose. The shorter distance measurements are evidently greatly affected by the ground interference effects, therefore little information about the attenuation due to other woodland elements can be gained, so small scale differences in vegetation cannot be assessed.

Section 6.3 describes some results, from Wetleys Wood, in which the interference patterns can still be determined at 48m separation, in the mid-frequencies, whereas in the measurements described from Bucknell Wood, 26m is considered to be sufficient distance to eliminate the interference effects. This phenomenon is related to the disruption of the interference patterns by scattering, thus the scattering effects are considerably greater in the dense, mixed coniferous wood than the more open spruce monoculture. The loss of the interference peaks in the high frequencies could also prove to be a useful indicator of the density of the stand. It should, however, be noted that the loss of these peaks is likely to be affected by turbulence effects which would be greater in the more open, dense, mixed coniferous stand than under the closed canopy of the spruce monoculture.

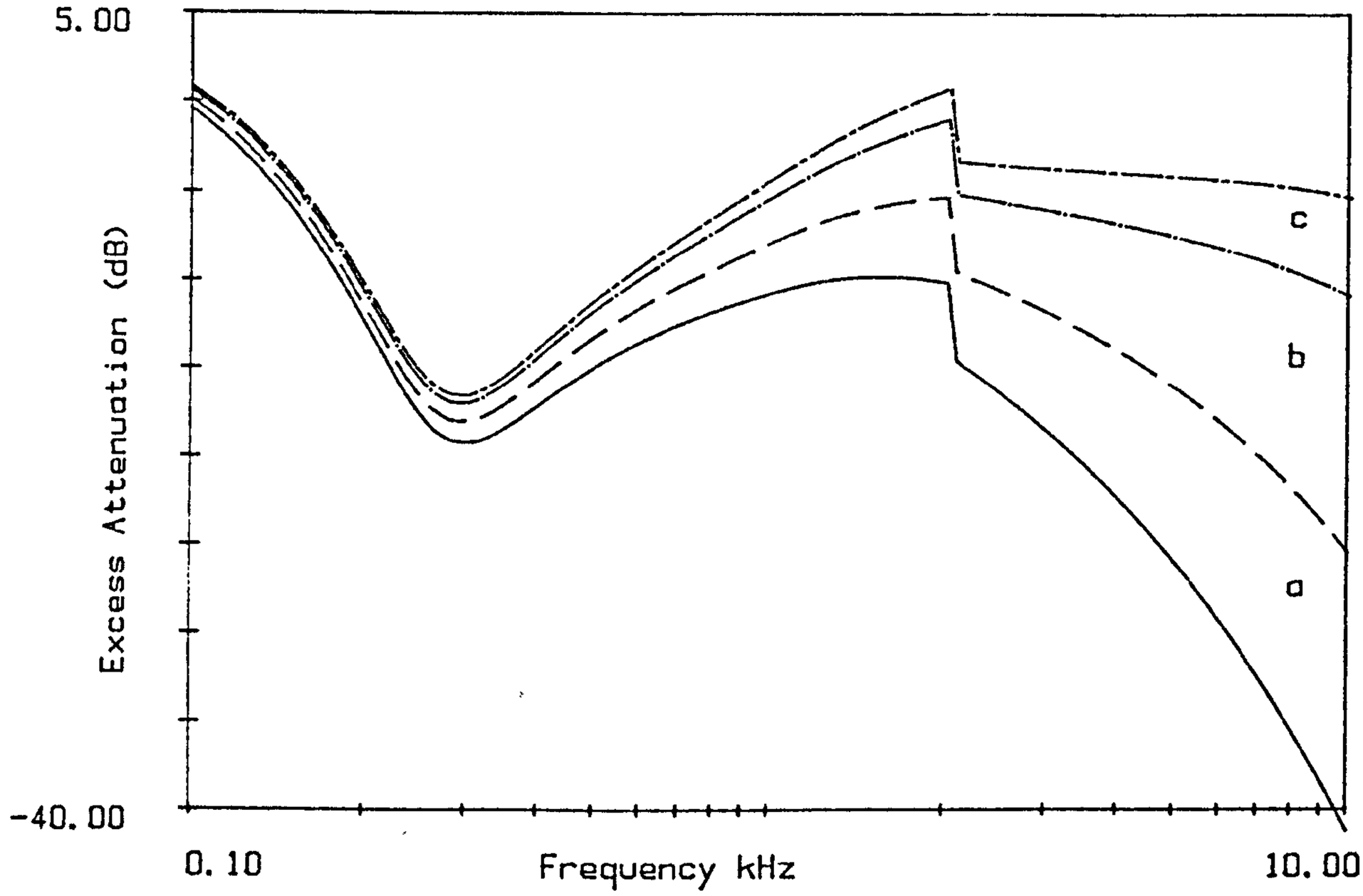

Figure 8.49
Excess attenuation at 50m, source and receiver height 1.2m.
Prediction using homogeneous approximation σe = 68,000; to 2kHz.
+ scattering radius= 0.057, density = 0.1, rigid cylinders
+ radius= 0.001, density = 100, o e = ——— 860,000.
— — — 1,900,000, ——— 10,000,000 ——— rigid.

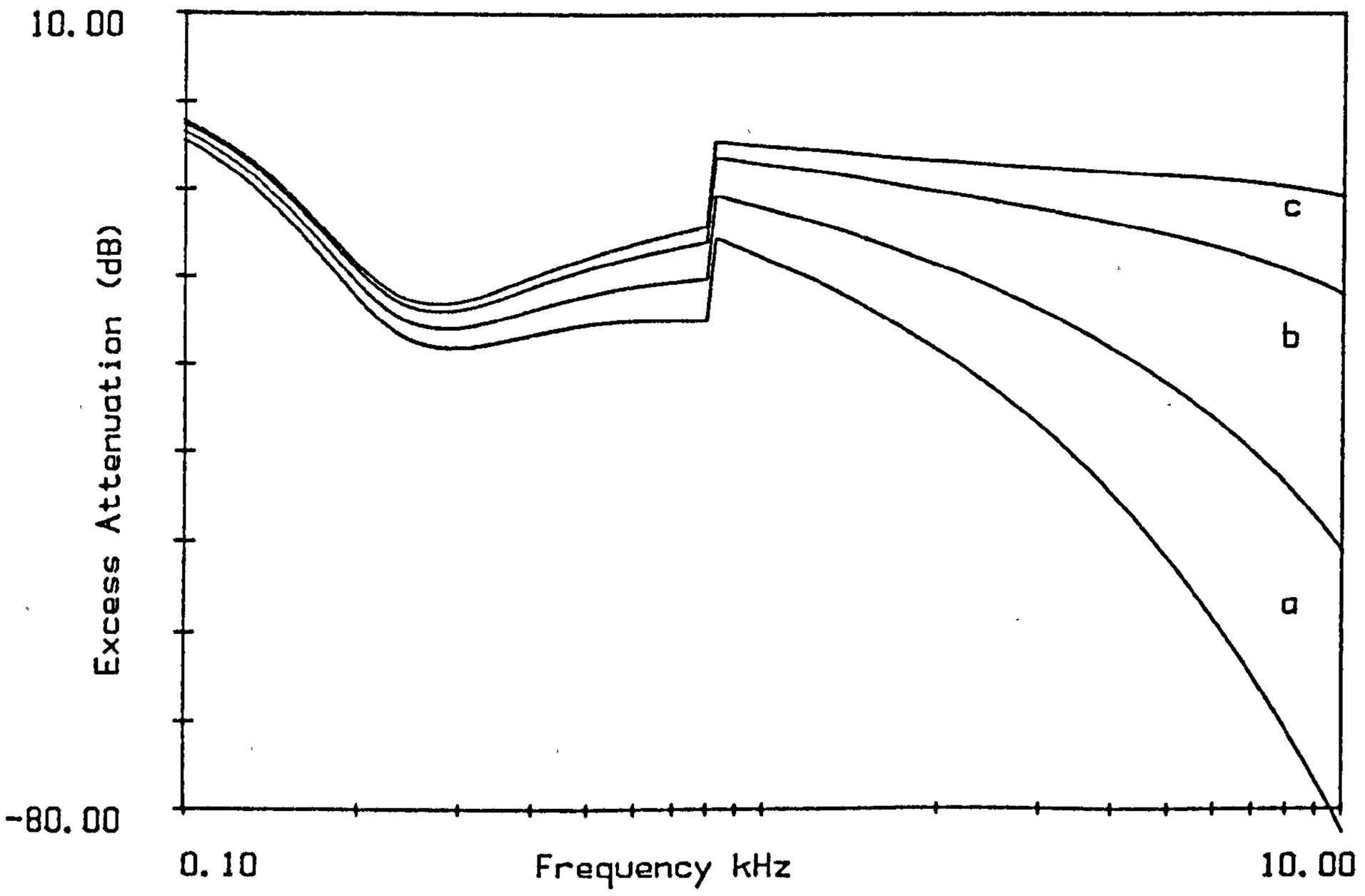

Figure 8.50
Excess attenuation at 100m, source and receiver height 1.2m.
Prediction input parameters as in figure 8.46.
The ground model prediction is only used to 800Hz.

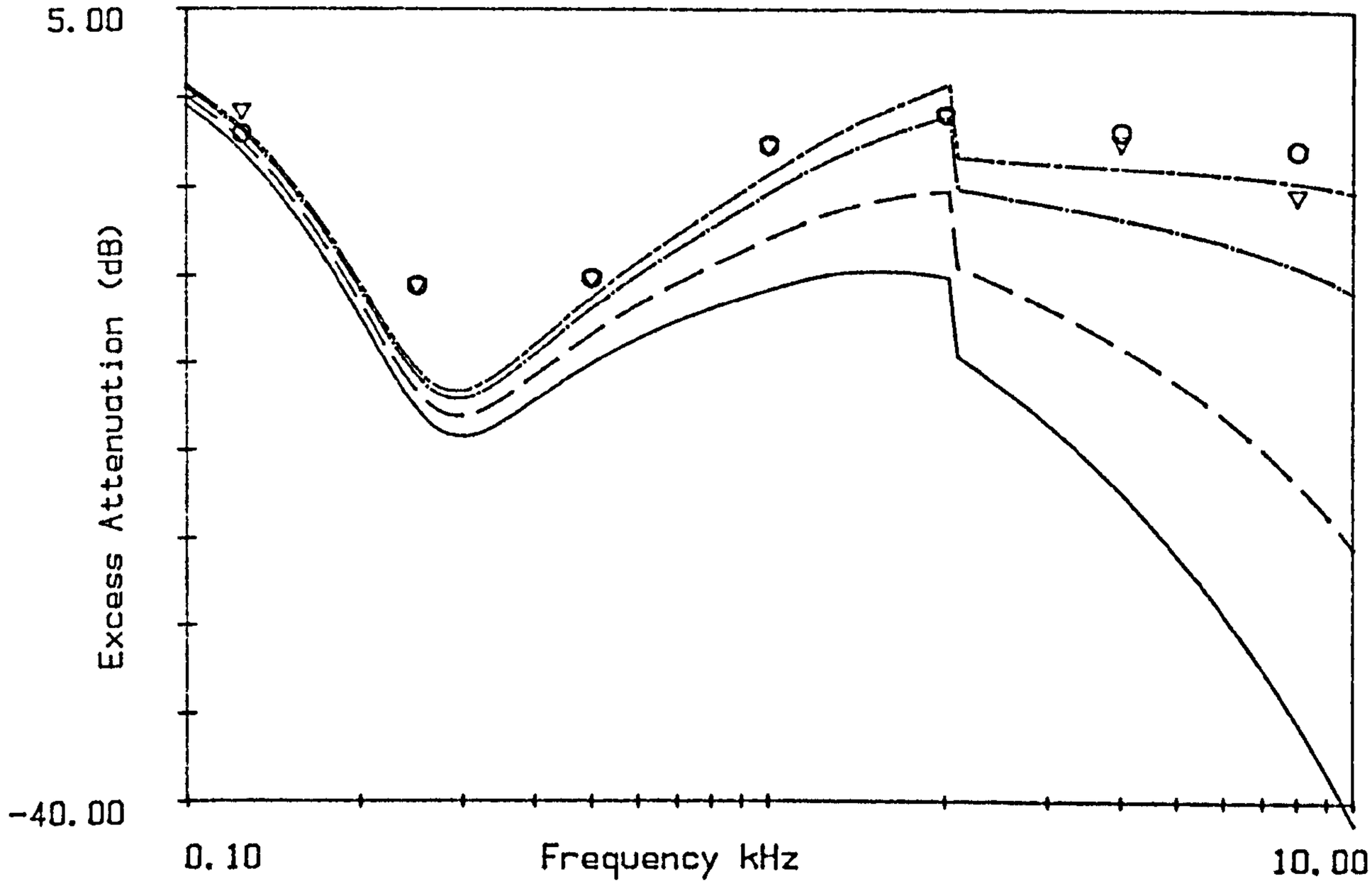

Figure 8.51
Excess attenuation at 50m, as in figure 8.49.
o Prediction from Kragh et al (1982)
∇ Prediction from ISO (1986).

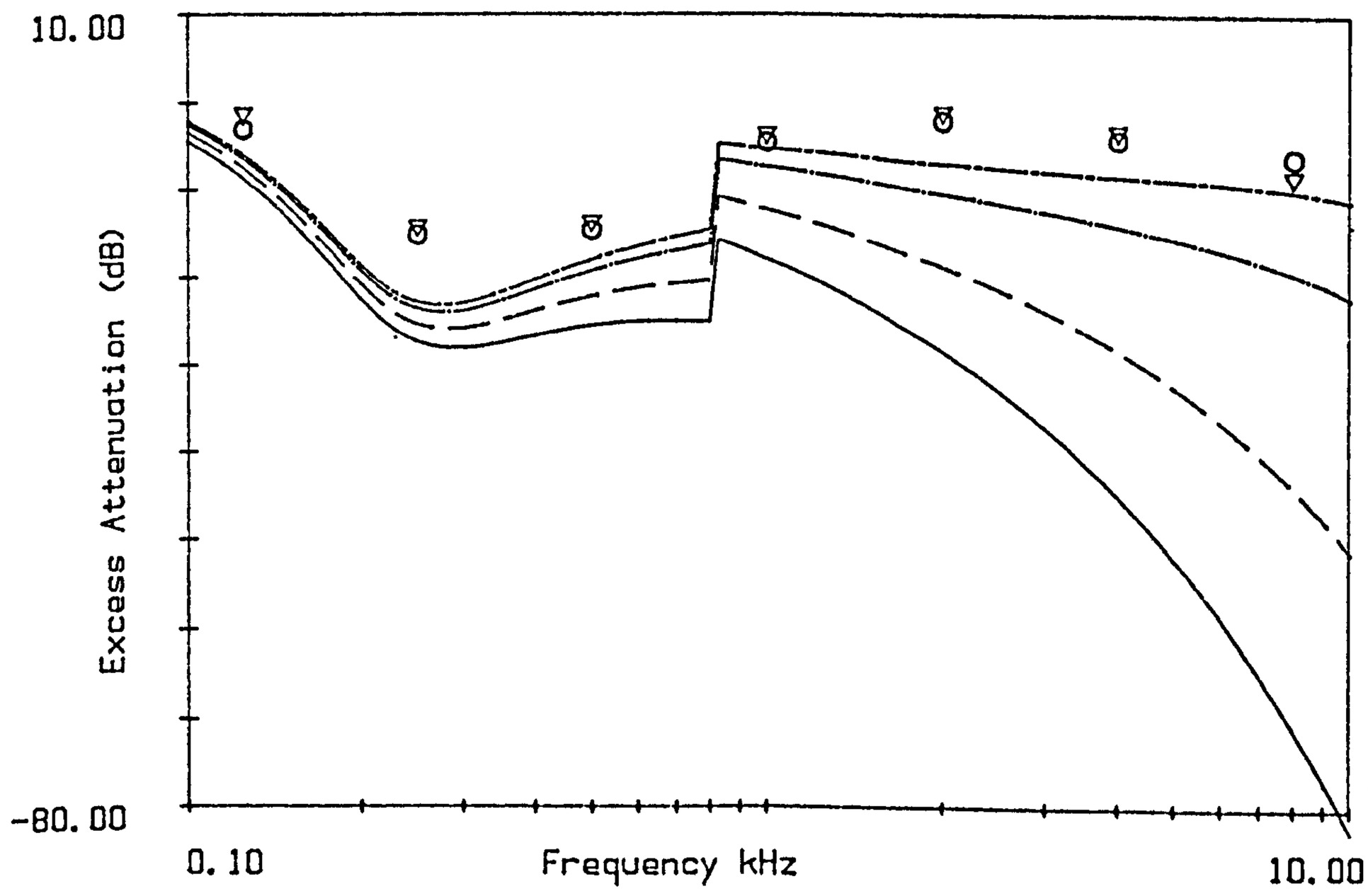

Figure 8.52
Excess attenuation at 100m, as in figure 8.50.
o Prediction from Kragh et al (1982)
∇ Prediction from ISO (1986).

8.6 Suggestions for Further Work.

Further model experiments could usefully be carried out using a larger array and more microphone locations as this would give an overall view of the attenuation. Any prediction of the type presented here must represent an average over a more extensive line of closer receiver locations since there is no consideration of the interference peaks and dips which are still observed in the mean values of the four locations used. Other predictive models could be assessed in the same way and modifications made to account for the distribution of different diameter cylinders within a wood.

This study has demonstrated that the mechanisms of ground interference and absorption, and scattering and absorption by the trunks, foliage and branches affect the acoustical properties of woodland, and that the proportion of the high frequency attenuation attributable to each of these effects depends on the types, and density of trees present. The difficulties of relating measured attenuation to physical and cultural parameters of woodlands has been pointed out by many researchers. Experiments designed to elucidate ways in which physical parameters of trees can be measured and related to their acoustical properties would therefore be advantageous in studies of sound propagation in woodland. These could take the form of measurements through smaller stands which could be effectively sampled for measurements of total biomass and the distribution of different sized elements, a stand such as a coppice could provide such an opportunity.

Experiments to determine the frequency range at which interference effects can be observed, and the extent to which they affect the attenuation, in various woodland situations, would be useful in the further development of the proposed prediction model. Such information could be used to determine the appropriate cutoff frequency for the combined prediction and the way in which the predictions could be combined to give a more realistic spectrum, without the sharp step in the mid-frequencies.

References: Chapter 8.

[1] Attenborough, K. and Hess, H. 1985. Acoustical Surveying of Porous Soils. in ACOUSTICAL IMAGING PROCEEDINGS OF THE FOURTEENTH INTERNATIONAL SYMPOSIUM. 111 - 122.

[2] Aylor, D.E. 1972. Noise Reduction by Vegetation and Ground. J. ACOUST. SOC. AM. 51(1) 197 - 205

[3] Embleton, T.F.W 1966. Scattering by an Array of Cylinders as a Function of Surface Impedance. J. ACOUST. SOC. AM. 40(3). 667 - 670.

[4] Frank, L.D. 1976. Tree Bark and the Forest Floor as Sound Absorbing Elements Within a Forest. MSc THESIS PENNSYLVANIA STATE UNIVERSITY.

[5] Heap, N.W. 1982. Sound Propagation over Mixed Impedances. PhD THESIS. OPEN UNIVERSITY.

[6] Kragh, J. Andersen, and Jakobsen 1982. Environmental Noise From Industrial Plants - General Prediction Method. DANISH ACOUSTICAL LABORATORY REPORT No. 32.

[7] ISO Working Group No 24. 1986. Prediction of Sound Propagation Outdoors. FIRST TEXT PROPOSAL FOR ISO/TC43/SC1/WG24.

[8] Yamada, S., Watanabe, T., Nakamara, S., Yokoyama, H. and Takeoka, S., 1977. Noise Reduction by Vegetation. PROCEEDINGS OF INTERNOISE 1977.

APPENDIX A: FORTRAN Source Code for Programs Referred to in the Text.

A.1 Routines for Analysis of Experimental Data.

Program DIF2MK

```
c     program to calculate field at two microphones in dB
c     and difference between them.
c
      character*35 ifile1,ifile2,ofile1,ofile2,infl
      dimension df(400,4),dn(400,4),an(250),af(250),dbn(250),dbf(250)
      dimension diff(250),fr(250)
      common/head/idat(3),itim(3),sh,rh,sd,rmh,rmd,iav
      common/hed2/fsa,ga,amks,fsb,gb,bmks

      type*,'Run  difin first'
      type*,'input filename containing input data (from DIFIN)'
      read(5,2)infl
      infl='difin.dat'
      ichi=10
      open(unit=10,name=infl,type='old')

c
c     Read in data and put data required for analysis into arrays:
c       i.e.  216 points every  point from 100Hz to 1kHz (25Hz apart)
c             and every other point from 1050hz to 10kHz (50Hz apart)
c

      type*,'first (near) microphone data filename?'
      read(ichi ,2)ifile1
      ifile1='[heap.margaret.d1]'//ifile1
      type*,'nicolet channel?  A=1  B=2'
      read(ichi ,*)ichn
      type*,' sound level meter used? 1=old,2=new  0=none'
      read(ichi ,*)islmn
      call slmset(ichi,islmn,vrefn,attn,itrn)
      type*,'
      type*,'islmn=',islmn,' vrefn=',vrefn,' attn=',attn,' itrn=',itrn


      type*,'second (far) microphone data filename?'
      read(ichi,2)ifile2
      ifile2='[heap.margaret.d1]'//ifile2
      type*,'channel? A=1, B=2'
      read(ichi,*)ichf
      type*,'sound level meter used? 1=old,2=new  0=none'
      read(ichi,*)islmf
      call slmset(ichi,islmf,vreff,attf,itrf)
      type*,'islmf=',islmf,'vreff=',vreff,' attf=',attf,' itrf=',itrf


      type*,'output file for dB difference?'
      read(ichi,2)ofile1
      type*,'output file dB at microphones'
      read(ichi,2)ofile2
      ofile1='[heap.margaret.d1]'//ofile1
      ofile2='[heap.margaret.d1]'//ofile2
```

```
2     format(a)


      open(unit=2,name=ifile1,type='old')
      open(unit=3,name=ofile1,type='new')
      open(unit=4,name=ofile2,type='new')



      call rddat
      gainn=ga
      if(ichn.eq.2) gainn=gb
      read(2,40)((dn(j,k),k=1,4),j=1,400)
40    format(1x,4e10.3)
      close(unit=2)

c     set up arrays for near microphone data and frequencies.
      jk2=4
      freq=75.0
      do 45 k2=1,216
      if(k2.gt.37)goto 46
      freq=freq+25
      jk2=jk2+1
      fr(k2)=freq
      goto 47
46    freq=freq+50
      jk2=jk2+2
      fr(k2)=freq

47    an(k2)=dn(jk2,ichn)
45    continue

      open(unit=2,name=ifile2,type='old')
      call rddat
      gainf=ga
      if(ichf.eq.2) gainf=gb
      read(2,50)((df(j,k),k=1,4),j=1,400)
50    format(1x,4e10.3)
      close(unit=2)

c     set up array for far microphone data
      jk3=4
      do 55 k3=1,216
      if(k3.gt.37)goto 56
      jk3=jk3+1
      goto 57
56    jk3=jk3+2
57    af(k3)=df(jk3,ichf)
55    continue

c
c     Input required parameters for corrections for free field
c     atmospheric absorption.

      type*,'correction for free field and atmos. abs?'
      type*,'      yes=1'
      read(ichi,*)ifaa
```

```
      if(ifaa.ne.1)goto 60
      type*,'input reference then test distances'
      read(ichi,*)rr,tr
      type*,'input relative humidity then temperature'
      read(ichi,*)arh,at

c
c     Use data to calculate field at microphones first adjusting
c       data for gain of tape recorder and S.L.M.
c

60    pref=2.000e-05
c     sprn=0.0
c     sprf=0.0

      do 200 j=1,216

      fre=fr(j)

c     Adjust for gain on nagra tape recorder.

      if(itrn.ne.0) an(j)=an(j)*gainn
      if(itrf.ne.0) af(j)=af(j)*gainf


c     convert from volts to dB
      dbn(j)=attn+20*alog10(an(j)/vrefn)

      dbf(j)=attf+20*alog10(af(j)/vreff)
      diff(j)=dbn(j)-dbf(j)

Correct for free field and atmospheric absorption.

      if(ifaa.ne.1) goto 90
      call corffaa(fre,rr,tr,at,arh,ffaa)
      diff(j)=diff(j)-ffaa

c     Write data to files.

90    write(3,100)alog10(fre),diff(j)
100   format(1x,3f12.6)
      write(4,150)alog10(fre),dbn(j),dbf(j)
150   format(1x,3f12.6)


200   continue


      stop
      end
```

```
      subroutine slmset(ichi,islm,vref,att,itr)
      type*,'tape recorder used? uher=0'
      read(ichi,*)itr
      type*,'tape recorder output voltage of calibration tone?'
      read(ichi,*)vo
      if(itr.eq.0) goto 10
      type*,'at tape attenuator setting?'
      read(ichi,*)tatt
      gain=10**(tatt/20.)
      vi=vo*gain
10    if(itr.eq.0)vi=vo
      type*,'vi=',vi
      type*,'calibrator used? 124dB=1,94dB=2'
      read(ichi,*)ical
      type*,'ical=',ical
      if(ical.eq.1)vref=vi/(10**0.2)
      if(ical.eq.2)vref=vi/(10**-1.3)
      if(islm.eq.2) goto 310
      if(islm.eq.0)goto 320
      type*,' slm attenuator setting for measurement?'
      read(ichi,*)att
      return
310   type*,'slm scale used for measurement?'
      type*,'   lower  - 25 to 105 = 1'
      type*,'   middle - 45 to 125 = 2'
      type*,'   upper  - 65 to 145 = 3'
310   read(ichi,*)att
      if(att.eq.1) vref=vref*100.
      if(att.eq.2) vref=vref*10.
      att=120
      return
320   att=120
      return
      end
```

Subroutines for the calculation of atmospheric absorption.

Subroutine Corffaa(freq,rr,tr,at,arh,ffaa)

```
c  subroutine to calculate the correction for free field and
c  atmospheric absorption for the difference between two
c  microphones at distances rr and tr

      ap=1
      call preat(at,ap,arh,f0,c0,h0,cv)
      ff=20*alog10(tr/rr)
      call atmos(freq,ap,at,h0,c0,f0,aa)
      ffaa=ff+(tr-rr)*aa
      return
      end
```

Subroutine Preat(at,ap,arh,f0,c0,h0,cv)

```
c
c routine to calculate constants for air absorption
c
      tk=273.15+at
      a=20.5318-2939./tk
      b=1./(tk**4.922)
      h0=(arh/ap)*b*(10.**a)
      f0=30560.*ap*(h0**1.3)
      c0=4.2425e-6+8.8168e-8*at+5.4834e-10*at*at
      cv=331.55*sqrt(1.+at/273.15)
      return
      end
```

subroutine atmos(f,ap,at,h0,c0,f0,aa)

```
c
c routine to calculate air absorption
c
      amo=2.*c0*(f/(f/f0+f0/f))
      b1=1.7e-8/sqrt(1.+3.66e-3*at)
      b2=h0*ap*f*f/(2.77e-5*f*f+h0*h0*ap*ap)
      amn=b1*b2
      amc=3.6e-11*(1.+1.e-3*at)*f*f/ap
      aa=(amo+amn+amc)*4.343
      return
      end
```

```
      program DIF2MKFIT
c     Program to fit level difference with Keith's two parameter models
c     (variable porosity, rigid backed layer or homogeneous) or with
c     Delaney and Bazely homogeneous model.
c     Fits to files of 100Hz to 1000Hz in 25Hz spacing (or first il
c     points) Corrects for free field and atmospheric absorption.
c
          common/ch1/k0,pi,j
          complex p1n,p1f,j,k1,zr,beta,ptotn,ptotf,zl,zl1
          character*35 ifile,ifile1
          dimension ameas(216,2)
          real k0
          pi=3.141592653
          topi=2*pi
          j=(0.0,1.0)
c
          type*,'interactive or from df2.dat?   interactive=1'
          accept*,int
          if(int.eq.1)ichi=5
          if(int.ne.1)ichi=2
          if(int.ne.1)open(unit=2,name='dif2.dat',type='old')
c
          if(int.eq.1)type*,'output file?'
          read(ichi,2)ifile1
5         if(int.eq.1)type*,'input filename for measured data'
          read(ichi,2)ifile
          if(int.eq.1)type*,'number of points used?'
          read(ichi,*)il
2         format(a)
          open(unit=3,name=ifile1,type='new')
          open(unit=1,name=ifile,type='old')
          read(1,*)((ameas(l,k),k=1,2),l=1,il)
          close(unit=1)
c
c     Enter geometry of the system
c
          if(int.eq.1)type*,'geometry for near microphone'
          if(int.eq.1)type*,'source ht,receiver ht,separation distance'
          read(ichi,*)hs,hrn,rn
          if(int.eq.1)type*,'geometry for far microphone'
          if(int.eq.1)type*,'source ht,receiver ht,separation distance'
          read(ichi,*)hs,hrf,rf
          ff=20*alog10(rf/rn)
          if(int.eq.1)type*,'correct for atmospheric absorption yes=1?'
          read(ichi,*)icorr
          if(icorr.ne.1)goto 7
          if(int.eq.1)type*,'relative humidity and temperature?'
          read(ichi,*)arh,at
c
7         if(int.eq.1)type*,'Model Required?'
          if(int.eq.1)type*,'Keiths homogeneous = 1'
          if(int.eq.1)type*,'D&B homogeneous   =2'
          if(int.eq.1)type*,'Variable porosity  = 3'
          if(int.eq.1)type*,'rigid-backed layer = 4'
          if(int.eq.1)type*,'freq.dependent RBL = 5'
          read(ichi,*)im
c
          if(int.eq.1)type*,' first flow resistivity, and increment?'
```

```
      read(ichi,*)flr,finc
      tflr=flr
      if(im.ge.3) goto 10
      its=0
      goto 15
c
10    its=20
      if(im.ne.3)goto 20
      if(int.eq.1)type*,'first alpha and increment?'
      read(ichi,*)de,dinc
      td=de
      goto 15
20    if(int.eq.1)type*,'first depth and increment'
      read(ichi,*)de,dinc
      td=de
      goto 15
c
15    in=0
      id=0
      small=1000.0
c
50    sumsq=0.0
      do 100 i1=1,il
      fr=10**ameas(i1,1)
      aa=0
      if(icorr.eq.1)call corffaa(fr,rn,rf,at,arh,ffaa)
      if(icorr.eq.1)aa=ffaa-ff
      amd=ameas(i1,2)
      om=topi*fr
      k0=om/343
      if(im.eq.1)call vpzr(fr,flr,0,zr)
      if(im.eq.2)call dbzr(fr,flr,zr)
      if(im.eq.3)call vpzr(fr,flr,de,zr)
      if(im.eq.4)call rblzr(fr,flr,de,zr)
      if(im.eq.5)call fdrblzr(fr,flr,de,zr)
      beta=1/zr
      call chen1(hs,hrn,rn,beta,p1n,ptotn,ap1n,aptotn)
      cn=20*alog10(aptotn/ap1n)
      call chen1(hs,hrf,rf,beta,p1f,ptotf,ap1f,aptotf)
      cf=20*alog10(aptotf/ap1f)
      pred=cn-cf-aa
      sumsq=sumsq+(amd-pred)**2

100   continue
      sumsq=sumsq/il
      if(sumsq.gt.small) goto 70
      if(sumsq.eq.small) goto 75
      if(sumsq.lt.small) goto 80

75    write(3,*),'sumsq=',sumsq,'  de=',de,'  flr=',flr
      goto 70
80    small=sumsq
      smflr=flr
      smd=de

70    id=id+1
      de=de+dinc
```

```
      if(id.lt.its) goto 50

60       in=in+1
      flr=flr+finc
      if(int.eq.1)type*,'flr=', flr
      dl=de

      de=td
      id=0
      if(in.lt.20) goto 50

c     if model 5 is being used check whether the best fit value is in fact
c     a semi infinite case.
      if(im.ne.5)goto 150
      ffr=10**ameas(1,1)
      call fdrblzr(ffr,smflr,smd,zl)
      call vpzr(ffr,smflr,0,zl1)
      test=real(zl)-real(zl1)
      atest=abs(test)

150    write(3,*)'    '
      write(3,910)ifile

      write(3,*)il,'  points'
      write(3,*)'   smallest mean squared difference=',small
      write(3,*)'    '
      if(im.eq.1)goto 901
      if(im.eq.2)goto 902
      if(im.eq.3)goto 903
      if(im.eq.4)goto 904
      if(im.eq.5)goto 905
901    write(3,800)smflr
      write(3,810)tflr,flr-finc,finc
      goto 999
902    write(3,820)smflr
      write(3,810)tflr,flr-finc,finc
      goto 999
903    write(3,840)smflr,smd
      write(3,810)tflr,flr-finc,finc
      write(3,860)td,dl-dinc,dinc
      goto 999
904    write(3,880)smflr,smd
      write(3,810)tflr,flr-finc,finc
      write(3,890)td,dl-dinc,dinc
      goto 999
905    write(3,881)smflr,smd
      write(3,810)tflr,flr-finc,finc
      write(3,890)td,dl-dinc,dinc
      if(atest.le.1.0)write(3,891)
      goto 999
999   write(3,*)'          ---*-*-*-*-*-*-*-*-*-*-*-*-*-*-*-*---'
      write(3,*)'    '
c
      if(int.eq.1)type*,'ANOTHER?     '
      if(int.eq.1)type*,'same file = 1,  different file = 2'
      read(ichi,*)ianov
      if(ianov.eq.1)goto 7
      if(ianov.eq.2)goto 5
```

```
c
910    format(4x,a)
800    format(' HOMOGENEOUS-effective flow resistivity =',f10.1)
810    format(' flow resistivities',f10.1,' to',f10.1,' increment=',f7.1)
820    format(' DELANEY & BAZELY -flow resistivity=',f10.1)
840    format(' VARIABLE POROSITY eff flow res=',f10.1,' alpha(e)=',f6.1)
860    format(' alpha(e)=',f6.1,' to',f6.1,'    increment=',f5.1)
880  format(' RIGID-BACKED LAYER-flow resistivity=',f10.1,' effective depth=',f6.3)
881  format(' NEW RIGID-BACKED LAYER-flow resistivity=',f10.1,' effective depth=',f6.3)
890    format(' depths=',f6.3,' to ',f6.3,'   increment=',f6.3)
891    format(' THIS IS IN FACT A SEMI INFINITE MODEL BEST FIT")

900    stop
       end
```

A.2 Routines for the Prediction of Attenuation.

```
      Program PREDDIFF
c     Calculates a prediction of the attenuation function ie. the difference
c     between the excess attenuation at two microphone positions.
c
c     Impedance is calculated using the following models which are identified
c     by the integer variable im thus:
c
c  im              model                          inputs              variable name
c
c  1     Delany and Bazely model          flow resistivity          fres
c
c  2     4 parameter model for rigid      flow resistivity          phib
c        porous medium (Rayliegh-         tortuosity                q2
c        Attenborough model)              shape factor              n
c                                         porosity                  capom
c
c  3     Talaske's 2 -layered model       flow resistivity
c        using Delany and Bazely          for each layer            fres1,fres2
c        to calculate impedance and
c        propagation constant.            layer depth               d
c
c  4     Talaske's 2 -layered model       for each layer
c        using 4 parameter model          flow resistivity          ph1,ph2
c        to calculated impedance and      porosity                  cap1,cap2
c        propagation constant.            tortuosity                q21,q22
c                                         shape factor              n1,n2
c                                         top layer depth           d
c
c  5     No model used but a file of      Arrays containing
c        impedance vs frequency read      frequency                 afr
c        into program.                    and impedance             azr
c
c  6     Variable porosity
c        approximation (= homogeneous     effective flow resistivity efr
c        approximation if alphe=0)        effective alpha           alphe
c
c  7     Rigid-backed layer
c        approximation with flat          effective flow resistivity efr
c        real part                        effective depth           de
c
c  8     4 parameter model for rigid      flow resistivity          phib
c        porous medium (Rayliegh-         tortuosity                q2
c        Attenborough model) over-        shape factor              n
c        lying rigid backing              porosity                  capom
c                                         layer depth               d
c
c  9     Rigid-backed layer
c        approximation with frequency-    effective flow resistivity efr
c        dependent real part              effective depth           de
c
c

      common/ch1/k0,pi,j
      complex j,beta,zr,p1n,ptotn,p1f,ptotf,azr
      character*20 ofile,frfil,ofile2,ofile3,ofile4
```

```
      dimension c(5),sig(5),afr(220),azr(22)
      real k0,n,n1,n2

      pi=3.141592653
      j=(0.0,1.0)
      at=17.0
      cv=331.55*sqrt(1+at/273.15)

      type*,'interactive or from predin.dat?'
      type*,'interactive=1'
      accept*,int
      ichi=5
      if(int.eq.1)goto 4
      ichi=10
      open(unit=10,name='predin.dat',type='old')
4     if(int.eq.1)type*,'output file? - difference'
      read(ichi,2)ofile
2     format(a)
      open(unit=2,name=ofile,type='new')
      if(int.eq.1)type*,'write impedance to file? yes=1'
      read(ichi,*)iwri

      if(iwri.eq.1)open(unit=3,name='zr.dat',type='new')

      if(int.eq.1)type*,'model required?'
      if(int.eq.1)type*,'      Delaney and Bazely infinite     = 1'
      if(int.eq.1)type*,'      Rayliegh-Attenborough infinite  = 2'
      if(int.eq.1)type*,'      D&B - Talaske 2-layered         = 3'
      if(int.eq.1)type*,'      R-A  Talaske 2-layered          = 4'
      if(int.eq.1)type*,'      measured impedance data         = 5'
      if(int.eq.1)type*,'      variable porosity 2 parameter   = 6'
      if(int.eq.1)type*,'      rigid-backed layer 2 parameter  = 7'
      if(int.eq.1)type*,'      rigid-backed layer Rayl-Atten   = 8'
      if(int.eq.1)type*,'    RBL 2 param - freq dependant Re(zr)=9'
      read(ichi,*)im
c
c Call appropriate input subroutine which simply accepts all the relevant
c input parameters
c
      if(im.eq.1)call delbaz(ichi,fres)
      if(im.eq.2)call zkkb(ichi,phib,q2,capom,n)
      if(im.eq.3)call dbtal(ichi,fres1,d,fres2)
      if(im.eq.4)call zkkbtal(ichi,ph1,ph2,q21,q22,cap1,cap2,n1,n2,d)
      if(im.eq.5)call mesd(ichi,it,azr,afr)
      if(im.eq.6)call vp(ichi,efr,alphe)
      if(im.eq.7)call rbl(ichi,efr,de)
      if(im.eq.8)call zkkbl(ichi,phib,q2,capom,n,d)
      if(im.eq.9)call rbl(ichi,efr,de)
      if(im.eq.5)goto 45
c
c     Set up frequencies to be used.
c
      if(int.eq.1)type*,'
      if(int.eq.1)type*,'iopt=1  50 Hz steps'
      if(int.eq.1)type*,'iopt=2  third octaves.'
      if(int.eq.1)type*,'iopt=3  frequency range with log spacing(134 points)'
      if(int.eq.1)type*,'iopt=5  frequency read from 2 column data file'
```

```
      if(int.eq.1)type*,'    '
      if(int.eq.1)type*,'input iopt'
      read(ichi,*)iopt
      if(int.eq.1)type*,'    '
      if(iopt.ne.5)goto 16
      if(int.eq.1)type*,'75 frequencies? or another file yes=1'
      read(ichi,*)ifrfil
      if(ifrfil.eq.1)goto 11
      if(int.eq.1)type*,'filename containing frequencies?'
      read(ichi,2)frfil
      goto 12
11     frfil='d1:dif165m_b48.dat'
12     open(unit=11,name=frfil,type='old')
      if(int.eq.1)type*,'number of frequencies?'
      read(ichi,*)ifre
      do 14 i=1,ifre
      read(11,*)afr(i),xxx
      afr(i)=10**afr(i)
14     continue
      it=ifre
      close(unit=11)
      goto 45

16     if(int.eq.1)type*,'first frequency?'
      read(ichi,*)fr

      if(iopt.eq.1) it=199
      if(iopt.eq.2) it=21
      if(iopt.eq.3) it=134
      if(iopt.eq.4) it=68

45     if(int.eq.1)type*,'geometry for near microphone?'
      if(int.eq.1)type*,'source height, receiver height and separation distance?'
      read(ichi,*)hsn,hrn,rn

      if(int.eq.1)type*,'    '
      if(int.eq.1)type*,'geometry for far microphone'
      if(int.eq.1)type*,'source height,receiver height and separation distance?'
      read(ichi,*)hsf,hrf,rf
      if(int.eq.1)type*,'correction for atmospheric absorption? no=0'
      read(ichi,*)ic
      if(ic.eq.0)goto 30
      at=20
      arh=60
30     ff=20*alog10(rf/rn)

      do 200 i=1,it
      if(im.eq.5.or.iopt.eq.5) fr=afr(i)
      if(ic.eq.0) goto 50
      call corffaa(fr,rn,rf,at,arh,ffaa)
      aa=ffaa-ff
      goto 60
50     aa=0
60     om=2*pi*fr
      k0=om/cv
c
c  Calculate impedance according to the model selected
```

```
c
      if(im.eq.1)call dbzr(fr,fres,zr)
      if(im.eq.2)call czkzr(fr,phib,q2,capom,n,zr)
      if(im.eq.3)call dbtlzr(fr,om,cv,fres1,d,fres2,zr)
      if(im.eq.4)call cztlzr(fr,ph1,ph2,q21,q22,cap1,cap2,n1,n2,d,zr)
      if(im.eq.5)zr=azr(i)
      if(im.eq.6)call vpzr(fr,efr,alphe,zr)
      if(im.eq.7)call rblzr(fr,efr,de,zr)
      if(im.eq.8)call czklzr(fr,phib,q2,capom,n,d,zr)
      if(im.eq.9)call fdrblzr(fr,efr,de,zr)
      rzr=real(zr)
      xzr=-1*aimag(zr)
      if(iwri.eq.1)write(3,5)alog10(fr),rzr,xzr
5     format(1x,3f12.6)
      beta=1/zr

      if(fr.ge.3000.) hs=hsn+0.2
      if(fr.lt.3000.) hs=hsn
c
c Calculate excess attenuation for each microphone and difference
c between them, corrected for atmospheric absorption if required.
c
      call chen1(hs,hrn,rn,beta,p1n,ptotn,apn,aptn)
      cn=20*alog10(aptn/apn)
      call chen1(hs,hrf,rf,beta,p1f,ptotf,apf,aptf)
      cf=20*alog10(aptf/apf)
      cin=cn-cf+aa
c
c  Write results and increment frequency
c
      write(2,2001)alog10(fr),cin
      if(im.eq.5.or.iopt.eq.5) goto 200
      if(iopt.eq.1) fr=fr+50.0
      if(iopt.eq.2) fr=fr*2**0.3333333
      if(iopt.eq.3) fr=fr*2**0.05
      if(iopt.eq.4) fr=fr*2**0.1
200     continue
2001    format(1x,2f12.6)
      stop
      end
```

Subroutines for the calculation of impedance using various prediction models as used in PREDDIFF.

subroutine czklzr(fr,phib,q2,capom,n,d,zr)

calculation of impedance using rigid backed layer model (equation 4.14)
c with bulk propagation constant and characteristic impedance calculated by
c Attenborough 4-parameter model (equation 4.13).

```
real n
complex zr
nv=13
np=1
call ordinate(fr,nv,np,q2,n,phib,capom,d,ord1)
np=2
call ordinate(fr,nv,np,q2,n,phib,capom,d,ord2)
zr=cmplx(ord1,ord2)
return
end
```

subroutine czkzr(fr,phib,q2,capom,n,zr)

calculation of impedance using Attenborough 4-parameter model (equation 4.13)

```
real n
complex zr
nv=10
np=1
d=.01
call ordinate(fr,nv,np,q2,n,phib,capom,d,ord1)
np=2
call ordinate(fr,nv,np,q2,n,phib,capom,d,ord2)
zr=cmplx(ord1,ord2)
return
end
```

```
      subroutine cztlzr(fr,ph1,ph2,q21,q22,cap1,cap2,n1,n2,d,zr)
calculation of impedance using 2-layered model described by Talaske (1980)
c   characteristic impedance of layers calculated using equation (4.13).
      complex z1,z2,zr,k1
      real n1,n2
      dd=1
c
calculate propagation constant in upper layer (k1).
c
      nv=1
      np=1
      call ordinate(fr,nv,np,q21,n1,ph1,cap1,dd,orda)
      np=2
      call ordinate(fr,nv,np,q21,n1,ph1,cap1,dd,ordb)
      k1=cmplx(orda,ordb)
c
calculate characteristic impedance of each layer (z1 and z2).
c
      nv=10
      np=1
      call ordinate(fr,nv,np,q21,n1,ph1,cap1,dd,ordc)
      np=2
      call ordinate(fr,nv,np,q21,n1,ph1,cap1,dd,ordd)
      z1=cmplx(ordc,ordd)

      np=1
      call ordinate(fr,nv,np,q22,n2,ph2,cap2,dd,orde)
      np=2
      call ordinate(fr,nv,np,q22,n2,ph2,cap2,dd,ordf)
      z2=cmplx(orde,ordf)
c
calculate surface impedance
c
      d2kj=j*2.0*k1*d
      zrn=z1+z2+(z2-z1)*cexp(d2kj)
      zrd=z1+z2+(z1-z2)*cexp(d2kj)
      zr=z1*zrn/zrd
      return
      end
```

```
      subroutine dbrblzr(fr,om,cv,fres,d,zr)
calculation of impedance using rigid backed layer impedance model
c equation (4.14) characteristic impedance of layer calculated using
c Delany and Bazely model equation (4.11)
      complex zl,zc,z2,j,k1
      sbyf=fres/(fr*1000.)
      flbyfr=fres/fr
      j=(0.0,1.0)
      call dbzr(fr,fres,zc)
c
calculate propagation constant in upper layer (k1).
c
      rho=1.21
      a=1.+0.0978*(flbyfr/rho)**0.7
      b=0.189*(flbyfr/rho)**0.595
      a=a*om/cv
      b=b*om/cv
      k1=cmplx(a,b)
c
calculate surface impedance (zl)
c
      z2=-j*k1*d
c
check for values of z2 which are too large for ccoth
c
      if(real(z2).le.44.3)goto 10
      cth=cmplx(1.0,0.0)
      goto 20
10    cth=ccoth(z2)
20    zl=zc*cth
      return
      end
```

```
      subroutine dbtlzr(fr,om,cv,fres1,d,fres2,zr)
calculation of impedance using 2-layered model described by Talaske (1980)
characteristic impedance of layers calculated using equation (4.11).
      complex z1,z2,k1,zr,zrn,zrd,j,d2kj,cn
      real n
      pi=3.141592653
      j=(0.0,1.0)
c
calculate characteristic impedance of each layer (z1 and z2).
c
      call dbzr(fr,fres1,z1)
      call dbzr(fr,fres2,z2)
c
calculate propagation constant in upper layer (k1).
c
      flbyfr=fres1/fr
      rho=1.21
      a=1.+0.0978*(flbyfr/rho)**0.7
      b=0.189*(flbyfr/rho)**0.595
      a=a*om/cv
      b=b*om/cv
      k1=cmplx(a,b)
c
calculate surface impedance
c
      d2kj=j*2.0*k1*d
      zrn=z1+z2+(z2-z1)*cexp(d2kj)
      zrd=z1+z2+(z1-z2)*cexp(d2kj)
      zr=z1*zrn/zrd
      return
      end



      subroutine dbzr(fr,fres,zr)
calculation of impedance using Delany and Bazley model (equation 4.11)
      complex zr
      flbyf=fres/fr
      rho=1.21
      r=1.+0.0571*(flbyf/rho)**0.754
      x=0.087*(flbyf/rho)**0.732
      zr=cmplx(r,x)
      return
      end
```

```
      subroutine fdrblzr(fr,efr,de,zr)
calculation of impedance using rigid backed layer approximation
c with frequency dependant resistance equation 4.19
      complex zr,arg,cth,ccoth,zh,i
      i=cmplx(0.0,1.0)
      frbyf=sqrt(efr/fr)
      rzh=0.218*frbyf
      xzh=0.218*frbyf
      zh=cmplx(rzh,xzh)
      arg=-1*i*5.59e-03*de*sqrt(efr*fr)*(1+i)
c
check for values of arg which are too large for ccoth
c
      if(real(arg).le.44.3)goto 10
      cth=cmplx(1.0,0.0)
      goto 20
10     cth=ccoth(arg)
20     zr=zh*cth
      return
      end
```

```
      subroutine ordinate(f,nv,np,q2,n,phib,capom,dd,ord)
c This routine returns the value (ord) of a requested variable at
c a given value of frequency (f).
c nv is the number of the variable.
c if np = 1 real part is selected. if np = 2 imaginary part is
c selected.
c        .... Uses cmpbj.for to calculate bessels functions ....
c
      real mu,nuf,n,lambdap,lambdas,mikb1
      complex i,y,tp,zkkb,j0,j1,rhobzk,rhobs,mikb,ct,rhobmi
      complex czk,cmi,npy,ccc,ccs,npys,zdzk,ikbd
      q=sqrt(q2)
      pi=3.141592653
      i=cmplx(0.0,1.0)
      cf=34000.0
      gamma=1.4
      prandtl=0.76
      sqrtnp=sqrt(prandtl)
      mu=181e-6
      rhof=1.2e-3
      nuf=mu/rhof
c
      ae=8*mu*(q**2)/(capom*phib)
      ae=ae**0.5
      omega=2*pi*f
      lambdap=(ae/n)*((omega/nuf)**0.5)
      y=sqrtnp*lambdap*(i**0.5)
      npy=y
      re6=real(npy)
      if(nv.eq.6.and.np.eq.1) ord=re6
      aim6=aimag(npy)
      if(nv.eq.6.and.np.eq.2) ord=aim6
c
      n1=0
      call cmpbj(y,n1,j0)
      n1=1
      call cmpbj(y,n1,j1)
      tp=j1/j0
      zkkb=1+2*((gamma-1)/y)*tp
      ccc=zkkb
      re7=real(ccc)
      if(nv.eq.7.and.np.eq.1) ord=re7
      aim7=aimag(ccc)
      if(nv.eq.7.and.np.eq.2) ord=aim7
c
c  variable no 1 - propagation constant.
c
      y=lambdap*(i**0.5)
      n1=0
      call cmpbj(y,n1,j0)
      n1=1
      call cmpbj(y,n1,j1)
      tp=j1/j0
      zkkb=zkkb/(1-(2/y)*tp)
      zkkb=zkkb*(q*omega/cf)**2
      zkkb=zkkb**0.5
      re1=real(zkkb)
      if(nv.eq.1.and.np.eq.1) ord=re1
```

```
      aim1=aimag(zkkb)
      if(nv.eq.1.and.np.eq.2) ord=aim1
c
c  variable 2 propagation constant using low frequency approximation.
c
      mikb1=(omega/cf)**2*gamma/rhof
      mikb=mikb1*(rhof*(1.33-0.2857*prandtl)*q**2)
      mikb=mikb+(i*phib*capom*n**2/omega)*mikb1
      mikb=mikb**0.5
      re2=real(mikb)
      if(nv.eq.2.and.np.eq.1) ord=re2
      aim2=aimag(mikb)
      if(nv.eq.2.and.np.eq.2) ord=aim2
c
c  variable no 3 - complex density.
c
      rhobzk=q**2*rhof/((1-(2/y)*tp)*capom)
      re3=real(rhobzk)
      if(nv.eq.3.and.np.eq.1) ord=re3
      aim3=aimag(rhobzk)
      if(nv.eq.3.and.np.eq.2) ord=aim3
c
c  variable no 4 - complex density using low freq. approx.
c
      rhobmi=rhof*q**2/capom
      rhobmi=1.33*rhobmi+i*phib*n**2/omega
      re4=real(rhobmi)
      if(nv.eq.4.and.np.eq.1) ord=re4
      aim4=aimag(rhobmi)
      if(nv.eq.4.and.np.eq.2) ord=aim4
c
c  variable no 5 - complex density if all pores were slits.
c
      b=(12*mu*(q**2)/(capom*phib))**0.5
      lambdas=b*((omega/nuf)**0.5)
      y=lambdas*(i**0.5)*i
      rhobs=(rhof*q**2)/capom
      call ctanh(y,ct)
      rhobs=rhobs/(1-ct/y)
      re5=real(rhobs)
      if(nv.eq.5.and.np.eq.1) ord=re5
      aim5=aimag(rhobs)
      if(nv.eq.5.and.np.eq.2) ord=aim5
c
c  variable no 10 - characteristic impedance.
c
      czk=(rhobzk*omega)/(zkkb*rhof*cf)
      rczk=real(czk)
      if(nv.eq.10.and.np.eq.1) ord=rczk
      xczk=aimag(czk)
      if(nv.eq.10.and.np.eq.2) ord=xczk
c
c  variable no 11 - low frequency approximation.
c
      cmi=(rhobmi*omega)/(mikb*rhof*cf)
      rcmi=real(cmi)
      if(nv.eq.11.and.np.eq.1) ord=rcmi
      xcmi=aimag(cmi)
```

```
      if(nv.eq.11.and.np.eq.2) ord=xcmi
c
c  variable no 9 - parameter for slits.
c
      npys=sqrtnp*lambdas*(i**0.5)*i
      re9=real(npys)
      if(nv.eq.9.and.np.eq.1) ord=re9
      aim9=aimag(npys)
      if(nv.eq.9.and.np.eq.2) ord=aim9
      call ctanh(npys,ct)
      ccs=1+(gamma-1)*ct/npys
      re8=real(ccs)
      if(nv.eq.8.and.np.eq.1) ord=re8
      aim8=aimag(ccs)
      if(nv.eq.8.and.np.eq.2) ord=aim8
c
c  variable no 12 - attenuation
c
      re12=20*aimag(zkkb)*dd/alog(10.0)
      if(nv.eq.12.and.np.eq.1) ord=re12
c
c  variable no 13 - impedance of a rigid-backed layer.
c
      ikbd=zkkb*dd*i
      call ctanh(ikbd,ct)
      zdzk=(-1.0)*czk/ct
      re13=real(zdzk)
      aim13=aimag(zdzk)
      if(nv.eq.13.and.np.eq.1) ord=re13
      if(nv.eq.13.and.np.eq.2) ord=aim13
      return
      end


      subroutine rblzr(fr,efr,de,zr)
calculation of impedance using rigid-backed layer approximation (equation 4.18)
      complex zr
      rzr=0.00082*efr*de
      xzr=38.99/(fr*de)
      zr=cmplx(rzr,xzr)
      return
      end


      subroutine vpzr(fr,efr,alphe,zr)
calculation of impedance using variable porosity approximation (equation 4.17)
      complex zr
      frbyf=sqrt(efr/fr)
      rzr=0.218*frbyf
      xzr=0.218*frbyf+9.74*(alphe/fr)
      zr=cmplx(rzr,xzr)
      return
      end
```

```
      complex function ccoth(z)
calculates hyperbolic cotangent (coth) of a complex number
      complex z,i
      i=cmplx(0.0,1.0)
      rz2=2.*real(z)
      az2=2.*aimag(z)
      c1=cosh(rz2)-cos(az2)
      ccoth=(sinh(rz2)-i*sin(az2))/c1
      return
      end
```

Subroutines for the Prediction of Propagation.

```
      subroutine chen1(hs,hr,r,beta,p1,ptot,ap1,aptot)
c Propagation model, returns the total and direct field at a given
c location for the calculation of excess attenuation  (equation 4.20)
c Q is calculated as in equation 4.5.
c Inputs to the subroutine are: the source height(hs), receiver height(hr),
c separation distance (r), complex admittance (beta=1/impedance).
c Outputs are complex value and magnitude of the total and direct field
c
      common/ch1/k0,pi,j
      complex j,ck,cg,cr1,cr2,cpi,rp,beta,p1,p2,p3,ptot
      complex pe,pe2,wiz,f,c1,c2,c4
      real k0

      h=hs+hr
      r1=sqrt((hs-hr)**2+r*r)
      r2=sqrt(h*h+r*r)
      cth=h/r2

      c1=(1.0,0.0)
      c2=(2.0,0.0)
      c4=(4.0,0.0)
      cg=cmplx(cth,0.0)
      ck=cmplx(k0,0.0)
      cr1=cmplx(r1,0.0)
      cr2=cmplx(r2,0.0)
      cpi=cmplx(pi,0.0)
      rp=(cg-beta)/(cg+beta)
      p1=cexp(j*ck*cr1)/(c4*cpi*ck*cr1)
      p2=rp*cexp(j*ck*cr2)/(c4*cpi*ck*cr2)
      pe=csqrt(j*ck*cr2/c2)*(cg+beta)
      pe2=-c1*j*pe
      call w(pe2,wiz)
      f=c1+j*csqrt(cpi)*pe*wiz
      p3=(c1-rp)*f*cexp(j*ck*cr2)/(c4*cpi*ck*cr2)

      ptot=p1+p2+p3
      ap1=cabs(p1)
      aptot=cabs(ptot)
      return
      end
```

```
      subroutine extend(FREQ,hs,hr,r,beta,zkkb1,cth,b,p1,ptot,ap1,aptot)
c     Calculation of total field and direct field at a given location over
c     an externally reacting boundary for the calculation of excess
c     attenuation. The error function term
c     is calculated according to the method of Chien and Soroka(1975),(1980)
c     (JSV 43(1) p9-20 and JSV 69 p340-343).
c     Total field calculated according to Attenborough-Hayek and
c     Lawther as corrected by Quartararo(Penn State MS Thesis 1983).
c     Inputs - source height(hs), receiver height(hr), separation distance(r)
c     Admittance=1/characteristic impedance(beta).
c     Outputs- total field(ptot), direct field (p1), absolute values of
c     total and direct field (aptot, ap1)
c
      complex j,ck,cg,cr1,cr2,cpi,rp,beta,p1,p2,p3,ptot,reflind
      complex pe,pe2,wiz,f,c1,c2,c4,cssqth,ktheta,kthetam,A
      complex numa,dena,bnum1,bnum2,bden1,bden2,zkkb1,b,wsquared
      real k0,ssqth
      PI=3.141592653
      K0=2.0*PI*FREQ/344.
      h=hs+hr
      r1=sqrt((hs-hr)**2+r*r)
      r2=sqrt(h*h+r*r)
      cth=h/r2
      J  =CMPLX(0.0,1.0)

      c1=(1.0,0.0)
      c2=(2.0,0.0)
      c4=(4.0,0.0)
      cg=cmplx(cth,0.0)
      ck=cmplx(k0,0.0)
      cr1=cmplx(r1,0.0)
      cr2=cmplx(r2,0.0)
      cpi=cmplx(pi,0.0)

      ssqth  =  1.-cth**2
      cssqth =  cmplx(ssqth,0.0)
      reflind = zkkb1/ck
      ktheta =  cssqth/reflind**2
      kthetam=  c1-ktheta
      kthetam=  csqrt(kthetam)

      rp=(cg-beta*kthetam)/(cg+beta*kthetam)

      p1=cexp(j*ck*cr1)/(c4*cpi*ck*cr1)
      p2=rp*cexp(j*ck*cr2)/(c4*cpi*ck*cr2)
      numa   =  c1-c1/reflind**2
      numa   =  numa**0.5
      dena   =  c1-(beta*ck/zkkb1)**2
      dena   =  dena**0.5
      A      =  j*beta*ck*numa/(zkkb1*dena)
c
c     If the real part of the arguement pe2 is negative, the
c     subroutine w returns a large value of wiz which tends to cause
c     an overflow in the following calculations or a sharp discontinuity in
c     the attenuation result. Therefore steps are taken
c     to avoid this occuring. A negative imaginary part of wsquared gives
c     a negative real part of pe2, a negative imaginary part of wsquared is
```

```
c       therefore set to 0.
c
c       This is evidently an approximation but does seem to give 'sensible'
c       results.
c
        wsquared = j*ck*cr2*(c1+A*cg-cssqth*csqrt(c1-A**2))
        wtestr=real(wsquared)
        wtesti=aimag(wsquared)
        if(wtesti.lt.0.0)wtesti=0.0
        wsquared=cmplx(wtestr,wtesti)
        pe2    =  -j*csqrt(wsquared)

        call w(pe2,wiz)

        f      =  c1+j*csqrt(cpi)*csqrt(wsquared)*wiz
        bnum1  =  (cg+beta*kthetam)*numa
        bden1  =  (cg+beta*numa/dena)*kthetam
        bnum2  =  dena+beta*numa*cg+cssqth*(c1-beta**2)**0.
5
        bnum2  =  csqrt(bnum2)
        bden2  =  dena**3*csqrt(c2*cssqth)*csqrt(csqrt(c1-beta**2))
        b      =  (bnum1*bnum2)/(bden1*bden2)
        p3=b*(c1-rp)*f*cexp(j*ck*cr2)/(c4*cpi*ck*cr2)

        ptot=p1+p2+p3
        ap1=cabs(p1)
        APTOT=CABS(PTOT)

        return
        end
```

```
      subroutine w(z,wiz)
c calculation of error function following the method of Chien and Soroka(1975)
c modified by the same authors in 1980.
c
c  subroutine W is modified from 'cderfc' developed at Pennsylvannia State
c  University.
      logical lx,ly
      complex*8 z,wiz,cefw,s,t1,t2,t3
      data cons/1.128379167095/
      x=-aimag(z)
      y=real(z)
c
      x1=y
      y1=-x
c
c      determine quadrant for z
c
10     lx=x.ge.0.0
      ly=y.ge.0.0
      if(lx.and.ly)iq=1
      if(.not.lx.and.ly)iq=2
      if(.not.lx.and..not.ly)iq=3
      if(lx.and..not.ly)iq=4
c
c      convert to 1st quadrant
c
      x=abs(x)
      y=abs(y)
      s=cmplx(x,y)
      xs=x
      ys=y
c
100    if(y.ge.4.29.or.x.ge.5.33)goto 110
      s=(1.0-y/4.29)*sqrt((1.0-(x*x)/28.41))
      h=1.6*s
      h2=2.0*h
      ncap=6.5+23.0*s
      alamda=h2**ncap
      nu=9.5+21.0*s
      goto 120
110    t1=4.613135e-1/(s*s-1.901635e-1)
      t2=9.999216e-2/(s*s-1.7844927)
      t3=2.883894e-3/(s*s-5.5253437)
      wiz=s*(t1+t2+t3)
      v=real(wiz)
      u=-aimag(wiz)
      goto 180
120    r1=0.0
      r2=0.0
      s1=0.0
      s2=0.0
      n=nu
130    if(n.lt.0)goto 150
      p1=n+1
      t1=y+h+p1*r1
      t2=x-p1*r2
      c=0.5/(t1*t1+t2*t2)
      r1=c*t1
```

```
      r2= c*t2
      if(h.eq.0.0.or.n.gt.ncap)goto 140
      t1=alamda+s1
      s1=r1*t1-r2*s2
      s2=r2*t1+r1*s2
      alamda=alamda/h2
140     n=n-1
      goto 130
150     if(alamda.eq.0.0)goto 160
      u=cons*s1
      v=cons*s2
      goto 180
160     u=cons*r1
      v=cons*r2
180     cefw=cmplx(u,v)
c
c       test for underflow and overflow
c
      test=-xs*xs+ys*ys
      if(test.lt.-85.0)test=-85.0
      if(test.gt.87.)test=87.0
c test for quadrant
      goto(230,220,210,210),iq
210     cefw=2.0*cexp(cmplx(test,-2.*xs*ys))-cefw
      if(iq.eq.3)goto 230
      if(iq.eq.4)goto 220
c       for 2nd and 4th quads conjugate cefw
c
220     cefw=conjg(cefw)
c
c
230     wiz=cefw
      return
      end
```

A.3 Calculation of Attenuation Due to Scattering.

Subroutine Scatter

```
      subroutine SCATTER(dens,rad,ifr,flres,scdi,fr,att)
c     Program to calculate attenuation
c     for an array of vertical cylindrical scatterers
c     ie. the difference in sound pressure level between two points within
c     the array.
c
c     Method taken from Embleton(1966) JASA.40(3) p667-670
c
      dimension aj(400),ah(400),dj(400),dh(400),aa(400)
      complex i,zb,kb,g,ga,ah,aa,dh
      real k,ka,kan
      pi=3.141593
      i=cmplx(0.0,1.0)
c
      om=2*pi*fr
      k=om/343.
      ka=k*rad
c
Calculate number of iterations required to calculate An.
c
      kan=(ka+5.8)/0.8
      itt=kan
c
Calculate surface impedance of cylinders(using Delaney & Bazely model)
c
      if(ifr.ne.0)goto 10
      flo=flres/(fr*1.21)
      r=1.+0.0571*(flo)**0.754
      x=0.087*(flo)**0.732
      zb=cmplx(r,x)
c
Calculate zero and first order values of Bessel and Hankel functions
c     and their derivitives.
c
10    call jyh(0,ka,1,aj(1),aim)
      call jyh(0,ka,3,rh0,xh0)
      ah(1)=cmplx(rh0,xh0)
      call jyh(1,ka,1,aj(2),aim)
      call jyh(1,ka,3,rh1,xh1)
      ah(2)=cmplx(rh1,xh1)
      dj(1)=-1*aj(2)
      dh(1)=-1*ah(2)
      dj(2)=aj(1)-aj(2)/ka
      dh(2)=ah(1)-ah(2)/ka
c
Calculate Bessel and Hankel functions  for positive values of n.
c     (negative not required as An for n=-n equals An)
c
      do 200 i1=3,itt
      aj(i1)=(2*(i1-2)*aj(i1-1)-ka*aj(i1-2))/ka
      dj(i1)=(ka*aj(i1-1)-(i1-1)*aj(i1))/ka
      ah(i1)=(2*(i1-2)*ah(i1-1)-ka*ah(i1-2))/ka
      dh(i1)=(ka*ah(i1-1)-(i1-1)*ah(i1))/ka
200       continue
c
```

```
Calculate An for each value of n.
c
      do 300 i2=1,itt
      if(ifr.ne.0) goto 301
      aa(i2)=-1*((i*aj(i2)+zb*dj(i2))/(i*ah(i2)+zb*dh(i2)))
      goto 300
301     if(ifr.eq.1)aa(i2)=-1*(i*aj(i2))/(i*ah(i2))
      if(ifr.eq.2)aa(i2)=-1*dj(i2)/dh(i2)
300     continue
c
Calculate scattering parameters g and ga.
c
      g=aa(1)
      ga=aa(1)
      do 350 i3=2,itt
      n=i3-1
      g=g+(2*aa(i3))
      ga=ga+(2*aa(i3)*(-1)**n)
350     continue
c
Calculate bulk propagation constant kb.
c
      cn=dens*2/k
      kb=csqrt(k*k-4*i*dens*g+(ga*ga-g*g)*((2*dens/k)**2))
      qc=aimag(kb)
c
Calculate attenuation within array.
c
      att=(20*qc*scdi)/alog(10.0)
c
      return
      end
```

```
      SUBROUTINE JYH(iord,x,nv,res,xes)
c     returns value of j,y or h for real x.
c     nv=1   is j i.e. bessel function first kind.
c     nv-2   is y i.e. bessel function second kind.
c     nv=3   is h i.e. hankel function.
c     iord is order.
      complex han01,han11,cres
      if(iord.eq.0.and.nv.eq.1)res=bj01(x)
      if(iord.eq.1.and.nv.eq.1)res=bj11(x)
      if(iord.eq.0.and.nv.eq.2)res=by01(x)
      if(iord.eq.1.and.nv.eq.2)res=by11(x)
      if(iord.eq.0.and.nv.eq.3)cres=han01(x)
      if(iord.eq.1.and.nv.eq.3)cres=han11(x)
      if(nv.ne.3) goto 10
      res=real(cres)
      xes=aimag(cres)
10    return
      end


      function bj01(x)
      common /flags/ ifjin,ifyin,ifjout,ifyout
      ifj = 1
      ify = 1
      ifjin = ifj
      yj = s17aef(x,ifj)
      bj01=yj
      if(ifj.ne.0)type*,'error ifj.ne.0 - bj01'
      return
      end


      function bj11(x)
      common /flags/ ifjin,ifyin,ifjout,ifyout
      ifj = 1
      ify = 1
      ifjin = ifj
      yj = s17aff(x,ifj)
      bj11=yj
      if(ifj.ne.0)type*,'error ifj.ne.0 - bj11'
      return
      end

      function by01(x)
      common /flags/ ifjin,ifyin,ifjout,ifyout
      ifj = 1
      ify = 1
      ifjin = ifj
      yj = s17acf(x,ifj)
      by01=yj
      if(ifj.ne.0)type*,'error ifj.ne.0 -by01'
      return
      end


      function by11(x)
      common /flags/ ifjin,ifyin,ifjout,ifyout
```

```
ifj = 1
ify = 1
ifjin = ifj
yj = s17adf(x,ifj)
by11=yj
if(ifj.ne.0)type*,'error ifj.ne.0 - by11'
return
end
```

```
complex function han01(x)
common /flags/ ifjin,ifyin,ifjout,ifyout
complex i
ifj = 1
ify = 1
ifjin = ifj
ifyin = ify
yj = s17aef(x,ifj)
yy=s17acf(x,ify)
i=cmplx(0.0,1.0)
han01=yj+i*yy
if(ifj.ne.0)type*,'error ifj.ne.0 - han01'
if(ify.ne.0)type*,'error ify.ne.0 - han01'
return
end
```

```
complex function han11(x)
common /flags/ ifjin,ifyin,ifjout,ifyout
complex i
i=cmplx(0.0,1.0)
ifj = 1
ify = 1
ifjin = ifj
ifyin= ify
yj = s17aff(x,ifj)
yy = s17adf(x,ify)
han11=yj+i*yy
if(ifj.ne.0)type*,'error ifj.ne.0 - han11'
if(ify.ne.0)type*,'error ify.ne.0 - han11'
return
end
```

A.4 Calculation of Significant Differences Using Pairwise T-Tests.

```
      PROGRAM TTEST
c     to calculate pairwise t-tests to determine whether 2 means are
c     significantly different.
c
      dimension dat(2,100,2),n(2),an(2),sum(2),sumsq(2),amean(2),ss(2)
      dimension table(30,3)
      character*20 ifile
      character*1 ask
      character*3 sig
      ichi=3
      open(unit=3,name='ts.dat',type='old')
100   sum(1)=0
      sum(2)=0
      sumsq(1)=0
      sumsq(2)=0
      n(1)=0
      an(1)=0
      n(2)=0
      an(2)=0
      do 110 i10=1,100
      dat(1,i10,1)=0.0
      dat(1,i10,2)=0.0
      dat(2,i10,1)=0.0
      dat(2,i10,2)=0.0
110   continue
2     format(a)

      open(unit=2,name='t_table.dat',type='old')
      read(2,*)((table(j,k),k=1,3),j=1,30)
      close(unit=2)

      do 20 i1=1,2
      i2=1
      type*,'filename for data set',i1
      read(ichi,2)ifile
      write(6,2)ifile
      type*,'column required 1=HOM  2=D&B'
      read(ichi,*)ic
      write(6,*)ic
      open(unit=2,name=ifile,type='old')
5     read(2,*),dat(i1,i2,1),dat(i1,i2,2)
      if(dat(i1,i2,ic).eq.999)goto 10
      i2=i2+1
      goto 5

10    n(i1)=i2-1
      an(i1)=i2-1

      close(unit=2)
20    continue


      do 40 i3=1,2
      do 30 i4=1,n(i3)
```

```
      sum(i3)=sum(i3)+dat(i3,i4,ic)
      sumsq(i3)=sumsq(i3)+(dat(i3,i4,ic)*dat(i3,i4,ic))

30    continue

      amean(i3)=sum(i3)/an(i3)
      ss(i3)=sumsq(i3)-(sum(i3)**2/an(i3))

40    continue

      df=(an(1)+an(2)-2)
      adf=df
      if(df.gt.30)adf=30
      ssq=(ss(1)+ss(2))/df
      ese=sqrt(ssq*(1/an(1)+1/an(2)))
      amd=amean(1)-amean(2)

      lsig=1
      type*,'df=',df
50    if(lsig.ne.1) goto 60
      t=table(adf,1)
      type*,'t=',t
      goto 80

60    if(lsig.ne.2)goto 70
      t=table(adf,2)
      goto 80

70    t=table(adf,3)

80    tese=t*ese
      al=amd-tese
      au=amd+tese
      type*,'CI=',al,',',au
      sig='not'

      if(al.gt.0.and.au.gt.0)sig='yes'
      if(al.lt.0.and.au.lt.0)sig='yes'

      if(sig.eq.'not'.and.lsig.eq.1)goto 101
      if(sig.eq.'not'.and.lsig.eq.2)goto 102
      if(sig.eq.'not'.and.lsig.eq.3)goto 103
      if(lsig.eq.3)goto 104
      lsig=lsig+1
      goto 50

101   type*,'not significant at 5% level'
      goto 500
102   type*,'significant at 5% but not at 1%'
      goto 500
103   type*,'significant at 1% but not at 0.1%'
      goto 500
104   type*,'significant at 0.1% level'
500   type*,' '
      if(amean(1).gt.amean(2))type*,'mean of data set 1 is higher'
      if(amean(2).gt.amean(1))type*,'mean of data set 2 is higher'
      if(amean(2).eq.amean(1))type*,'means identical!!'
      type*,'mean(1)=',amean(1),'mean(2)=',amean(2)
```

```
99    stop
      end
```

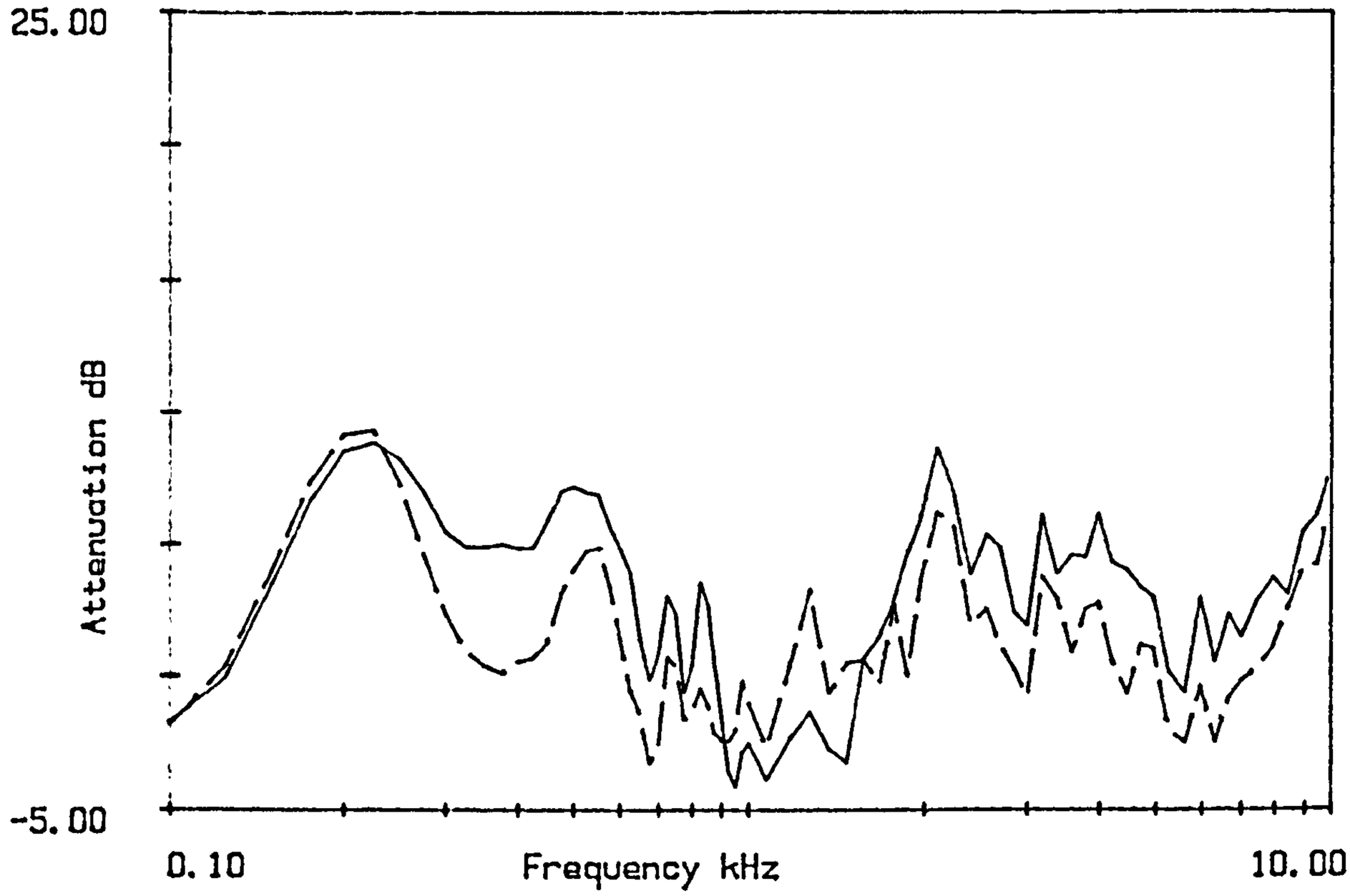

APPENDIX B1 Results from Mixed Oak/Spruce Wood - Hazelborough Wood.
Figure B1.1
Attenuation at C24 on 10/8/83.
Microphone heights 1.2m and 2.5m(----).

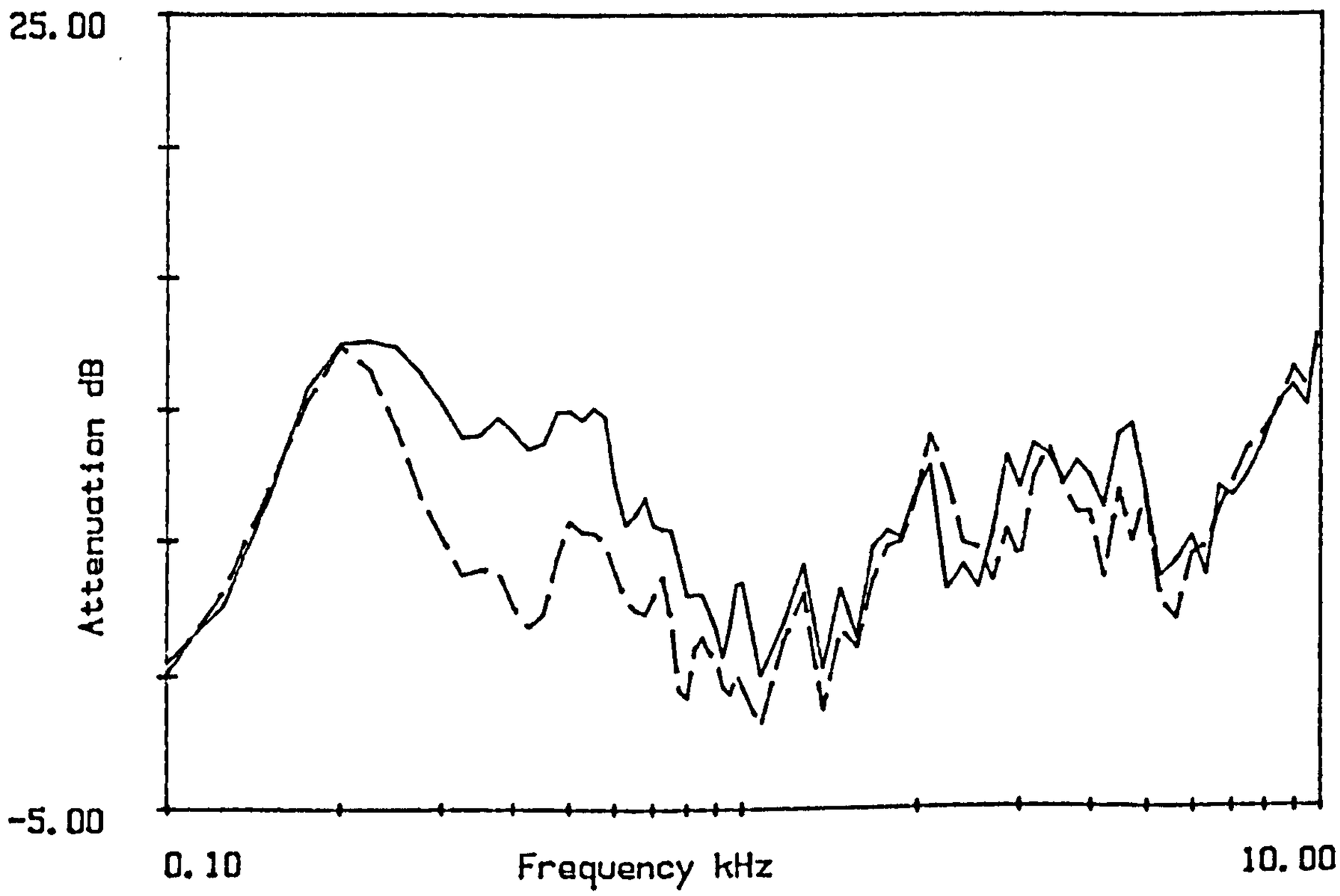

Figure B1.2
Attenuation at C48 on 10/8/83.
Microphone heights 1.2m and 2.5m(----).

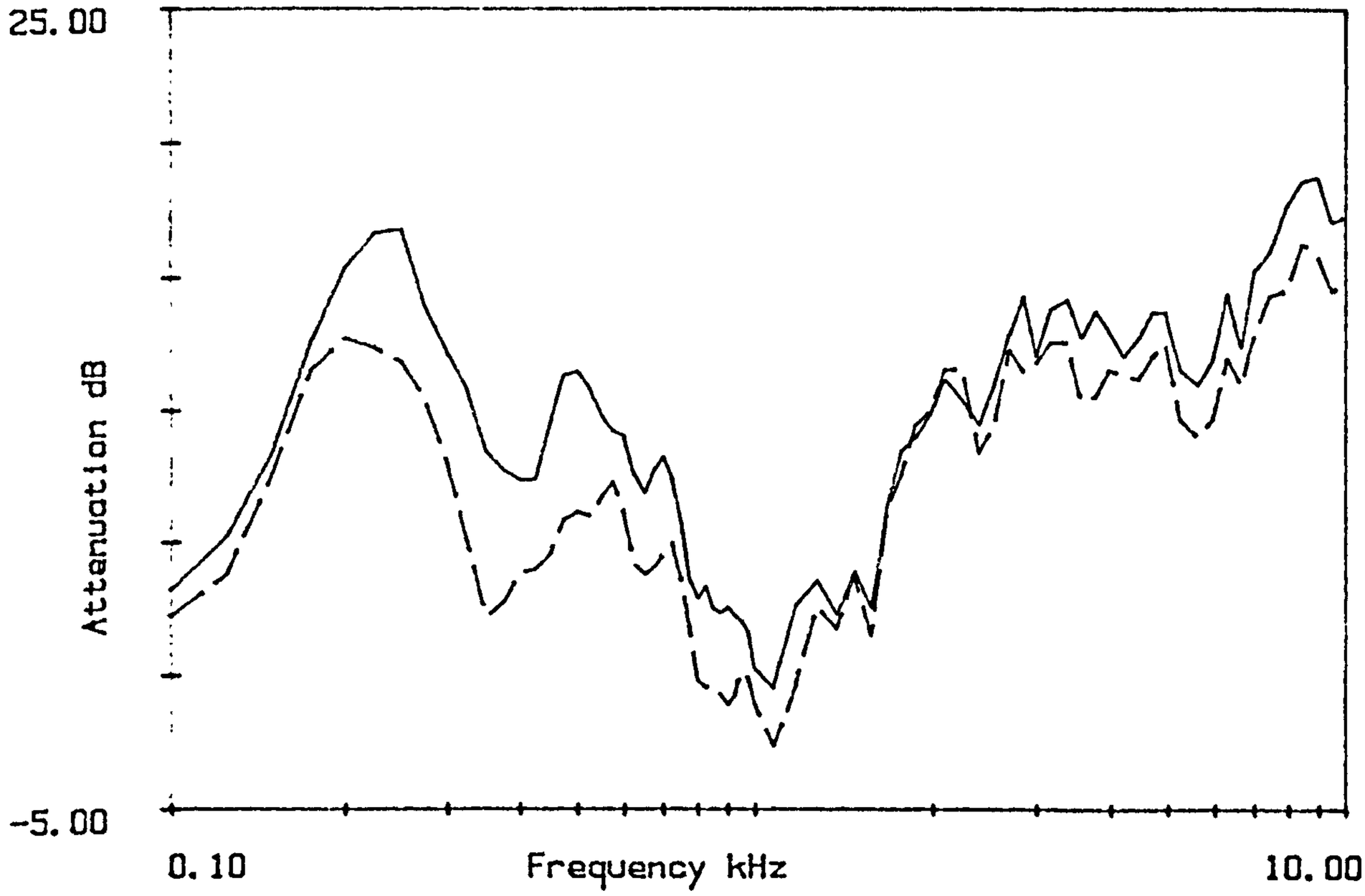

Figure B1.3
Attenuation at C72 on 10/8/83.
Microphone heights 1.2m and 2.5m(----).

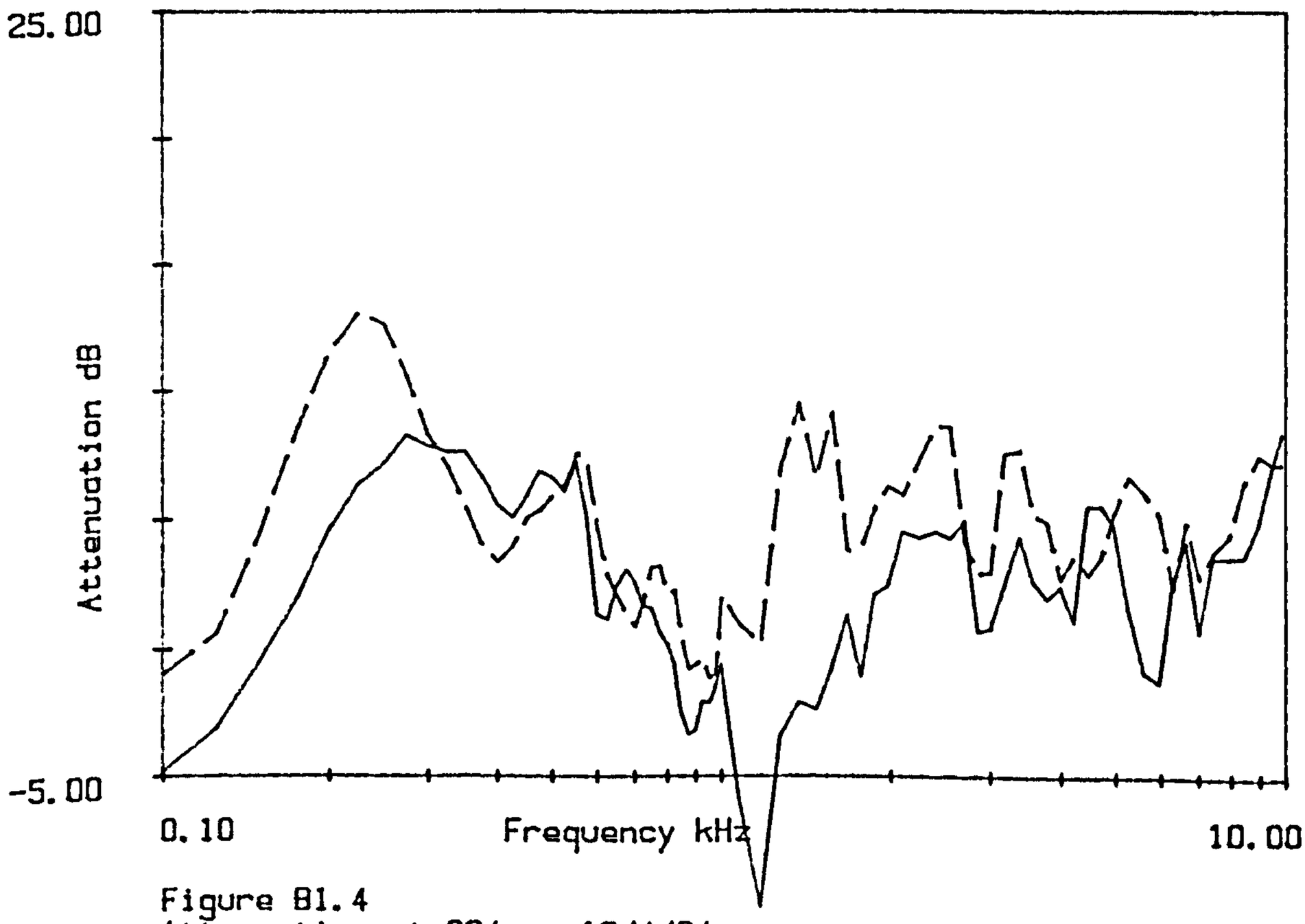

Figure B1.4
Attenuation at C24 on 10/4/84.
Microphone heights 1.2m and 2.5m(----).

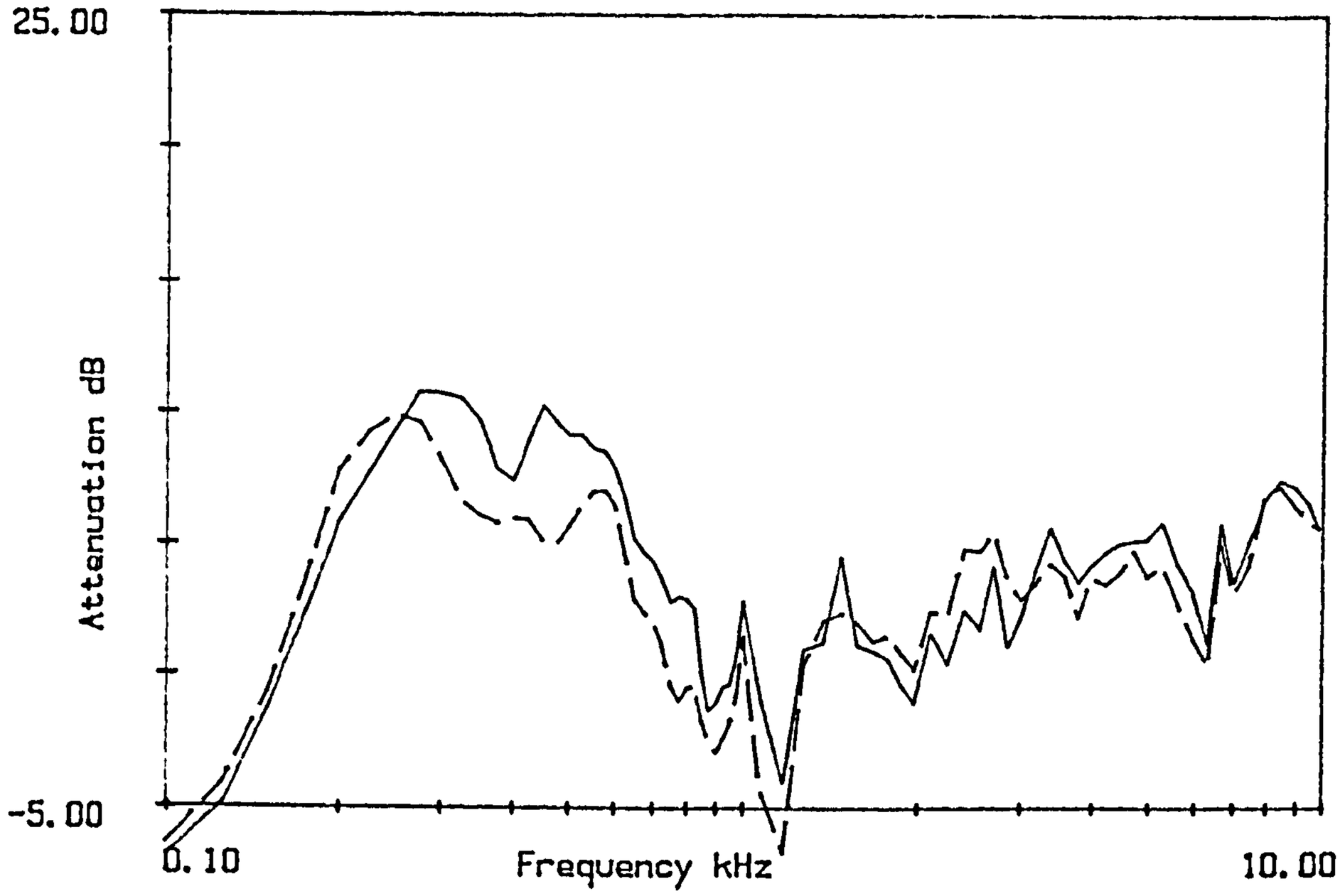

Figure B1.5
Attenuation at C48 on 10/4/84.
Microphone heights 1.2m and 2.5m(-----).

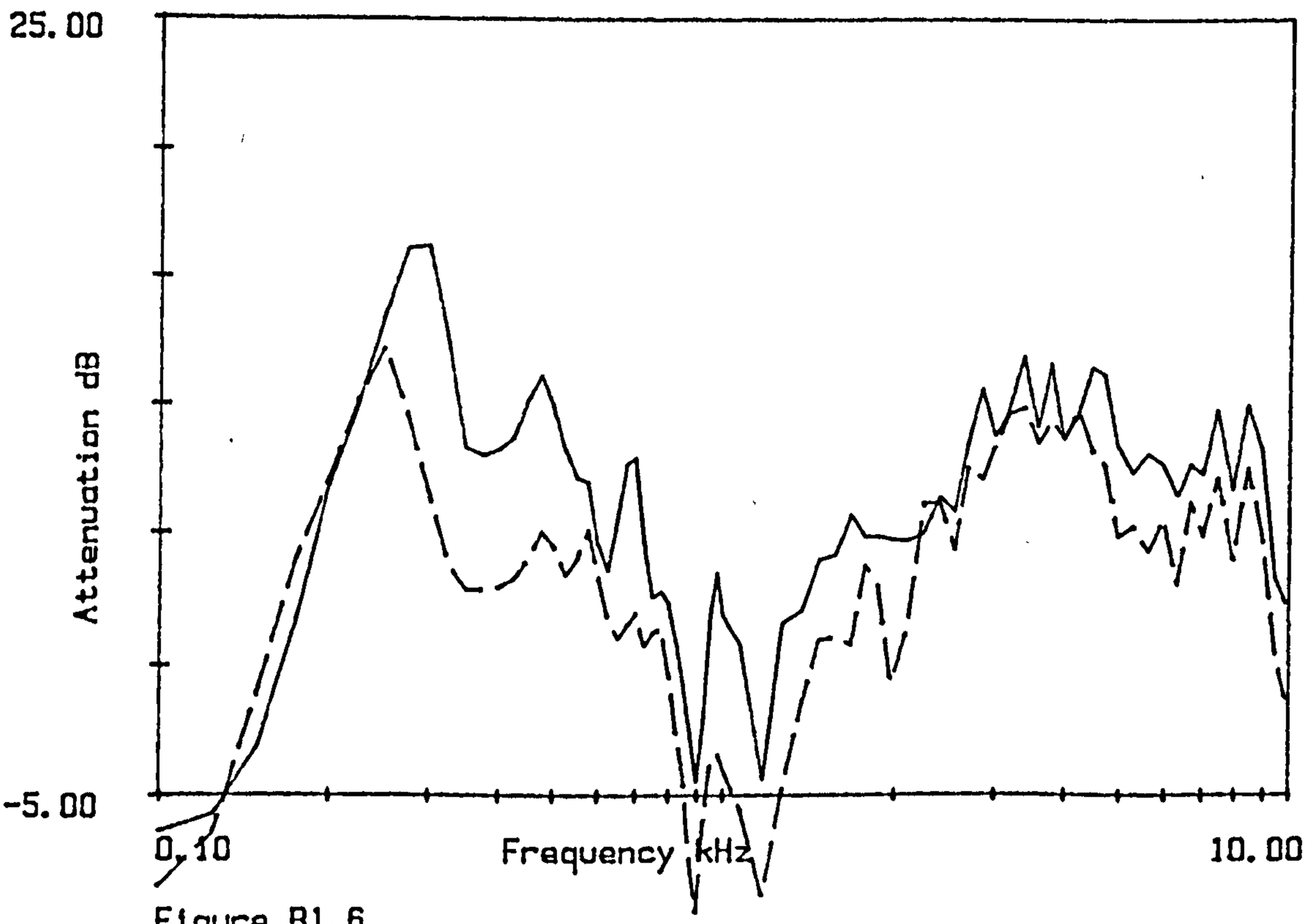

Figure B1.6
Attenuation at C72 on 10/4/84.
Microphone heights 1.2m and 2.5m(-----).

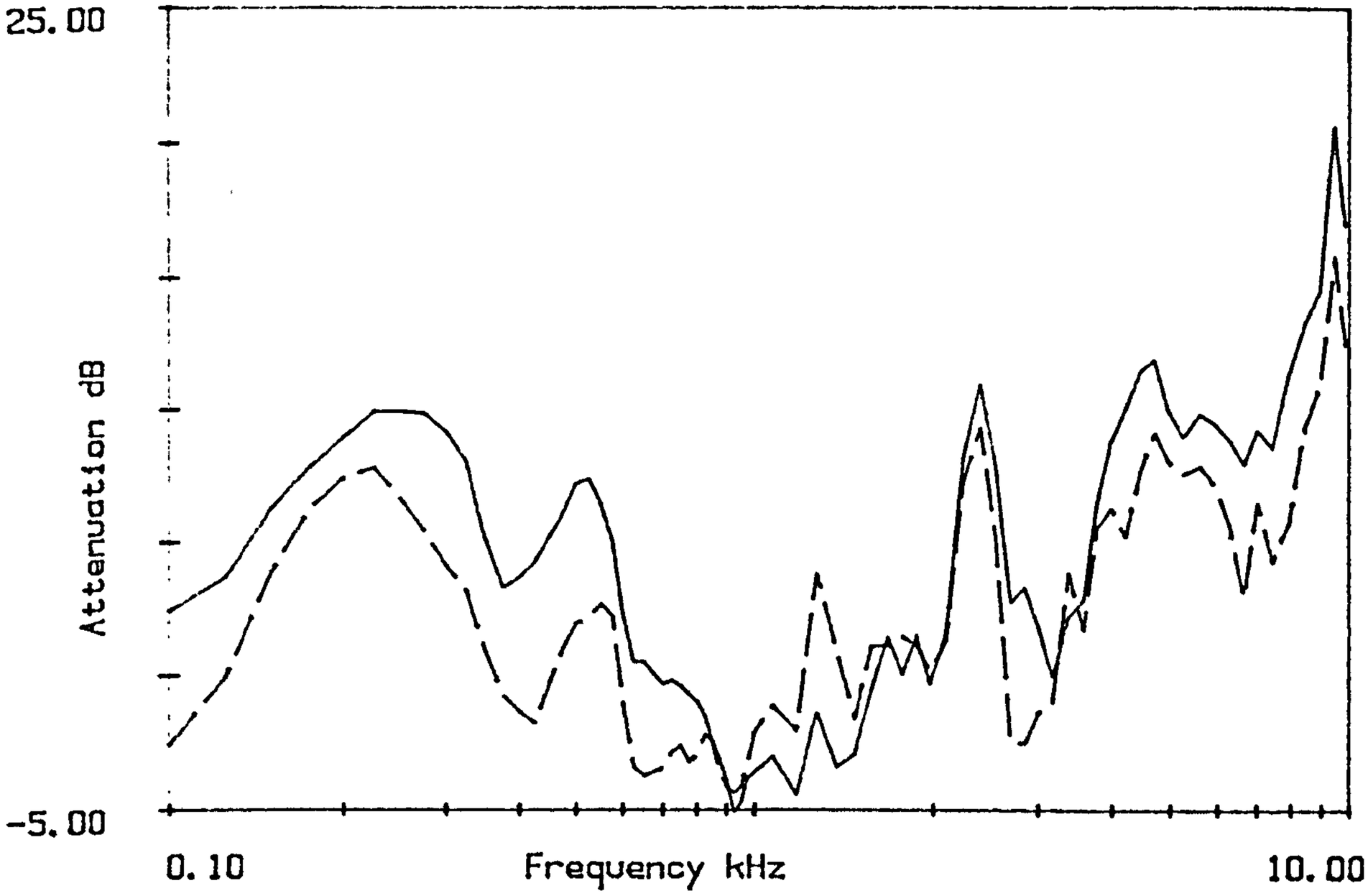

Figure B1.7
Attenuation at C24 on 5/7/84.
Microphone heights 1.2m and 2.5m(----).

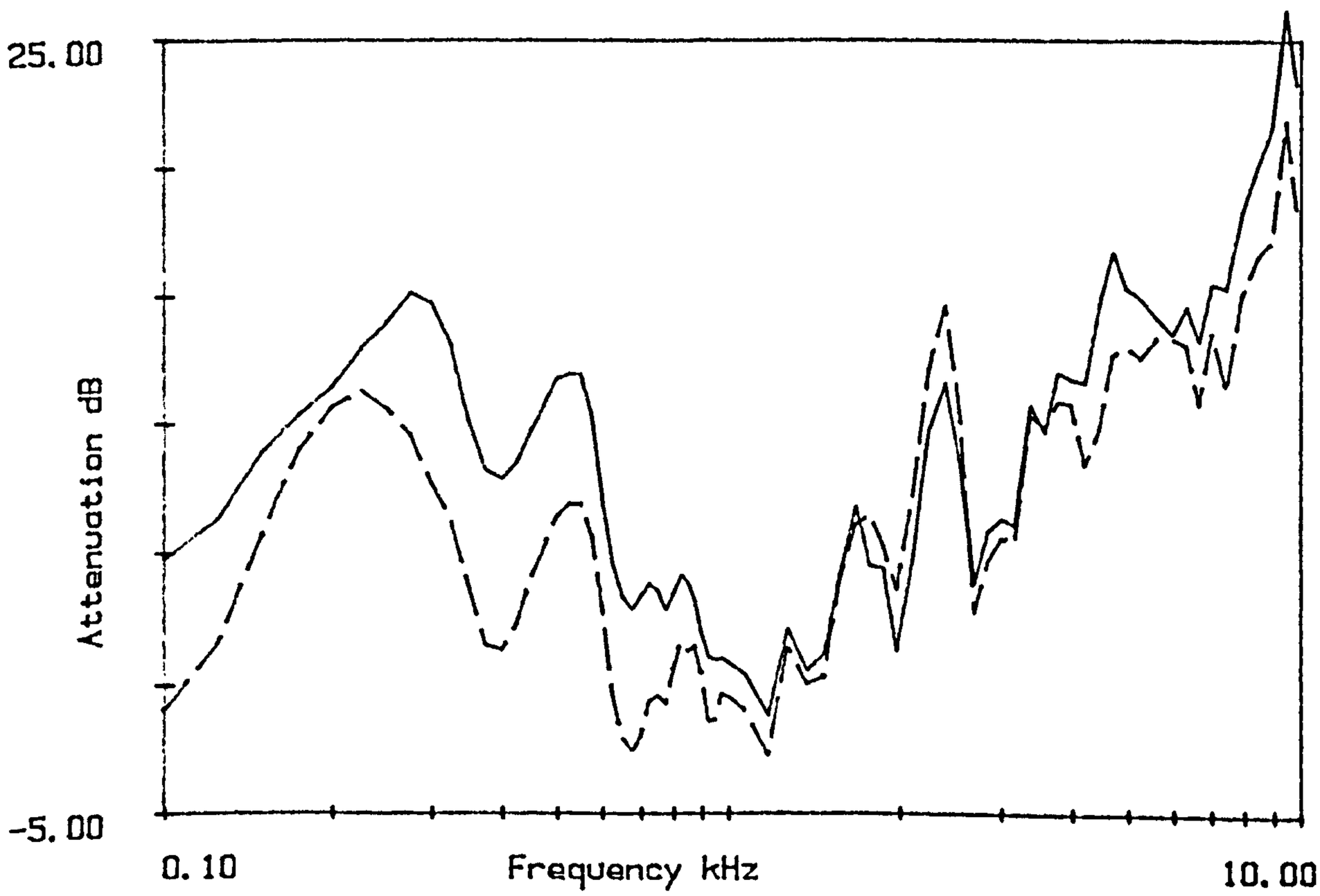

Figure B1.8
Attenuation at C48 on 5/7/84.
Microphone heights 1.2m and 2.5m(----).

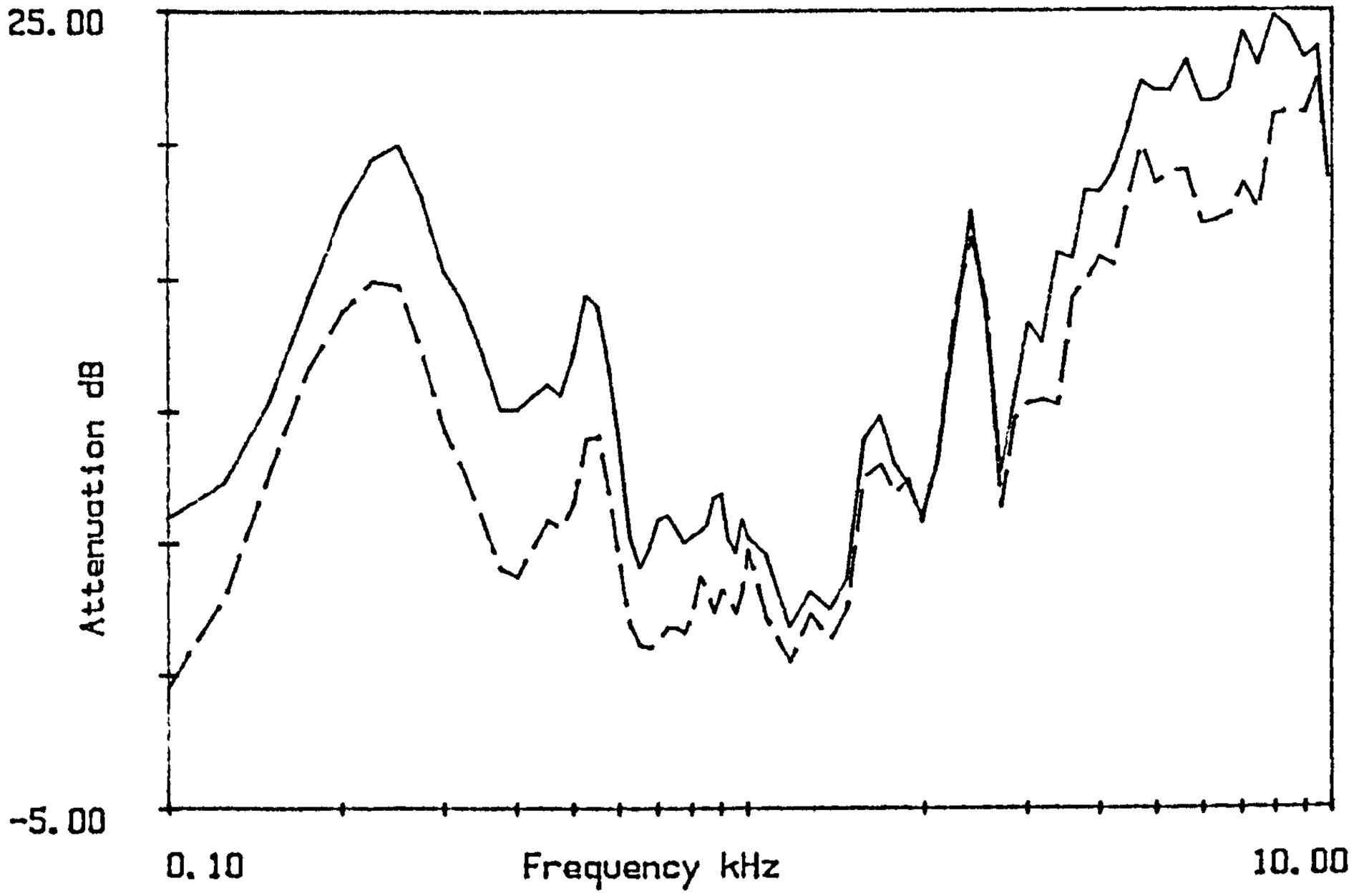

Figure B1.9
Attenuation at C72 on 5/7/84.
Microphone heights 1.2m and 2.5m(----).

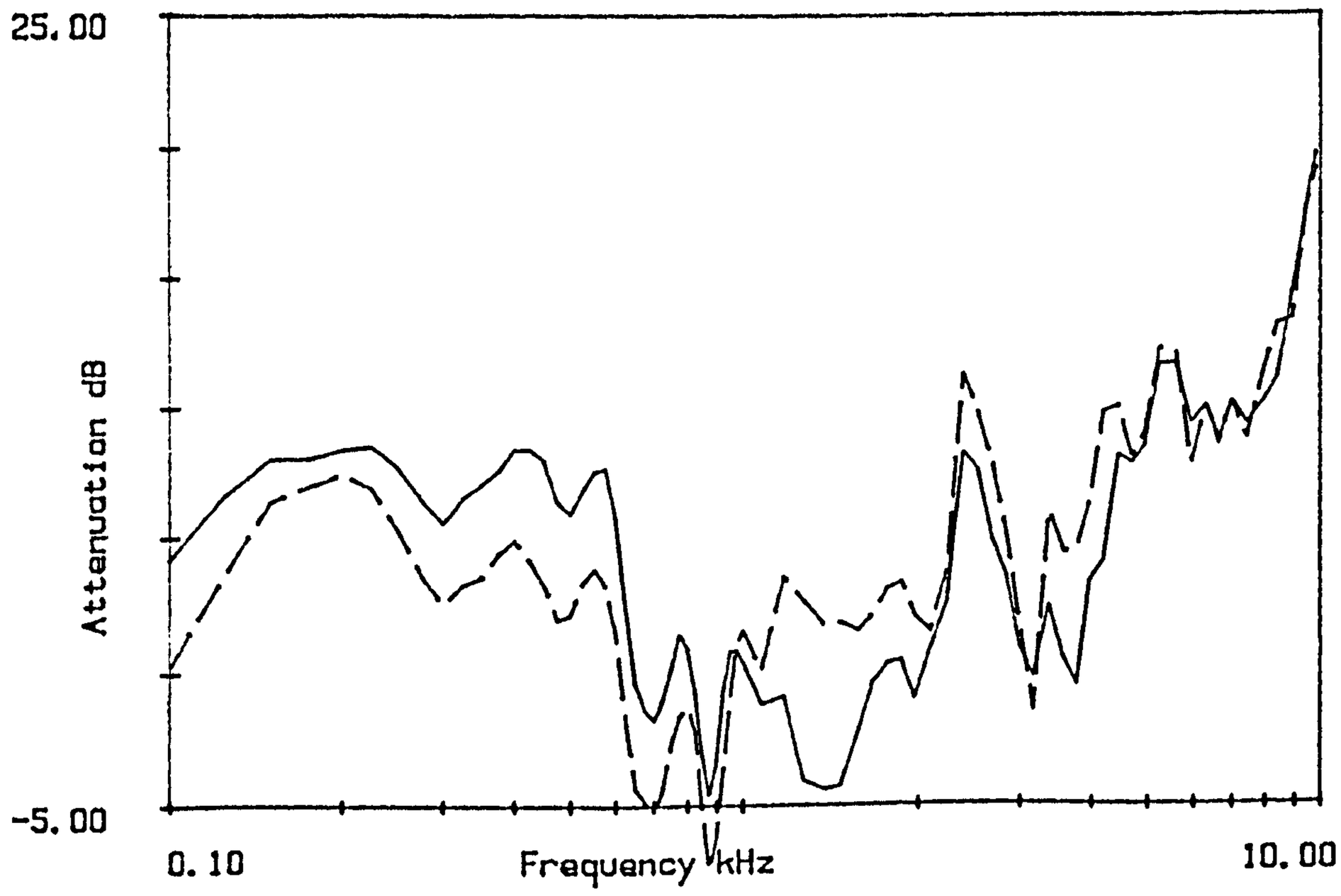

Figure B1.10
Attenuation at D24 on 5/7/84.
Microphone heights 1.2m and 2.5m(----).

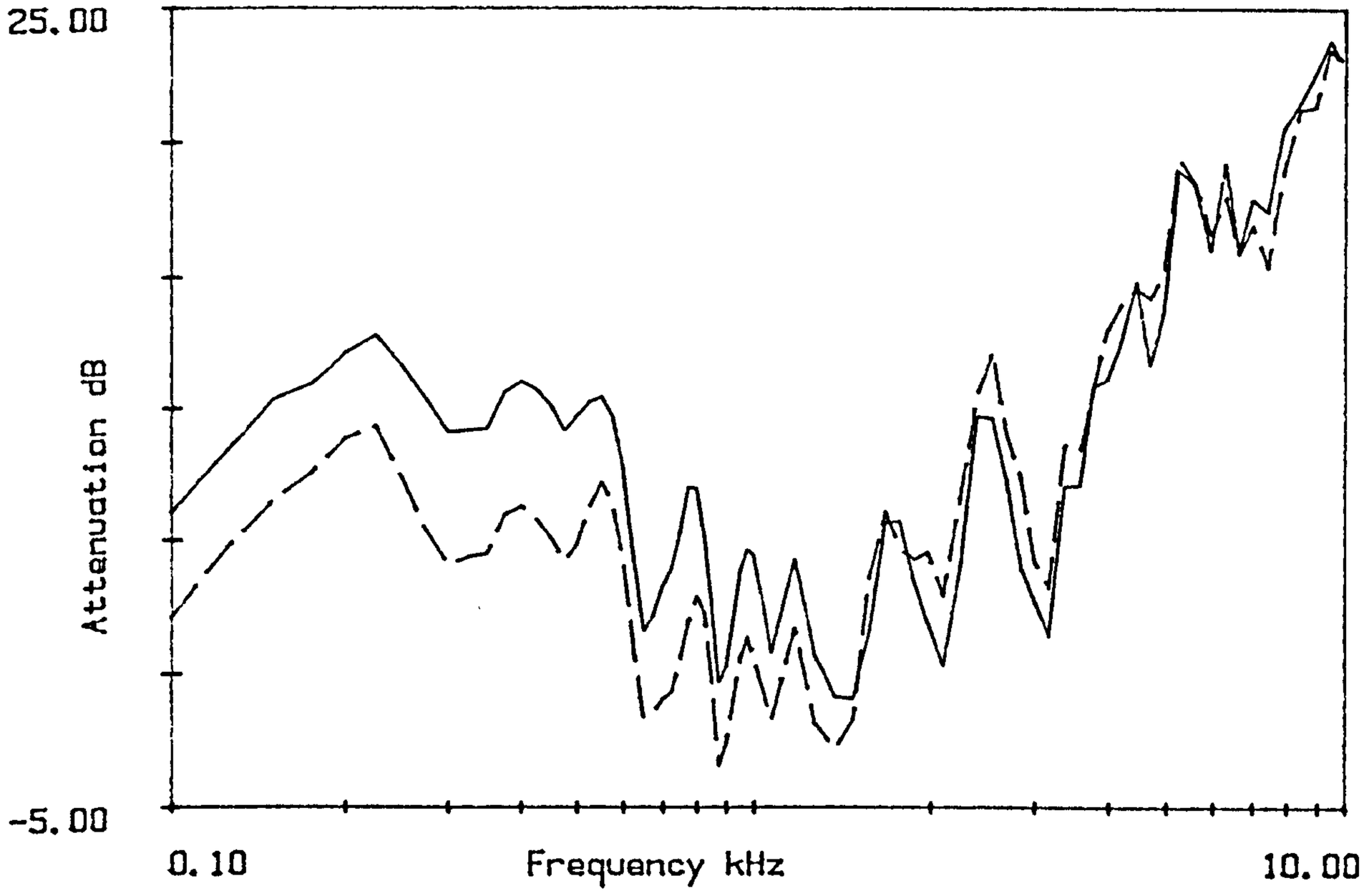

Figure B1.11
Attenuation at D48 on 5/7/84.
Microphone heights 1.2m and 2.5m(----).

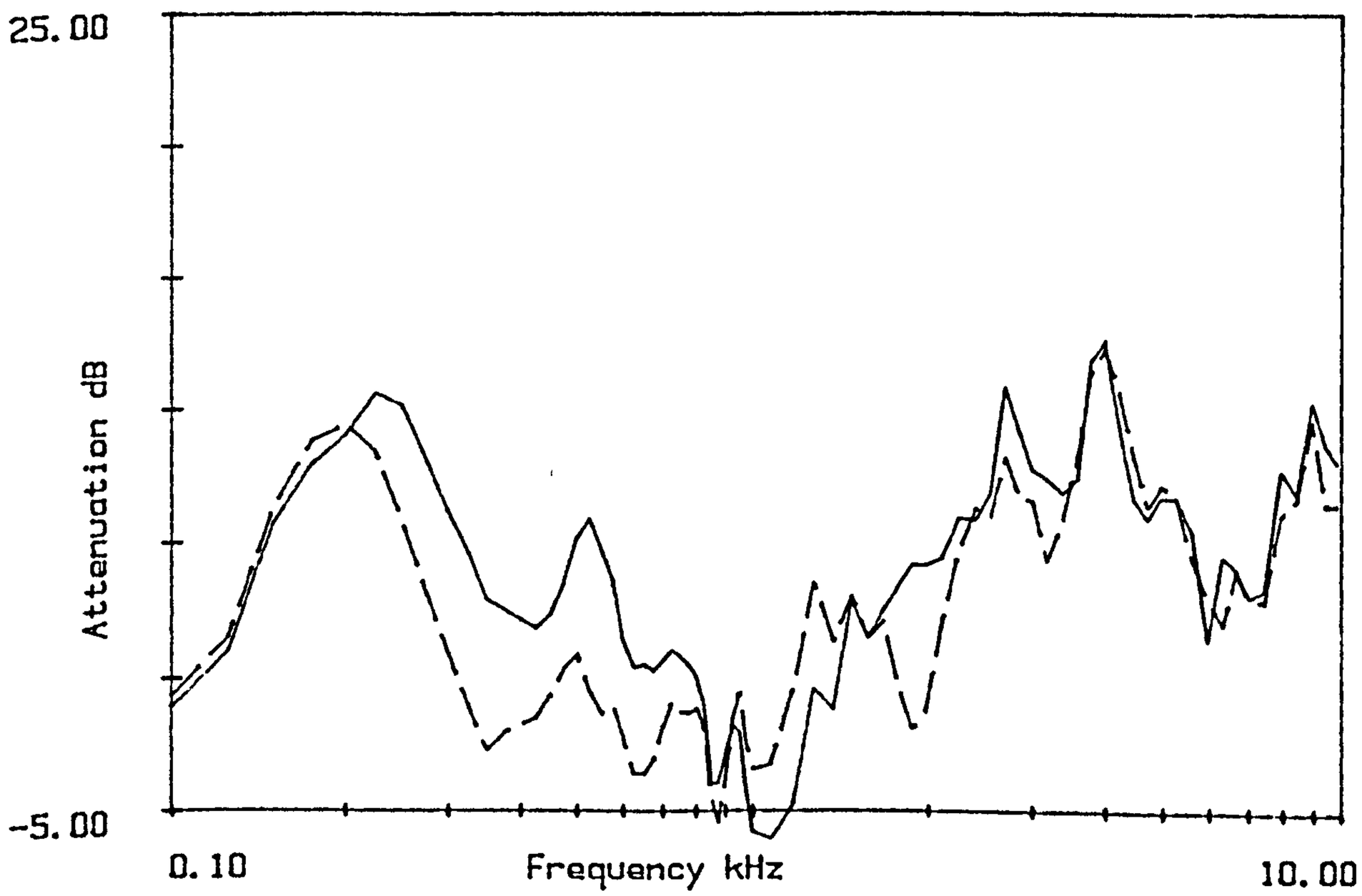

Figure B1.12
Attenuation at H24 on 9/8/84.
Microphone heights 1.2m and 2.5m(----).

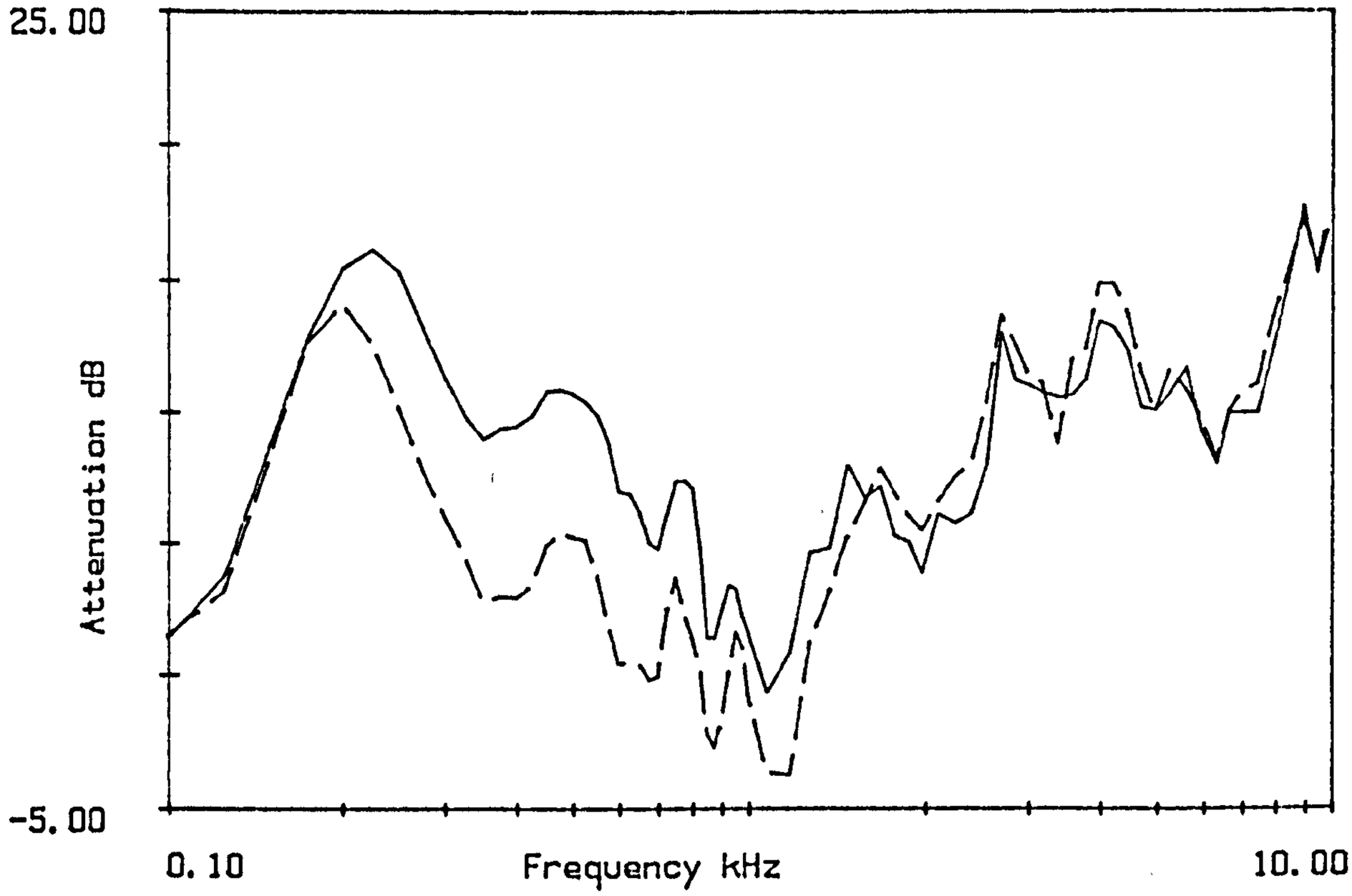

Figure B1.13
Attenuation at H48 on 9/8/84.
Microphone heights 1.2m and 2.5m(----).

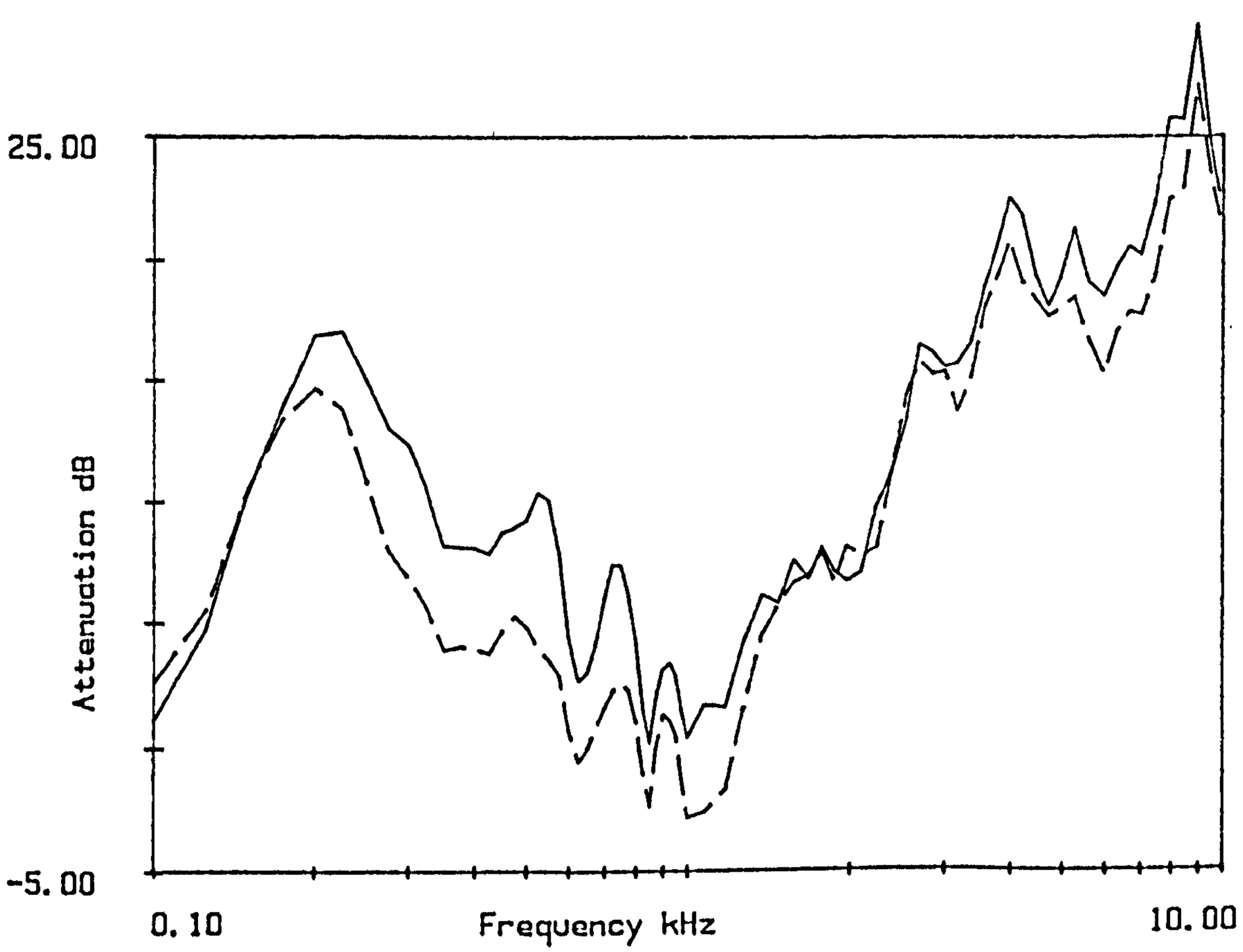

Figure B1.14
Attenuation at H72 on 9/8/84.
Microphone heights 1.2m and 2.5m(----).

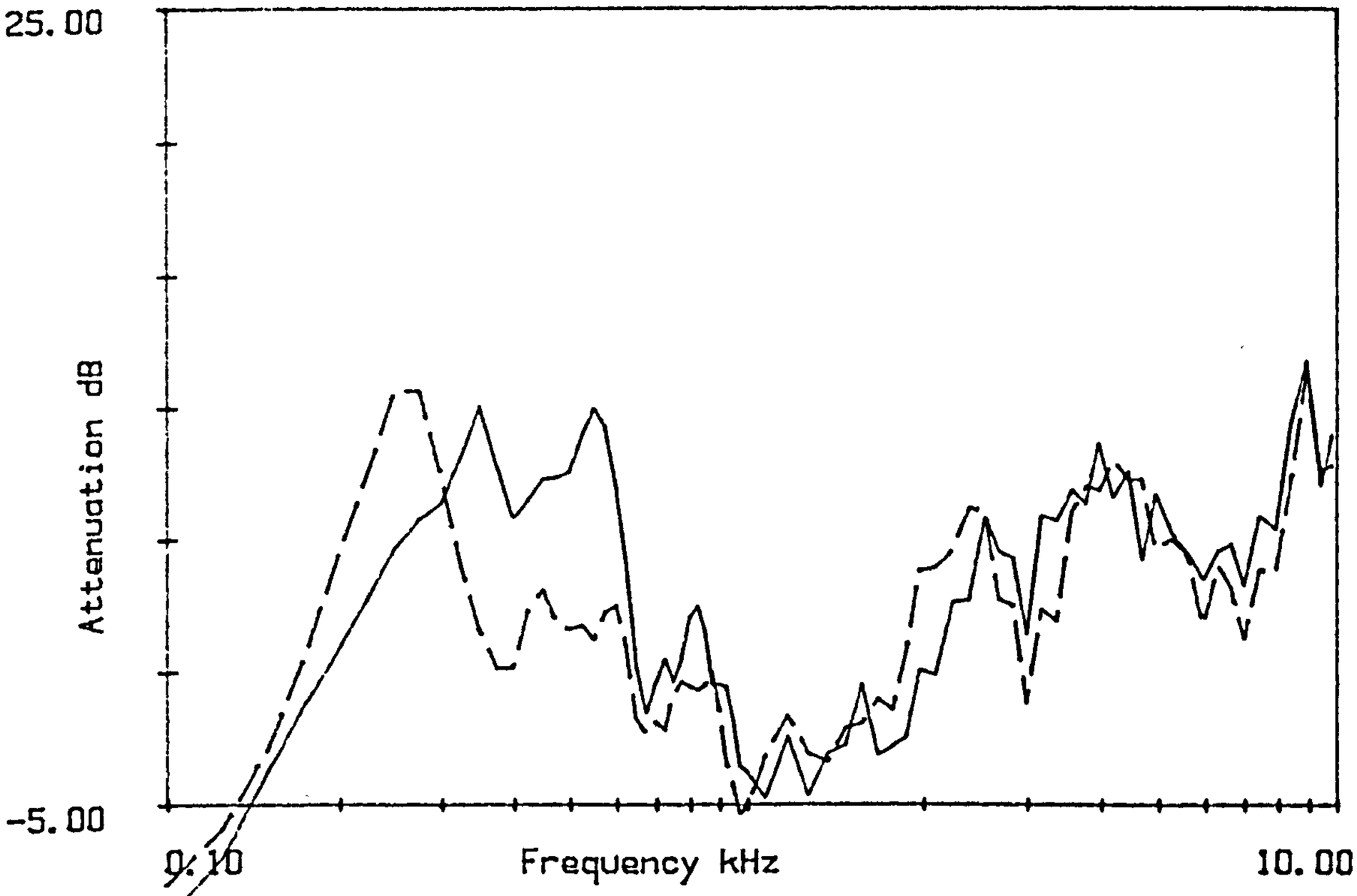

Figure B1.17
Attenuation at C48 on 20/6/85. at 14.30
Microphone heights 1.2m and 2.5m(----).

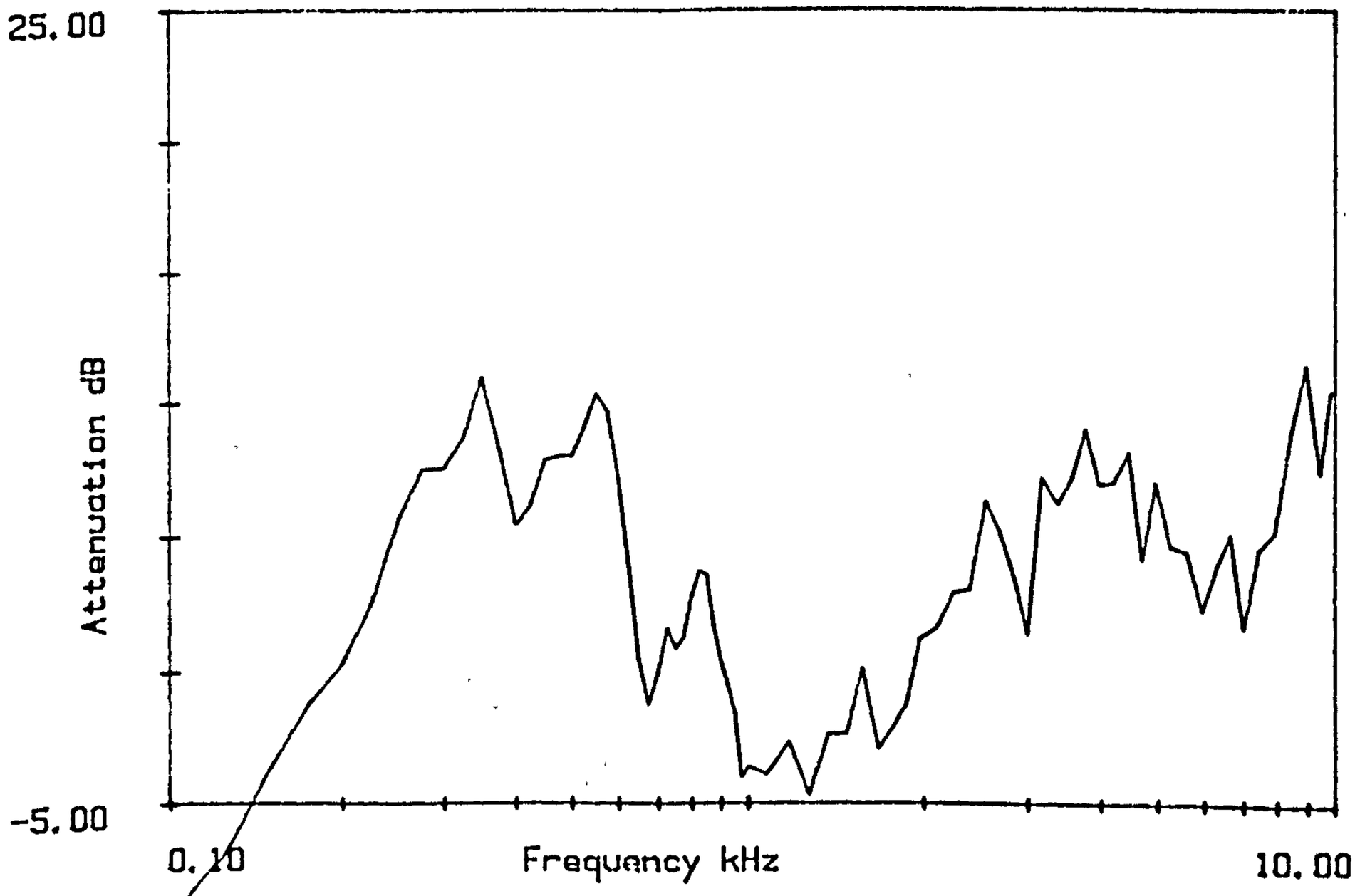

Figure B1.18
Attenuation at C48 on 20/6/85. at 15.50
Microphone height 1.2m.

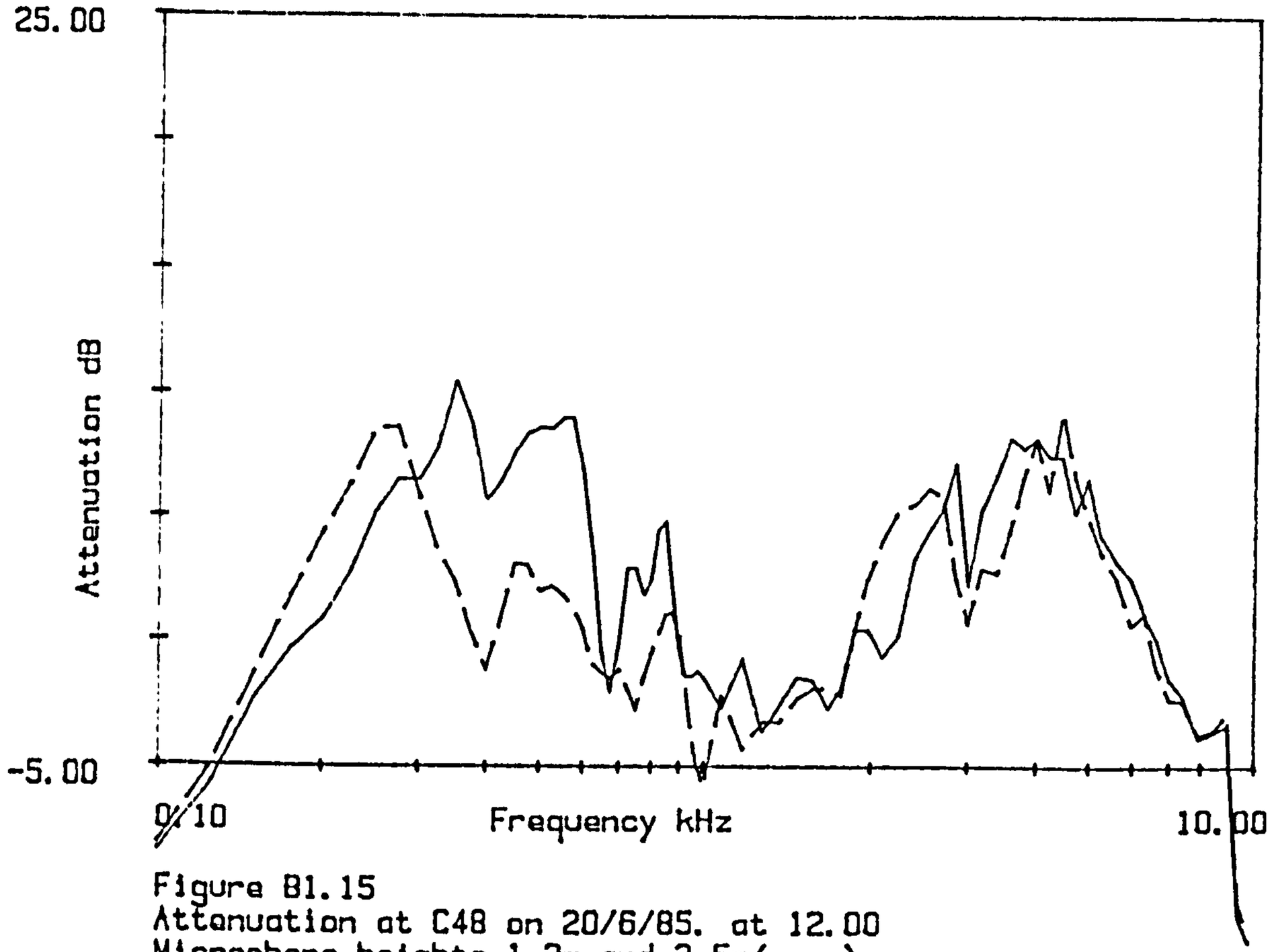

Figure 81.15
Attenuation at C48 on 20/6/85. at 12.00
Microphone heights 1.2m and 2.5m(----).

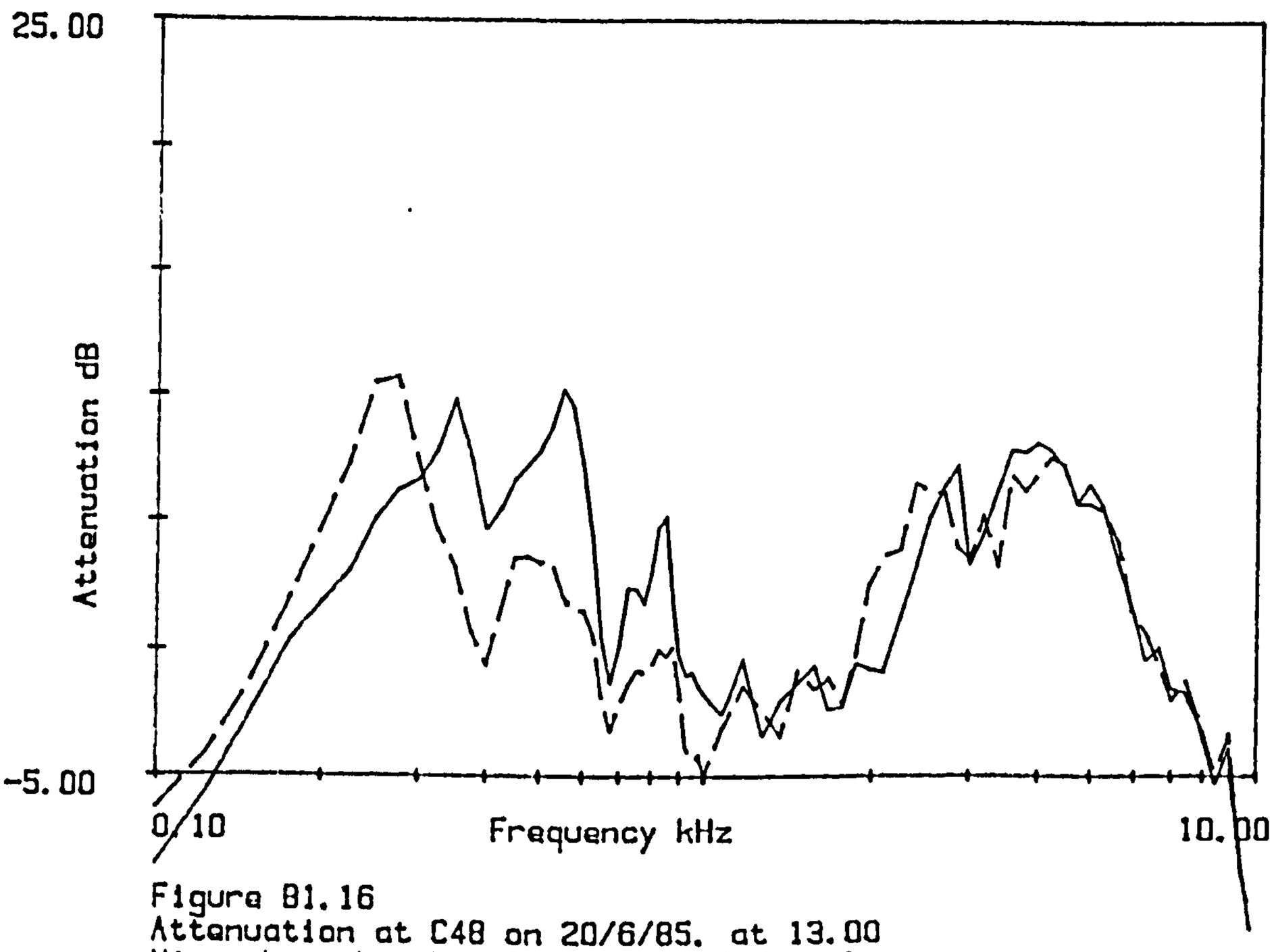

Figure 81.16
Attenuation at C48 on 20/6/85. at 13.00
Microphone heights 1.2m and 2.5m(----).

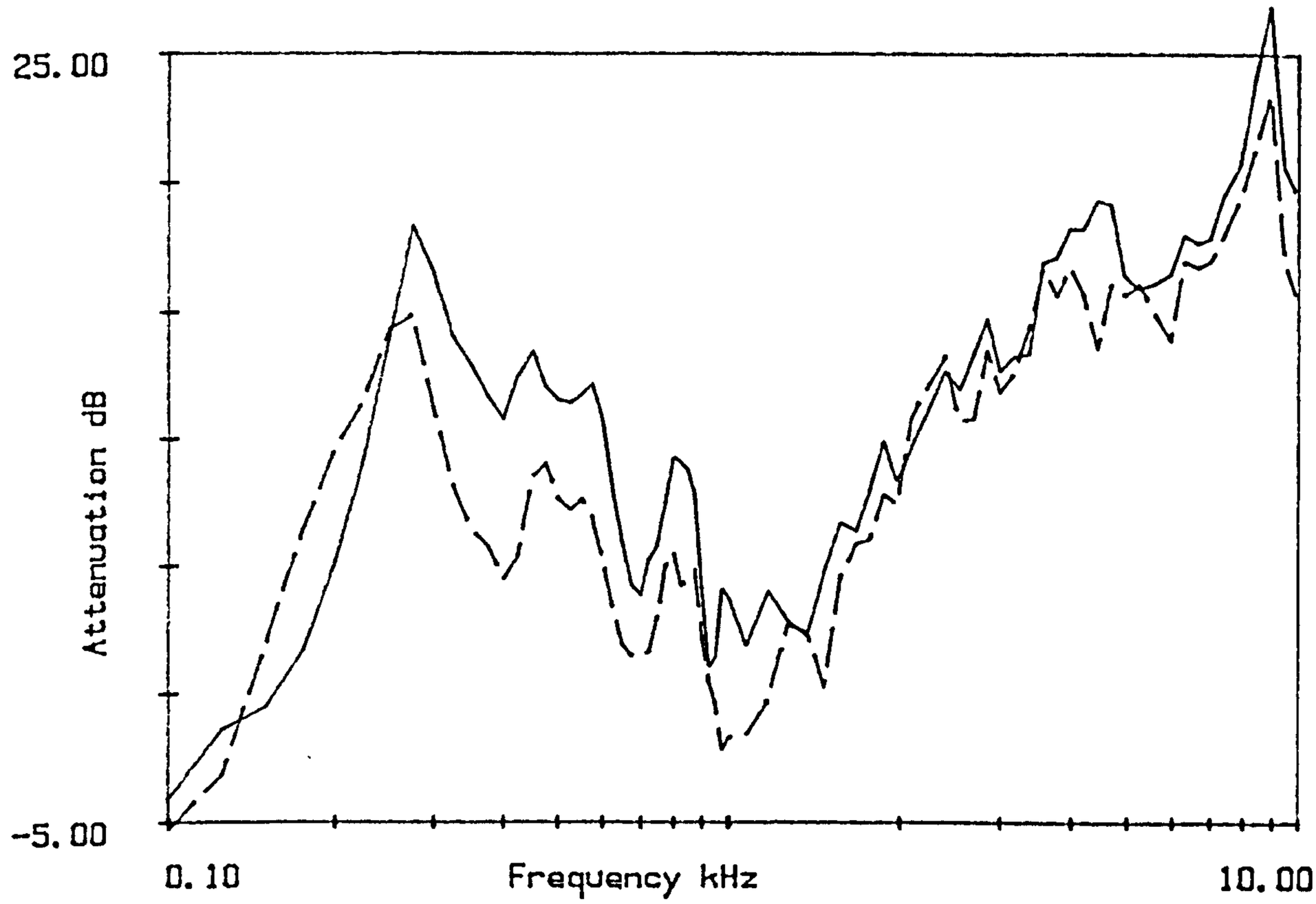

Figure 81.19
Attenuation at C72 on 20/6/85. at 12.00
Microphone heights 1.2m and 2.5m(----).

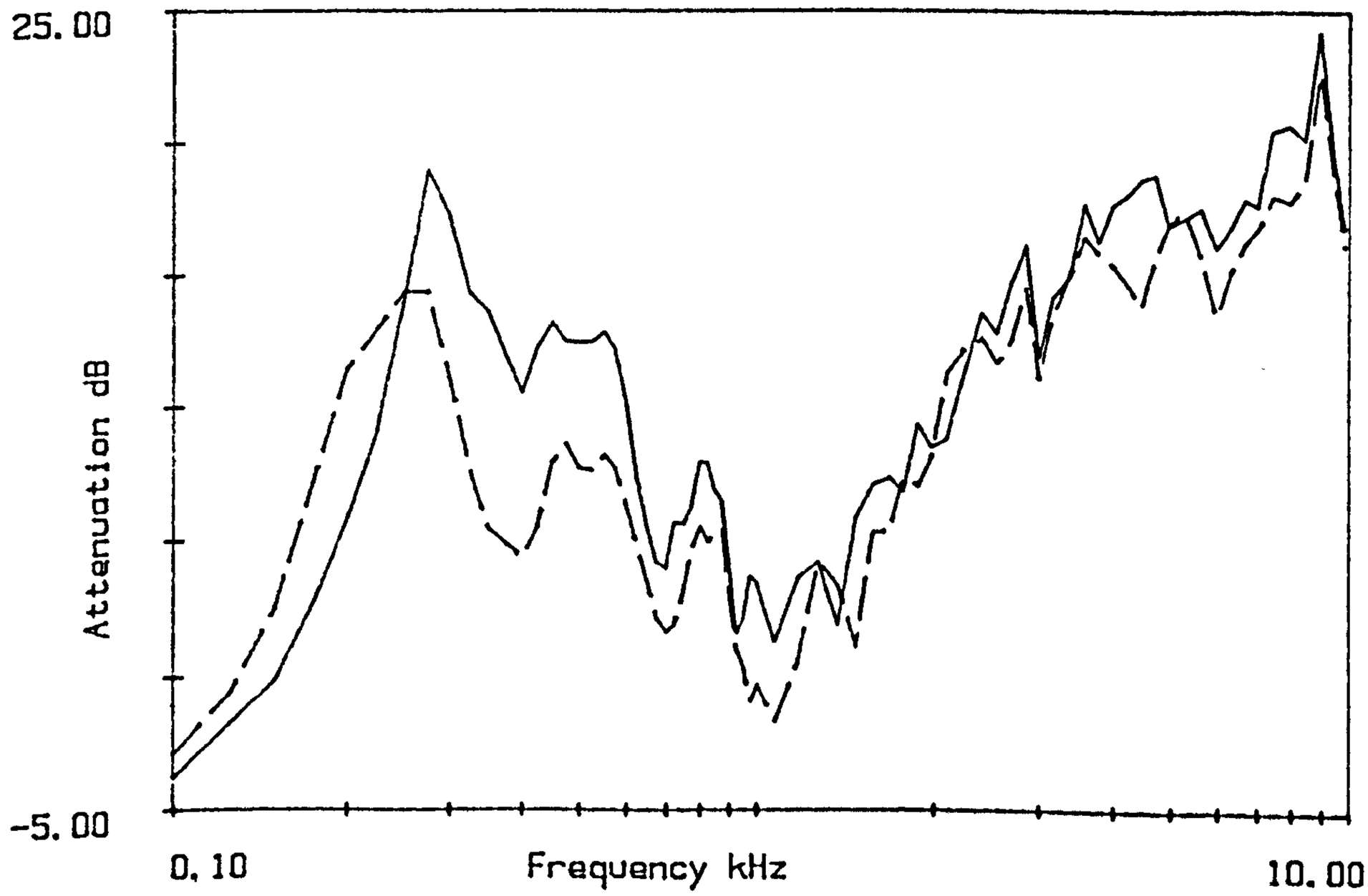

Figure 81.20
Attenuation at C72 on 20/6/85. at 13.00
Microphone heights 1.2m and 2.5m(----).

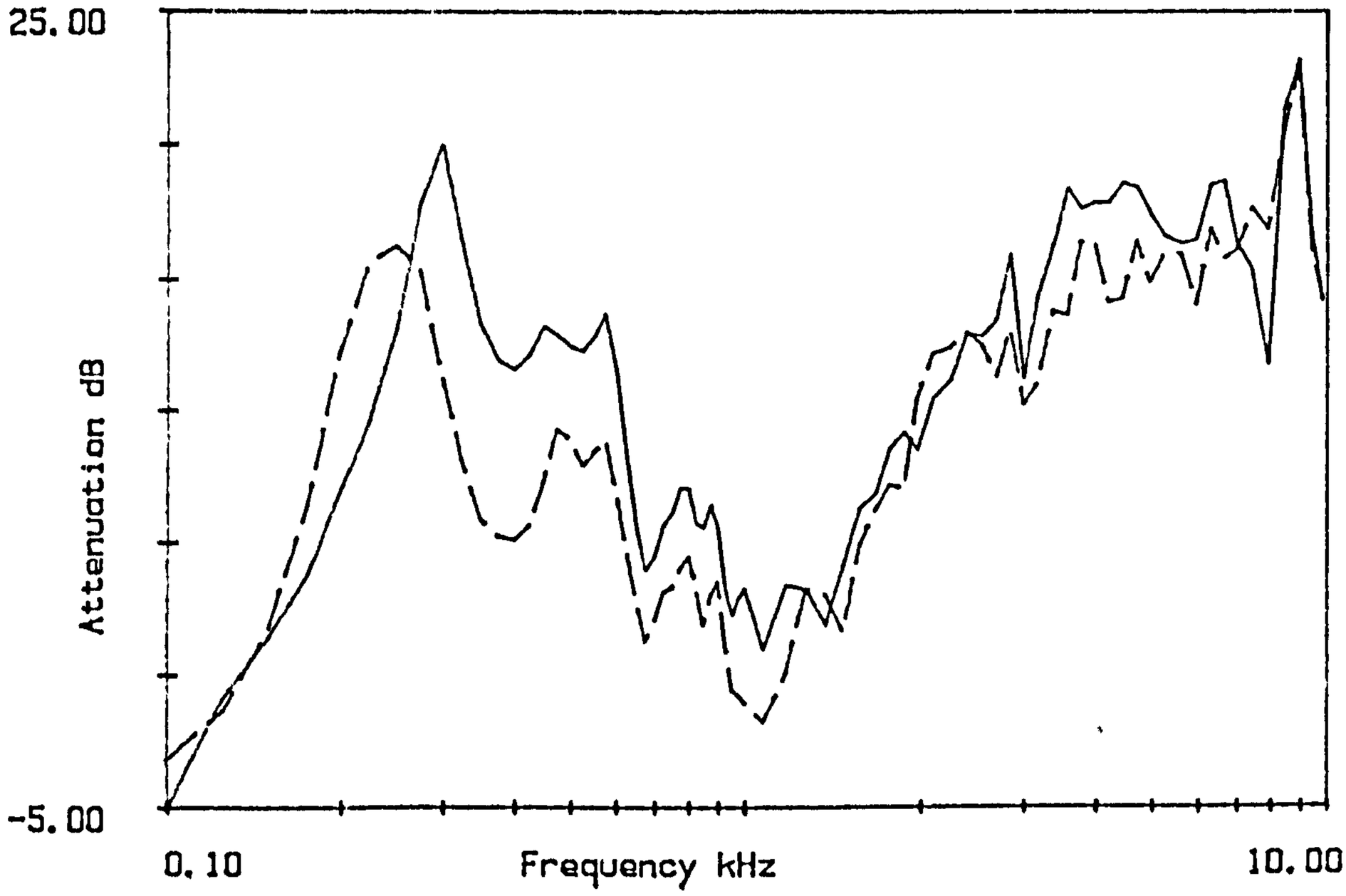

Figure B1.21
Attenuation at C72 on 20/6/85. at 14.30
Microphone heights 1.2m and 2.5m(----).

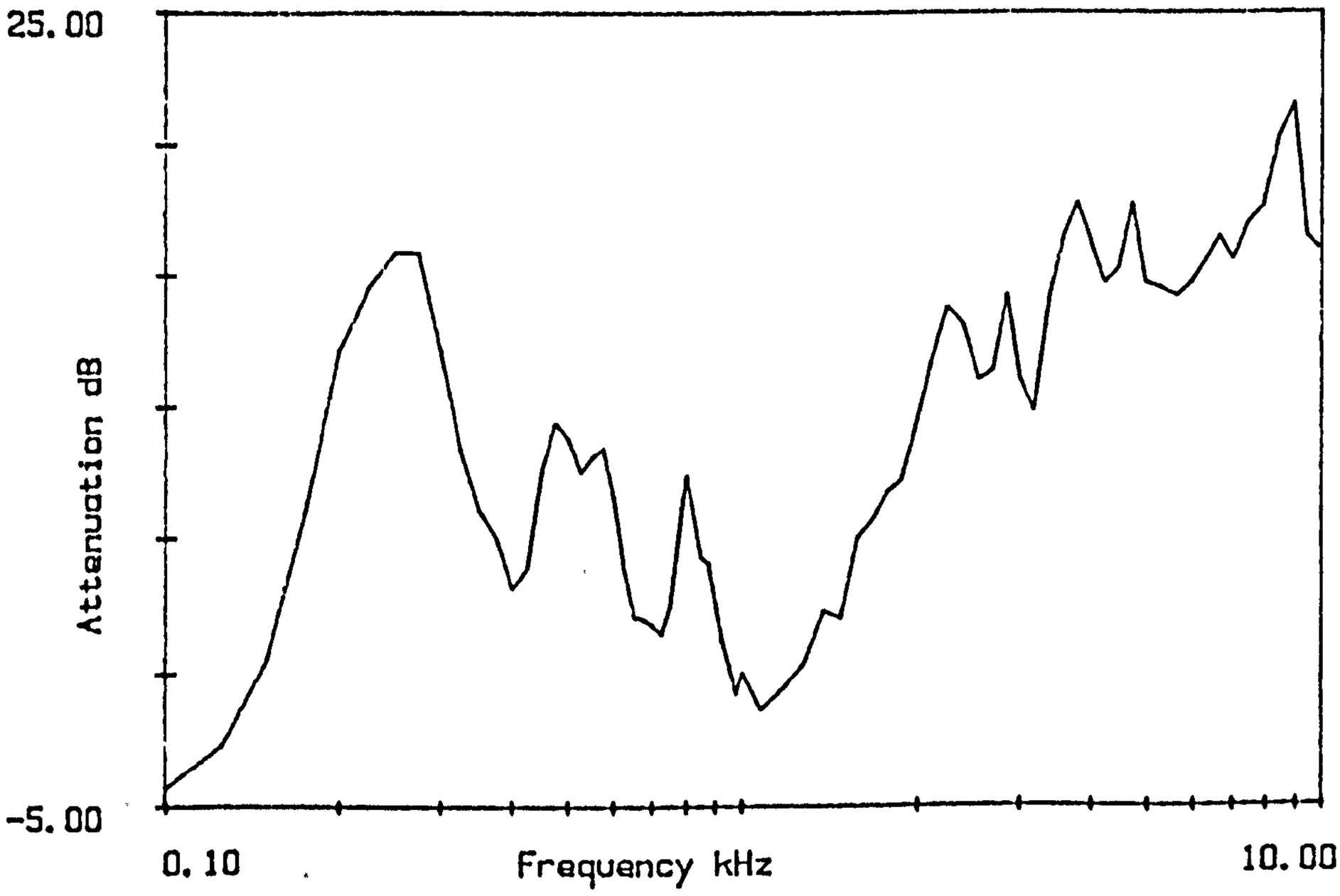

Figure B1.22
Attenuation at C72 on 20/6/85. at 15.50
Microphone height 2.5m.

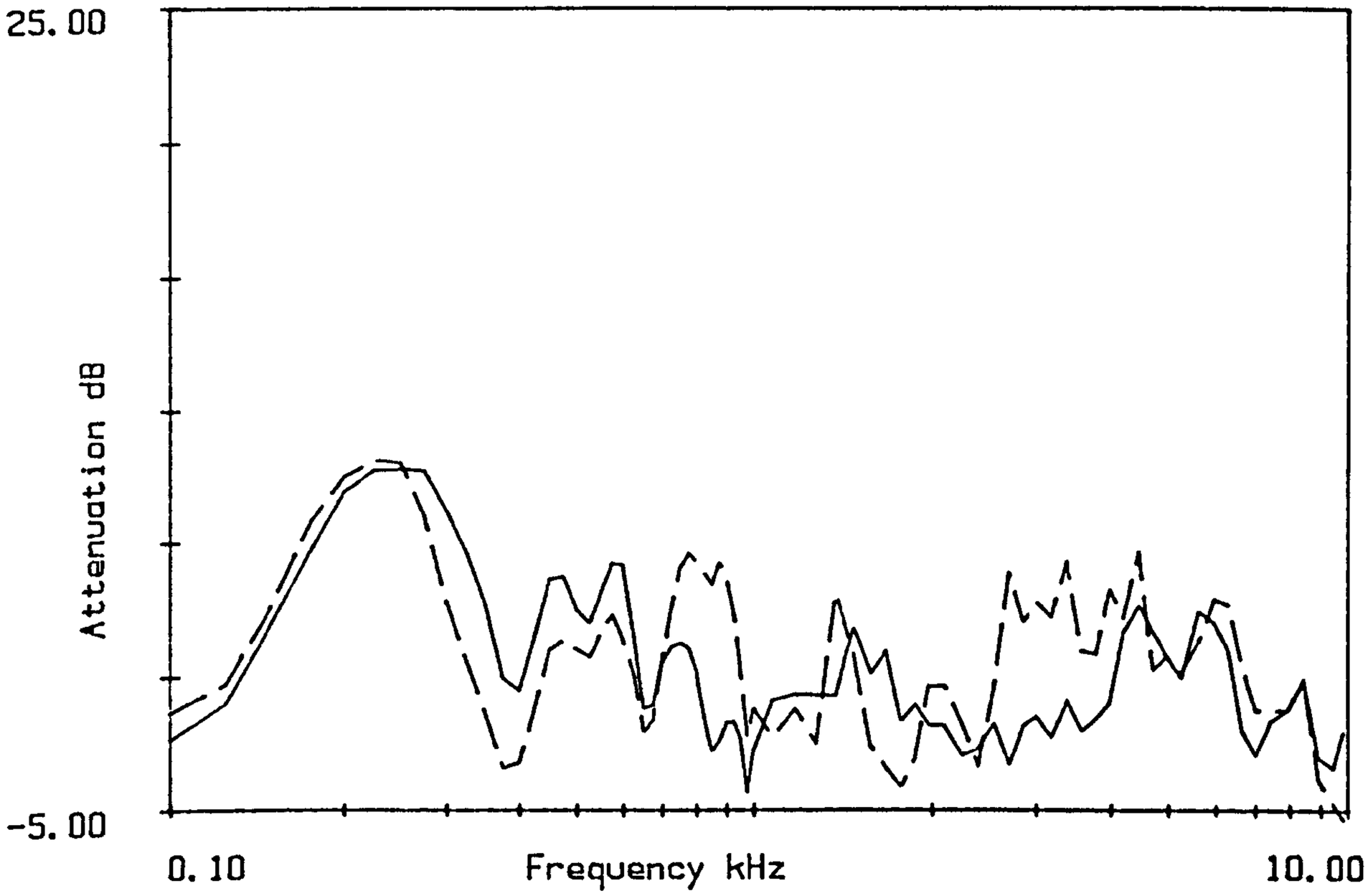

APPENDIX B2 Results from Spruce Monoculture - Wetleys Wood.
Figure B2.1
Attenuation at A12 on 28/7/83.
Microphone heights 1.2m and 2.5m(----).

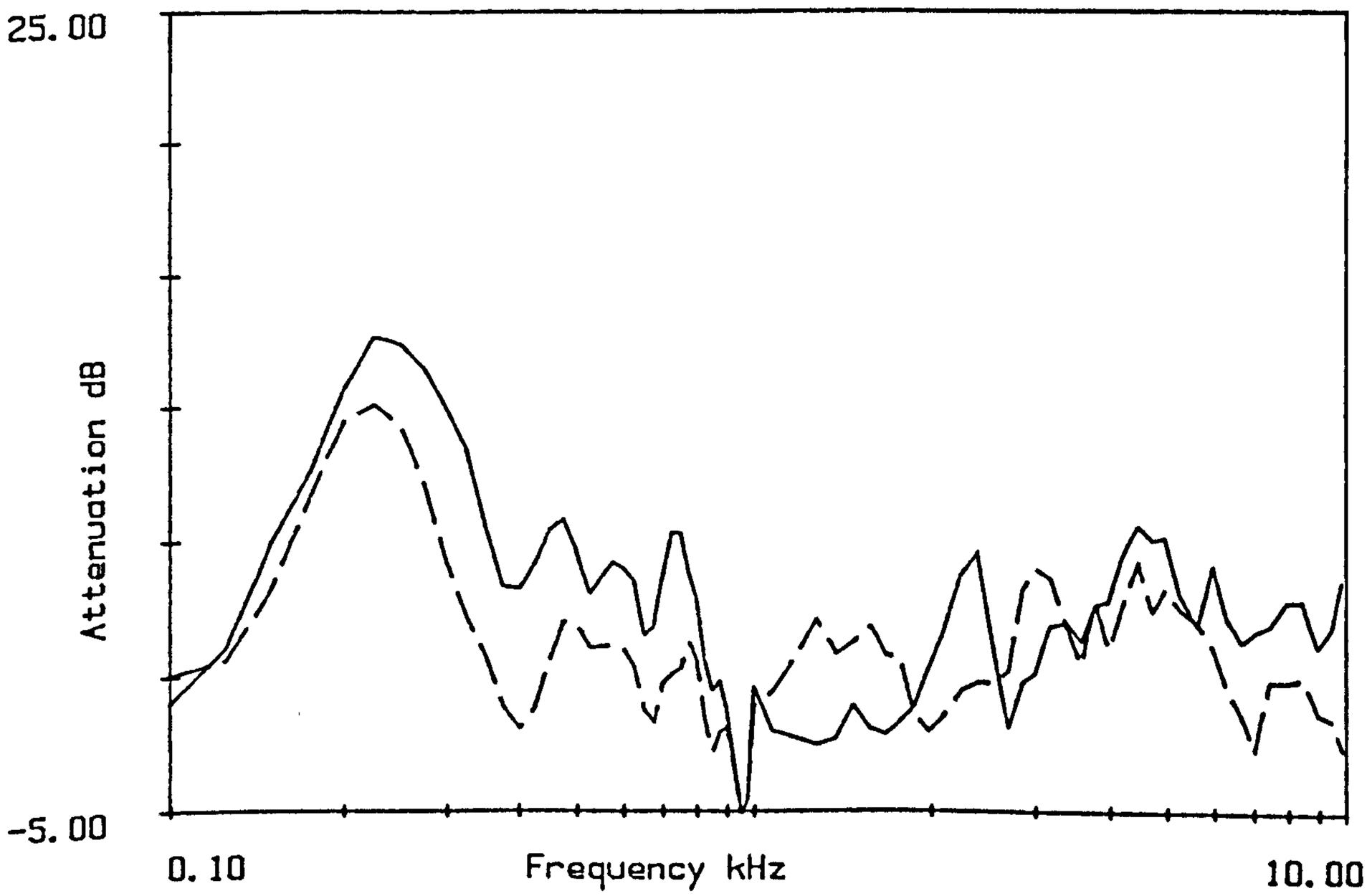

Figure B2.2
Attenuation at A24 on 28/7/83.
Microphone heights 1.2m and 2.5m(----).

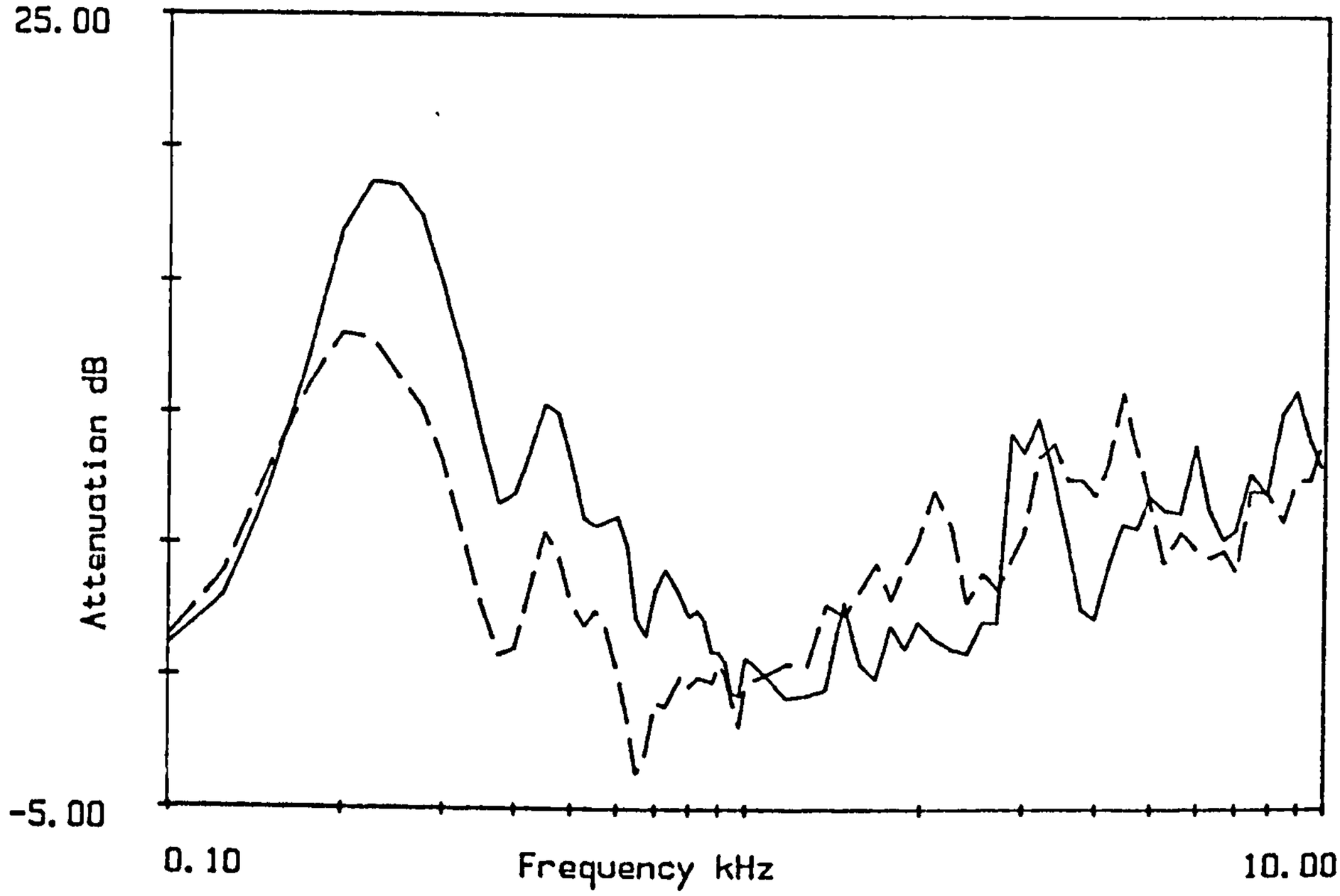

Figure B2.3
Attenuation at A48 on 28/7/83.
Microphone heights 1.2m and 2.5m(----).

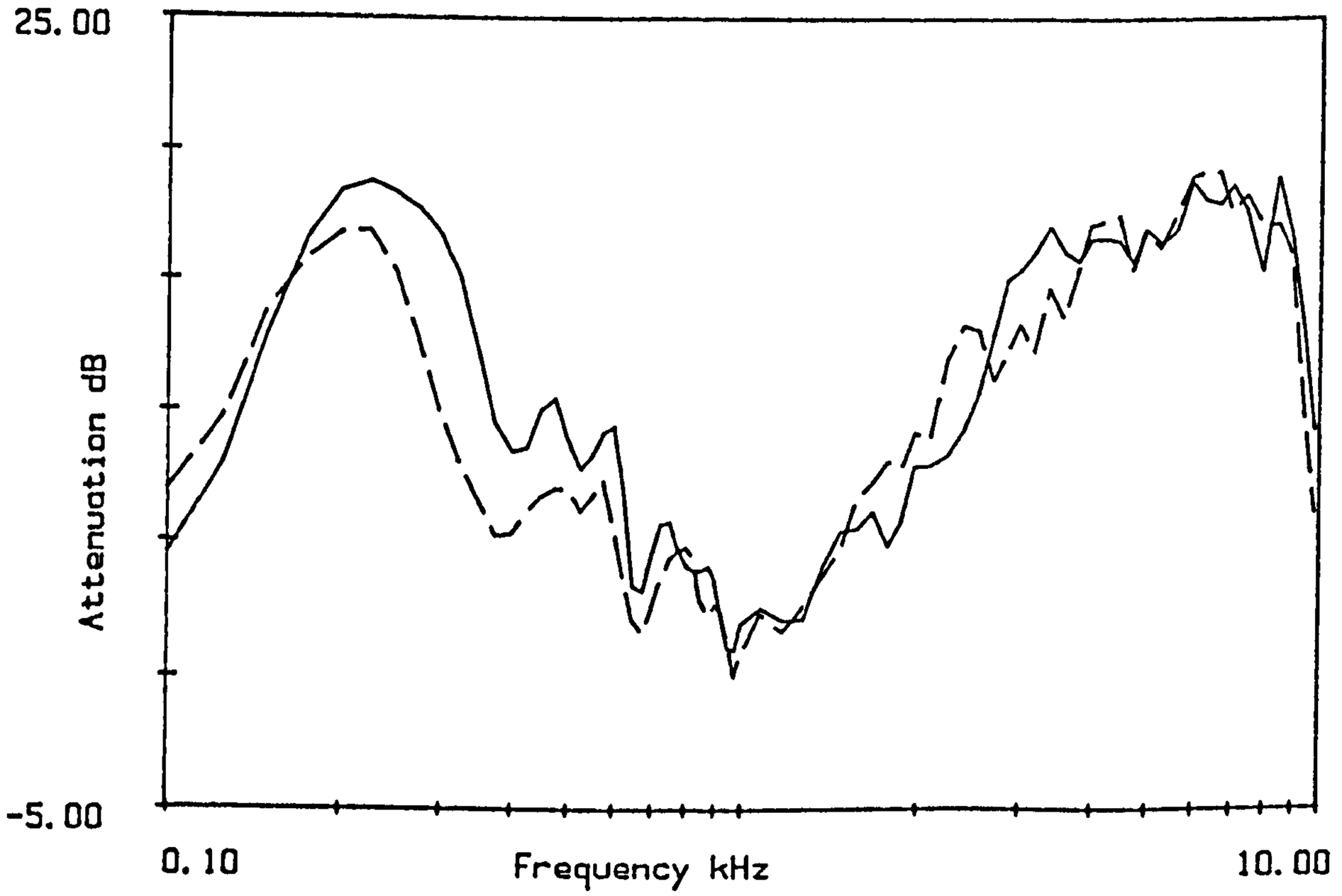

Figure B2.4
Attenuation at A96 on 28/7/83.
Microphone heights 1.2m and 2.5m(----).

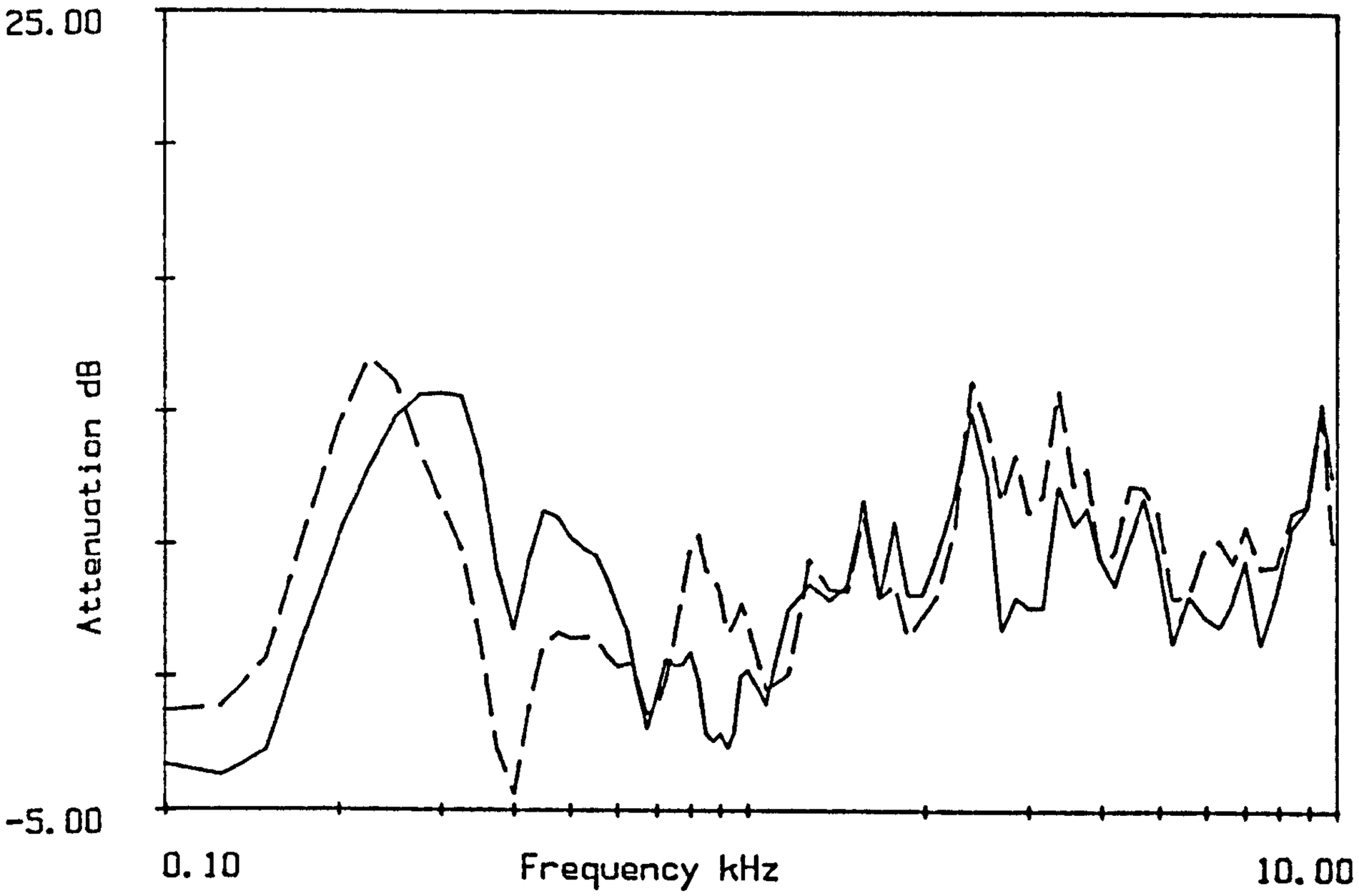

Figure 82.5
Attenuation at A12 on 26/6/84.
Microphone heights 1.2m and 2.5m(----).

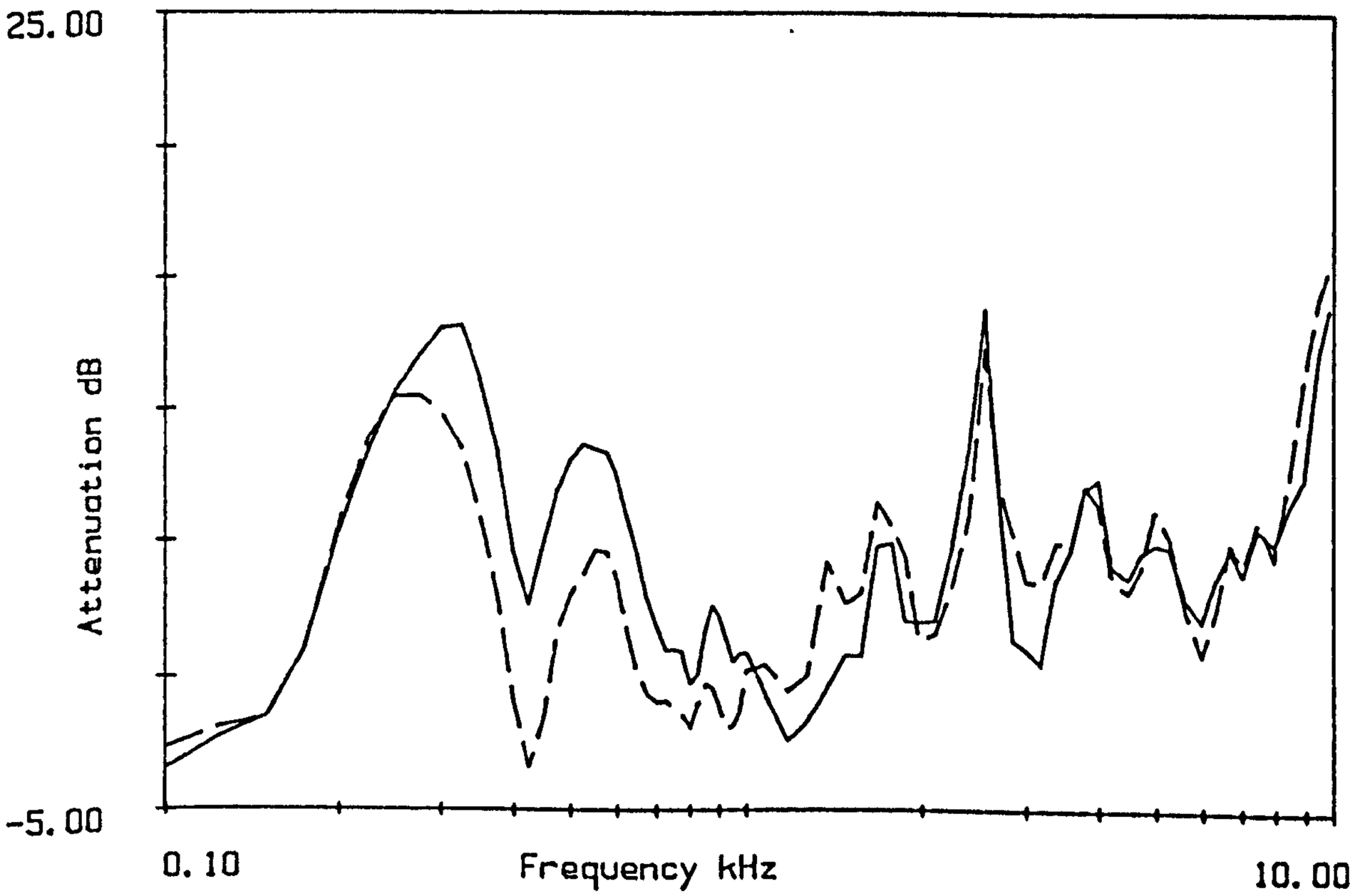

Figure 82.6
Attenuation at A24 on 26/6/84.
Microphone heights 1.2m and 2.5m(----).

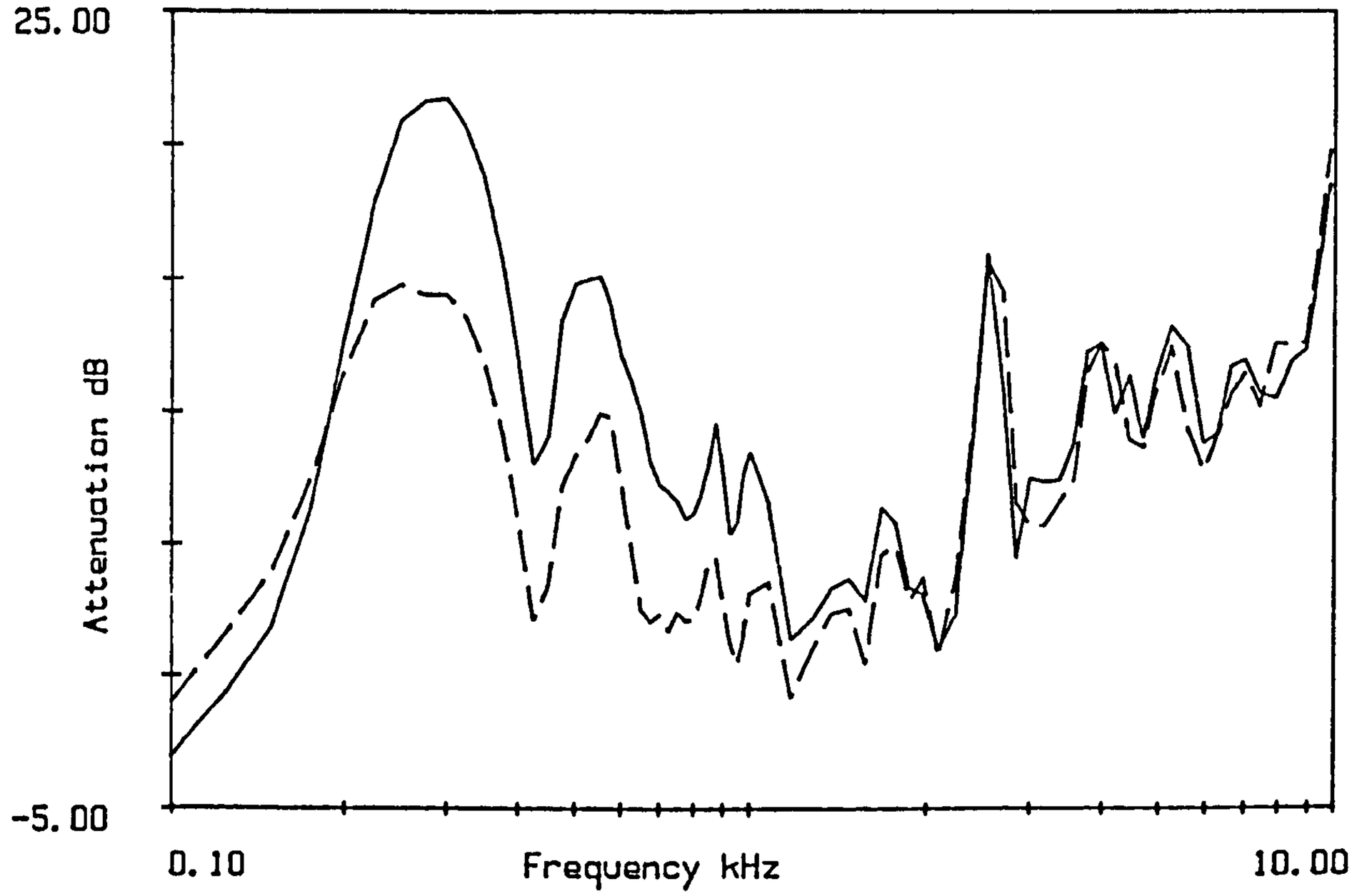

Figure B2.7
Attenuation at A48 on 26/6/84.
Microphone heights 1.2m and 2.5m(----).

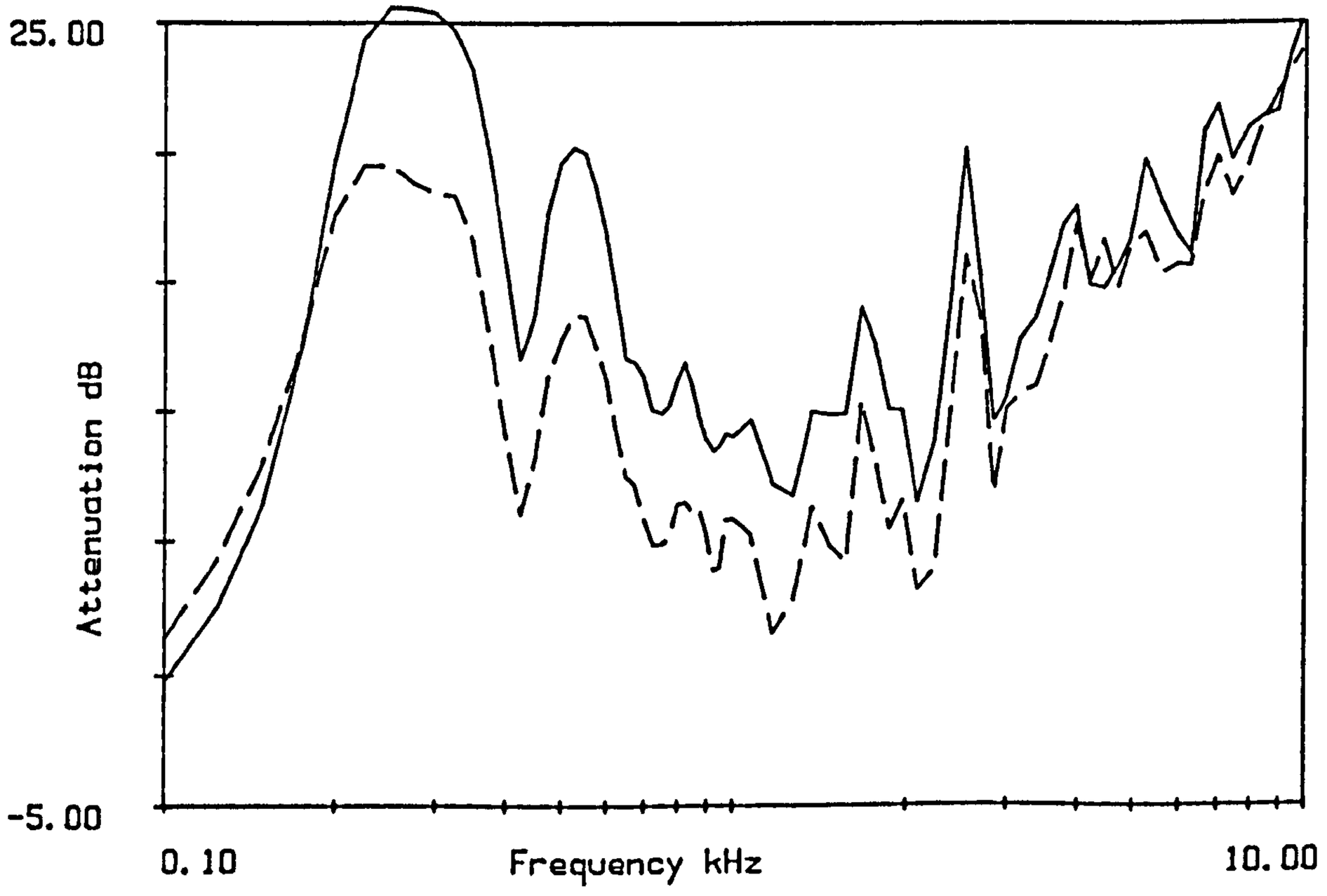

Figure B2.8
Attenuation at A96 on 26/6/84.
Microphone heights 1.2m and 2.5m(----).

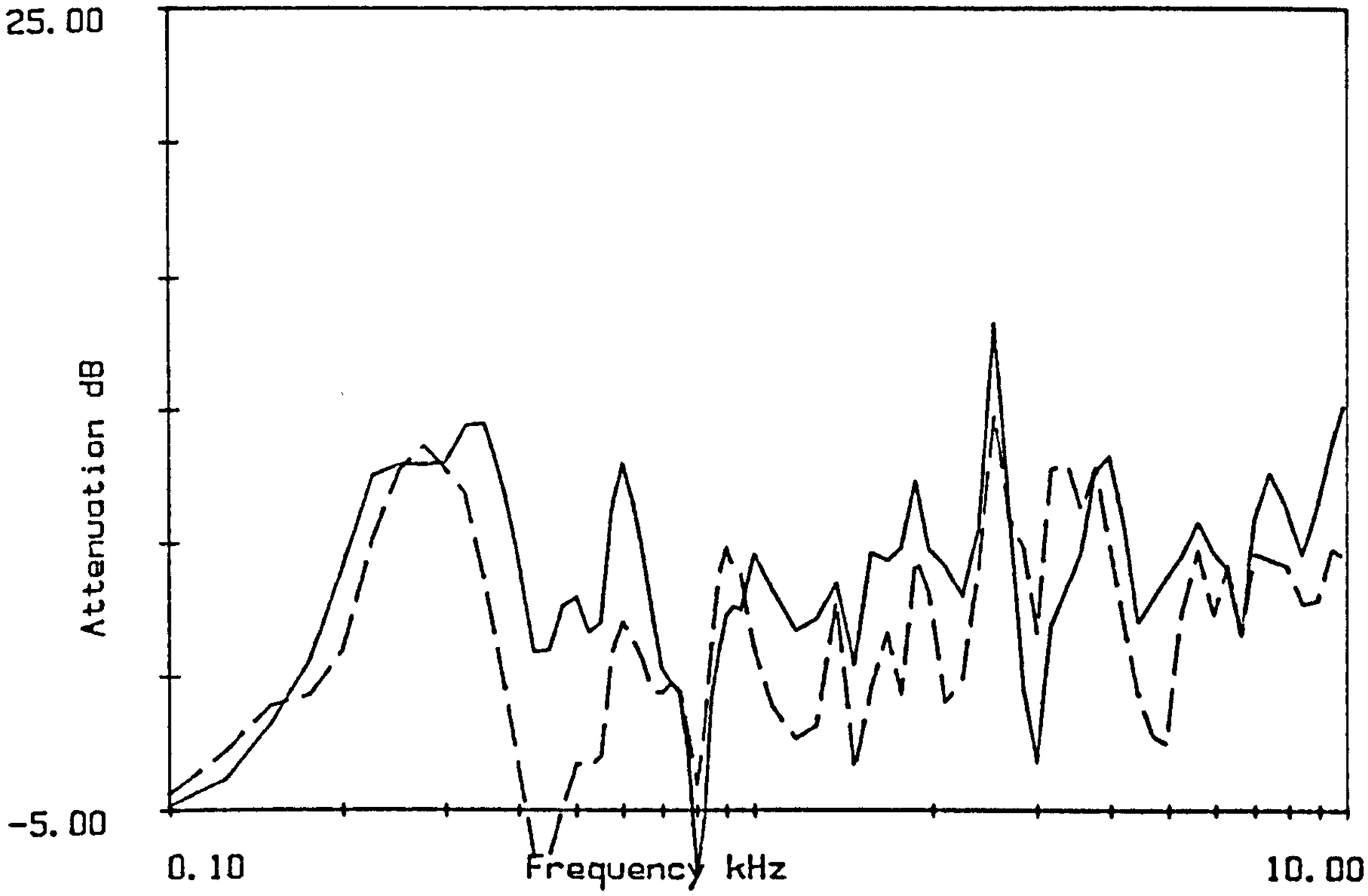

Figure B2.9
Attenuation at B12 on 26/6/84.
Microphone heights 1.2m and 2.5m(----).

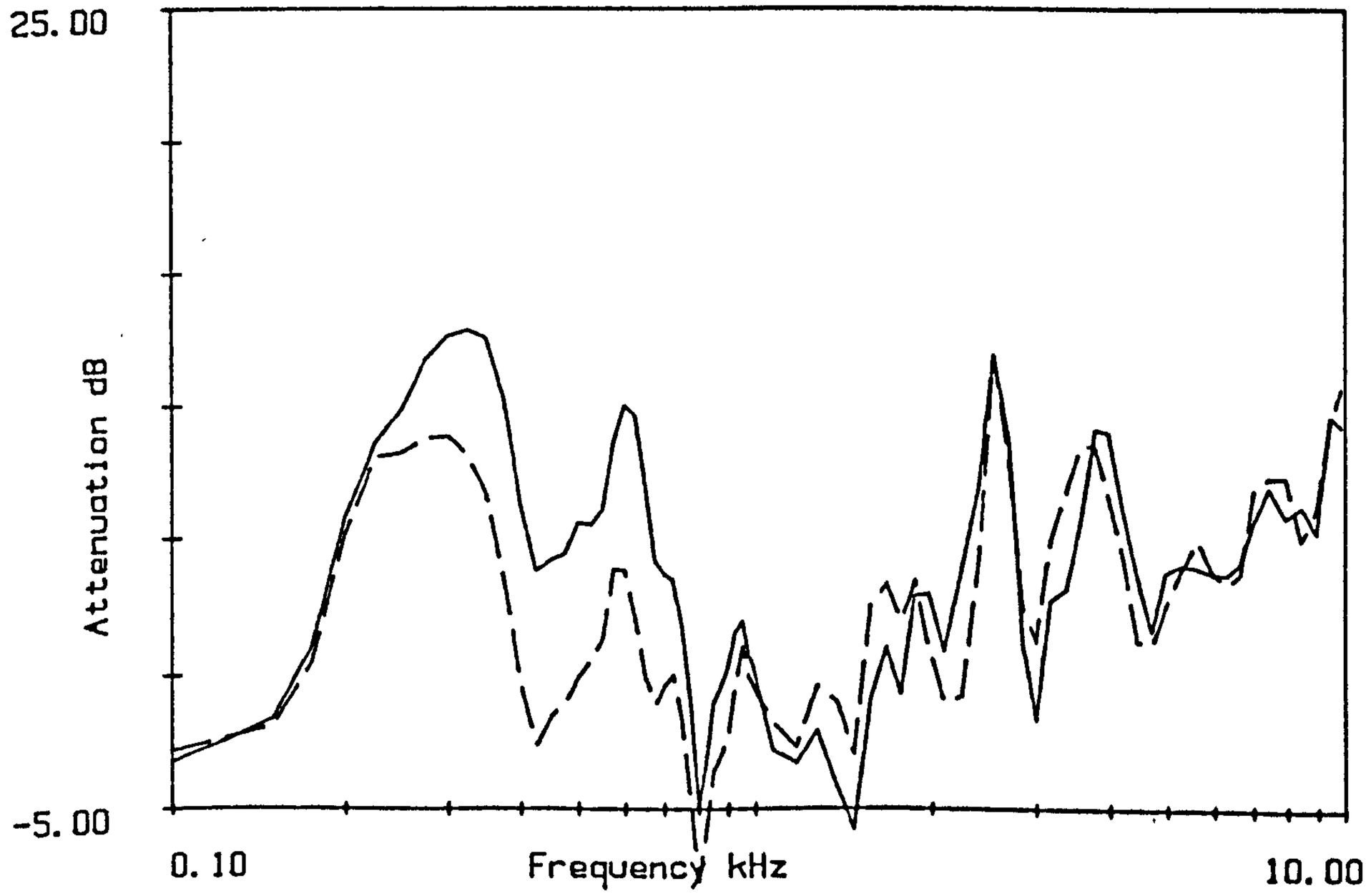

Figure B2.10
Attenuation at B24 on 26/6/84.
Microphone heights 1.2m and 2.5m(----).

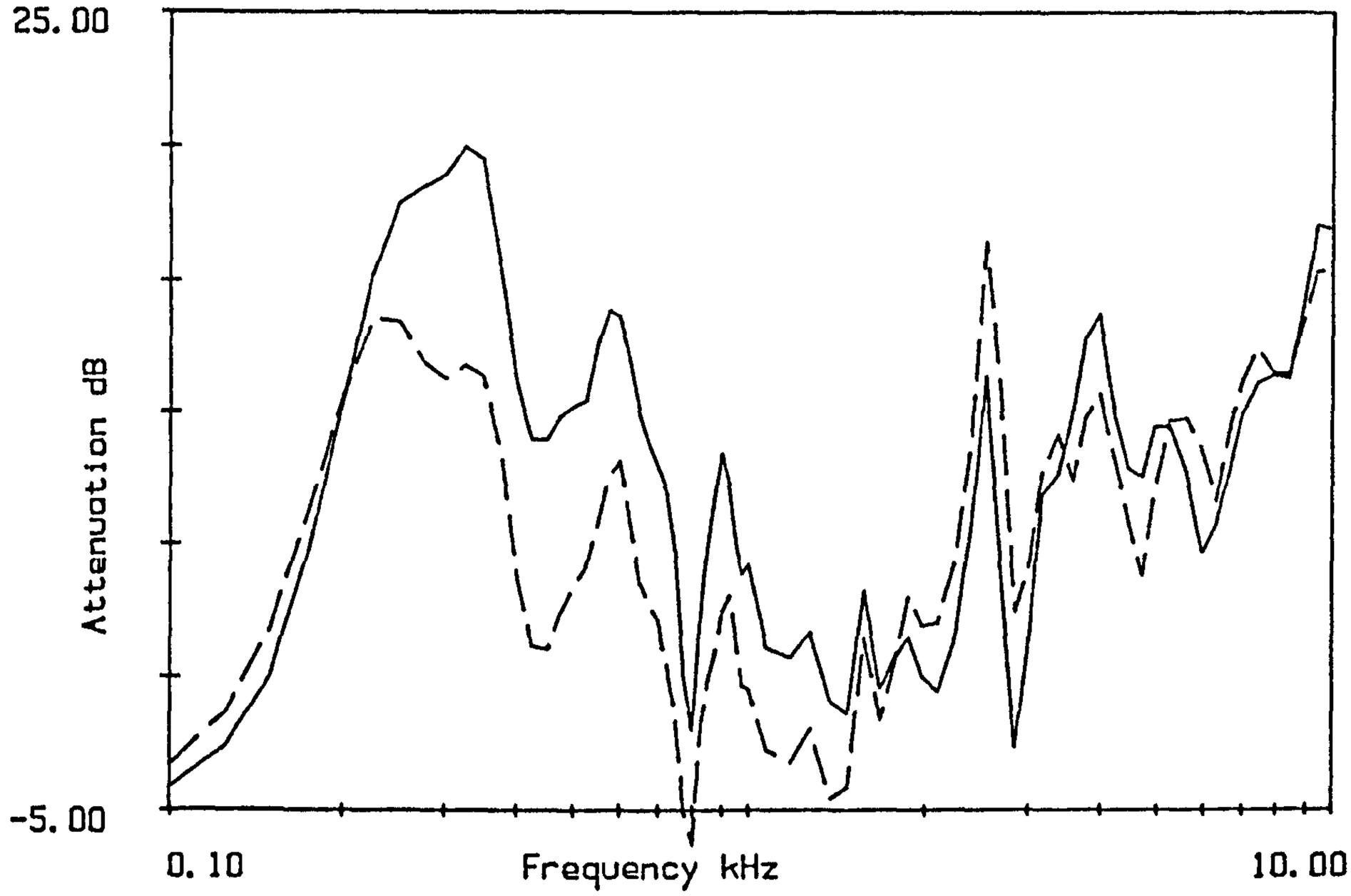

Figure B2.11
Attenuation at B48 on 26/6/84.
Microphone heights 1.2m and 2.5m(----).

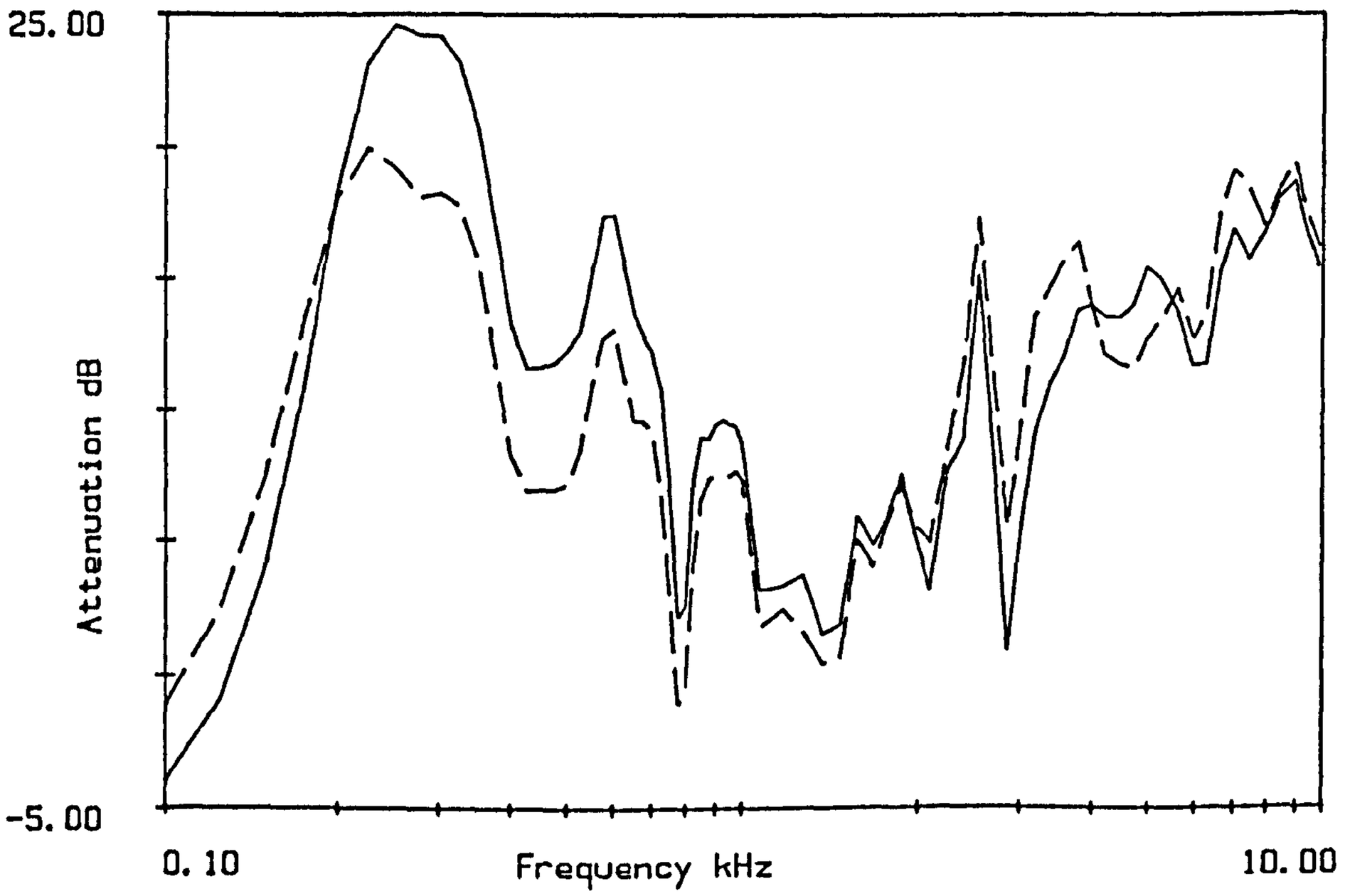

Figure B2.12
Attenuation at B96 on 26/6/84.
Microphone heights 1.2m and 2.5m(----).

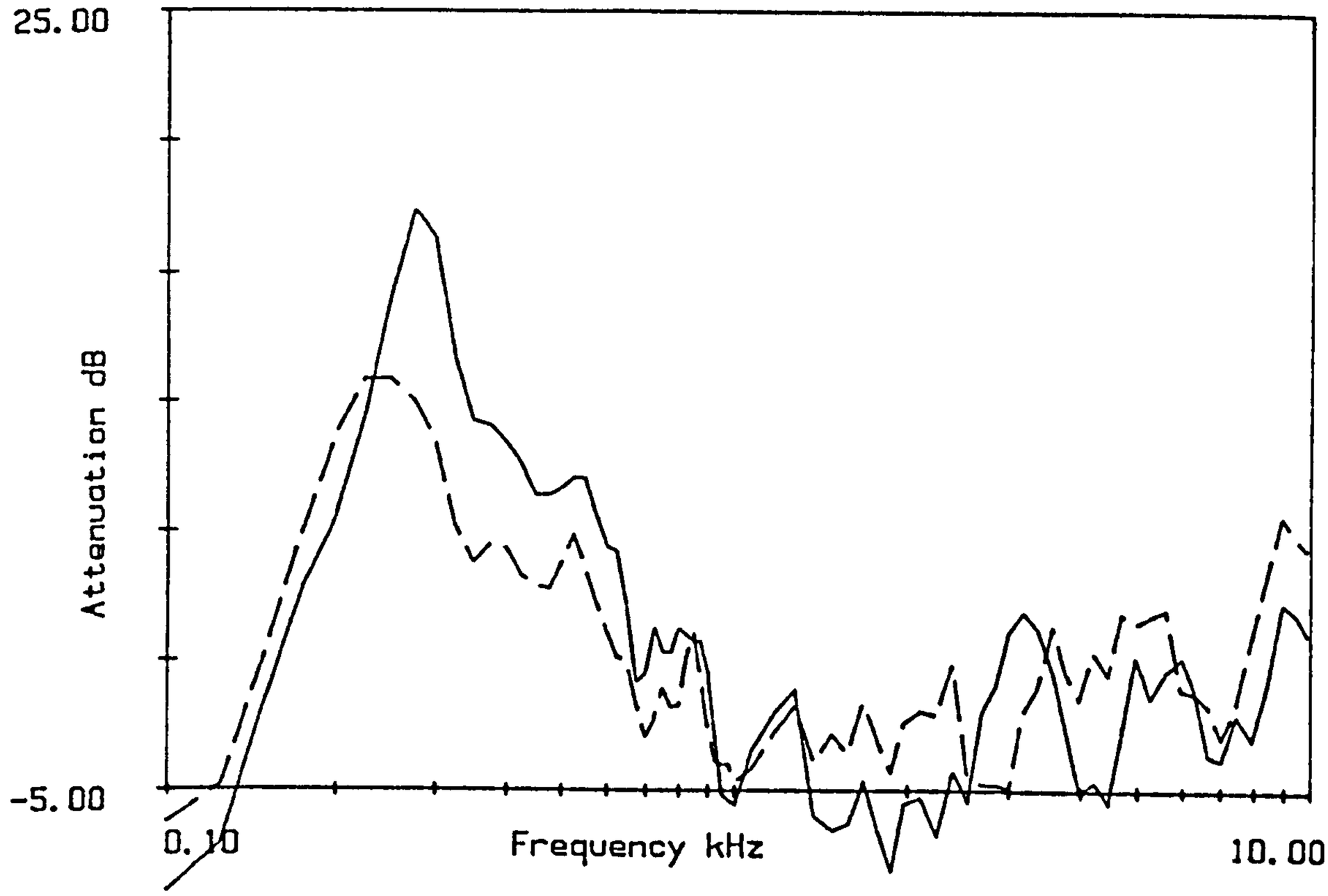

Figure B2.13
Attenuation at A48 on 16/5/85 at 13.00
Microphone heights 1.2m and 2.5m(----).

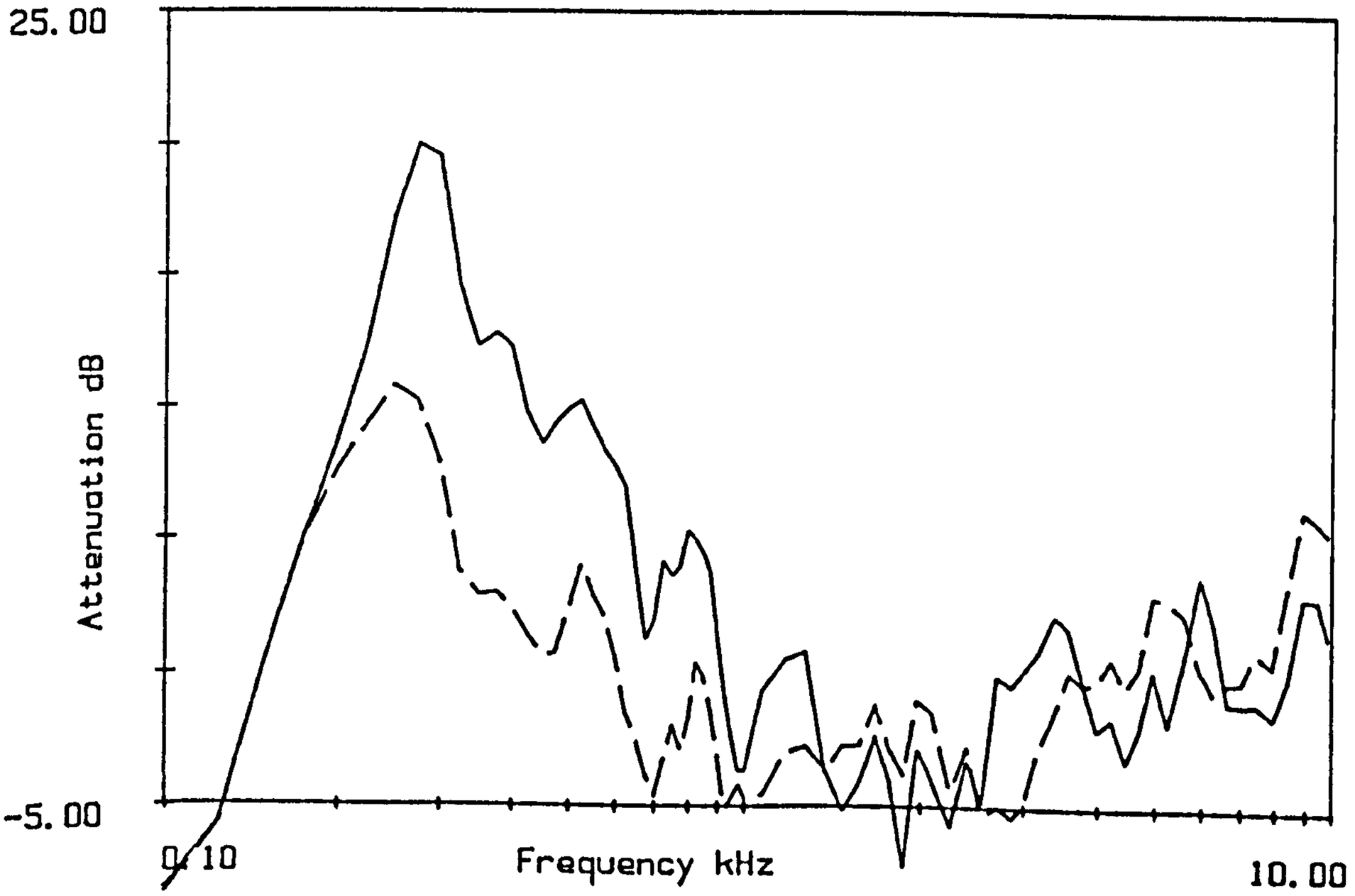

Figure B2.14
Attenuation at A48 on 16/5/85 at 14.00
Microphone heights 1.2m and 2.5m(----).

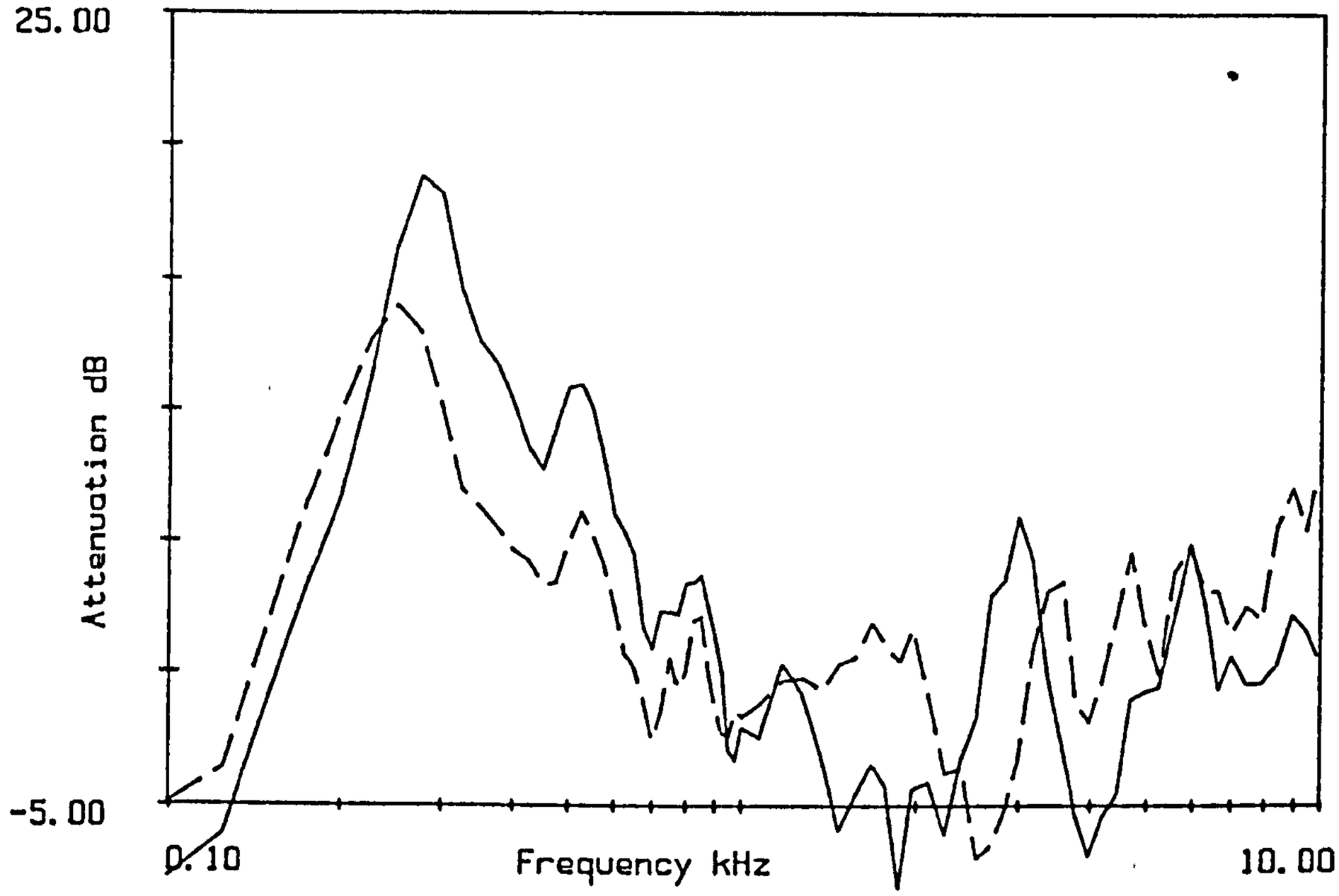

Figure B2.15
Attenuation at A48 on 16/5/85 at 15.00
Microphone heights 1.2m and 2.5m(----).

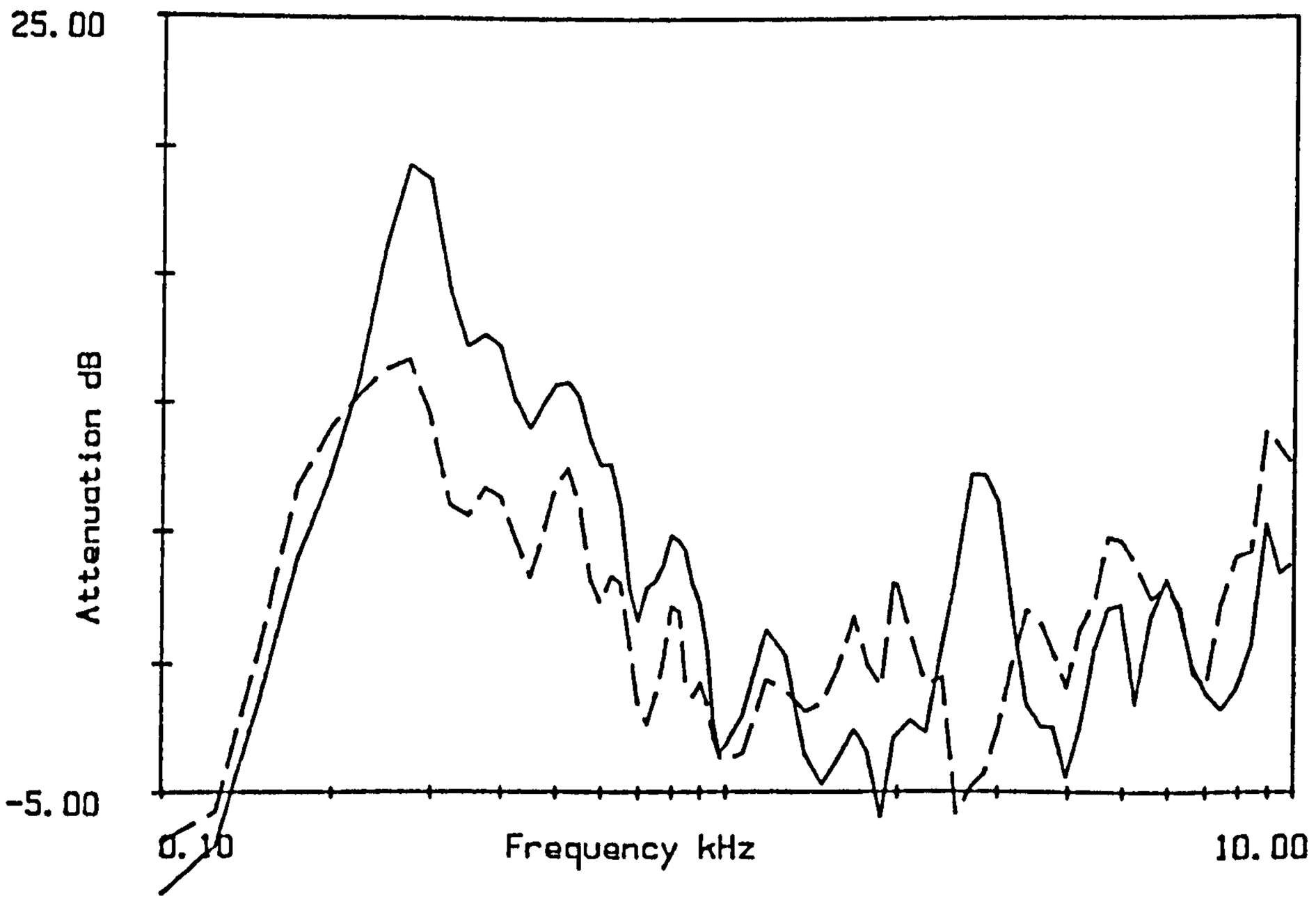

Figure B2.16
Attenuation at A48 on 16/5/85 at 16.00
Microphone heights 1.2m and 2.5m(----).

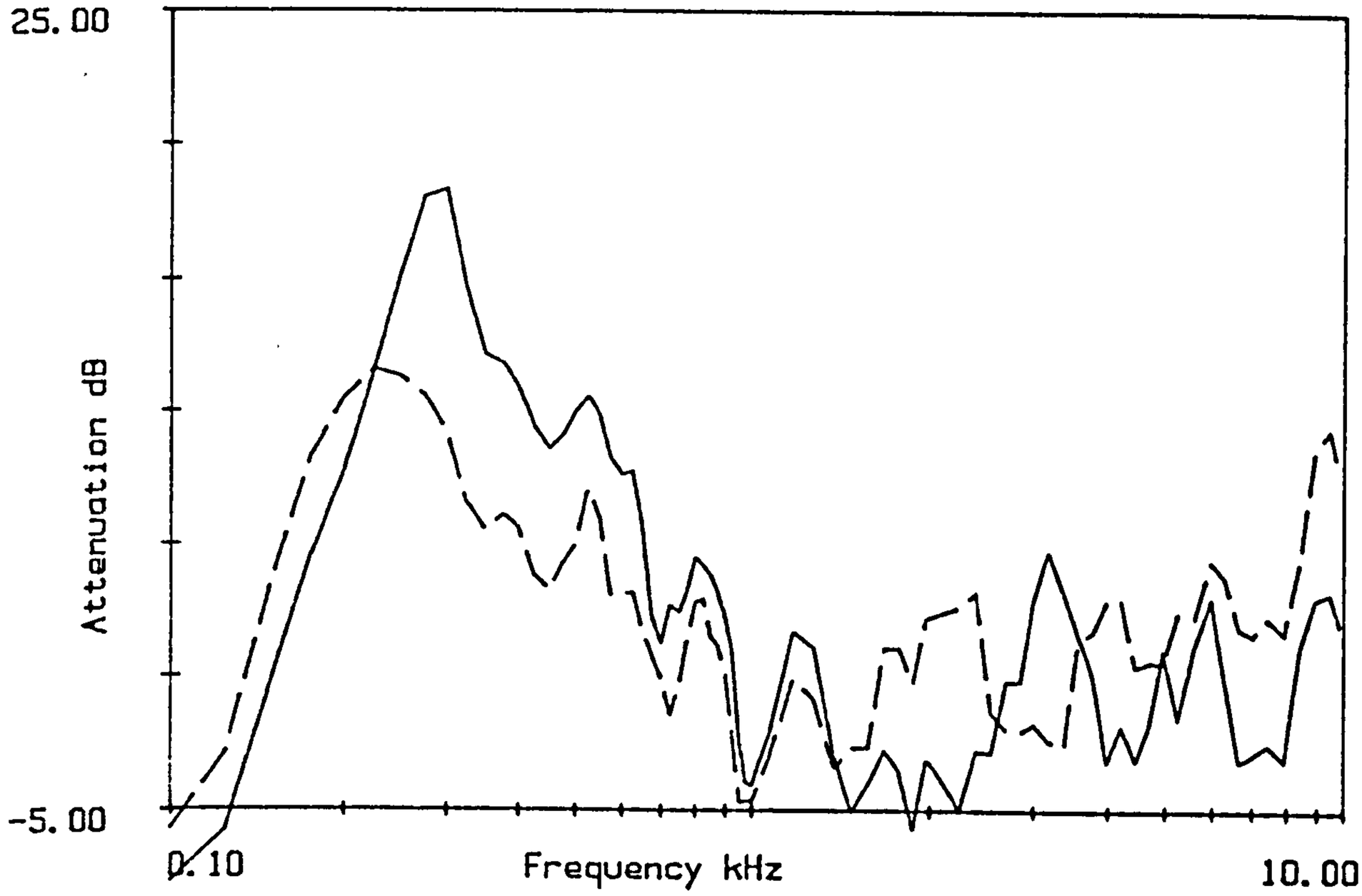

Figure 82.17
Attenuation at A48 on 16/5/85 at 16.30
Microphone heights 1.2m and 2.5m(----).

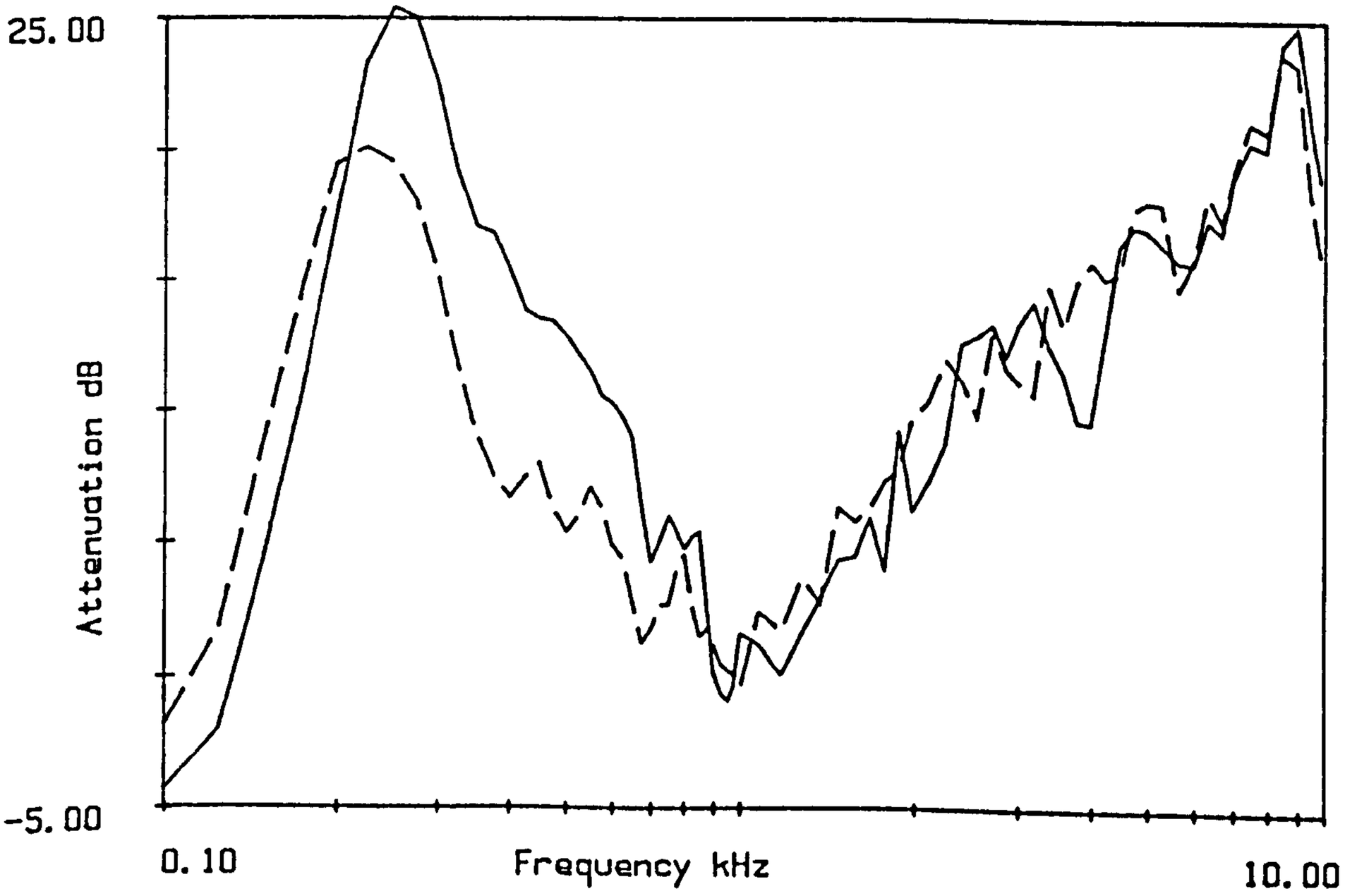

Figure 82.18
Attenuation at A96 on 16/5/85 at 13.00
Microphone heights 1.2m and 2.5m(----).

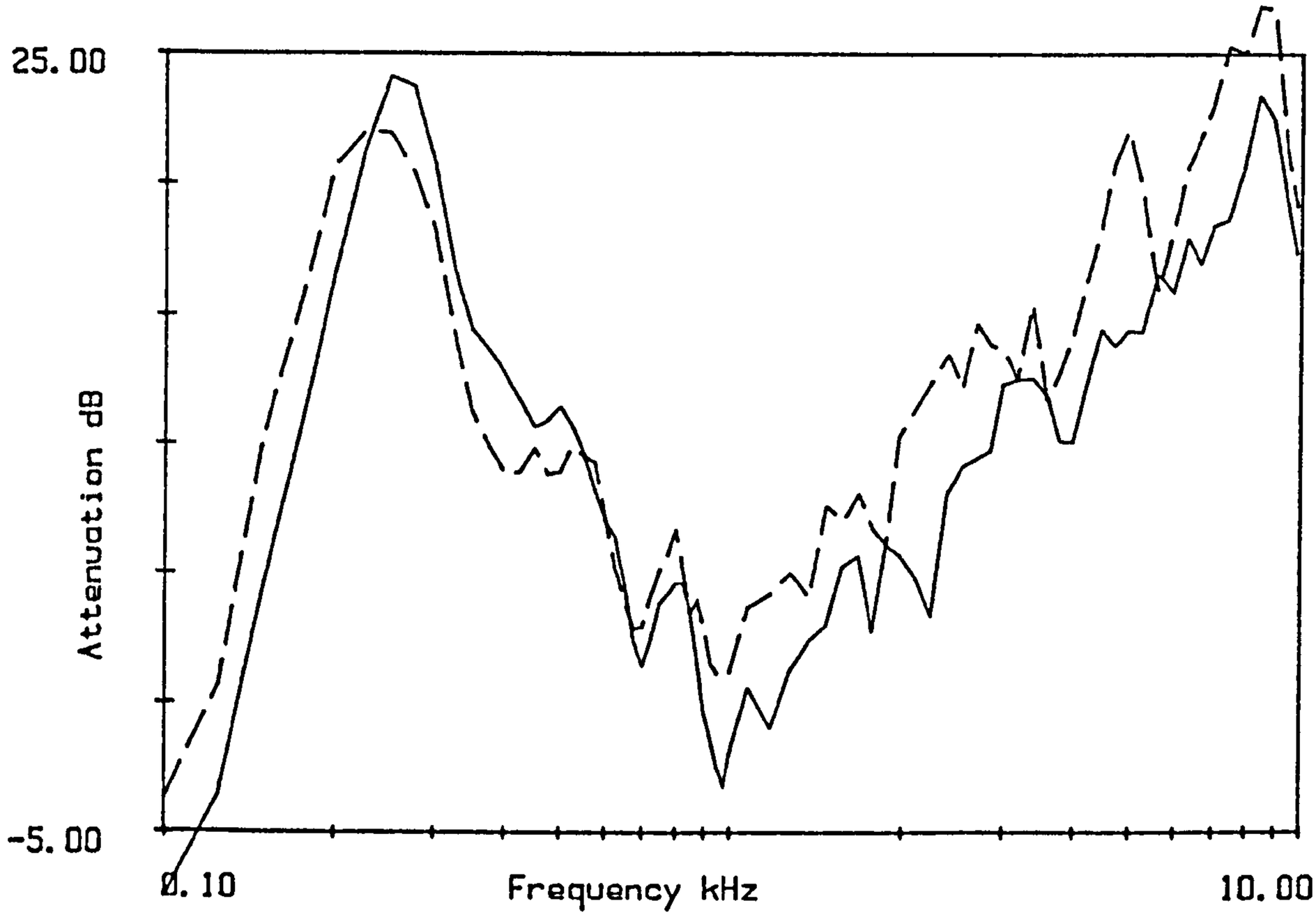

Figure B2.19
Attenuation at A96 on 16/5/85 at 14.00
Microphone heights 1.2m and 2.5m(----).

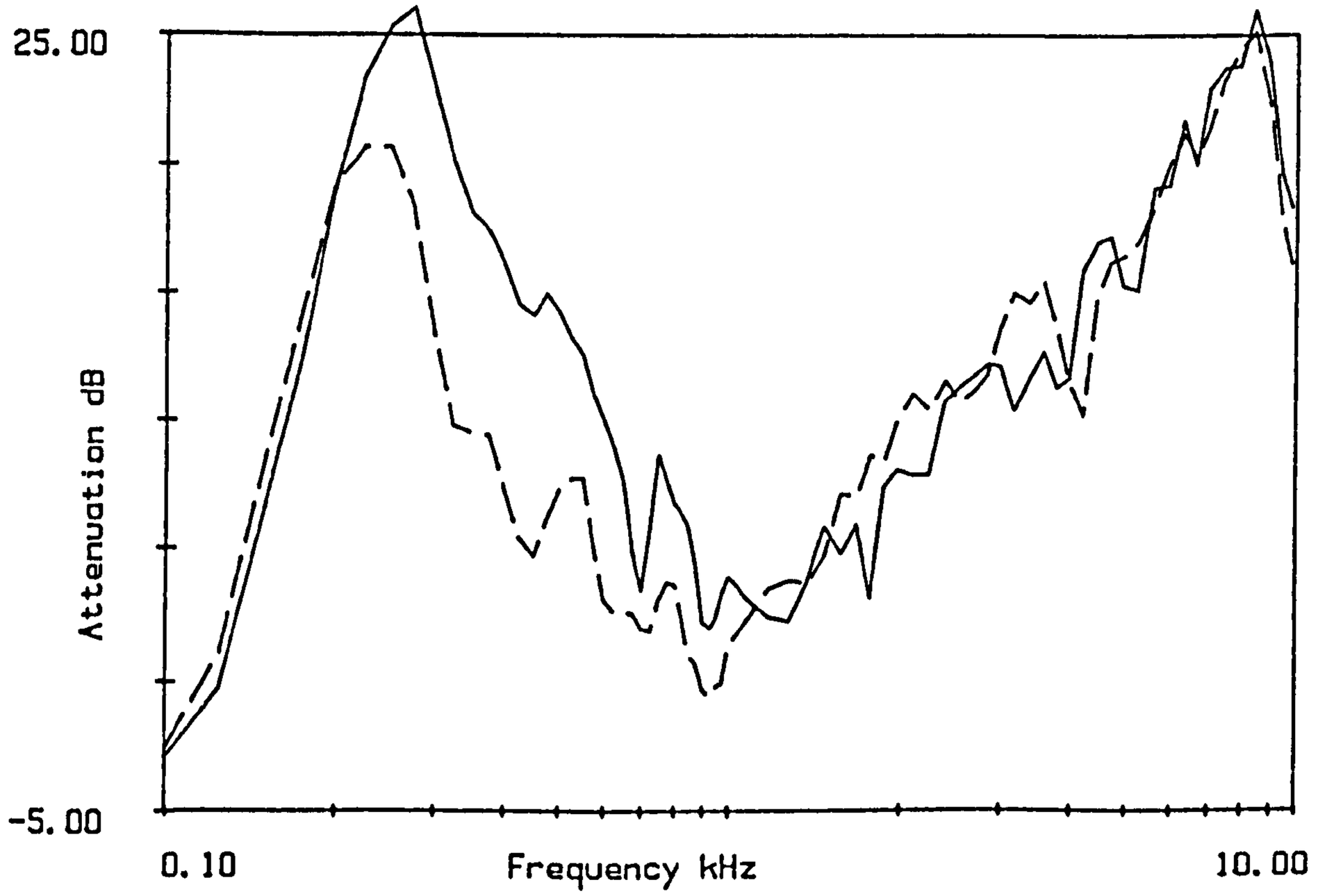

Figure B2.20
Attenuation at A96 on 16/5/85 at 15.00
Microphone heights 1.2m and 2.5m(----).

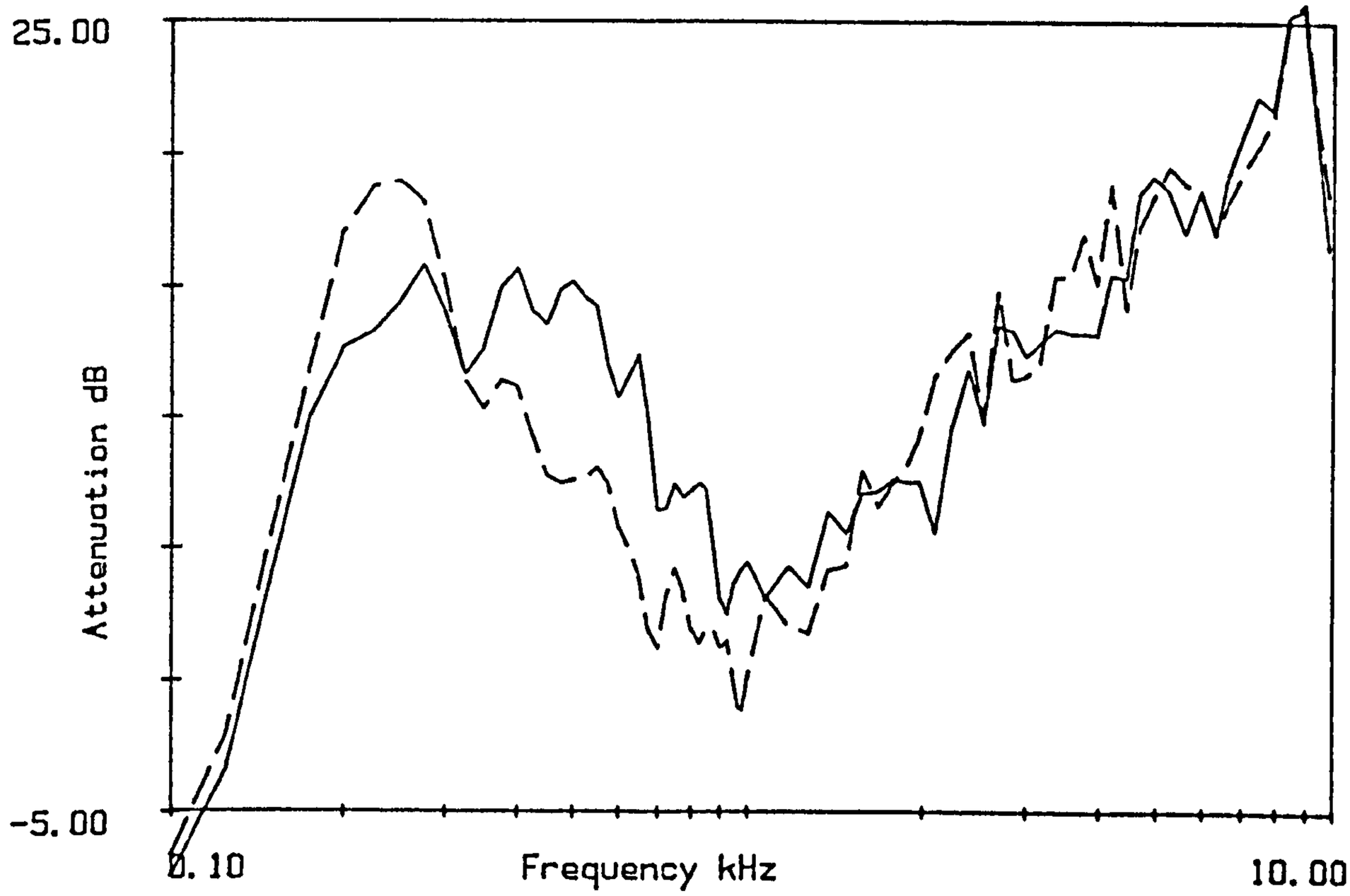

Figure B2.21
Attenuation at A96 on 16/5/85 at 16.00
Microphone heights 1.2m and 2.5m(----).

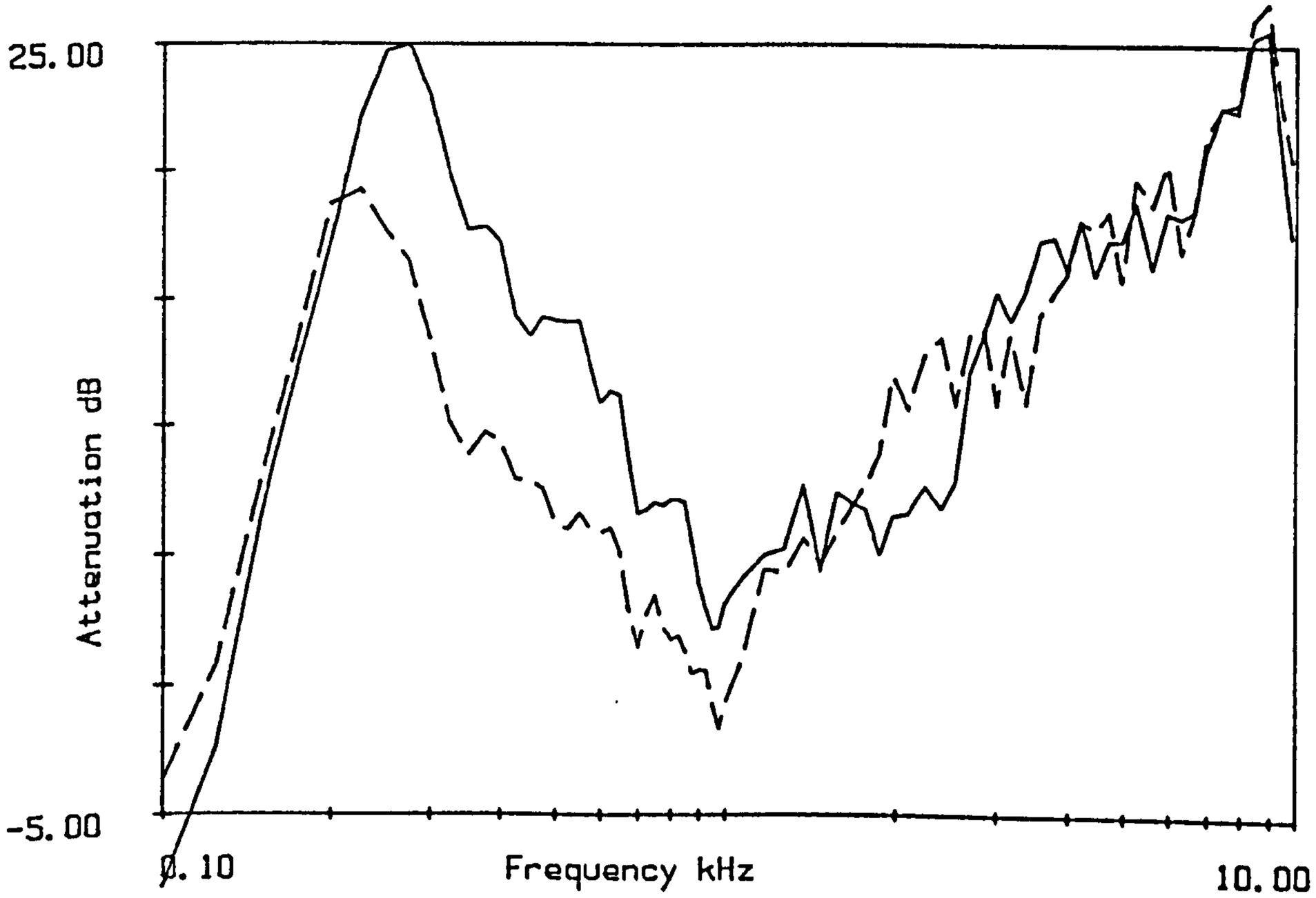

Figure B2.22
Attenuation at A96 on 16/5/85 at 16.30
Microphone heights 1.2m and 2.5m(----).

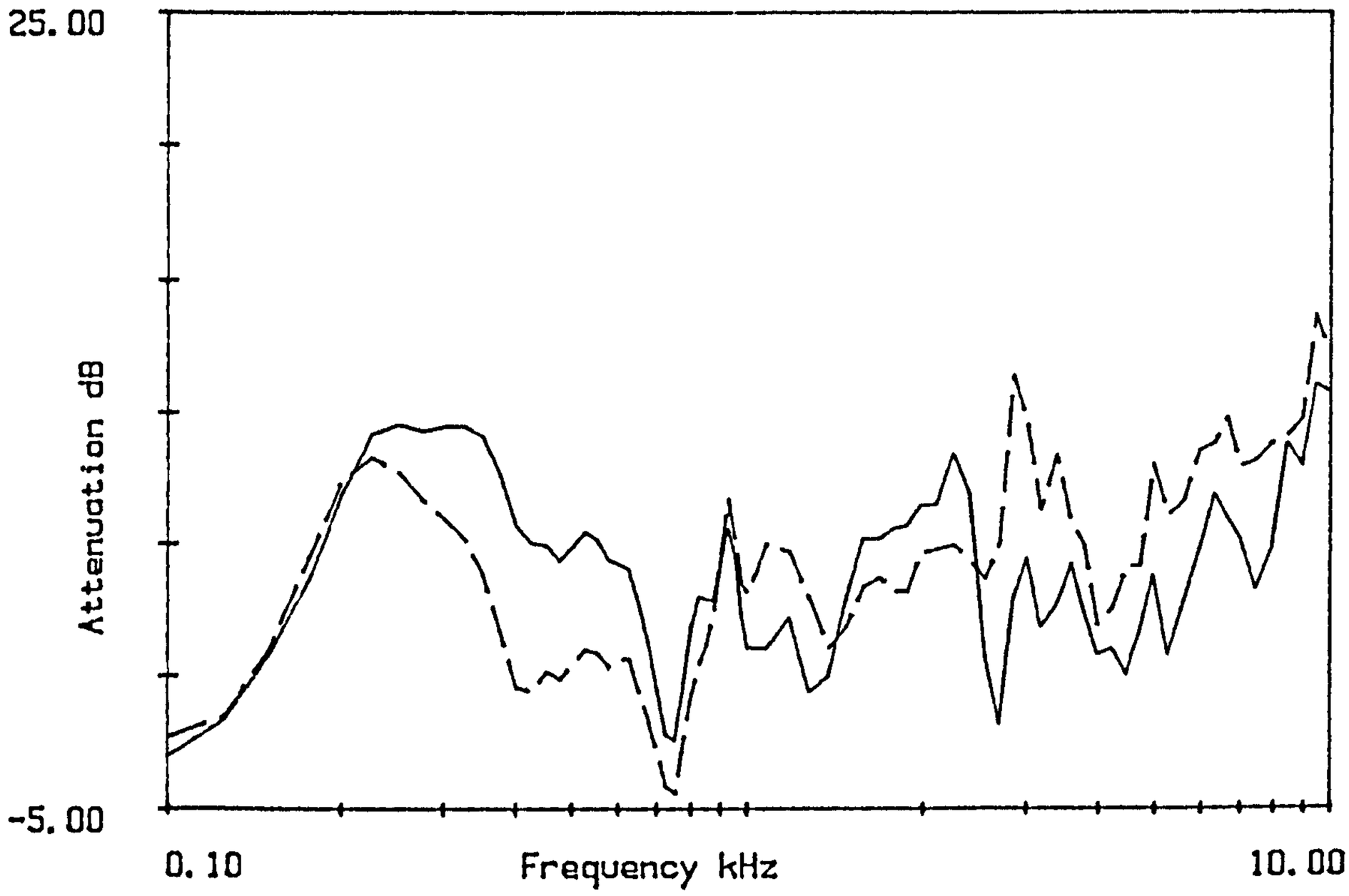

APPENDIX B3 Results from Mixed Coniferous Wood.
Figure B3.1
Attenuation on 9/7/84 source at F26 microphones at F12
Microphone heights 1.2m and 2.5m(----).

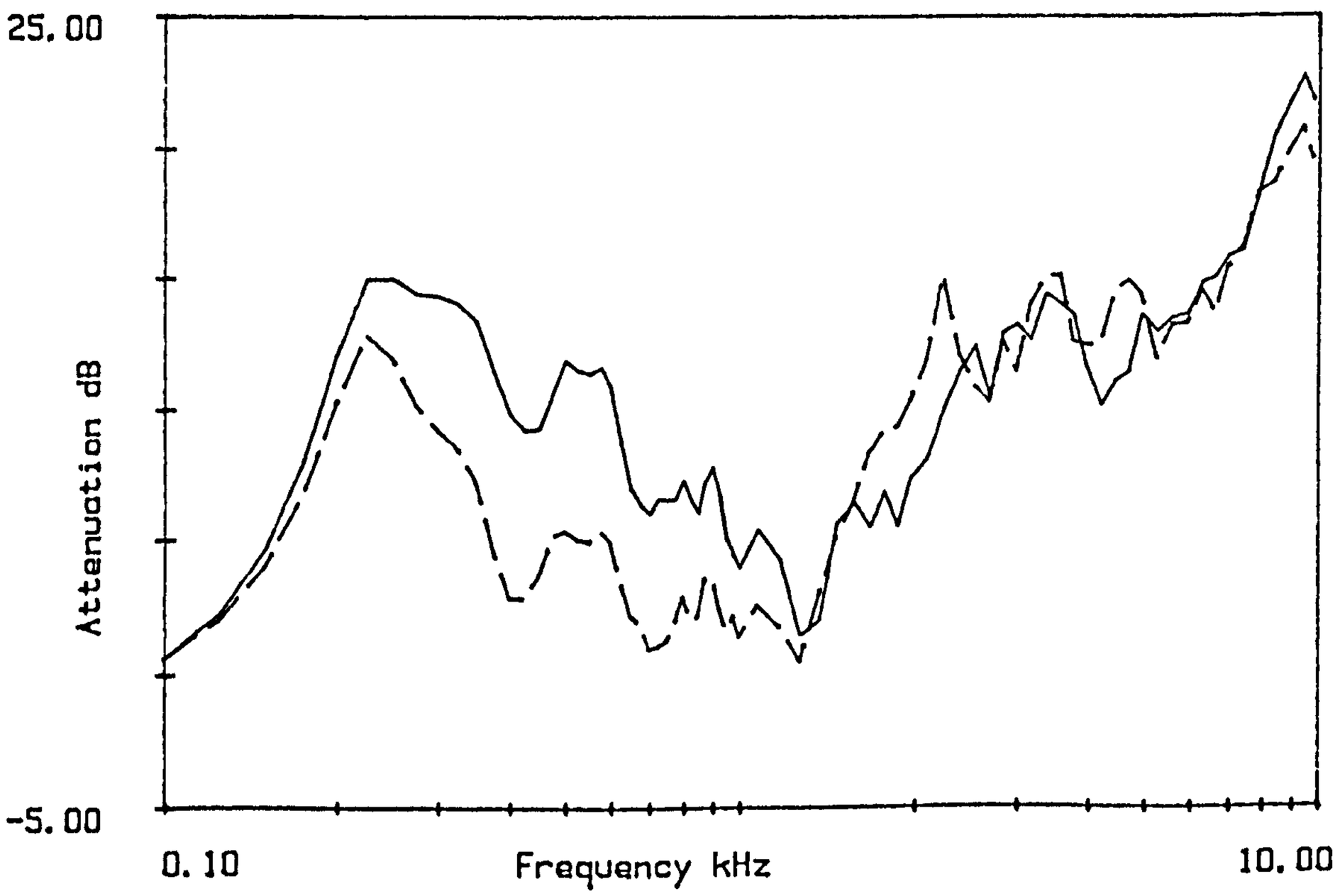

Figure B3.2
Attenuation on 9/7/84 source at F26 microphones at G24.
Microphone heights 1.2m and 2.5m(----).

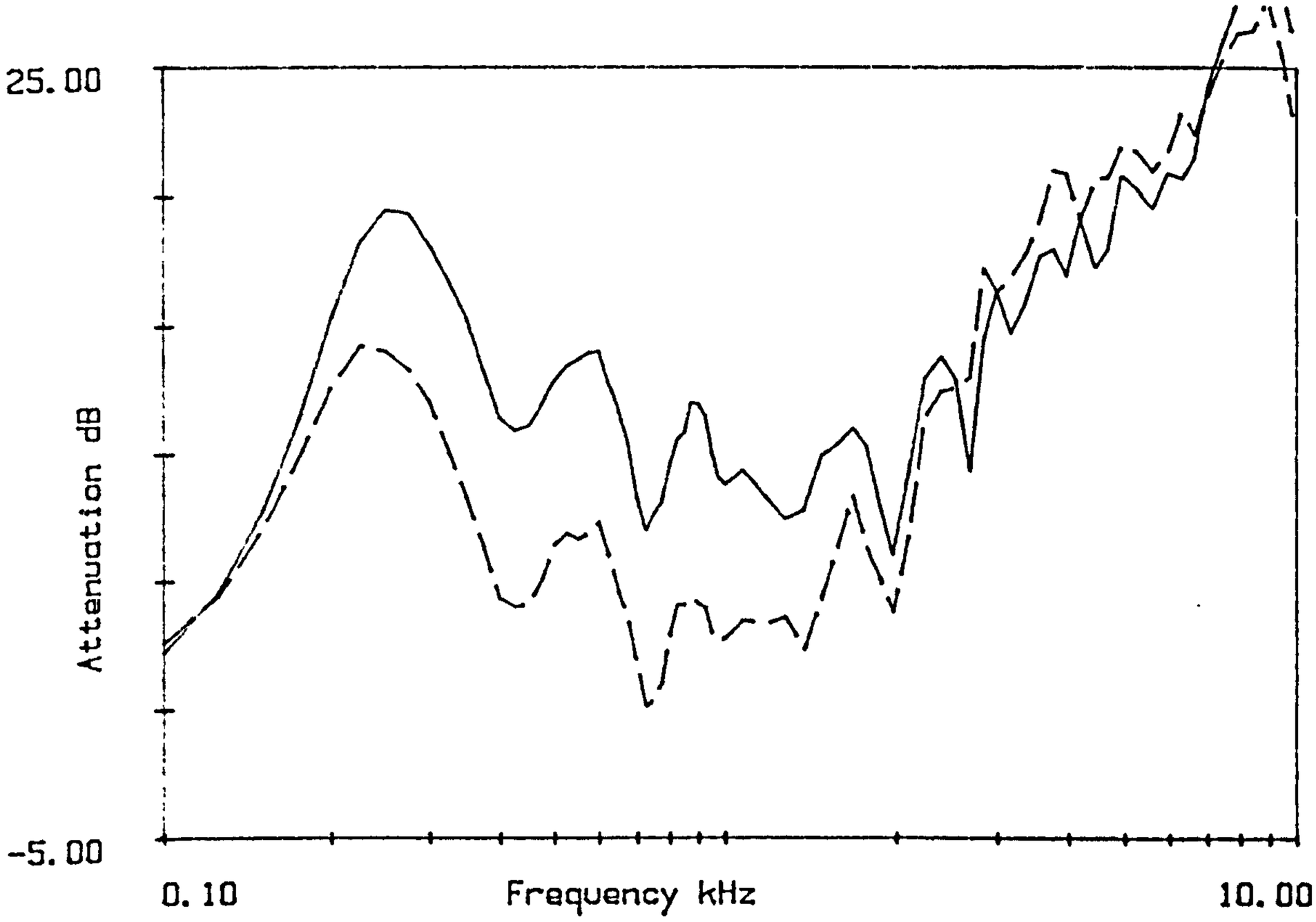

Figure B3.3
Attenuation on 9/7/84 source at F26 microphones at G40
Microphone heights 1.2m and 2.5m(----).

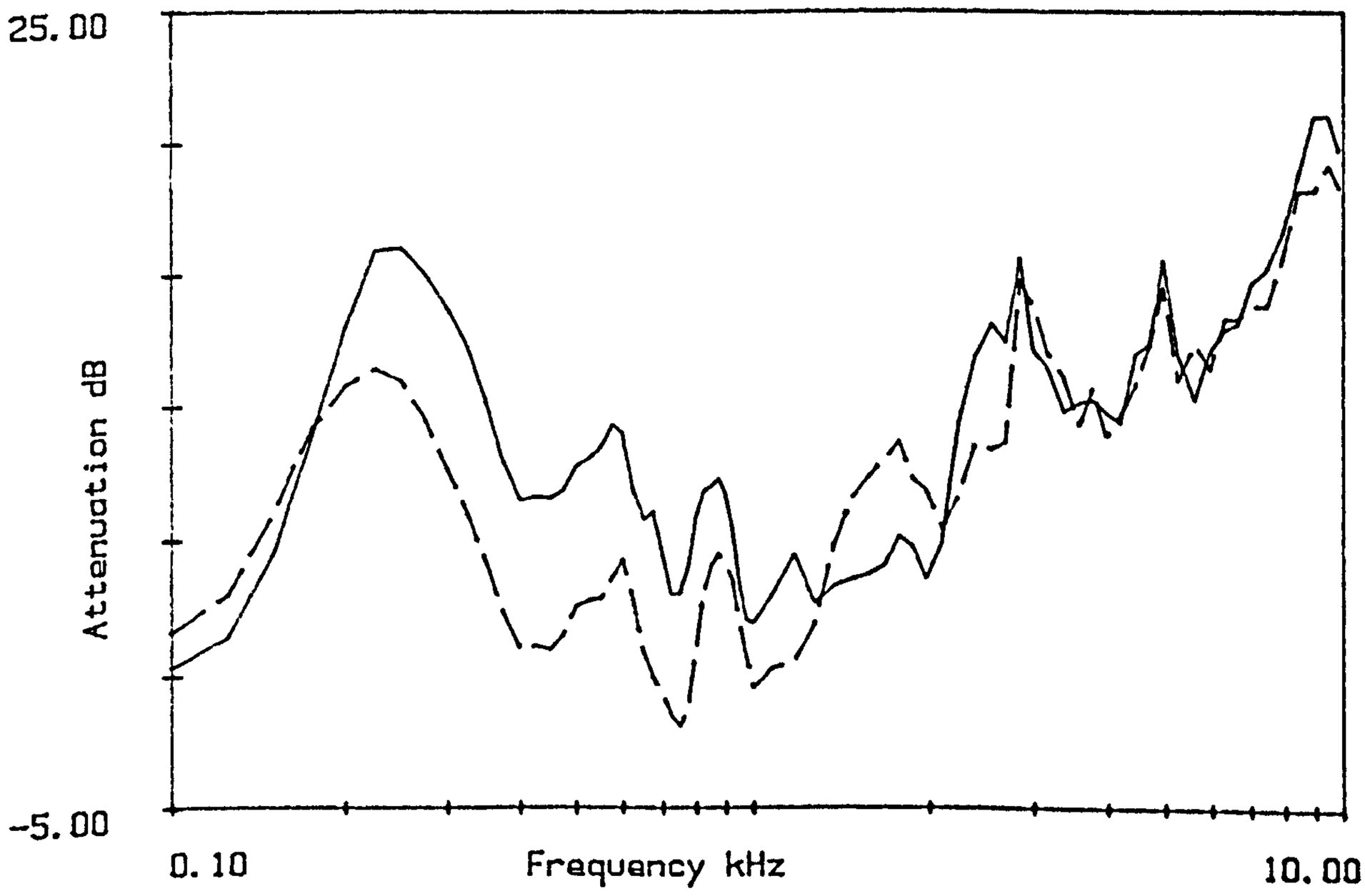

Figure B3.4
Attenuation on 9/7/84 source at F26 microphones at FS
Microphone heights 1.2m and 2.5m(----).

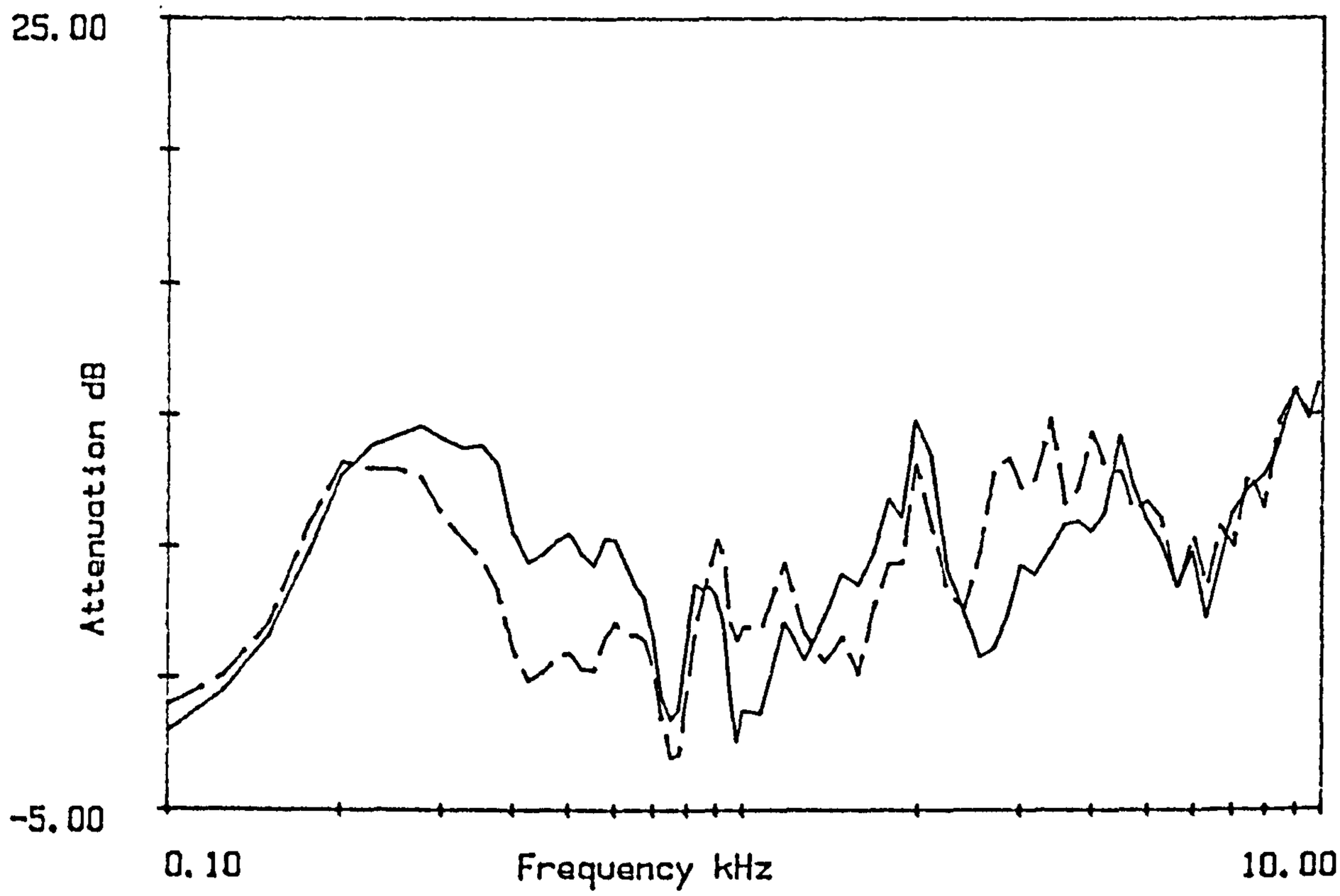

Figure B3.5
Attenuation on 8/8/84 source at F26 microphones at F12
Microphone heights 1.2m and 2.5m(----).

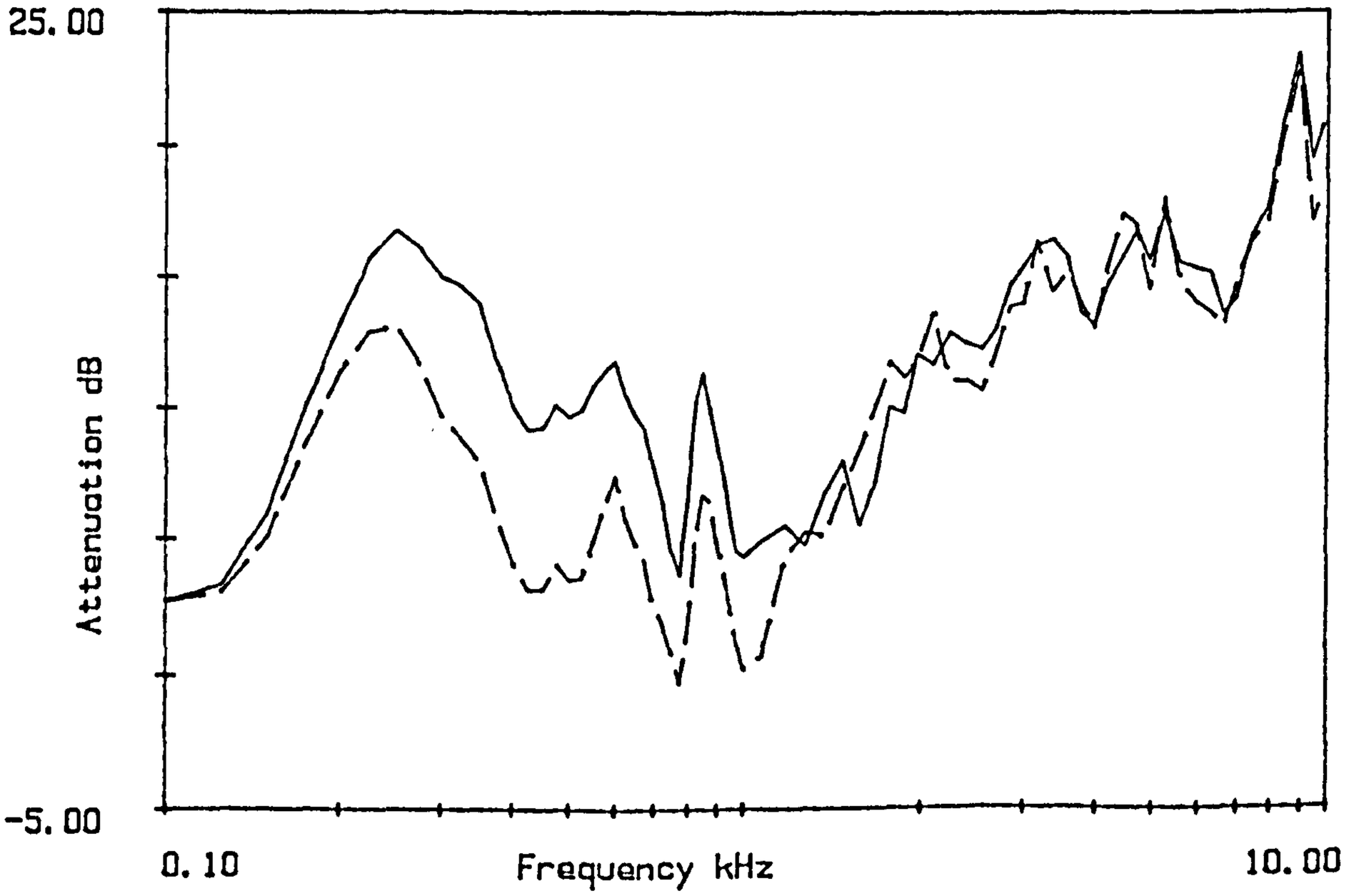

Figure B3.6
Attenuation on 8/8/84 source at F26 microphones at G24.
Microphone heights 1.2m and 2.5m(----).

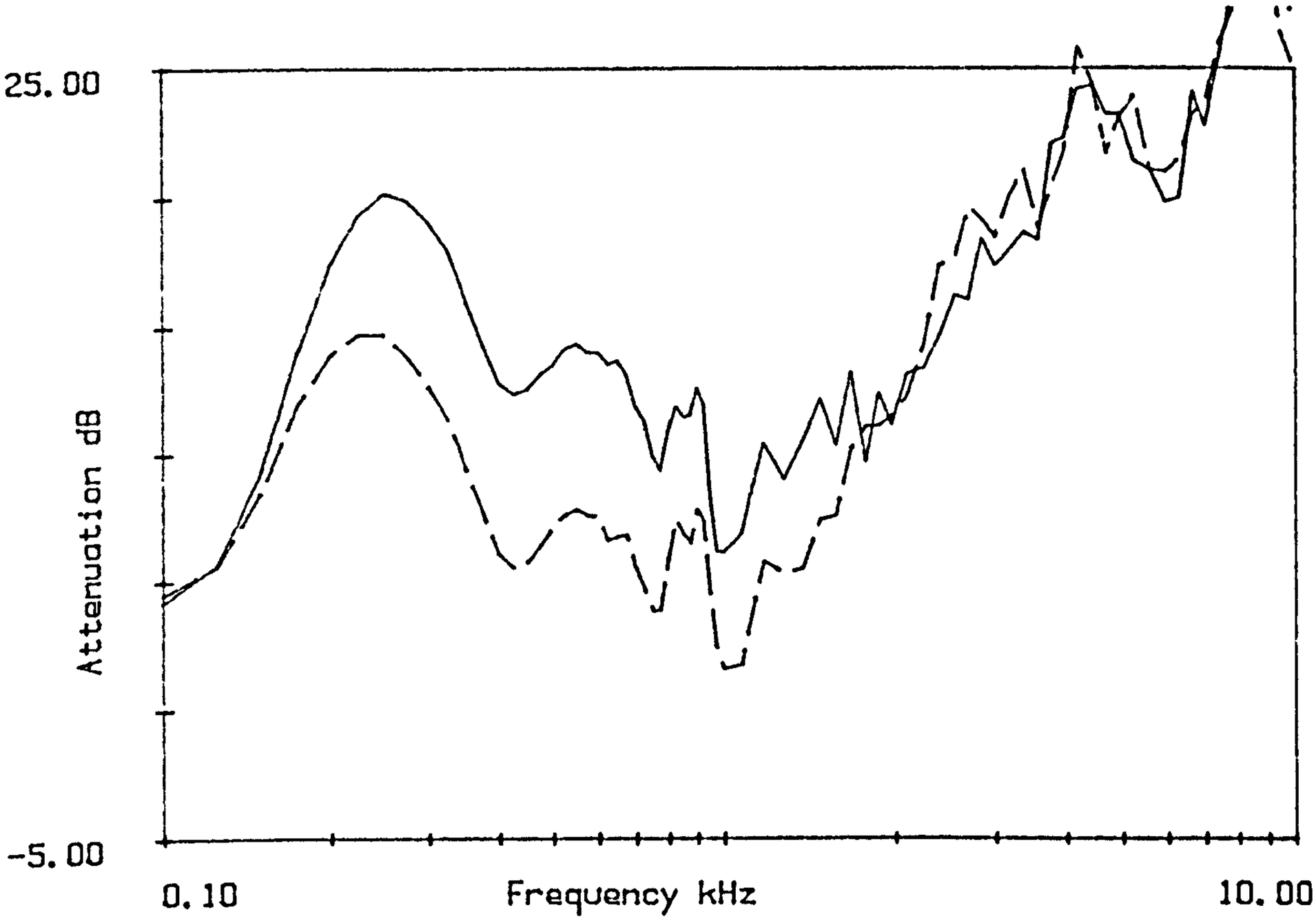

Figure B3.7
Attenuation on 8/8/84 source at F26 microphones at G40
Microphone heights 1.2m and 2.5m(----).

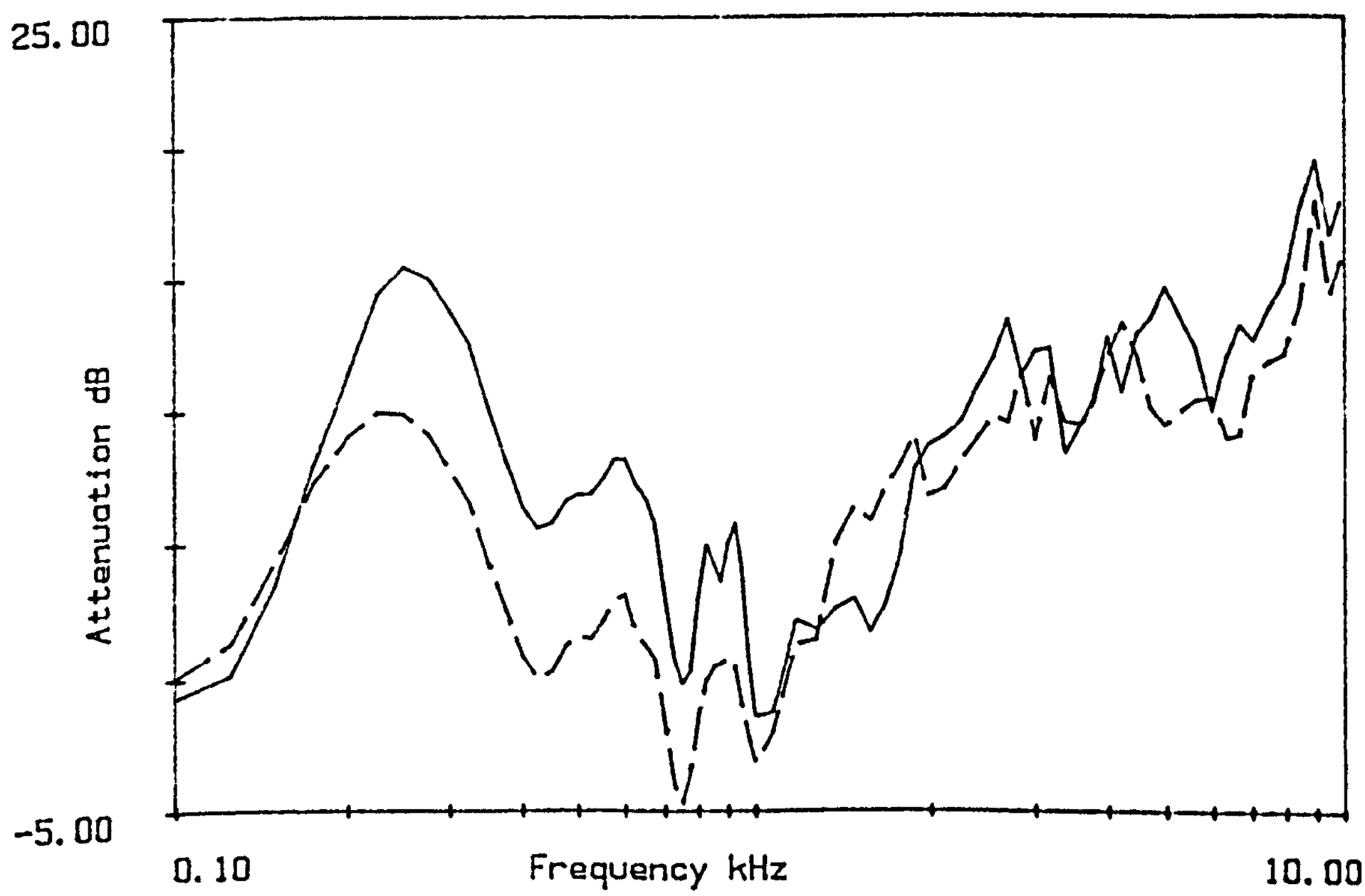

Figure B3.8
Attenuation on 8/8/84 source at F26 microphones at F5
Microphone heights 1.2m and 2.5m(----).

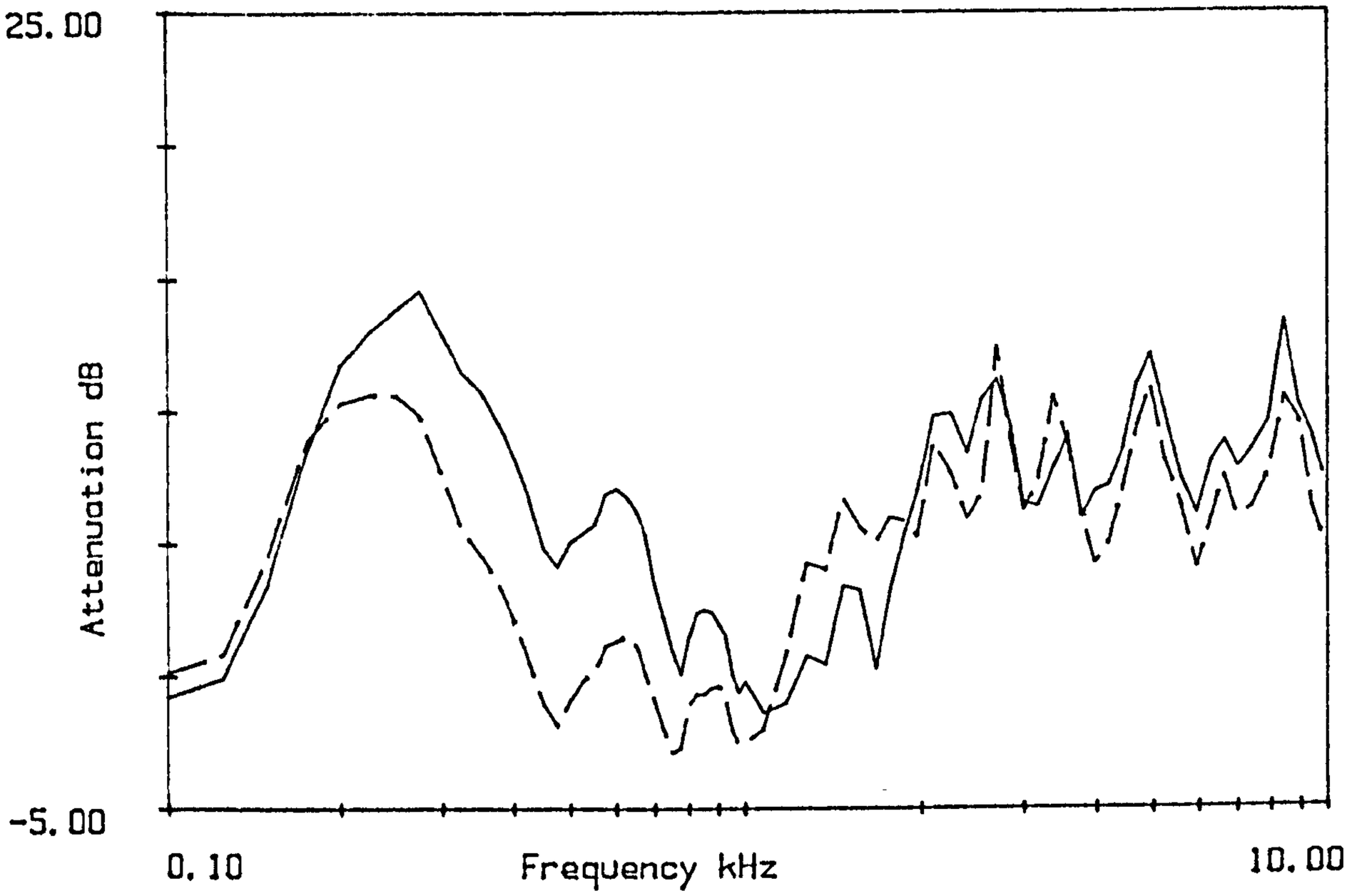

Figure B3.9
Attenuation on 8/8/84 source at FS microphones at F26
Microphone heights 1.2m and 2.5m(----).

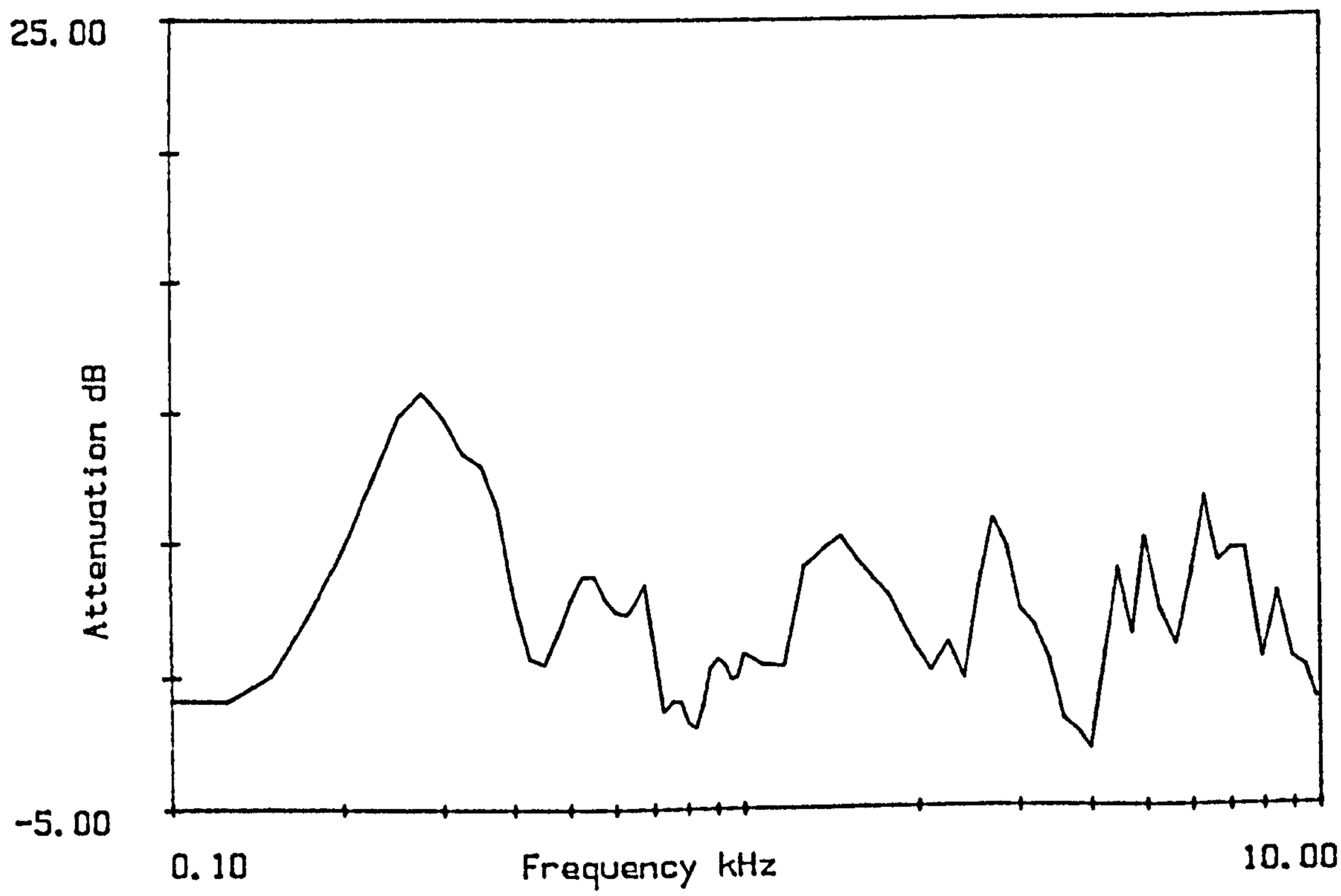

Figure B3.10
Attenuation on 8/8/84 source at F26 microphones at FS
Microphone height 1.2m.

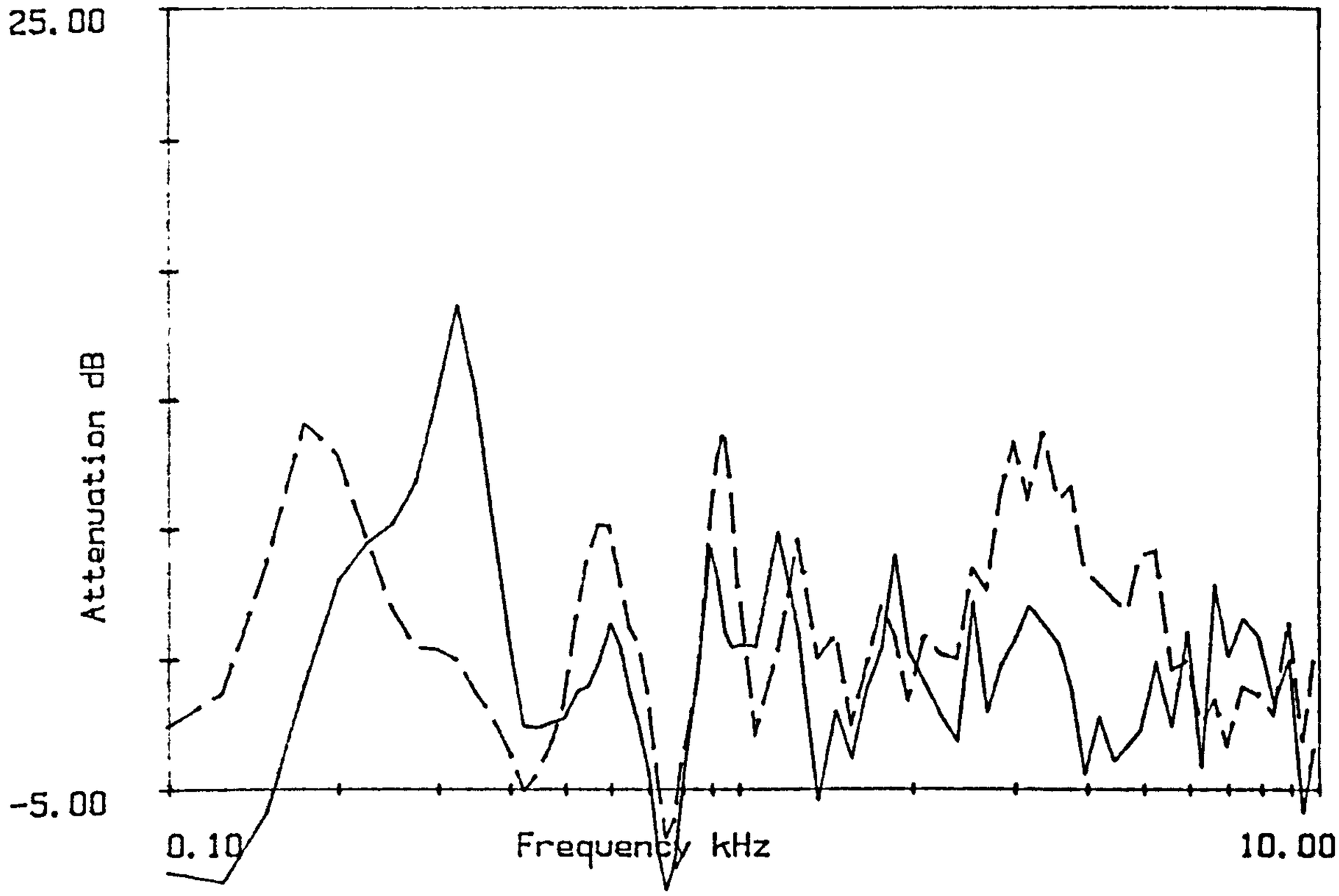

Figure B3.11
Attenuation on 2/7/85 source at FS microphones at b.
Microphone heights 1.2m and 2.5m(----).
7m Without Trees. Source height 1.3m.

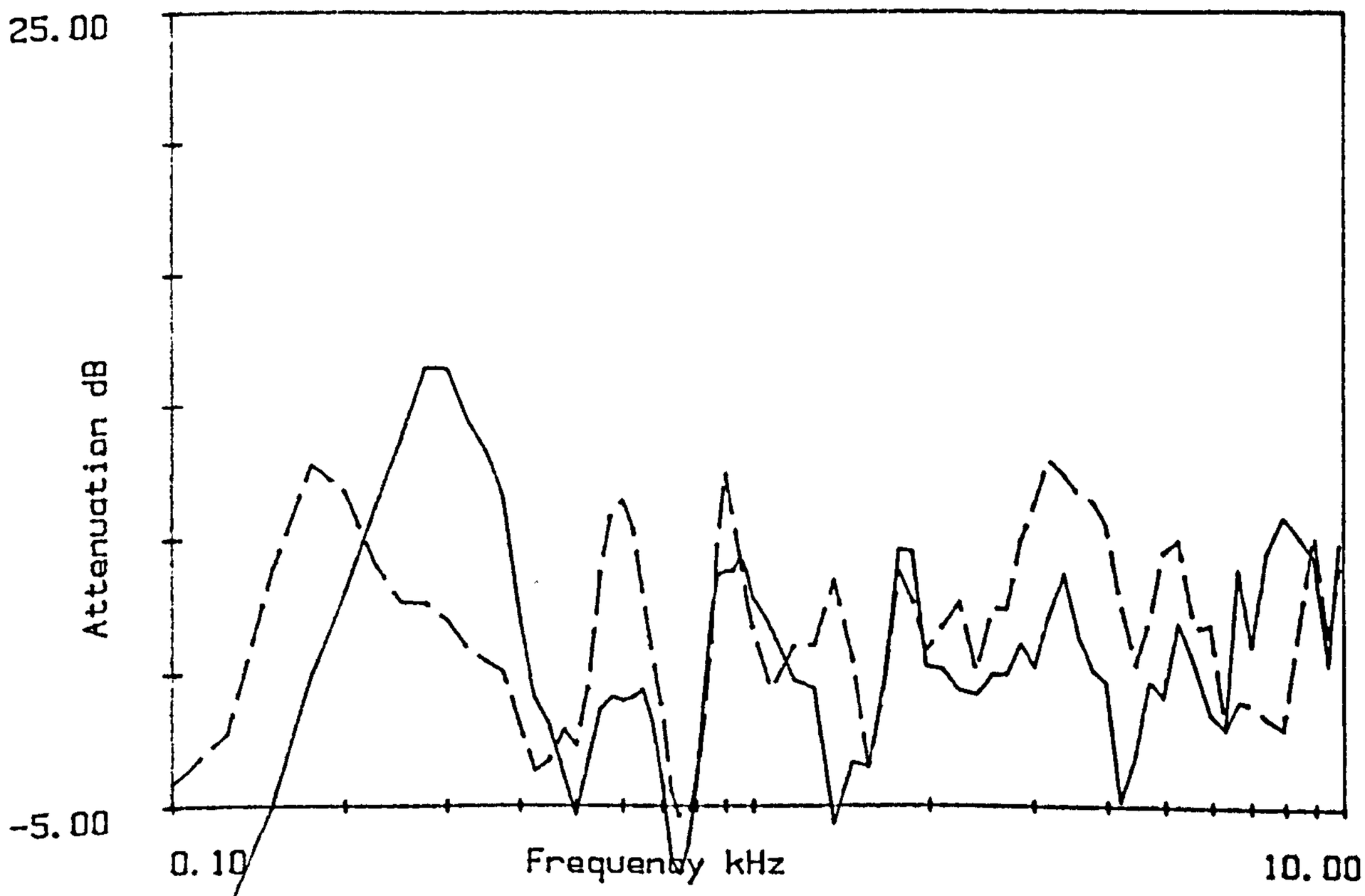

Figure B3.12
Attenuation on 2/7/85 source at FS microphones at c (7m).
Microphone heights 1.2m and 2.5m(----).
Source Height 1.3m.

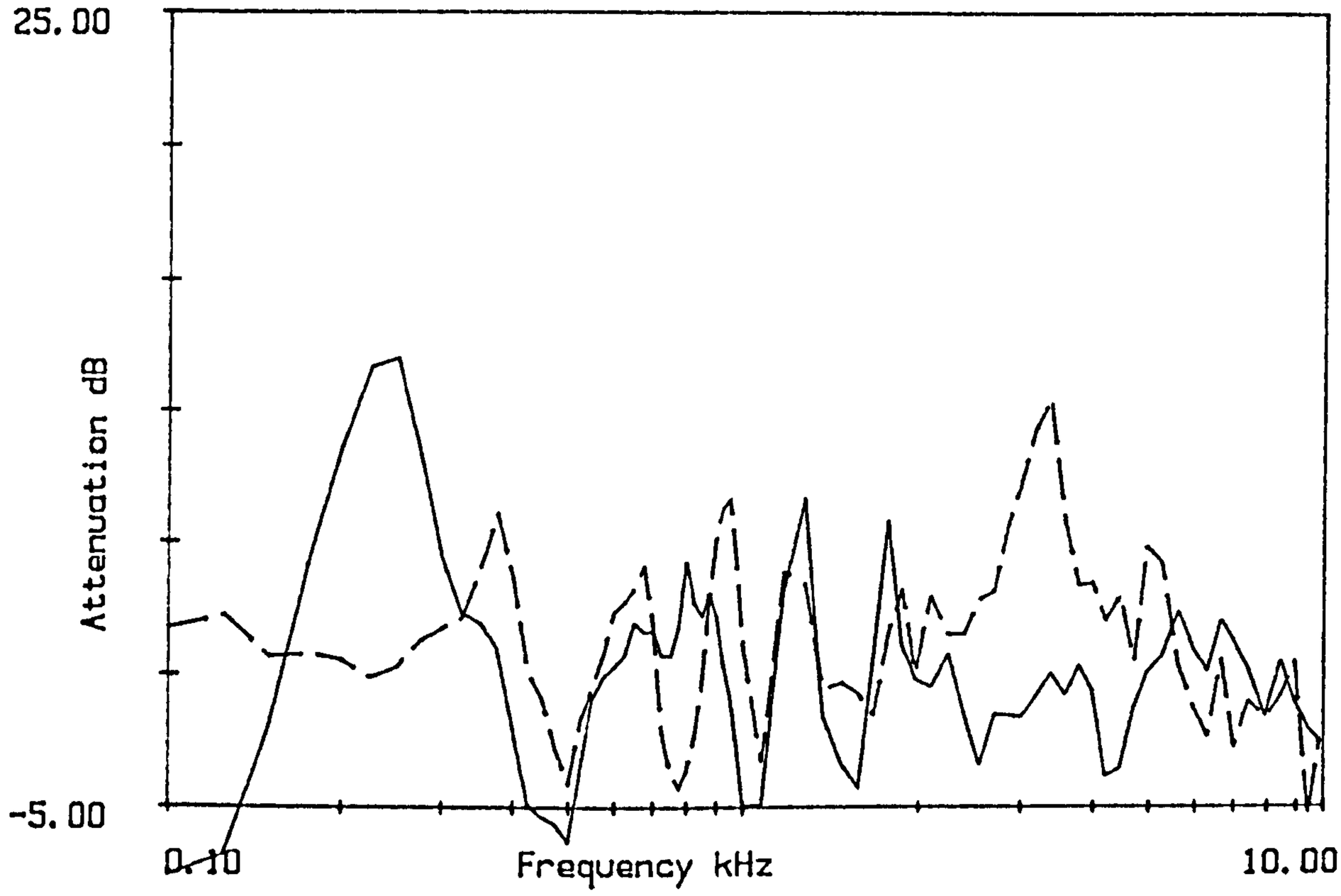

Figure 83.13
Attenuation on 2/7/85 source at FS microphones at c(7m)
Microphone heights 1.2m and 2.5m(----).
Source Height 1.75m.

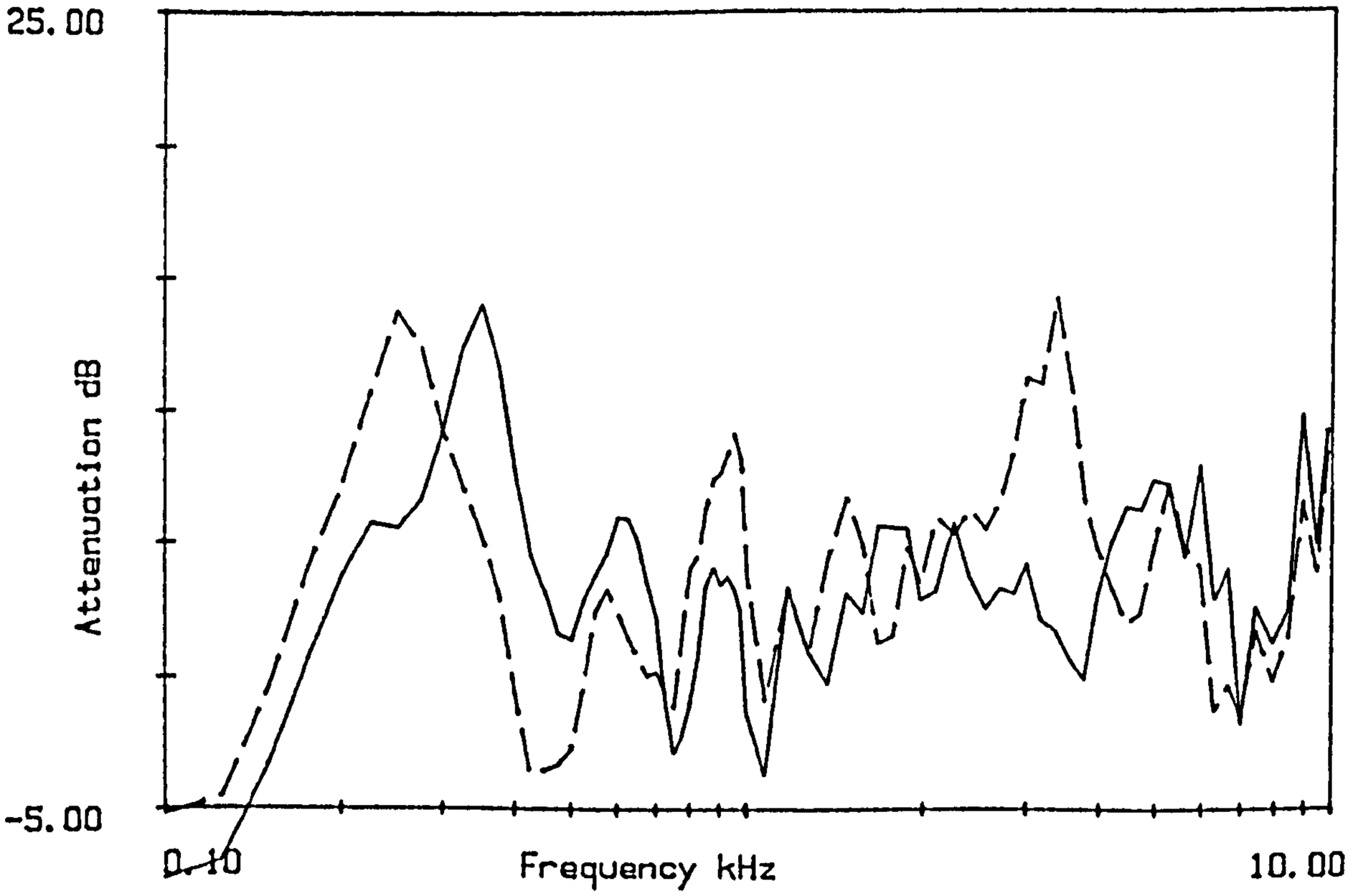

Figure 83.14
Attenuation on 2/7/85 source at FS microphones at F12.
Microphone heights 1.2m and 2.5m(----).
Source Height 1.3m.

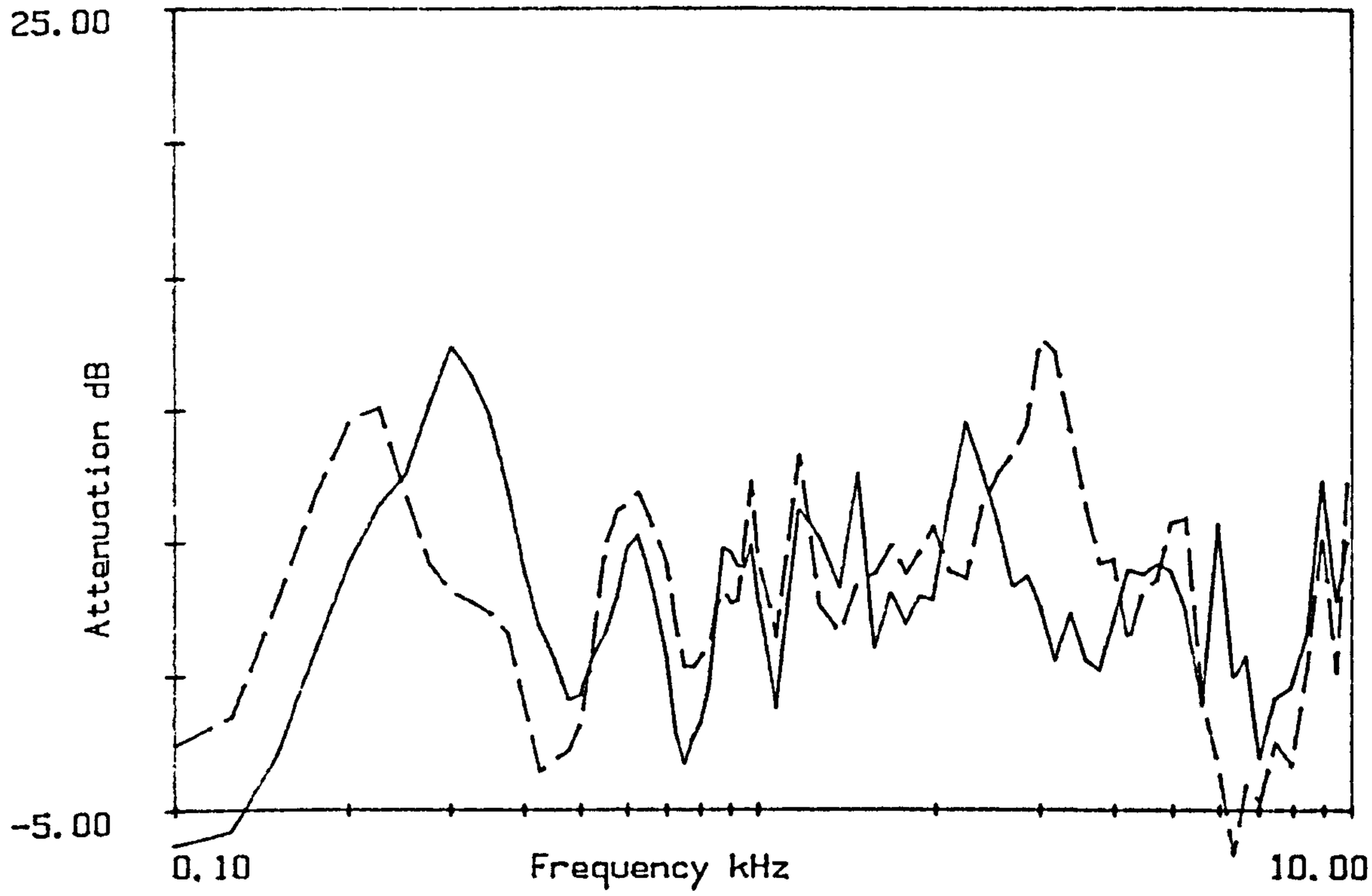

Figure B3.15
Attenuation on 2/7/85 source at FS microphones at F12.
Microphone heights 1.2m and 2.5m(----).
Source Height 1.75m.

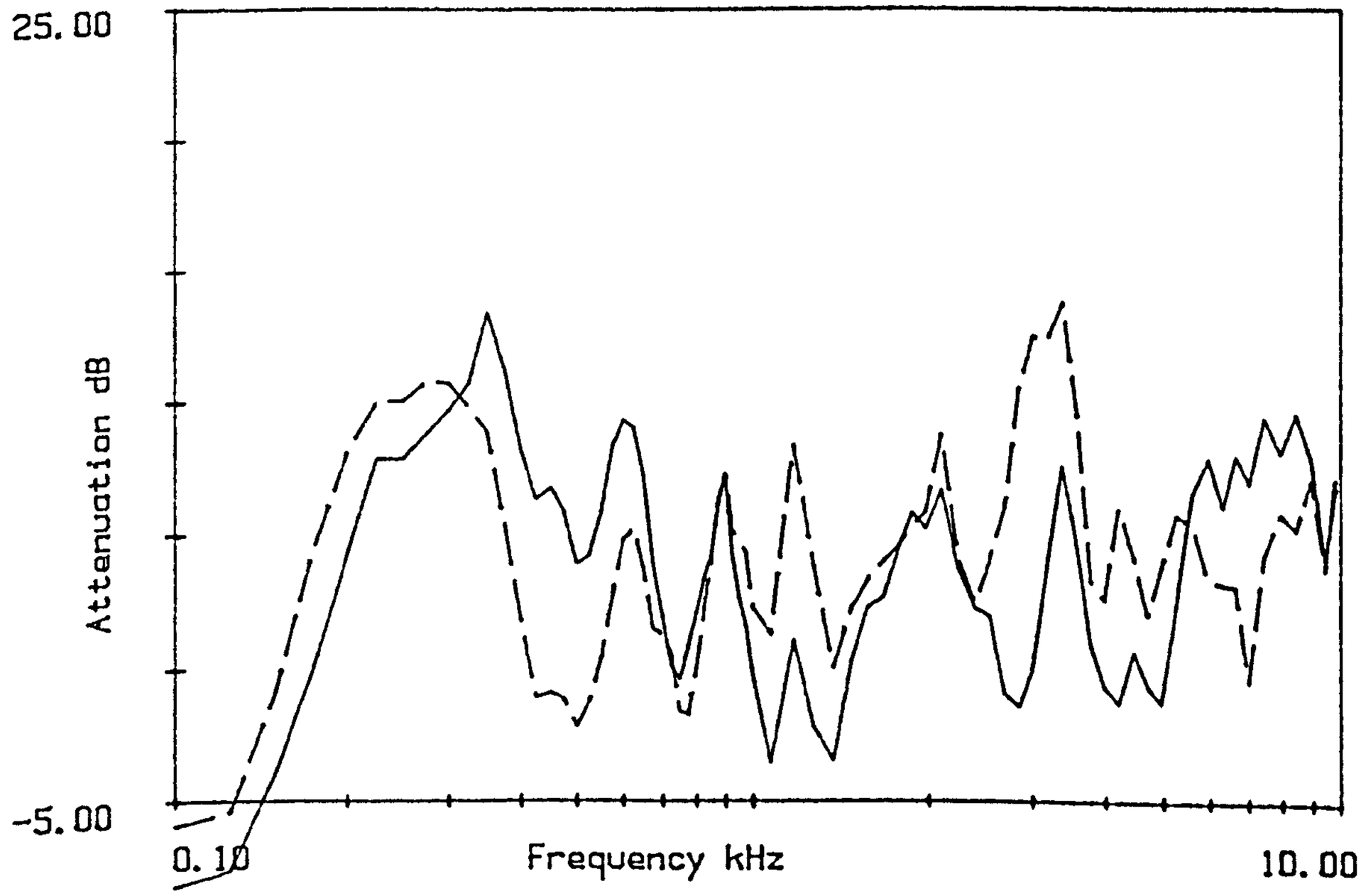

Figure B3.16
Attenuation on 2/7/85 source at FS microphones at d(16.8m).
Microphone heights 1.2m and 2.5m(----).
Source Height 1.3m.

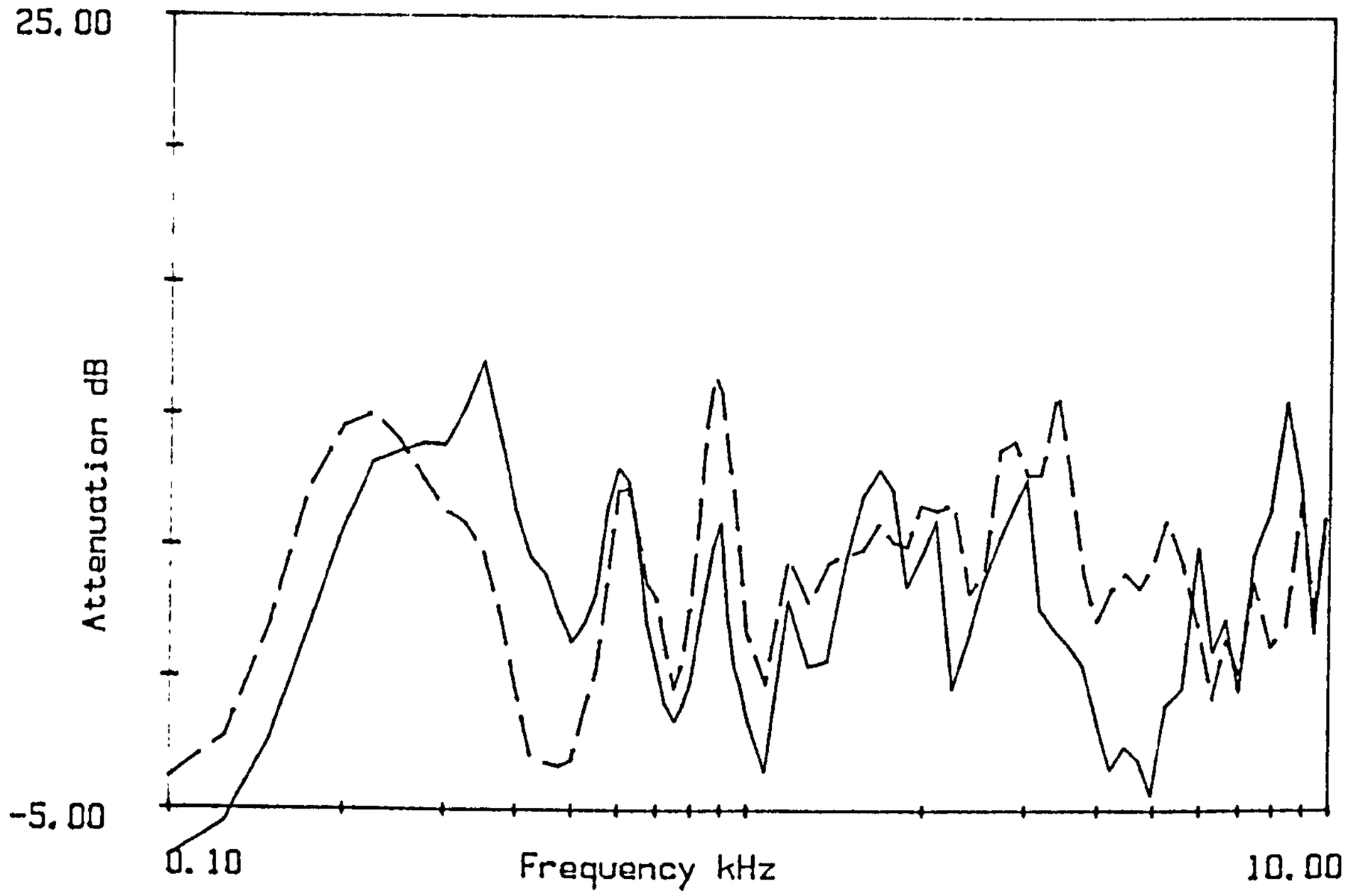

Figure B3.17
Attenuation on 2/7/85 source at FS microphones at d(16.8m).
Microphone heights 1.2m and 2.5m(----).
Source Height 1.75m.

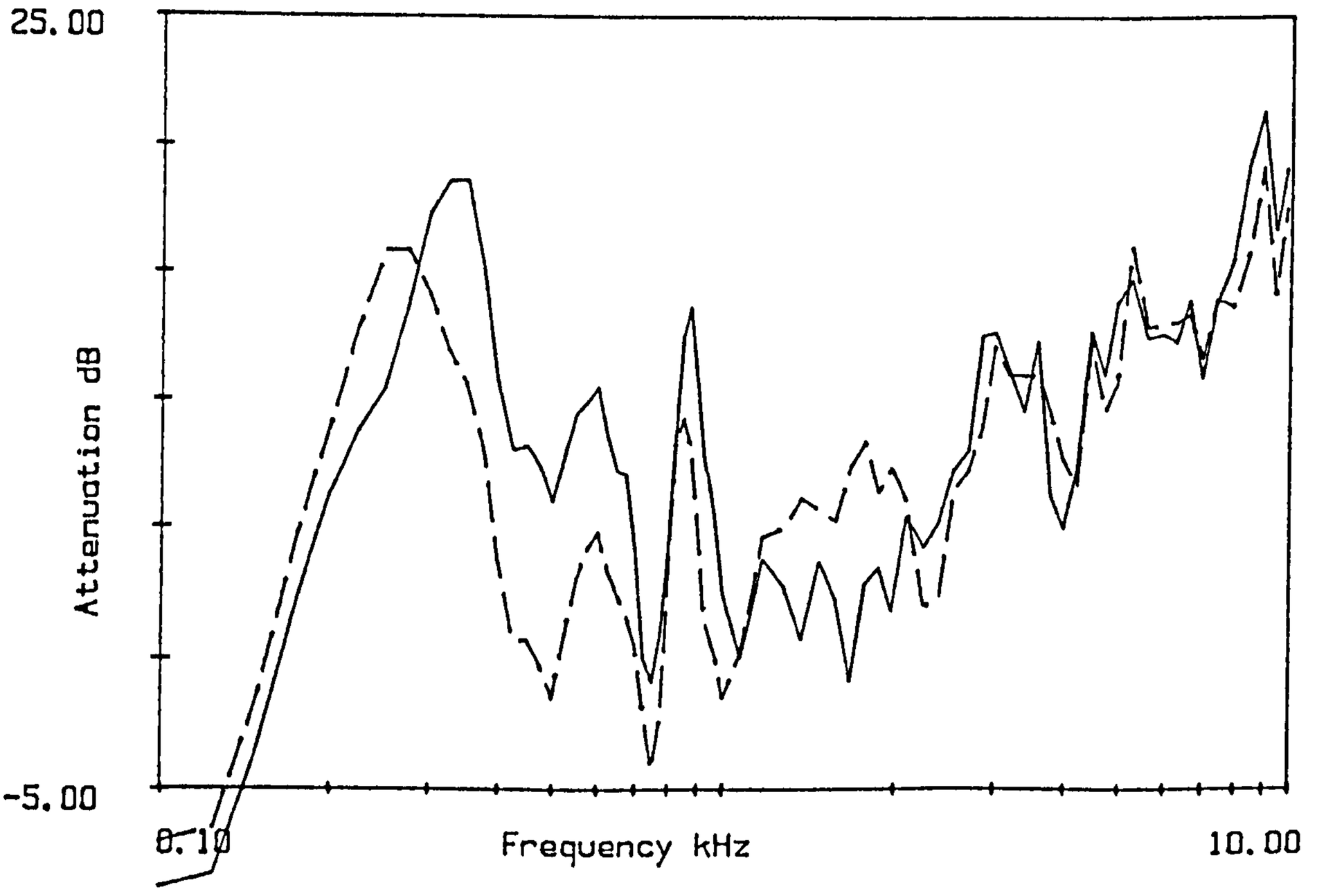

Figure B3.18
Attenuation on 2/7/85 source at FS microphones at F26
Microphone heights 1.2m and 2.5m(----).
Source Height 1.3m.

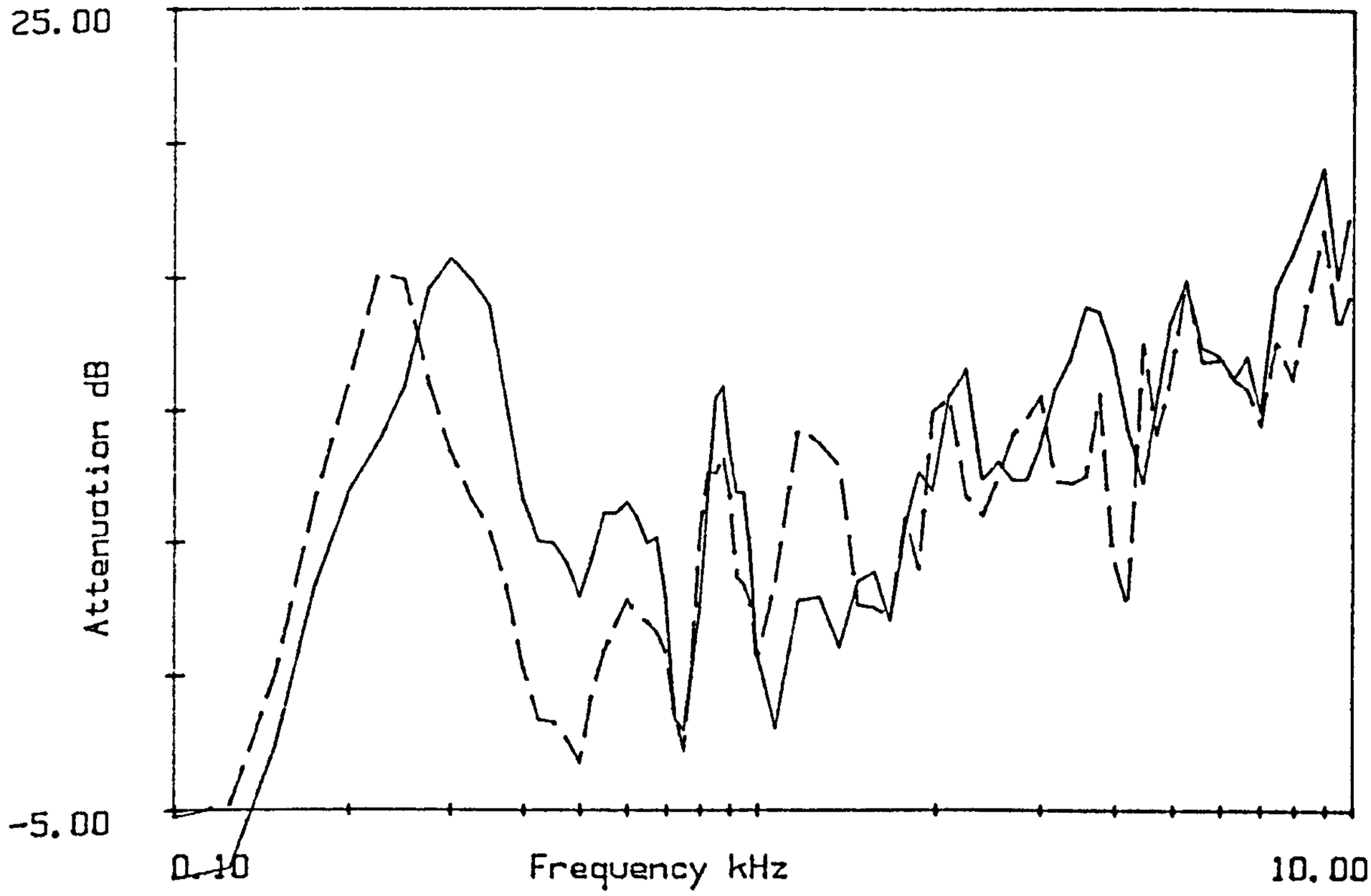

Figure B3.19
Attenuation on 2/7/85 source at FS microphones at F26
Microphone heights 1.2m and 2.5m(----).
Source Height 1.75m.

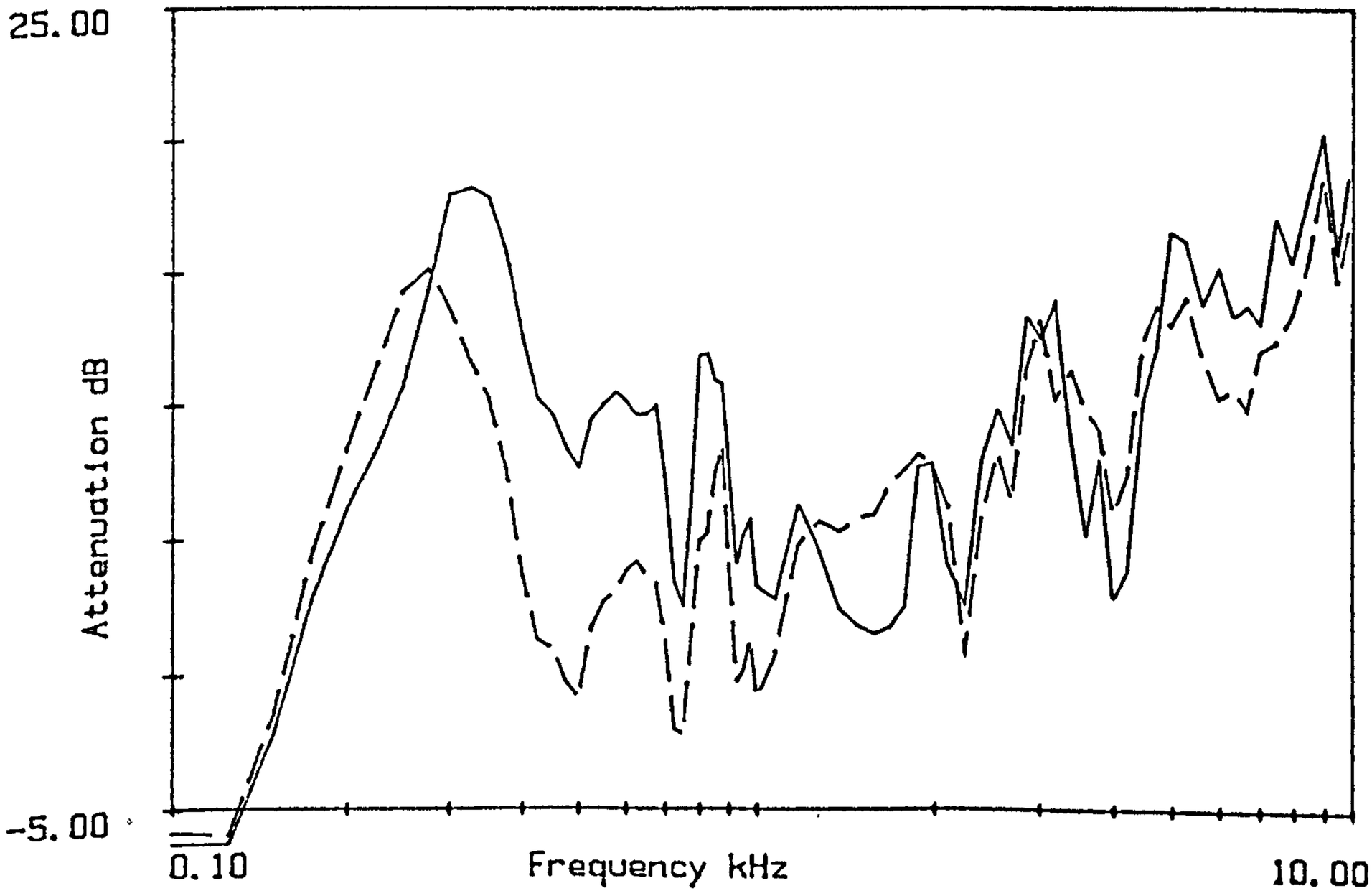

Figure B3.20
Attenuation on 2/7/85 source at FS microphones at F26
Microphone heights 1.2m and 2.5m(----).
Source Height 1.3m.

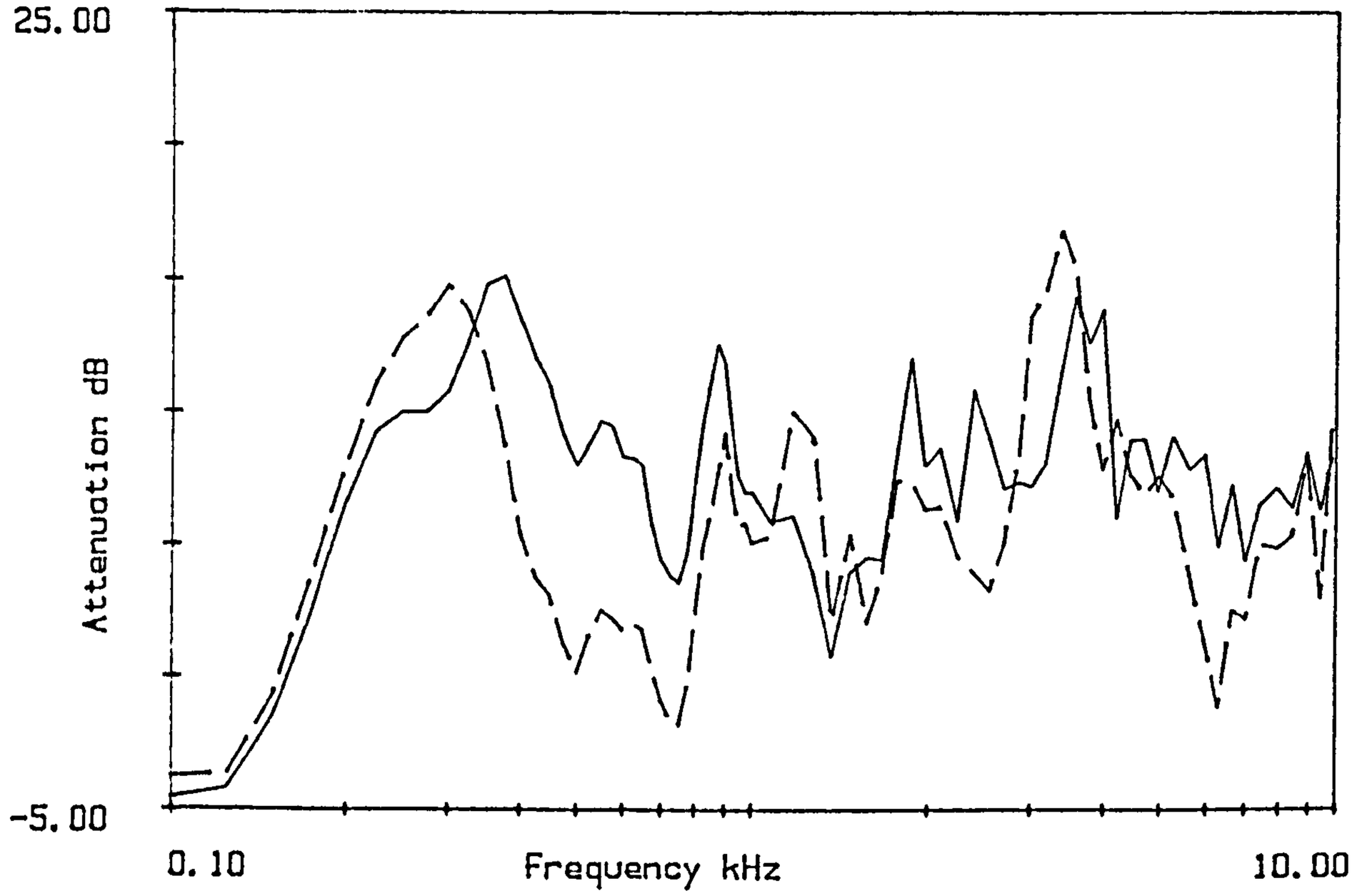

Figure B3.21
Attenuation on 2/7/85 source at F12 microphones at F26.
Microphone heights 1.2m and 2.5m(----).
Source Height 1.3m.

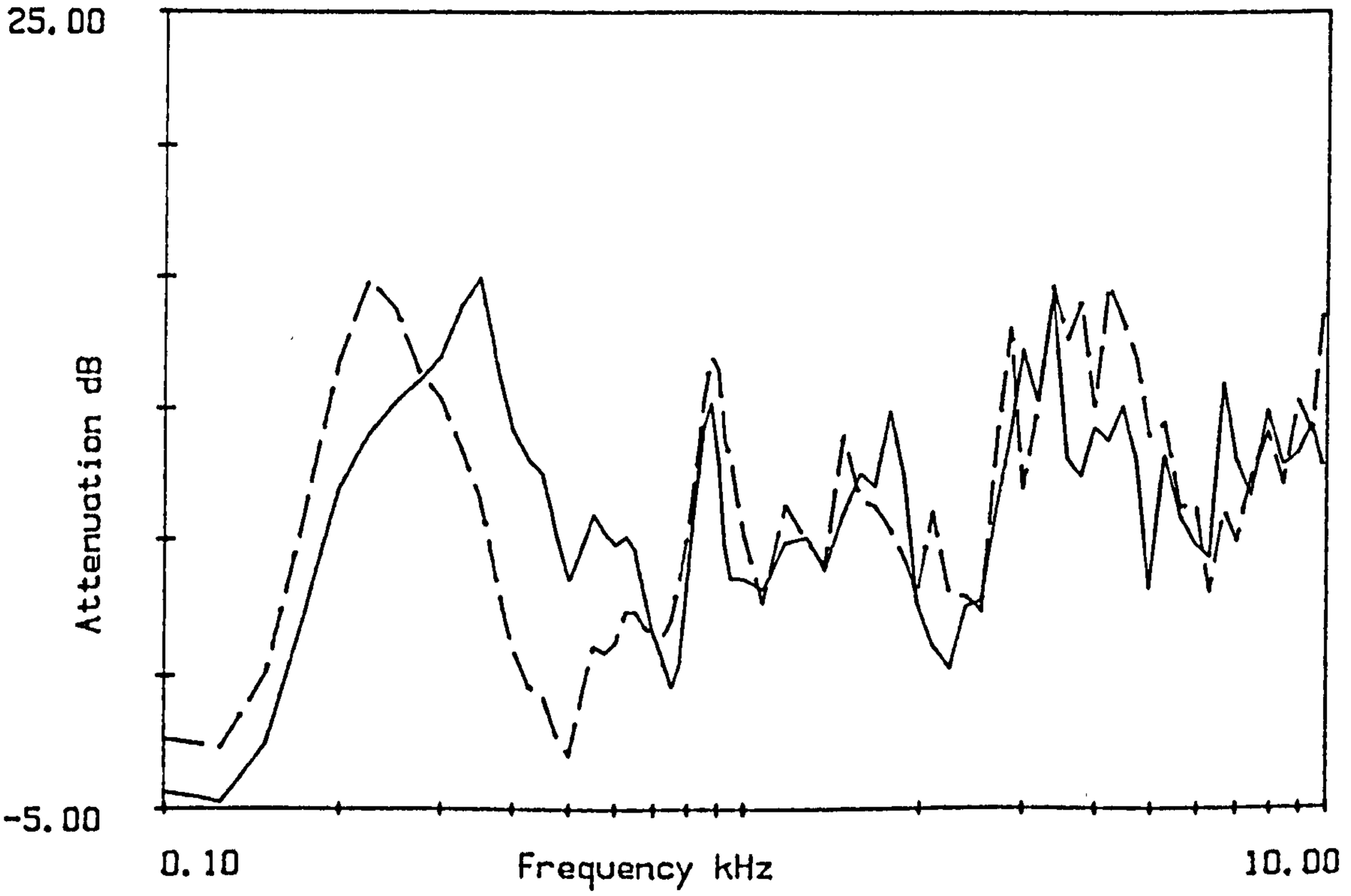

Figure B3.22
Attenuation on 2/7/85 source at F12 microphones at F26
Microphone heights 1.2m and 2.5m(----).
Source Height 1.75m.

Appendix C: Best Fit Ground Parameters.

All the data sets were fitted to predictions of sound propagation using a least mean squares fit. The results presented in this appendix are the ground parameters which gave the best fit to the data (lowest mean squared difference) and the mean difference obtained using those parameters (md). The column labelled hr gives the test microphone height. The letters SI in the final column indicate that the rigid-backed layer approximation gave an almost identical impedance value to the homogeneous model, ie. the layer approximates to a semi-infinite medium. This is checked by the fitting routine which subtracts the real part of the impedance obtained using the rigid backed layer from that using the same value of σ_e in the homogeneous model. if there is less than 1 ρc unit between the two the semi-infinite case (SI) is indicated.

Appendix C1: Data from Hazelborough Wood.

Hazelborough Wood 10/8/83

Microphone Position		Homogeneous Approximation		Delany and Bazely		Rigid-Backed Layer Approximation			
Site	hr	σ_e	md	σ_e	md	σ_e	d_e	md	
C24	1.2	59000	3.22	26000	2.23	80000	0.08	3.06	
	2.5	34000	3.40	23000	3.18	50000	0.09	3.19	
C48	1.2	39000	3.44	24000	3.08	50000	0.11	3.01	SI
	2.5	34000	3.83	23000	3.63	50000	0.095	3.67	
C72	1.2	35000	4.13	23000	3.43	40000	0.14	3.99	SI
	2.5	36000	3.36	24000	3.01	40000	0.145	3.09	SI
Mean		39500	3.56	23833	3.26	51667	0.11	3.33	

Hazelborough Wood 10/4/84

Microphone Position		Homogeneous Approximation		Delany and Bazely		Rigid-Backed Layer Approximation			
Site	hr	σ_e	md	σ_e	md	σ_e	d_e	md	
C24	1.2	93000	2.16	63000	2.33	90000	0.085	2.06	SI
	2.5	111000	5.27	51000	5.40	110000	0.055	5.08	
C48	1.2	127000	2.57	77000	2.46	120000	0.070	2.59	
	2.5	153000	2.91	85000	3.16	160000	0.050	2.77	
C72	1.2	116000	4.91	68000	4.48	120000	0.105	5.08	SI
	2.5	113000	3.84	62000	3.57	130000	0.060	3.97	
Mean		118833	3.61	67667	3.57	121667	0.071	3.59	

Hazelborough Wood 5/7/84

Microphone Position		Homogeneous Approximation		Delany and Bazely		Rigid-Backed Layer Approximation			
Site	hr	σ_e	md	σ_e	md	σ_e	d_e	md	
C24	1.2	30000	2.48	20000	2.31	40000	0.109	2.47	
	2.5	30000	1.93	20000	1.75	40000	0.105	1.81	
C48	1.2	40000	2.88	20000	2.67	50000	0.109	2.71	SI
	2.5	50000	2.72	30000	2.65	50000	0.100	2.60	
C72	1.2	30000	2.83	20000	2.35	40000	0.109	2.83	
	2.5	50000	3.08	30000	2.88	50000	0.108	3.03	SI
D24	1.2	20000	4.16	10000	3.82	40000	0.109	4.23	
	2.5	20000	3.76	20000	3.62	30000	0.121	3.66	SI
D48	1.2	20000	3.86	10000	3.47	40000	0.109	3.96	
	2.5	30000	3.93	20000	3.74	40000	0.109	3.84	
Mean		32000	3.16	20000	2.93	42000	0.1088	3.11	

Hazelborough Wood 9/8/84

Microphone Position		Homogeneous Approximation		Delany and Bazely		Rigid-Backed Layer Approximation			
Site	hr	σ_e	md	σ_e	md	σ_e	d_e	md	
H24	2.5	20000	1.89	20000	1.65	20000	0.185	1.90	SI
	1.2	30000	2.52	20000	2.08	30000	0.140	2.40	SI
H48	2.5	30000	2.79	20000	2.82	40000	0.110	2.75	SI
	1.2	40000	2.69	20000	2.63	40000	0.120	2.51	SI
H72	2.5	30000	2.58	20000	2.05	30000	0.185	2.58	SI
	1.2	30000	4.15	20000	3.43	40000	0.130	4.11	SI
Mean		30000	2.77	20000	2.44	33333	0.145	2.71	

Hazelborough Wood 20/6/85

Microphone Position		Homogeneous Approximation		Delany and Bazely		Rigid-Backed Layer Approximation			
Site C72									
Time	hr	σ_e	md	σ_e	md	σ_e	d_e	md	
12.00	1.2	130000	2.55	80000	2.55	130000	0.075	2.48	SI
	2.5	110000	2.30	60000	2.48	120000	0.060	2.15	
13.00	1.2	120000	2.41	70000	2.36	120000	0.080	2.34	SI
	2.5	90000	2.74	50000	2.93	110000	0.065	2.61	
14.15	1.2	120000	2.33	70000	2.32	120000	0.075	2.24	SI
	2.5	90000	2.39	50000	2.54	100000	0.065	2.31	SI
16.00	2.5	100000	2.47	60000	2.62	120000	0.055	2.36	
Mean		108571	2.46	62857	2.54	117143	0.068	2.36	
C48									
12.00	1.2	180000	3.60	110000	3.39	180000	0.065	2.48	SI
	2.5	110000	3.13	60000	2.98	130000	0.06	2.15	
13.00	1.2	190000	3.57	110000	3.43	190000	0.06	2.34	
	2.5	90000	2.37	60000	2.22	100000	0.075	2.61	
14.15	1.2	180000	4.07	110000	3.78	180000	0.065	2.24	
	2.5	100000	2.75	60000	2.52	120000	0.06	2.31	
16.00	1.2	180000	3.53	100000	3.26	180000	0.065	2.36	SI
Mean		147143	3.29	87143	3.08	154286	0.064	3.26	

Appendix C2: Data from Wetleys Wood.

Wetleys Wood 28/7/83

Microphone Position		Homogeneous Approximation		Delany and Bazely		Rigid-Backed Layer Approximation			
Site	hr	σ_e	md	σ_e	md	σ_e	d_e	md	
A12	1.2	55000	3.26	30000	3.16	60000	0.085	3.13	
	2.5	58000	2.80	35000	2.62	60000	0.080	2.70	
A24	1.2	38000	2.95	26000	3.02	40000	0.115	2.79	SI
	2.5	43000	2.97	28000	2.83	50000	0.095	2.83	
A48	1.2	34000	1.73	25000	1.35	40000	0.130	1.77	SI
	2.5	32000	2.43	23000	2.29	40000	0.115	2.30	SI
A96	1.2	33000	4.82	22000	3.99	40000	0.135	5.05	SI
	2.5	29000	2.43	20000	2.03	30000	0.175	2.36	SI
Mean		38125	2.92	26125	2.66	45000	0.116	2.87	

Wetleys Wood 26/6/84

Microphone Position		Homogeneous Approximation		Delany and Bazely		Rigid-Backed Layer Approximation			
Site	hr	σ_e	md	σ_e	md	σ_e	d_e	md	
A12	1.2	89000	3.20	60000	3.27	90000	0.070	3.13	
	2.5	77000	3.03	50000	2.94	90000	0.055	2.95	
A24	1.2	89000	3.26	59000	3.51	90000	0.080	3.17	
	2.5	10700	3.18	64000	3.21	110000	0.065	3.07	
A48	1.2	69000	4.43	48000	4.83	80000	0.070	4.28	
	2.5	91000	4.60	55000	4.93	100000	0.065	4.35	
A96	1.2	69000	2.87	46000	3.35	70000	0.100	2.59	SI
	2.5	74000	3.93	46000	4.28	80000	0.080	3.55	
B96	1.2	73000	3.72	47000	3.57	80000	0.075	3.74	
	2.5	72000	4.99	44000	5.07	80000	0.070	4.73	
B48	1.2	79000	4.18	52000	4.35	80000	0.100	4.09	SI
	2.5	82000	4.19	48000	4.23	90000	0.070	4.04	
B24	1.2	84000	4.19	56000	4.31	80000	0.095	4.12	SI
	2.5	90000	3.67	54000	3.57	90000	0.085	3.61	SI
B12	1.2	107000	5.04	62000	4.98	110000	0.060	4.99	SI
	2.5	255000	3.98	94000	4.09	200000	0.050	3.96	*
Mean		83467	3.89	52733	4.03	88000	0.076	3.76	

* Mean excludes measurement at B12, 2.5m as it gives a very different result to the other measurements.

Wetleys Wood 16/5/85

Microphone Position		Homogeneous Approximation		Delany and Bazely		Rigid-Backed Layer Approximation			
Site A96									
Time	hr	σ_e	md	σ_e	md	σ_e	d_e	md	
13.00	1.2	70000	3.54	40000	3.08	70000	0.095	3.62	Sl
	2.5	50000	1.65	40000	1.35	70000	0.070	1.75	
14.00	1.2	60000	5.18	40000	4.60	80000	0.065	5.25	
	2.5	60000	2.10	40000	2.24	70000	0.060	1.80	
15.00	1.2	60000	2.45	40000	2.04	70000	0.095	2.59	Sl
	2.5	50000	1.97	40000	1.58	70000	0.065	2.07	
16.00	1.2	130000	4.11	60000	4.08	140000	0.060	3.93	
	2.5	70000	2.14	50000	1.85	90000	0.055	2.02	
16.30	1.2	70000	2.46	50000	2.10	80000	0.065	2.44	
	2.5	60000	2.19	40000	1.77	70000	0.070	2.20	
Mean		68000	2.78	44000	8.78	81000	0.070	2.77	
A48									
13.00	1.2	80000	3.62	50000	3.13	80000	0.095	3.65	Sl
	2.5	80000	2.04	50000	1.85	90000	0.070	1.98	
14.00	1.2	70000	1.68	50000	1.56	90000	0.060	1.70	
	2.5	70000	2.37	50000	2.06	80000	0.075	2.37	
15.00	1.2	80000	1.73	50000	1.46	80000	0.095	1.79	Sl
	2.5	70000	2.13	50000	2.20	90000	0.065	2.04	
16.00	1.2	90000	1.72	60000	1.60	100000	0.055	1.69	
	2.5	100000	2.49	60000	2.61	110000	0.055	2.32	
16.30	1.2	80000	1.71	50000	1.62	90000	0.070	1.72	
	2.5	70000	2.56	40000	2.70	90000	0.065	2.36	
Mean		79000	2.20	51000	2.08	90000	0.070	2.16	

Appendix C3: Data from Bucknell Wood.

Bucknell Wood 9/7/84

Microphone Position		Homogeneous Approximation		Delany and Bazely		Rigid-Backed Layer Approximation		
Site	hr	σ_e	md	σ_e	md	σ_e	d_e	md
Source at F26.								
F12	1.2	110000	4.94	60000	5.04	110000	0.060	4.90
	2.5	100000	3.21	60000	3.38	100000	0.060	3.10
G24	1.2	80000	6.94	50000	7.39	80000	0.070	6.91
	2.5	90000	5.63	40000	5.67	100000	0.060	5.59
G40	1.2	50000	6.95	30000	7.33	60000	0.085	6.98
	2.5	60000	5.68	30000	5.85	70000	0.075	5.67
FS	1.2	50000	5.27	30000	5.50	50000	0.090	5.23
	2.5	50000	5.03	30000	4.88	50000	0.085	4.98
Mean		73750	5.41	41250	5.63	77500	0.073	5.42

Bucknell Wood 8/8/84

Microphone Position		Homogeneous Approximation		Delany and Bazely		Rigid-Backed Layer Approximation			
Site	hr	σ_e	md	σ_e	md	σ_e	d_e	md	
Source at F26.									
F12	1.2	110000	4.59	60000	4.78	110000	0.060	4.50	
	2.5	80000	3.74	40000	3.71	80000	0.069	3.63	
G24	1.2	70000	7.91	40000	8.25	70000	0.075	7.81	
	2.5	100000	6.64	40000	6.69	110000	0.056	6.54	
FS	1.2	50000	4.48	30000	4.64	50000	0.095	4.39	
	2.5	50000	3.73	30000	3.60	60000	0.083	3.61	
G40	1.2	50000	7.72	30000	8.10	50000	0.096	7.60	
	2.5	50000	4.62	30000	4.12	60000	0.109	4.64	SI
Source at FS									
F26	1.2	40000	3.78	30000	3.88	50000	0.097	3.67	
	2.5	40000	3.49	30000	3.32	50000	0.087	3.39	
F12	1.2	70000	4.04	40000	3.98	70000	0.089	4.00	
Mean		64545	4.98	36364	5.01	69091	0.083	4.89	

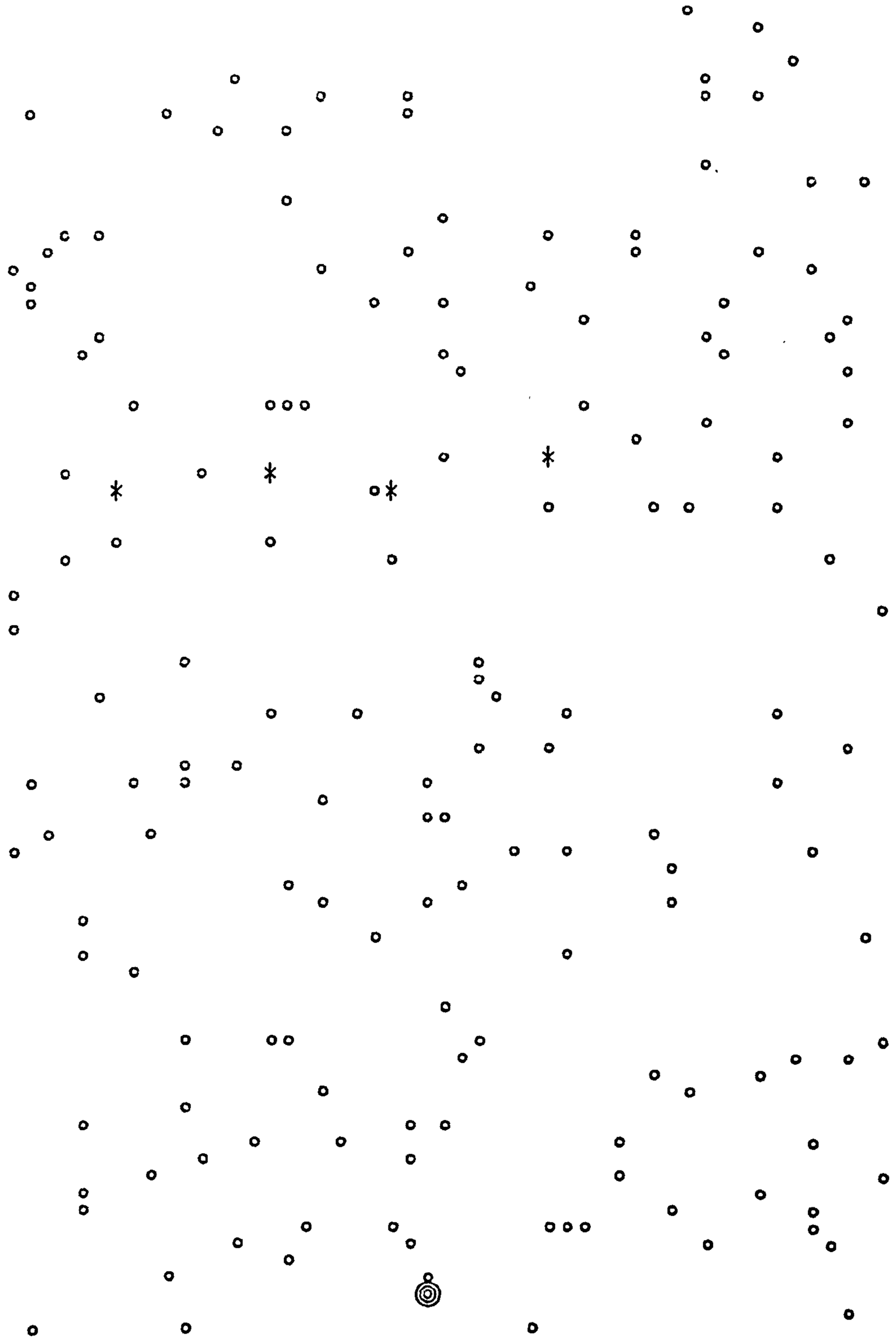

Figure D.1
Measurement A-6 Array Density 240 Rod Diameter 6mm.

◎ Air jet sound source

* Microphone.

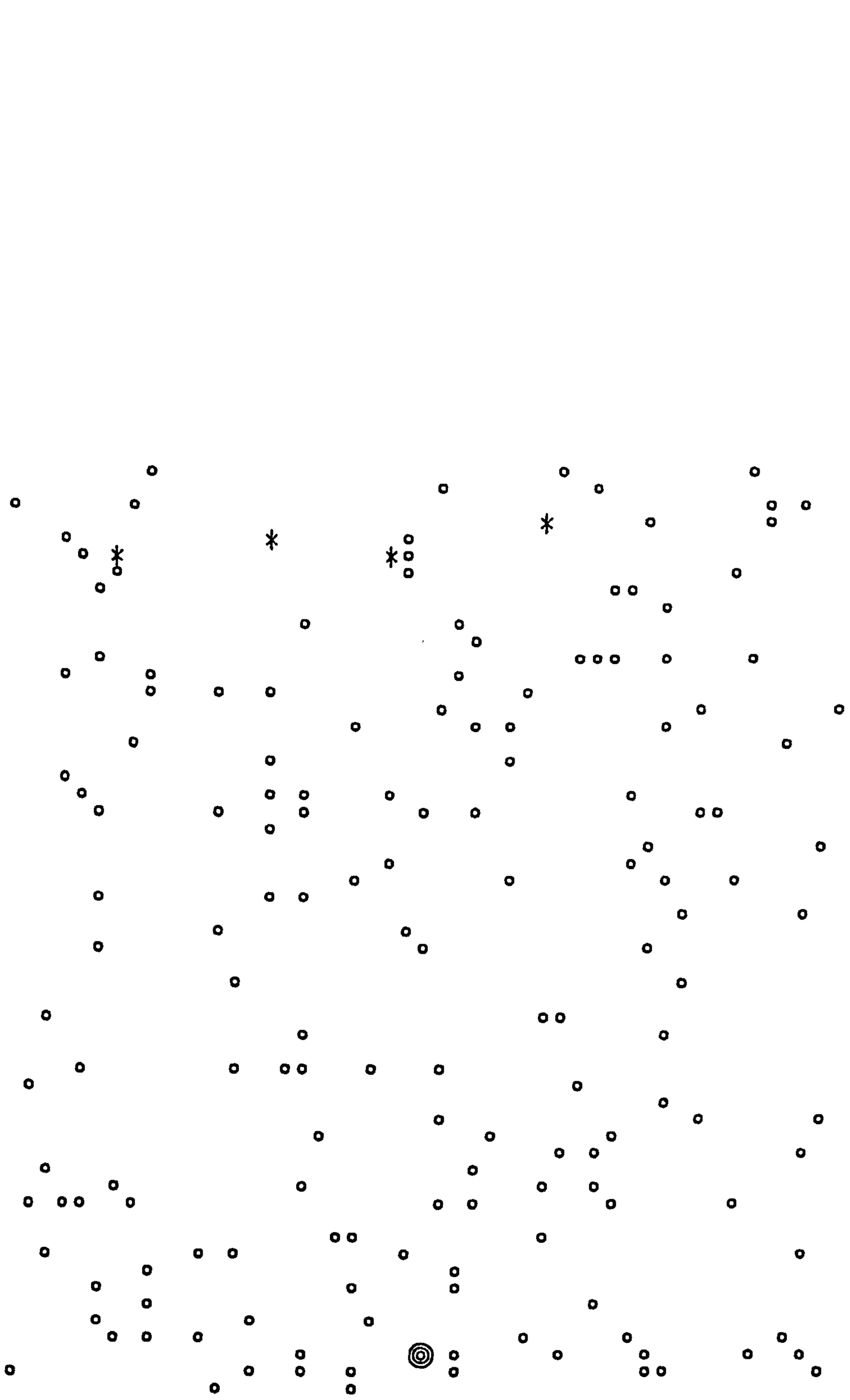

Figure D.2
Measurement B-6 Array Density 360 Rod Diameter 6mm.

◎ Air jet sound source

* Microphone.

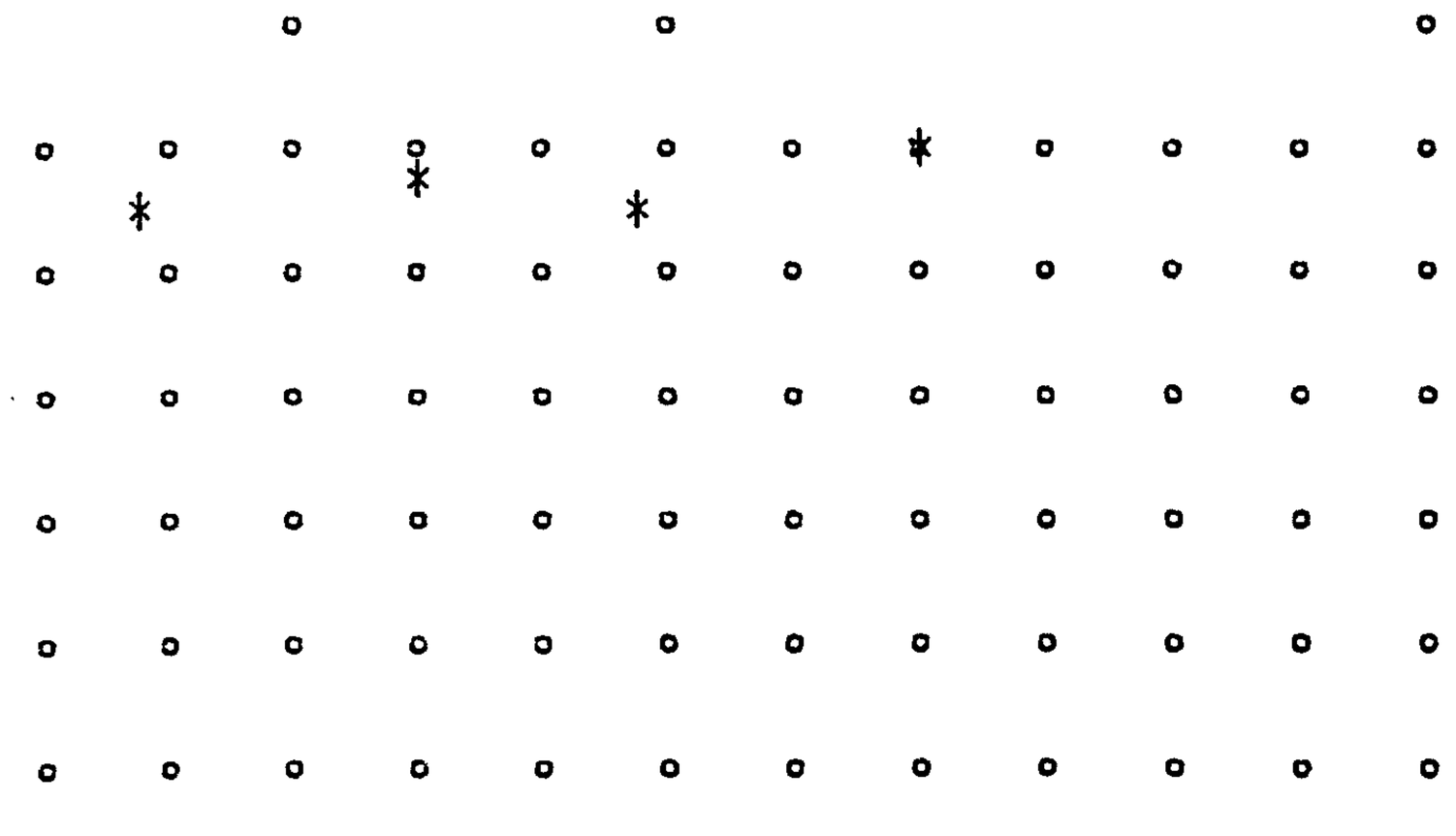

Figure D.3
Measurement C-6 Array Density 400 Rod Diameter 6mm.

◎ Air jet sound source

* Microphone.

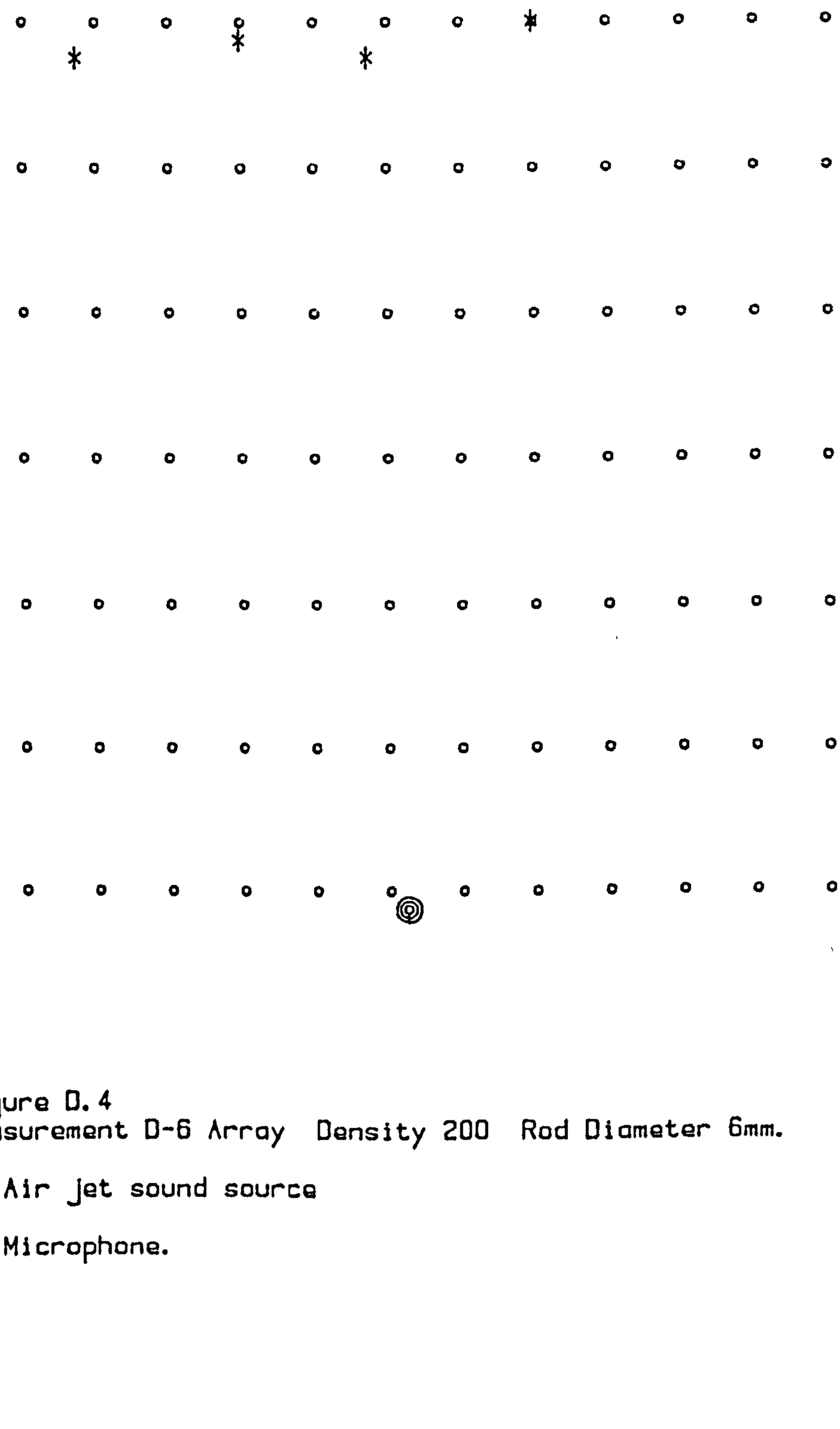

Figure D.4
Measurement D-6 Array Density 200 Rod Diameter 6mm.

◎ Air jet sound source

* Microphone.

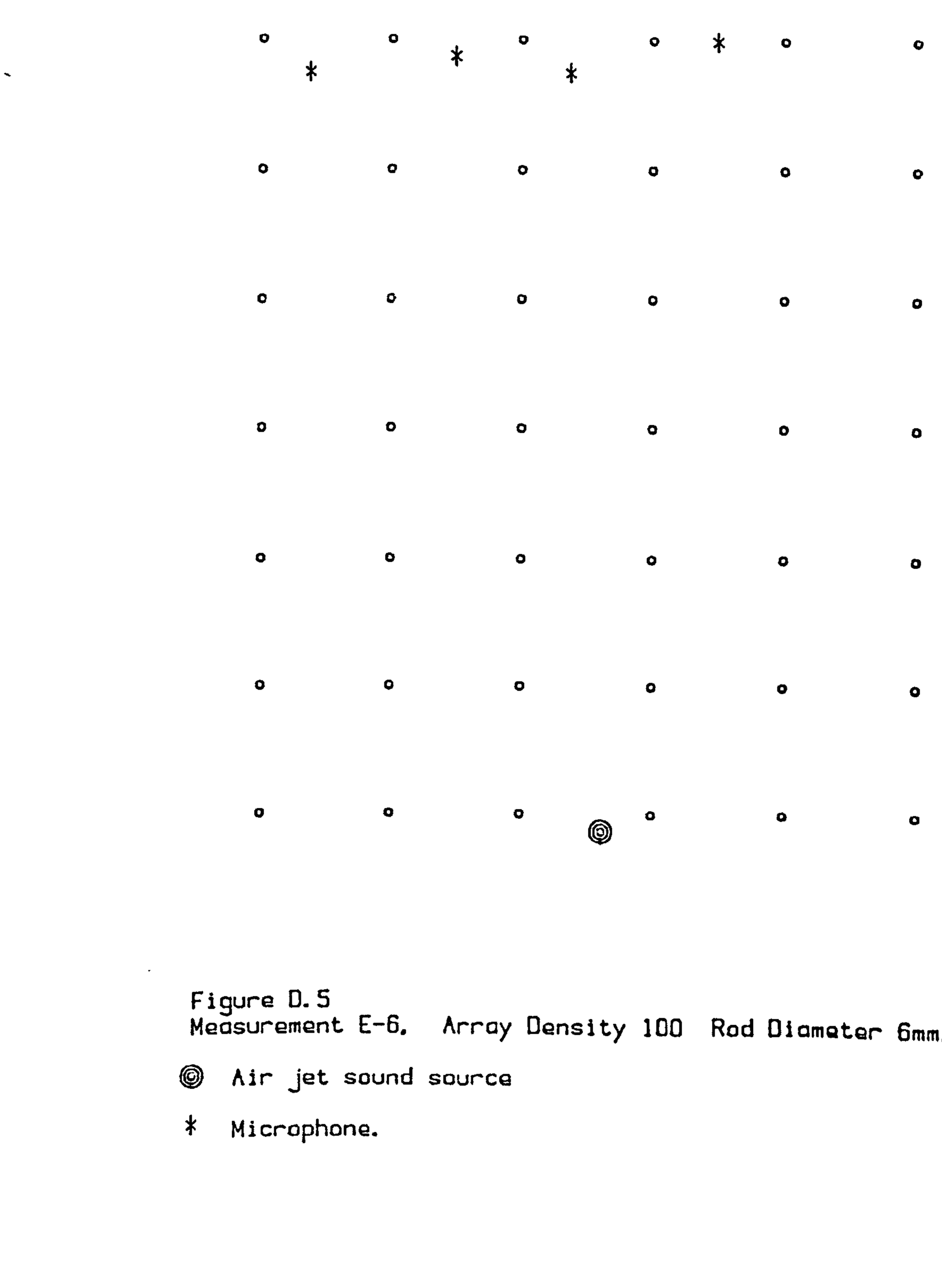

Figure D.5
Measurement E-6. Array Density 100 Rod Diameter 6mm.

◎ Air jet sound source

* Microphone.

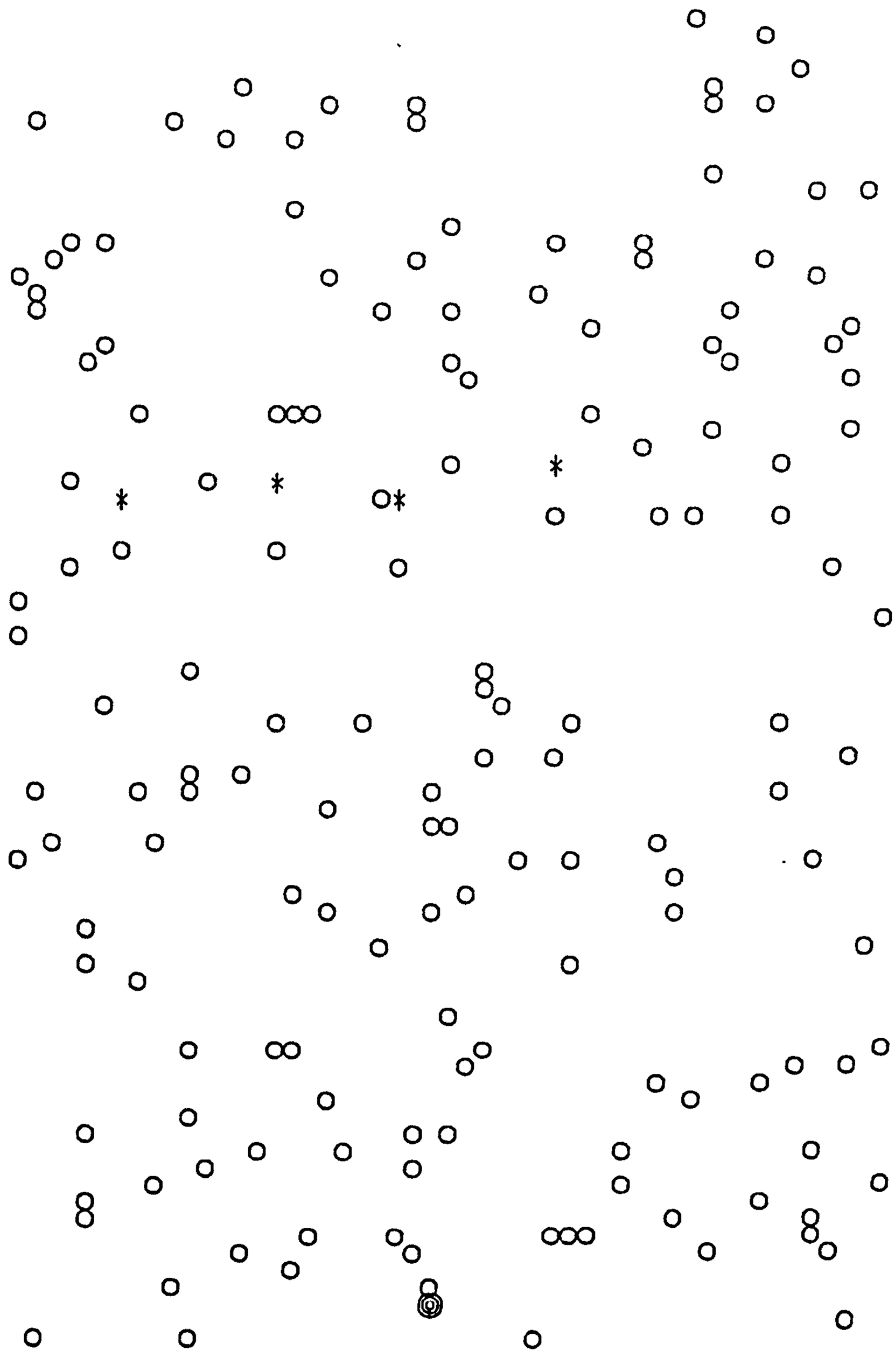

Figure D.6
Measurement A-12 Array Density 240 Rod Diameter 12mm.

◎ Air jet sound source

* Microphone.

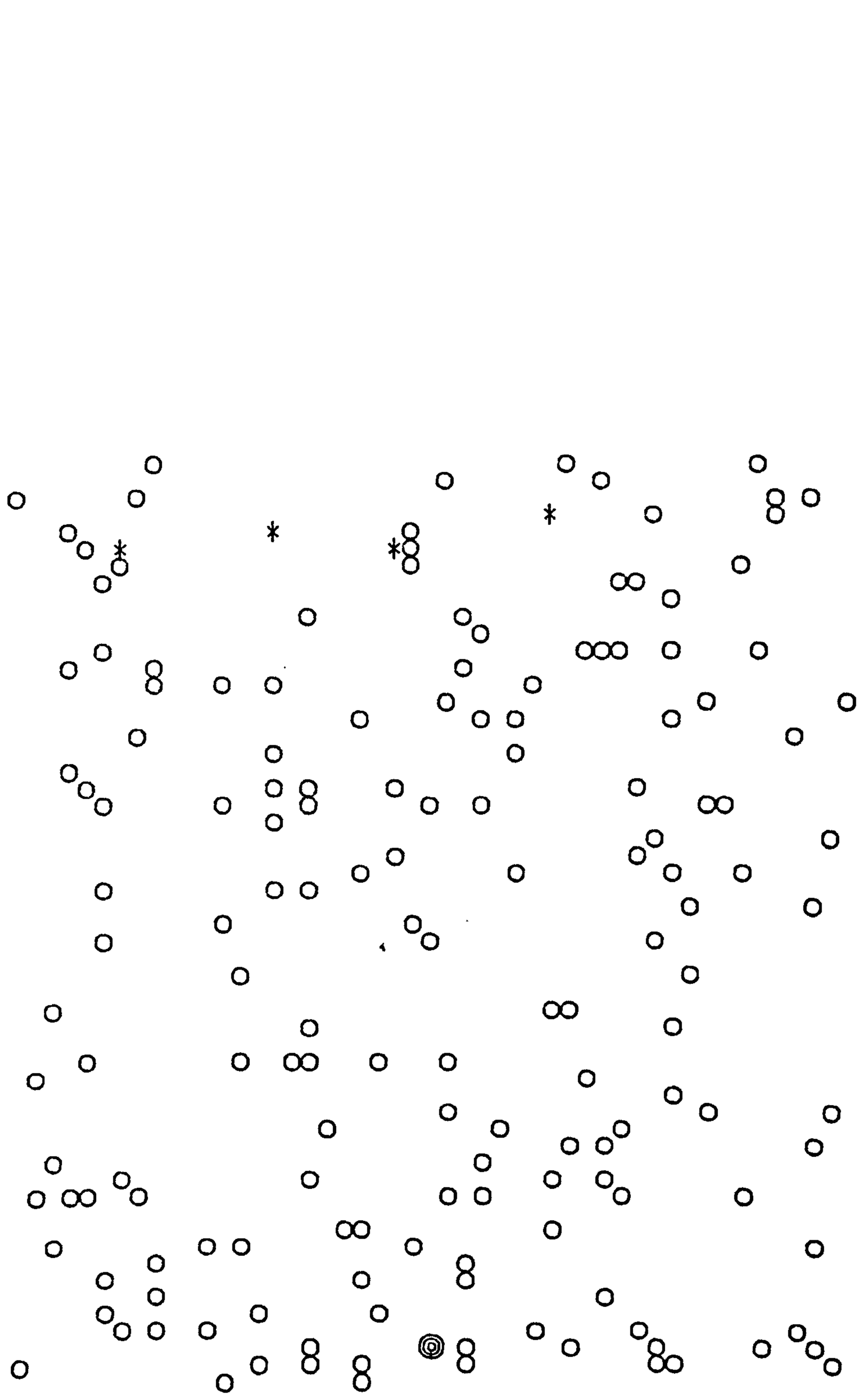

Figure D.7
Measurement B-12 Array Density 360 Rod Diameter 12mm.

◎ Air jet sound source

* Microphone.

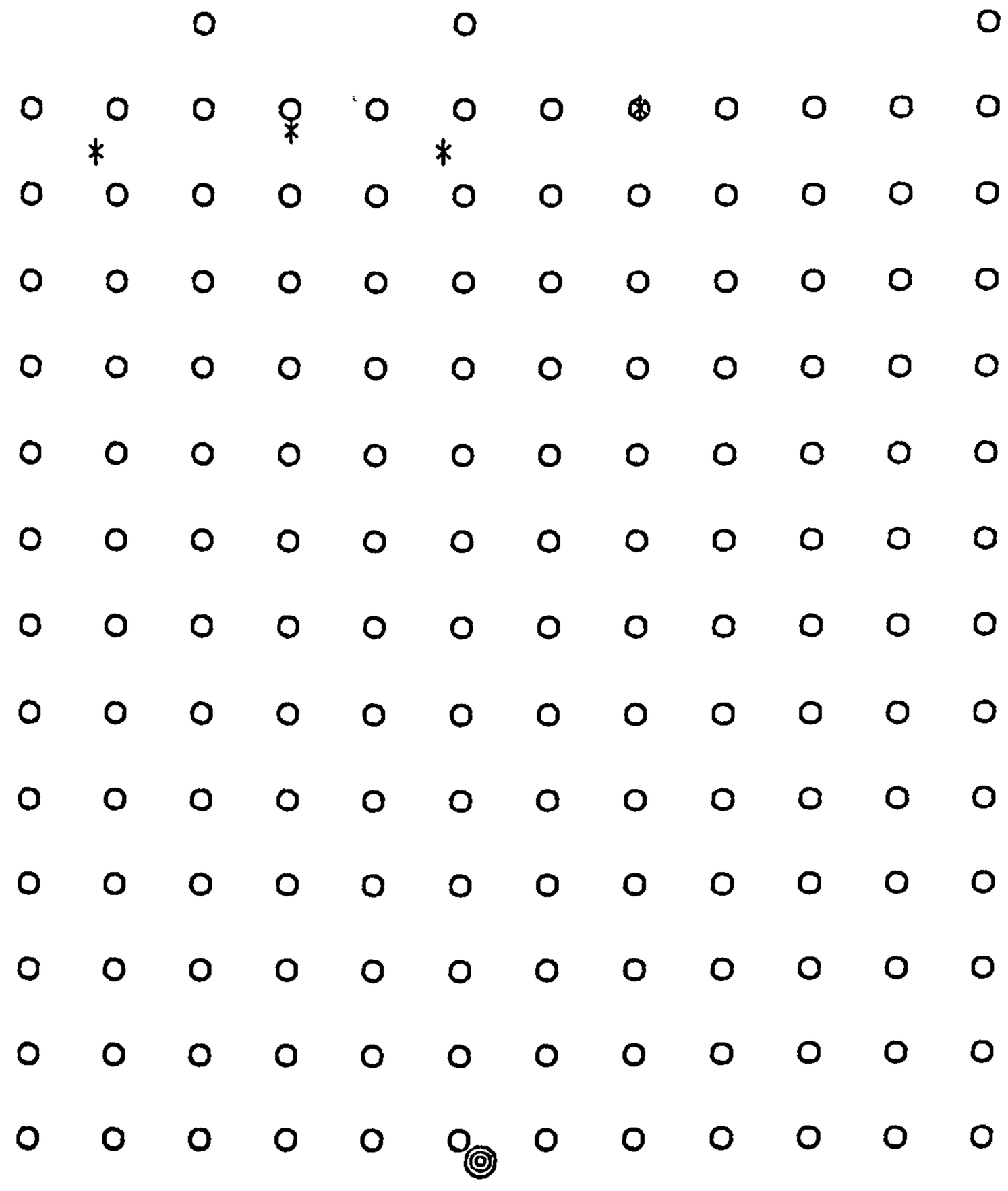

Figure D.8
Measurement C-12 Array Density 400 Rod Diameter 12mm.

◎ Air jet sound source

* Microphone.

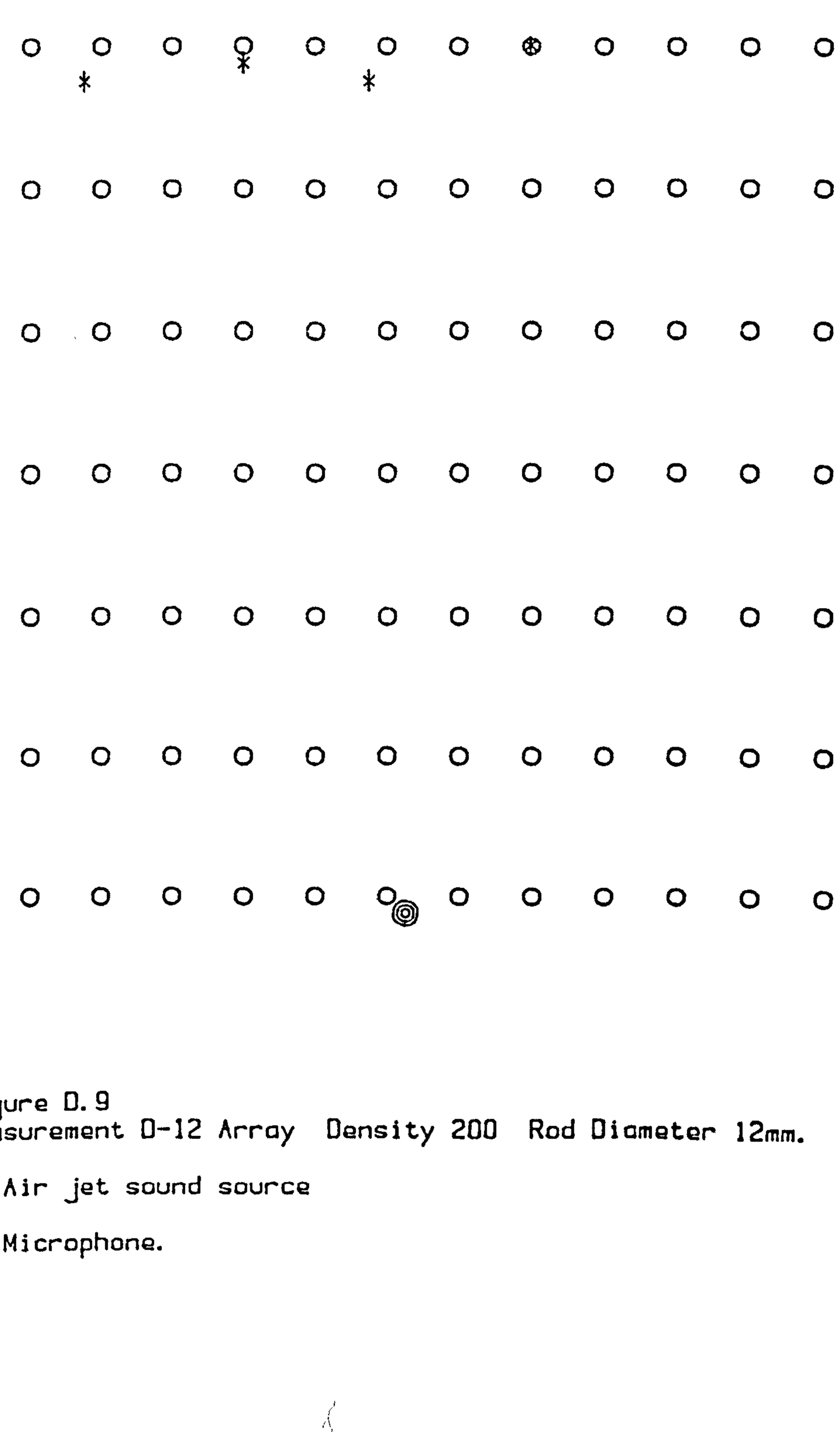

Figure D.9
Measurement D-12 Array Density 200 Rod Diameter 12mm.

◎ Air jet sound source

* Microphone.

Figure D.10
Measurement E-12 Array Density 100 Rod Diameter 12mm.

◎ Air jet sound source

* Microphone.

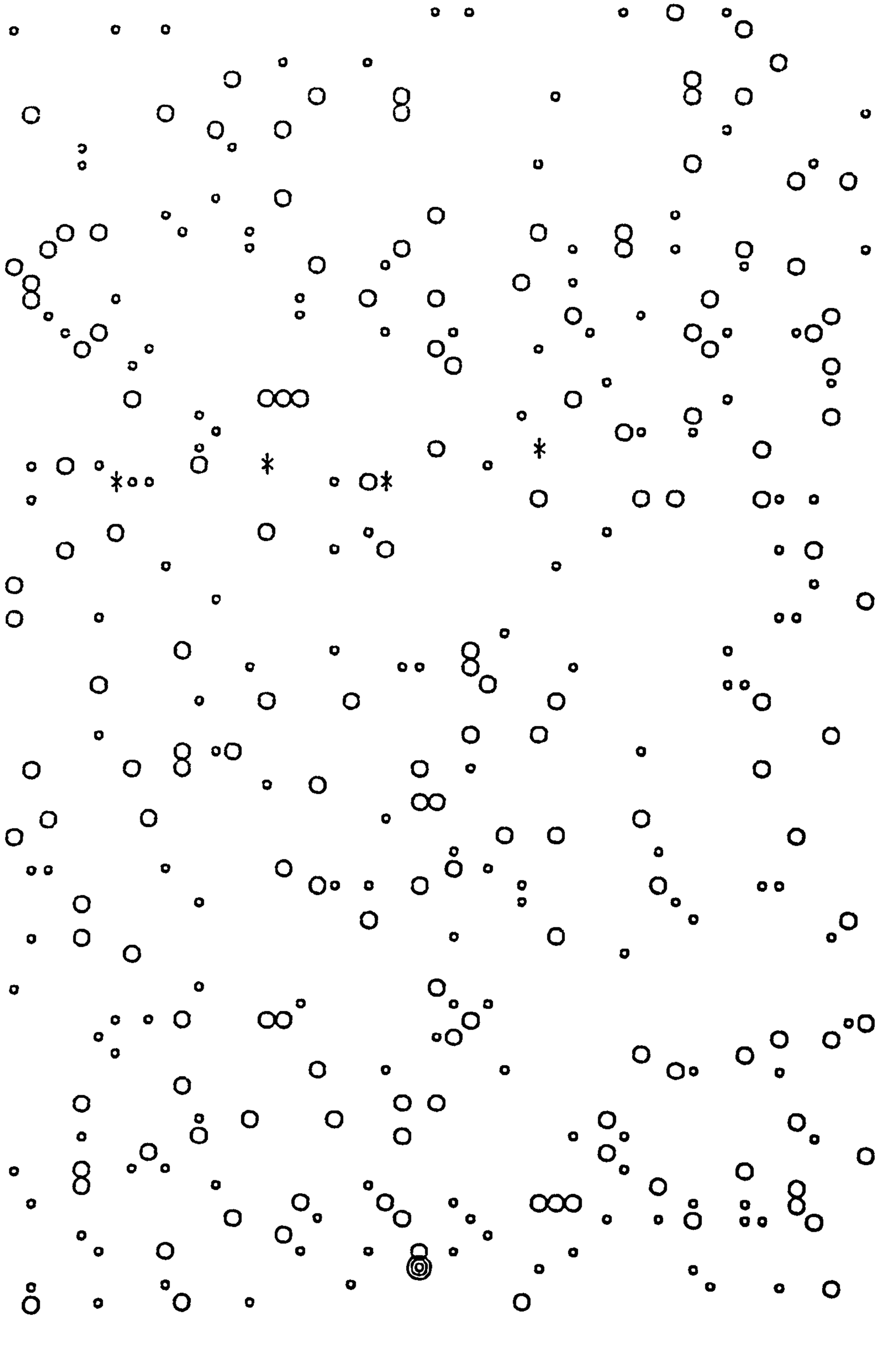

Figure D.11
Measurement F. Total Array Density 480 Diameter 6mm/12mm.

◎ Air jet sound source

* Microphone.

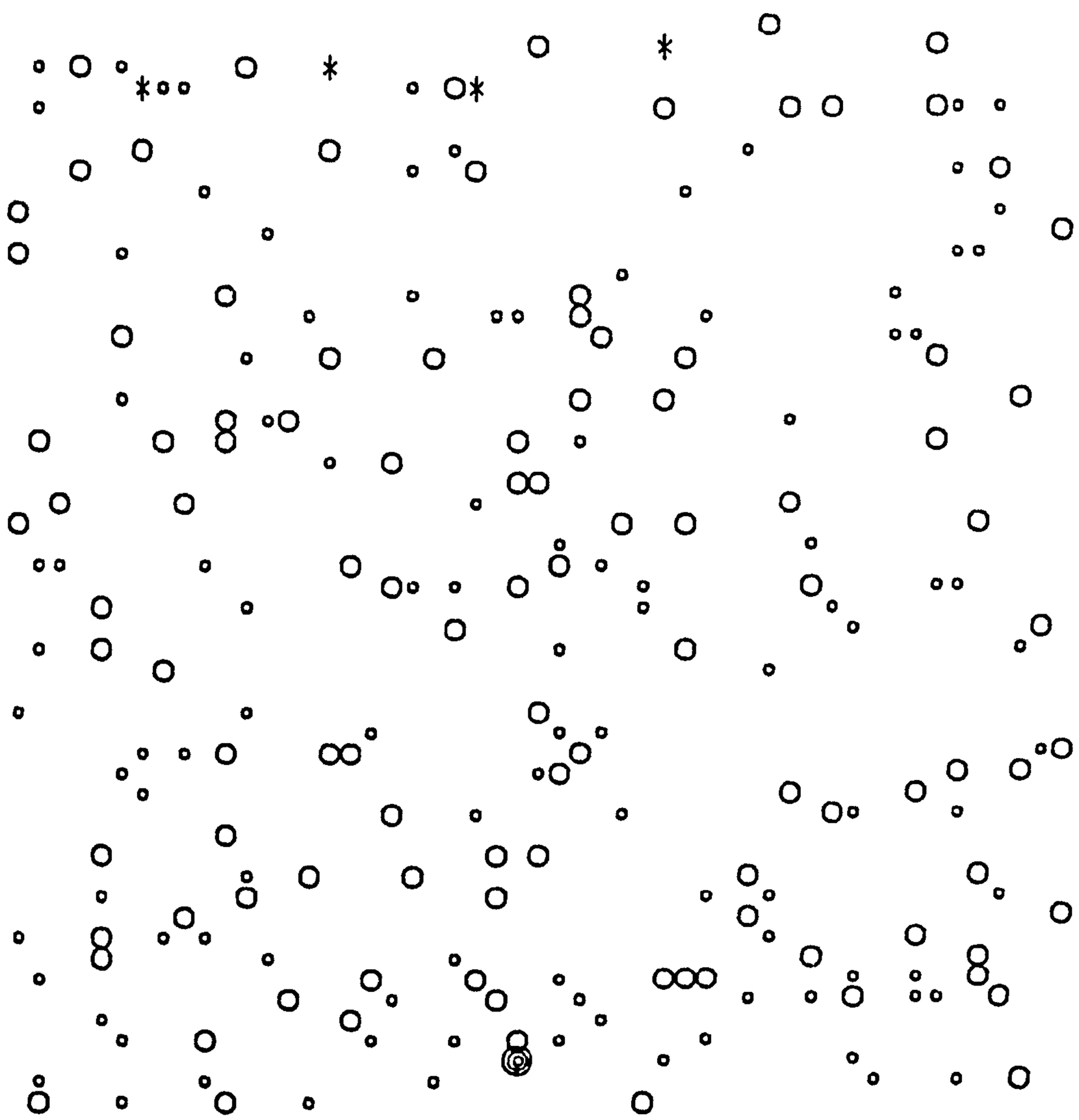

Figure D.12 Measurement F, with part of array behind microphones removed. Array Density 480 Diameter 6mm/12mm.

◎ Air jet sound source

* Microphone.

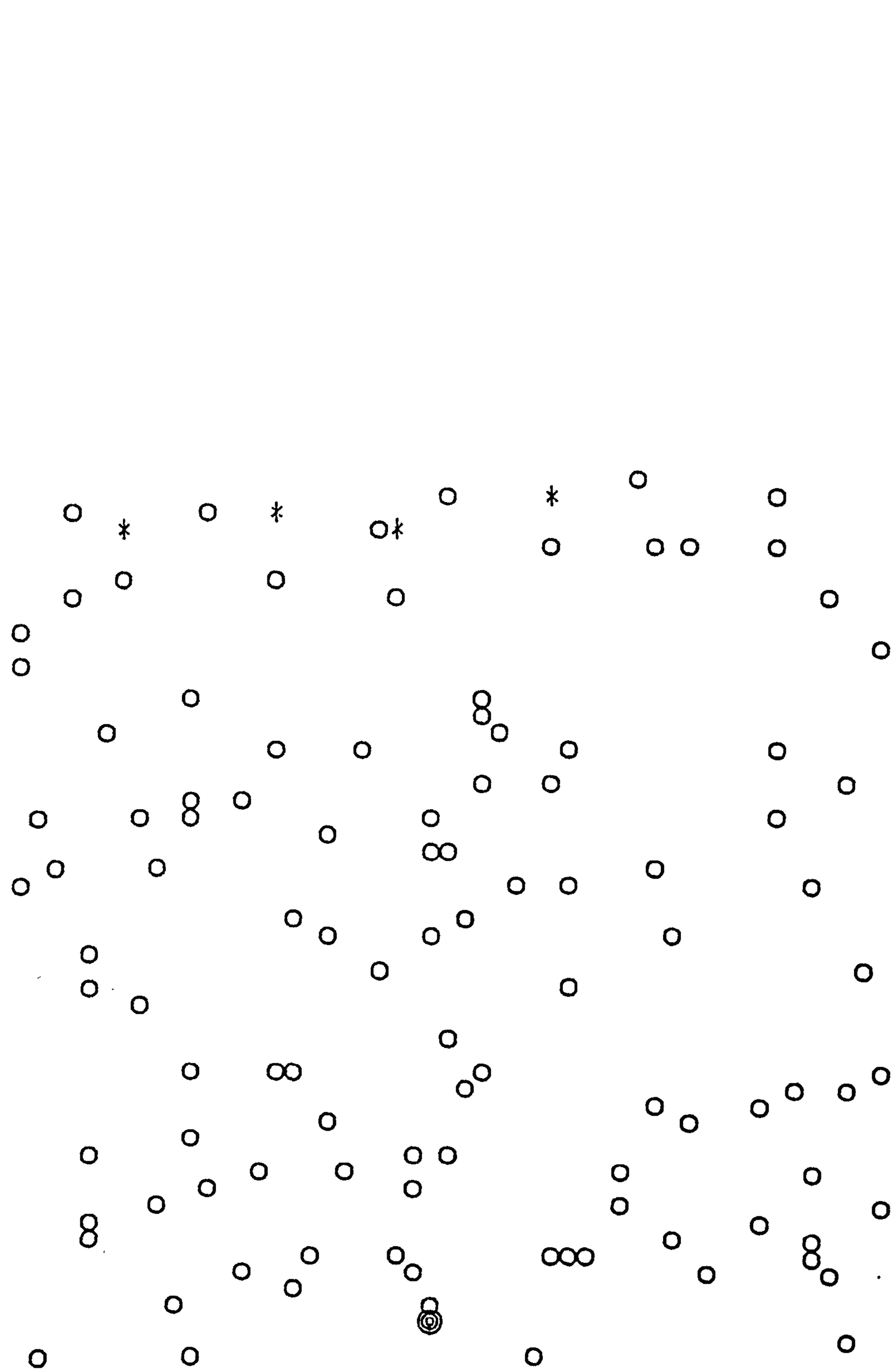

Figure D.13 Measurement A-12, with part of array behind microphones removed. Array Density 240 Diameter 12mm.

◎ Air jet sound source

* Microphone.

Figure D.14
6 row narrow belt of array C-12 rows 1-6

◎ Air jet sound source

* Microphone.

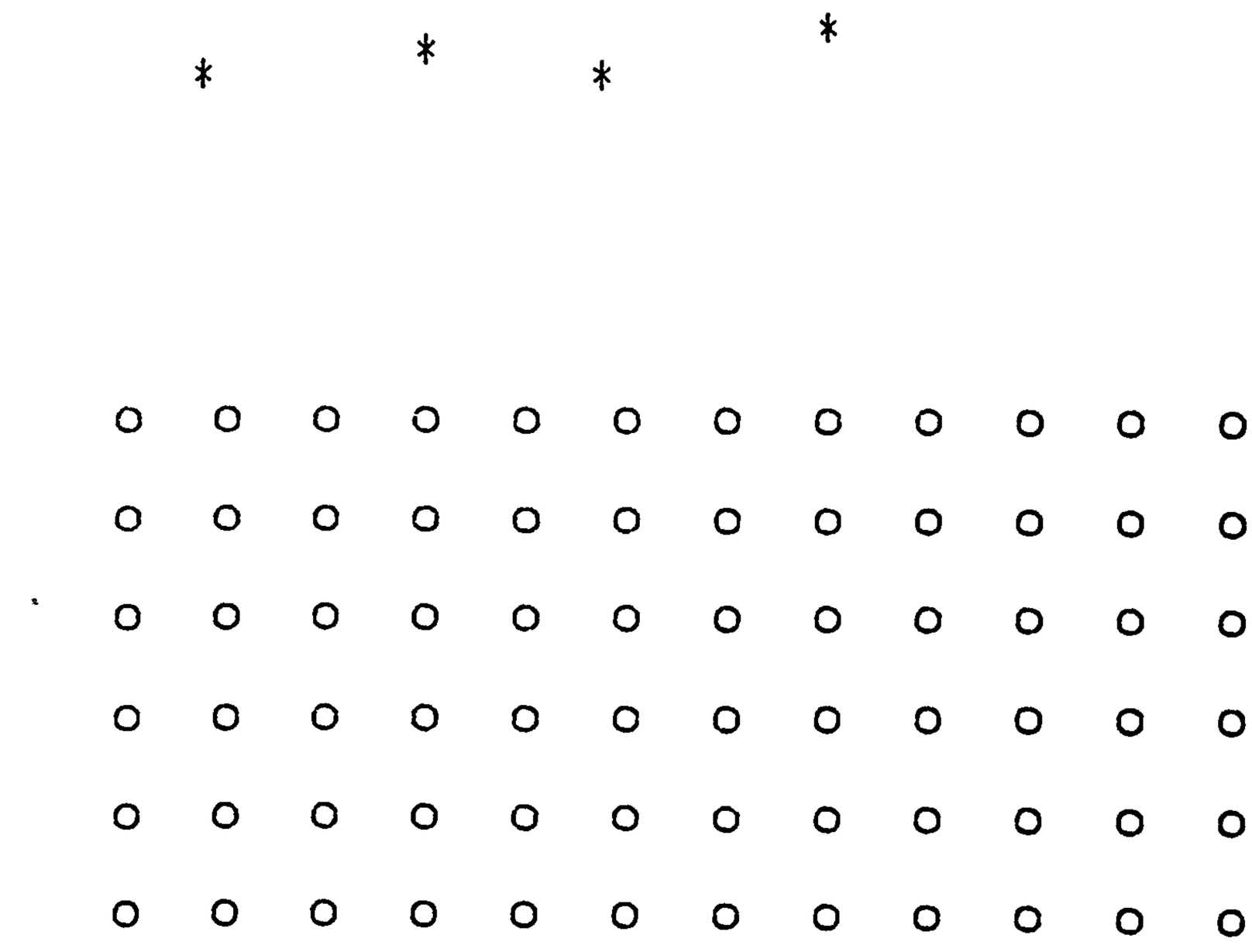

Figure D.15
6 row narrow belt of array C-12 rows 4-9

◎ Air jet sound source

* Microphone.

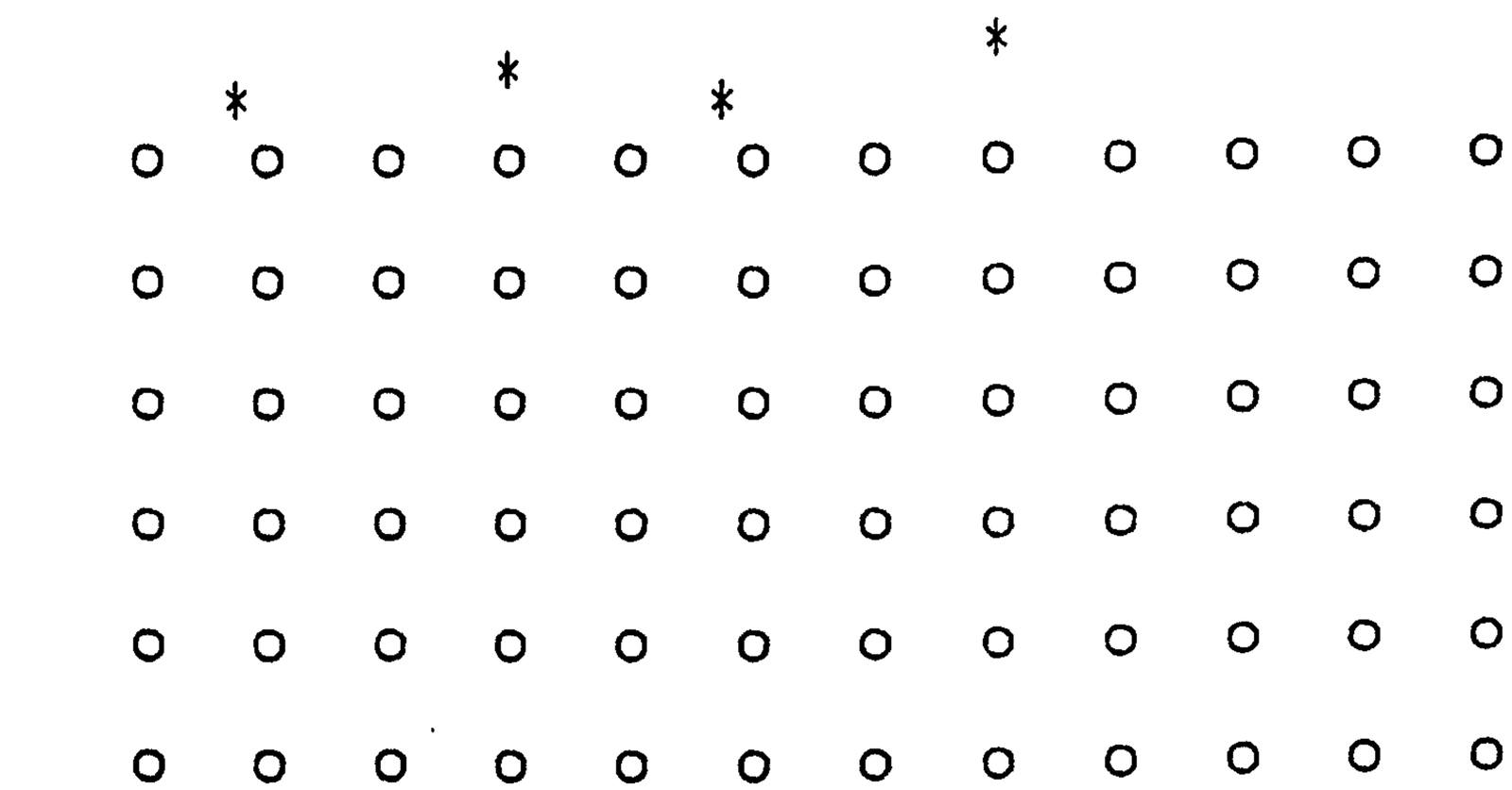

Figure D.16
6 row narrow belt of array C-12 rows 7-12

◎ Air jet sound source

* Microphone.

Figure D.17
4 row narrow belt of array C-12; rows 1-4

◎ Air jet sound source

* Microphone.

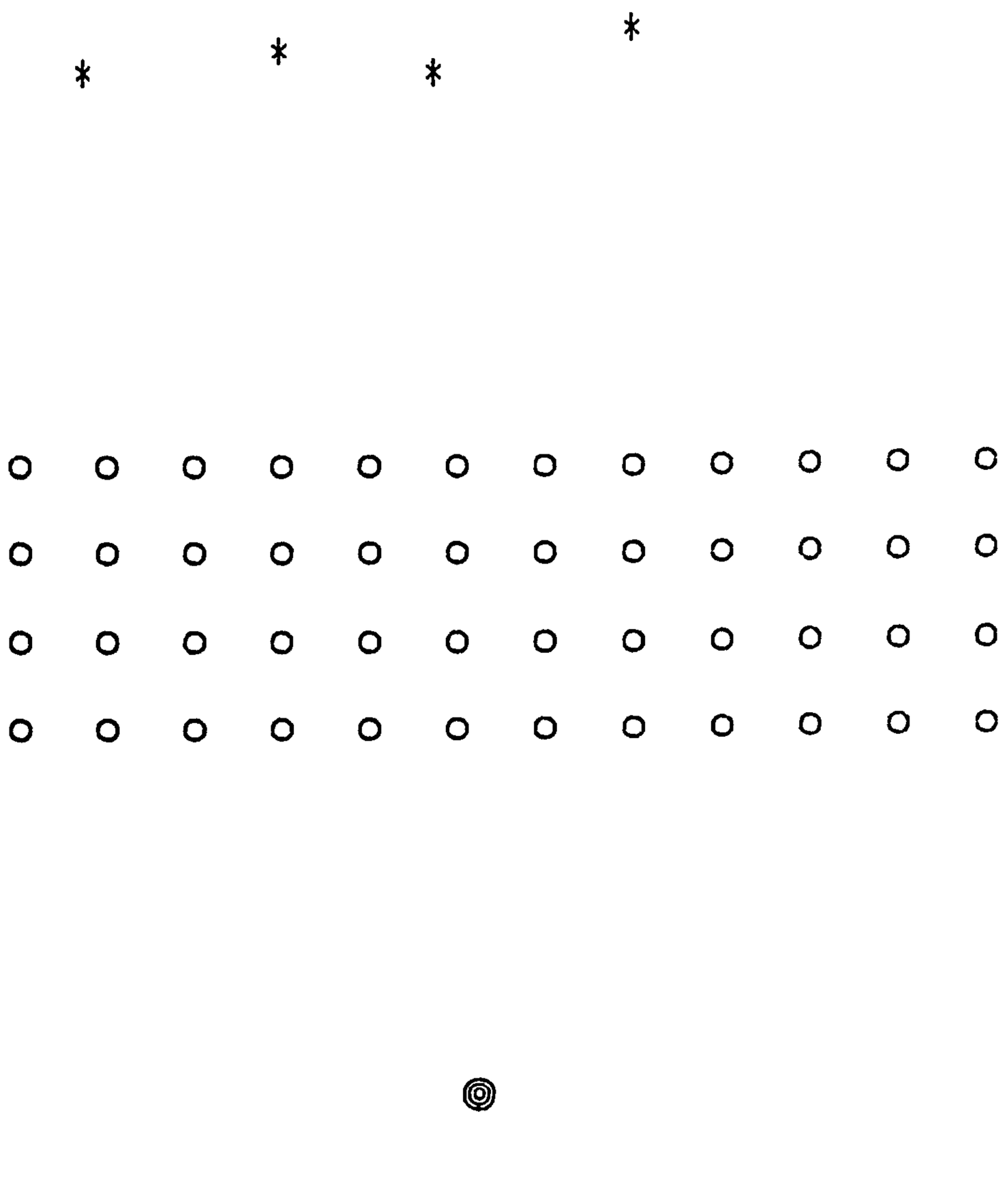

Figure D.18
4 row narrow belt of array C-12 rows 5-8

◎ Air jet sound source

* Microphone.

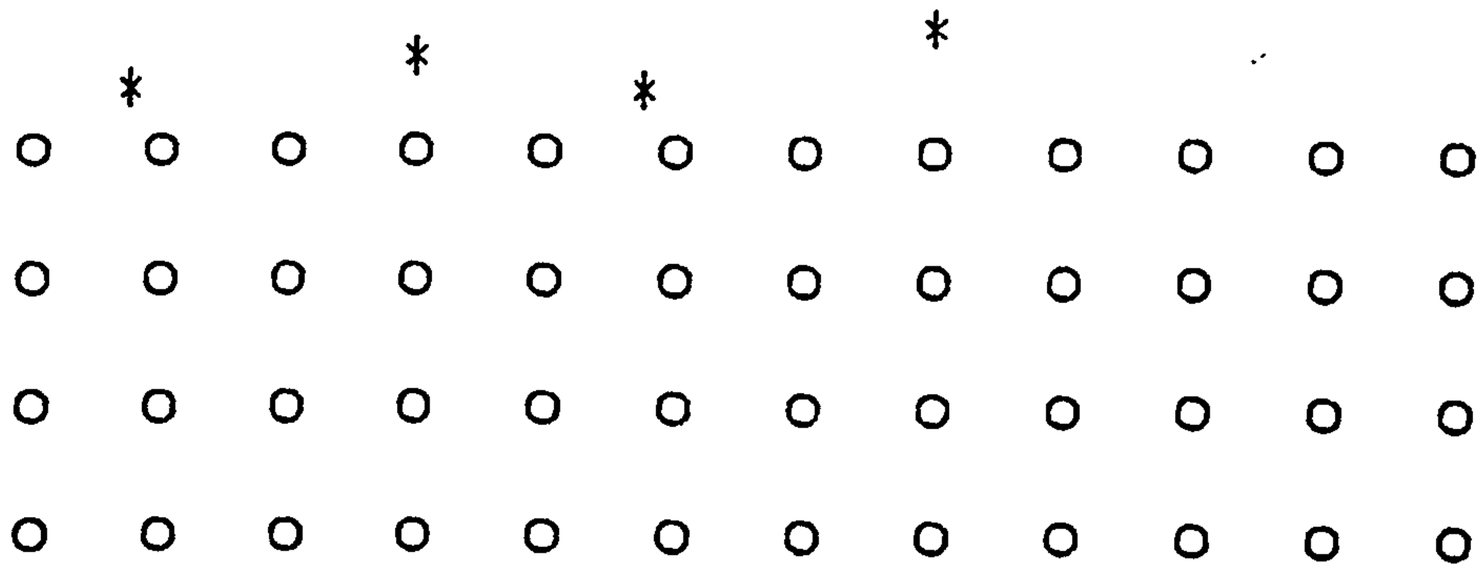

Figure D.19
4 row narrow belt of array C-12 rows 9-12

◎ Air jet sound source

* Microphone.

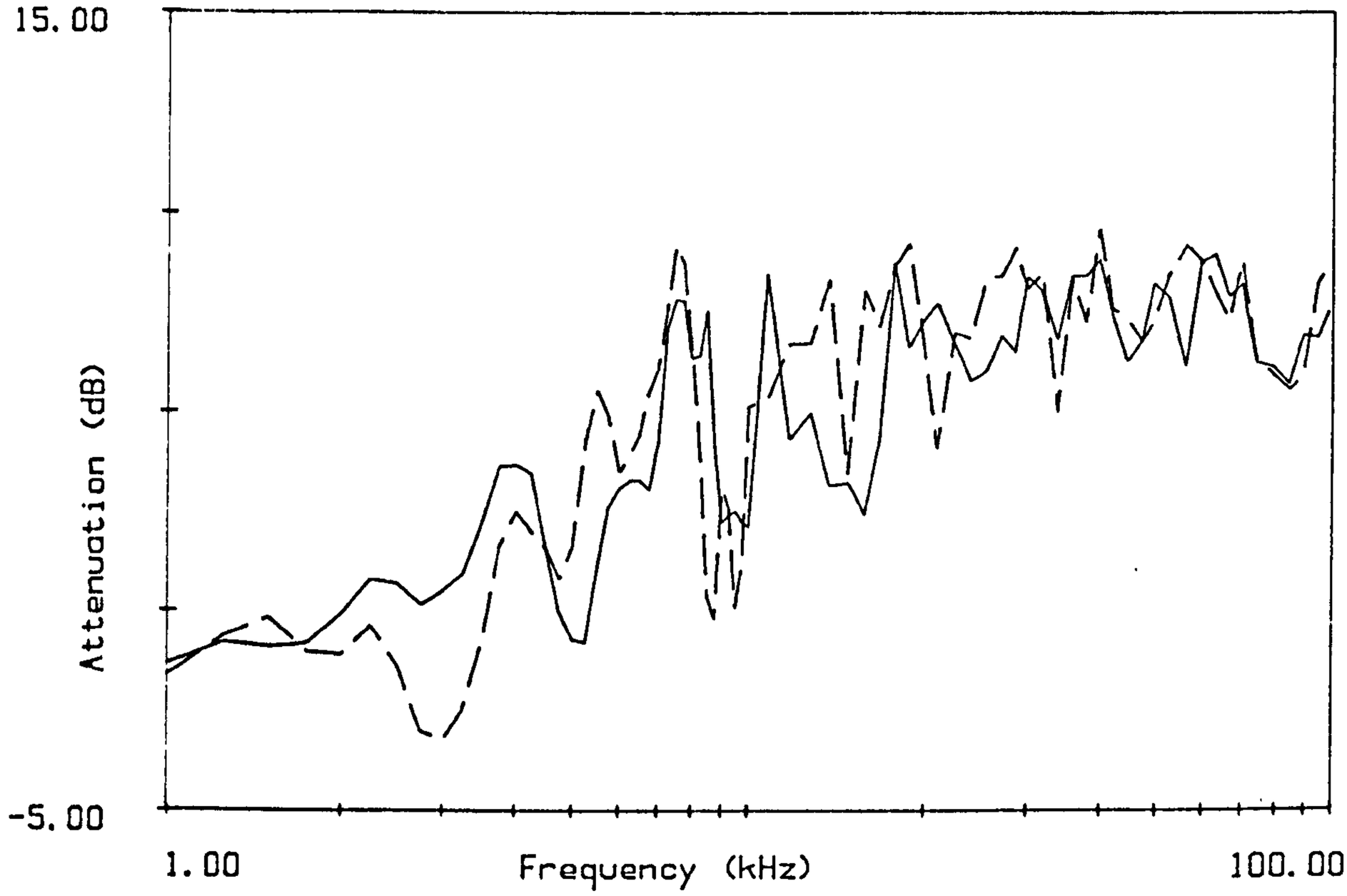

Figure D.20 microphone 1
Attenuation through array B-12 with the rods displaced slightly between measurements (array density 360).

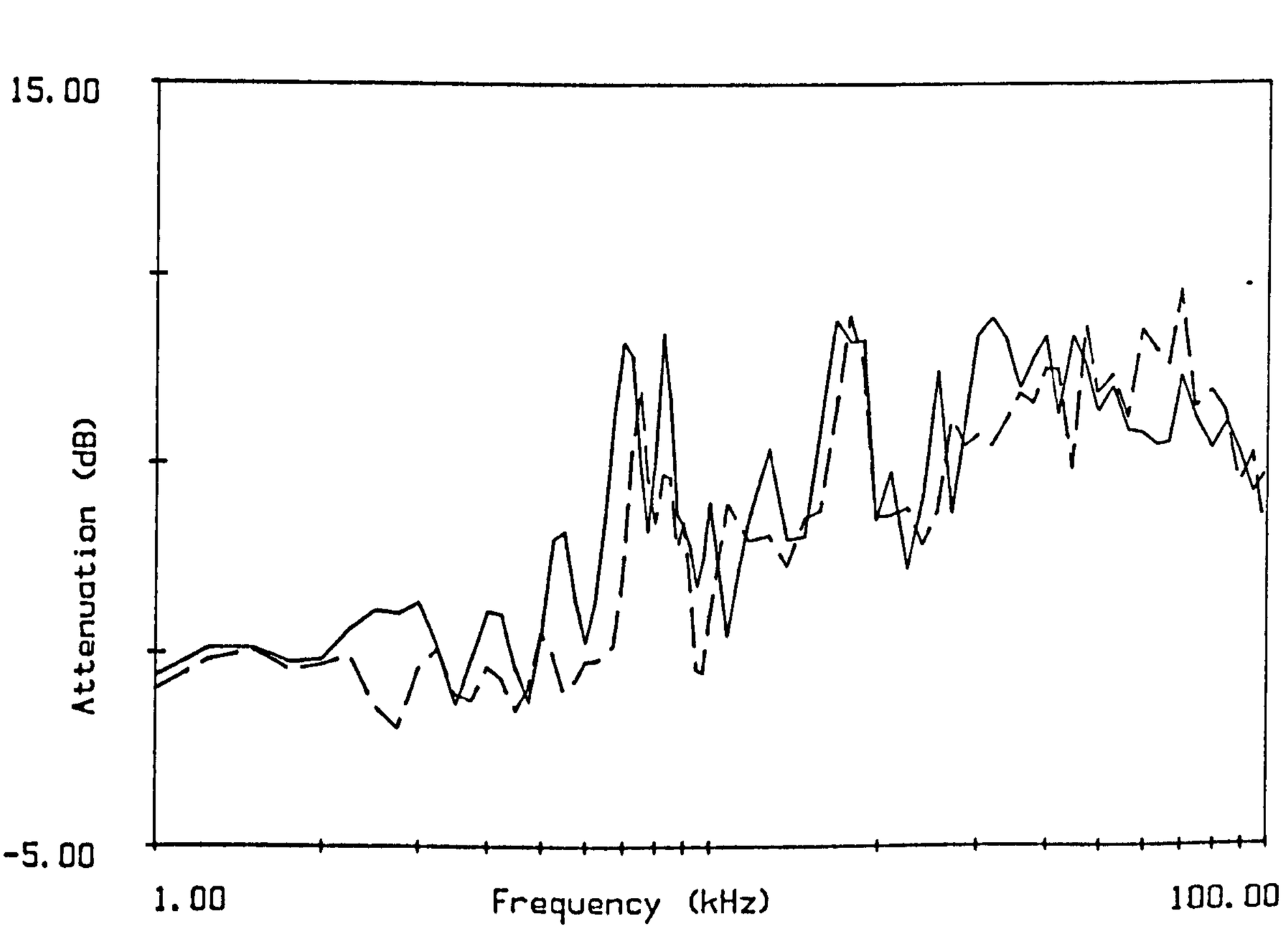

Figure D.21 microphone 2
Attenuation through array B-12 with the rods displaced slightly between measurements (array density 360)

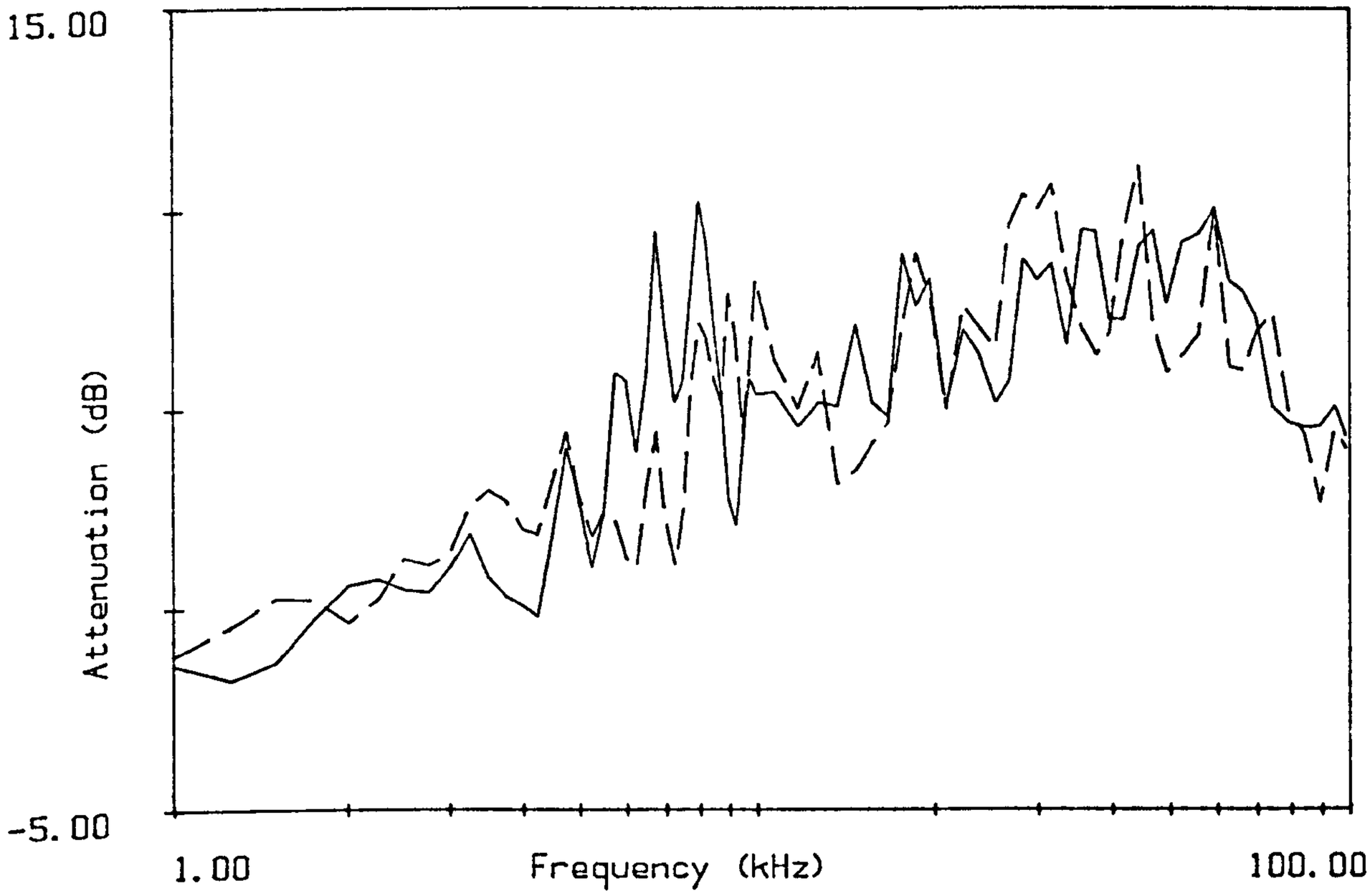

Figure D.22 microphone 3
Attenuation through array B-12 with the rods displaced slightly between measurements (array density 360)

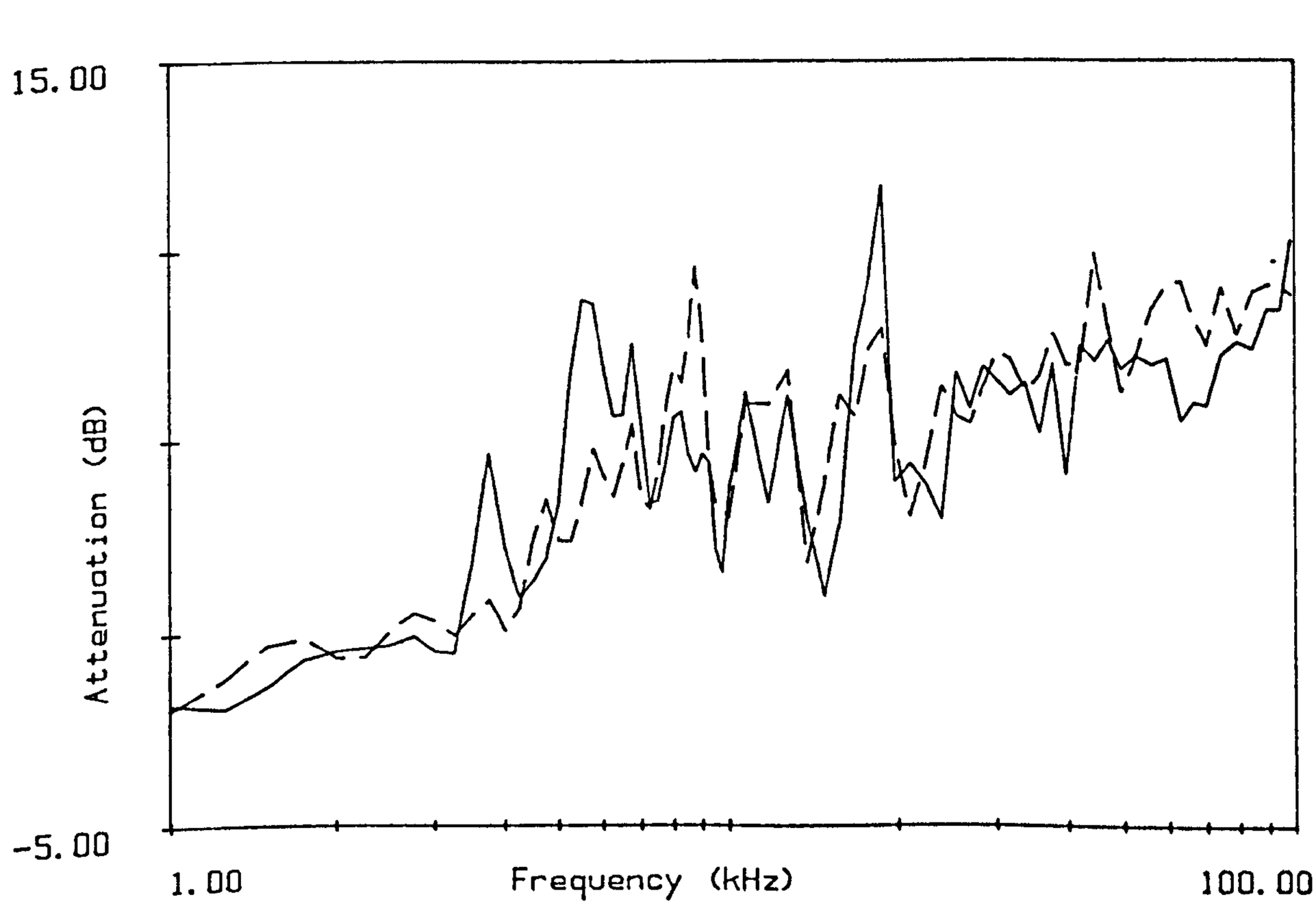

Figure D.23 microphone 4
Attenuation through array B-12 with the rods displaced slightly between measurements (array density 360)

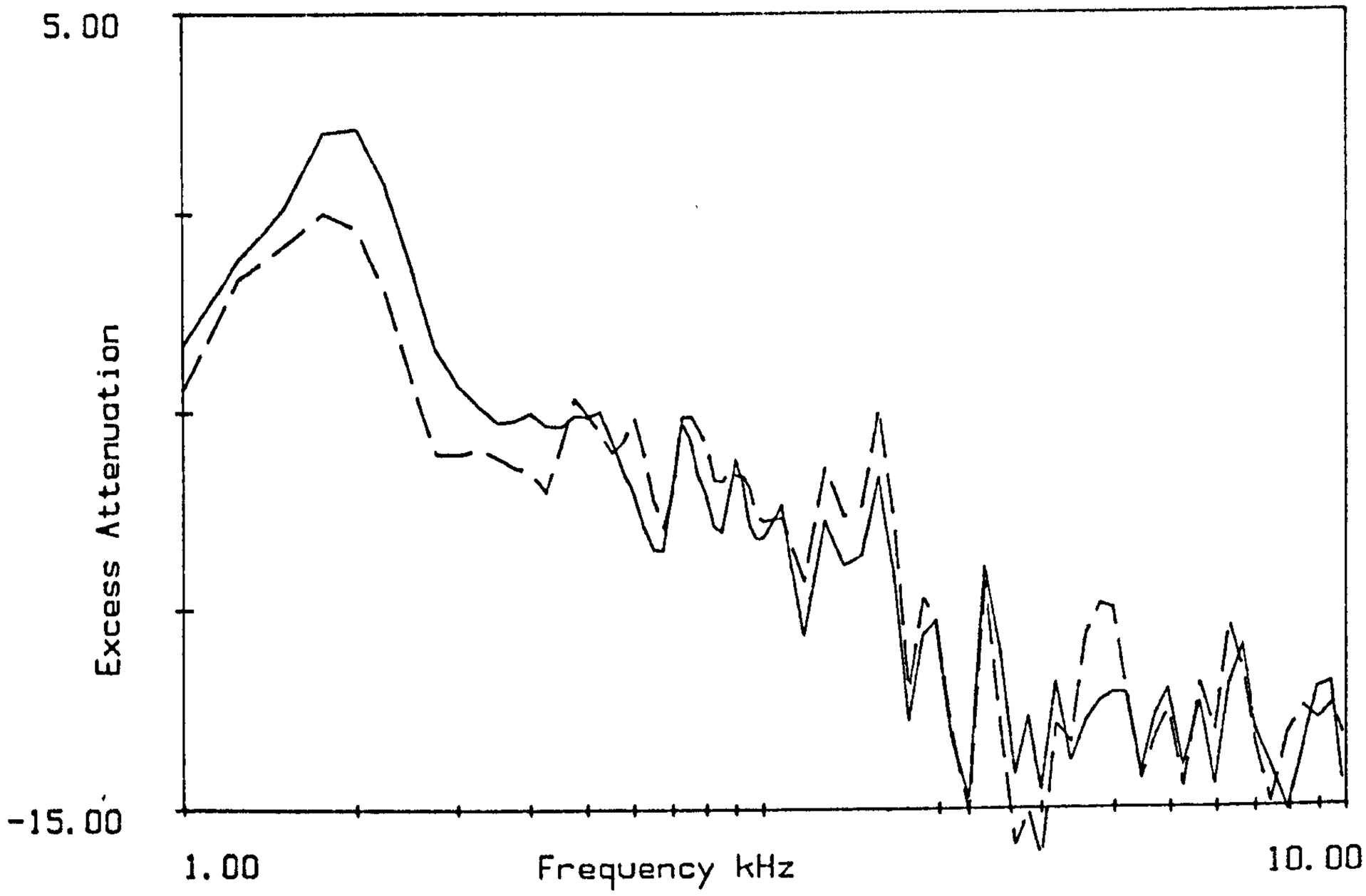

Figure D.24 microphone 1
Measured Excess Attenuation over Sand.
— — · with the holes left by the rods.
——— with the surface flattened

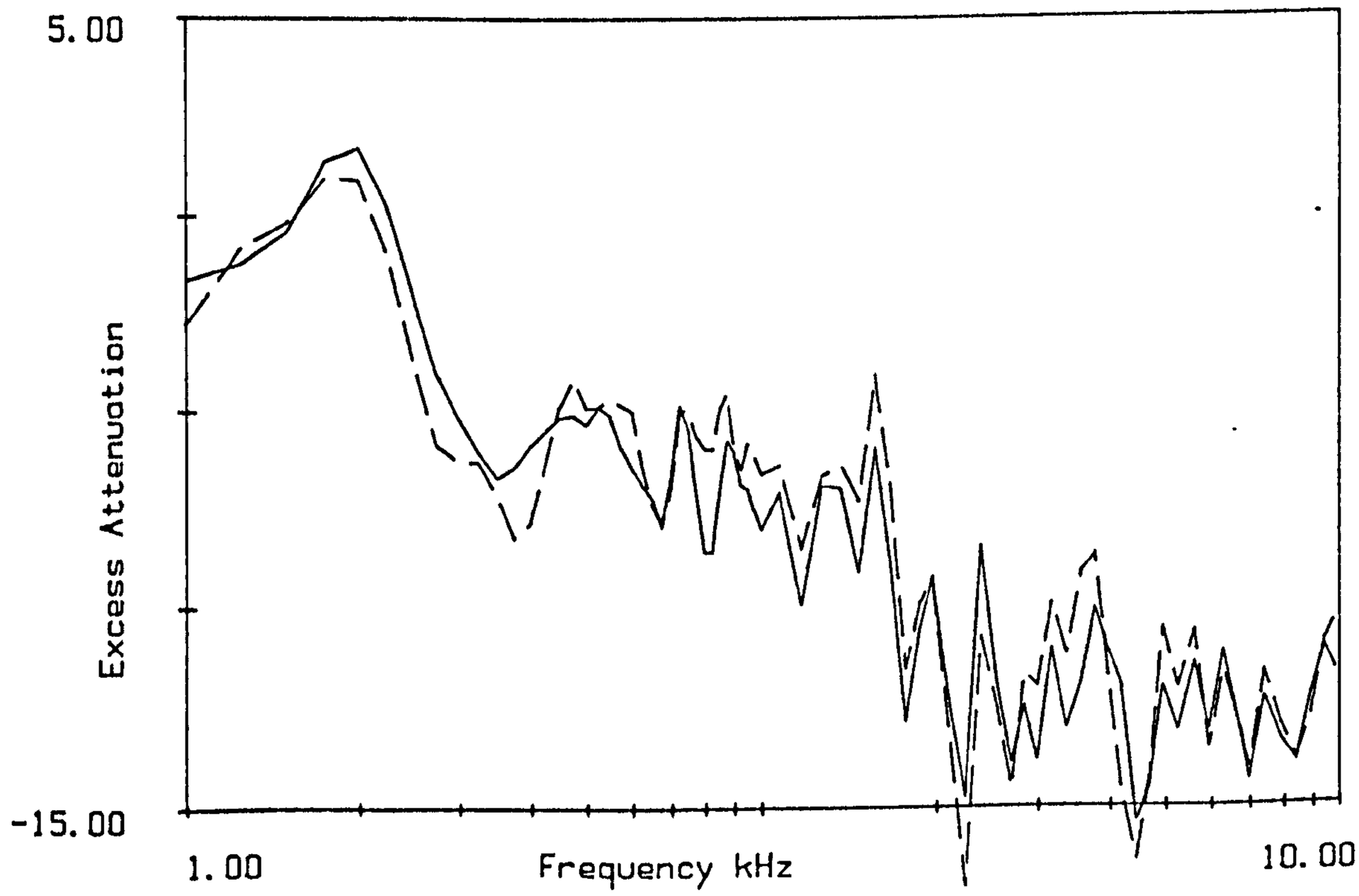

Figure D.25 microphone 2
Measured Excess Attenuation over Sand.
— — · with the holes left by the rods.
——— with the surface flattened

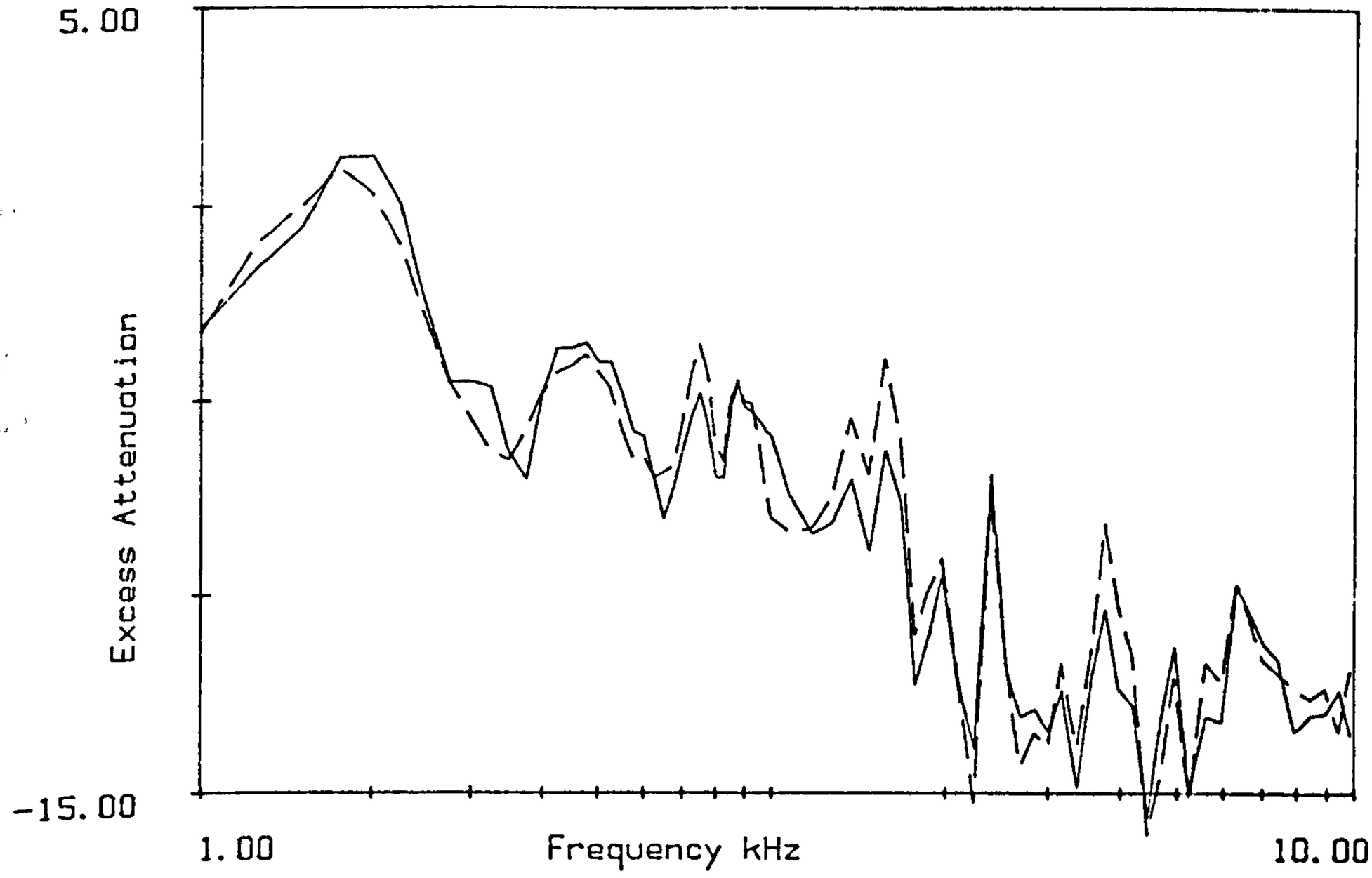

Figure D.26 microphone 3
Measured Excess Attenuation over Sand.
— — · with the holes left by the rods.
——— with the surface flattened

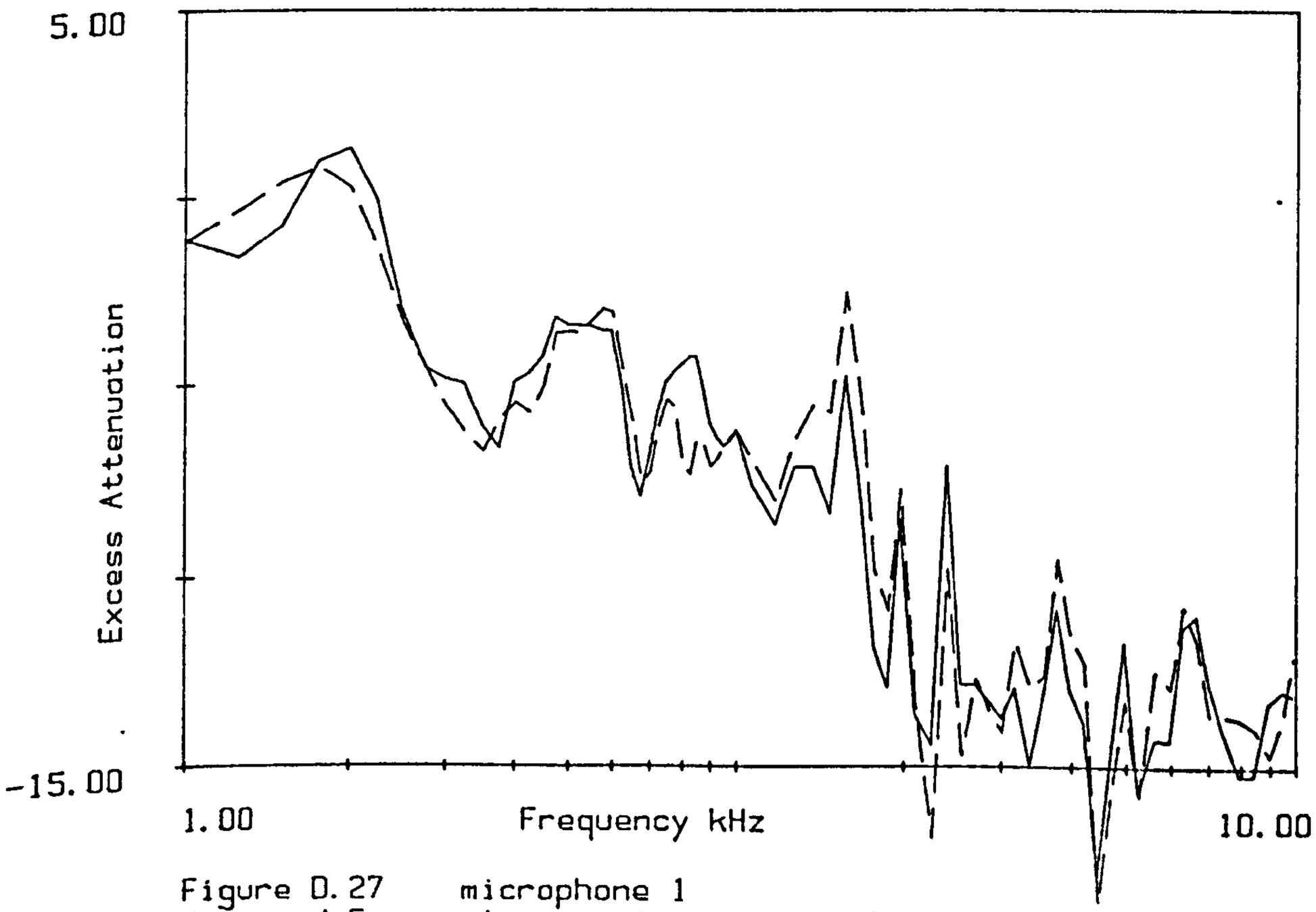

Figure D.27 microphone 1
Measured Excess Attenuation over Sand.
— — · with the holes left by the rods.
——— with the surface flattened

Appendix E: Papers presented at Meetings.

E1: "The Use of Trees for Noise Control." Presented at Internoise 85 Munich, September 1985.

E2: "Sound Propagation Results from Three British Woodlands." Presented at a workshop on "Sound Propagation in Forests and Shelterbelts." Nijmegen, Netherlands, March 1986.

THE USE OF TREES FOR NOISE CONTROL

M.A. Price, N.W. Heap and K. Attenborough
Department of Engineering Mechanics, Faculty of Technology
The Open University, Walton Hall, Milton Keynes, England

INTRODUCTION

The use of a belt of woodland as a barrier to screen a problematic noise source such as road traffic, is an attractive proposition from an aesthetic and ecological point of view, but the actual acoustical effectiveness has long been a matter of debate. A related problem is that of noise propagation prediction where there is an existing wooded area.

Measurements were made at various woodland sites in Buckinghamshire, England to investigate the vegetation characteristics important in the prediction of noise propagation. The results of some of these measurements are presented here.

EXPERIMENTAL METHOD

The sound source used was an audio system emitting broad-band pseudorandom noise. the source was monitored by a reference microphone at a distance of 2 metres. Recordings were made at various distances (12 to 96 m) from the source, at 1.2 m and 2.5 m above the ground. The recordings were analysed by means of a digital spectrum analyser to give a spectrum of level vs frequency for each microphone position.

The result can be expressed as a level difference function corrected for free field attenuation as shown in Figures 1 and 2. The attenuation due to spherical spreading and atmospheric absorption are subtracted from the difference in level between the reference and test microphones. The corrected level difference is a measure of the effectiveness of the woodland, or any other terrain, in attenuating noise; a higher value indicating greater attenuation.

The temperature and relative humidity were measured and used to calculate the atmospheric absorption correction. Measurements were restricted to calm conditions ie windspeeds of less than 2 ms^{-1} (measured at 2.5 m above the ground).

The results presented here are from three forestry stands:

1) Monoculture of Norway spruce (Picea abies), 30 years old, full canopy dead lower branches, no ground vegetation, litter layer of needles.

2) Mixed Norway spruce/oak with a dense deciduous understorey of hawthorn (Crataegus monogyna), 38 years old, litter layer of oak and hawthorn leaves and spruce needles.

3) Mixed coniferous stand of alternate rows of red cedar (Thuja plicata) Norway spruce, and Scots pine (Pinus sylvestris) 15 years old, incomplete canopy, foliage along whole length of trunk. Ground vegetation mainly of long grass.

RESULTS

Figure 1 shows the corrected level difference for a measurement in stand 2 (Mixed oak/spruce) compared with that for a measurement over a grass sports field, using the same geometry. The woodland data shows the typical pattern of level difference found in these measurements. The function peaks at low frequencies and increases with increasing frequency, after a mid frequency dip. The sport field data also has a low frequency peak but it occurs at a higher frequency than in the woodland. The high frequency values are considerably less for the sports field than the woodland.

GROUND EFFECT

It is widely accepted that the low frequency peak in these types of curves is due to the 'ground effect' (the interference between the direct and ground reflected wave) which is highly dependent on the properties of the ground surface.

The data presented in Figures 1 and 2, and other measurements, have been fitted to predictions of corrected level difference based on the widely used Weyl-van der Pol formulation for point source propagation over a finite impedance boundary [1]. Two ground impedance models were used; a) the Delaney and Bazley model in which impedance is characterised by flow resitivity (σ)[2]. And b) the variable porosity model presented by Attenborough [3], characterised by effective flow resistivity (σe) and a factor describing the porosity gradient in the soil (αe). ($\alpha e = 0$ for homogenous ground). The model parameters which gave a prediction closest to the measured spectra in the frequency range 100 Hz-1 kHz (least mean-squared-difference test), were calculated for the level difference measured at several source-receiver geometries. The mean values are presented in table 1.

Table 1 Best fit parameters for different ground surfaces.

Terrain	Delaney and Bazley	Variable Porosity	
	σ (mks rayls)	σe (mks rayls)	αe
Spruce Monoculture	52700	77100	0
Mixed oak/spruce	23800	39500	0
Mixed coniferous	45500	73500	0
Sports field	384700	435700	238

These results show that all three woodland types have significantly lower effective flow resistivities than the sports field, ie acoustically 'softer' ground surfaces. Thus the ground effect peak is at a lower frequency. The stand with the thick layer of deciduous leaves (stand 2 - oak/spruce) has a lower flow resistivity than either of the pure coniferous stands which have a thinner litter layer composed solely of needles (stand 1) or a dense covering of long grass (stand 3).

SCATTERING

Embleton [4] presents a theory for the prediction of attenuation due to scattering of sound by an array of vertical cylinders of infinite length (given their radius, surface impedance and the density of the array). As an attempt to predict the level difference due to the combination of the ground effect and scattering by tree trunks, predictions from the two models were added together. The result of one such addition is shown in Figure 2, compared with measured data from the spruce monoculture and the prediciton from the Weyl-van der Pol formulation. The ground parameters used are the best fit values (100 Hz to 1kHz range only) for this measurement, and the scattering parameters were estimated from a small sample area within the stand.

The simple addition of the two models does not predict the overall pattern of the measured level difference, but does predict significantly more attenuation at high frequencies than the ground effect alone. It is evident that a more complex situation exists than that described by simple addition perhaps involving some interaction between the ground and scattering effects. In particular, the extent to which the ground interference patterns are perturbed by the presence of scatterers and micrometeorological effects is unknown. The fact that the high frequency attenuation is greater in the measurement than the prediction suggests that the foliage and branches may also attenuate some sound.

CONCLUDING REMARKS

The effectiveness of a tree stand in reducing noise levels is highly dependent on the spectrum of the noise with high and low frequencies attenuated more than mid-frequencies. In the mid-frequencies the reduction may be less with woodland than with the grass sports field. The low frequency peak depends on the woodland type, as demonstrated above, and differences between stands were also observed in the high frequency range.

REFERENCES

[1] K. Attenborough, S.I. Hayek and J.M. Lawther 1980. J Acoust Soc Am 68 (5) 1493-1501 Propagation of Sound Above a Porous Half-space.

[2] M.E. Delaney and E.N. Bazley 1970. Appl Acoust 3 105. Acoustical properties of Fibrous Materials.

[3] K. Attenborough, J Sound Vib (in press; Acoustical Impedance Models for Outdoor Ground Surfaces.

[4] T.F.W. Embleton 1966. J Acoust Soc Am 40 (3) 667-670, Scattering by an Array of Cylinders as a Function of Surface Impedance.

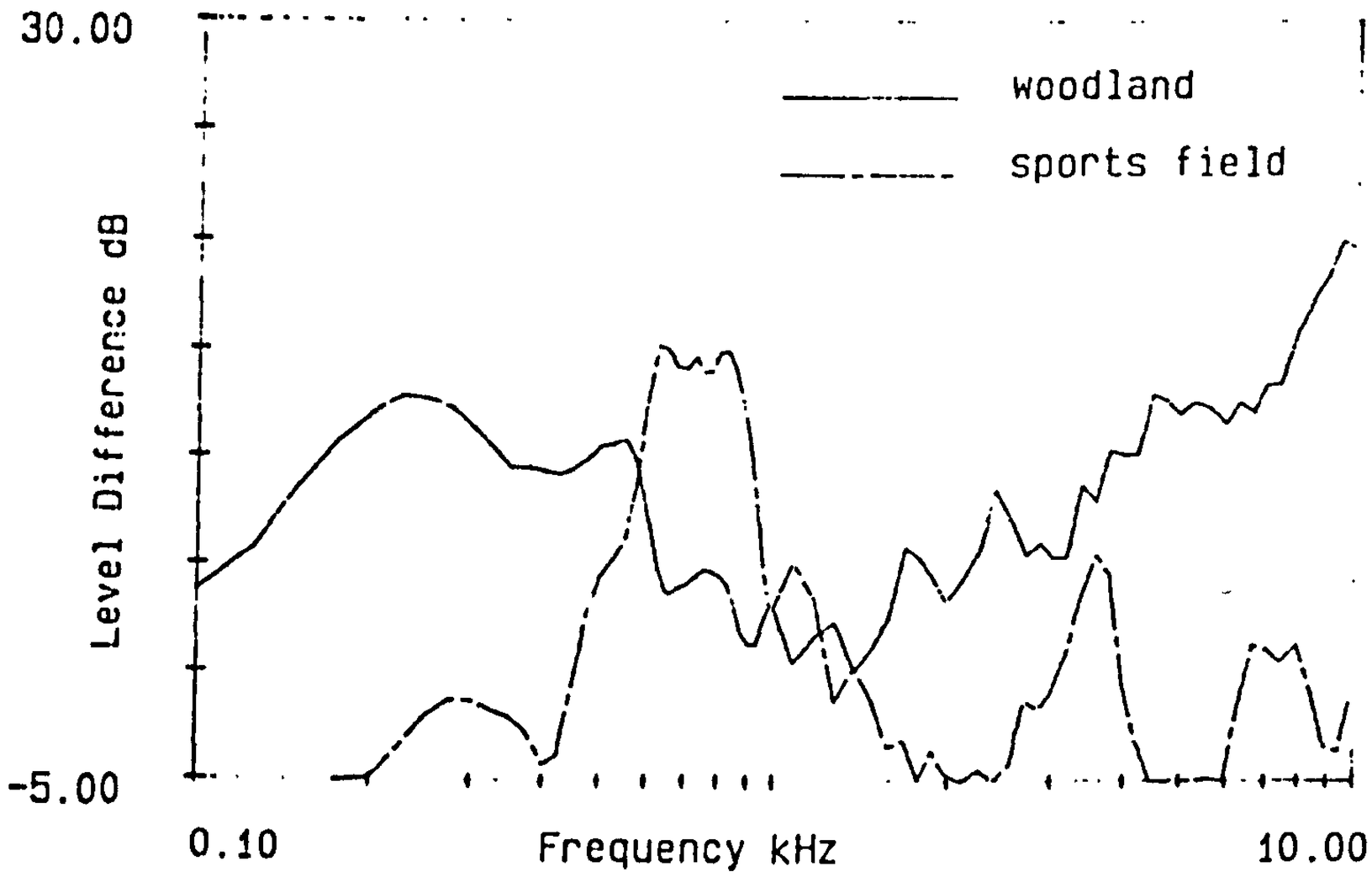

FIGURE 1

Corrected level difference at 48m separation, microphone height 1.2m.

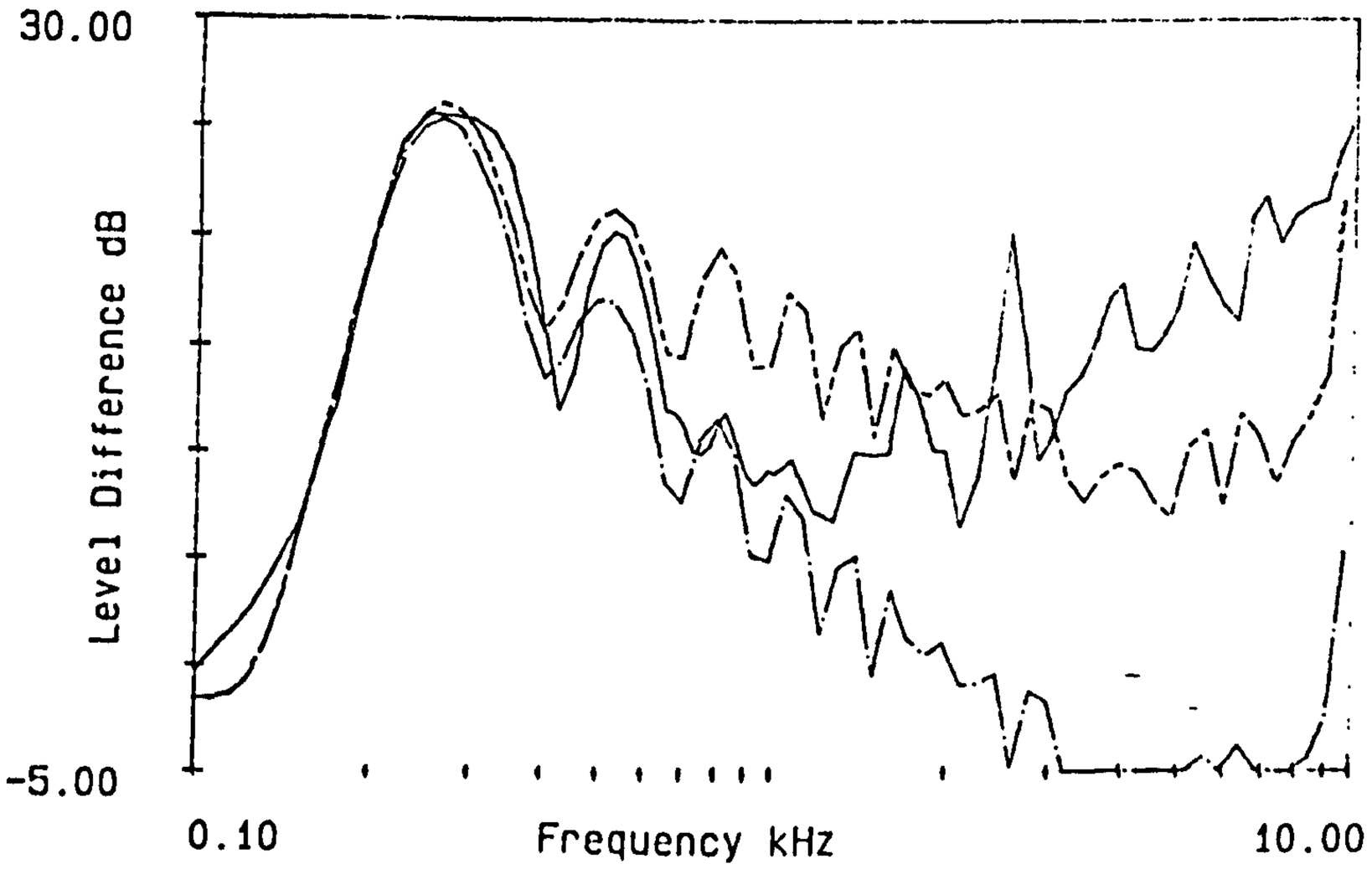

FIGURE 2

Comparisons of corrected level difference, 96m separation 1.2m microphone height.
——·—— measured (spruce monoculture)
——·— ground effect: - σ e = 67000, α e = 0
——·-·— sum of ground effect and scattering

SOUND PROPAGATION RESULTS FROM THREE BRITISH WOODLANDS.

M.A.Price, K.Attenborough and N.Heap.

Department of Engineering Mechanics,
Faculty of Technology,
The Open University,
Milton Keynes MK7 6AA,
England.

Introduction

Sound propagation measurements were made in three woodlands in order to compare the effects of different types of woodland, and assess the use of theoretical models to predict sound propagation. Small scale model experiments were also carried out to investigate the scattering of sound by an array of cylinders.

The woodlands investigated were all forestry stands planted on relatively flat land in southern Northamptonshire, England. The important characteristics of the stands are:

[1] Monoculture of Norway spruce (Picea abies), 30 years old, full canopy, dead lower branches, no ground vegetation, litter layer of needles. Mean radius 0.059m, stem density $0.303m^{-2}$.

[2] Mixed Norway spruce and oak, with a dense deciduous understorey of hawthorn (Crataegus monogyna), 38 years old, litter layer of oak and hawthorn leaves and spruce needles. Mean radius 0.045m, stem density $0.267m^{-2}$.

[3] Mixed coniferous stand of alternate rows of red cedar (Thuja plicata), Norway spruce, and Corsican pine (Pinus nigra) 15 years old, incomplete canopy, foliage along the whole length of the trunk. Ground vegetation mainly of long grass. Mean radius 0.066m, stem density $0.181m^{-2}$

The mean radii and densities were calculated in small sample areas within the experimental plots and used in the calculations of attenuation due to scattering described below.

Experimental Method

The sound source used was an audio system emitting broad-band pseudorandom noise. The source was monitored by a reference microphone at a distance of 2 metres. Recordings were made at various distances (12m to 96m) from the source, at 1.2m and 2.5m above the ground. The recordings were analysed by means of a digital spectrum analyser to give a spectrum of level vs frequency for each microphone position.

The results are expressed as 'attenuation' calculated by subtracting the attenuation due to spherical spreading and atmospheric absorption from the difference in level between the reference and test microphones. The temperature and relative humidity were measured and used to calculate the atmospheric absorption according to the formulae described by Bazley (1976). Measurements were restricted to calm conditions ie windspeeds of less than $2ms^{-1}$ (measured at 2.5m above the ground).

Ground Effect

The so-called ground effect has been discussed elsewhere in the workshop. eg by Dr T. Embleton Dr K. Attenborough and Ms H. Hess. In this study the Weyl-van der Pol formulation was used to calculate predictions of the attenuation function resulting from the interference pattern between the ground reflected wave and direct wave, and the ground and surface waves, (as described in Attenborough et al 1980). The impedance was calculated using the following three models:

a) Delany and Bazley (1970) described a formula for the surface impedance which was derived empirically from impedance measurements of fibrous materials and has been widely used in the prediction of surface impedance of ground surfaces.

$$Z_s = 1 + 0.05(\sigma_e / f)^{0.75} + i\,0.077(\sigma_e / f)^{0.73}$$

where Z_s is the surface impedance, f is the frequency and σ_e is the effective flow resistivity.

b) Attenborough (1985) deduced approximations for the calculation of ground impedance for a ground with porosity decreasing exponentially with depth.

$$Z_s = 0.218(\sigma_e / f)^{0.5} + i\left[0.218(\sigma_e / f)^{0.5} + 9.74(\alpha_e / f)\right]$$

c) It is evident that for a homogeneous ground the value of α_e is zero and the real and imaginary parts are equal. This homogeneous model can be used in the standard formula for the surface impedance of a rigid-backed layer to give the following equation for the surface impedance.

$$Z_s = 0.218(1+i)(\sigma_e / f)^{0.5} \coth\left[-i\,5.59\times10^{-5}(1+i)(\sigma_e f)^{0.5} d_e\right]$$

the variables σ_e, α_e and d_e (the effective depth) are defined in these two models as:

$$\sigma_e = \frac{S_f^2 \sigma}{\Omega} \qquad \alpha_e = \frac{n'\alpha}{\Omega} \qquad d_e = d\,\Omega$$

where

σ = flow resistivity

α = rate of decrease of porosity

S_f = a pore shape factor

n' = a grain shape factor

Ω = air porosity

d = layer depth.

The predicted attenuation was fitted to the measured data to obtain the values of the ground parameters, which give the least mean squared difference, ie the 'best fit values'; over the frequency range 100Hz to 1kHz.

Scattering

The second mechanism investigated by means of a theoretical model is scattering of sound by the tree trunks. Embleton (1966) presents a theory describing the scattering of plane waves by a random array of locally reacting cylinders, of infinite length. This model is based on the multiple-scattering theory due to Twersky. The cylinders are characterised by their radius and surface impedance, and the number of scatterers per unit area is also used in the calculations. The bulk propagation constant is calculated as

$$k_b = \left| k_0^2 - 4iNg + \left(g_1^2 - g^2\right)\left|\frac{2N}{k_0}\right|^2 \right|^{0.5}$$

where k_0 = propagation constant in air $\frac{\omega}{c_0}$

N = average number of scatterers per unit area

$$g = \sum_{n=-\infty}^{n=\infty} A_n \quad \text{and} \quad g_1 = \sum_{n=-\infty}^{n=\infty} (-1)^n A_n$$

and

$$A_n = -\left|\frac{iJ_n(ka) + Z_b J'_n(ka)}{iH_n(ka) + Z_b H'_n(ka)}\right|$$

a = radius of the cylinders

Z_b = The normalised surface impedance of the cylinders.

The attenuation is calculated from the imaginary part of the bulk propagation constant by means of a standard formula for attenuation in a porous medium;

$$Attenuation = \frac{20 \times \mathrm{Im}(k_b) \times depth}{\log_e(10.0)}$$

Results

Figure 1 shows a typical example of the measurements made on two different days in the mixed oak/spruce woodland. The pattern of attenuation is typical of that obtained in all the results in this study and also that described by other authors (eg. Martens 1981): ie it has a marked peak in attenuation at the low frequency part (200 to 250 Hz) a dip in the mid frequencies, and rises again in the high frequency part. It is widely accepted that the low frequency peak of such attenuation spectra is due to the ground effect. The difference in the location of the low frequency peak in the two spectra of figure 1 is thought to arise from a difference in the moisture content of the ground on the two days. A similar result to that of the winter measurement was obtained on a day in the summer of 1985 after a spell of wet weather but all the results from drier days gave a result similar to the summer measurement of figure 1. The wetter conditions gave a higher best fit effective flow resistivity than the dry days (see table 1), as might be expected.

The difference in the high frequency part of the two spectra of figure 1 appears to be due to the effect of foliage since the measuring path used was the same for both, the only difference being in the absence of leaves in the deciduous understorey in the winter measurement.

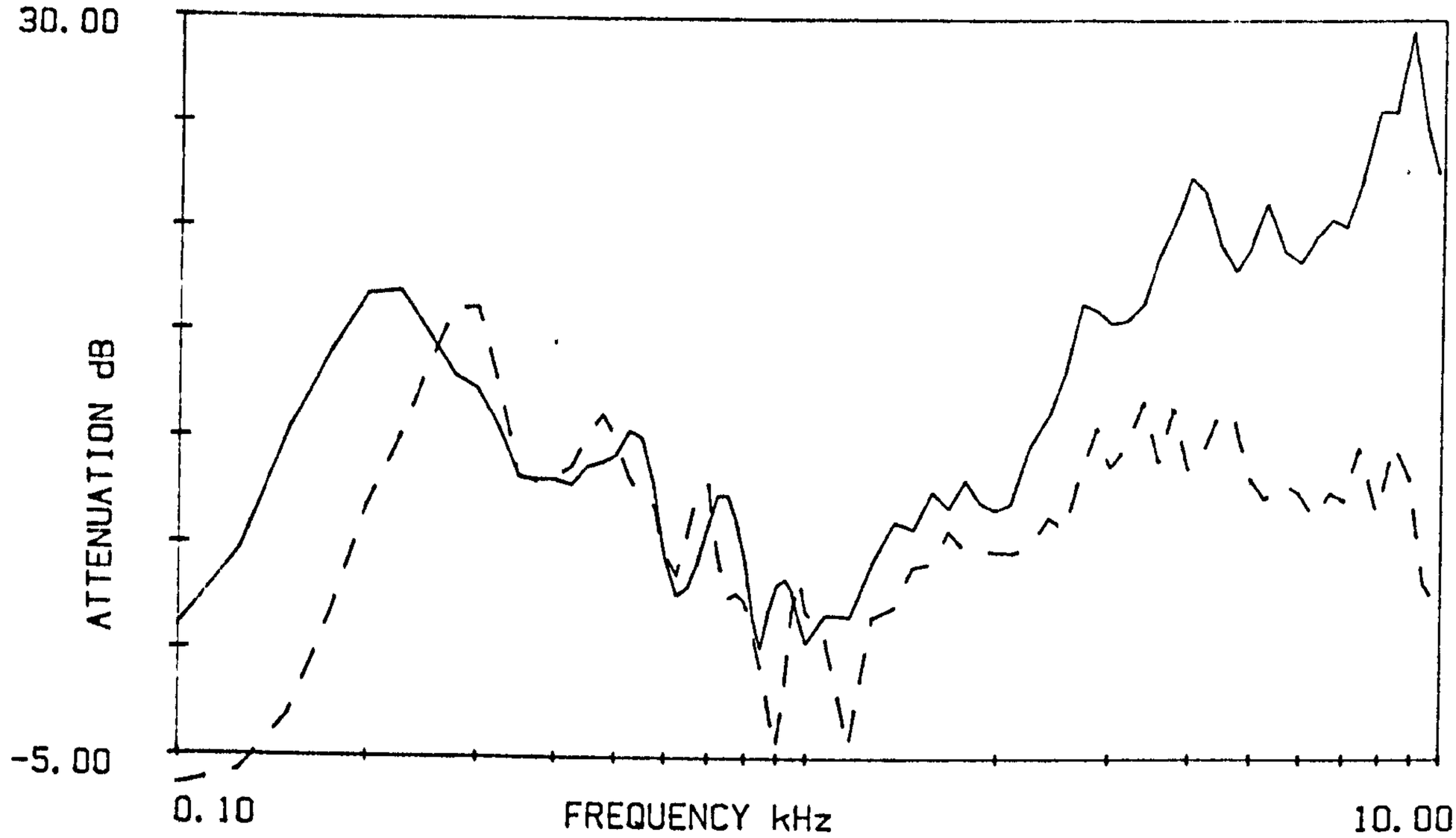

Figure 1 : Summer and Winter (-----) measurements in mixed oak/spruce wood.
Source Height = 1.3m, Test Microphone Height = 1.2m, Separation Distance = 72m.

TABLE 1 Best Fit Ground Parameters

Stand	Delany and Bazley	Attenborough Approximations: Homogeneous	Rigid-Backed Layer	
	σ_e	σ_e	σ_e	d_e
Spruce	40,000	61,000	63,000	0.09
Oak/Spruce dry	21,000	34,000	40,000	0.12
wet	65,000	114,000	119,000	0.07
Mixed Conifers	39,000	69,000	73,000	0.08

Table 1 shows the result of fitting the three predictive models to the attenuation spectra. The result of fitting the variable porosity model was, in practically all cases, identical to the homogeneous model ie α=0. The rigid-backed layer model generally gave a large value of effective depth and a similar effective flow resistivity to the homogeneous model. This indicates that this model also gives a best fit in virtually the homogeneous condition despite the fact that the ground has a layered structure.

The three woodlands do not have significantly different best fit ground parameters, although the two different cases (wet and dry) for the oak/spruce are significantly different, (significance assessed by means of a studentised T-test).

Figure 2 is a comparison between typical results from the three woodlands, the experimental geometry was approximately the same for each of the measurements and the mixed woodland result is from a summer measurement. The pattern of attenuation is clearly different in the different woodlands. The low frequency ground effect peak is at a similar frequency in the three woodlands although it is at a rather different magnitude in the mixed oak/spruce. The mixed oak/spruce wood gives a rather lower mean flow resistivity from all the measurements which does not appear to be reflected in this example.

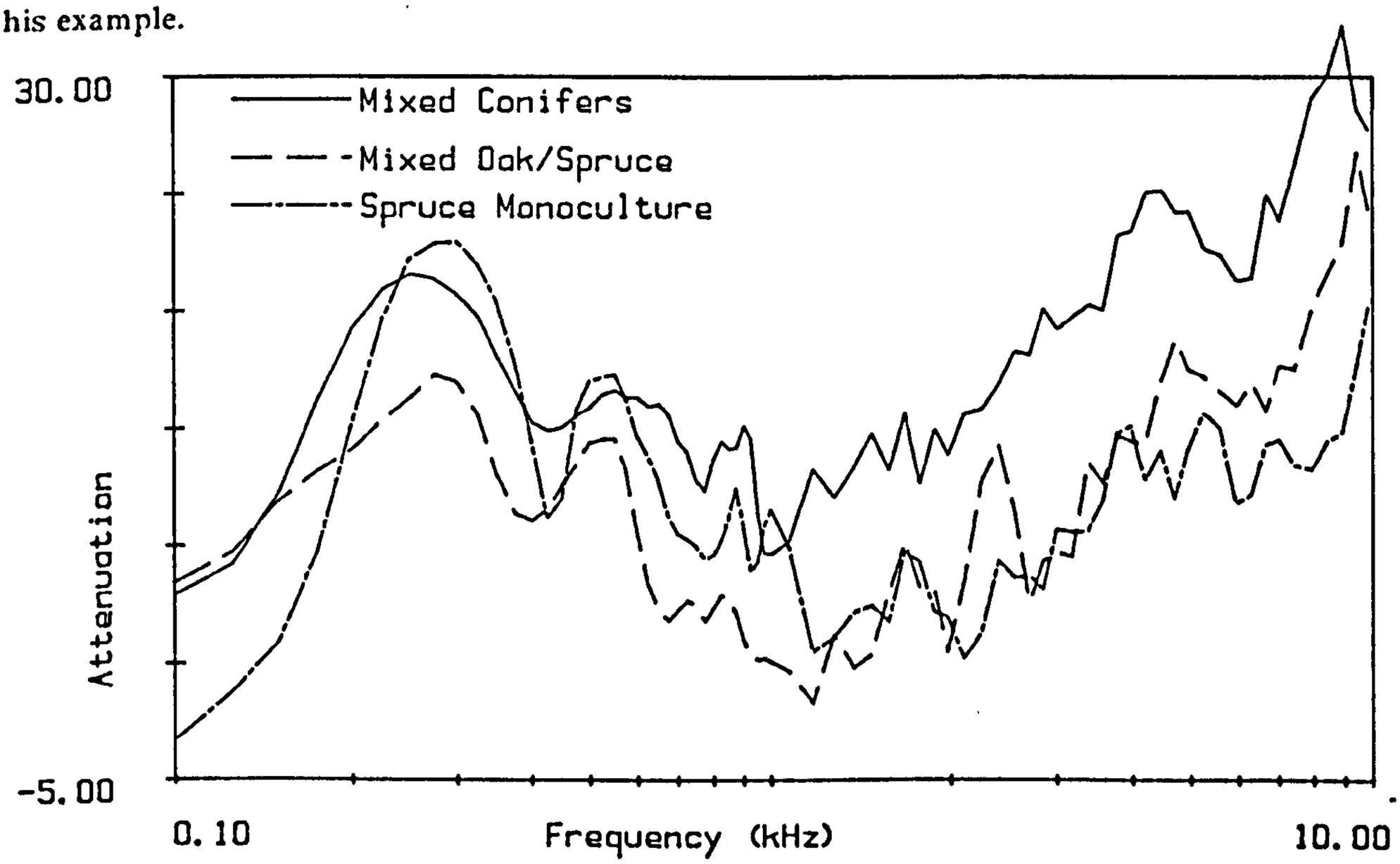

Figure 2 : Typical Attenuation Spectra for the Three Woodlands.
Source Height = 1.3m, Test Microphone Height = 1.2m, Separation Distance = 48m.

The mixed coniferous wood gives a higher value than the other two woods for most of the frequency range. This woodland had an extremely dense structure of foliage and branches especially in the red cedar rows. Which could account for the higher high- and mid-frequency attenuation in this stand. The mixed oak/spruce woodland gives a higher value of attenuation in the high frequency part than the spruce woodland. The winter oak/spruce measurements generally give a similar value of high frequency attenuation to that in the spruce.

Figure 3 shows an example of the use of the ground effect model calculated using the the best fit value of σ_e in the Homogeneous approximation of Attenborough (1985), and the result of adding predictions from the ground model to that from the scattering model. The scattering prediction is calculated using the mean radii and densities detailed above, and assuming that the cylinders are rigid. This assumption is based on the results of impedance tube measurements made by Frank (1976) which showed that trees have a very low absorption coefficient. It is evident that the ground effect model

predicts the low frequency part of the attenuation spectra quite well, but the high frequency part of the measurement diverges rapidly from the prediction and the sharp peak of the prediction is not seen in the measurement. Adding the scattering prediction does not significantly improve the comparison between prediction and measurement, causing over-prediction at some frequencies and under-prediction at others.

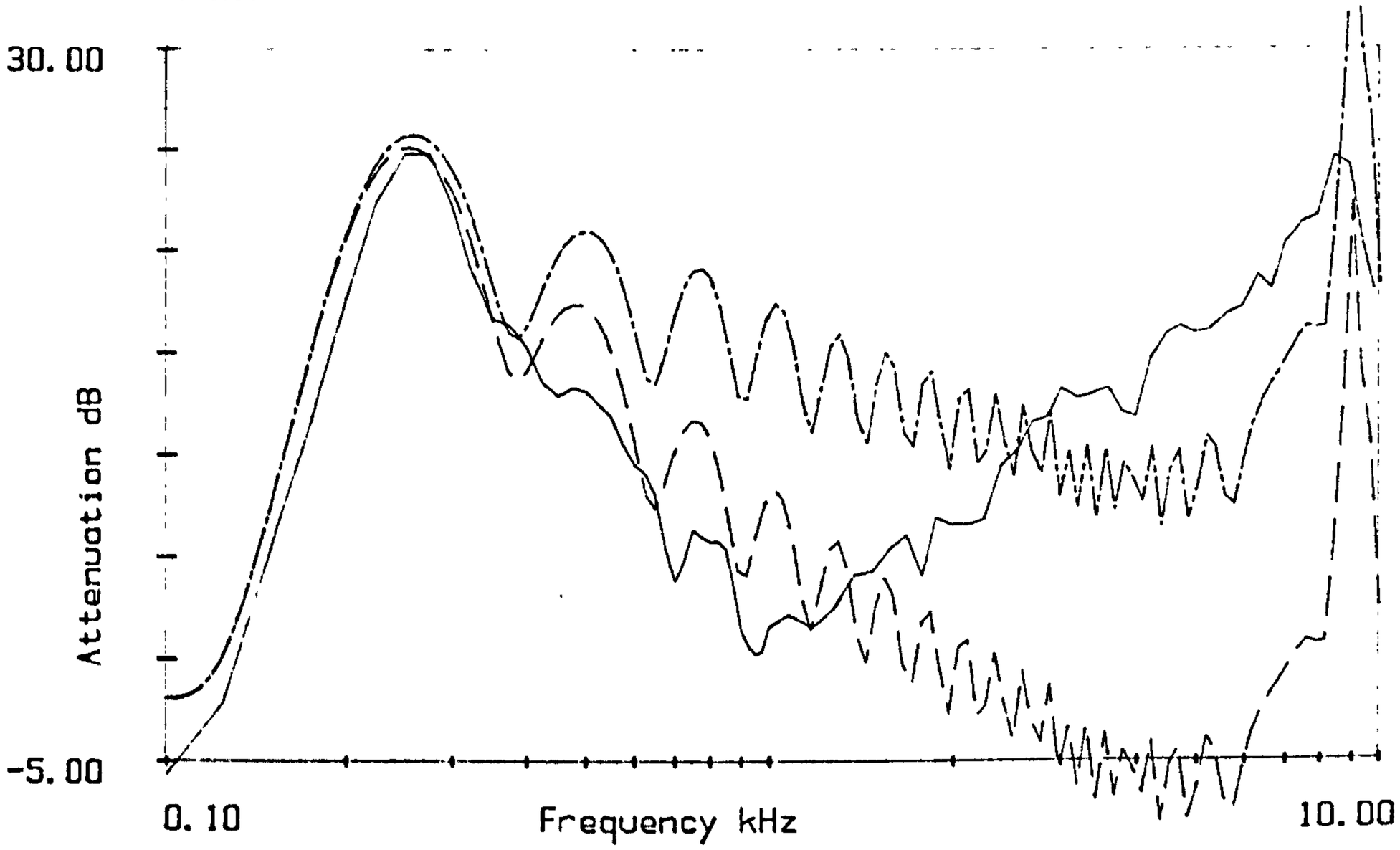

Figure 3.
——— Measurement from the Spruce monoculture, separation distance 96m, microphone height 1.2m.
— — — Ground effect prediction σe = 64,000.
—·—·— Ground + scattering prediction.

Investigation of the high frequency part of the measurements made at 40m separation or greater shows that the attenuation has a linear relationship with distance, and that the marked high frequency interference peaks are only very rarely observed. These facts indicate that the attenuation is not related to ground interference and can be expressed as the attenuation for a certain distance to compare results from different distances. Figure 4 is a comparison between the mean values of high frequency attenuation from all the longer distance measurements corrected to the value of attenuation per 25m. The mixed coniferous wood evidently gives considerably greater attenuation than the other two woods, with a smaller difference between the spruce and mixed woods. Figure 5 shows the attenuations from the scattering model corresponding to the predicted trunk attenuation, assuming rigid cylinders and using the sampled mean trunk radius and density given above. The predictions do not have the same frequency dependence as the measurements although they do increase with frequency. The attenuation is greatly under-predicted for the mixed coniferous wood and also for most of the mixed oak/spruce spectrum. The spruce monoculture attenuation is, however over-predicted over the whole range.

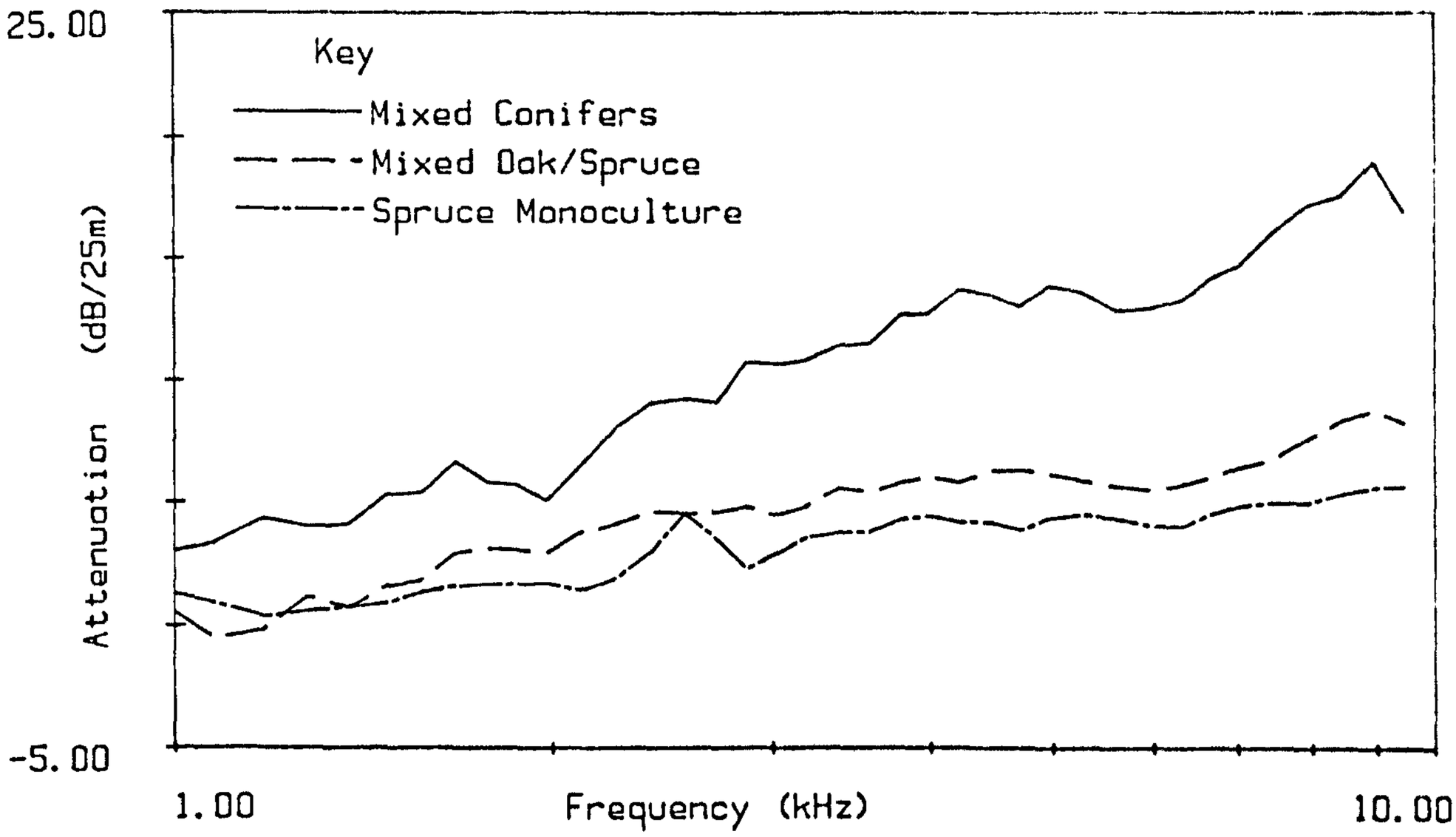

Figure 4

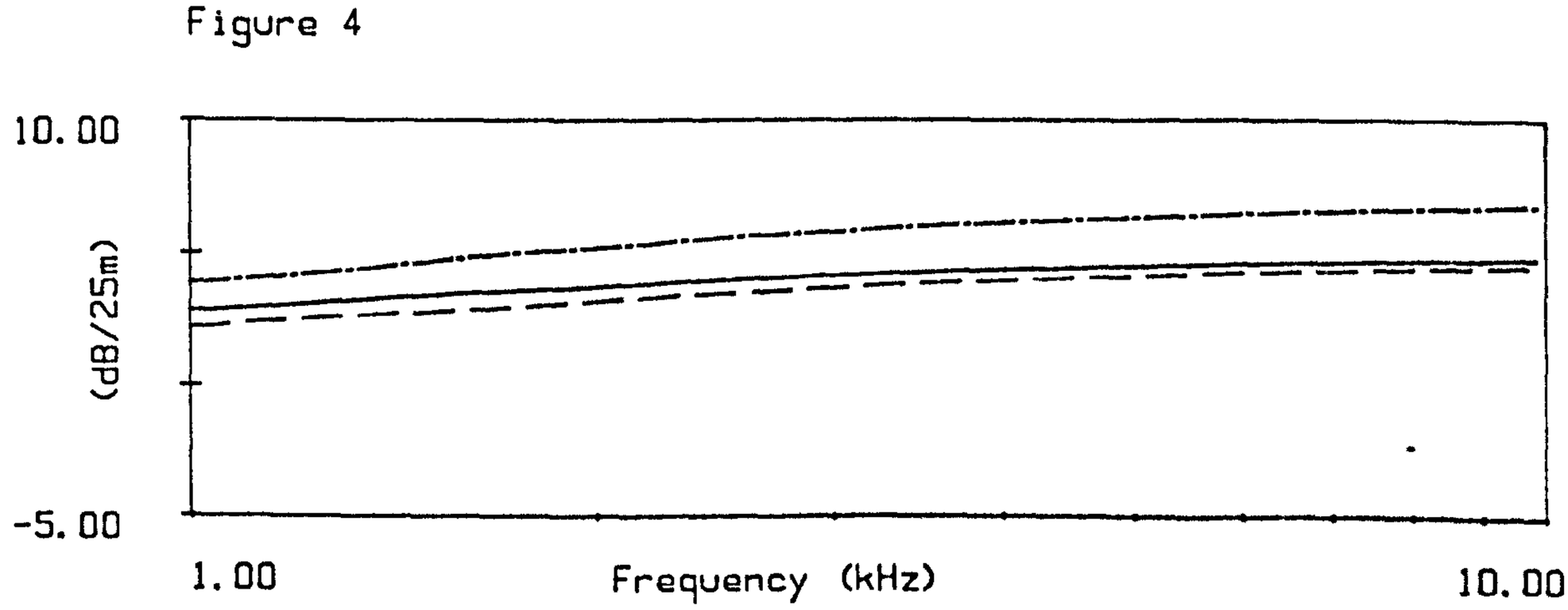

Figure 5

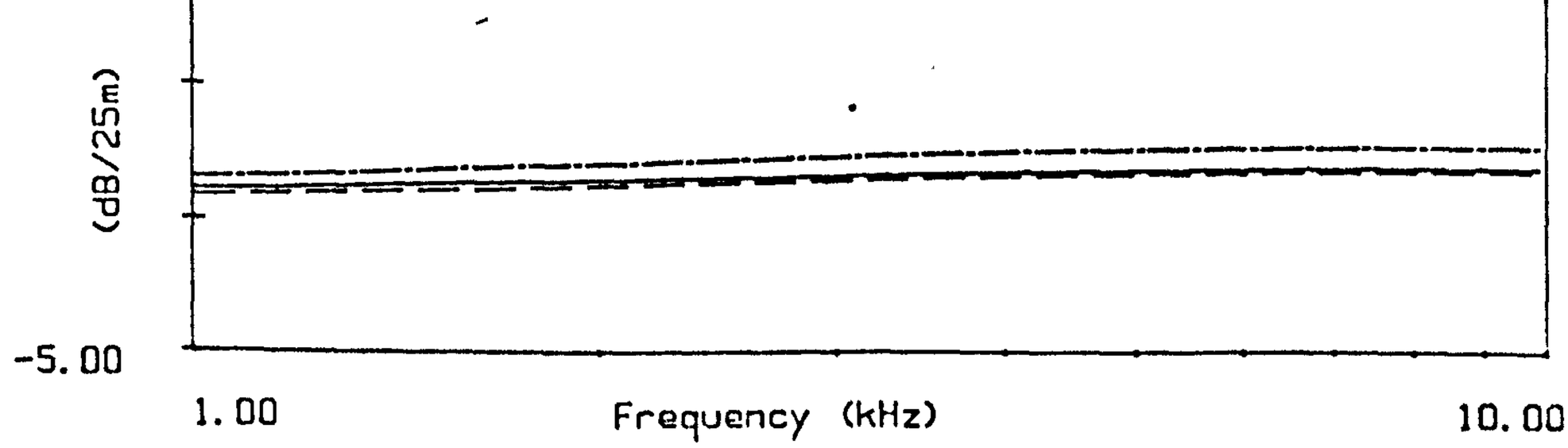

Figure 5a

Model Experiments

In order to investigate the scattering prediction model further, and determine its validity in the presence of a ground surface, a small scale model experiment was carried out in an anechoic chamber. An air jet sound source producing a broad-band signal with much energy in the high frequency range (1kHz to 100kHz) was used. The analysis of the results was carried out between 1kHz and 100kHz thus the experiment assesses the case of small wavelengths and small scatterers to compare with the larger wavelengths and larger scatterers of the woodland experiments. Wooden dowel rods with diameters of 6mm and 12mm were used to create random or regular arrays, of varying densities between the air jet and an array of microphones and the resulting signal at the microphones analysed. The rods were then removed and the measurement repeated. The continuous line of figure 6 shows an example of the attenuation calculated by subtracting the 'with scatters' measurement from the 'without scatterers' case, this is from an experiment using long scatterers, with no ground surface, and a random array. The broken line of figure 6 is the result of an experiment using the same array but the rods were inserted into a tray of sand in the anechoic chamber and the source and microphones were close to the sand surface. The insertion loss shown here is the result of subtracting the signal recorded with the scatterers in the sand from that with the sand surface alone. This measurement and others carried out in the same way show that the insertion loss from the sand tray and the attenuation from the semi-infinite length case are similar, ie that there is no detectable interaction between the ground and scattering effect which could not be accounted for by simply adding the effects of the ground and the scatterers.

Figure 7 shows a comparison between the attenuation measurement of figure 6 and the predicted attenuation from the scattering model described above. It is evident that the model greatly over-predicts the attenuation. The prediction uses the rigid cylinder assumption. Altering the surface impedance of the cylinders in the prediction only increases the predicted attenuation. In order to fit the prediction to the measurement either the assumed radius or density may be altered. Fitting all the results to the prediction by altering each of the parameters showed that, on average, a reduction in density of 60% while maintaining the measured radius gives a considerably better fit to the measured data. The second prediction line in figure 7 shows this correction to the model, it is evident that this prediction matches the measurement quite well.

Scattering Predictions for Woodland Measurements

The assumption is made that a similar correction could be made to the prediction for the woodland measurements. Figure 5a shows the resulting predictions in dB/25m for the high frequency part of the woodland results, ie the mean sampled radii given above, are used, but the density is reduced by 60%. It is evident from comparisons with figure 4 that all the attenuation spectra are under-predicted except for the lower frequencies in the spruce and mixed oak/spruce woodlands.

In an attempt to predict the part of the high frequency attenuation not accounted for by trunk scattering, a further calculation using the scattering model was carried out. Figures 8 and 9 show the result of putting a radius of 1mm and a surface impedance calculated using a high flow resistivity (10,000,000 mks), rather than the rigid assumption, into the model. The sum of the 'trunk prediction' and the small scatterers prediction gives a good fit to the high frequency part. The density of 1mm scatterers used for the mixed coniferous wood ($600m^{-1}$) is 6 times greater than that for the spruce monoculture. Since the prediction assumes a non-rigid surface this accounts for the absorption of sound at the surface. Figures 8a and 9a show the two predictions added together in figures 8 and 9. It is evident that the trunk scattering prediction (continuous lines) contributes a greater proportion of the total in the spruce monoculture, particularly in the mid frequencies, than in the mixed coniferous wood. The amount of foliage and branches is considerably greater in the younger mixed coniferous

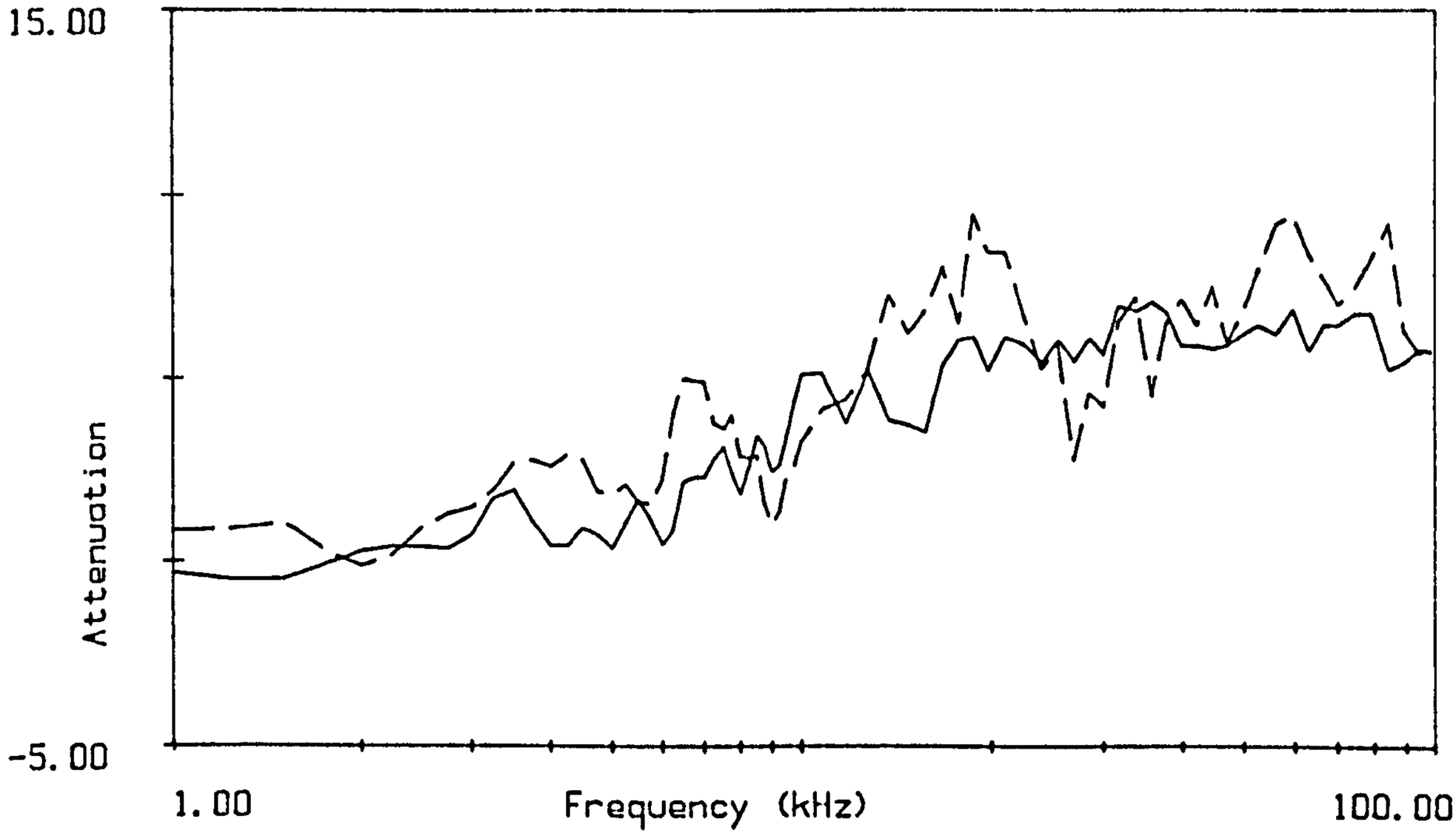

Figure 6
Attenuation and Insertion Loss(----) from an array of cylinders density = 240 rod per square metre, radius = 0.006m, separation distance = 0.65m

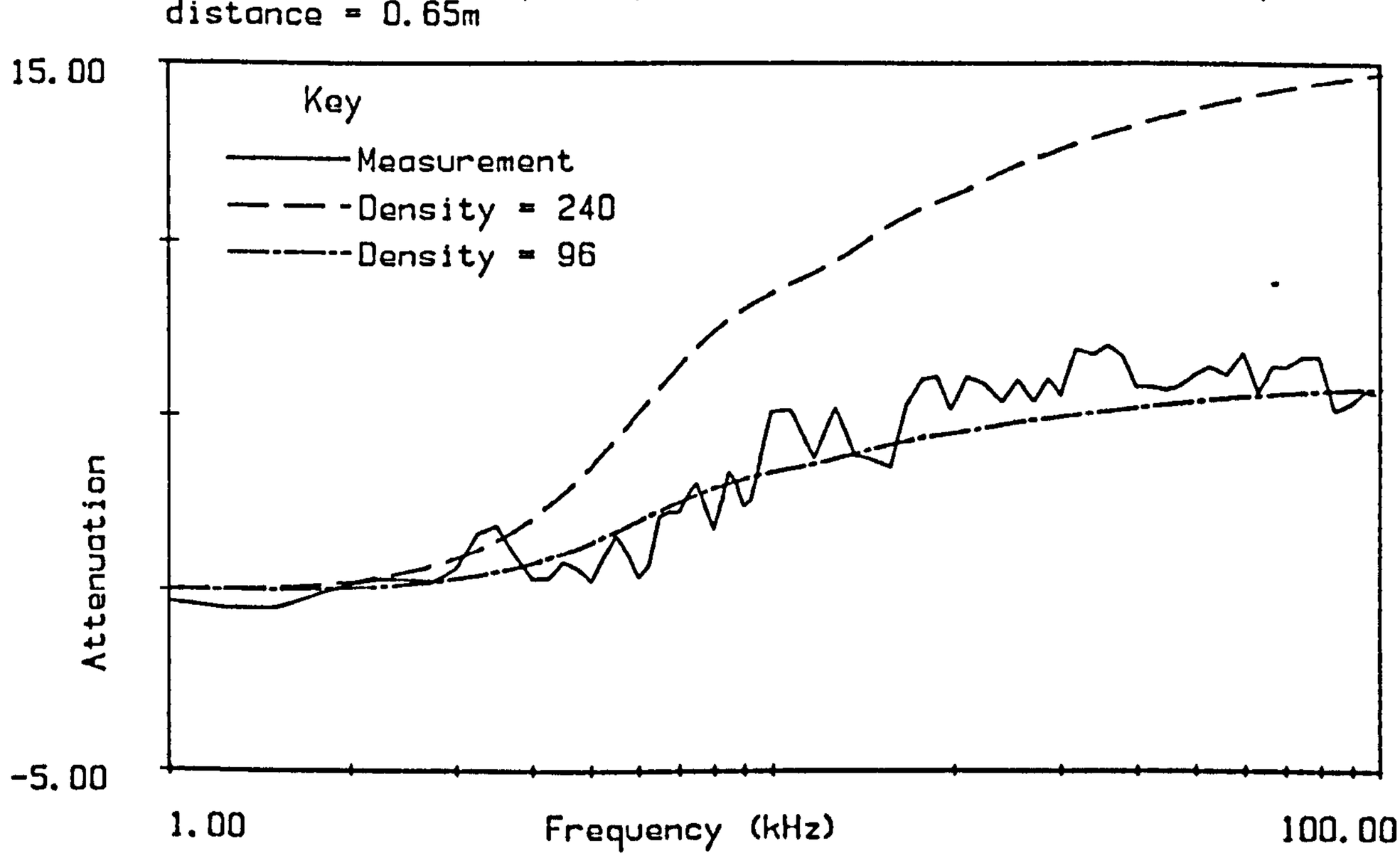

Figure 7
Measured attenuation of figure 6 compared with predictions using measured and modified (-60%) densities.

wood than the spruce monoculture, so the prediction from the 1mm non-rigid scatterers could be regarded as a way of accounting for the scattering and absorbing effects of these woodland elements. The two parts of the prediction could relate, conceptually, to the scattering and absorbing cross sections described by Bullen and Fricke (1982), since the rigid assumption for the trunks confines their effect to scattering rather than absorption whereas some absorption is accounted for in the small scatterers prediction.

Figures 8 and 9 indicate that a combination of ground effect (low frequencies only), scattering by trunks and scattering and absorption by smaller woodland elements, both characterised by the multiple scattering model described by Embleton (1966), could be used to predict the measured attenuation in woodlands.

References

[1] Attenborough, K., Hayek, S.I. and Lawther J.M. 1980. J. ACOUST. SOC. AM. 68 (5) 1493-1501 Propagation of Sound Above a Porous Half-space.

[2] Attenborough K. 1985 J. SOUND VIB. Acoustical Impedance Models for Outdoor Ground Surfaces.

[3] Bazley, E.N. 1976 NPL ACOUSTICS REPORT AC74. Sound absorption in air at frequencies up to 100kHz.

[4] Bullen, R. and Fricke, F. 1982 J. SOUND VIB. 80(1) 11-23 Sound Propagation Through Vegetation.

[5] Delany, M.E. and Bazley, E.N. 1970. APPLIED ACOUSTICS 3 105. Acoustical properties of Fibrous Materials.

[6] Embleton, T.F.W. 1966 J. ACOUST. SOC. AM. 40 (3) 667-670, Scattering by an Array of Cylinders as a Function of Surface Impedance.

[7] Frank, L.D. 1976 MS THESIS PENNSYLVANIA STATE UNIVERSITY. Tree Bark and Forest Floor as Sound Absorbing Elements Within a Forest.

[8] Martens, M.J.M. 1981, APPLIED ACOUSTICS 14 167- 189. Noise Abatement in Plant Monocultures and Plant Communities.

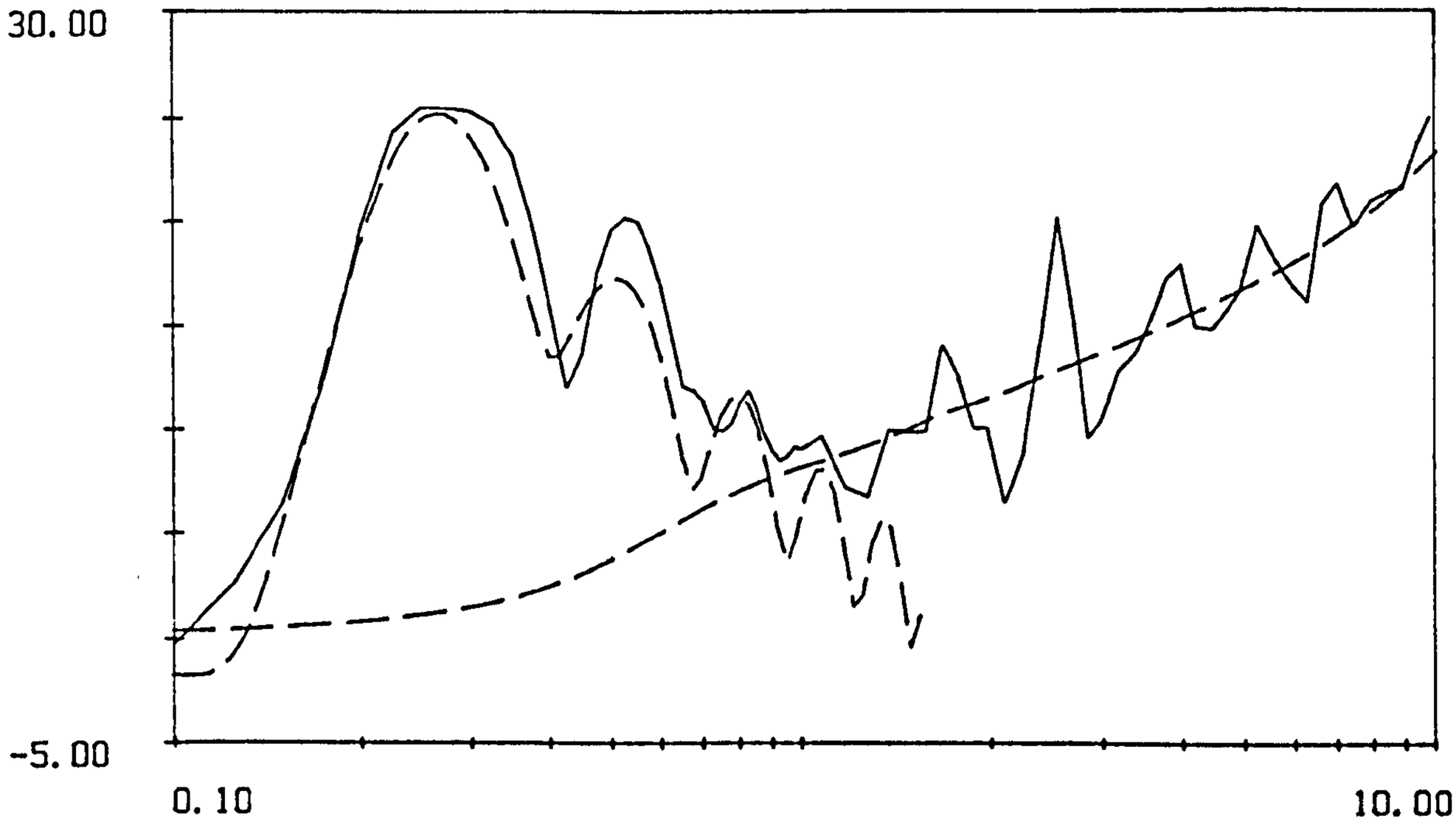

Figure 8 Attenuation at 96m in Spruce monoculture
(-----) predictions - ground effect σ_e =69,000
and sum of scattering predictions of Figure 8a.

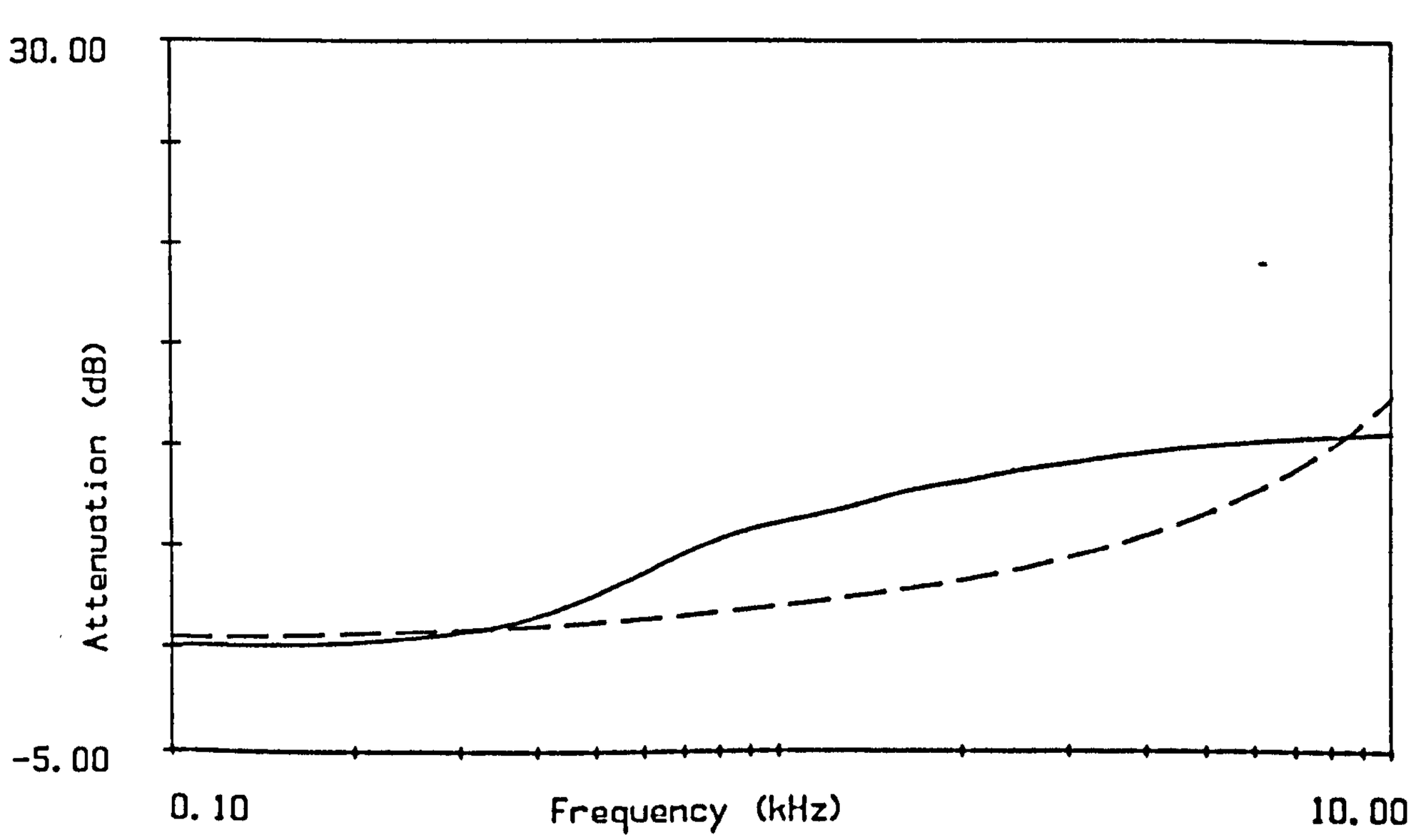

Figure 8a
Scattering Predictions:
——— Radius = 0.059, Density = 0.1212, Rigid Cylinders
------ Radius = 0.001, Density = 100 ,
Surface Impedance calculated using σ_e = 10,000,000

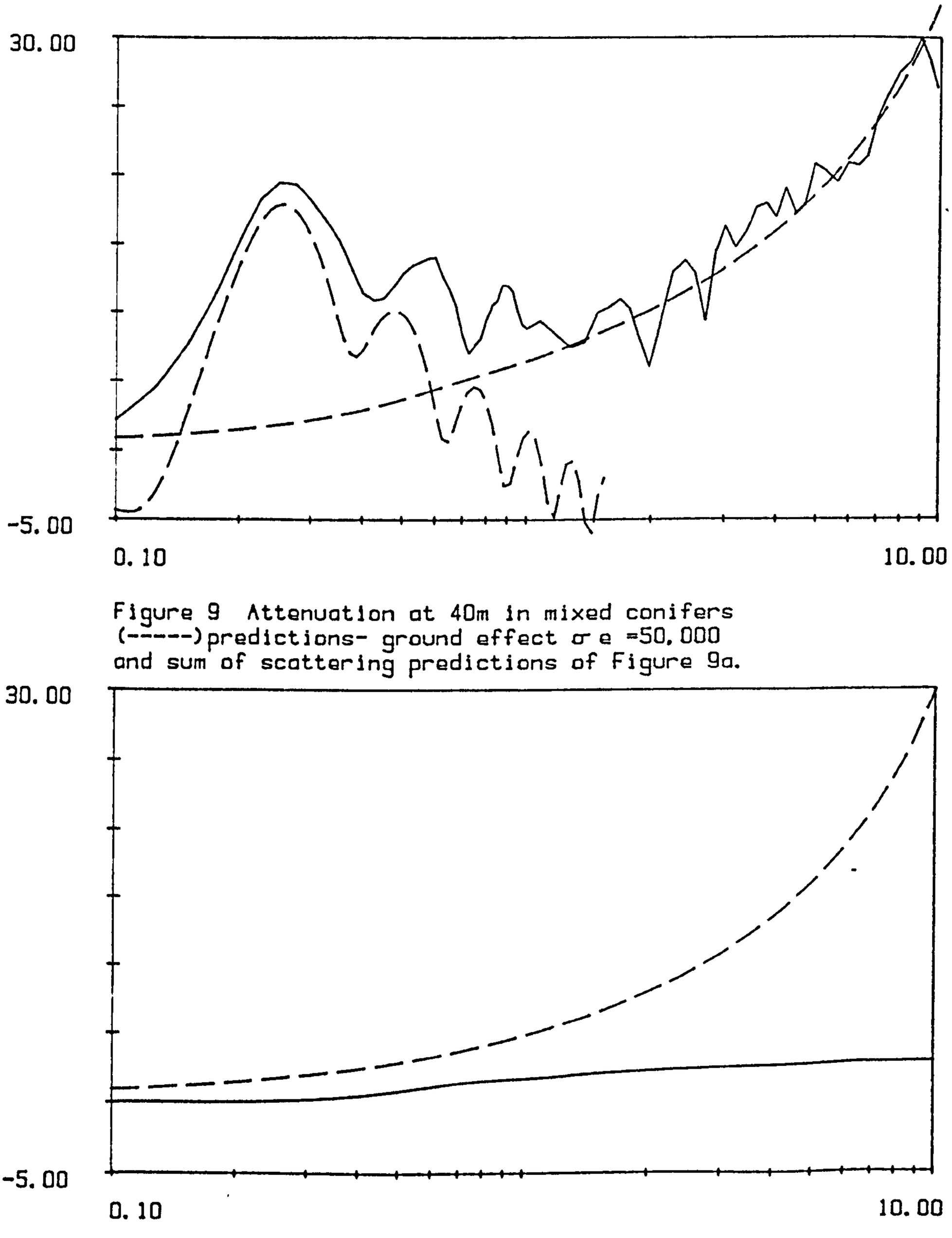

Figure 9 Attenuation at 40m in mixed conifers
(-----)predictions- ground effect σ e =50,000
and sum of scattering predictions of Figure 9a.

Figure 9a
Scattering Predictions:
——— radius = 0.066, density = 0.0724, rigid cylinders
------ radius = 0.001, density = 600,
surface impedance calculated using σ e = 10,000,000.

Appendix F: Glossary of Acoustical Terms.

Absorption Coefficient: the ratio of sound energy absorbed by by a surface to the total sound energy which strikes it.

Acoustics: the science of sound.

Acoustical: relating to acoustics.

Amplitude: the maximum value, the peak.

Anechoic: almost totally sound-absorbent at a very wide range of frequencies. An anechoic chamber gives almost **Free Field** conditions.

Audio Frequency: a frequency within the audible range of about 20 Hz to 20,000 Hz.

A-weighting: a weighting applied electronically, or numerically, which reduces the contribution of the low and high frequencies to the overall sound pressure level, in order to approximately simulate the response of the human ear. The resulting level is expressed as dBA.

Band: a segment of the frequency spectrum, eg. an octave or third octave.

Bel ten decibels (not normally used).

Characteristic Impedance (ρc): a measure of the qualities possessed by a substance carrying sound waves which indicates the ratio of the root mean square (rms) sound pressure at a point to the rms particle velocity. It is equal to the product of the density 'ρ' and the speed of sound 'c' in the substance.

Decibel (dB): (one tenth of a Bel) a means of denoting the ratio of two quantities when the range of the values is very great. A Bel can be described as the number of tenfold increases the lower quantity must be given to equal the higher, ie $\log_{10}\left[\frac{i_1}{i_2}\right]$; Sound pressure level is the commonest quantity expressed in decibels, in which case the lower quantity is usually $2\times10^{-5}Nm^{-2}$, known as the reference pressure.

Diffraction: the diversion of the direction of travel of a wave other than by reflection or refraction.

Echo: reflected sound which arrives a long enough time after its direct equivalent to be heard as a separate sensation.

Field: region of acoustical interest.

Free Field: a region in which no significant reflections of sound occur.

Frequency: the number of times a vibrating system or particle completes a repetitive cycle of movement in a period of one second, expressed in Hertz or 'cycles per second'. Non-periodic waves can also be defined in terms of frequency, in which case the rates of rise and fall of pressure for a given amplitude govern the frequencies in the wave.

Gradient: a variation of the local speed of sound with height above ground, or other measure of distance, causing **refraction** of sound. It is most commonly caused by rising or falling temperature with altitude or by differences in wind speed.

Impedance: a measure of the complex ratio of force (or pressure) to velocity see also **Characteristic Impedance.**

Natural Frequency: the frequency at which a system oscillates freely after suitable excitation.

Noise: Unwanted sound.

Octave: the interval between two sounds one of which has a frequency twice that of another.

Oscillation: variation in the magnitude of a quantity above and below a certain level over a period of time (or distance).

Particle: a theoretical infinitesimally small part of a substance or medium.

Peak Sound Pressure Level: the value in decibels of the maximum sound pressure level.

Periodic: repeating in an identical form after a constant and repetitive period of time. The classic example is a **sine wave.**

Phase: a measure or whether a sound or other periodic function is 'in step' or 'out of step'. It is measured as an angle in degrees or (usually) in radians. If, for example, one sine wave lags behind another so that it is always at its minimum when the other is at its maximum it is π radians or 180/(de out of phase.

Plane Wave: A wave in which the **wave fronts** are parallel with one another and at right angles to the direction of propagation.

Pure Tone: A sound whose waveform is **sinusoidal.**

Random Noise: Strictly speaking, a fluctuating quantity (sound or electronic) whose amplitude distribution with time is Gaussian. Generally, noise due to random pressure or other fluctuations resulting in a continuous spectrum.

Refraction: the bending of sound by passage from one medium to another or in a gradient.

Resonance: when a system is vibrating as a result of a forced excitation at a certain frequency, if the amplitude of vibration deminishes as a result of raising or lowering the frequency of the exciting force then the system is in resonance.

Resonant: capable of being excited into resonance.

Resonant Frequency: a frequency at which resonance occurs.

Reverberation: sound (eg. in a room) which builds up owing to multiple reflections from surrounding surfaces. It will persist after the source has stopped emitting sound.

Reverberation Time: the time it takes for reverberant sound of a given frequency to decay by 60dB after the source is cut off.

Root-mean-square (rms) Value: the values of a fluctuating quantity are squared, averaged and then the square root is extracted. The peak sound pressure of a sine wave is equal to the rms sound pressure multiplied by $\sqrt{2}$. The rms sound pressure level is the best measure of continuous sound but the peak level is necessary for the assessment of impulsive sound.

Sine wave: a wave which varies with time or distance as the trigonometric function, the sine.

Sinusoidal: varying as the sine of an angle.

Sound: wave motion in an elastic medium, or the sensation of hearing this may produce.

Sound Power Level: the total energy per second emitted by the source as sound expressed as decibels, normally referenced to 10^{-12} Watts.

Sound Pressure Level: the rms (usually) values of the pressure fluctuations above and below atmospheric pressure caused by the passage of a sound wave, expressed in decibels re $2\times10^{-5}Nm^{-2}$.

Sound Shadow: the acoustical equivalent to a light shadow, usually partially penetrated as a result of diffraction.

Spherical Wave: A wave in which the wave fronts form concentric spheres.

Transmission Loss: a measure of the sound insulation of a layer of material in decibels. It is equal to the arithmetic difference between the level in decibels of the incident and transmitted waves.

Wave: a disturbance propagated in a medium.

Wave Front: a theoretical surface which is made up of points at which the phase of a wave is the same. In the case of a sine wave the wave front joins points of equal amplitude and phase.

Wavelength: the perpendicular distance between two wave fronts in which the phases differ by one complete period. It is equal to the speed of sound divided by the frequency and is usually represented by λ.

White Noise: noise of a statistically random nature having equal energy at every frequency over a particular band.